LAMINATION RESIDUAL STRESSES IN FIBER COMPOSITES
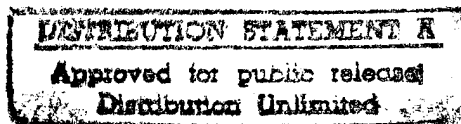
INTERIM REPORT

by I. M. Daniel and T. Liber

IIT RESEARCH INSTITUTE

19960206 049

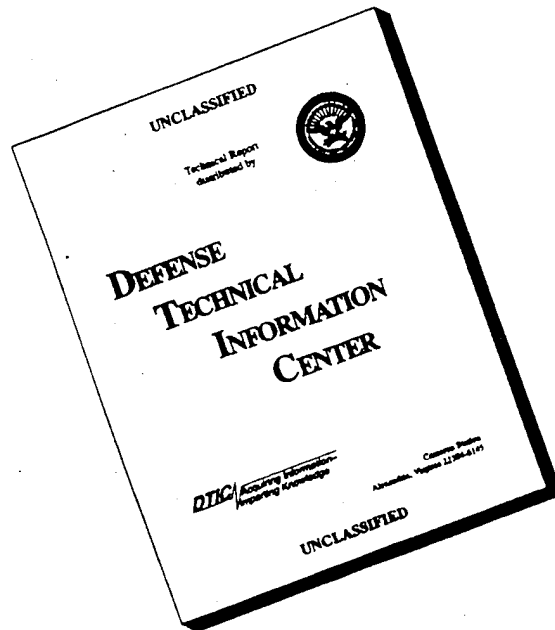Prepared for

DISCLAIMER NOTICE

UNCLASSIFIED

Technical Report
distributed by

**DEFENSE
TECHNICAL
INFORMATION
CENTER**

DTIC Acquiring Information—
Imparting Knowledge

Cameron Station
Alexandria, Virginia 22304-6145

UNCLASSIFIED

THIS DOCUMENT IS BEST QUALITY AVAILABLE. THE COPY FURNISHED TO DTIC CONTAINED A SIGNIFICANT NUMBER OF PAGES WHICH DO NOT REPRODUCE LEGIBLY.

ADD 420299

1. Report No. NASA CR-134826	2. Government Accession No.	3. Recipient's Catalog No.
4. Title and Subtitle Lamination Residual Stresses In Fiber Composites–Interim Report		5. Report Date March 1975
		6. Performing Organization Code
7. Author(s) I. M. Daniel and T. Liber		8. Performing Organization Report No. D6073-I
9. Performing Organization Name and Address IIT Research Institute 10 West 35 Street Chicago, IL 60616		10. Work Unit No. IITRI R.P. No. D6073
		11. Contract or Grant No. NAS3-16766
12. Sponsoring Agency Name and Address National Aeronautics and Space Administration Washington, DC 20546		13. Type of Report and Period Covered Interim 8-72 to 6-74
		14. Sponsoring Agency Code

15. Supplementary Notes
Project Manager, C. C. Chamis
Materials and Structures Division
NASA-Lewis Research Center
Cleveland, OH 44135

16. Abstract
An experimental investigation was conducted to determine the magnitude of lamination residual stresses in angle-ply composites and to evaluate their effects on composite structural integrity. The materials investigated were Boron/Epoxy, Boron/Polyimide, Graphite/Low Modulus Epoxy, Graphite/High Modulus Epoxy, Graphite/Polyimide and S-Glass/Epoxy. These materials were fully characterized. Static properties of $[0_2/\pm45]_s$ laminates were also determined. Experimental techniques using embedded strain gages were developed and used to measure residual strains during curing. The extent of relaxation of lamination residual stresses was investigated. It was concluded that the degree of such relaxation is low. The behavior of angle-ply laminates subjected to thermal cycling, tensile load cycling, and combined thermal cycling with tensile load was investigated. In most cases these cycling programs did not have any measurable influence on residual strength and stiffness of the laminates. The only exceptions were the Graphite/Low Modulus Epoxy and S-Glass/Epoxy which failed during elevated temperature thermal cycling under load and showed degradation during low temperature thermal cycling under load. In the tensile load cycling tests, the Graphite/Polyimide showed the highest endurance with 10 million cycle runouts at loads up to 90 percent of the static strength. The S-Glass/Epoxy had the lowest endurance failing to survive 10 million cycles even at 25 percent of ultimate. The effects of fiber volume ratio, ply orientation and ply stacking sequence were also investigated for Graphite/Polyimide. Residual strains during curing, static strength and residual properties after thermal cycling under load were determined. The $[0_2/\pm15]_s$ specimens with the lowest residual stresses showed somewhat higher residual strength. The $[0_2/90_2]_s$ laminate, having the highest residual stresses, showed a reduction in residual stiffness and strength. No significant changes were observed in residual properties of the three stacking sequence variations of the $[0_2/\pm45]_s$ laminate.

17. Key Words (Suggested by Author(s)) angle-ply fiber composites, lamination-residual stresses, embedded gages, stress relaxation, thermal load cycling, tensile load cycling, residual strength and stiffness, acoustic emission	18. Distribution Statement Unclassified, Unlimited

19. Security Classif. (of this report) Unclassified	20. Security Classif. (of this page) Unclassified	21. No. of Pages 467	22. Price* $11.50

* For sale by the National Technical Information Service, Springfield, Virginia 22151

NASA-C-168 (Rev. 6-71)

FOREWORD

This is the First Interim report on IIT Research Institute Project No. D6073 "Lamination Residual Stresses in Fiber Composites," prepared by IITRI for NASA-Lewis Research Center, under Contract No. NAS3-16766. The work described herein was conducted in the period 1 August 1972 to June 30, 1974. Dr. C.C. Chamis was the NASA-Lewis Project Manager. IIT Research Institute personnel who made material contributions to the work reported herein include: Drs. I.M. Daniel, T. Liber and Messrs K.E. Hofer, N.P. Rao, L.C. Bennett, M. Iyengar, R. LaBedz, H. Lane, R. Lebeter and T. Niiro.

Respectfully submitted,
IIT RESEARCH INSTITUTE

I.M. Daniel
Science Advisor
Mechanics of Materials Division

APPROVED:

R.H. Cornish
Director
Mechanics of Materials Division

IMD/djc

iii

LAMINATION RESIDUAL STRESSES IN FIBER COMPOSITES

ABSTRACT

An experimental investigation was conducted to determine the magnitude of lamination residual stresses in angle-ply composites and to evaluate their effects on composite structural integrity. The materials investigated were Boron/Epoxy, Boron/Polyimide, Graphite/Low Modulus Epoxy, Graphite/High Modulus Epoxy, Graphite/Polyimide and S-Glass/Epoxy. These materials were fully characterized. Static properties of $[0_2/\pm45]_s$ were also determined. Experimental techniques using embedded strain gages were developed and used to measure residual strains during curing. The extent of relaxation of lamination residual stresses was investigated. It was concluded that the degree of such relaxation is low. The behavior of angle-ply laminates subjected to thermal cycling, tensile load cycling and thermal cycling with tensile load was investigated. In most cases these cycling programs did not have any measurable influence on residual strength and stiffness of the laminates. The only exceptions were the Graphite/Low Modulus Epoxy and S-Glass/Epoxy which failed during elevated temperature thermal cycling under load and showed degradation during low temperature thermal cycling under load. In the tensile load cycling tests, the Graphite/Polyimide showed the highest endurance with 10 million cycle runouts at loads up to 90 percent of the static strength. The S-Glass/Epoxy had the lowest endurance failing to survive 10 million cycles even at 25 percent of ultimate. The effects of fiber volume ratio, ply orientation and ply stacking sequence were also investigated for Graphite/Polyimide. Residual strains during curing, static strength and residual properties after thermal cycling under load were determined. The $[0_2/\pm15]_s$ specimens with the lowest residual stresses showed somewhat higher residual strength. The $[0_2/90_2]_s$ laminate, having the highest residual stresses, showed a reduction in residual stiffness and strength. No significant changes were observed in residual properties of the three stacking sequence variations of the $[0_2/\pm45]_s$ laminate.

TABLE OF CONTENTS

TABLE OF CONTENTS (Cont.)

LIST OF TABLES

LIST OF TABLES (Cont.)

LIST OF FIGURES

LIST OF FIGURES (Cont.)

LIST OF FIGURES (Cont.)

LIST OF FIGURES (Cont.)

LIST OF FIGURES (Cont.)

LIST OF FIGURES (Cont.)

IITRI Research Project No. D6073

LAMINATION RESIDUAL STRESSES IN FIBER COMPOSITES

1.0 INTRODUCTION

Advanced filamentary composites, such as boron and graphite reinforced plastics, are finding increasing applications in more critical aircraft components such as fan blades. The evaluation of a given structural component from the point of view of stiffness and load carrying capacity requires exact knowledge of the loading conditions, stress and strain distributions, material properties and failure criteria. Similar information is required in the synthetic approach where a structural and material design is sought to meet a desired function with its concomitant loading on the component.

In conducting the stress analysis step in this process it is very important to add to the externally induced stresses the pre-existing state of residual stress. The type of residual stresses that are of critical importance are those stresses produced during curing and caused by the different coefficients in thermal expansion of the various plies of a laminate. An extensive analysis of lamination residual stresses was given by Chamis.[1] Using a linear laminate theory he presented results on residual stresses as a function of constituent properties, ply-stacking sequence and orientation, fiber content, cure temperature and other variables. It was shown that residual stresses can reach values comparable to the transverse strength of the ply and thus induce cracking across the plies.[1,2] They can also cause interlaminar separation.

Before the theory above can be generally applied to design of critical components, it must be verified experimentally. A systematic experimental program is needed to measure residual stresses directly, their possible decay with time, and their dependence on composite design variables. An experimental study is also needed of the influence of residual stresses on the structural integrity, stiffness and strength of the composite.

To meet the needs above, the NASA-Lewis Research Center is sponsoring the current program with IIT Research Institute under Contract No. NAS3-16766. The objectives of the present investigation are: (1) to experimentally determine the magnitude of lamination residual stresses in fiber-composite angle-ply laminates, (2) to evaluate their effects on composite structural integrity, and (3) to provide experimental data for verification of existing lamination residual stress theory.

The investigation described in this interim report consists of the following five tasks:

TASK I - Literature Survey and Materials Selection

The objective of this task was to conduct a selective literature survey to obtain thermal and mechanical properties of unidirectional composites and their constituent matrix and fiber materials and to select six fiber/matrix systems for the experimental investigation.

TASK II - Residual Strains and Static Strength

The objective of this task was to fabricate and characterize the six composite materials selected, to develop instrumentation procedures and measure residual strains during curing, and to determine the static strength of angle-ply laminates.

TASK III - Evaluation of Stress Relaxation

The objective of this task was to evaluate the magnitude of relaxation of residual stresses and its effect on strength.

TASK IV - Cyclic Loading and Residual Strength

The objective of this task was to measure degradation and residual strength of angle-ply laminates subjected to cyclic thermal loading, cyclic mechanical loading and cyclic thermal loading under tension.

TASK V - Effects of Laminate Configuration Variables

The objective of this task was to determine the effects of fiber volume ratio, ply stacking sequence and ply orientation on the magnitude of residual stress and residual strength after thermal cycling under tensile load.

2.0 TASK I - LITERATURE SURVEY AND MATERIALS SELECTION

2.1 Literature Survey

The following six fiber/matrix material systems were investigated in this program:

A. Boron/Intermediate Modulus Epoxy

B. Boron/Polyimide

C. Graphite/Low Modulus Epoxy

D. Graphite/High Modulus Epoxy

E. Graphite/Polyimide

F. S-Glass/Intermediate Modulus Epoxy

To aid in the selection of the final material systems, a literature survey was performed of candidate systems aimed at collecting data on thermal, mechanical and physical properties of unidirectional composites and their constituent matrix and fiber materials. The survey was conducted with a view to selecting materials with the following approximate values for the moduli of the constituents:

Boron fibers:	380-415 GPa (55-60 x 10^6 psi)
Graphite fibers:	345-415 GPa (50-60 x 10^6 psi)
Low modulus epoxy:	2.1 GPa (300,000 psi)
Intermediate modulus epoxy:	3.5 GPa (500,000 psi)
High modulus epoxy:	4.8 GPa (700,000 psi)

The boron epoxy system was found to be one of the best characterized materials with a great deal of data available. Several matrices have been used with boron fibers, such as AVCO 5505 (formerly NARMCO 5505) and SP272, a product of 3M Company. Some properties for the constituent materials and the unidirectional laminate are tabulated

in Tables 2-1, 2-2, 2-3 and 2-4. The principal properties of the two laminates are quite similar. The AVCO 5505 epoxy matrix has a modulus of approximately 3.5 GPa (500,000 psi), while the SP272 matrix has a modulus of approximately 4.8 GPa (700,000 psi). For this reason, plus the fact that it is better characterized and more commonly used, the AVCO 5505 system was selected as material system A.

The following Boron/Polyimide systems were investigated as candidates for material system B:

(1) Boron/Skybond 703, compression molded

(2) Boron/P13N, compression molded

(3) Boron/P13N, autoclave molded

(4) Hercules 6001B

(5) Boron/WRD 9371

Of the above, Boron/P13N was found to have the most available data. Some of these are shown in Figures 2-1 through 2-8 which are taken from Reference 9. Tables 2-5 and 2-6 list properties for the Boron/6001B and Boron/WRD9371 systems as published by the manufacturers, 10,11. Workability and pertinent fabrication properties for Skybond 703 and Ciba-Geigy P13N polyimide resins were found in References 12 and 13. However, few mechanical property data were found for the cast resins. From the information obtained in the survey it was decided to select the 4 mil Boron/WRD9371 as the material system B.

References 9, 10, 11, and 14 through 22 were used to establish mechanical properties of various high modulus graphite/epoxy candidate systems for selecting a Graphite/Low Modulus Epoxy and a Graphite/High Modulus Epoxy. Reference 14 presented the results of an extensive literature survey and was used in the construction of comparative tables for our selection purposes. Table 2-7 shows the relative performance of several graphite fibers. Of the commercially available fibers (excluding the Celanese Gy-70 and Thornel 75) the highest specific modulus material is the Modmor I graphite fiber with a 415 GPa

Table 2-1

PROPERTIES OF BORON FILAMENT (United Aircraft)(Ref. 3)

Density, ρ, kg/m^3 (1bm/in.^{3})	2,644 (0.095)
Modulus, E, GPa (psi)	403 (58.5 x 10^6)
Tensile Strength, S_T, MPa (psi)	2930 (426,000)

Table 2-2

PROPERTIES OF NARMCO (AVCO) 5505 RESIN (Ref. 3)

Density, ρ, kg/m^3 (1bm/in.^{3})	1,257 (0.0457)
Modulus, E, GPa (psi)	3.84 (557,000)
Shear Modulus, G, GPa (psi)	1.36 (197,000)
Poisson's Ratio, ν	0.41
Tensile Strength, S_T, kPa (psi)	55,800 (8,100)
Compressive Strength, S_C, kPa (psi)	127,600 (18,500)

Table 2-3

PROPERTIES OF UNIDIRECTIONAL BORON/EPOXY (AVCO 5505)
(Fiber Volume Ratio: 0.50)

Property	Temperature degK (°F)	SI Units	English Units	Reference Number[*]
Density, ρ	-	2,005 kg/m^3	0.0725 lb/in.^{3}	-
Longitudinal Thermal Coefficient, α_{11}	297 (75)	4.5×10^{-6} K^{-1}	2.5 μ ϵ/°F	4
	450 (350)	4.5×10^{-6} K^{-1}	2.5 μ ϵ/°F	4
Transverse Thermal Coefficient, α_{22}	297 (75)	23.5×10^{-6} K^{-1}	13.1 μ ϵ/°F	4
	450 (350)	39.6×10^{-6} K^{-1}	22.0 μ ϵ/°F	4
Longitudinal Modulus, E_{11}	297 (75)	207 GPa	30×10^6 psi	5
	400 (260)	207 GPa	30×10^6 psi	5
	450 (350)	200 GPa	29×10^6 psi	5,6
Transverse Modulus, E_{22}	297 (75)	18.6 GPa	2.7×10^6 psi	5,7
	400 (260)	12.4 GPa	1.8×10^6 psi	5
	450 (350)	7.6 GPa	1.1×10^6 psi	5
Shear Modulus, G_{12}	297 (75)	13.8 GPa	2×10^6 psi	8
	450 (350)	1.4 GPa	0.2×10^6 psi	8
Major Poisson's Ratio, ν_{12}	297 (75)	0.20	-	3
Minor Poisson's Ratio, ν_{21}	297 (75)	0.06	-	3
Longitudinal Tensile Strength, S_{11T}	297 (75)	1,325 MPa	192,000 psi	3,5
	400 (260)	1,102 MPa	160,000 psi	5
	450 (350)	1,000 MPa	145,000 psi	5,7
Longitudinal Compressive Strength, S_{11C}	297 (75)	1,792 MPa	260,000 psi	3,4
	450 (350)	896 MPa	130,000 psi	4
Transverse Tensile Strength, S_{22T}	297 (75)	63,400 kPa	9,200 psi	3,5,7
	400 (260)	52,400 kPa	7,600 psi	5
	450 (350)	38,500 kPa	5,600 psi	5
Transverse Compressive Strength, S_{22C}	297 (75)	310,000 kPa	45,000 psi	5
	450 (350)	108,000 kPa	15,700 psi	6
Intralaminar Shear Strength, S_{12}	297 (75)	119,000 kPa	17,300 psi	8
	450 (350)	37,200 kPa	5,400 psi	8

[*]Numbers refer to list of references at end of report.

Table 2-4

PROPERTIES OF UNIDIRECTIONAL BORON/EPOXY (SP272)
(Fiber Volume Ratio: 0.50)

Property	Temperature degK (°F)	SI Units	English Units	Reference Number*
Density, ρ	-	2,005 kg/m^3	0.0725 lb/in.^{3}	-
Longitudinal Thermal Coefficient, α_{11}	-	-	-	-
Transverse Thermal Coefficient, α_{22}	-	-	-	-
Longitudinal Modulus, E_{11}	297 (75)	207 GPa	30×10^6 psi	8
	400 (260)	200 GPa	29×10^6 psi	8
	450 (350)	200 GPa	29×10^6 psi	8
Transverse Modulus, E_{22}	297 (75)	22 GPa	3.2×10^6 psi	8
Shear Modulus, G_{12}	297 (75)	12.4 GPa	1.8×10^6 psi	8
Major Poisson's Ratio, ν_{12}	297 (75)	0.23	-	-
Minor Poisson's Ratio, ν_{21}	297 (75)	0.025	-	-
Longitudinal Tensile Strength, S_{11T}	297 (75)	1,283 MPa	186,000 psi	8
	400 (260)	1,283 MPa	186,000 psi	8
	450 (350)	1,115 MPa	162,000 psi	8
Longitudinal Compressive Strength, S_{11C}	297 (75)	3,050 MPa	443,000 psi	8
	400 (260)	1,870 MPa	272,000 psi	8
	450 (350)	592 MPa	86,000 psi	8
Transverse Tensile Strength, S_{22T}	297 (75)	80,600 kPa	11,700 psi	8
	400 (260)	55,100 kPa	8,000 psi	8
	450 (350)	24,800 kPa	3,600 psi	8
Transverse Compressive Strength, S_{22C}	-	-	-	-
Intralaminar Shear Strength, S_{12}	297 (75)	129,000 kPa	18,700 psi	8
	450 (350)	34,500 kPa	5,000 psi	8

*Numbers refer to list of references at end of report.

Table 2-5

PROPERTIES OF UNIDIRECTIONAL BORON/POLYIMIDE HERCULES 6001B (Ref. 10)

Fiber Volume Ratio, FVR	0.60
Density, ρ	2,100 kg/m^3 (0.076 lb/in.^{3})
Longitudinal Modulus, E_{11} (Flexural)	
298 deg K (77°F)	223 GPa (32.4 x 10^6 psi)
590 deg K (600°F)	210 GPa (30.4 x 10^6 psi)
Longitudinal Flexural Strength, S_{11F}	
298 deg K (77°F)	1,950 MPa (283,000 psi)
590 deg K (600°F)	1,270 MPa (184,000 psi)
Interlaminar Shear Strength, S_{13}	47,500 kPa (6,900 psi)

Table 2-6

PROPERTIES OF UNIDIRECTIONAL BORON/POLYIMIDE WRD 9371 (Ref. 11)

Fiber Volume Ratio, FVR	0.55
Density, ρ	1,960 kg/m^3 (0.071 lb/in.^{3})
Flexural Modulus, E_{11}	172 GPa (24.9 x 10^6 psi)
Flexural Strength, S_{11F}	
297 deg K (75°F)	1,730 MPa (251,000 psi)
560 deg K (550°F)	1,300 MPa (188,000 psi)
Interlaminar Shear Strength, S_{13}	90,300 kPa (13,100 psi)

(60×10^6 psi) modulus. Furthermore, this fiber has been prepregged with a wide variety of epoxy and polyimide resin systems. It was selected as the reinforcement for the current study. A comparison of domestic and foreign fiber composite properties for several resin systems is shown in Tables 2-8, 2-9 and 2-10. Unfortunately, little or no data was available on the cast resin properties for these systems.

In addition to the literature search, several prepreggers were contacted for their capabilities in producing prepreg tape with such resins employing the Modmor I high modulus graphite fiber. Two commercially available systems were detailed by Whittaker R&D Laboratories employing ERLA 4289 (average elastic modulus of approximately 2.1 GPa (300,000 psi) and ERLA 4617 (average elastic modulus of the resin in the range of 5.5 to 6.2 GPa (800,000 to 900,000 psi).

Matrix resin bulk properties for the ERLA 4289 are shown in Table 2-11. Properties of unidirectional laminates with S-glass are shown in Table 2-12. The void contents for flat laminates of ERLA 4289 with S-glass were respectable at 1.8 percent and 2.2 percent for uni-directional and bidirectional plates, respectively. The 0° strengths and stiffnesses of S-glass/ERLA 4289 would depend primarily on the filament properties but the transverse modulus of 10 GPa (1.45×10^6 psi) would not differ much from that of the Modmor I/ERLA 4289 system. On the basis of the above information, Modmor I/ERLA 4289 was selected as material system C.

The following Graphite/Polyimide systems were investigated as candidates for material system E:

 (1) HMG 50 Graphite/P13N, compression molded
 (2) HMS Graphite/P13N, autoclave molded
 (3) HTS Graphite/P13N, compression molded
 (4) Hercules HM Graphite/6001 Polyimide
 (5) Modmor II/Gemon L
 (6) Modmor II/WRD 9371
 (7) Modmor I/WRD 9371

Table 2-7

TYPICAL STRENGTH PROPERTIES AND RELATIVE MERITS OF GRAPHITE FILAMENTS (Ref. 14)

Properties	Graphite Filaments							
			Morganite		Courtaulds			
	HMG-50	Thornel 50-S	Type I	Type II	HM-S	HT-S	Celanese GY-70	Thornel 75
Modulus (10^6 psi)	50	50	60	40	50	32	75	75
Specific Modulus (10^6 in.)	819	814	833	635	721	504	1027	1150
Tensile Strength (10^3 psi)	287	280	250	350	250	300	300	320
Specific Tensile Strength (10^6 in.)	4.7	4.75	3.47	5.55	3.47	4.72	4.11	4.93
Density (gm/cc) (lb/cu in)	1.70 0.061	1.63 0.059	1.94 0.072	1.75 0.063	1.90 0.069	1.76 0.063	1.95 0.070	1.86 0.067
Relative Merits	1. Continuous 2. Specific moduli & strength	1. Continuous 2. Specific moduli & strength	1. Fiber Surface 2. Specific modulus	1. Fiber Surface 2. Specific strength	1. Continuous 2. Cost	1. Continuous 2. Cost 3. Specific strength	1. Continuous 2. High modulus 3. High strength	1. Continuous 2. High modulus 3. High strength

Table 2-8

COMPARISON OF COMPOSITES MADE WITH DOMESTIC GRAPHITE FIBERS (Ref. 14)

Fiber	Epoxy Resin	0° Tension σ, ksi	0° Tension E, msi	90° Tension σ, ksi	90° Tension E, msi	0° Flexure σ, ksi	Horizontal Shear, ksi	Reference
Thornel 50*	Narmco 2387	132	24.0	6.8	1.6	–	–	23
HMG-50*	E-787	93	19.4	6.1	1.3	–	–	23
Thornel-50S*	Narmco 2387	134	31.2	–	–	–	–	23
HMG-50	4617	124	30.1	2.5	1.1	100	5.2	24
HMG-50	E-715	108	24.9	1.7	0.8	–	5.1	25
HMG-50	BP-907	134	28.5	–	–	–	6.6	24
Thornel 50	ERL-2256	102	23.0	2.6	0.8	–	3.0	26
Thornel 50	E-798	118	22.5	0.9	0.7	–	–	24
HMG-50	X-05	(130)	22.9	–	–	–	–	24

*Sandwich data

( ) Data includes some specimens that failed improperly.

Table 2-9

COMPARISON OF COMPOSITES MADE WITH HIGH MODULUS GRAPHITE FIBERS (Ref. 14)

Fiber	Epoxy Resin	0° Tension		90° Tension		0°Flexure	90°Flexure	Horizontal	Reference
		σ, ksi	E, msi	σ, ksi	E, msi	σ, ksi	σ, ksi	Shear, ksi	
Celanese	Epi-Rez 508	121	47.5	5.0	1.0	124	3.7	9.7	23
Celanese	Fiberite X-904	(117)	46.1	1.6	1.1	—	—	—	27
Celanese*	Epi-Rez 508	93	34.5	8.4	1.4	—	—	—	25
Celanese	Epi-Rez 508	129	47.0	—	—	—	—	8.3	28
Celanese	Celanese R-350A	117	44.0	4.2	0.8	95	—	—	28
Celanese	Celanese R-350A	(80)	40.7**	3.3	0.8	—	—	8.9	24
HMS	Hercules 3002	(102)	25.6	4.7	1.1	123	—	10.0	24
Morganite I	Narmco 1004	(76)	23.7	5.8	0.9	111	—	8.1	24
HMS	Fiberite X-904	(74)	28.2	(2.6)	0.8	112	—	9.7	24
HMS	3M's P2-287	(105)	27.9	5.0	1.1	130	—	10.2	24
HMS	ERLA 4317	114	28.0	4.5	1.3	—	—	11.4	24
Morganite I	ERLA 4617	126	25.5	5.9	1.2	141	10.2	8.6	24
Morganite I	Narmco XHB178	106	32.8	4.0	0.9	95	5.2	7.1	24
Morganite I	Narmco 2387	95	32.0	4.0	1.0	96	5.7	7.2	24
Celanese	Celanese R-350A	—	—	—	—	125	6.0	8.5	29

*45 v/o Celanese plus asbestos carrier

**50.4 msi in compression

( ) Data includes some specimens that failed improperly.

2-10

Table 2-10

COMPARISON OF 350F RESIN SYSTEMS WITH GRAPHITE FIBERS (Ref. 14)

Epoxy Resin	Fiber	0° Tensile Strength RT, ksi	0° Tensile Strength % Ret. @350F	90° Tensile Strength RT, ksi	90° Tensile Strength % Ret. @350F	0° Flexural Strength RT, ksi	0° Flexural Strength % Ret. @350F	90° Flexural Strength RT, ksi	90° Flexural Strength % Ret. @350F	Horizontal Shear RT, ksi	Horizontal Shear % Ret. @350F	Reference
F&H 4617	Type II	–	–	–	–	260.9	55.1*	17.0	39.4*	15.3	39.3*	23
Fiberite 4617	Type II	–	–	–	–	212.8	85.8*	10.9	–	13.7	43.1*	23
3M's PR-287	Type II	–	–	–	–	149	100.0*	11.0	81.8*	12.8	68.8*	23
Ciba 95	Type II	–	–	–	–	196.2	86.4*	15.5	63.2*	16.1	60.3*	23
Fiberite X-904	HTS	181	87.6	–	–	–	–	–	–	14.6	(36.0)	27
Fiberite X-904	Celanese	117	94.0	–	–	–	–	–	–	5.5	66.0	27
Fiberite X-904	Morganite II	172.8	103.4	–	–	–	–	–	–	12.0	(44.4)	27
Ferro E-293**	Morganite II	(111.5)	90.5	3.2	25.0	–	–	–	–	–	–	27
BXP-2401**	Morganite II	(108.0)	98.7	2.5	117	–	–	–	–	–	–	27
Narmco 2387**	Morganite II	(103.6)	120.6	4.7	61.4	–	–	–	–	–	–	27
Narmco 1004**	Morganite II	(125.2)	101.4	6.9	63.6	–	–	–	–	11.7	6.1	27
Fiberite X-904	HMS	–	–	–	–	111.8	65.5	–	–	9.7	54.7	24
3M's PR-287	HMS	–	–	–	–	129.6	62.0	–	–	10.2	50.0	24
Narmco 1004	Morganite I	–	–	–	–	111.2	57.6	–	–	8.1	59.4	24
Hercules 3002	HMS	–	–	–	–	122.5	70.2	–	–	10.0	72.0	24
Fiberite X-904	HTS	–	–	–	–	150.7	61.9	–	–	12.7	53.5	24
BXP 2401	Morganite II	–	–	–	–	157.0	70.0	–	–	14.4	43.0	24
Celanese R350A	Celanese	–	–	–	–	94.8	72.0	–	–	8.9	59.5	24
Epon 1031/828/CPDA	HMG-50	–	–	–	–	89.7	56.2	–	–	–	–	24
Fiberite X-903	HMS	–	–	–	–	99.3	80.0	–	–	5.2	67.4	24
Fiberite X-904	HTS	–	–	–	–	163.3	73.7	–	–	11.7	56.5	24
Fiberite X-904	HMS	–	–	–	–	124.5	83.3	–	–	6.9	79.8	24
Narmco 2387	Morganite II	–	–	–	–	152.7	–	–	–	12.4	47.0	24

*High-temperature tests conducted at 300F.

**Made with some very early continuous Morganite II.

( ) Data includes some specimens that failed improperly.

Table 2-11

PROPERTIES OF LOW-MODULUS MATRIX RESIN ERLA 4289 (Ref. 19)

Modulus, E	
(Tensile)	1.55 GPa (225,000 psi)
(Compressive)	2.56 GPa (371,000 psi)
Tensile Strength, S_T	33,800 kPa (4,900 psi)
Compressive Yield Point, S_{YC}	92,500 kPa (13,400 psi)
Ultimate Tensile Elongation, ϵ_{UT}	0.185
Compressive Yield Strain, ϵ_{YC}	0.064
Heat Distortion Temperature (at 1820 Pa, 264 psi)	316°K (109°F)

Table 2-12

PROPERTIES OF UNIDIRECTIONAL S-GLASS/LOW-MODULUS EPOXY
994 "S" HTS/ERLA 4289 (Ref. 19)

Fiber Volume Ratio, FVR	0.36
Void Volume Ratio	0.018
Longitudinal Modulus, E_{11}	56.2 GPa (8.15×10^6 psi)
Transverse Modulus, E_{22}	10 GPa (1.45×10^6 psi)
Longitudinal Flexural Strength, S_{11T}	1.27 GPa (184,000 psi)
Longitudinal Compressive Strength, S_{11C}	600,000 kPa (87,200 psi)
Transverse Tensile Strength, S_{22T}	21,400 kPa (3,100 psi)
Interlaminar Shear Strength, S_{31}	38,000 kPa (5,500 psi)

Properties for the high-modulus resin, ERLA 4617, are tabulated in Table 2-13 (Ref. 20). Modmor I/ERLA 4617 was selected as material system D.

Table 2-13

PROPERTIES OF HIGH-MODULUS MATRIX RESIN ERLA 4617
(With m-PDA Hardener) (Ref. 20)

Modulus, E (Tensile)	5.4×10^6 kN/m^2 (783,000 psi)
(Compressive)	6.1×10^6 kN/m^2 (890,000 psi)
(Flexural)	5.6×10^6 kN/m^2 (815,000 psi)
Tensile Strength, S_T	132,000 kN/m^2 (19,200 psi)
Compressive Strength, S_C	226,000 kN/m^2 (32,800 psi)
Flexural Strength, S_F	214,000 kN/m^2 (31,000 psi)
Ultimate Tensile Elongation, ε_{UT}	0.028
Heat Distortion Temperature	448°K (175°C) (347°F)

Typical data of some of the above candidate systems are given in Tables 2-14, 2-15 and 2-16 and Figures 2-9 and 2-10. Based on the available data, Modmor I/WRD 9371 was selected as material system E. The specific gravity of this material at a fiber volume ratio of 50 percent is 1.62.

Three commercially available systems were reviewed for material system F (S-glass/intermediate modulus epoxy). These systems, all products of 3M Company, are 1002S, 1009S and XP-251 with S-glass fibers. Property data for these three materials are tabulated in Tables 2-17, 2-18 and 2-19. The temperature limitations of 1002S and the difficulty in obtaining the XP-251-S within the time frame of the program were factors in the decision to select the 1009-26S as the material system F.

2.2 Materials Selection

The literature survey of candidate materials resulted in the selection of six final material systems for investigation in this program. They are tabulated in Table 2-20 together with typical values for constituent fiber and matrix moduli, as obtained in the survey. Also listed are the suppliers from which these materials were purchased.

Table 2-14

PROPERTIES OF UNIDIRECTIONAL GRAPHITE/POLYIMIDE HERCULES 6001M (Ref. 10)

Fiber Volume Ratio, FVR	0.61
Density, ρ	1,690 kg/m^3 (0.061 lb/in.^{3})
Flexural Modulus, E_{11}	
297 deg K (75°F)	194 GPa (28.1 x 10^6 psi)
590 deg K (600°F)	164 GPa (23.8 x 10^6 psi)
Flexural Strength, S_{11F}	
297 deg K (75°F)	1.08 GPa (156,000 psi)
590 deg K (600°F)	0.63 GPa (92,000 psi)
Interlaminar Shear Strength, S_{13}	
297 deg K (75°F)	65,000 kPa (9,390 psi)
590 deg K (600°F)	40,800 kPa (5,910 psi)

Table 2-15

PROPERTIES OF UNIDIRECTIONAL GRAPHITE/POLYIMIDE MODMOR II/WRD 9371

Fiber Volume Ratio, FVR	0.55
Density, ρ	1,540 kg/m^3 (0.056 lb/in.^{3})
Longitudinal Modulus, E_{11}	156.5 GPa (22.7 x 10^6 psi)
Transverse Modulus, E_{22}	15 GPa (2.18 x 10^6 psi)
Longitudinal Tensile Strength, S_{11T}	1,500 MPa (218,000 psi)
Longitudinal Compressive Strength, S_{11C}	1,210 MPa (175,000 psi)
Transverse Tensile Strength, S_{22T}	65,500 kPa (9,500 psi
Transverse Compressive Strength, S_{22C}	132,500 (19,200 psi)
Flexural Strength, S_{11F}	
297 deg K (75°F)	1,380 MPa (200,000 psi)
560 deg K (550°F)	925 MPa (134,300 psi)
Interlaminar Shear Strength, S_{13}	
297 deg K (75°F)	85,000 kPa (12,300 psi)
560 deg K (550°F)	41,700 kPa (6,050 psi)

Table 2-16

PROPERTIES OF UNIDIRECTIONAL MODMOR II/GEMON L POLYIMIDE (Ref. 30)

Fiber Volume Ratio, FVR	0.62
Density, ρ	1,510 kg/m^3 (0.055 lb/in.^{3})
Resin Content, Percent by Weight	32
Longitudinal Thermal Coefficient, α_{11} (-300°F to 75°F)	-0.68 x 10^{-6}K^{-1}(-0.38 x 10^{-6} in./in./°F)
α_{11} (75°F to 500°F)	0.14 x 10^{-7}K^{-1}(0.08 x 10^{-7} in./in./°F)
Transverse Thermal Coefficient, α_{22} (-300°F to 75°F)	27 x 10^{-6}K^{-1} (15 x 10^{-6} in./in./°F)
α_{22} (75°F to 500°F)	45 x 10^{-6}K^{-1} (25 x 10^{-6} in./ir./°F)

Table 2-17

PROPERTIES OF UNIDIRECTIONAL S-GLASS/EPOXY SCOTCHPLY 1002S (Ref. 31)

Longitudinal Modulus, E_{11}	44 GPa (6.4×10^6 psi)
Longitudinal Tensile Strength, S_{11T}	1,340 MPa (195,000 psi)

Table 2-18

PROPERTIES OF UNIDIRECTIONAL S-GLASS/EPOXY SCOTCHPLY 1009-26S (Ref. 32)

Longitudinal Modulus, E_{11}	61.3 GPa (8.9×10^6 psi)
Longitudinal Tensile Strength, S_{11T}	1,270 MPa (185,000 psi)
Longitudinal Compressive Strength, S_{11C}	620,000 kPa (90,000 psi)
Intralaminar Shear Strength, S_{12}	14,500 kPa (2,100 psi)

Table 2-19

PROPERTIES OF UNIDIRECTIONAL S-GLASS/EPOXY SCOTCHPLY XP251-S (Ref. 33)

Longitudinal Modulus, E_{11}	57.8 GPa (8.4×10^6 psi)
Longitudinal Tensile Strength, S_{11T}	1,720 MPa (250,000 psi)

Table 2-20

MATERIAL SYSTEMS SELECTED FOR INVESTIGATION

Material Systems		Typical Moduli			
		Fiber		Matrix	
Generic Description	Commercial Description	psix10^6	GPa	psix10^6	GPa
A Boron/Intermediate Modulus Epoxy	4 mil Boron/AVCO 5505[1]	58.5	403	0.557	3.84
B Boron/Polyimide	4 mil Boron/WRD 9371[2]	58.5	403	-	-
C Graphite/Low Modulus Epoxy	Modmor I/ERLA 4289[2]	55.0	396	0.225	1.55
D Graphite/High Modulus Epoxy	Modmor I/ERLA 4617[3]	55.0	396	0.783	5.40
E Graphite/Polyimide	Modmor I/WRD 9371[2]	55.0	396	-	-
F S-Glass/Intermediate Modulus Epoxy	Scotchply 1009-26S[4]	12.4	85.6	-	-

Suppliers:

[1] Whittaker Corporation, Narmco Division, Costa Mesa, California.

[2] Whittaker Corporation, R&D Division, San Diego, California.

[3] Fothergill and Harvey Ltd. Composite Materials Division, Summit Littleborough, Lancashire, England.

[4] 3M Company, St. Paul, Minnesota.
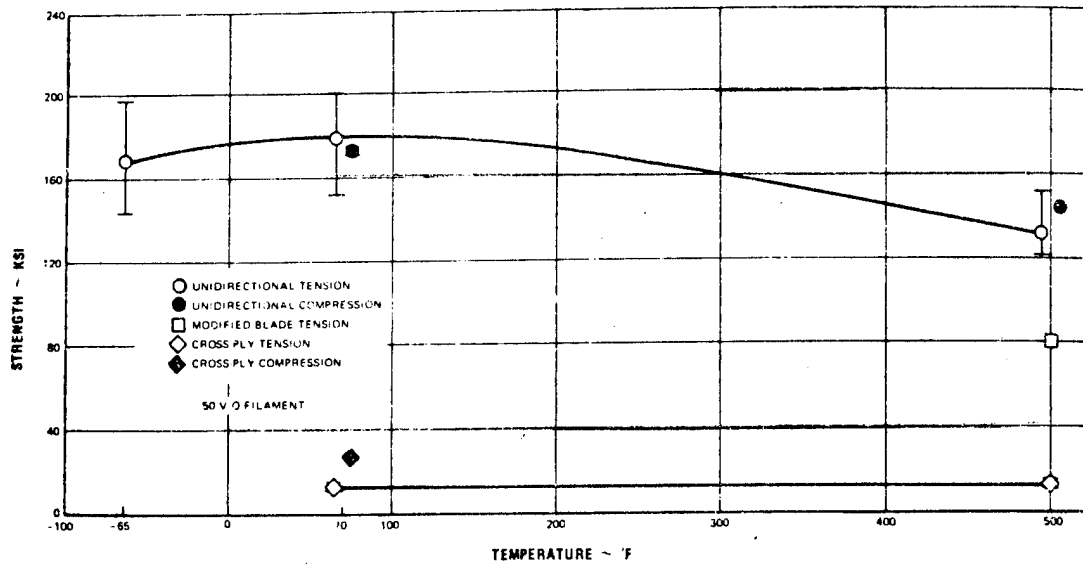
Fig. 2-1 TENSILE AND COMPRESSIVE STRENGTH AS A FUNCTION OF TEMPERATURE
FOR BORON/POLYIMIDE (Boron/P13N) (Ref. 9)
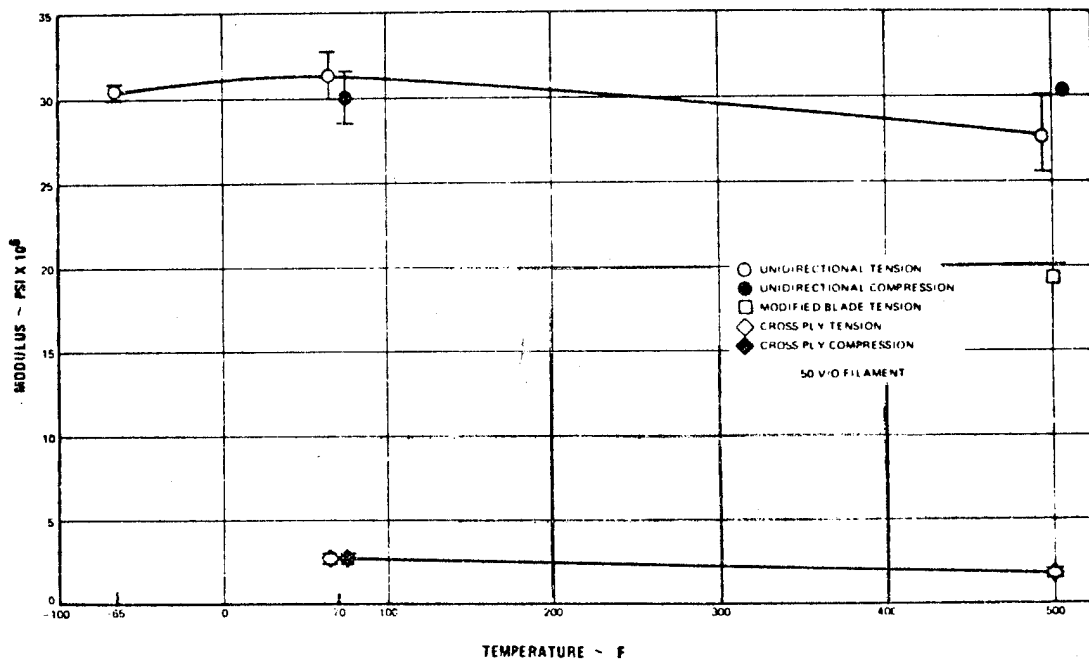
Fig. 2-2 TENSILE AND COMPRESSIVE MODULUS AS A FUNCTION OF TEMPERATURE
FOR BORON/POLYIMIDE (Boron/P13N) (Ref. 9)

2-19
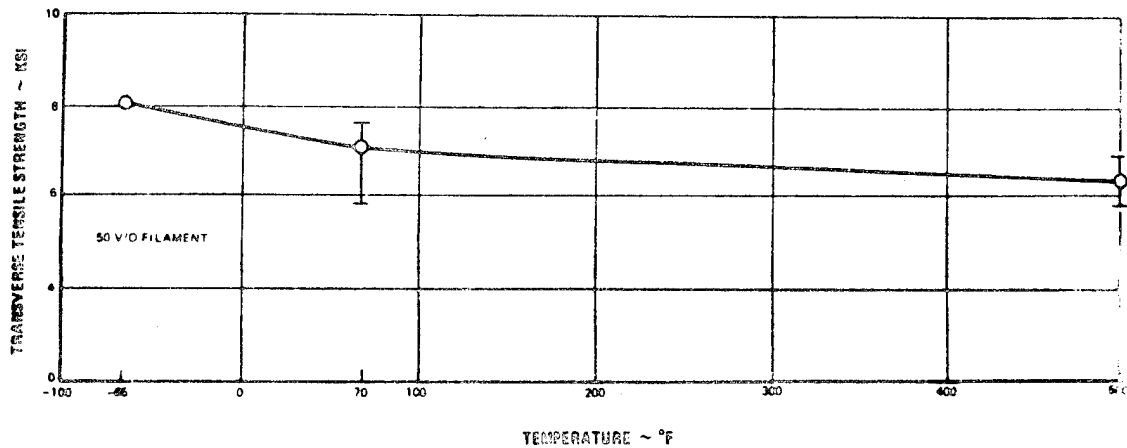
Fig. 2-3   TRANSVERSE TENSILE STRENGTH OF UNIDIRECTIONAL BORON/
POLYIMIDE (Boron/P13N) AS A FUNCTION OF TEMPERATURE
(Ref. 9)
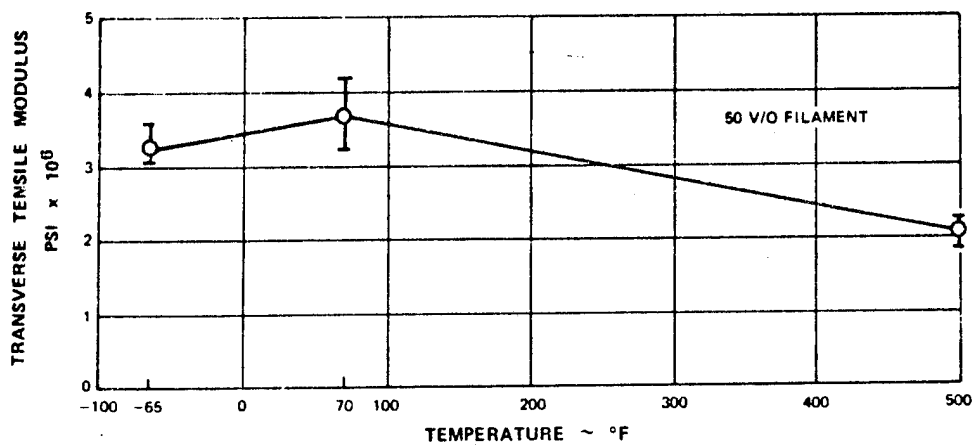
Fig. 2-4   TRANSVERSE TENSILE MODULUS OF UNIDIRECTIONAL BORON/
POLYIMIDE (Boron/P13N) AS A FUNCTION OF TEMPERATURE
(Ref. 9)

2-20
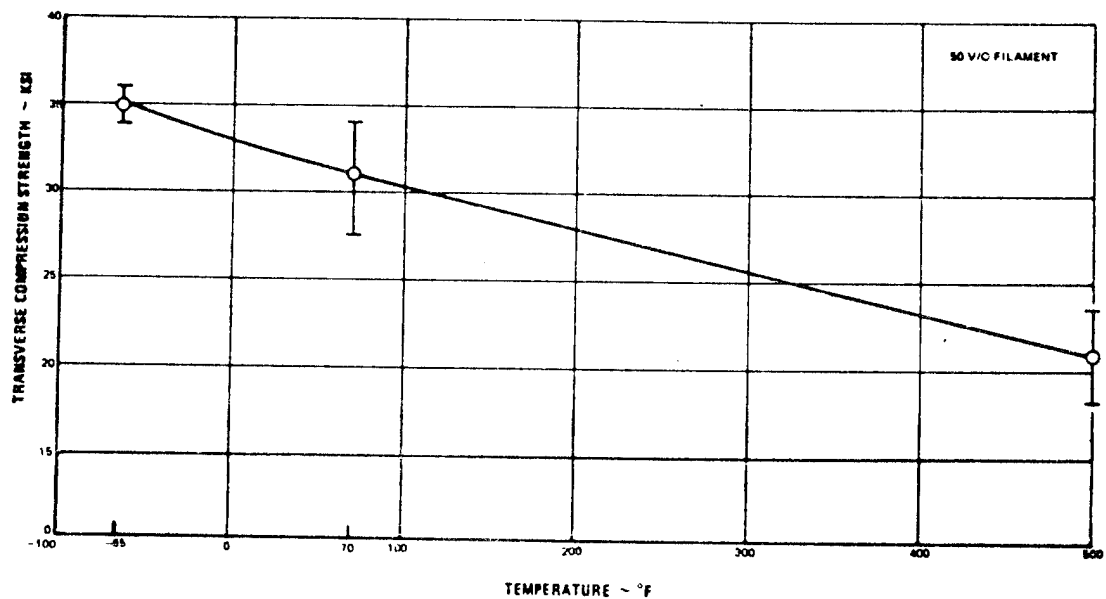
Fig. 2-5 TRANSVERSE COMPRESSIVE STRENGTH OF UNIDIRECTIONAL BORON/
POLYIMIDE (Boron/P13N) AS A FUNCTION OF TEMPERATURE
(Ref. 9)
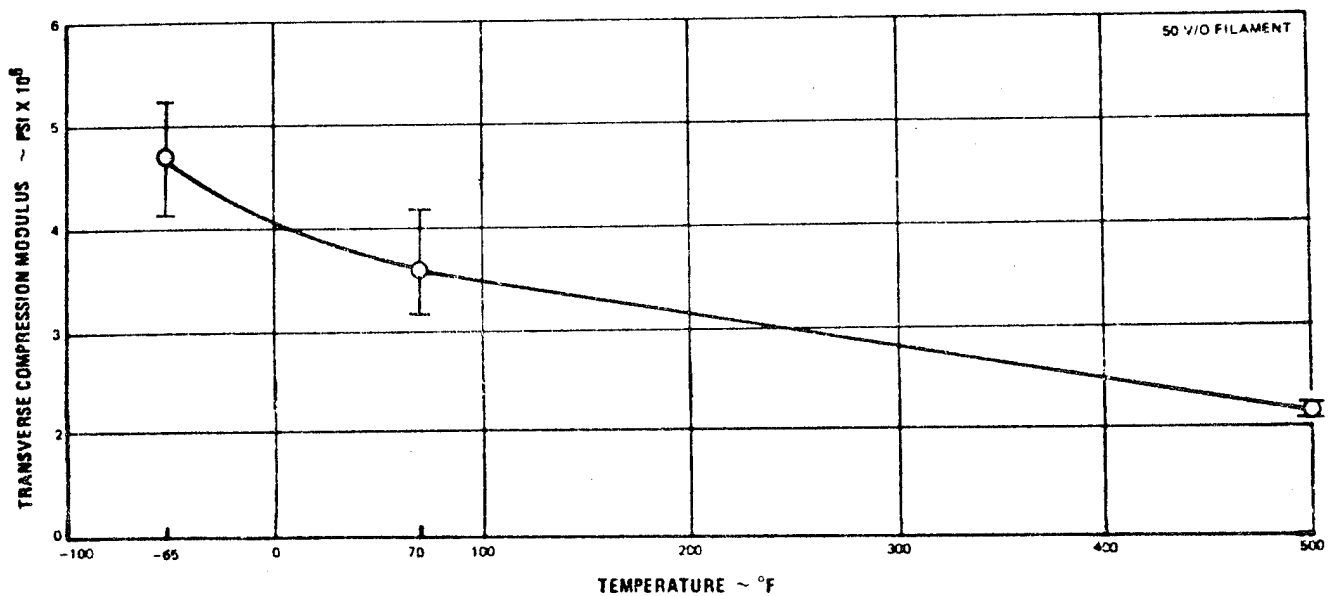
Fig. 2-6 TRANSVERSE COMPRESSIVE MODULUS OF UNIDIRECTIONAL BORON/
POLYIMIDE (Boron/P13N) AS A FUNCTION OF TEMPERATURE
(Ref. 9)
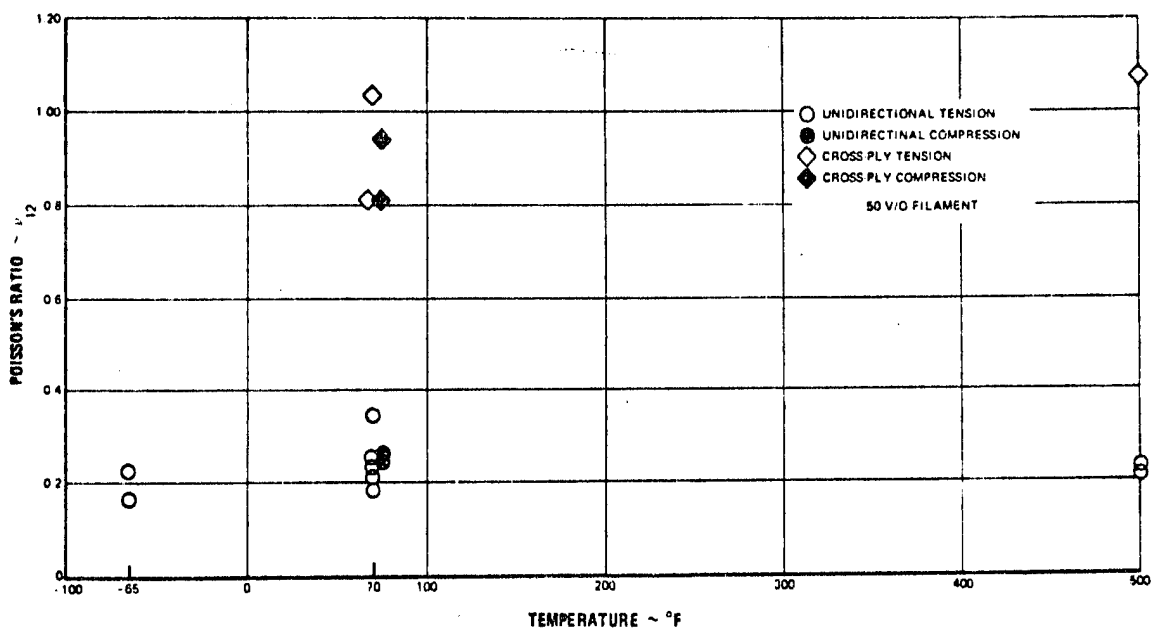
Fig. 2-7 POISSON'S RATIO DETERMINED IN TENSION AND COMPRESSION AS
A FUNCTION OF TEMPERATURE FOR BORON/POLYIMIDE (Boron/P13N)
(Ref. 9)
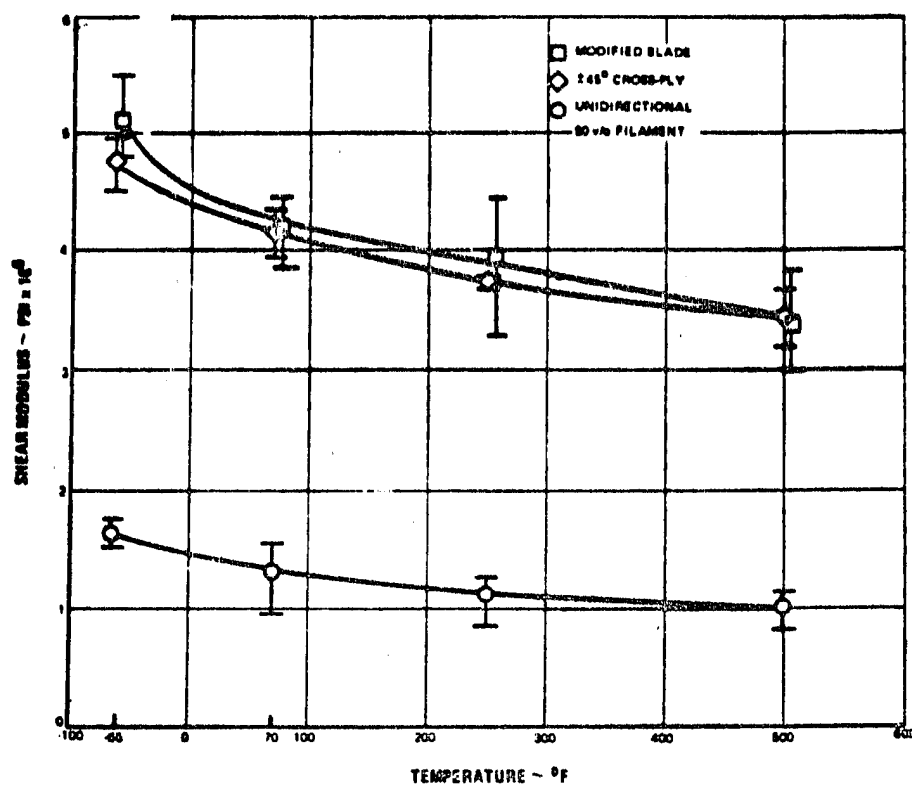
Fig. 2-8 SHEAR MODULUS OF BORON/POLYIMIDE (Boron/P13N) LAMINATES
AS A FUNCTION OF TEMPERATURE (Ref. 9)

2-22
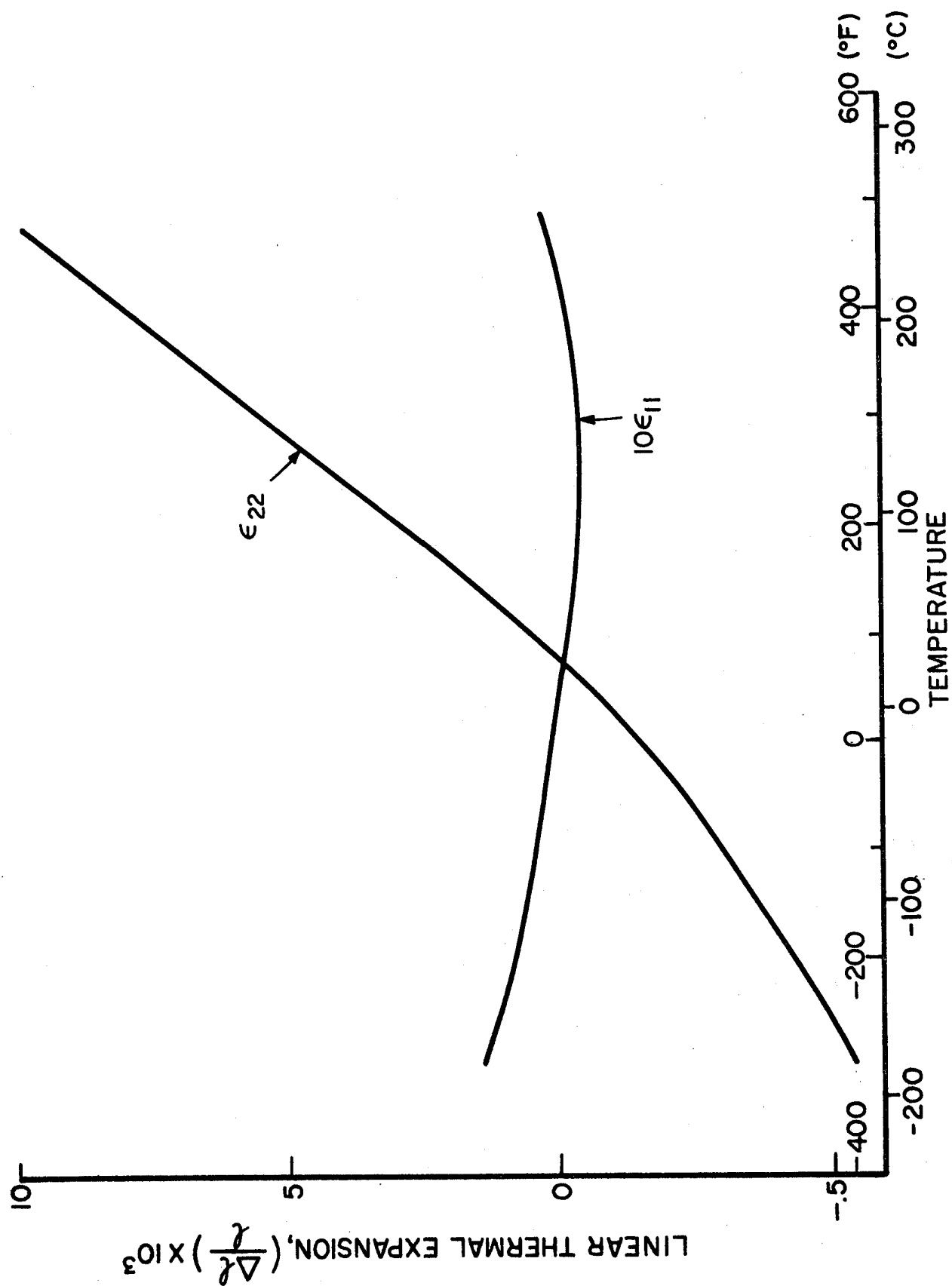
Fig. 2-9 THERMAL EXPANSION OF UNIDIRECTIONAL GRAPHITE/POLYIMIDE AS A FUNCTION OF TEMPERATURE (MODMOR II WITH GEMON L POLYIMIDE; AFTER STRIEPENS, Ref. 30)
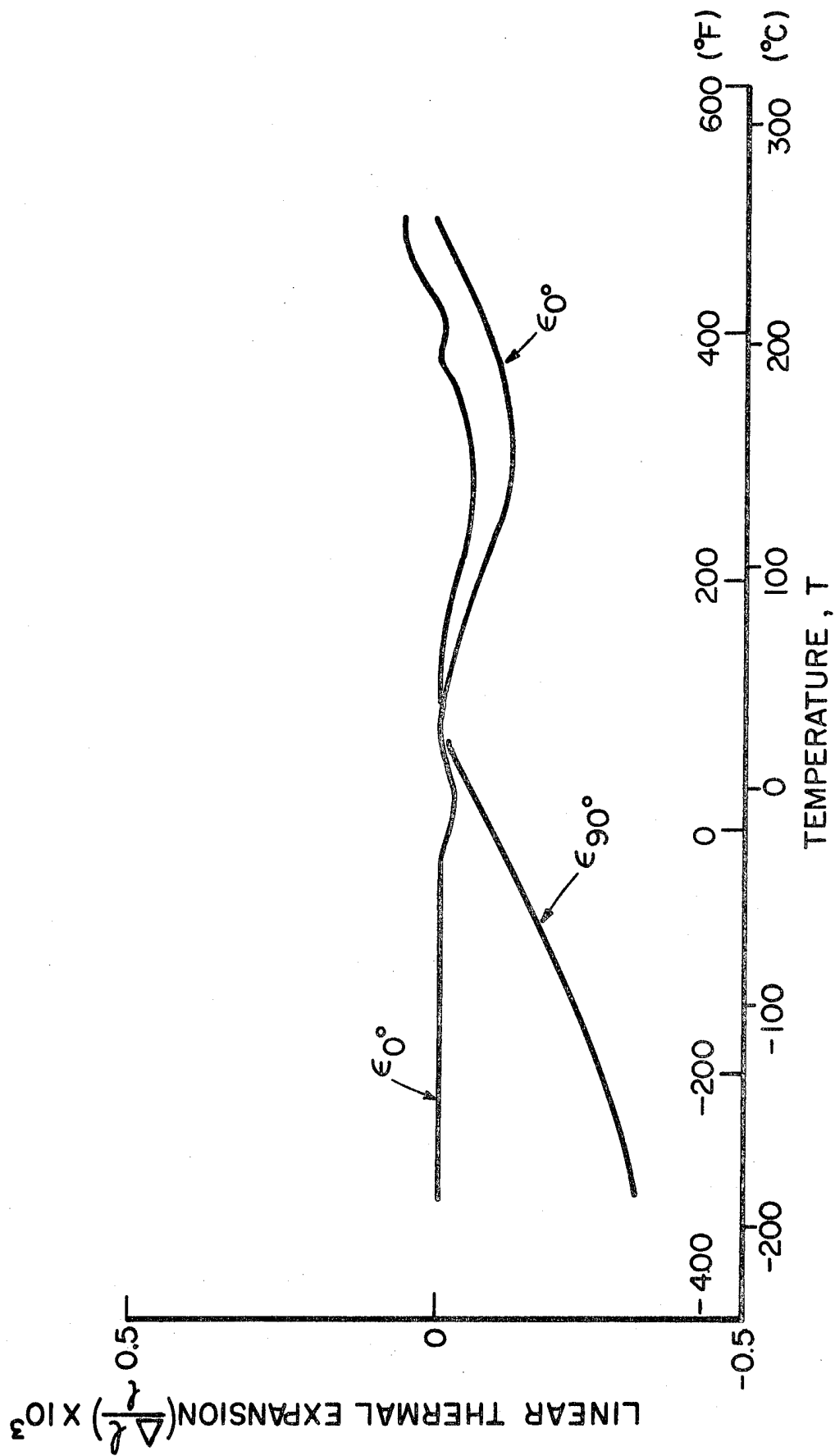
Fig. 2-10 THERMAL EXPANSION OF $[0_3/\pm45/90_2/\mp45/0_3]_s$ GRAPHITE/POLYIMIDE LAMINATE AS A FUNCTION OF TEMPERATURE (MODMOR II WITH GEMON L POLYIMIDE; AFTER STRIEPENS, Ref. 30)

2-24

3.0   TASK II - RESIDUAL STRAIN AND STATIC STRENGTH

3.1   Material Qualification

The selected materials were ordered and received in prepreg form.   The material was inspected visually prior to specimen fabrication.   Prepreg sections having large fiber gaps, broken fibers, fiber cross-overs, resin-rich or resin-poor areas were discarded during this inspection.   The materials were qualified by determining their flexural and interlaminar shear strengths from unidirectional coupons, and comparing them with published values for these materials, if available, or with values for similar materials.

The qualification testing was done by means of beams subjected to three-point bending.   The test specimens were 15-ply thick unidirectional coupons cut from a plate cured according to manufacturer's specifications.   Flexural strength test coupons were 10.2 cm (4 in.) long with a 6.3 cm (2.5 in.) span length.   Shear strength coupons were 1.5 cm (0.6 in.) long with a span length of 1 cm (0.4 in.).   The standard beam formulas below were used to determine the strength values.

$$\sigma = \frac{3P\ell}{2wt^2}$$

for flexural strength, and

$$\tau = \frac{3P}{4wt}$$

for interlaminar shear strength.

Here, P is the load on the beam, w is beam width and t is the thickness.   The fiber orientation in these tests is in the direction of the beam axis.

For material A, 47 m (160 ft) of Boron/Epoxy (Boron/AVCO 5505) 7.6 cm (3 in.) wide prepreg tape was ordered and received.   The Whittaker Corporation certified that this material conformed to General Dynamics Spec. FMS-2001A.   Results of the qualification tests are shown in Tables 3-1 and 3-2.   The FMS-2001 Specification requires a flexural strength of 1550 MPa (225 ksi).

Table 3-1

QUALIFICATION FLEXURE TESTS ON BORON/AVCO 5505

Specimen Number	Thickness cm, (in.)	Width cm, (in.)	Flexural Strength MPa, (ksi)
73-0-A-1	0.203 (0.080)	1.273 (0.501)	1600 (232)
-2	0.203 (0.080)	1.273 (0.501)	1630 (236)
-3	0.203 (0.080)	1.273 (0.501)	1690 (245)
-4	0.201 (0.079)	1.273 (0.501)	1700 (246)
-5	0.201 (0.079)	1.273 (0.501)	1790 (259)
		Average:	1680 (244)

Table 3-2

QUALIFICATION INTERLAMINAR SHEAR TESTS ON BORON/AVCO 5505

Specimen Number	Thickness cm, (in.)	Width cm, (in.)	Shear Strength MPa (ksi)
73-0-A-1	0.201 (.079)	0.632 (.249)	61.8 (8.96)
-2	0.203 (.080)	0.630 (.248)	53.4 (7.74)
-3	0.201 (.079)	0.635 (.250)	62.1 (9.00)
-4	0.201 (.079)	0.632 (.249)	55.2 (8.00)
-5	0.203 (.080)	0.635 (.250)	57.7 (8.36)
		Average:	58.0 (8.41)

For material B, an order was placed for 1.1 kg (2.4 lb, approximately 37.5 ft^2) of 4 mil Boron/WRD 9371. The results of the flexure and interlaminar shear qualification tests are shown in Tables 3-3 and 3-4.

Table 3-3

QUALIFICATION FLEXURE TESTS ON BORON/POLYIMIDE WRD 9371

Specimen Number	Thickness cm, (in.)	Width cm, (in.)	Flexural Strength MPa, (ksi)
73-0-B-1	0.185 (0.073)	1.283 (0.505)	1340 (194)
-2	0.188 (0.074)	1.285 (0.506)	1240 (180)
-3	0.188 (0.074)	1.280 (0.504)	1500 (217)
-4	0.180 (0.071)	1.270 (0.500)	1430 (207)
-5	0.183 (0.072)	1.278 (0.503)	1490 (216)
		Average:	1400 (203)

Table 3-4

QUALIFICATION INTERLAMINAR SHEAR TESTS ON BORON/POLYIMIDE WRD 9371

Specimen Number	Thickness cm, (in.)	Width cm, (in.)	Shear Strength MPa (ksi)
73-0-B-1	0.180 (0.071)	0.638 (0.251)	43.5 (6.31)
-2	0.185 (0.073)	0.638 (0.251)	40.9 (5.93)
-3	0.180 (0.071)	0.640 (0.252)	41.3 (5.99)
-4	0.185 (0.073)	0.640 (0.252)	41.6 (6.03)
-5	0.188 (0.074)	0.640 (0.252)	42.2 (6.11)
		Average:	41.9 (6.07)

The order for material C consisted of 45.7 m (150 ft) of
7.62 cm (3 in.) wide prepreg tape of Modmor I/ERLA 4289. The material
was received and qualification laminates prepared in accordance with
the manufacturer's recommended procedure. The cured laminates were
of unacceptable quality with almost no interply integrity. An exami-
nation of the prepreg material showed absolutely no tack to the
material although drape appeared to be evident. The 4289 system is a
low viscosity system and according to Cole[19] generally has a great
deal of flow in the molding operation. Indeed, Cole found it useful
to advance the resin prior to curing in order to minimize the flow of
resin. This experience was completely contrary to our own with the
material received since a visual examination of the glass bleeder cloth
showed some areas completely dry. The qualification plates bleeder
cloth delaminated with a slight pull of the hand. Furthermore, the
resin powdered away from the bleeder cloths during flexural folding
of an individual ply. The dry, low tack, state of the material
received was interpreted as indicating an advanced state of curing
of the prepreg, unsuitable for acceptable laminate fabrication. Upon
consultation with the manufacturer a second order was placed to replace
the first. This arrived in tackier condition and with a modified
curing schedule specified by the manufacturer.

For material system D, 54.9 m (180 ft) of Modmor I/ERLA 4617
was ordered and received. Tables 3-5 and 3-6 show the results of the
qualification tests.

Table 3-5

QUALIFICATION FLEXURE TESTS ON MODMOR I/ERLA 4617

Specimen Number	Thickness cm, (in.)	Width cm, (in.)	Flexural Strength MPa, (ksi)
73-0-D-1	0.185 (0.073)	1.275 (0.502)	1140 (166)
-2	0.185 (0.073)	1.278 (0.503)	1140 (165)
-3	0.178 (0.070)	1.273 (0.501)	930 (135)
-4	0.188 (0.074)	1.278 (0.503)	1100 (159)
-5	0.183 (0.072)	1.270 (0.500)	1100 (159)
		Average:	1080 (157)

Table 3-6

QUALIFICATION INTERLAMINAR SHEAR TESTS ON MODMOR I/ERLA 4617

Specimen Number	Thickness cm, (in.)	Width cm, (in.)	Shear Strength MPa, (ksi)
73-0-D-1	0.185 (0.073)	0.645 (0.254)	89.0 (12.9)
-2	0.188 (0.074)	0.645 (0.254)	90.4 (13.1)
-3	0.188 (0.074)	0.645 (0.254)	90.4 (13.1)
-4	0.188 (0.074)	0.645 (0.254)	96.6 (14.0)
-5	0.188 (0.074)	0.643 (0.253)	89.7 (13.0)
		Average:	91.2 (13.2)

For material system E, an order was placed for 3.1 kg (6.8 lb, approximately 400 ft) of 7.62 cm (3 in.) wide Modmor I/WRD 9371 prepreg tape. Results of the qualification tests are shown in Tables 3-7 and 3-8.

Table 3-7

QUALIFICATION FLEXURE TESTS ON MODMOR I/WRD 9371

Specimen Number	Thickness cm, (in.)	Width cm, (in.)	Flexural Strength MPa, (ksi)
73-0-E-1	0.218 (0.086)	1.275 (0.502)	697 (101.0)
-2	0.226 (0.089)	1.278 (0.503)	491 (71.2)
-3	0.224 (0.088)	1.275 (0.502)	604 (87.5)
-4	0.218 (0.086)	1.275 (0.502)	538 (78.0)
-5	0.218 (0.086)	1.278 (0.503)	697 (101.0)
		Average:	605 (87.8)

Table 3-8

QUALIFICATION INTERLAMINAR SHEAR TESTS ON MODMOR I/WRD 9371

Specimen Number	Thickness cm, (in.)	Width cm, (in.)	Shear Strength MPa, (ksi)
73-0-E-1	0.224 (0.088)	0.643 (0.253)	24.4 (3.54)
-2	0.224 (0.088)	0.643 (0.253)	26.0 (3.77)
-3	0.226 (0.089)	0.643 (0.253)	21.1 (3.06)
-4	0.224 (0.088)	0.643 (0.253)	22.1 (3.20)
-5	0.224 (0.088)	0.640 (0.252)	28.0 (4.06)
		Average:	24.3 (3.53)

For material system F, an order was placed for 65.8 m (72 yards) of 10.16 cm (4 in.) wide Scotchply S-Glass/Epoxy 1009-26S-5901 prepreg tape. The results of the qualification tests are shown in Tables 3-9 and 3-10.

Table 3-9

QUALIFICATION FLEXURE TESTS ON SCOTCHPLY S-GLASS/EPOXY-1009-26S-5901

Specimen Number	Thickness cm, (in.)	Width cm, (in.)	Flexural Strength MPa, (ksi)
73-0-F-1	0.246 (0.097)	1.262 (0.497)	1610 (233)
-2	0.246 (0.097)	1.262 (0.497)	1630 (236)
-3	0.246 (0.097)	1.262 (0.497)	1590 (231)
-4	0.246 (0.097)	1.262 (0.497)	1570 (227)
		Average:	1600 (232)

Table 3-10

QUALIFICATION INTERLAMINAR SHEAR TESTS ON SCOTCHPLY
S-GLASS/EPOXY-1009-26S-5901

Specimen Number	Thickness cm, (in.)	Width cm, (in.)	Shear Strength MPa, (ksi)
73-0-F-1	0.246 (0.097)	0.635 (0.250)	54.4 (7.89)
-2	0.246 (0.097)	0.638 (0.251)	58.5 (8.47)
-3	0.244 (0.096)	0.645 (0.248)	59.1 (8.57)
-4	0.246 (0.097)	0.635 (0.250)	55.7 (8.07)
-5	0.246 (0.097)	0.635 (0.250)	56.5 (8.19)
		Average:	56.8 (8.24)

3.2 Laminate Fabrication

Laminate plates were fabricated from each material system to provide specimens for the qualification testing, characterization of unidirectional laminates, and residual stress studies. Specimens for the latter did not have embedded instrumentation. Table 3-11 shows the plate dimensions, laminate constructions and number and type of specimens fabricated from these plates for each material system.

Each plate was layed up from prepreg tape on a flat metal base in accordance with established procedures. As required, the Boron/Epoxy and Boron/Polyimide laminates were layed up with one mil thick glass scrim cloth between each ply and on the top and bottom surfaces of the plate. The other material systems had no scrim cloth. The layed up plate on its metal base was then placed in an autoclave for curing, Fig. 3-1.

All plates were cured in the autoclave. Postcuring, when required, was done in an air circulating oven. All curing schedules required vacuum application in addition to heat and pressure. Vacuum bagging to the table was done using teflon film as the bagging material which was sealed to the autoclave table by means of "Prestight"

Table 3-11

PLATE FABRICATION FOR CHARACTERIZATION
AND RESIDUAL STRESS STUDIES

Plate No.	Length cm, (in.)	Width cm, (in.)	Laminate Construction	Number and Type of Specimens
73-0-X**	15.2 (6)	15.2 (6)	$[0_{15}]$	5 Flexural Strength Qualification Coupons 5 Interlaminar Shear Strength Qualification Coupons 2 90-Degree Compression Characterization Coupons
73-1-X	25.4 (10)	7.6 (3)	$[0_6]$	2 Tension Characterization Coupons
73-2-X	30.5 (12)	15.2 (6)	$[90_8]$	2 Tension Characterization Coupons, 1 Relaxation Coupon 2 0-Degree Compression Characterization Coupons
73-3-X	33.6 (14)	10.2 (4)	$[0_6]$	2 10-Degree Off-Axis Intralaminar Shear Characterization Coupons
73-4-X	25.4 (10)	30.5 (12)	$[0_2/\pm 45]_s$	15 Coupons for Residual Stress Studies

**X stands for material systems A, B, C, D, E, and F.

tape vacuum sealant. After closing the autoclave, programmed heat and pressure could be applied to the plate layup while a desired vacuum level was maintained inside the bag by means of an external vacuum pump and a tube line.

Following are the specific curing schedules used for the six material systems. Heating was applied at a rate of 2.8 deg K (5 deg F) per minute unless otherwise noted.

Boron/Epoxy (Boron/AVCO 5505)

1. Apply full vacuum to bagged layup.

2. Pressurize autoclave to 587 kPa (85 psi).

3. Heat to 450 deg K (350 deg F).

4. Release vacuum and hold temperature for 2 hours.

5. Allow to cool to room temperature.

Boron/Polyimide (Boron/WRD 9371)

Precuring in air circulating oven:

1. "B"-stage prepreg layup for 3 hours at 375 ±1 deg K (215 ±2 deg F).

2. Allow to cool to room temperature.

Autoclave Curing:

1. Apply full vacuum to bagged layup.

2. Heat to 375 deg K (215 deg F) and hold for 1 hour.

3. Heat to 386 deg K (235 deg F) and hold for 1 hour. After 15 minutes at this temperature, pressurize autoclave to 587 kPa (85 psi).

4. Heat to 450 deg K (350 deg F) and hold for 1 hour.

5. Cool to 322 deg K (120 deg F) under pressure.

6. Release pressure and vacuum and allow to cool to room temperature.

Postcuring in Air Circulating Oven:

1. Bag layup in "Silastic" vacuum tight bag and apply vacuum.

2. Heat to 589 deg K (600 deg F) in 24 hours.

3. Hold at 589 deg K (600 deg F) for 60 hours.

4. Cool to room temperature in 12 hours.

Graphite/Low Modulus Epoxy (Modmor I/ERLA 4289)

Prestaging:

1. Apply 38 cm (15 in.) Hg vacuum to bagged layup.

2. Heat to 325 deg K (125 deg F) and hold for 3 hours.

Curing:

1. Increase temperature to 393 deg K (250 deg F).

2. Pressurize autoclave to 276 kPa (40 psi), maintain vacuum and hold for 2 hours.

Postcuring:

1. Increase temperature to 448 deg K (350 deg F) and hold for 4 hours with vacuum and pressure.

2. Allow to cool to room temperature.

Graphite/High Modulus Epoxy (Modmor I/ERLA 4617)

Autoclave Curing:

1. Apply full vacuum to bagged layup.

2. Pressurize autoclave to 587 kPa (85 psi).

3. Heat to 444 deg K (340 deg F) and hold for 1 hour with vacuum and pressure.

4. Allow to cool to room temperature.

Postcuring in Air Circulating Oven:

1. Heat to 444 deg K (340 deg F) and hold for 6 hours.

2. Allow to cool to room temperature.

Graphite/Polyimide (Modmor I/WRD 9371)

Precuring in Air Circulating Oven:

1. "B"- stage prepreg layup for 1 hour at 366 ±3 deg K (200 ±5 deg F).

2. Allow to cool to room temperature.

Autoclave Curing:

1. Apply 12.7 cm (5 in.) Hg vacuum to bagged layup.

2. Heat to 366 deg K (200 deg F) at 1.5-2 deg K/min (3-4 deg F/min) and hold for 30 minutes.

3. Heat to 394 deg K (250 deg F) at 1.5-2 deg K/min (3-4 deg F/min).

4. Apply full vacuum.

5. Heat to 408 deg K (275 deg F) and pressurize auto-clave to 587 kPa (85 psi).

6. Heat to 450 deg K (350 deg F) and hold for 2 hours.

7. Cool to 322 deg K (120 deg F) under pressure.

8. Release pressure and vacuum and allow to cool to room temperature.

Postcuring in Air Circulating Oven:

1. Bag layup in "Silastic" vacuum-tight bag and apply vacuum.

2. Heat to 450 deg K (350 deg F) in 4 hours.

3. Heat to 589 deg K (600 deg F) in 30 hours.

4. Hold at 589 deg K (600 deg F) for 10 hours.

5. Cool to room temperature in 14 hours.

S-Glass/Epoxy (Scotchply 1009-26S)

1. Apply full vacuum to bagged layup.

2. Heat to 422 deg K (300 deg F).

3. Pressurize autoclave to 173 kPa (25 psi), release vacuum and hold at temperature and pressure for 30 minutes.

4. Heat to 436 deg K (325 deg F) and hold for 4 hours.

5. Allow to cool to room temperature.

The thickness of each finished plate was measured at various plate locations. The average ply thicknesses, determined from these measurements for the six material systems are listed below. All subsequent stress computations for the various test specimens were based on these average ply thicknesses.

Material System	Average Per Ply Thickness	
	cm,	(in.)
A. Boron/AVCO 5505	0.0130	(0.0051)
B. Boron/WRD 9371	0.0127	(0.0050)
C. Modmor I/ERLA 4289	0.0137	(0.0055)
D. Modmor I/ERLA 4617	0.0127	(0.0050)
E. Modmor I/WRD 9371	0.0147	(0.0058)
F. S-Glass/Epoxy	0.0165	(0.0065)

3.3 Characterization of Unidirectional Laminates

3.3.1 Tensile Properties

The tensile properties of the unidirectional laminates were determined by testing tensile coupons instrumented with surface strain gages. For this purpose, two coupons for each fiber orientation, longitudinal and transverse, were cut from the fabricated plates from each of the six material systems. The longitudinal coupons were 6-ply thick, 1.27 cm (0.5 in.) wide and 23 cm (9 in.) long, with the fibers

oriented along the coupon axis. The transverse coupons were 8-ply thick, 2.54 cm (1 in.) wide and 23 cm (9 in.) long, with the fibers oriented transversely to the coupon axis.

The test specimens were prepared by bonding gripping tabs to the ends of the coupons and strain gages to the test sections. The tabs were Fiberglass/Epoxy crossply laminates, each 10-ply thick, 3.8 cm (1.5 in.) long with a 0.32 cm (1/8 in.) long taper at one end, and a width equal to that of the coupon. The strain gages on each specimen were two 2-gage 90-degree rosettes bonded to the specimen at the center of the test section, one on each side.

The testing was done by applying incrementally an axial tensile load to the specimens in an Instron universal testing machine and recording the strain from the gages. A crosshead rate of 0.127 cm (0.05 in.) per minute was selected as representing static loading. The loading was carried to specimen failure. Typical fractures of unidirectional tensile specimens are shown in Figs. 3-2 and 3-3. The laminate properties obtained from these test data are: longitudinal tensile strength S_{11T}, longitudinal modulus E_{11}, major Poisson's ratio ν_{12}, transverse tensile strength S_{22T}, transverse modulus E_{22} and minor Poisson's ratio ν_{21}. Stress-strain curves were plotted from the recorded data and are shown in Figs. 3-4 through 3-17. The strain data were averaged for the pairs of gages on opposite sides to compensate for any possible bending effects. The moduli and Poisson's ratios were determined from the initial slopes of the curves fitted to the data points. The unidirectional laminate properties obtained from the data for the six material systems are summarized in Tables 3-13 through 3-18 presented at the end of this section. *

The axial strains in the Boron/Epoxy unidirectional specimens show noticeable nonlinearities (Figs. 3-4, 3-5). In the Boron/ Polyimide some nonlinearity exists in the axial strain of the 0-degree uniaxial specimens (Figs. 3-6, 3-7), but the axial strain in the 90-degree specimen as well as all transverse strains appear linear to failure. Although the longitudinal modulus is approximately the

*Table 3-12 is cited later

same in both materials above, since it is a fiber-governed property, the longitudinal tensile strength of Boron/Polyimide is significantly lower than that of Boron/Epoxy. In the transverse direction, both modulus and strength of Boron/Polyimide are appreciably lower than corresponding properties of Boron/Epoxy.

The strains in the 0-degree Graphite/Low Modulus Epoxy specimen are linear to failure (Figs. 3-10 and 3-11). Transverse data were difficult to obtain because the 90-degree plates were extremely fragile and broke prematurely. The strains in the Graphite/High Modulus Epoxy were also linear to failure. The transverse strength is reasonably high (41.9 MPa; 6.07 ksi), approximately two-thirds of that of Boron/Epoxy. The Graphite/Polyimide shows some nonlinearity near failure in the longitudinal strain. The longitudinal modulus is higher than that of the Graphite/High Modulus Epoxy. The longitudinal strength, governed by the fibers, is approximately equal to that of Graphite/High Modulus Epoxy and significantly lower than that of Graphite/Low Modulus Epoxy. In the transverse direction, the Graphite/Polyimide has a modulus appreciably lower than that of Boron/Polyimide and somewhat lower than that of Graphite/High Modulus Epoxy. Its transverse strength is somewhat higher than that of Boron/ Polyimide but appreciably lower than that of Graphite/High Modulus Epoxy.

The strains in the S-glass/Epoxy are fairly linear to failure except in the case of the longitudinal strain in one specimen (Fig. 3-16). The transverse modulus is the highest of all such moduli in the other material systems, and is equal to approximately forty percent of its tensile modulus. The longitudinal tensile strength is fairly high, comparable to that of Boron/Epoxy.

3.3.2 Compressive Properties

Characterization of unidirectional laminates in compression was done using the IITRI designed compression test fixture, Figs. 3-18 and 3-19, incorporating some recent improvements in alignment.

Although this fixture is not ideal, it represents the best features of compression coupon fixtures available elsewhere. The development of the IITRI compression test is based on a survey of many available systems including the TEI test, a system combining the best features of the TEI and the sandwich beam tests, Narmco Test Method No. 303, Federal Test Method Standard No. 406, ASTM compression test, and the Celanese test.

The Celanese test uses split conical collet grips which fit into matching sleeves which in turn fit into a snugly fitting cylindrical shell. One major disadvantage of this fixture is that it requires a perfect cone-to-cone contact. This contact is not normally achieved due to small variations in tab thickness. Instead, contact is limited to two lines on opposite sides of the specimen. This unstable condition causes a lateral shift in the seat grips which then contact the enveloping cylinder and produce high frictional forces. The result is that the Celanese fixture, tested at IITRI, results in erroneously high values for the stiffness and compressive strength.

The IITRI fixture represents a modification of the Celanese one. The conical grips have been replaced with trapezoidal wedges. This eliminates the problem of line contact, since surface-to-surface contact can be attained at all positions of the wedges. Furthermore, it permits precompression of the specimen tabs to prevent slippage early in the load cycle. This is especially important at high strain rates. Finally, the lateral alignment of the fixture top and bottom halves is assured by a guidance system consisting of two parallel roller bushings.

Two coupons for each fiber orientation, loongitudinal and transverse, were used for the compression testing of each of the six material systems. The longitudinal coupons were cut from the 8-ply plates and the transverse from the 15-ply plates. Each coupon was nominally 0.64 cm (0.25 in.) wide and 14.0 cm (5.5 in.) long. The test specimens were prepared by bonding pairs of 6.35 cm (2.5 in.)

long tabs to each end of the specimen, making the specimen test section 1.27 cm (0.5 in.) long. The tabs were Glass/Epoxy crossply laminates, 10-ply thick, with a 0.32 cm (1/8 in.) long taper at the test section end.

The tests conducted on these specimens determined the longitudinal compressive strength S_{11C} and the transverse compressive strength S_{22C}. The results for the six material systems obtained from these tests are listed in Tables 3-13 to 3-18.

In three material systems, Boron/Epoxy, Boron/Polyimide and Graphite/High Modulus Epoxy, the longitudinal compressive strength is higher (up to 15 percent) than the tensile strength, as expected. The validity of the opposite result for the other three material systems is questioned. The measured transverse compressive strength (S_{22C}) is in all cases appreciably higher than the corresponding tensile strength. It ranges from 2.2 to 5.7 times the transverse tensile strength.

3.3.3   Intralaminar Shear Properties

The intralaminar shear properties were determined by testing off-axis unidirectional coupons in tension. Two coupons per material system were tested. These specimens were 6-ply thick with the fibers oriented at 10-degrees with the loading axis, made by machining the coupons from unidirectional plates at a 10-degree angle with the fibers. They were 1.27 cm (0.5 in.) wide and 33 cm (13 in.) long with specially made tapered loading tabs.

These tabs were 7.6 cm (3 in.) long made of similarly (10-degree) oriented 6-ply glass/epoxy material. The taper was approximately 4.6 cm (1.8 in.) long, making a taper angle of about 1.3-degrees. The reason for the long specimen with the long tapered and similarly oriented tabs, was to produce a uniform known state of stress in the test section by minimizing end effects. The specimens were instrumented with surface strain gages, a 3-gage rosette on one side and an axial gage on the other. The 3-gage rosette had one gage oriented axially one at 45-degrees and one transversely to the loading axis.

The testing was done in the Instron testing machine. The specimens were loaded in tension at a rate of 0.127 cm (0.05 in.) per minute. The load was applied at increments until failure. At each increment of load, the strains and load were recorded.

The intralaminar properties determined from these data are the intralaminar shear strength S_{12} and intralaminar shear modulus G_{12}. The S_{12} is determined from the relation

$$S_{12} = S_{xxT} \sin\theta \cos\theta$$

where S_{xxT} is the axial tensile strength. For $\theta = 10$-degrees the formula becomes

$$S_{12} = 0.171 S_{xxT}$$

There are two alternate but equivalent ways for determining G_{12}. The first makes use of the transformation equation for orthotropic materials:

$$\frac{1}{G_{12}} = \frac{1}{E_{xx}\sin^2\theta \cos^2\theta} - \frac{\cos^2\theta}{E_{11}\sin^2\theta} + \frac{2\nu_{12}}{E_{11}} - \frac{\sin^2\theta}{E_{22}\cos^2\theta}$$

where θ = angle between loading and fiber direction and E_{xx} the tensile modulus in the loading direction. For $\theta = 10$ degrees the relation above becomes

$$\frac{1}{G_{12}} = \frac{34.20}{E_{xx}} + \frac{2\nu_{12} - 32.16}{E_{11}} - \frac{0.03}{E_{22}}$$

By plotting the axial stress σ_{xx} versus the axial strain ϵ_{xx} the modulus E_{xx} can be determined from the slope of the curve fitted to the data. Figures 3-20 through 3-25 show the plots obtained from the test data for the six material systems. For each specimen the longitudinal strains measured on the two sides of the specimen were averaged to eliminate any possible bending effects. Each figure shows the data obtained for both specimens of each material. The value of E_{xx} listed in each figure is the average for the two specimens.

The modulus G_{12} was determined from the above formula using E_{xx} as determined in Figs. 3-20 to 3-25, and E_{11}, E_{22}, ν_{12} determined in the tensile characterization tests. The values of G_{12} and S_{12} determined from the test data are summarized in Tables 3-13 through 3-18.

The alternate method for determining G_{12} requires the use of all three strains recorded by the 3-gage rosette as follows.

The three strains measured as a function of applied load are: the axial strain (ϵ_x), transverse strain (ϵ_y) and 45-degree strain (ϵ_{45}). The shear strain ϵ_{xy} referred to the axes of the specimen is computed from the relation

$$\epsilon_{xy} = \epsilon_{45} - \left(\frac{\epsilon_x + \epsilon_y}{2}\right)$$

and the shear strain referred to the material axes of the specimen (parallel and normal to the fibers) is obtained from the relation

$$\epsilon_{12} = -\frac{\epsilon_x - \epsilon_y}{2} \sin 2\theta + \epsilon_{xy} \cos 2\theta$$

where $\theta = 10$ deg., the angle between the load and fiber directions. The shear stress referred to the material axes is given by

$$\sigma_{12} = \sigma_x \sin\theta \cos\theta$$

This shear stress is plotted versus the corresponding shear strain. The initial slope of this curve yields the in-plane shear modulus, G_{12} and the ultimate value of σ_{12} is the intralaminar in-plane shear strength. Figures 3-26 and 3-27 show shear stress versus shear strain curves for the Boron/Polyimide and the S-Glass/Epoxy materials determined by this method.

3.3.4 Coefficients of Thermal Expansion

The thermal expansion coefficients for the unidirectional laminates were determined in the residual strain task presented in Section 3.4. The details of the method used are presented in that section with only a brief description given here.

The coefficients of thermal expansion were determined by monitoring longitudinal and transverse strains with temperature in uniaxial $[0_8]$ specimens for each of the six material systems. The specimens were 12.7 cm (5 in.) long and 2.4 cm (1 in.) wide. They were instrumented with embedded strain gages and an embedded thermocouple for strain and temperature monitoring and recording. The thermal expansion strain was established from the strain readings by correcting for the pure thermal output of the gages. The slope of this thermal strain versus temperature curve for the longitudinal and transverse directions yielded the thermal expansion coefficients α_{11} and α_{22}. The results for the six material systems are listed in Tables 3-13 to 3-18.

3.3.5 Density and Fiber Volume Fraction

The laminate densities for the six composite systems were determined by the displacement method in accordance with the ASTM-D792 recommended procedure. Briefly, the method involves three steps. The composite laminate sample is first weighed in air. Next, the sample is suspended by a wire on the weighing scale and weighed while totally immersed in a liquid of known density and good wettability. The liquid selected for our tests was alcohol. For the final step, the suspended wire is weighed immersed in the liquid to the same depth as during the sample weighing. Using these data the composite laminate density is obtained from the formula

$$\rho_c = \frac{\rho_\ell W_c}{W_c - W + W_w}$$

where

ρ_c = density of composite

ρ_ℓ = density of immersion liquid

W_c = weight of composite sample in air

W = weight of sample and wire while immersed
in liquid

W_w = weight of wire while immersed in liquid

The densities determined for the six material systems are presented in Table 3-12. During immersion the liquid cannot penetrate into the interior voids of the specimen. Consequently, the absolute density determined by this method is in error by the amount of voids present in the interior.

The fiber volume ratios, FVR, were determined by the gravimetric method. This involves a computation using the known densities of the constituent materials. The fiber volume ratio is given by the following relation:

$$FVR = \frac{\rho_c - \rho_r}{\rho_f - \rho_r} - \delta_s \left(\frac{\gamma_s N_s}{\rho_s t_c} \right) \left(\frac{\rho_s - \rho_r}{\rho_f - \rho_r} \right)$$

where

ρ_c, ρ_r, ρ_f = densities of composite, resin, and
fiber, respectively

ρ_s = density of scrim cloth fiber

γ_s = weight per unit area of a single scrim cloth ply

N_s = number of scrim cloth plies in composite

t_c = composite specimen thickness

δ_s = 1 if composite contains scrim cloth

δ_s = 0 for composite without scrim cloth

Table 3-12

DENSITIES AND FIBER VOLUME RATIOS OF COMPOSITE SYSTEMS

| Material System | Densities, ρ, kg/m^3 (lb/in.^{3}) | | | Fiber Volume Ratio, FVR | Scrim Cloth Volume Ratio |
	Composite ρ_c	Fiber ρ_f	Resin ρ_r		
A. Boron/Epoxy (Boron/AVCO 5505)	2034 (0.073)	2680 (0.097)	1220 (0.044)	0.50	0.06
B. Boron/Polyimide (4 Mil Boron/WRD 9371)	2000 (0.072)	2680 (0.097)	1180 (0.043)	0.49	0.06
C. Graphite/Low Modulus Epoxy (Modmor I/ERLA 4289)	1560 (0.056)	1980 (0.071)	1125 (0.041)	0.51	-
D. Graphite/High Modulus Epoxy (Modmor I/ERLA 4617)	1540 (0.056)	1980 (0.071)	1180 (0.043)	0.45	-
E. Graphite/Polyimide (Modmor I/WRD 9371)	1540 (0.056)	1980 (0.071)	1180 (0.043)	0.45	-
F. S-Glass/Epoxy (Scotchply 1009-26-5901)	2130 (0.077)	2480 (0.090)	1230 (0.044)	0.72	-

Table 3-13
PROPERTIES OF UNIDIRECTIONAL BORON/EPOXY
(Boron/AVCO 5505)

Property (Room Temperature Unless Otherwise Specified)	SI Units	English Units
Fiber Volume Ratio, FVR	0.50	-
Density, ρ	2034 kg/m^3	0.073 lb/in.^{3}
Longitudinal Thermal Coefficient, α_{11}		
297 deg K (75°F)	6.1×10^{-6} K^{-1}	3.4 $\mu\varepsilon$/°F
450 deg K (350°F)	6.1×10^{-6} K^{-1}	3.4 $\mu\varepsilon$/°F
Transverse Thermal Coefficient, α_{22}		
297 deg K (75°F)	30.3×10^{-6} K^{-1}	16.9 $\mu\varepsilon$/°F
450 deg K (350°F)	37.8×10^{-6} K^{-1}	21.0 $\mu\varepsilon$/°F
Longitudinal Modulus, E_{11}	201 GPa	29.2×10^6 psi
Transverse Modulus, E_{22}	21.7 GPa	3.15×10^6 psi
Shear Modulus, G_{12}	5.4 GPa	0.78×10^6 psi
Major Poisson's Ratio, ν_{12}	0.17	-
Minor Poisson's Ratio, ν_{21}	0.02	-
Longitudinal Tensile Strength, S_{11T}	1,375 MPa	199,000 psi
Longitudinal Compressive Strength, S_{11C}	1,600 MPa	232,000 psi
Transverse Tensile Strength, S_{22T}	56.0 MPa	8,100 psi
Transverse Compressive Strength, S_{22C}	123.7 MPa	17,900 psi
Intralaminar Shear Strength, S_{12}	62.3 MPa	9,100 psi

Table 3-14

PROPERTIES OF UNIDIRECTIONAL BORON/POLYIMIDE

(Boron/WRD 9371)

Property (Room Temperature Unless Otherwise Specified)	SI Units	English Units
Fiber Volume Ratio, FVR	0.49	-
Density, ρ	2000 kg/m^3	0.072 lb/in.^{3}
Longitudinal Thermal Coefficient, α_{11}		
297 deg K (75°F)	4.9×10^{-6} K^{-1}	2.7 $\mu\varepsilon$/°F
450 deg K (350°F)	4.9×10^{-6} K^{-1}	2.7 $\mu\varepsilon$/°F
Transverse Thermal Coefficient, α_{22}		
297 deg K (75°F)	28.4×10^{-6} K^{-1}	15.8 $\mu\varepsilon$/°F
450 deg K (350°F)	28.4×10^{-6} K^{-1}	15.8 $\mu\varepsilon$/°F
Longitudinal Modulus, E_{11}	221.5 GPa	32.1×10^6 psi
Transverse Modulus, E_{22}	14.5 GPa	2.1×10^6 psi
Shear Modulus, G_{12}	7.66 GPa	1.11×10^6 psi
Major Poisson's Ratio, ν_{12}	0.16	-
Minor Poisson's Ratio, ν_{21}	0.02	-
Longitudinal Tensile Strength, S_{11T}	1040 MPa	151,000 psi
Longitudinal Compressive Strength, S_{11C}	1090 MPa	158,000 psi
Transverse Tensile Strength, S_{22T}	10.8 MPa	1,600 psi
Transverse Compressive Strength, S_{22C}	62.8 MPa	9,100 psi
Intralaminar Shear Strength, S_{12}	25.9 MPa	3,750 psi

Table 3-15

PROPERTIES OF UNIDIRECTIONAL GRAPHITE/LOW MODULUS EPOXY
(Modmor I/ERLA 4289)

Property (Room Temperature Unless Otherwise Specified)	SI Units	English Units
Fiber Volume Ratio, FVR	0.51	-
Density, ρ	1560 kg/m^3	0.056 lb/in.^{3}
Longitudinal Thermal Coefficient, α_{11}		
297 deg K (75°F)	-1.1×10^{-6} K^{-1}	-0.6 $\mu\varepsilon$/°F
450 deg K (350°F)	3.2×10^{-6} K^{-1}	1.3 $\mu\varepsilon$/°F
Transverse Thermal Coefficient, α_{22}		
297 deg K (75°F)	31.5×10^{-6} K^{-1}	17.5 $\mu\varepsilon$/°F
450 deg K (350°F)	27.0×10^{-6} K^{-1}	15.0 $\mu\varepsilon$/°F
Longitudinal Modulus, E_{11}	188 GPa	27.3×10^6 psi
Transverse Modulus, E_{22}	4.14 GPa	600,000 psi
Shear Modulus, G_{12}	4.83 GPa	700,000 psi
Major Poisson's Ratio, ν_{12}	0.20	-
Minor Poisson's Ratio, ν_{21}	0.04	-
Longitudinal Tensile Strength, S_{11T}	1,115 MPa	162,000 psi
Longitudinal Compressive Strength, S_{11C}	990 MPa	144,000 psi
Transverse Tensile Strength, S_{22T}	4.15 MPa	600 psi
Transverse Compressive Strength, S_{22C}	-	-
Intralaminar Shear Strength, S_{12}	33.5 MPa	4,850 psi

Table 3-16

PROPERTIES OF UNIDIRECTIONAL GRAPHITE/HIGH MODULUS EPOXY
(Modmor I/ERLA 4617)

Property (Room Temperature Unless Otherwise Specified)	SI Units	English Units
Fiber Volume Ratio, FVR	0.45	-
Density, ρ	1,540 kg/m^3	0.056 lb/in.^{3}
Longitudinal Thermal Coefficient, α_{11} 297 deg K (75°F) 445 deg K (340°F)	-0.9×10^{-6} K^{-1}	-0.5 $\mu\varepsilon$/°F
Transverse Thermal Coefficient, α_{22} 297 deg K (75°F)	33.3×10^{-6} K^{-1}	18.5 $\mu\varepsilon$/°F
445 deg K (340°F)	58.9×10^{-6} K^{-1}	32.7 $\mu\varepsilon$/°F
Longitudinal Modulus, E_{11}	190 GPa	27.5×10^6 psi
Transverse Modulus, E_{22}	7.1 GPa	1.03×10^6 psi
Shear Modulus, G_{12}	6.2 GPa	0.9×10^6 psi
Major Poisson's Ratio, ν_{12}	0.10	-
Minor Poisson's Ratio, ν_{21}		-
Longitudinal Tensile Strength, S_{11T}	841 MPa	122,000 psi
Longitudinal Compressive Strength, S_{11C}	883 MPa	128,000 psi
Transverse Tensile Strength, S_{22T}	41.9 MPa	6,070 psi
Transverse Compressive Strength, S_{22C}	196.5 MPa	28,500 psi
Intralaminar Shear Strength, S_{12}	61.5 MPa	8,900 psi

Table 3-17

PROPERTIES OF UNIDIRECTIONAL GRAPHITE/POLYIMIDE
(Modmor I/WRD 9371)

Property (Room Temperature Unless Otherwise Specified)	SI Units	English Units
Fiber Volume Ratio, FVR	0.45	-
Density, ρ	1,540 kg/m^3	0.056 lb/in.^{3}
Longitudinal Thermal Coefficient, α_{11}		
297 deg K (75°F)	0 K^{-1}	0 $\mu\epsilon$/°F
589 deg K (600°F)	0 K^{-1}	0 $\mu\epsilon$/°F
Transverse Thermal Coefficient, α_{22}		
297 deg K (75°F)	25.3 x 10^{-6} K^{-1}	14.1 $\mu\epsilon$/°F
589 deg K (600°F)	25.3 x 10^{-6} K^{-1}	14.1 $\mu\epsilon$/°F
Longitudinal Modulus, E_{11}	216 GPa	31.3 x 10^6 psi
Transverse Modulus, E_{22}	4.97 GPa	720,000 psi
Shear Modulus, G_{12}	4.48 GPa	650,000 psi
Major Poisson's Ratio, ν_{12}	0.25	-
Minor Poisson's Ratio, ν_{21}	0.02	-
Longitudinal Tensile Strength, S_{11T}	807 MPa	117,000 psi
Longitudinal Compressive Strength, S_{11C}	652 MPa	94,500 psi
Transverse Tensile Strength, S_{22T}	14.9 MPa	2,150 psi
Transverse Compressive Strength, S_{22C}	70.5 MPa	10,200 psi
Intralaminar Shear Strength, S_{12}	21.7 MPa	3,150 psi

Table 3-18

PROPERTIES OF UNIDIRECTIONAL S-GLASS/EPOXY
(Scotchply 1009-26-5901)

Property (Room Temperature Unless Otherwise Specified)	SI Units	English Units
Fiber Volume Ratio, FVR	0.72	-
Density, ρ	2,134 kg/m^3	0.077 lb/in.^{3}
Longitudinal Thermal Coefficient, α_{11}		
297 deg K (75°F)	3.8 x 10^{-6} K^{-1}	2.1 $\mu\varepsilon$/°F
435 deg K (325°F)	3.8 x 10^{-6} K^{-1}	2.1 $\mu\varepsilon$/°F
Transverse Thermal Coefficient, α_{22}		
297 deg K (75°F)	16.7 x 10^{-6} K^{-1}	9.3 $\mu\varepsilon$/°F
435 deg K (325°F)	54.9 x 10^{-6} K^{-1}	30.5 $\mu\varepsilon$/°F
Longitudinal Modulus, E_{11}	60.7 GPa	8.8 x 10^6 psi
Transverse Modulus, E_{22}	24.8 GPa	3.6 x 10^6 psi
Shear Modulus, G_{12}	12.0 GPa	1.74 x 10^6 psi
Major Poisson's Ratio, ν_{12}	0.23	-
Minor Poisson's Ratio, ν_{21}	0.09	-
Longitudinal Tensile Strength, S_{11T}	1,290 MPa	187,000 psi
Longitudinal Compressive Strength, S_{11C}	822 MPa	119,000 psi
Transverse Tensile Strength, S_{22T}	46.0 MPa	6,670 psi
Transverse Compressive Strength, S_{22C}	174 MPa	25,300 psi
Intralaminar Shear Strength, S_{12}	45 MPa	6,500 psi

The resin and fiber densities, ρ_r and ρ_f, for the material systems were obtained from the manufacturers of the prepreg tapes. They are listed in Table 3-12. Glass scrim cloth was used in the material systems with boron fibers. Properties of this scrim cloth are

$$\rho_s = 2540 \text{ kg/m}^3 \ (0.0918 \text{ lb/in.}^3)$$

$$\gamma_s = 0.193 \text{ N/m}^2 \ (2.802 \times 10^{-5} \text{ lb/in.2})$$

The fiber volume ratios determined for the six material systems are listed in Table 3-12. These, together with the composite densities are also shown in the summary Tables 3-13 to 3-18.

3.4 Residual Strain

3.4.1 General Experimental Procedures

Residual strains were determined in eight-ply laminates of $[0_2/\pm45]_s$ construction for the six material systems selected. These specimens were 2.54 cm (1 in.) wide and 22.9 cm (9 in.) long. Unidirectional $[0_8]$ specimens were also used for reference purposes in determining the residual strain buildup and for measuring the basic coefficients of thermal expansion. These specimens were 2.54 cm (1 in.) wide and 12.7 cm (5 in.) long.

The specimens were fabricated and instrumented with surface and embedded gages and thermocouples following previously established procedures [3,34]. The embedded instrumentation requires lead exits through the specimen sides which precludes cutting specimens from a single plate. Each specimen was therefore layed up individually to final dimensions using 2.54 cm (1 in.) wide strips cut from the prepreg tape at the required fiber orientation. To assure uniformity in properties the specimens were fabricated from the same batch of material as the characterization and static strength specimen plates described in Section 3.2 and under the same quality control. To assure straight parallel sides and maintain width control the specimens

were laid up between a pair of parallel steel guides 2.54 cm (1 in.) apart mounted on a steel base plate. The guides contained markings and cutouts for locating the embedded gages and permitting the leads to exit through the sides. For curing, the laid up specimens were transferred to another steel plate with cork strips as the parallel guides. These served a dual purpose; to maintain width control by preventing spreading and shifting of specimen plies under pressure in the curing cycle, and as dams against edge flow of resin, forcing the resin to bleed during curing only through the top and bottom of the specimen. This control is required in order to maintain uniformity of resin content over the specimen width.

The foil strain gages used to instrument the specimens were three gage rosettes, used primarily as embedded instrumentation, and two gage rosettes, used primarily as surface gages. Special requirements on the gages were that they produce no significant local thickening when embedded and that they be electrically insulated from the conducting fibers.

In the case of the glass/epoxy specimens there are no insulation problems. Hence conventional open-face gages approximately 0.025 mm (0.001 in.) thick (Micro-Measurements EA Series) were used with nickel-clad copper ribbon leads attached. These ribbons are approximately 0.025 mm (0.001 in.) thick and 0.38 mm (0.015 in.) wide. The gages were laid down during specimen fabrication on the desired plies in accordance with the typical layouts shown in Figs. 3-28 and 3-29. The matrix resin served to bond the gages and no additional cement was necessary. The embedded gages in the $[0_2/\pm45]_s$ specimens were laid down in a staggered pattern (Figure 3-29) in order to minimize local specimen thickening. Each gage was checked for electrical continuity before it was emplaced and after layup.

A Chromel-Alumel (ANSI Type K) thermocouple was embedded in each specimen during layup. The thermocouple wires were 0.25 mm (0.01 in.) in diameter with fiberglass insulation beyond the sensing junction. Because of the thickness and stiffness of

the wires the thermocouple was located at the end of the specimen, embedded between the fourth and fifth plies.

Figure 3-30 illustrates a Glass/Epoxy specimen with embedded instrumentation after cure. The embedded gages and thermocouple are visible through the material.

For the boron and graphite fiber specimens, previously developed techniques were improved and refined. Fully encapsulated gages were used because these fibers are electrically conducting. To minimize local specimen thickening, special gages were procured with the backing and encapsulation only half as thick as on standard gages. The encapsulated gage thickness was therefore approximately 0.025 mm (0.001 in.). The attached ribbon leads were nickel-clad copper 0.025 mm (0.001 in.) thick and 0.38 mm (0.015 in.) wide. They were coated to fully insulate them from the conducting fibers. In addition, since the ribbon lead coating was not always available or effective, the leads were sandwiched between strips of 0.013 mm (0.0005 in.) thick polyimide sheet (Kapton) during gage layup. No cement was necessary to emplace the gages since the specimen matrix served as bonding material.

The gages were checked for electrical continuity and gage and lead shorts due to accidental contact with the fibers both before and after layup.

Gages in the $\left[0_2/\pm45\right]_s$ specimens were embedded in a staggered pattern in order to minimize local specimen thickening. For the uniaxial specimens gage staggering was not necessary since only one gage was embedded. In the case of the boron specimens local specimen thickening due to gage emplacement was minimized by removing an area of scrim cloth equal to the area of the gage and leads where the gage was laid down. Scrim cloth thickness, 0.025 mm (0.001 in.), is essentially the same as that of the gage.

For the epoxy matrix specimens, polyimide-encapsulated Constantan alloy gages (Micro-Measurements, Series QA) were used. An example of such gages are the three-gage rosette QA-06-125RD-350,

option B171 and the two-gage rosette QA-06-125TQ-350, option
B171. These gages are designed to operate in the temperature
range of 77 deg K (320°F) to 478 deg K (400°F). These gages could
not be used for the polyimide matrix specimens because of their
higher postcure temperature. The gages selected for the polyimide
specimens were the high temperature glass-fiber epoxy phenolic-
encapsulated nickel-chromium alloy gages (Micro-Measurements WK
Series). An example of such gages are the three-gage rosette
WK-06-125RA-350, option B156 and the two-gage rosette, WK-06-125TM-
350, option B156.

In addition to the gages, each boron and graphite specimen
was provided with an embedded thermocouple of the same type and
at the same location, as in the case of the Glass/Epoxy specimens.

In all cases above, all gages and thermocouples were
completely wired before specimen curing and connected to a multi-
channel Signal Conditioning and Data Acquisition system for monitoring
during curing. The instrumented specimens were bagged with the
gages and thermocouples completely wired and subjected to the
prescribed curing and postcuring cycles in the autoclave, Fig. 3-31,
and high temperature oven, Fig. 3-32.

The combinations of high temperature, pressure and vacuum
applications during curing and postcuring required special techniques
for wiring and lead emplacement for the specimen instrumentation.
The three-wire gage compensation technique, Fig. 3-33, was used to
compensate for the appreciable resistance changes taking place in
the portions of the lead wires exposed to the elevated temperatures
inside the autoclave or oven. As indicated in Fig. 3-33 these lead
wires must be of equal length for the compensation to be exact. The
use of high resistance strain gages reduces the errors due to de-
viations from this condition. For this reason 350 ohm strain gages
rather than the more common 120 ohm gages were selected for the
majority of the specimens.

The high curing and postcuring temperatures called for suitable lead wires and soldering techniques. In the case of the epoxy matrix specimens the lead wires were AWG 26 teflon-insulated copper wires suitable in the range between 73 deg K and 473 deg K (-328^OF and 392^OF). They were soldered to the gage leads with a tin-compound solder applicable up to 456 deg K (361^OF). For the polyimide matrix specimens the lead wires were AWG 26 fiberglass-braid insulated nickel-clad copper wires, suitable in the range from 4 deg K to 753 deg K (-452^OF to 900^OF). These were soldered to the gage leads with a silver compound recommended for temperatures up to 892 deg K (1145^OF). To prevent air leaks through the wire insulation and maintain vacuum during curing, it was necessary to bare the wires locally and embed them in the silicon rubber gasket used in bagging the specimens.

The completely wired and bagged specimens were connected to a data acquisition system for monitoring of strain buildup as a function of temperature during curing and postcuring (Fig. 3-31 and 3-32). The data acquisition system consisted of strain gage bridge balance boxes for signal conditioning plus a digital voltmeter with automatic scanning and printing units.

3.4.2 Determination of Residual Strains and Residual Stresses

Strain gage and thermocouple outputs were recorded in all specimens during curing, postcuring, and in some cases, during subsequent thermal cycling. To properly interpret the strain gage output ε_a (apparent strain), it is necessary to separate this output into the component ε_t due to the deformation of the specimen (thermal strain) and the component ε_g due to the change in resistivity of the gage with temperature (thermal output)

$$\varepsilon_t = \varepsilon_a - \varepsilon_g$$

To determine ε_g a fused quartz specimen of known thermal expansion, 0.7×10^{-6} K^{-1} (0.4 $\mu\varepsilon/^O$F), was instrumented with a strain gage and a thermocouple and included along with the laminate specimen in all tests. The gage used on the quartz was of the same

type and material as those used for the laminate specimens. The measured gage output from the quartz specimen ε_q is related to the thermal output of the gage by the expression

$$\varepsilon_g = \varepsilon_q - \varepsilon_{tq}$$

where ε_{tq} is the known thermal expansion strain in quartz. The measured thermal output of the gages was checked against similar data supplied by the manufacturer with each gage package and the agreement was found satisfactory. The true thermal strain ε_t in the composite laminates was obtained by subtracting algebraically from the apparent strain the output from the gage on the quartz and adding the known thermal expansion of quartz:

$$\varepsilon_t = \varepsilon_a - \varepsilon_q + \varepsilon_{tq}$$

The reference specimen used for measurement of the purely thermal output of the gage can be of any material with a known constant and stable coefficient of thermal expansion. Figure 3-34 shows the measured gage output from quartz and aluminum oxide (alumina) specimens.

The residual stresses in each ply correspond to the so-called restraint or residual strains, i.e., the difference between the unrestrained thermal expansion of that ply and the restraint expansion of the laminate. Given a ply with material axes 1, 2 at an angle θ with the laminate axes x,y, the residual strains at a temperature T are given by the relations

$$(\varepsilon_r)_{xx} = -\int_{T_o}^{T} \alpha_{xx} dT + \left[\varepsilon_{xx}(T) - \varepsilon_{xx}(T_o)\right]$$

$$(\varepsilon_r)_{xy} = -\int_{T_o}^{T} \alpha_{xy} dT + \left[\varepsilon_{xy}(T) - \varepsilon_{xy}(T_o)\right]$$

$$(\varepsilon_r)_{yy} = -\int_{T_o}^{T} \alpha_{yy} dT + \left[\varepsilon_{yy}(T) - \varepsilon_{yy}(T_o)\right]$$

where ε_r is the residual strain, ε_{xx}, ε_{xy}, ε_{yy} measured thermal strains,

$$\alpha_{xx} = m^2 \alpha_{11} + n^2 \alpha_{22}$$

$$\alpha_{xy} = mn(\alpha_{22} - \alpha_{11})$$

$$\alpha_{yy} = n^2 \alpha_{11} + m^2 \alpha_{22}$$

the transformed thermal coefficients of expansion referred to the x-y system ($m = \cos\theta$, $n = \sin\theta$). T_0 is the reference temperature, usually the curing temperature, at which residual strains and stresses are zero.

The expressions above can also be written in terms of apparent strains measured in the unidirectional and angle-ply laminates as follows:

$$(\varepsilon_r)_{\alpha\beta} = \left[(\varepsilon_u)_{\alpha\beta} - (\varepsilon_1)_{\alpha\beta} \right]_{T_0}^{T} =$$

$$= \left[(\varepsilon_{au})_{\alpha\beta} - (\varepsilon_{a1})_{\alpha\beta} \right]_{T_0}^{T}$$

where α, β = x,y, and subscripts a, u, 1 denote apparent unidirectional laminate and angle-ply laminate, respectively.

Residual stresses are computed from the residual or restraint strains above using the orthotropic constitutive relations, taking into consideration the temperature dependence of the stiffness and residual strains. The stress difference between two temperature levels T and T_0 is given by:

$$\left[\sigma_{ij} \right]_{T_0}^{T} = \int_{T_0}^{T} \left[Q \right] \frac{\partial}{\partial\tau} \left[\varepsilon_{ij} \right] d\tau$$

where $\left[Q \right]$, $\left[\sigma_{ij} \right]$ and $\left[\varepsilon_{ij} \right]$ are the temperature-dependent stiffness, residual stress, and residual strain matrices, respectively. When the directions i,j above are not principal material directions for the ply, the stiffness matrix $\left[\overline{Q} \right]$ referred to the reference axes i, j is used.

For the 0-degree plies of the $0_2/\pm45_s$ laminate, where the material axes of the ply coincide with the material axes of the laminate and the principal stress and strain directions,

$$\sigma_{11}(T) = \int_{T_o}^{T} \left[Q_{11}(\tau) \frac{\partial \varepsilon_{11}}{\partial \tau} + Q_{12}(\tau) \frac{\partial \varepsilon_{22}}{\partial \tau} \right] d\tau$$

$$\sigma_{22}(T) = \int_{T_o}^{T} \left[Q_{12}(\tau) \frac{\partial \varepsilon_{11}}{\partial \tau} + Q_{22}(\tau) \frac{\partial \varepsilon_{22}}{\partial \tau} \right] d\tau$$

$$\sigma_{12}(T) = 0$$

where subscripts 1 and 2 correspond to directions parallel and transverse to the fibers. The stiffness matrix components are related to measured quantities as follows:

$$Q_{11} = \frac{E_{11}}{1-\nu_{12}\nu_{21}}$$

$$Q_{12} = \frac{\nu_{21} E_{11}}{1-\nu_{12}\nu_{21}} = \frac{\nu_{12} E_{22}}{1-\nu_{12}\nu_{21}}$$

$$Q_{22} = \frac{E_{22}}{1-\nu_{12}\nu_{21}}$$

$$Q_{66} = G_{12}$$

3.4.3 Edge Effects

A test was conducted to establish whether thermal strains measured in the laminated specimens are uniform across the width of the specimen. A 2.54 cm x 22.9 cm (1 in. x 9 in.) $[0_2/\pm45]_s$ S-Glass/Epoxy specimen was instrumented with embedded gages (Micro-Measurements EA-05-062TT-120) at different locations across the width (Fig. 3-35). The specimen was cured and subsequently subjected

to a thermal cycle from room temperature to 435 deg K (325°F) and down to room temperature. Strain gages were recorded at frequent intervals and are plotted as a function of temperature in Figs. 3-36 to 3-39. The agreement among the three gages is very good, indicating that thermal strains are uniform across the width of the specimen.

3.4.4 Residual Strains in Boron/Epoxy

A 2.54 cm x 22.9 cm (1 in. x 9 in.) eight-ply laminate of $[0_2/\pm45]_s$ layup and a 2.54 cm x 12.7 cm (1 in. x 5 in.) $[0_8]$ specimen were fabricated and instrumented with surface and embedded gages and thermocouples following procedures discussed before. The angle-ply laminate was instrumented with encapsulated three-gage rosettes (Micro-Measurements QA-05-125RD-350, Option B110) on the third, fifth and seventh plies, two-gage rosettes (EA-06-125TF-120) on the top and bottom surfaces, and an embedded thermocouple between the fourth and fifth ply. The unidirectional specimen was instrumented with a three-gage rosette and a thermocouple in the middle surface and two-gage rosettes on the top and bottom surfaces. The embedded gages were fully encapsulated and the attached ribbon leads were coated to prevent any current leakage through the conducting boron fibers.

The instrumented Boron/Epoxy and quartz specimens with all wiring connected to a Digital Data Acquisition system were placed in the autoclave and subjected to the curing cycle described earlier. Strain gage and thermocouple readings were recorded at 5.5 deg K (10°F) intervals during the heating and cooling cycles.

To compare strains during curing with those due to purely thermal expansion, the same specimens above were subjected to a thermal cycle from room temperature to 450 deg K (350°F) and down to room temperature. Strain gages and thermocouples were recorded at 5.5 deg K (10°F) intervals.

The apparent strains recorded during the first part of the curing cycle (increasing temperature) showed a great deal of scatter and bore no resemblance to those of the second half (decreasing temperature). This is probably because no macroscopic stresses are built up while the matrix resin is in a fluid state. Residual stresses build up after curing is achieved at the peak temperature of 450 deg K(350^OF). Recorded apparent strains for the $[0_2/\pm45]_s$ laminate during the decreasing temperature stage of the curing cycle are shown in Fig. 3-40. These apparent strains in all cases were corrected for the purely thermal output of the gage, by subtracting algebraically the output from the gage on the quartz specimen and adding the known thermal expansion of quartz. Thus, thermal strains were obtained for the second part of the curing cycle (decreasing temperature) for the $[0_8]$ and $[0_2/\pm45]_s$ boron/epoxy specimens (Figs. 3-41 and 3-42). Also plotted in these figures are the thermal strains obtained during the subsequent thermal cycling of the specimens averaged for the ascending and descending parts of the cycle. The agreement between the two sets of strains is satisfactory and it indicates that the curing strains in the second half of the curing cycle are caused by thermal expansion of the material. Therefore, the residual strains induced during curing are caused by differential thermal expansion of the various plies. The small discrepancies between curing and thermal strains observed at the higher temperatures may be related to different rates of temperature variation. It is worth noting that the strain variation during curing is perfectly linear with temperature.

The slopes of the thermal strain versus temperature curves (Fig. 3-41) for the unidirectional laminate yields the coefficient of thermal expansion below:

At T = 297 deg K(75^OF)

α_{11} = 6.1 x 10^{-6} K^{-1} (3.4 $\mu\varepsilon$/^{O}F)

α_{22} = 30.3 x 10^{-6} K^{-1} (16.9 $\mu\varepsilon$/^{O}F)

3-37

At T = 450 deg K(350°)

α_{11} = 6.1 x 10^{-6} K^{-1} (3.4 $\mu\epsilon/^OF$)

α_{22} = 37.8 x 10^{-6} K^{-1} (21.0 $\mu\epsilon/^OF$)

The residual stresses induced in each ply correspond to
the so-called restraint strains, i.e., the difference between the
unrestrained thermal expansion of that ply and the restrained
expansion of the laminate. The restraint or residual strains for
the 0-degree ply of the $[0_2/\pm45]_s$ boron/epoxy laminate were obtained
by subtracting from the longitudinal, transverse and 45-degree
thermal strains of Fig. 3-42 the corresponding strain components
measured in the unidirectional laminate. These strains are plotted
as a function of temperature by setting the 450 deg K(350^OF)
temperature as the stress-free level (Fig. 3-43). The residual
strains in the 45-degree ply were obtained in a similar fashion and
plotted in Fig. 3-44.

Residual stresses in the 0-degree plies of the $[0_2/\pm45]_s$
laminate were obtained as a function of temperature by using the
residual strains of Fig. 3-43 and published values for temperature
dependent stiffness properties in the constitutive relations given
previously (Section 3.4.2). Here, the stress-free temperature of
450 deg K(350^OF) was taken as the reference temperature T_o in the
integral constitutive relations. The temperature variation of the
longitudinal, transverse and shear moduli, as given by the Advanced
Composites Design Guide is shown in Figs. 3-45 to 3-49.[35]

The results in Fig. 3-50 show that the 0-degree plies are
under compressive residual stress in the direction of the fibers
and under tensile stress in the transverse direction. The former
varies nearly linearly with temperature as it depends primarily on
the longitudinal modulus E_{11} which varies little with temperature.
The transverse residual stress is slightly nonlinear as shown in

Fig. 3-50 because it is related to the highly temperature-dependent transverse modulus E_{22}. This transverse stress is the more significant of the two because it is tensile and reaches a value of 32,400 kPa (4700 psi), or approximately 50 percent of the transverse strength of the unidirectional material.

3.4.5 Residual Strains in Boron/Polyimide

Boron/Polyimide specimens similar to the Boron/Epoxy specimens above were prepared. A 2.54 cm x 22.9 cm (1 in. x 9 in.) laminate of $0_2/\pm45_s$ layup was instrumented with three-gage rosettes (WK-06-125RA-350, Option B157) on the top and bottom surfaces and on the fourth and fifth plies. A unidirectional 0_8 2.5 cm x 12.7 cm (1 in. x 5 in.) control specimen was instrumented with similar three-gage rosettes on the top and middle surfaces and a two-gage rosette (WK-06-125TM-350, Option B157) on the bottom surface. Thermocouples were embedded in both specimens.

The instrumented specimens along with a reference quartz specimen instrumented with similar gages were subjected to the curing cycle described previously. This consisted of B-staging, autoclave curing, and postcuring in an air circulating oven under vacuum. Strain gages and thermo-couples were recorded throughout the curing and postcuring cycles.

Strains for the cooling stage of the curing cycle for the unidirectional specimen are shown in Fig. 3-51. They are linear with temperature. The coefficients of thermal expansion obtained as the slopes of these curves are:

$$\alpha_{11} = 4.9 \times 10^{-6} \text{ K}^{-1} \text{ (2.7 } \mu\varepsilon/^{\circ}\text{F)}$$

$$\alpha_{22} = 28.4 \times 10^{-6} \text{ K}^{-1} \text{ (15.8 } \mu\varepsilon/^{\circ}\text{F)}$$

Similar data for postcuring, during the heating and cooling stages, were analyzed and the strains are plotted in Fig. 3-52. The strains again vary linearly with temperature and have the same slopes as those during the curing cycle. This means that the

coefficients of thermal expansion are constant, at least up to 589 deg K(600°F).

Strains in the $[0_2/\pm45]_s$ laminate recorded during curing and postcuring seemed to be erroneous. Subsequent determinations of residual strains are based on strains recorded during thermal cycling of specimens in Task IV. Apparent strains recorded during this thermal cycling are shown in Fig. 3-53, and the corresponding true thermal strains in Fig. 3-54.

Restraint strains in the 0-degree and 45-degree plies of the $[0_2/\pm45]_s$ laminate were obtained as before by subtracting the unrestrained thermal strains of each ply from the corresponding strains in the laminate (Figs. 3-55 and 3-56). As in the case of the Boron/Epoxy these strains are linear with temperature. The true residual strains must be referred to the stress-free temperature level. In this case the stress-free level is at 450 deg K(350°F), the temperature at which the matrix solidifies. To obtain the true residual strains, the curves of Figs. 3-55 and 3-56 must be shifted parallel to the strain axis until they intersect the temperature axis at 450 deg K(350°F). The maximum residual strain in the ±45-degree plies occurs at room temperature in the transverse to the fiber direction and is equal to 2950με. The maximum residual strain in the 0-degree plies is 2260με in the transverse to the fiber direction at room temperature.

3.4.6 Residual Strains in Graphite/Low Modulus Epoxy

A 2.54 cm x 22.9 cm (1 in. x 9 in.) laminate of $[0_2/\pm45]_s$ layup was instrumented with a two-gage rosette (QA-06-125TQ-350, Option 171) on the top surface and three-gage rosettes (QA-06-125RD-350, Option 171) on the fourth and fifth plies. A 2.54 cm x 12.7 cm (1 in. x 5 in.) $[0_8]$ unidirectional control specimen was instrumented with two-gage rosettes on the top and bottom surfaces and a three-gage rosette and a thermocouple embedded between the fourth and fifth plies. The instrumented specimens

along with a similarly instrumented reference quartz specimen were subjected to the curing cycle described earlier. Strain gage and thermocouple readings were recorded throughout the curing and postcuring stages.

Thermal strains for the 0-degree unidirectional specimen are plotted in Fig. 3-57. The coefficients of longitudinal and transverse thermal expansion measured at the two ends of the temperature range are:

At $T = 297$ deg $K(75^\circ F)$

$$\alpha_{11} = -1.1 \times 10^{-6} \ K^{-1} \ (-0.6 \ \mu\varepsilon/^\circ F)$$

$$\alpha_{22} = 31.5 \times 10^{-6} \ K^{-1} \ (17.5 \ \mu\varepsilon/^\circ F)$$

At $T = 450$ deg $K(350^\circ F)$

$$\alpha_{11} = 2.3 \times 10^{-6} \ K^{-1} \ (1.3 \ \mu\varepsilon/^\circ F)$$

$$\alpha_{22} = 27.0 \times 10^{-6} \ K^{-1} \ (15.0 \ \mu\varepsilon/^\circ F)$$

Results from the $[0_2/\pm45]_s$ laminate were not meaningful. The test was repeated four times with new specimens each time, but with limited success. It is believed that the difficulties encountered are due to the very brief shelf life of the material.

3.4.7 Residual Strains in Graphite/High Modulus Epoxy

A 2.54 cm x 22.9 cm (1 in. x 9 in.) laminate of $[0_2/\pm45]_s$ layup and a 2.54 cm x 12.7 cm (1 in. x 5 in.) $[0_8]$ unidirectional specimen was instrumented exactly as the corresponding Graphite/ Low Modulus Epoxy specimens above. The instrumented specimens along with a quartz reference specimen were subjected to the curing and postcuring cycles described before.

Apparent strains during the curing and postcuring cycles for the unidirectional specimen are shown in Figs. 3-58 to 3-60. Thermal strains were obtained by correcting for the purely thermal output of the gages and plotted in Fig. 3-61. As can be seen, the transverse thermal expansion is nonlinear with temperature and the longitudinal expansion is very small and negative. The coefficients of thermal expansion measured as the slopes of these curves were obtained at the two ends of the temperature range.:

At T = 297 deg $K(75^{O}F)$

α_{11} = 0

α_{22} = 33.3 x 10^{-6} K^{-1} (18.5 $\mu\epsilon/^{O}F$)

At T = 444 deg $K(340^{O}F)$

α_{11} = -0.9 x 10^{-6} K^{-1} (-0.5 $\mu\epsilon/^{O}F$)

α_{22} = 58.9 x 10^{-6} K^{-1} (32.7 $\mu\epsilon/^{O}F$)

Apparent strains during the various stages of curing and postcuring for the $[0_2/\pm45]_s$ laminate are shown in Figs. 3-62 to 3-66. The longitudinal strains do not show any significant difference in the various stages of curing and postcuring (Figs. 3-62 to 3-64). The transverse strains recorded during the second part of the curing cycle and the heating stage of the postcuring are in good agreement (Fig. 3-65), but they are significantly different from those during the cooling stage of postcuring (Fig. 3-66). This can be explained by the fact that curing is not completed during the curing cycle, and that a substantial portion of it takes place during the dwell period (6 hours) of the post-curing cycle.

Thermal strains induced during curing in the angle-ply laminate are plotted in Fig. 3-67. The transverse strain reaches a maximum value of 675$\mu\varepsilon$. When the zero reference point for these curves is taken at 444 deg K (340°F), the stress-free temperature level, it can be seen that the transverse strain increases slowly down to approximately 378 deg K (220°F) and thereafter it varies at a higher rate. This is an indication that the matrix material is not fully cured and is still in a semi-solid state.

During postcuring, the specimen is heated again to its stress-free temperature level (444 deg K, 340°F). However, upon cooling a new set of residual strains are induced (Fig. 3-68). These strains are higher than those recorded during the curing cycle and vary nearly linearly with temperature at rates close to those of the curing strains at the low temperature end. This can be attributed to the fact that after the 6-hour dwell at 444 deg K (340°F) complete curing takes place and the matrix material attains thermal properties similar to those near room temperature prior to postcuring.

Residual (restraint) strains in the 0-degree and 45-degree plies of the $[0_2/\pm45]_s$ laminate were obtained as before by subtracting the unrestrained thermal expansion of each ply (Fig. 3-61) from the corresponding restrained expansion of the laminate (Fig. 3-68). These residual strains are plotted as a function of temperature in Figs. 3-69 and 3-70. Because of the large differences in transverse and 45-degree strains between the unidirectional and angle-ply laminate, the residual strains reflect essentially the same nonlinearities of the thermal strains in the unidirectional specimen.

3.4.8 Residual Strains in Graphite/Polyimide

A 2.54 cm x 22.9 cm (1 in. x 9 in.) laminate of $[0_2/\pm45]_s$ layup was instrumented with two-gage rosettes (WK-06-125TM-350, Option B157) on the top and bottom surfaces and three-gage rosettes (WK-06-125RA-350, Option B157) on the fourth and fifth plies. A

unidirectional $[0_8]$ 2.5 cm x 12.7 cm (1 in. x 5 in.) control specimen was instrumented with similar three-gage rosettes on the top and middle surfaces and a two-gage rosette on the bottom surface. Thermocouples were embedded in both specimens.

The instrumented specimens along with a reference quartz specimen instrumented with similar gages were subjected to the curing cycle described earlier. This consisted of B-staging in an air-conditioning oven, autoclave curing, and postcuring under vacuum. Strain gages and thermocouples were recorded throughout the curing and postcuring cycles. Additional data were obtained from similar specimens prepared subsequently for Task IV.

Thermal strains in the unidirectional laminate are shown in Fig. 3-71. They vary linearly with temperature thus indicating constant coefficients of thermal expansion. These coefficients are:

$$\alpha_{11} = 0$$

$$\alpha_{22} = 25.3 \times 10^{-6} \text{ K}^{-1} \ (14.1 \ \mu\epsilon/^{\circ}\text{F})$$

Strains in the angle-ply laminate are plotted in Fig. 3-72. They are an order of magnitude smaller than the thermal strains of the unidirectional material. This is due to the zero longitudinal thermal expansion of the unidirectional material which tends to restrain thermal expansion in the laminate along the 0- and ±45 deg directions. The observed scatter and apparent nonlinearity in strains is not significant, but appears pronounced because of the small magnitude of the strains.

Restrain strains in the 0-degree and 45-degree plies of the $[0_2/\pm45]_s$ laminate were obtained as before and plotted in Figs. 3-73 and 3-74. These strains are linear with temperature since the thermal strains in both the unidirectional and angle-ply

specimens are linear with temperature. The true residual strains are referred to the stress-free temperature level of 450 deg K (350°F) as in the case of the Boron/Polyimide. The maximum residual strain then at room temperature is 375 $\mu\epsilon$ in the ±45-degree plies normal to the fiber direction. The maximum residual strain in the 0-degree plies is 355 $\mu\epsilon$ in the transverse to the fiber direction.

3.4.9 Residual Strains in S-Glass/Epoxy

A 2.54 cm x 22.9 cm (1 in. x 9 in.) eight-ply laminate of $[0_2/\pm45]_s$ layup was instrumented with three-gage rosettes (EA-06-125RD-350) on the fourth, fifth and seventh plies, two-gage rosettes (EA-06-125TM-120) on the top and bottom surfaces and a thermocouple between the fourth and fifth ply. A uni-directional $[0_8]$ 2.54 cm x 12.7 cm (1 in. x 5 in.) control specimen was instrumented with a two-gage rosette (EA-06-125-TQ-350) and a thermocouple in the middle surface and two-gage rosettes on the top and bottom surfaces.

The instrumented specimens along with a reference quartz specimen were bagged and placed in the autoclave and subjected to the curing cycle described earlier.

Strain gage and thermocouple output was recorded through-out the curing cycle. Subsequently, the same specimens were sub-jected to a thermal cycle from room temperature to 435 deg K (325°F) and down to room temperature. Strain gages and thermo-couples were recorded at frequent intervals.

As in the case of the boron/epoxy specimens, the strain readings for the S-glass/epoxy specimens obtained in the first half of the curing cycle were not meaningful. However, a strain change, which must be partly attributed to the curing process, was observed during the dwell periods at 420 deg K (300°F) and 435 deg K (325°F).

Apparent strains during the decreasing temperature stage of curing and during thermal cycling are shown in Figs. 3-75, 3-76 and 3-77 for the unidirectional and angle-ply laminates. These strains were corrected as before for the purely thermal output of the gage. Thermal strains obtained for the second part of the curing cycle (decreasing temperature) for the $[0_8]$ and $[0_2/\pm45]_s$ S-glass/epoxy specimens are plotted in Figs. 3-78 and 3-79. Also plotted in these figures are the thermal strains obtained during thermal cycling of the specimens subsequent to curing. Again, the agreement between the two sets of strains is satisfactory, indicating that residual strains due to curing are primarily induced by the differential thermal expansion of the various plies. The strains in the unidirectional laminate are characteristically nonlinear, unlike those in the boron/epoxy specimen. However, the thermal strains in the $[0_2/\pm45]_s$ laminate are essentially linear with temperature.

The coefficients of thermal expansion of the unidirectional laminate were obtained as the slopes of the thermal strain versus temperature curves of Fig. 3-78. The following coefficients were obtained:

At T = 297 deg K (75°F)

α_{11} = 3.8 x 10^{-6} K^{-1} (2.1 $\mu\epsilon$/°F)

α_{22} = 16.7 x 10^{-6} K^{-1} (9.3 $\mu\epsilon$/°F)

At T = 435 deg K (325°F)

α_{11} = 3.8 x 10^{-6} K^{-1} (2.1 $\mu\epsilon$/°F)

α_{22} = 54.9 x 10^{-6} K^{-1} (30.5 $\mu\epsilon$/°F)

Residual strains in the 0-degree and 45-degree plies of the $\begin{bmatrix} 0_2/\pm 45 \end{bmatrix}_s$ S-Glass/Epoxy laminate were obtained as before by subtracting the unrestrained thermal expansion of each ply from the corresponding restrained expansion of the laminate. These residual strains were plotted as a function of temperature with 435 deg K (325°F) as the stress-free level (Figs. 3-80, 3-81). Unlike the residual strains in the Boron/Epoxy these strains for the S-Glass/Epoxy are nonlinear.

3.5 <u>Static Strength</u>

Two angle-ply $\begin{bmatrix} 0_2/\pm 45 \end{bmatrix}_s$ specimens of each material, including one with embedded instrumentation, were tested statically in tension. Embedded and surface gages were monitored at load intervals to failure. In some cases acoustic emission was also monitored.

Stress-strain curves for three Boron/Epoxy specimens are shown in Figs. 3-82 to 3-84. The acoustic emission output corresponding to the specimen of Fig. 3-84 is shown in Fig. 3-85. Pertinent results obtained from the stress-strain curves are the initial Young's modulus E_{xx}, Poisson's ratio ν_{xy} and tensile strength S_{xxT}. These results are tabulated in Table 3-19. The axial strain from Fig. 3-84 was also plotted next to the acoustic emission output in Fig. 3-85. The cumulative number of counts is low and increases slowly in the linear range of strain response. However, it increases at an accelerating rate with the onset of nonlinearity, which is related to microfailures.

The state of strain at any given time is the result of superposition of the residual strains induced during curing and the mechanical strains produced by external loading. The total strain history in the 0-degree and 45-degree plies of the specimen of Fig. 3-84 is given in Figs. 3-86 and 3-87. As can be seen the residual and mechanical strains in the 0-degree plies are additive only in the 45-degree direction and subtractive in the

longitudinal and transverse directions. In the 45-degree plies they are additive only in the longitudinal and -45-degree (normal to the fibers) directions.

Stress-strain curves to failure and acoustic emission output for Boron/Polyimide are shown in Figs. 3-88 and 3-89. The axial strain is linear to failure. The strength is appreciably lower than that of Boron/Epoxy. The acoustic emission level rises more abruptly than that of Boron/Epoxy, which indicates a more catastrophic type of failure.

Stress-strain curves to failure and acoustic emission output for Graphite/Low Modulus Epoxy are shown in Figs. 3-90 to 3-92. The axial strain is linear up to a point immediately preceding failure. The level of acoustic emission rises gradually until immediately preceding failure, where it shows a sudden jump. (Fig. 3-92).

Stress-strain curves to failure for Graphite/High Modulus Epoxy are shown in Figs. 3-93 and 3-94. The acoustic emission level recorded for the specimen of Fig. 3-93 was very low ($<10^4$ counts) and showed only a gradual rise. This is an indication that the specimen might have failed prematurely. A large discrepancy exists between the modulus values for the two specimens, without any evident reason.

Stress-strain curves to failure for Graphite/Polyimide are shown in Figs. 3-95 to 3-97. All strains are linear to failure. Acoustic emission for the specimen of Fig. 3-97 is shown in Fig. 3-98. Here, the rise is gradual and the level high, which indicates that the microfailure process is widespread and starts at a low load.

Stress-strain curves to failure for S-Glass/Epoxy are shown in Figs. 3-99 and 3-100. All strains show some nonlinearity even at low loads. An acoustic emission record was obtained for another specimen to be described under Task III.

The initial Young's modulus, Poisson's ratio, and tensile strength obtained from the tests above are tabulated in Table 3-19. A cursory look at this table shows that the S-Glass/Epoxy is the strongest, but has the lowest modulus. The Boron/Epoxy follows closely in strength and has the second highest modulus. The Boron/Polyimide with the highest modulus has a strength equal to approximately 80 percent of that of Boron/Epoxy. The Graphite/Low Modulus Epoxy seems to be some-what stronger than the Graphite/High Modulus Epoxy and much stronger than the Graphite/Polyimide. The average value of Poisson's ratio for the Boron and Graphite composites is 0.72 ± 0.02. Poisson's ratio for S-Glass/Epoxy is substantially lower (0.52).

Table 3-19

STATIC TENSILE STRENGTH OF $[0_2/\pm45]_s$ LAMINATES

Material	Specimen No.	Modulus, Exx GPa (10⁶ psi)		Poisson's Ratio, ν_{xy}	Tensile Strength MPa (ksi)	
Boron/Epoxy		117	(17.0)	0.71	750	(109)
		115	(16.6)	0.71	680	(99)
		114	(16.5)	0.67	745	(108)
Boron/Polyimide		117	(17.0)	0.72	563	(82)
		--	--	--	563	(82)
Graphite/Low Modulus Epoxy		109	(15.8)	0.74	583	(85)
		113	(16.4)	0.70	552	(80)
		--	--	--	552	(80)
Graphite/High Modulus Epoxy		112	(16.2)	0.71	407	(59)
		86	(12.4)	0.72	503	(73)
		--	--	--	517	(75)
		--	--	--	511	(74)
Graphite/Polyimide		104	(15.1)	0.73	303	(44)
		119	(17.3)	0.80	315	(46)
		117	(17.0)	0.60	412	(60)
S-Glass/Epoxy		36	(5.2)	0.47	675	(98)
		37	(5.4)	0.56	810	(117)
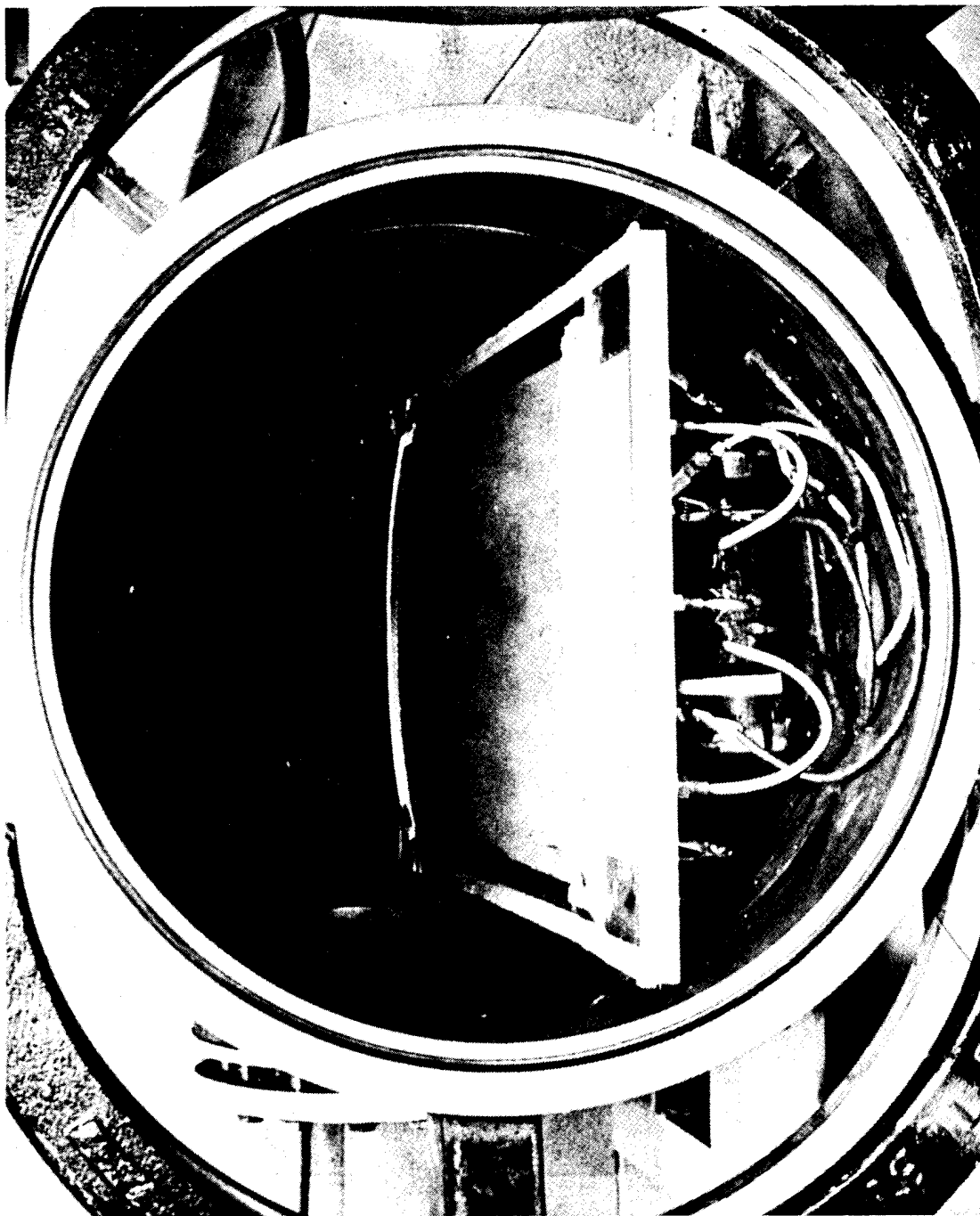
Fig. 3-1 CLOSEUP OF AUTOCLAVE WITH LAMINATE IN PLACE FOR CURING
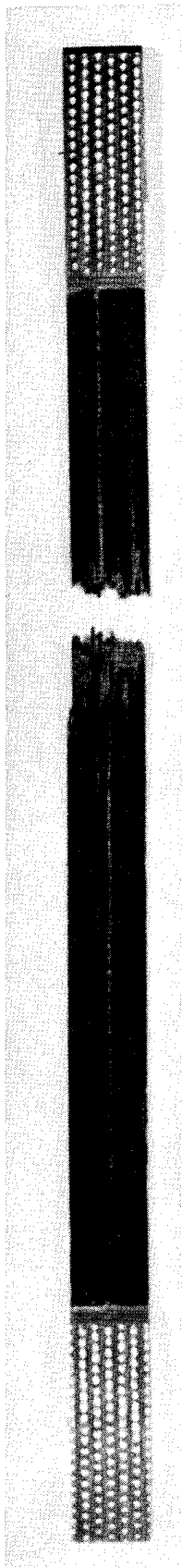
BORON/EPOXY
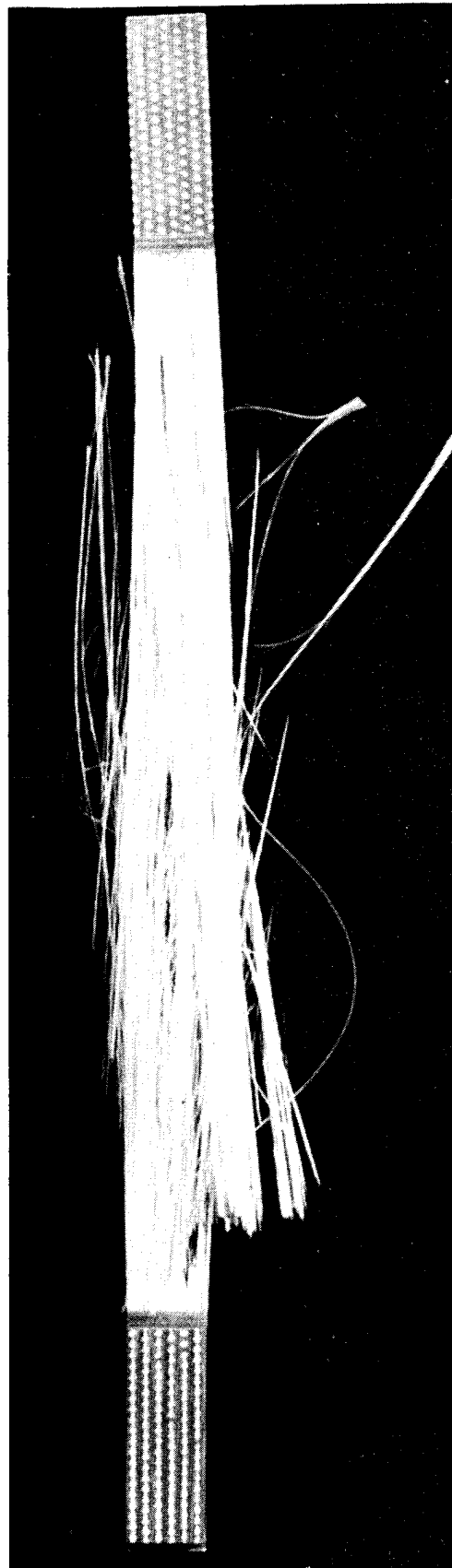
S-GLASS/EPOXY

Fig. 3-2 TYPICAL FRACTURES OF UNIDIRECTIONAL 0-DEGREE TENSILE SPECIMENS
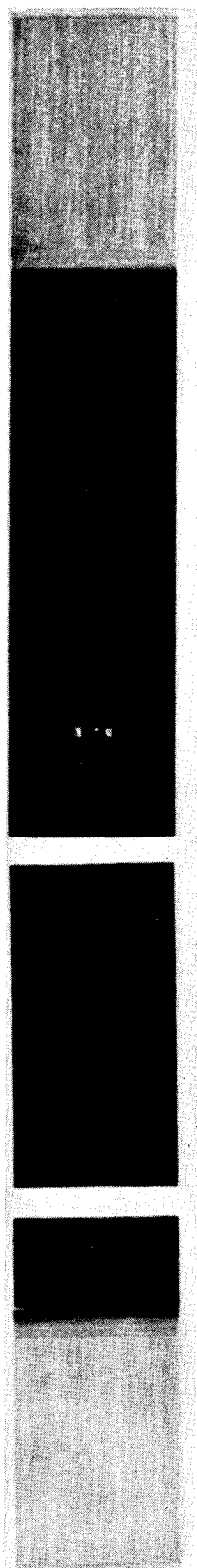
GRAPHITE/HIGH MODULUS EPOXY
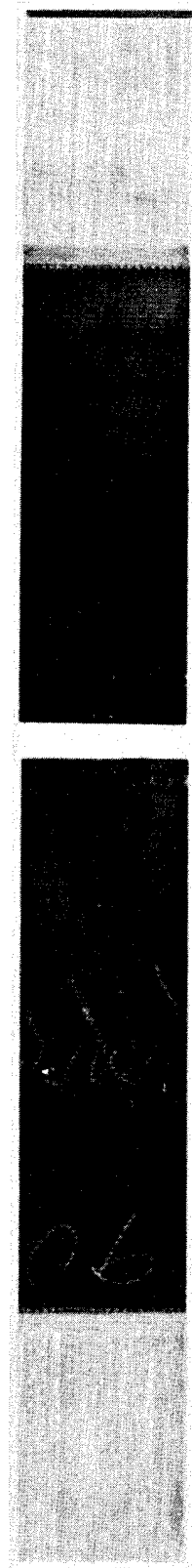
GRAPHITE/POLYIMIDE

Fig. 3-3 TYPICAL FRACTURES OF UNIDIRECTIONAL 90-DEGREE TENSILE SPECIMENS
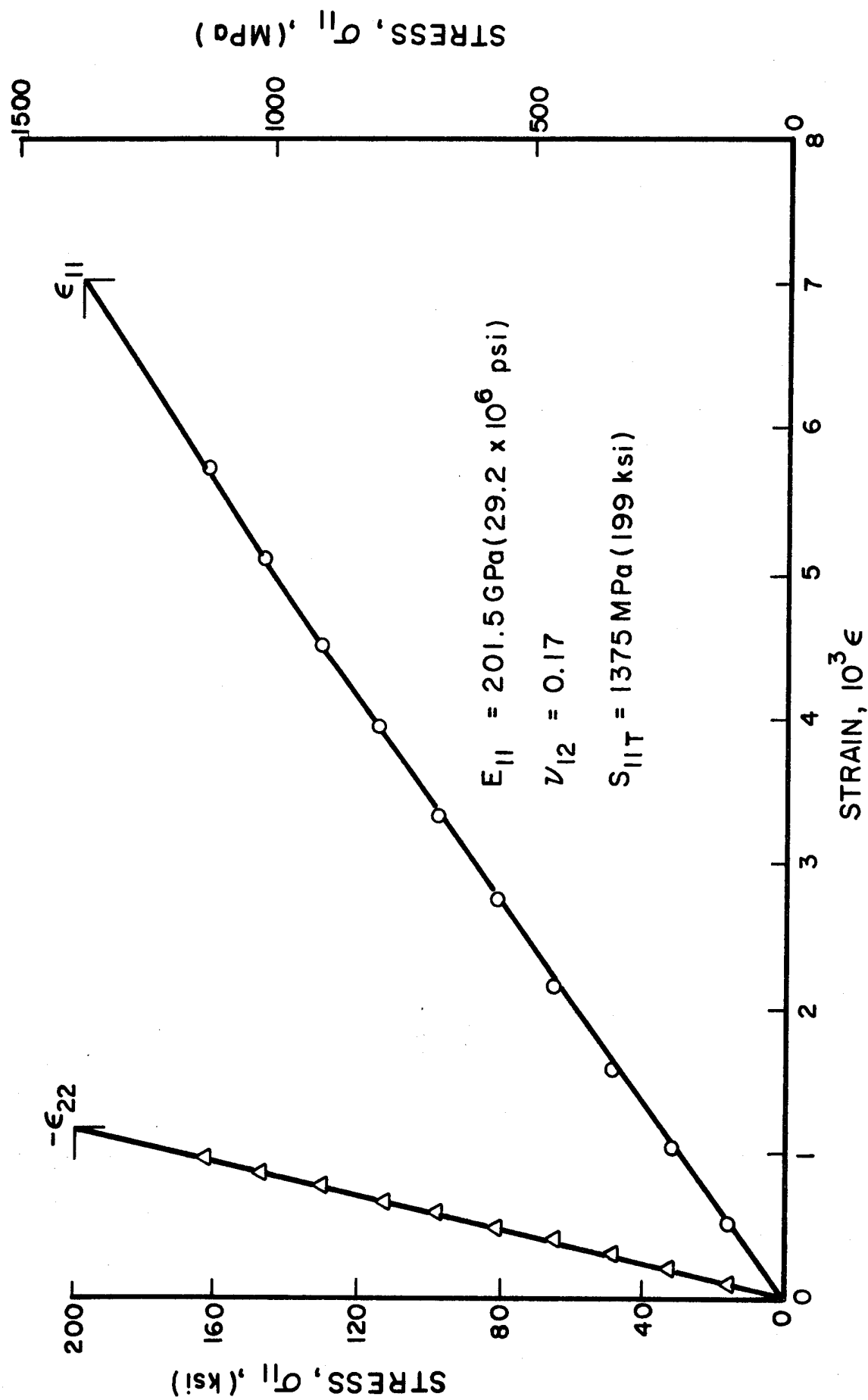
Fig. 3-4 STRAINS IN 0-DEGREE UNIDIRECTIONAL BORON/EPOXY SPECIMEN UNDER UNIAXIAL TENSION
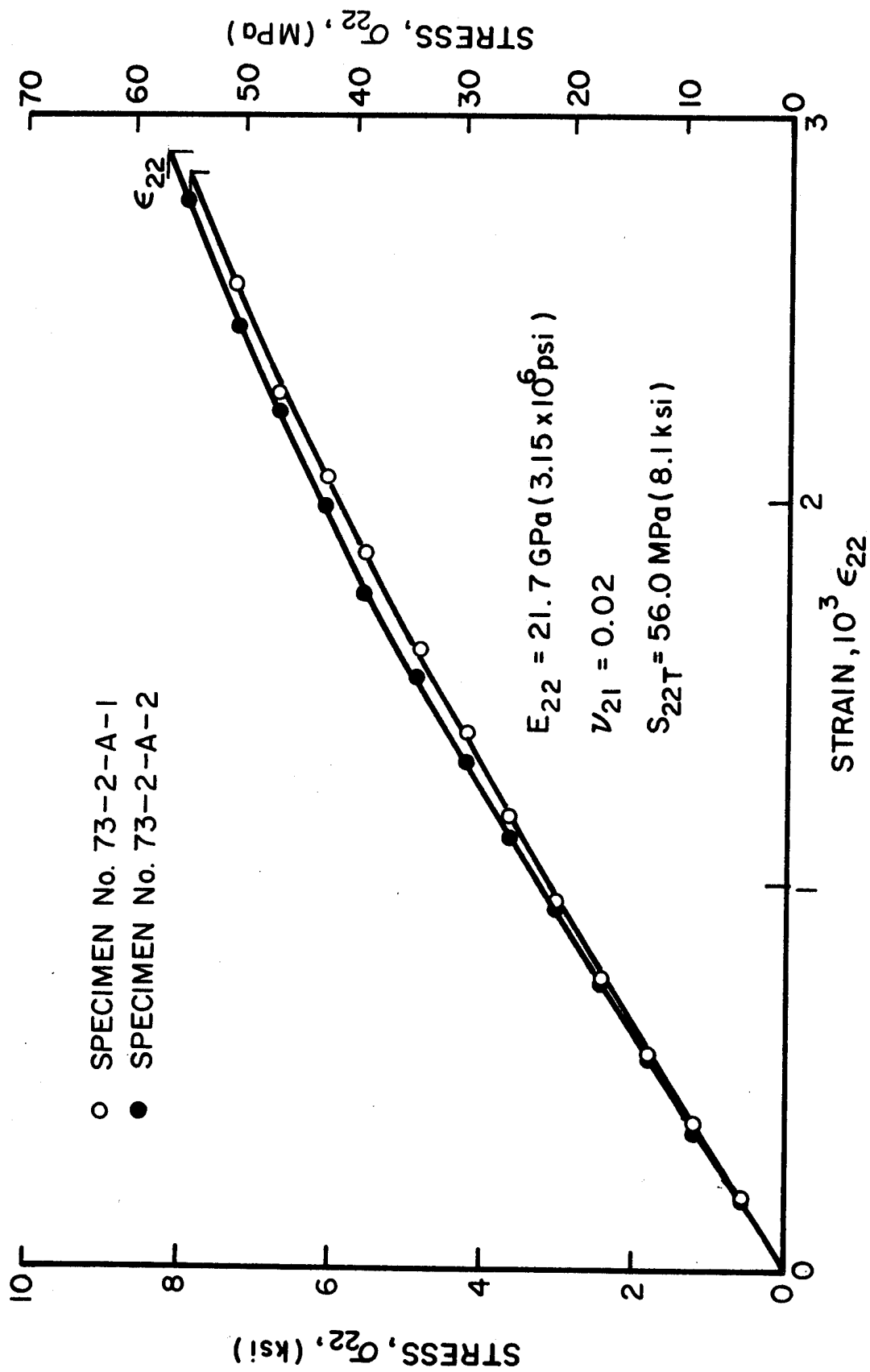
$E_{11} = 201.5 \, GPa \, (29.2 \times 10^6 \, psi)$

$\nu_{12} = 0.17$

$S_{11T} = 1375 \, MPa \, (199 \, ksi)$

3-54

Fig. 3-5 STRAINS IN 90-DEGREE UNIDIRECTIONAL BORON/EPOXY SPECIMENS UNDER UNIAXIAL TENSION

$E_{22} = 21.7 \, GPa \, (3.15 \times 10^6 \, psi)$

$\nu_{21} = 0.02$

$S_{22T} = 56.0 \, MPa \, (8.1 \, ksi)$

○ SPECIMEN No. 73-2-A-1

● SPECIMEN No. 73-2-A-2
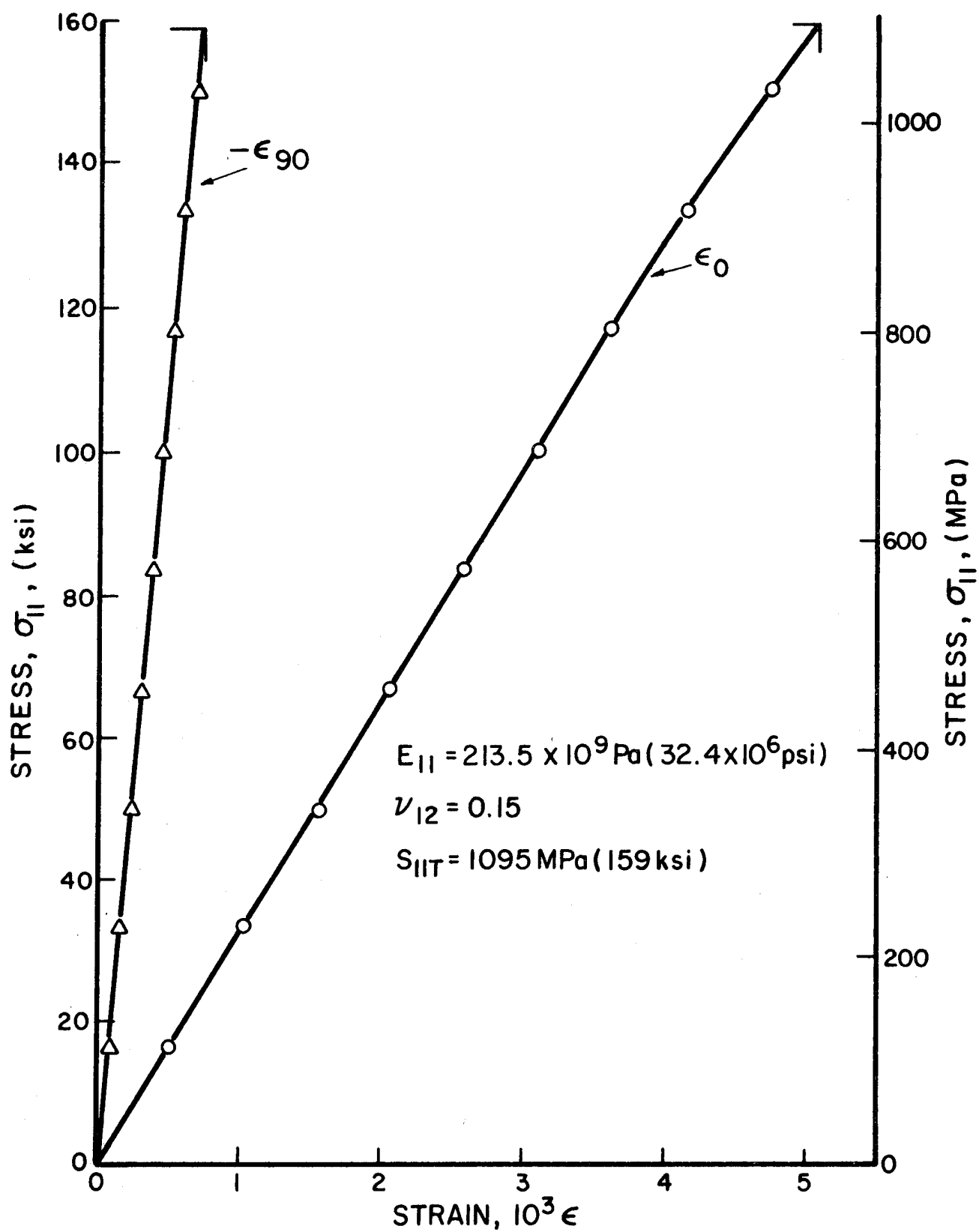
Fig. 3-6 STRAINS IN 0-DEGREE UNIDIRECTIONAL BORON/POLYIMIDE
SPECIMEN UNDER UNIAXIAL TENSION

3-56
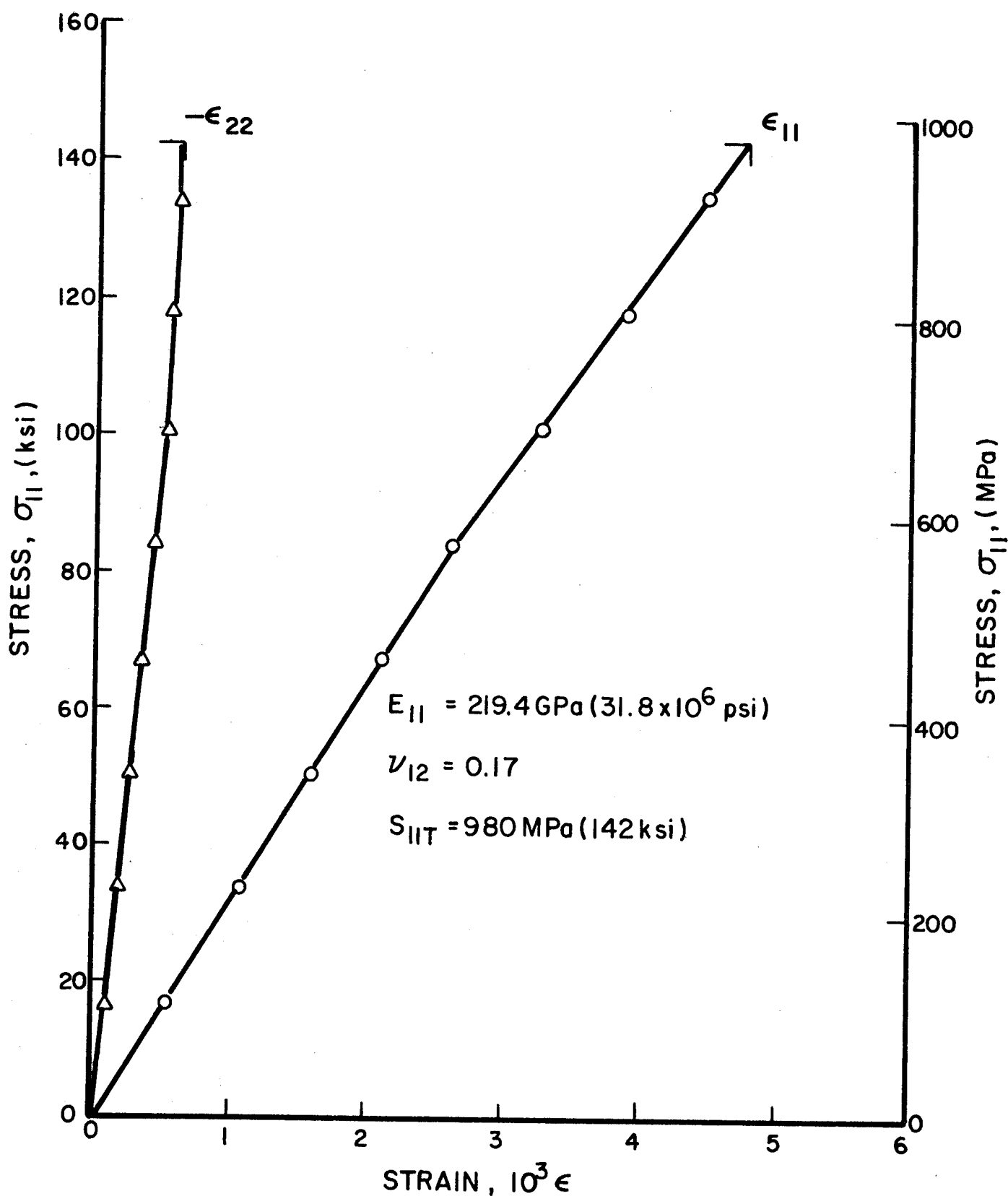
Fig. 3-7 STRAINS IN 0-DEGREE UNIDIRECTIONAL BORON/POLYIMIDE
SPECIMEN UNDER UNIAXIAL TENSION

3-57
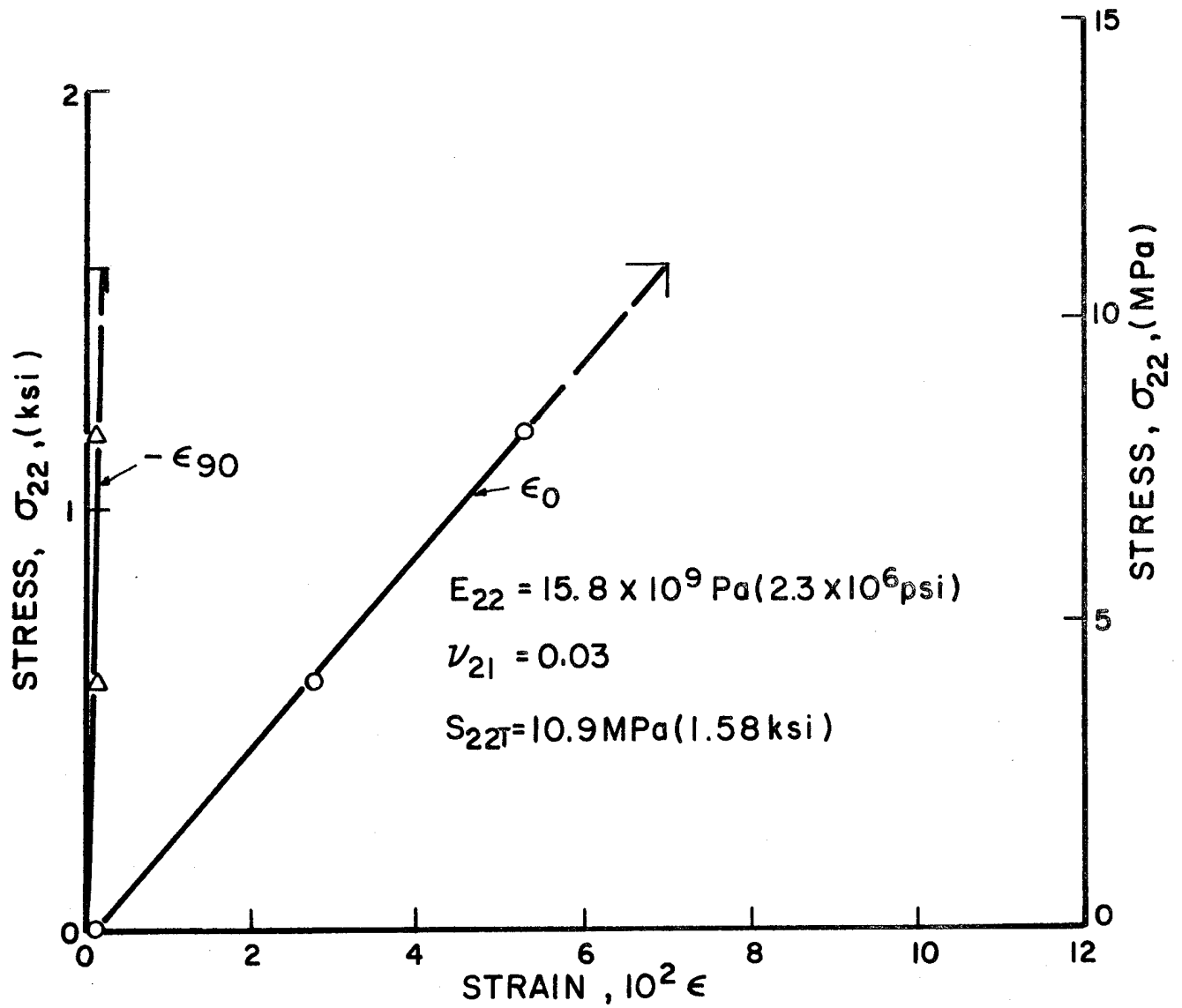
Fig. 3-8   STRAINS IN 90-DEGREE UNIDIRECTIONAL BORON/POLYIMIDE
SPECIMEN UNDER UNIAXIAL TENSION
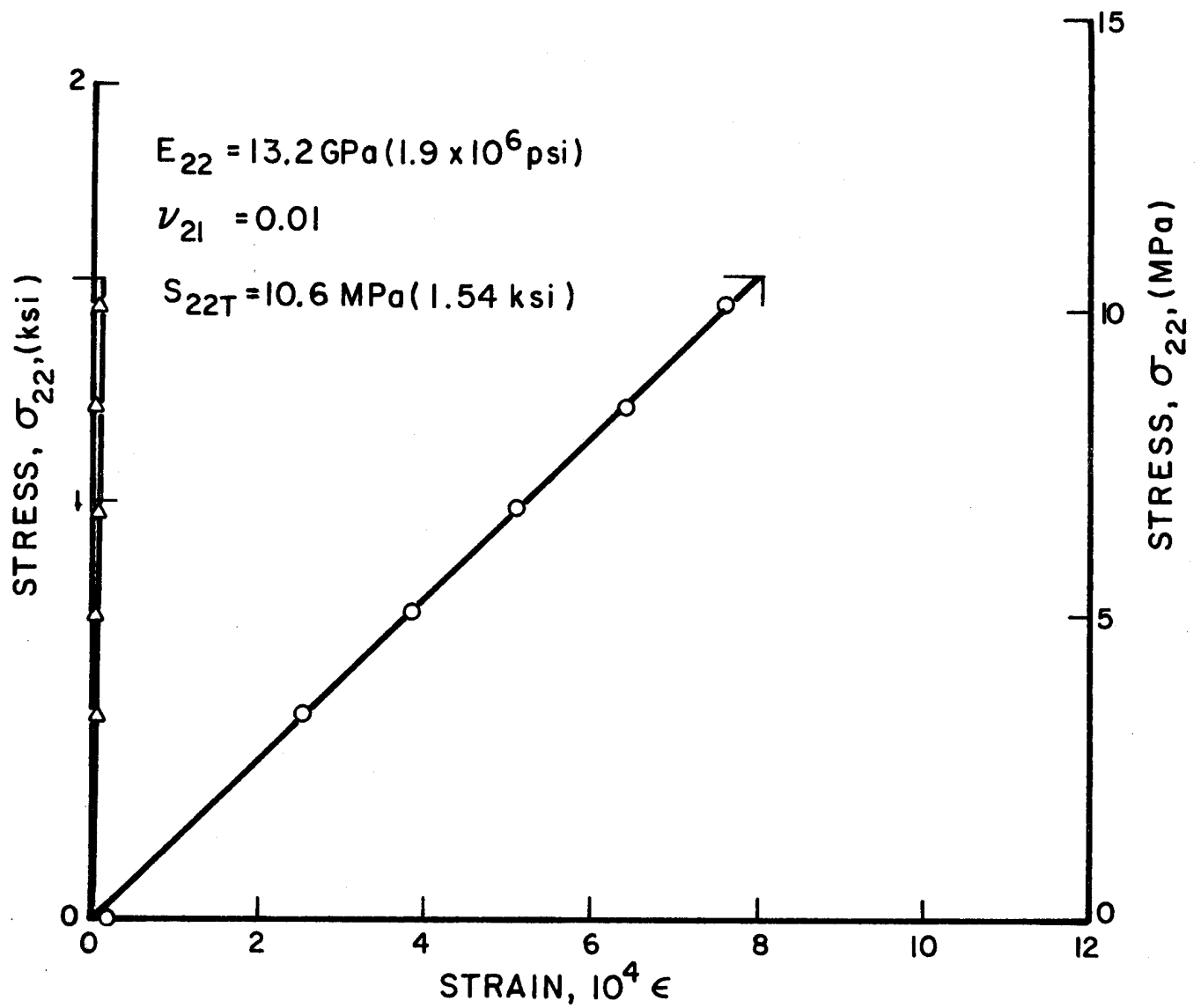
Fig. 3-9   STRAINS IN 90-DEGREE UNIDIRECTIONAL BORON/POLYIMIDE
            SPECIMEN UNDER UNIAXIAL TENSION
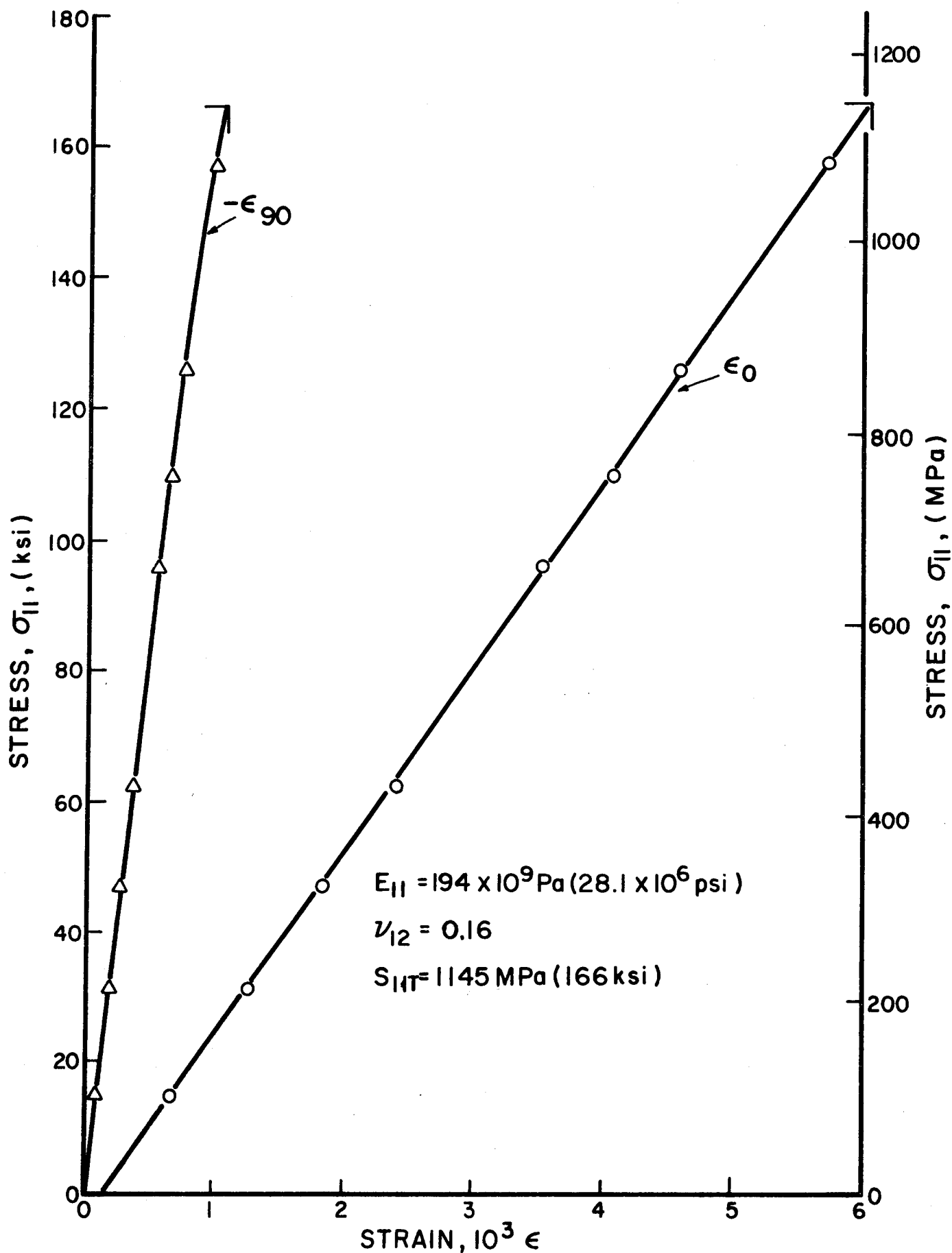
Fig. 3-10   STRAINS IN 0-DEGREE UNIDIRECTIONAL GRAPHITE/LOW-MODULUS
EPOXY UNDER UNIAXIAL TENSION

3-60
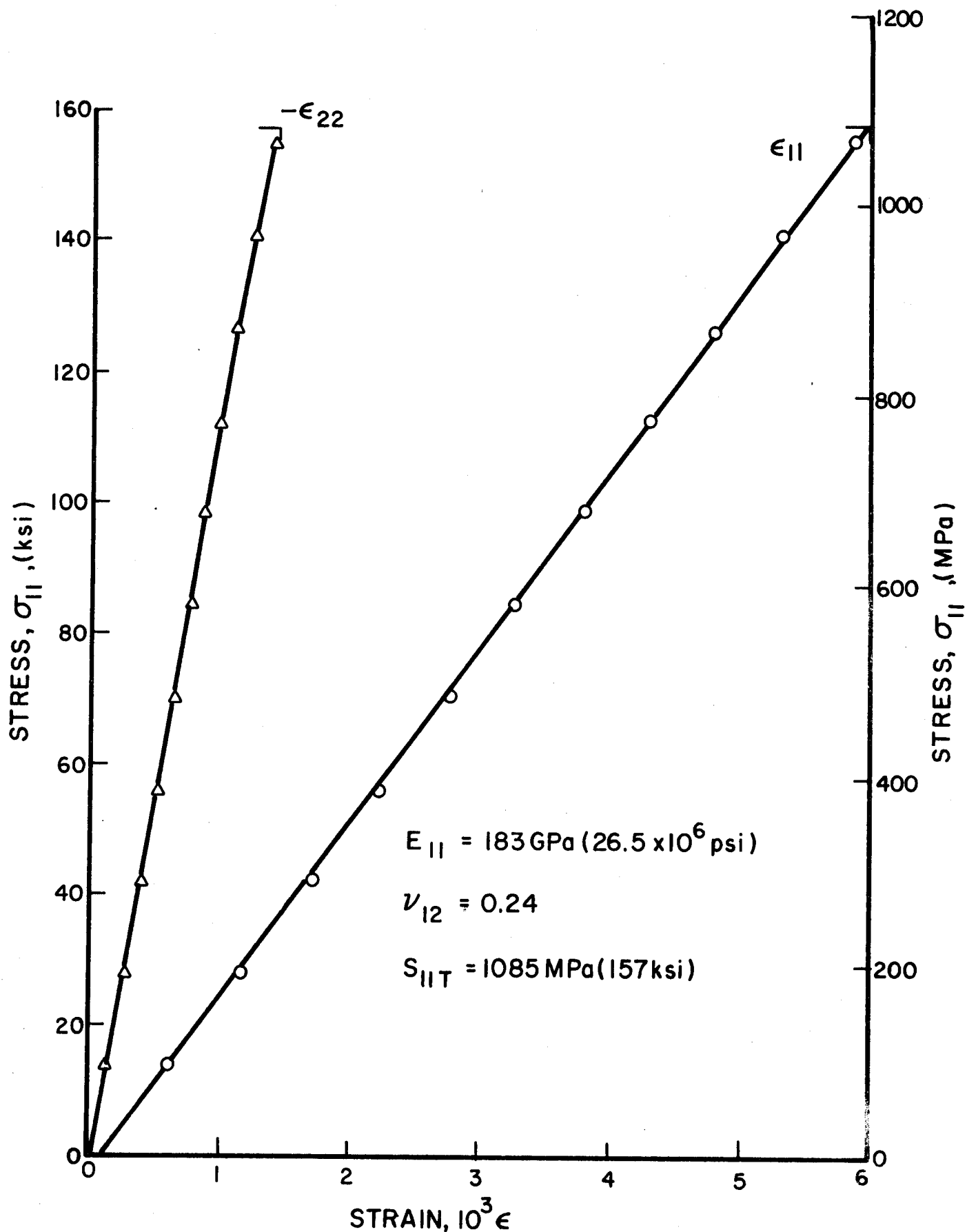
Fig. 3-11   STRAINS IN 0-DEGREE UNIDIRECTIONAL GRAPHITE/LOW MODULUS
EPOXY SPECIMEN UNDER UNIAXIAL TENSION

3-61
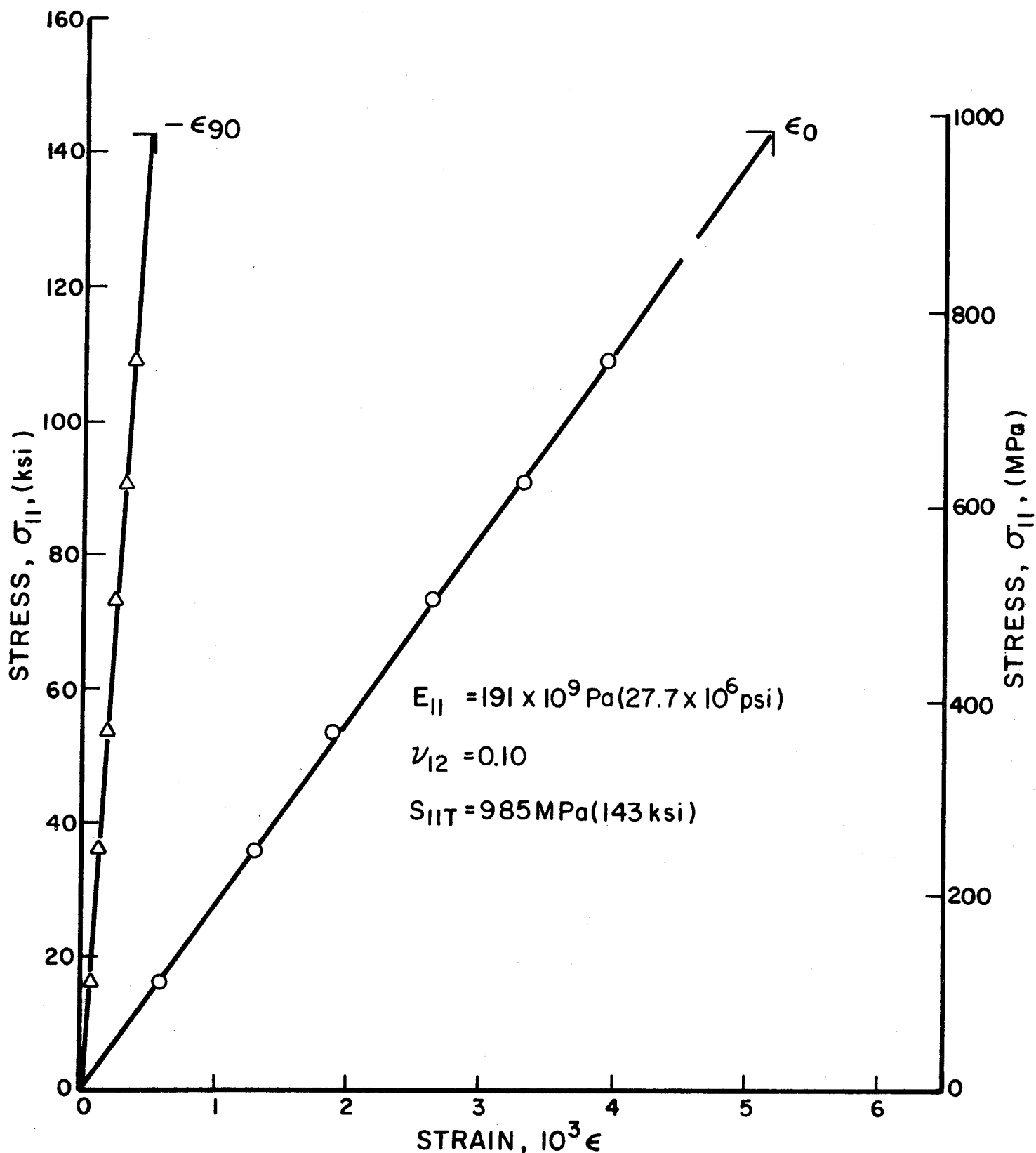
Fig. 3-12 STRAINS IN 0-DEGREE UNIDIRECTIONAL GRAPHITE/HIGH MODULUS
EPOXY SPECIMEN UNDER UNIAXIAL TENSION

E_{11} = 191 × 10⁹ Pa (27.7 × 10⁶ psi)

ν_{12} = 0.10

S_{11T} = 985 MPa (143 ksi)

3-62
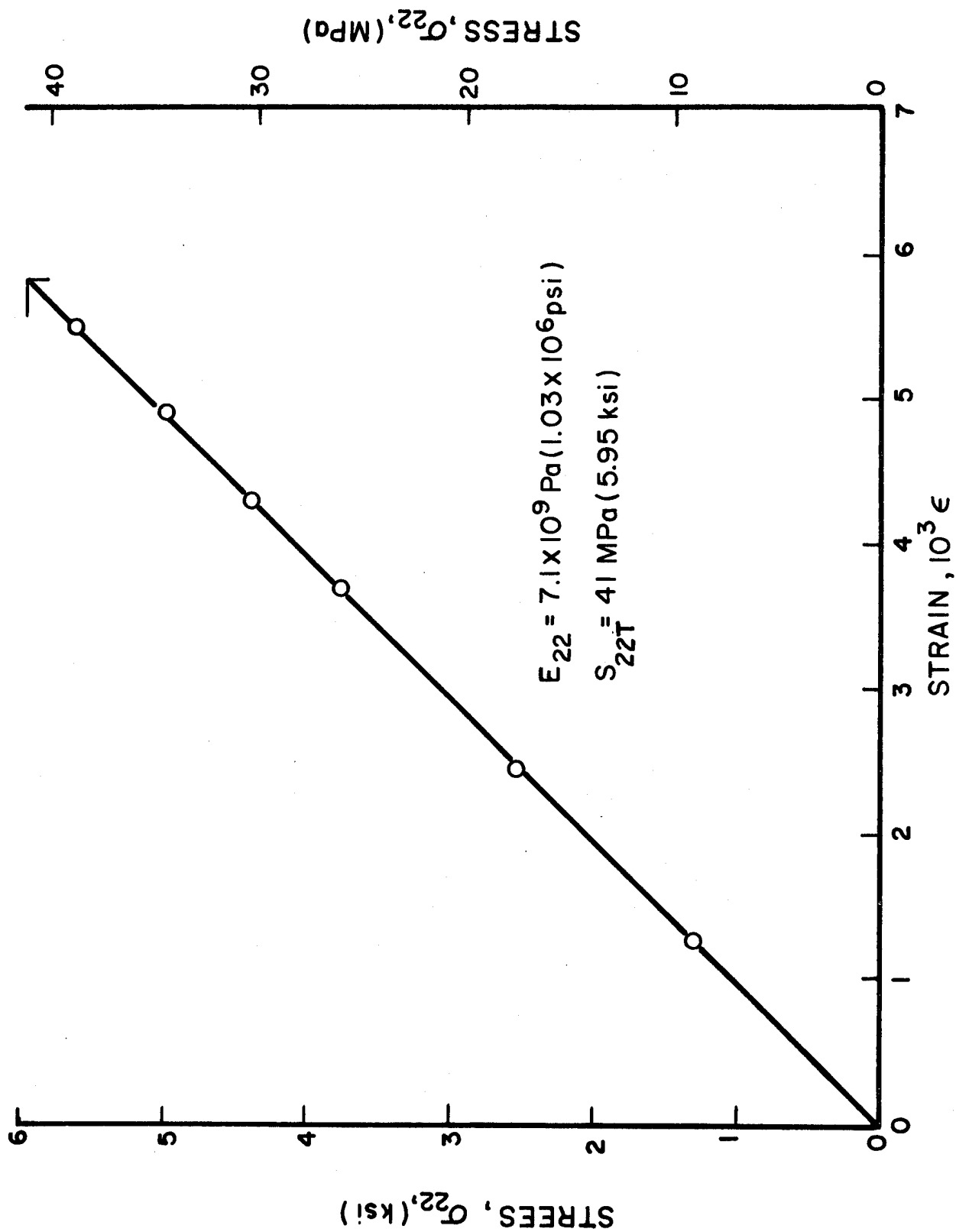
Fig. 3-13 STRAINS IN 90-DEGREE UNIDIRECTIONAL GRAPHITE/HIGH MODULUS EPOXY SPECIMEN UNDER UNIAXIAL TENSION

In the figure:

$E_{22} = 7.1 \times 10^9$ Pa$(1.03 \times 10^6$ psi$)$

$S_{22T} = 41$ MPa$(5.95$ ksi$)$

STRESS, σ_{22}, (MPa)

STRESS, σ_{22}, (ksi)

STRAIN, $10^3 \epsilon$

3-63
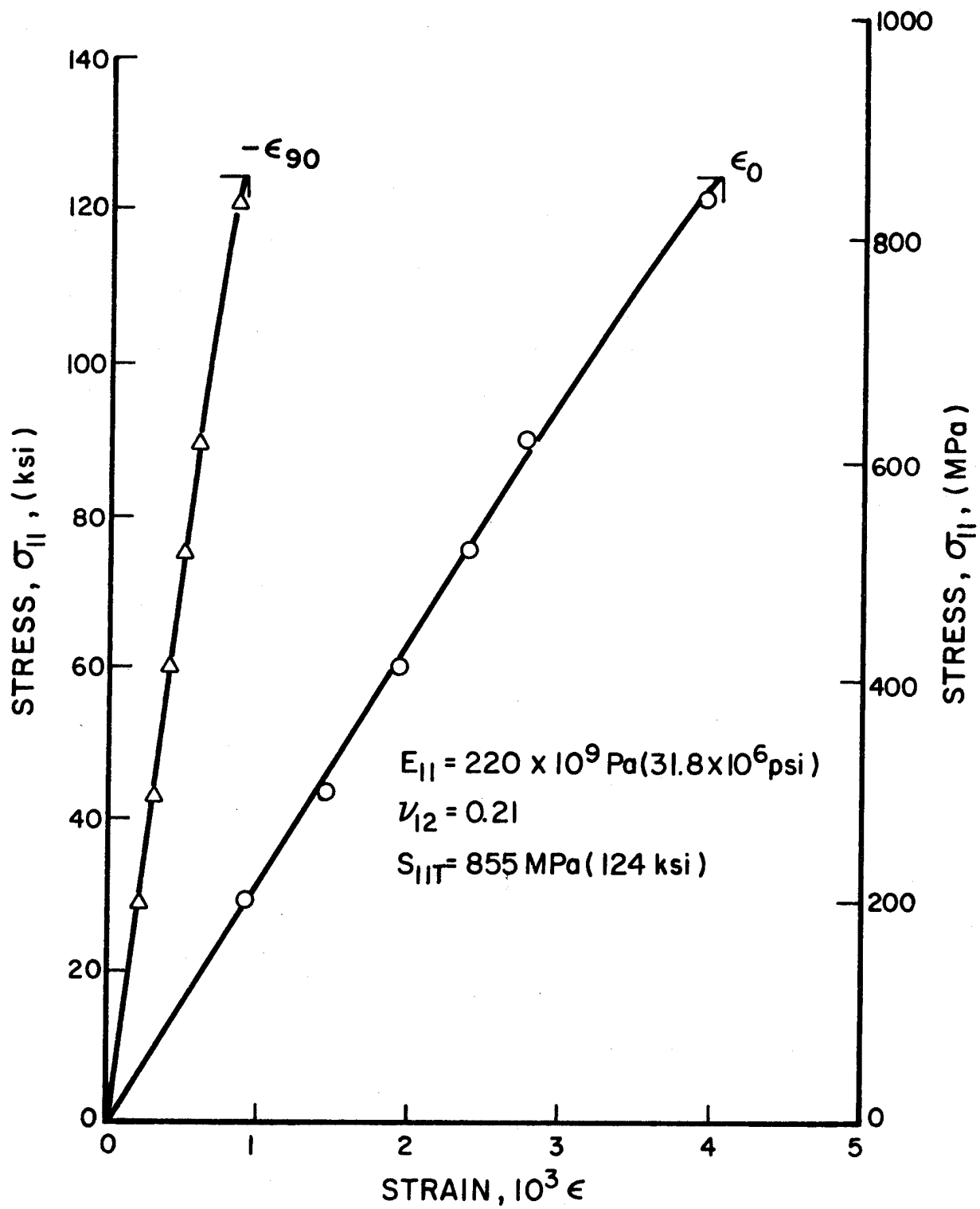
Fig. 3-14   STRAINS IN 0-DEGREE UNIDIRECTIONAL GRAPHITE/POLYIMIDE
SPECIMEN UNDER UNIAXIAL TENSION
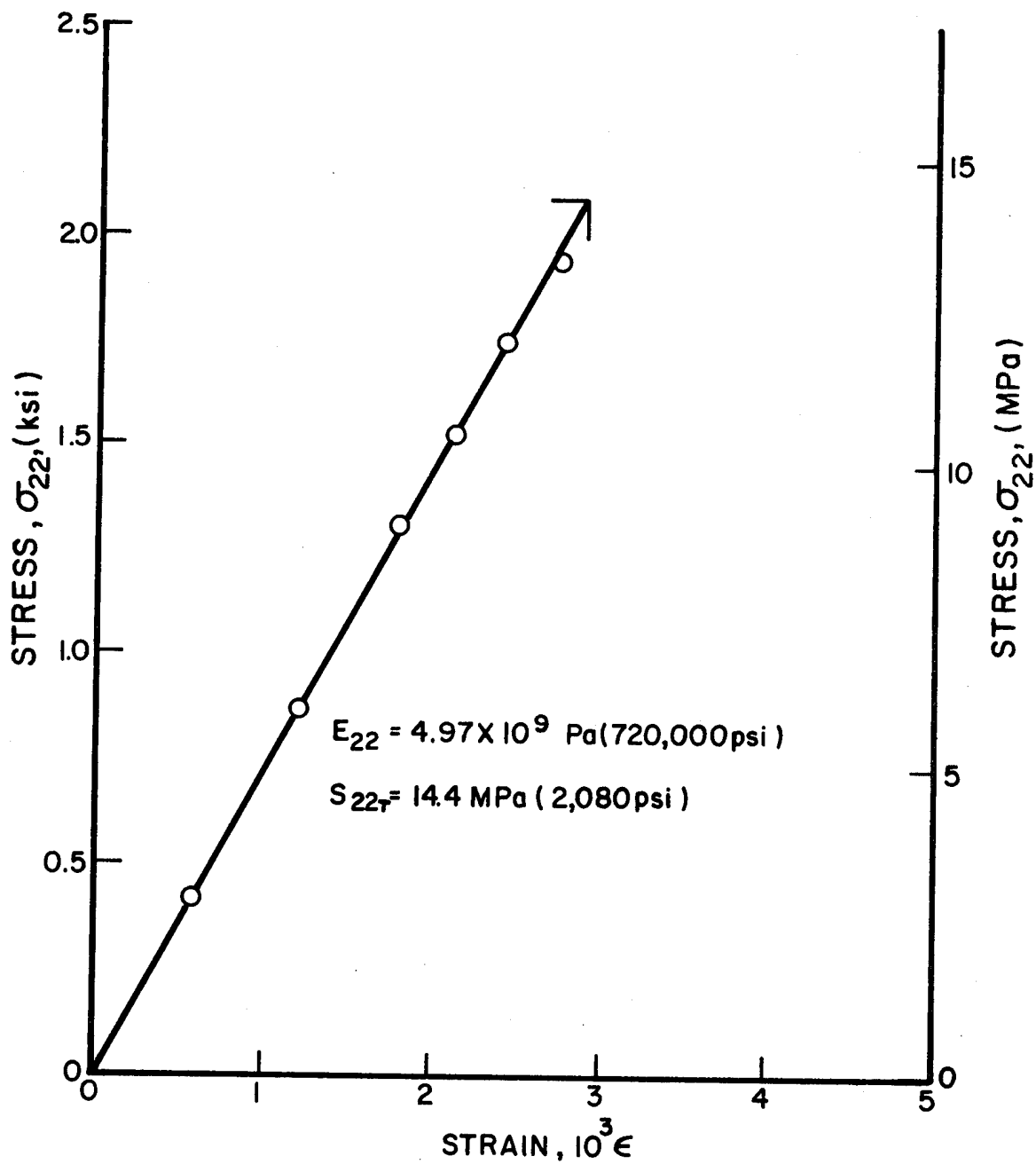
Fig. 3-15   STRAIN IN 90-DEGREE UNIDIRECTIONAL GRAPHITE/
POLYIMIDE SPECIMEN UNDER UNIAXIAL TENSION
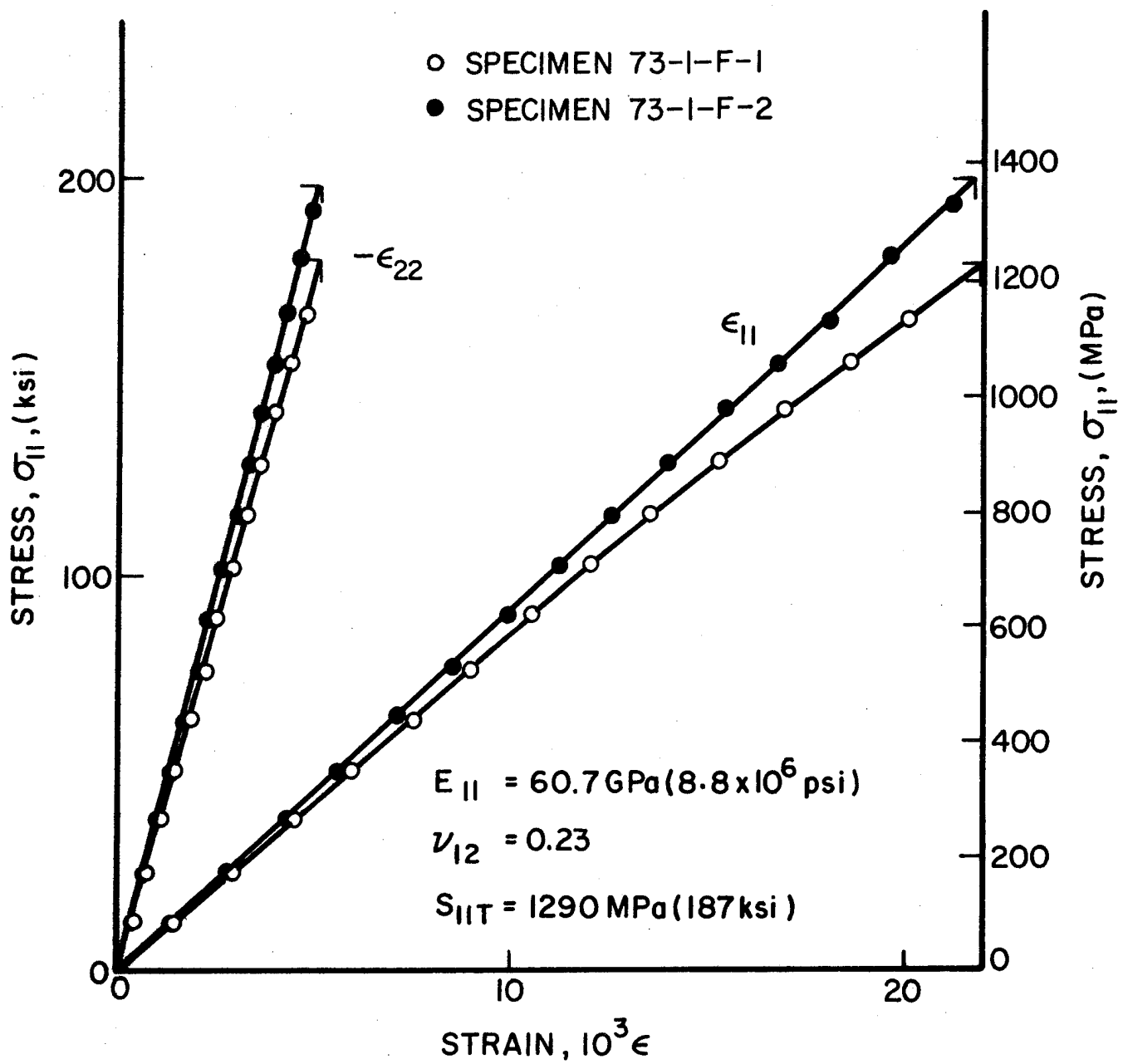
Fig. 3-16   STRAINS IN 0-DEGREE UNIDIRECTIONAL S-GLASS/EPOXY
SPECIMEN UNDER UNIAXIAL TENSION
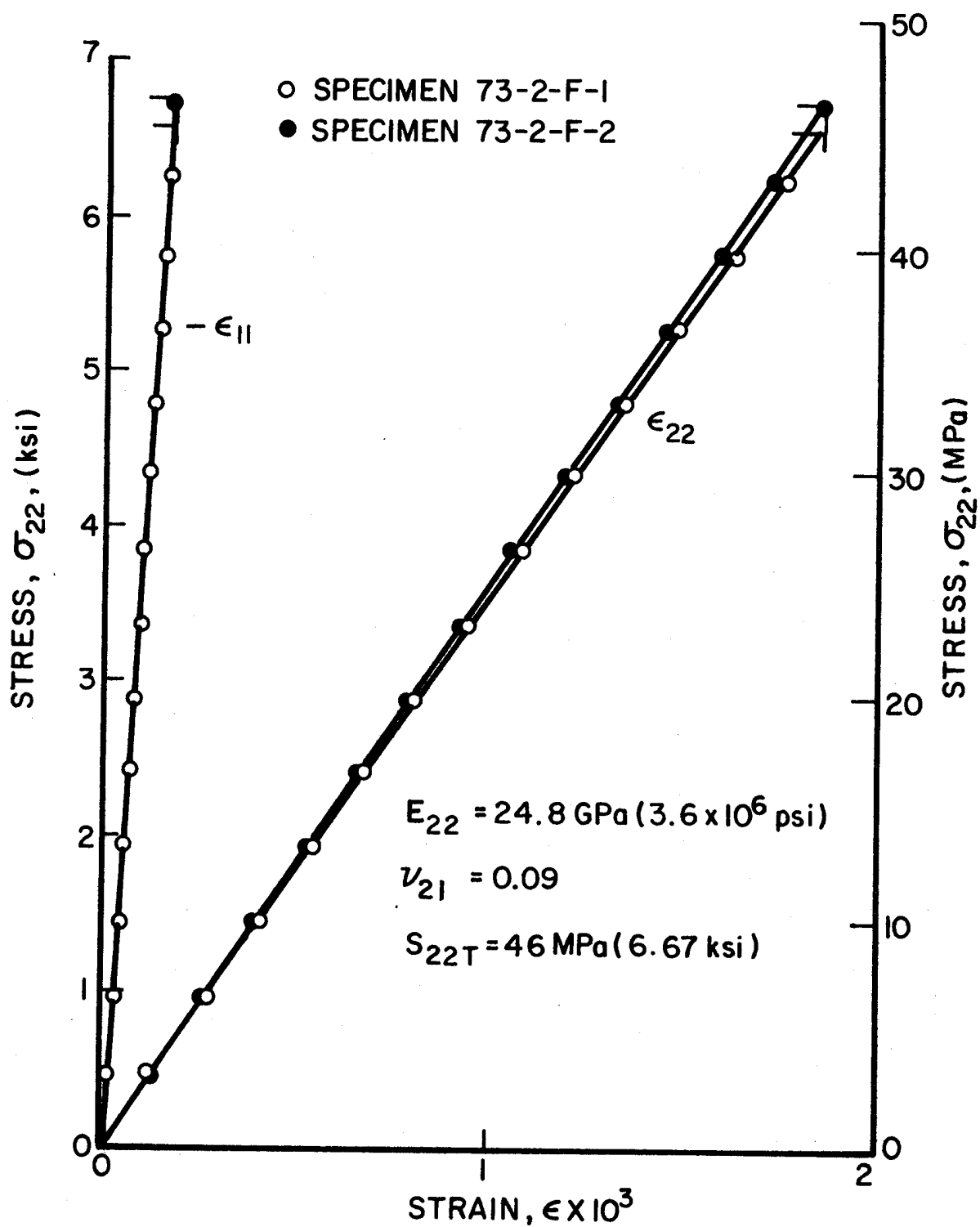
Fig. 3-17   STRAINS IN 90-DEGREE UNIDIRECTIONAL S-GLASS/EPOXY
SPECIMENS UNDER UNIAXIAL TENSION
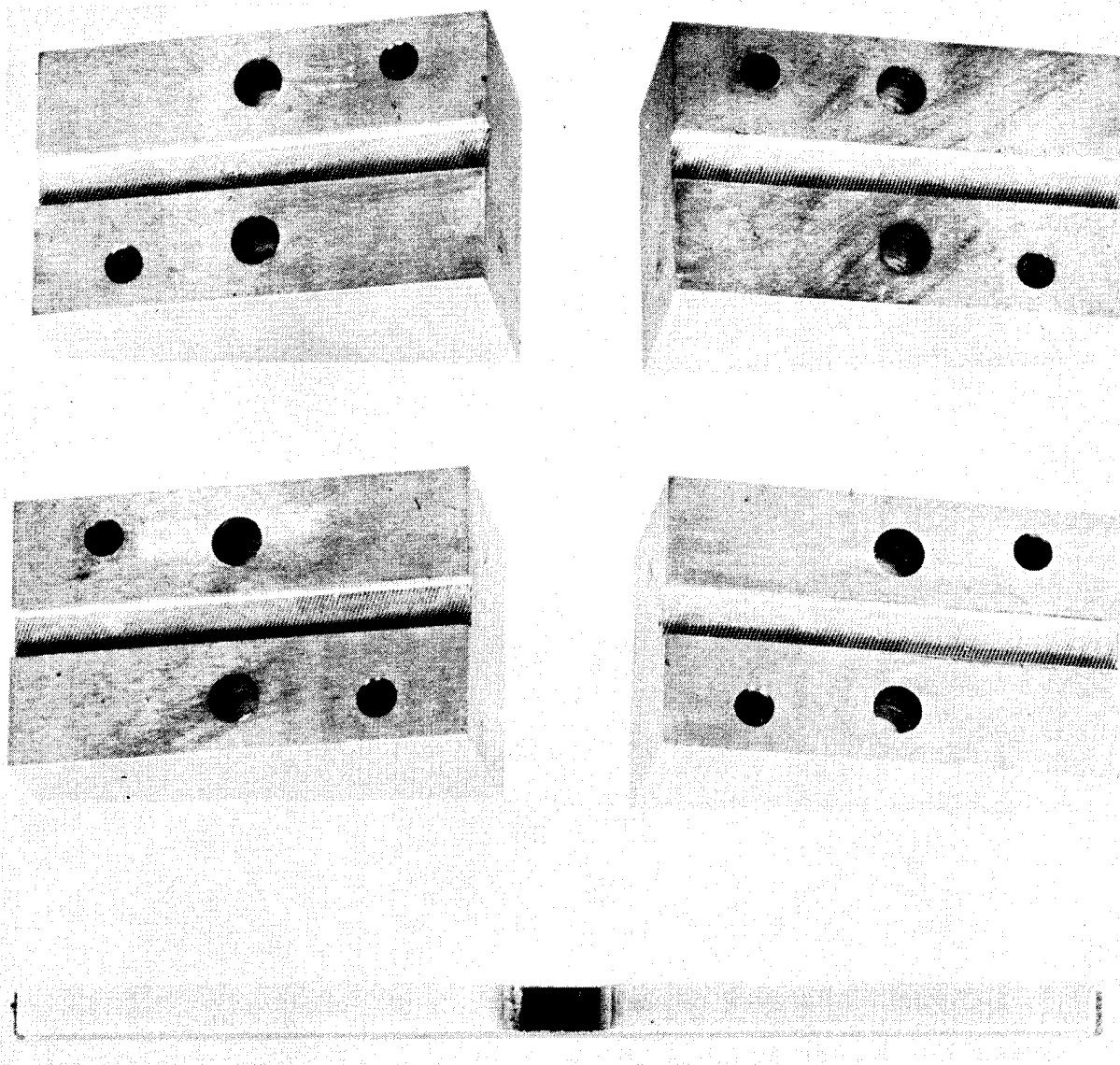
Fig. 3-18 IITRI COMPRESSION COUPON TEST FIXTURE - WEDGE
SHAPED SPECIMEN HOLDERS AND TEST SPECIMEN
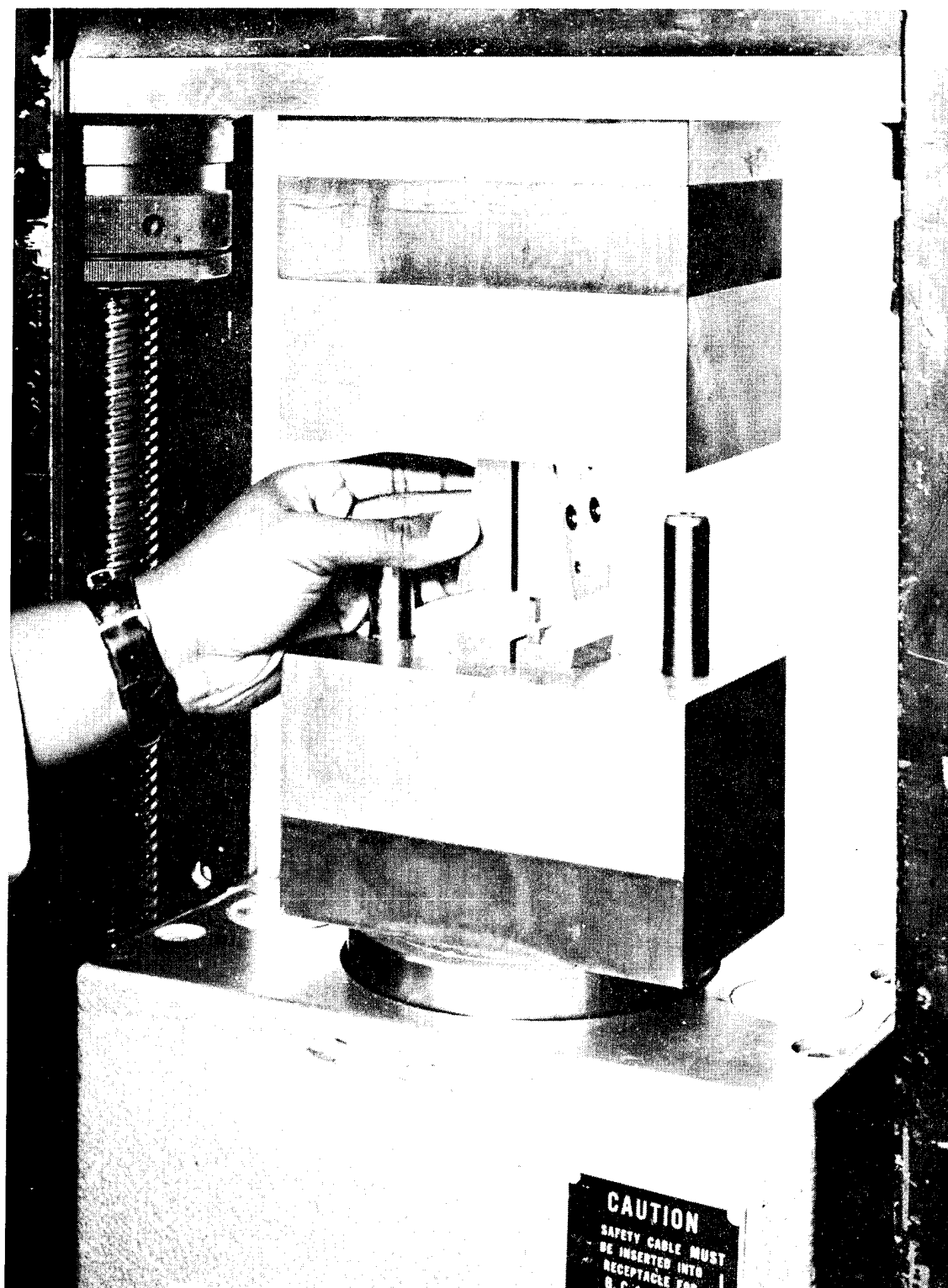
Fig. 3-19 IITRI COMPRESSION COUPON TEST FIXTURE SPECIMEN
ALIGNMENT
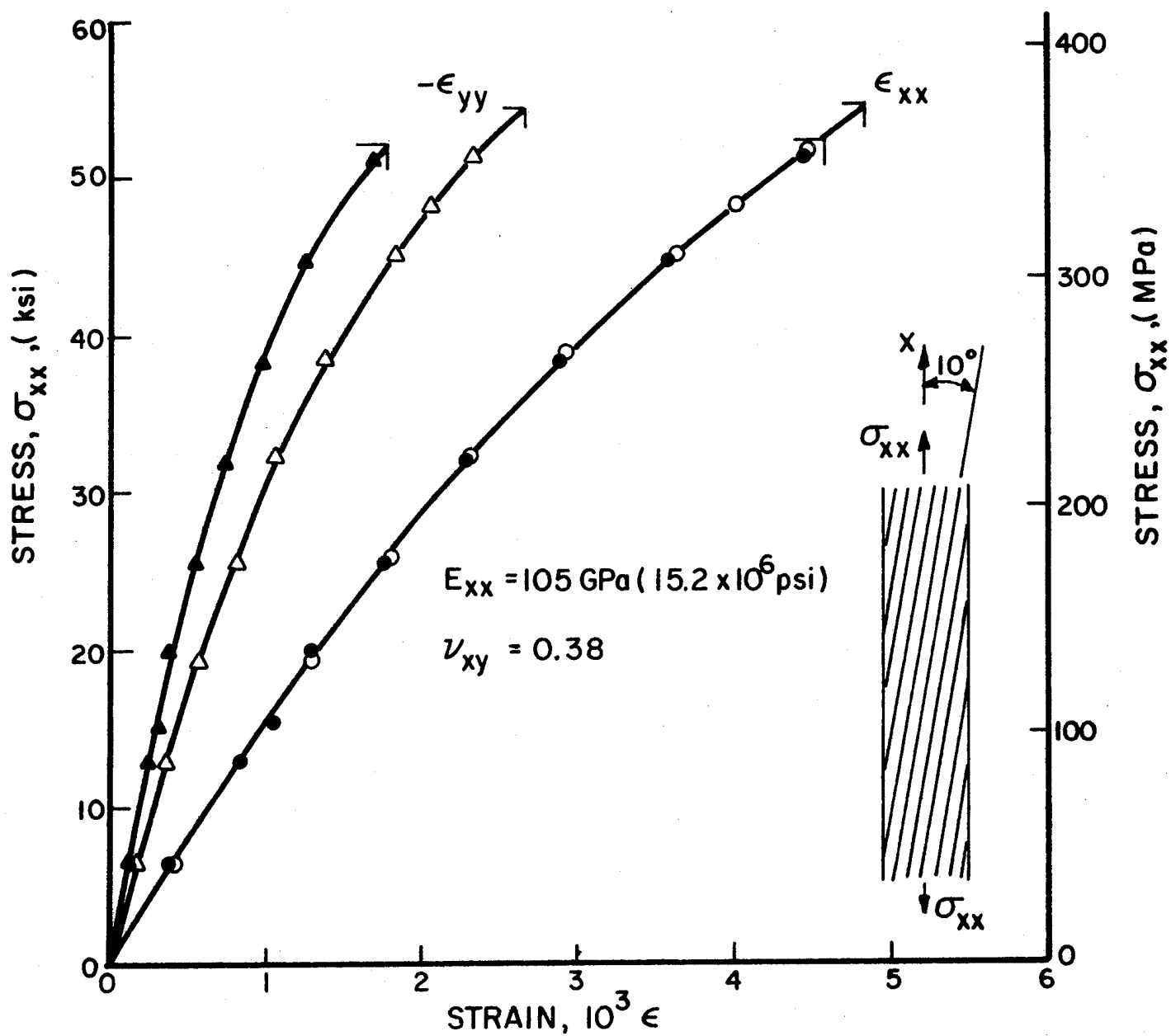
Fig. 3-20 STRESS-STRAIN CURVES IN 10-DEGREE OFF-AXIS UNIDIRECTIONAL
BORON/EPOXY SPECIMEN UNDER UNIAXIAL TENSION
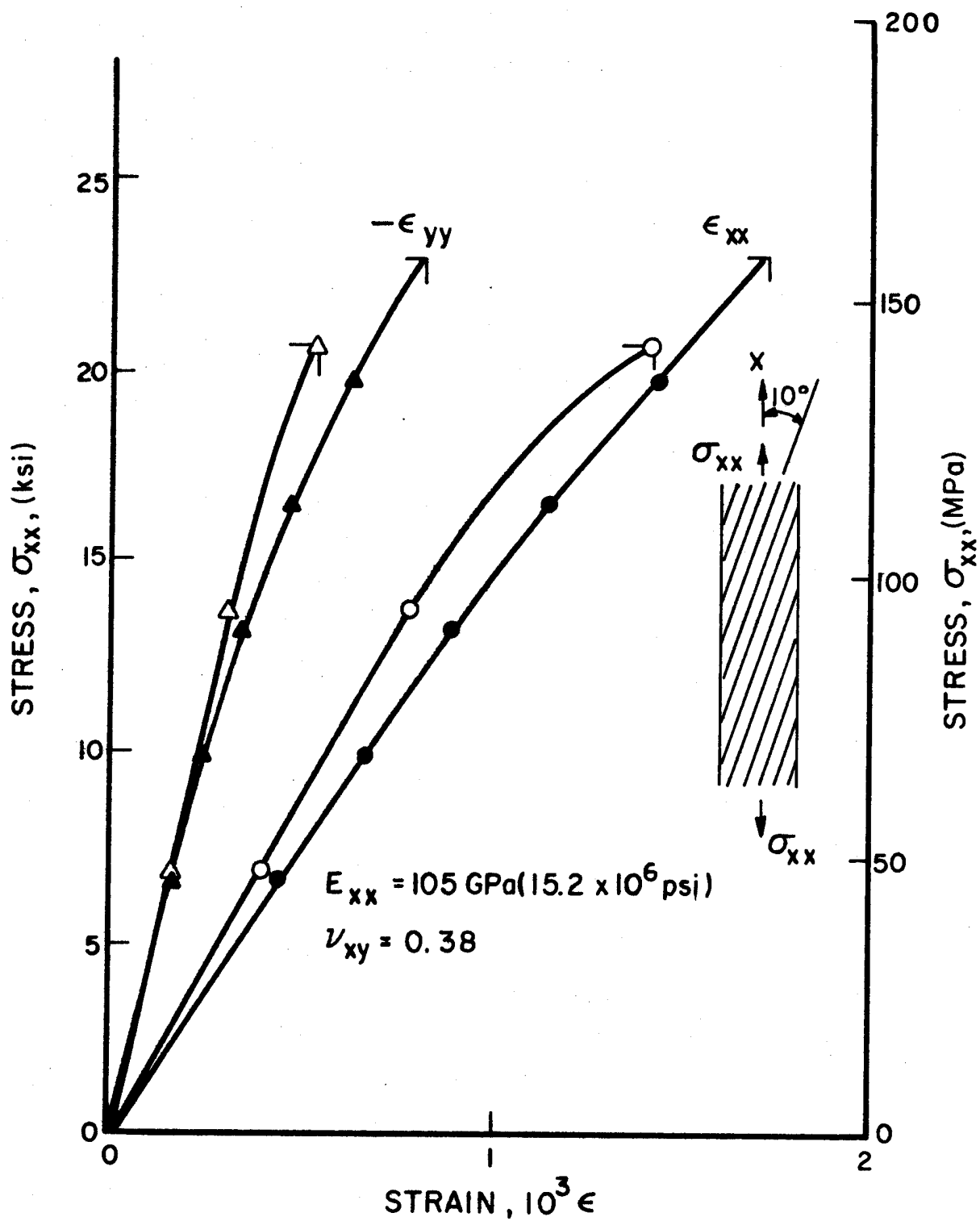
Fig. 3-21   STRESS-STRAIN CURVES IN 10-DEGREE OFF-AXIS UNIDIRECTIONAL
BORON/POLYIMIDE SPECIMEN UNDER UNIAXIAL TENSION

3-71
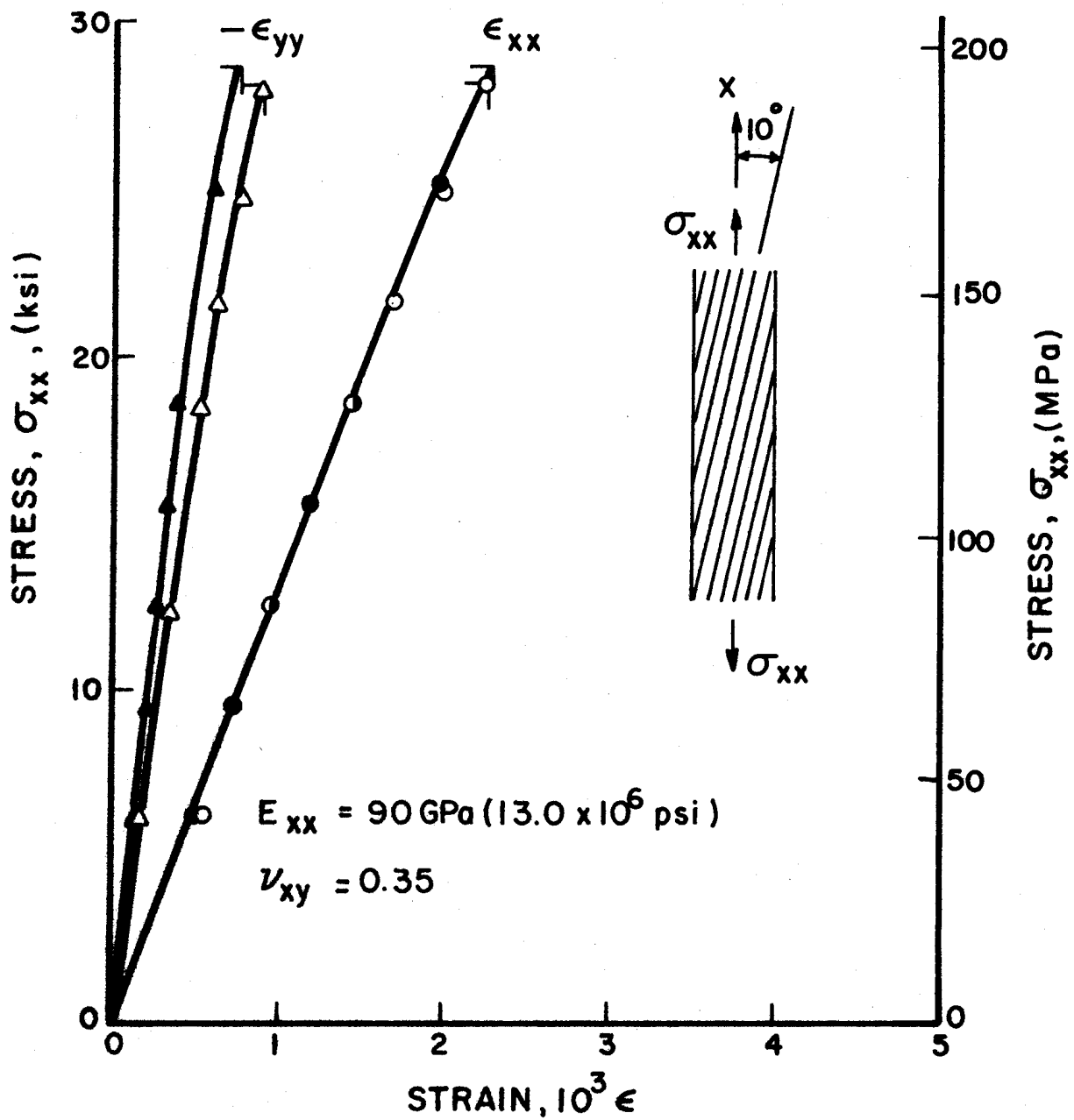
Fig. 3-22 STRESS-STRAIN CURVES IN 10-DEGREE OFF-AXIS UNIDIRECTIONAL
GRAPHITE/LOW MODULUS EPOXY SPECIMEN UNDER UNIAXIAL TENSION
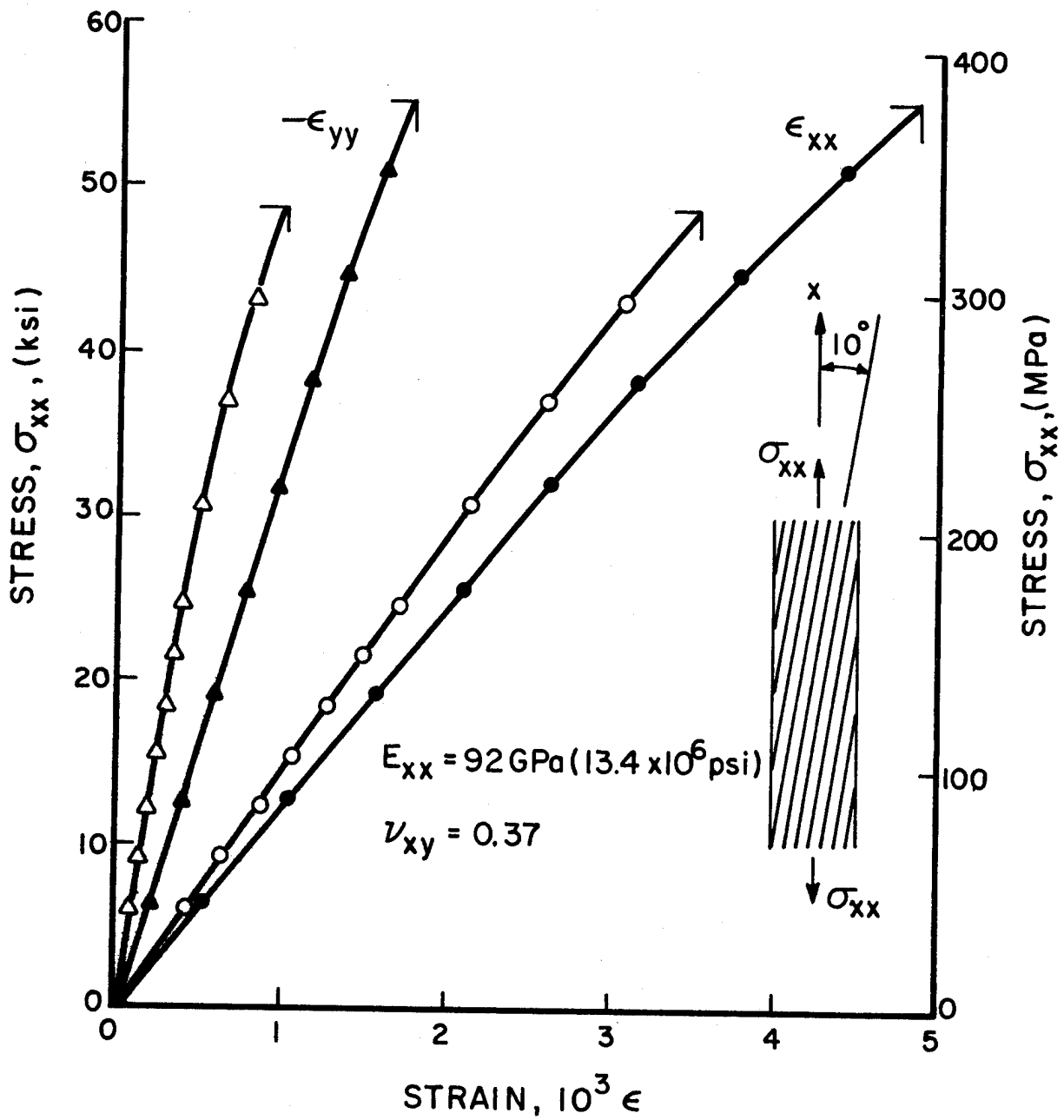
Fig. 3-23 STRESS-STRAIN CURVES IN 10-DEGREE OFF-AXIS UNIDIRECTIONAL
GRAPHITE/HIGH MODULUS EPOXY SPECIMEN UNDER UNIAXIAL TENSION
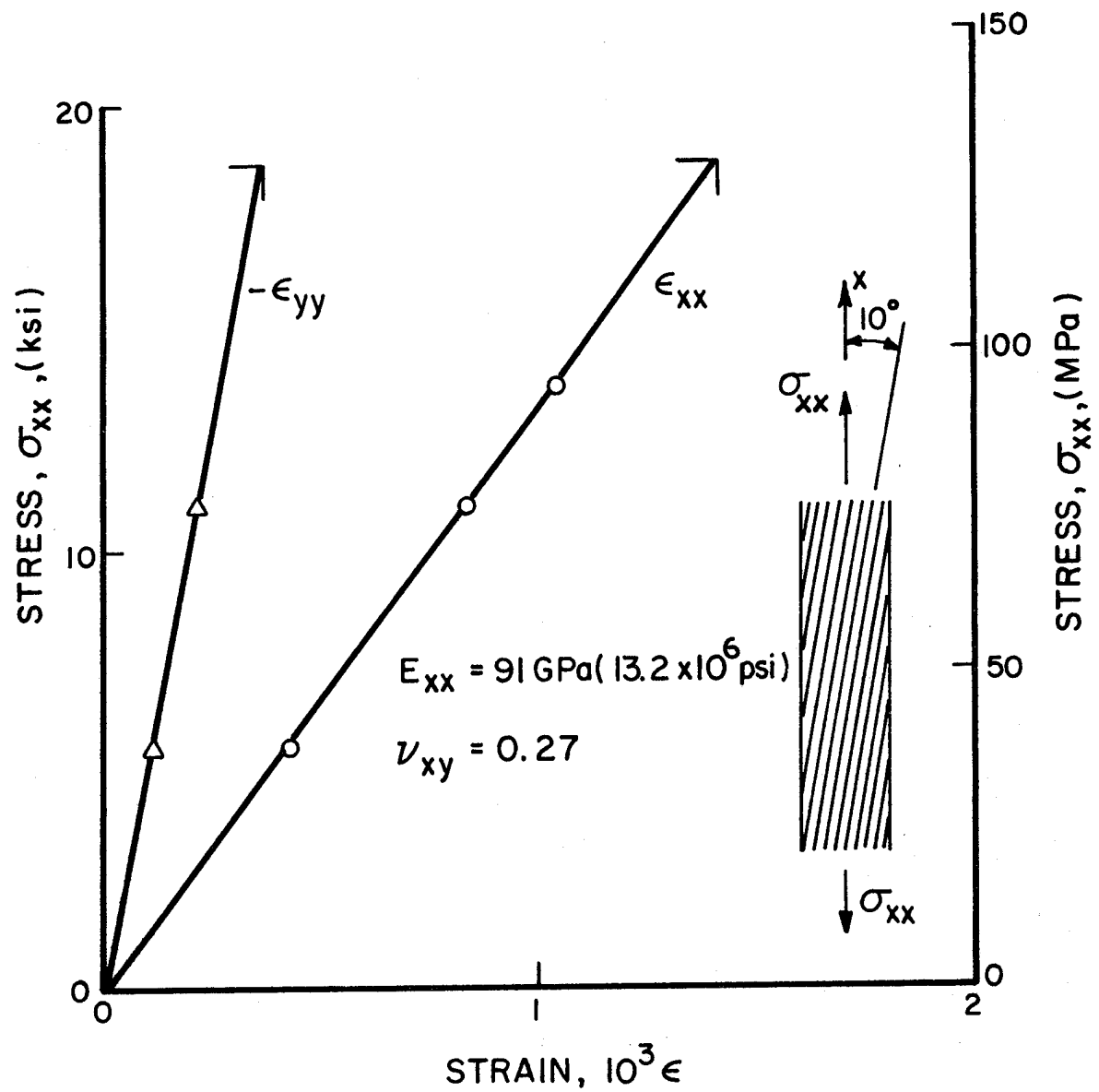
Fig. 3-24   STRESS-STRAIN CURVES IN 10-DEGREE OFF-AXIS UNIDIRECTIONAL
GRAPHITE/POLYIMIDE SPECIMEN UNDER UNIAXIAL TENSION
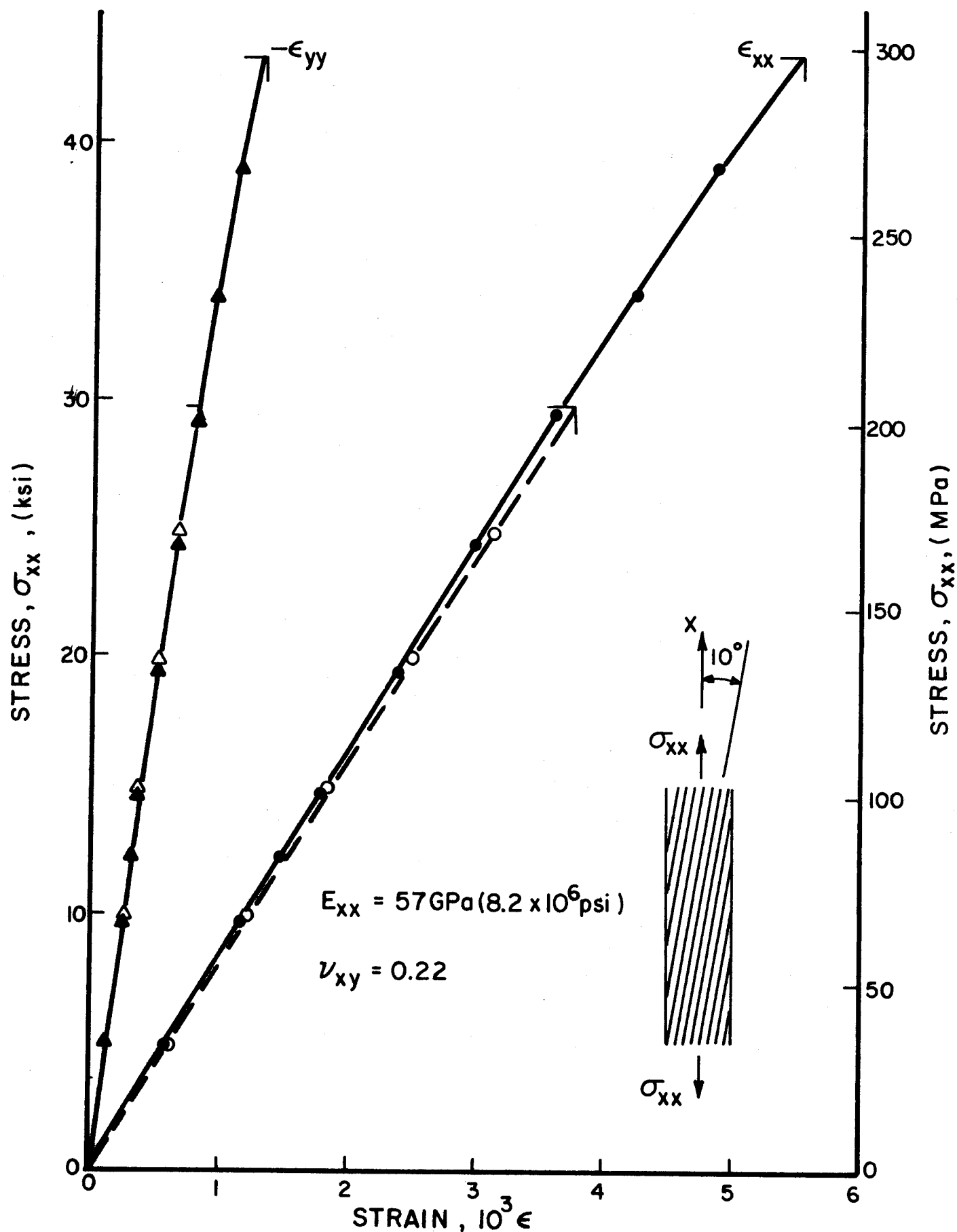
Fig. 3-25   STRESS-STRAIN CURVES IN 10-DEGREE OFF-AXIS UNIDIRECTIONAL
S-GLASS/EPOXY SPECIMEN UNDER UNIAXIAL TENSION
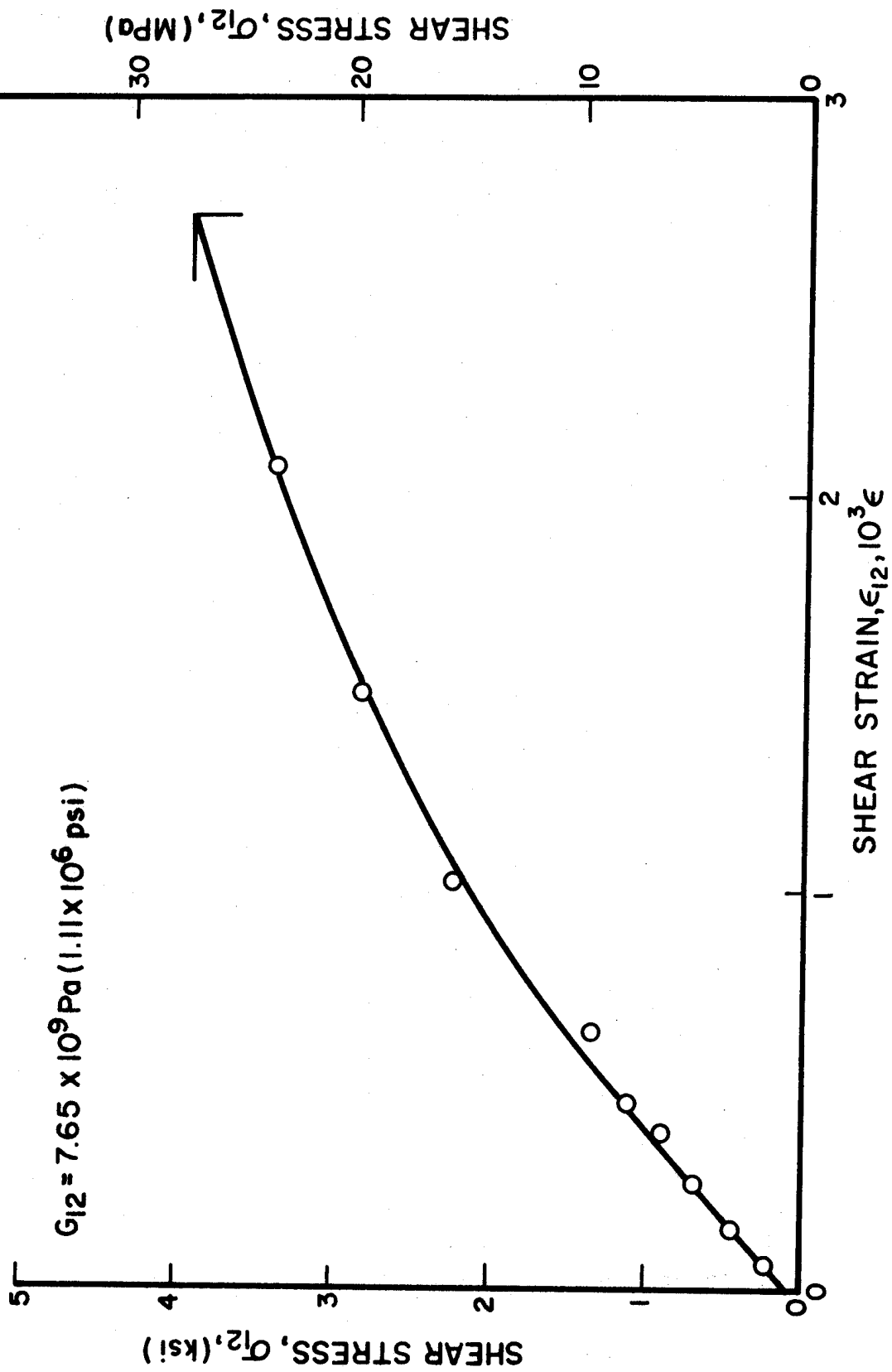
Fig. 3-26 SHEAR STRESS-SHEAR STRAIN IN 10-DEGREE OFF-AXIS BORON/POLYIMIDE SPECIMEN

$G_{12} = 7.65 \times 10^9 Pa (1.11 \times 10^6 psi)$

SHEAR STRESS, σ_{12}, (MPa)

SHEAR STRESS, σ_{12}, (ksi)

SHEAR STRAIN, ϵ_{12}, $10^3 \epsilon$
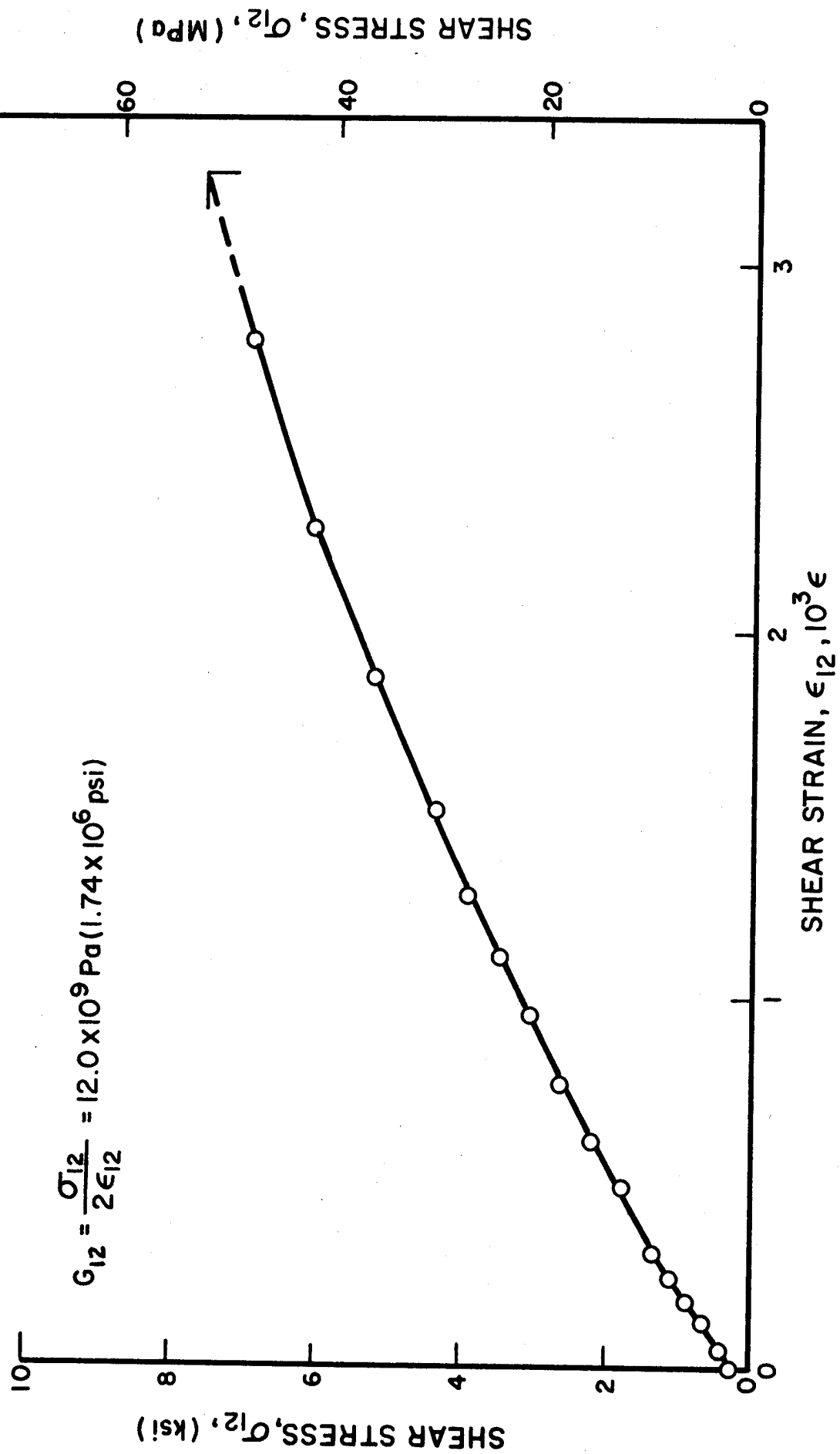
Fig. 3-27 SHEAR STRESS VERSUS SHEAR STRAIN IN 10-DEGREE OFF-AXIS UNIDIRECTIONAL S-GLASS/ EPOXY SPECIMEN

$$G_{12} = \frac{\sigma_{12}}{2\epsilon_{12}} = 12.0 \times 10^9 \, Pa (1.74 \times 10^6 \, psi)$$
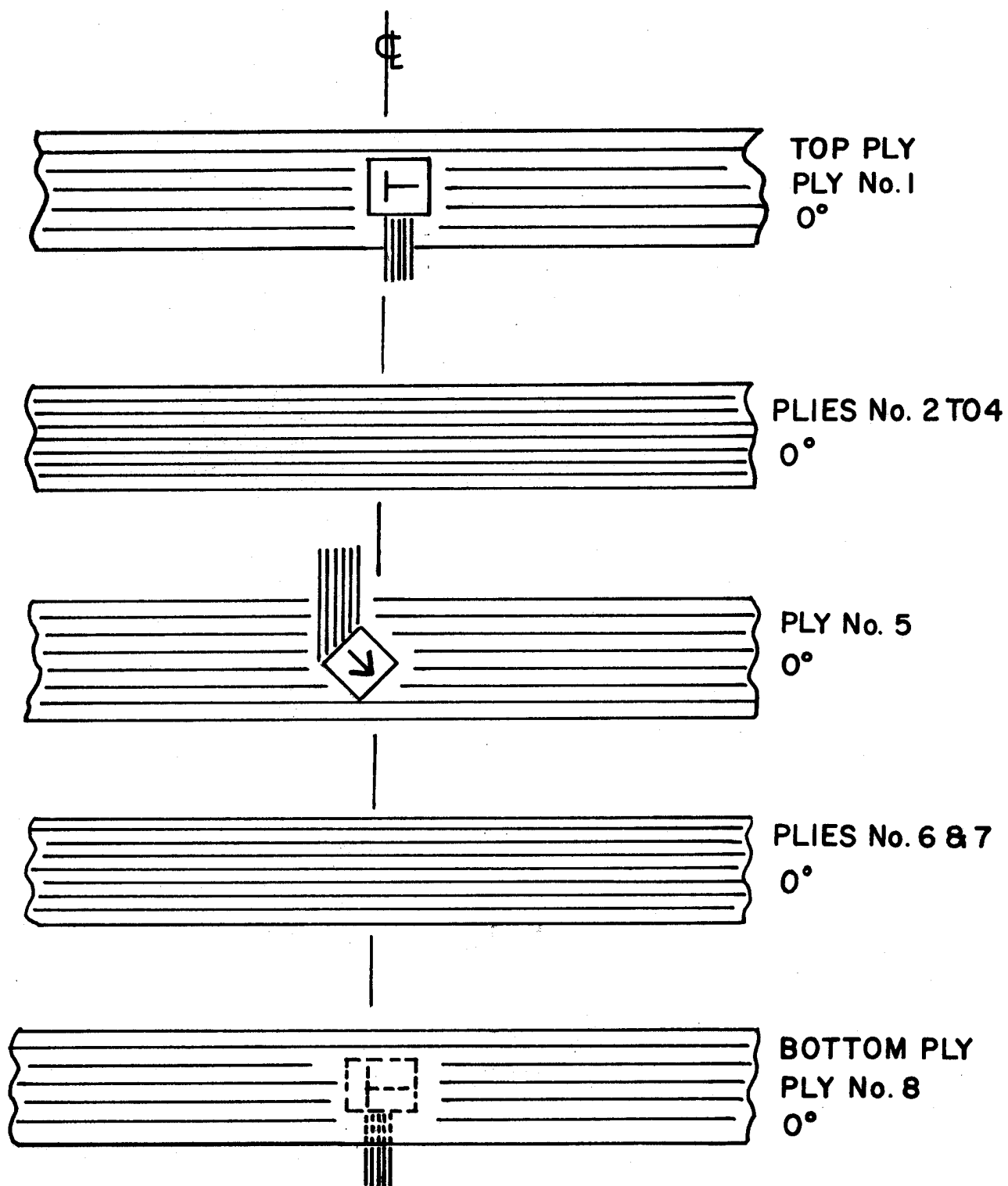
Fig. 3-28 TYPICAL STRAIN GAGE LAYOUT IN $[0_8]$ UNIDIRECTIONAL
SPECIMENS
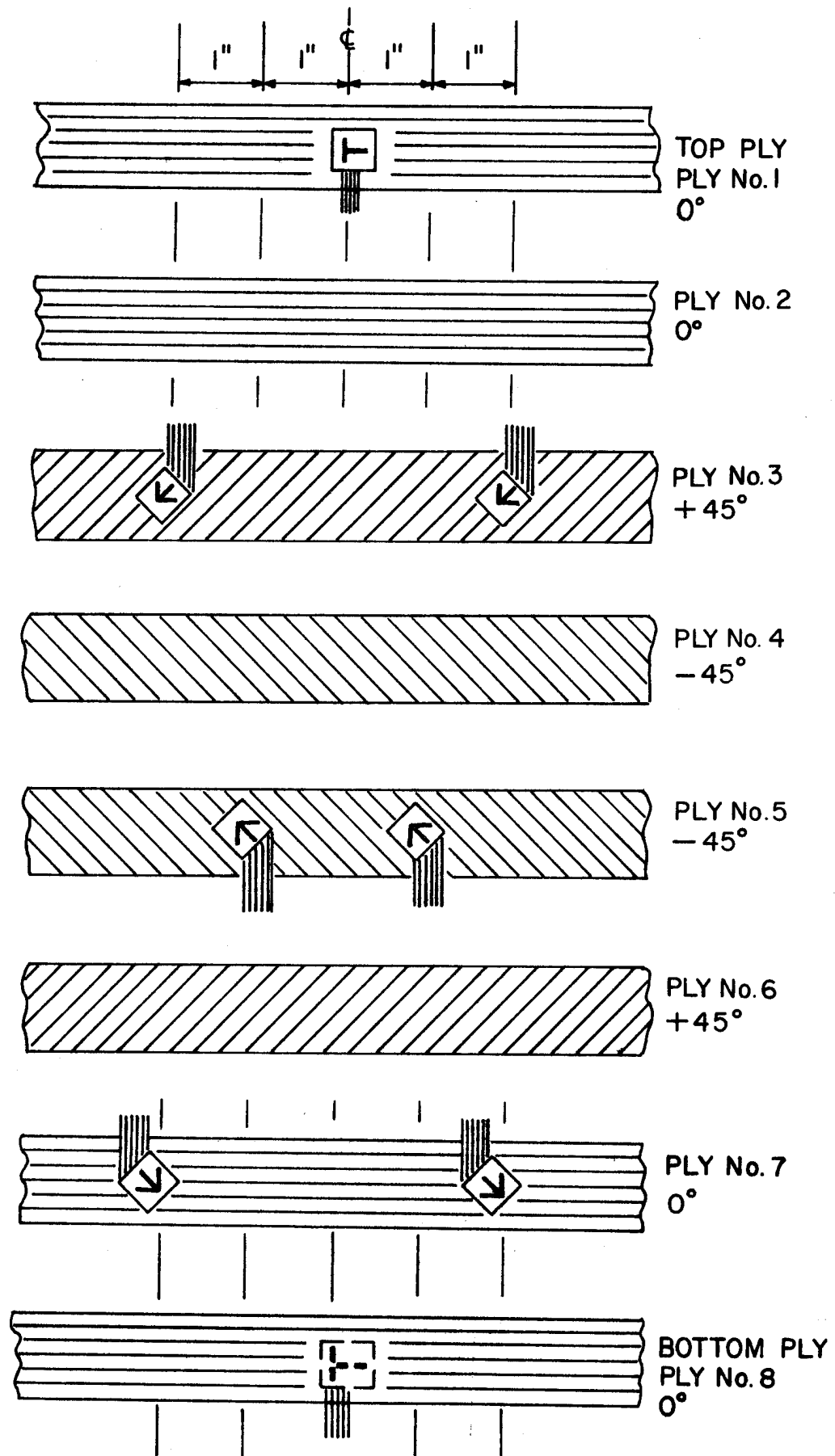
Fig. 3-29 STRAIN GAGE LAYOUT IN $[0_2/\pm 45]_s$ SPECIMEN

3-79
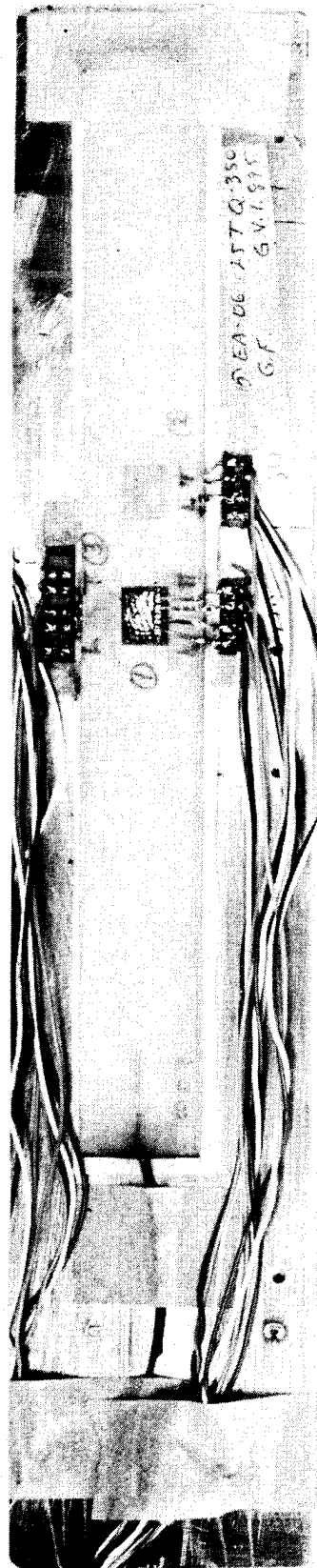
Fig. 3-30 GLASS/EPOXY UNIAXIAL SPECIMEN WITH SURFACE AND EMBEDDED GAGES AND THERMOCOUPLE AFTER CURING
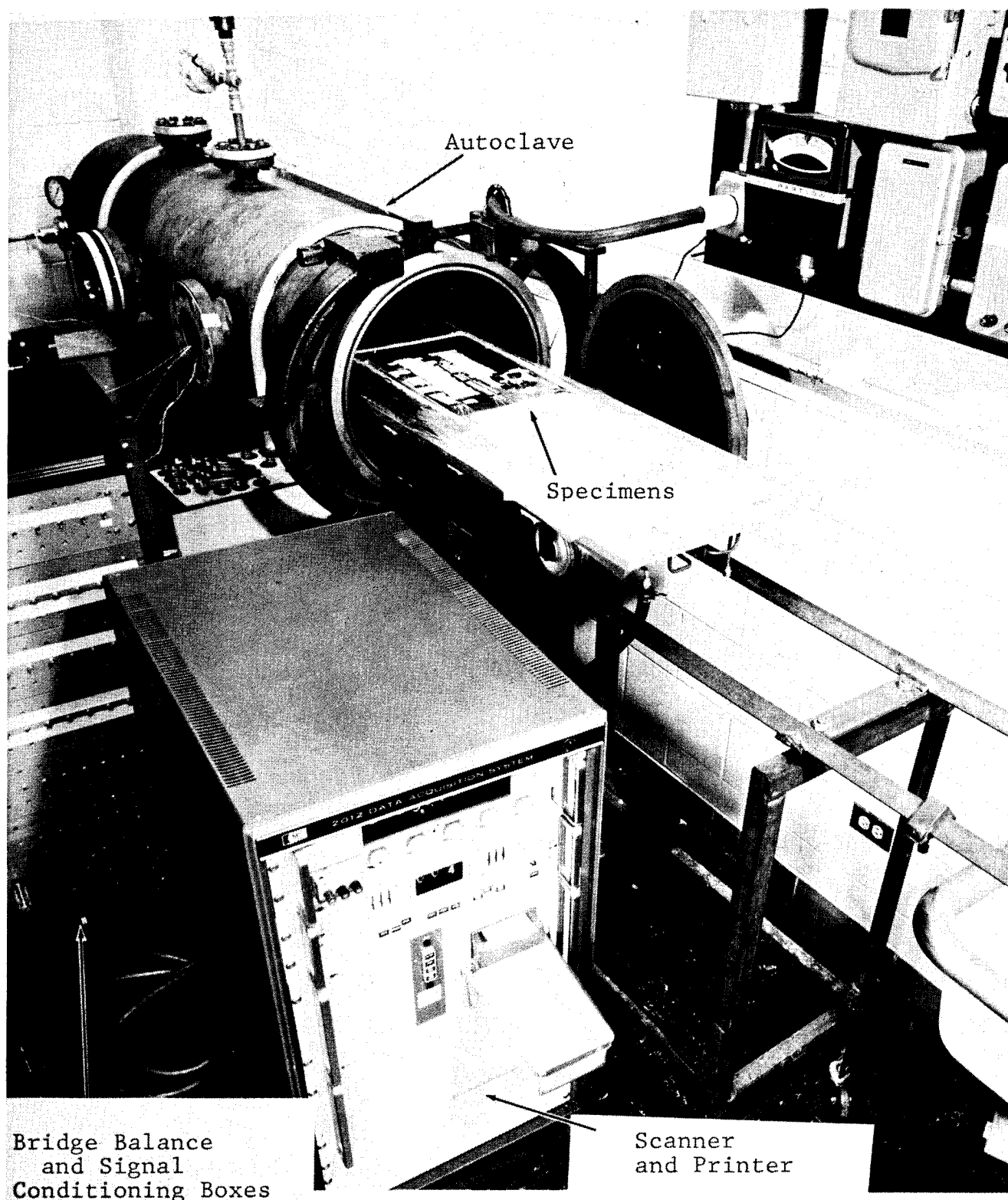
Fig. 3-31 INSTRUMENTED AND WIRED SPECIMENS WITH DATA
ACQUISITION SYSTEM BEING READIED FOR STRAIN
AND TEMPERATURE MONITORING DURING AUTOCLAVE
CURING

Fig. 3-32   INSTRUMENTED AND WIRED SPECIMENS WITH DATA
ACQUISITION SYSTEM BEING READIED FOR STRAIN
AND TEMPERATURE MONITORING DURING POSTCURING

Fig. 3-33 SCHEMATIC DIAGRAM OF SIGNAL CONDITIONING WITH THREE WIRE COMPENSATION FOR RECORDING STRAIN GAGE DATA WITH A DIGITAL DATA ACQUISITION SYSTEM.

NOTE:

Lead wire lengths
(a) and (c) exposed
to elevated temperature
must be of equal lengths.

R_1, R_2, R_3 are bridge
completion resistors.
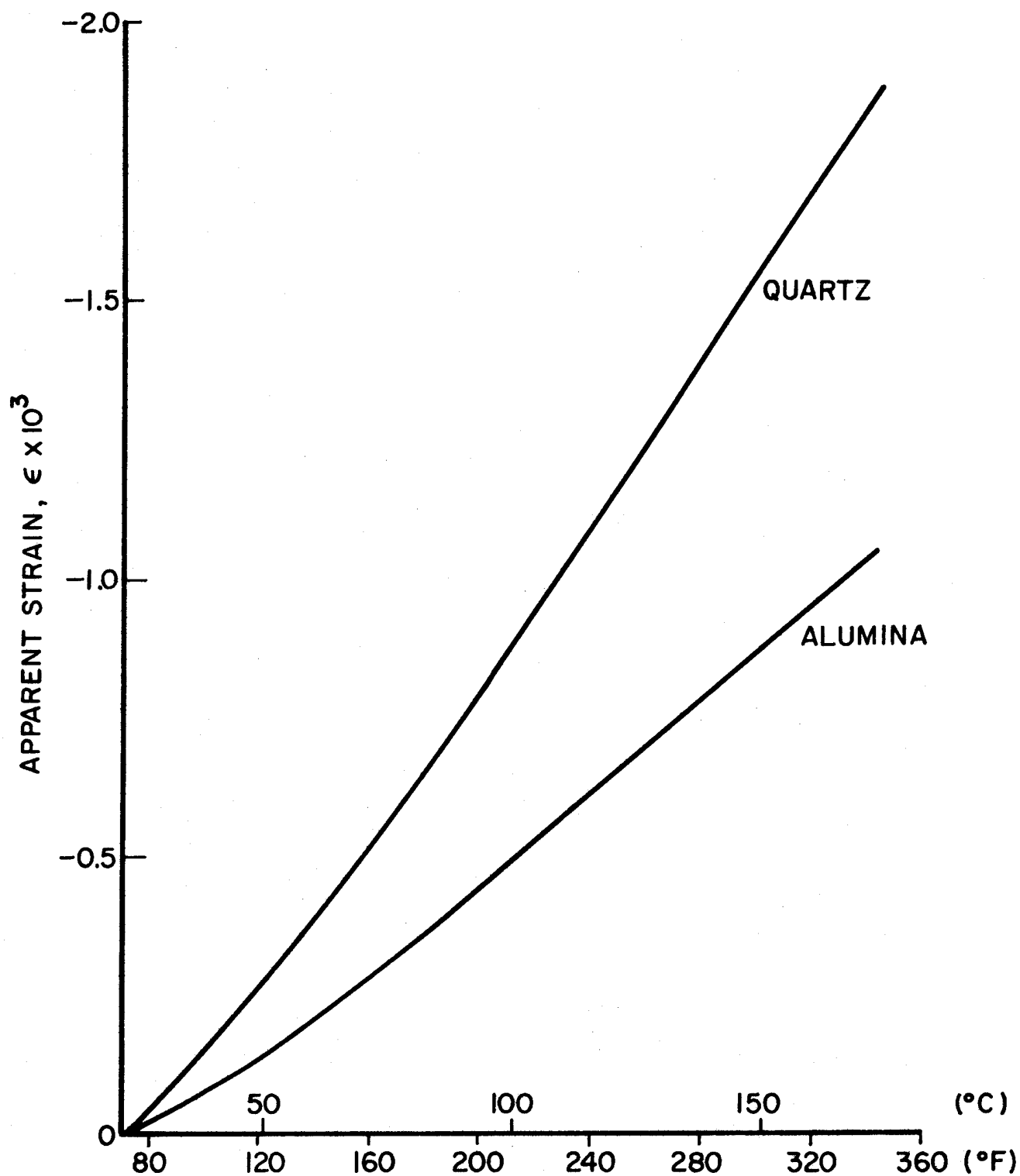
Figure 3-34

OUTPUTS OF STRAIN GAGES ATTACHED TO QUARTZ AND ALUMINUM OXIDE AS A
FUNCTION OF TEMPERATURE (COEFFICIENTS OF THERMAL EXPANSION FOR QUARTZ
AND ALUMINA ARE 0.7×10^{-6} K^{-1} (0.4×10^{-6} in/in./°F) AND 6.8×10^{-6} K^{-1}
(3.8×10^{-6} in./in./°F), RESPECTIVELY)

2.54 cm. (1 in.)

22.9 cm. (9 in.)

y

x

1
2
3
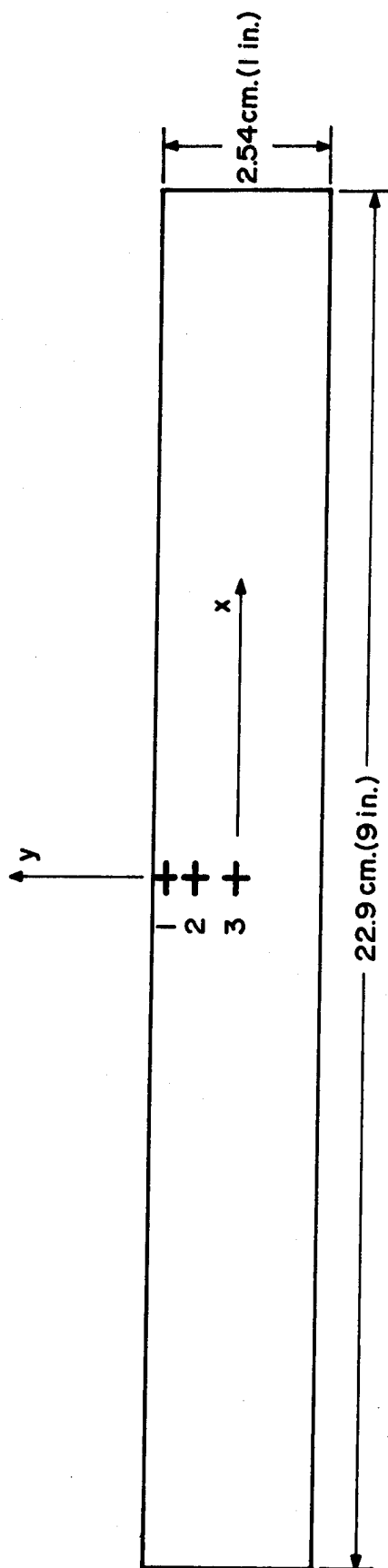
GAGE NO.	TYPE	LOCATION
1	EA-05-062TT-120	y = 0; Between 4th and 5th Ply
2	EA-05-062TT-120	y = 0.63 cm (0.25 in.); Between 4th and 5th Ply
3	EA-05-062TT-120	y = 1.14 cm (0.45 in.); Between 4th and 5th Ply

Fig. 3-35 SCHEMATIC ILLUSTRATING GAGE LOCATIONS IN $[0_2/\pm45]_s$ S-GLASS/EPOXY SPECIMEN USED IN STUDY OF EDGE EFFECTS
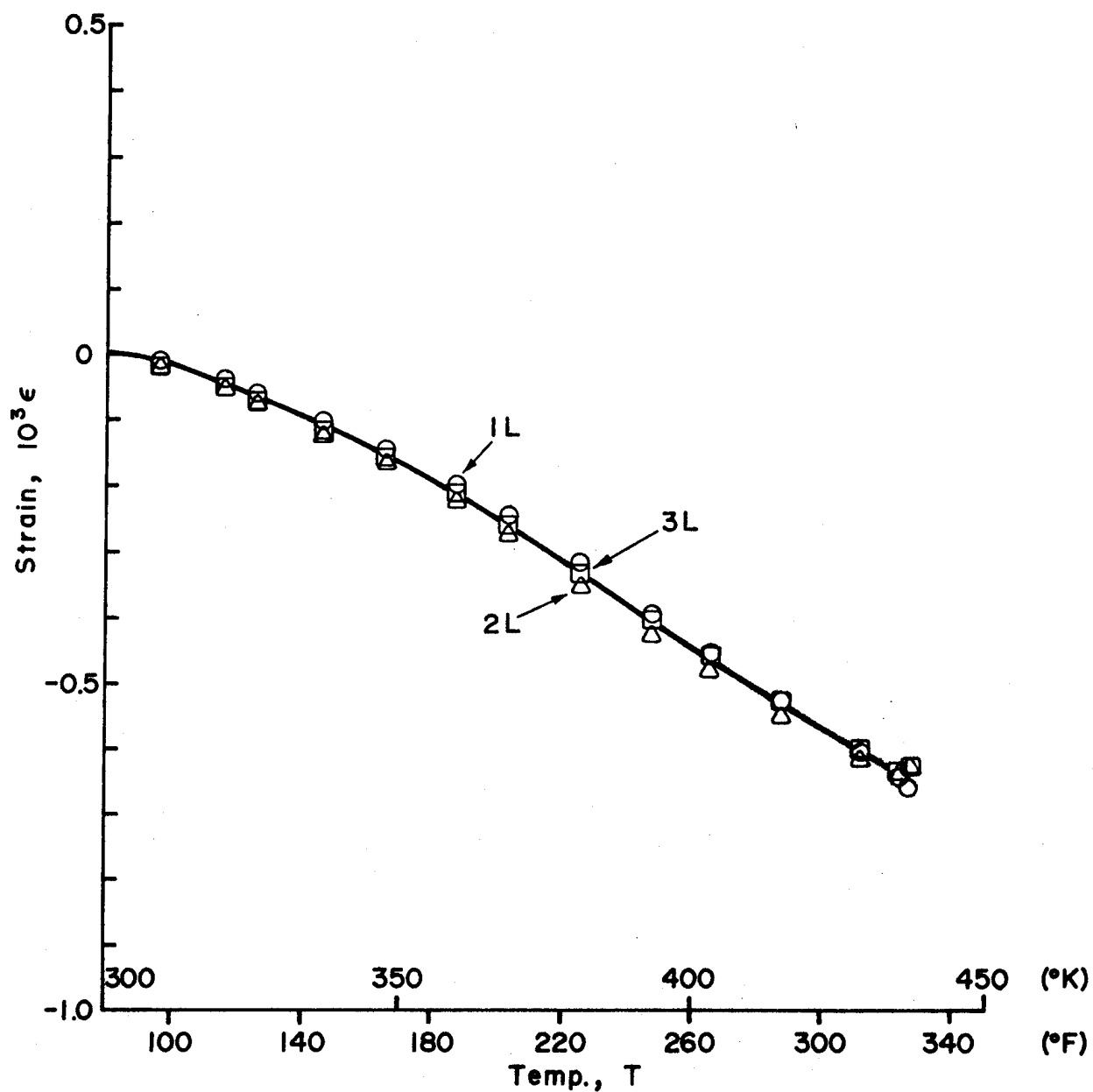
Fig. 3-36   APPARENT LONGITUDINAL STRAINS IN $\left[0_2/\pm45\right]_s$ S-GLASS/
EPOXY SPECIMEN DURING THERMAL CYCLING (Increasing
Temperature)
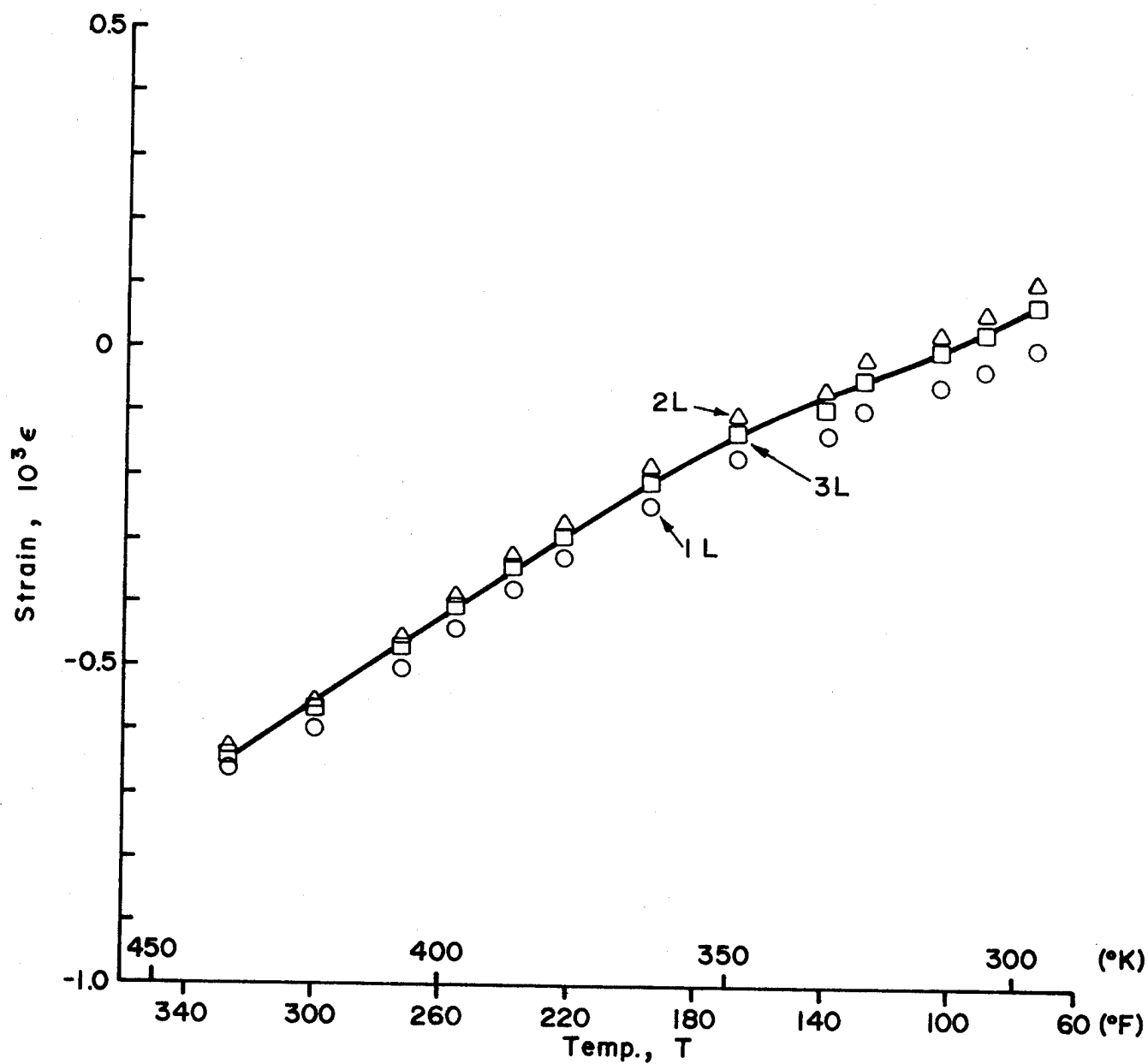
Fig. 3-37 APPARENT LONGITUDINAL STRAINS IN $[0_2/\pm45]_s$ S-GLASS/
EPOXY SPECIMEN DURING THERMAL CYCLING (Decreasing
Temperature)
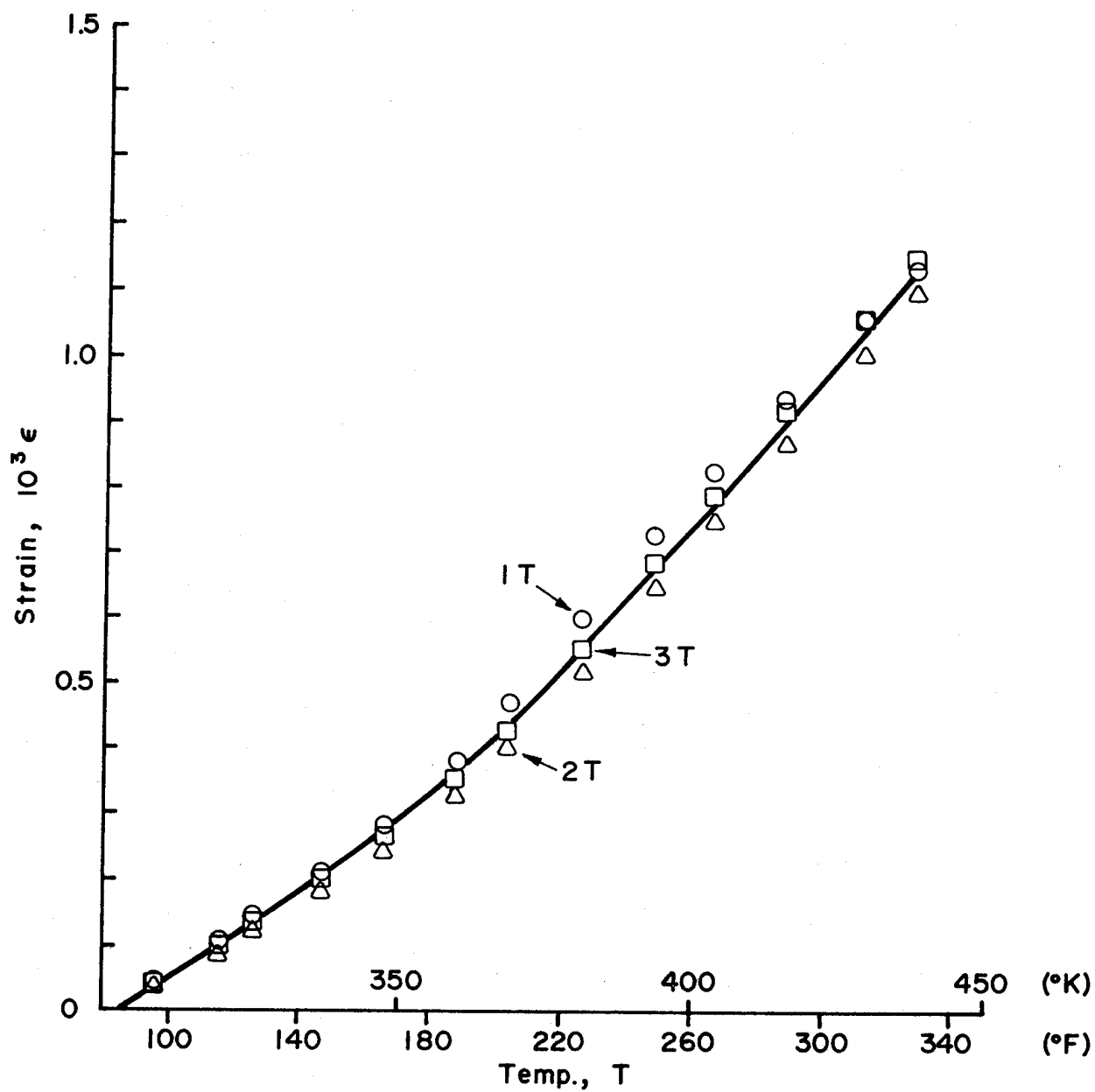
Fig. 3-38 APPARENT TRANSVERSE STRAINS IN $[0_2/\pm45]_s$ S-GLASS/
EPOXY SPECIMEN DURING THERMAL CYCLING (Increasing
Temperature)
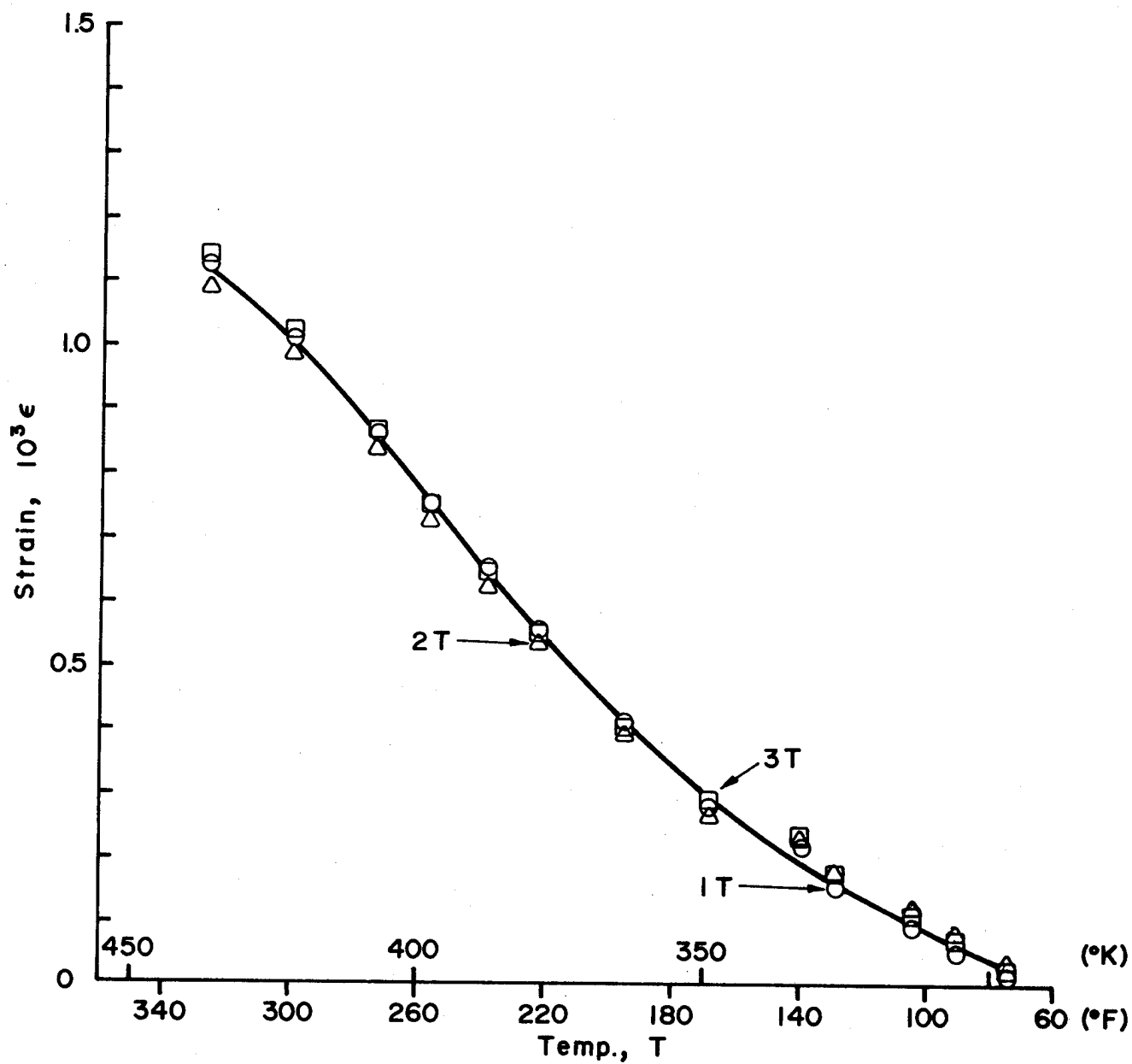
Fig. 3-39   APPARENT TRANSVERSE STRAINS IN $\begin{bmatrix} 0_2/\pm45 \end{bmatrix}_s$ S-GLASS/
EPOXY SPECIMEN DURING THERMAL CYCLING (Decreasing
Temperature)
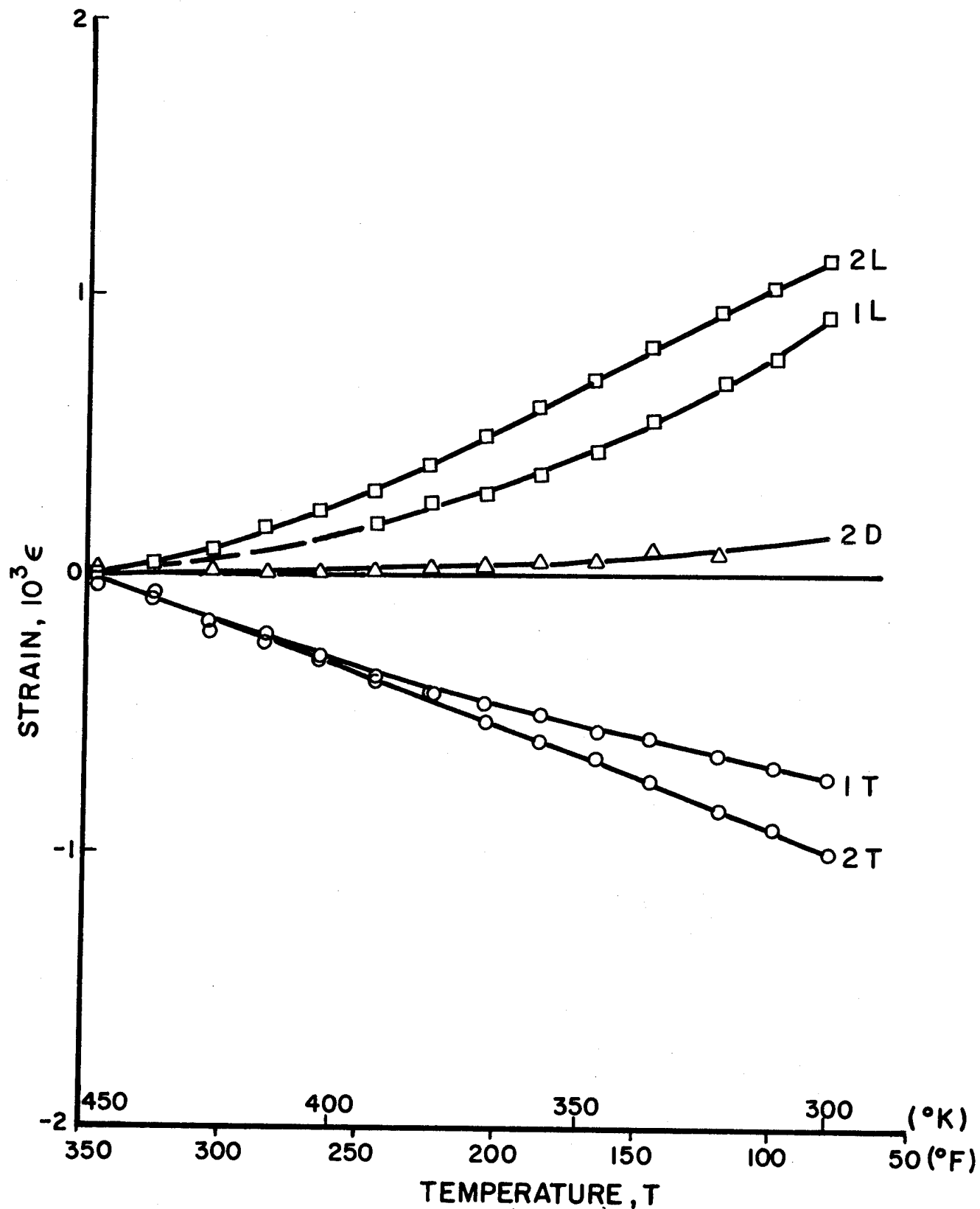
Fig. 3-40   APPARENT STRAINS IN $[0_2/\pm45]_s$ BORON/EPOXY SPECIMEN
DURING CURING (DECREASING TEMPERATURE).
(GAGE DESIGNATIONS: L,T,D: LONGITUDINAL, TRANSVERSE
AND 45-DEGREE; 1, 2: TOP SURFACE, MIDDLE SURFACE,
RESPECTIVELY)

3-90
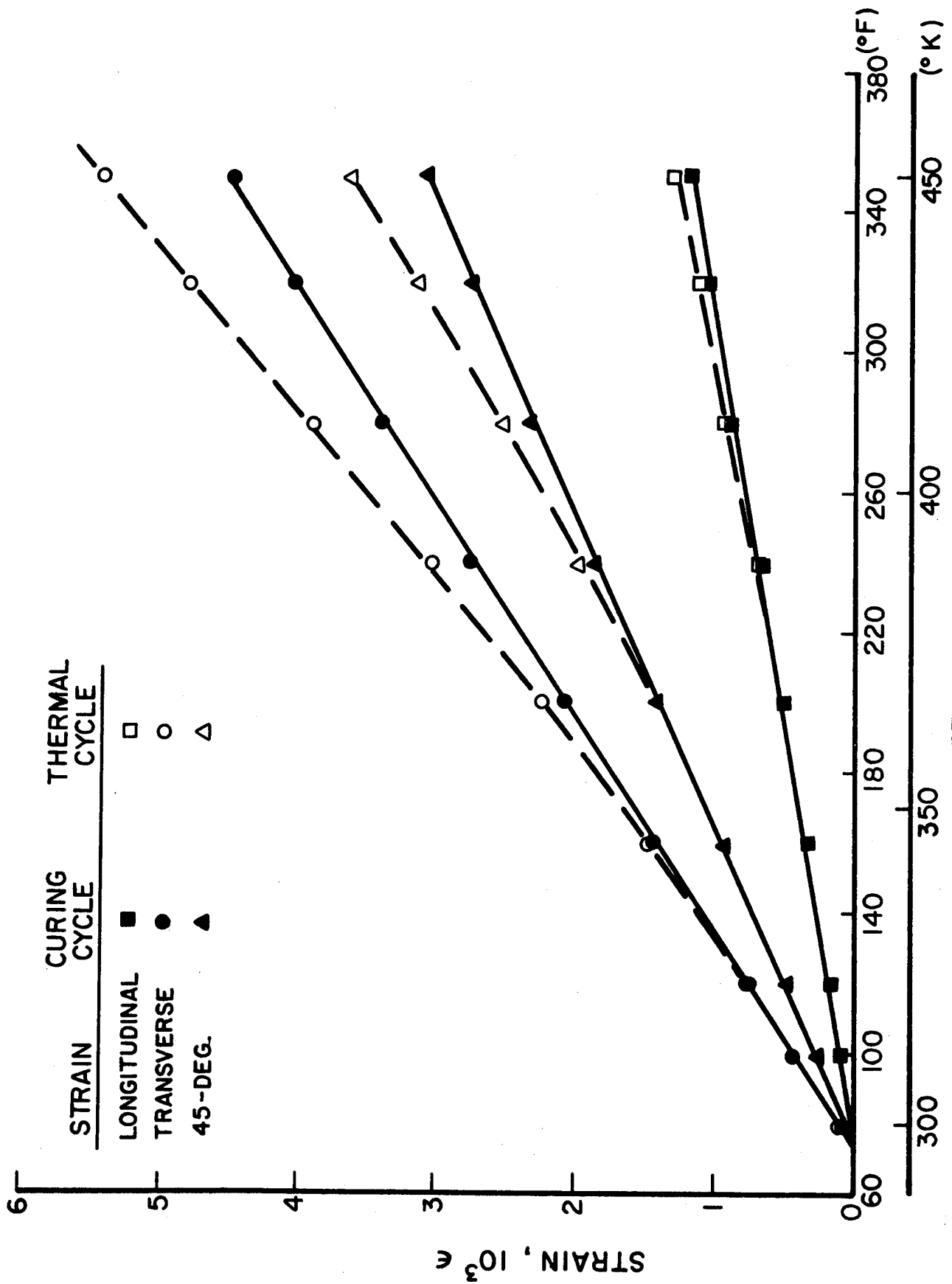
Fig. 3-41 STRAINS IN $[0_8]$ BORON/EPOXY SPECIMEN DURING CURING AND THERMAL CYCLE

16-3
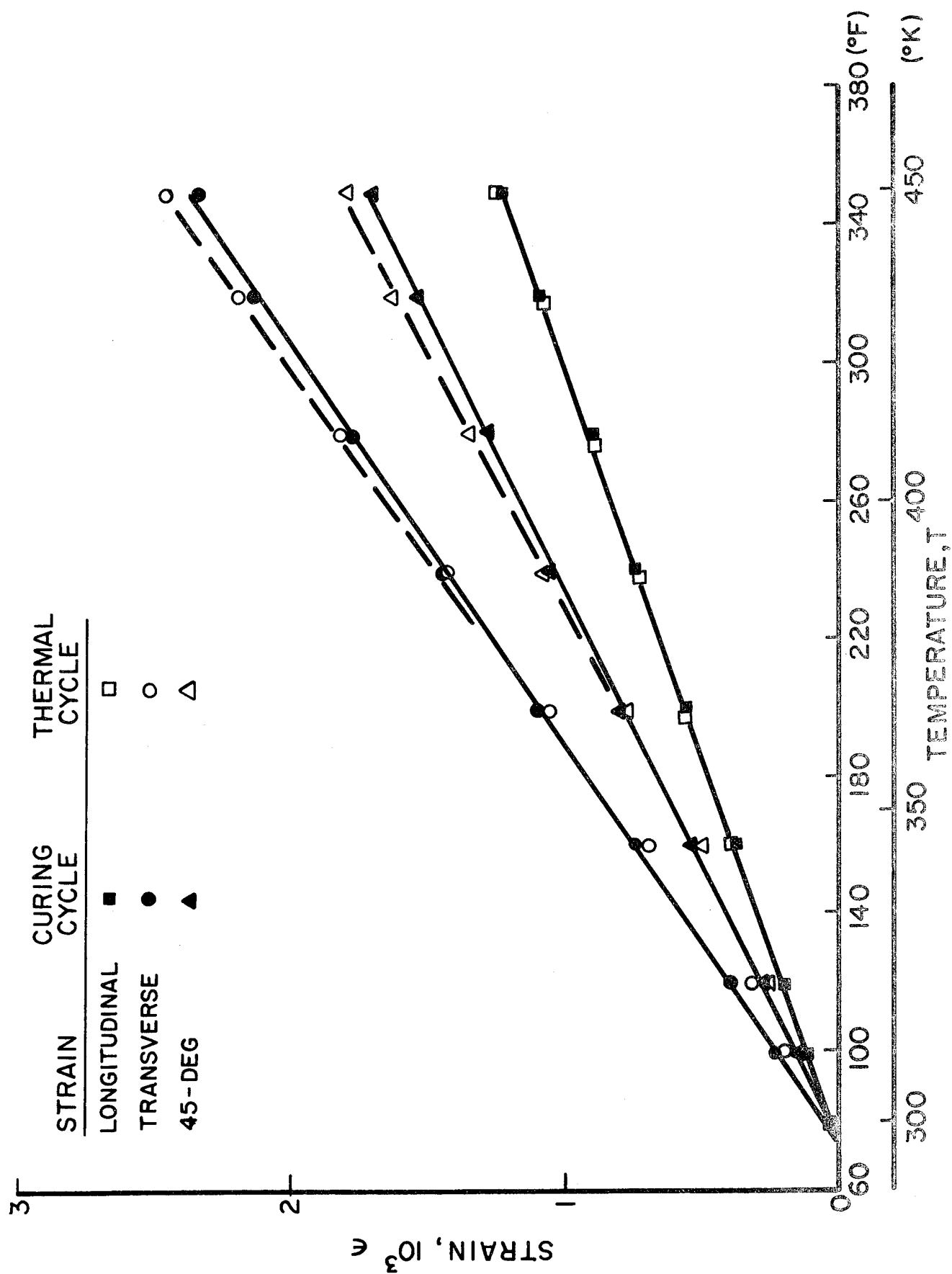
Fig. 3-4.2 STRAINS IN $[0_2/\pm45]_s$ BORON/EPOXY SPECIMEN DURING CURING AND THERMAL CYCLE
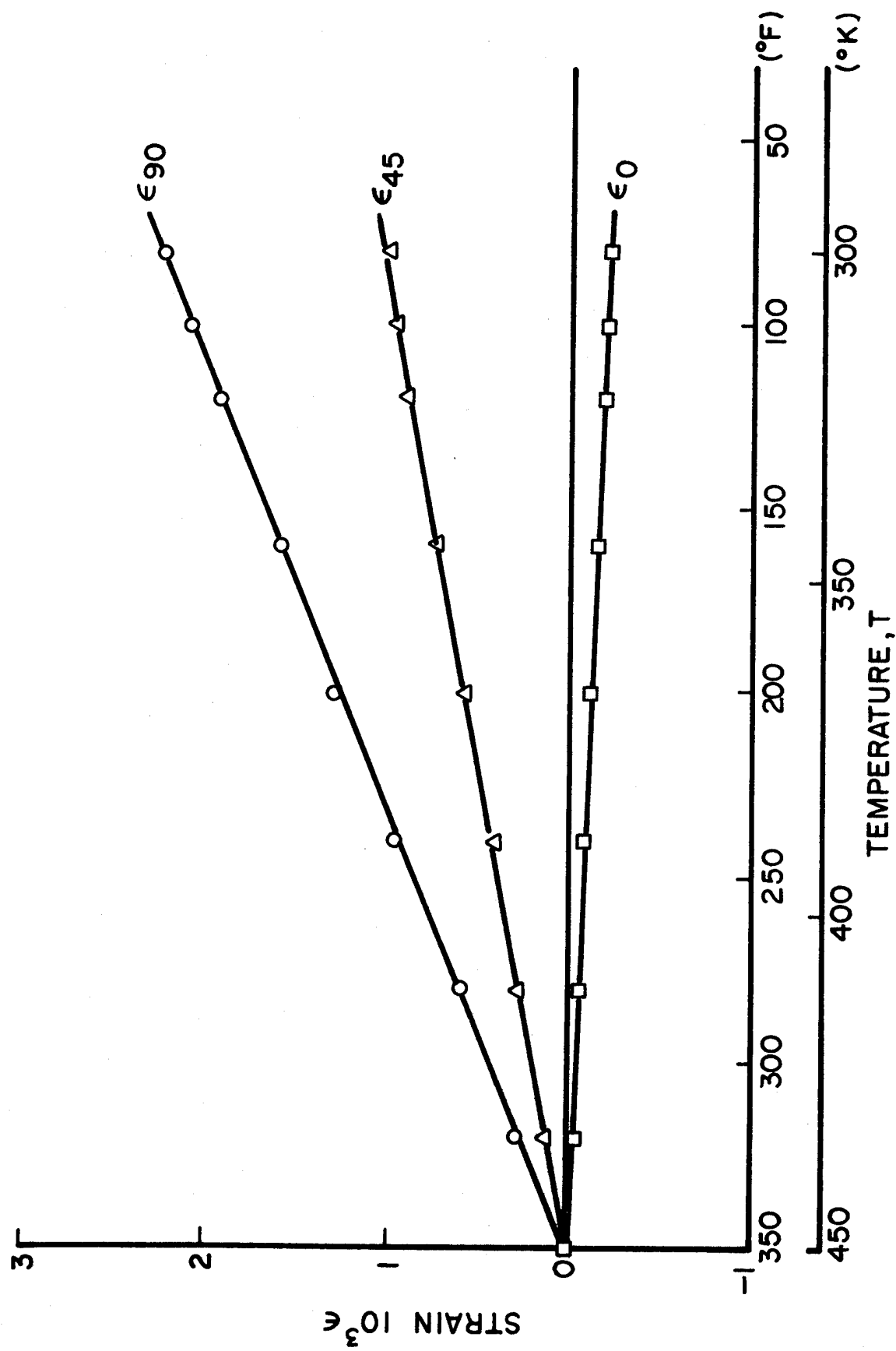
Fig. 3-43 RESIDUAL STRAINS IN 0-DEGREE PLIES OF $\left[0_2/\pm 45\right]_s$ BORON/EPOXY SPECIMEN
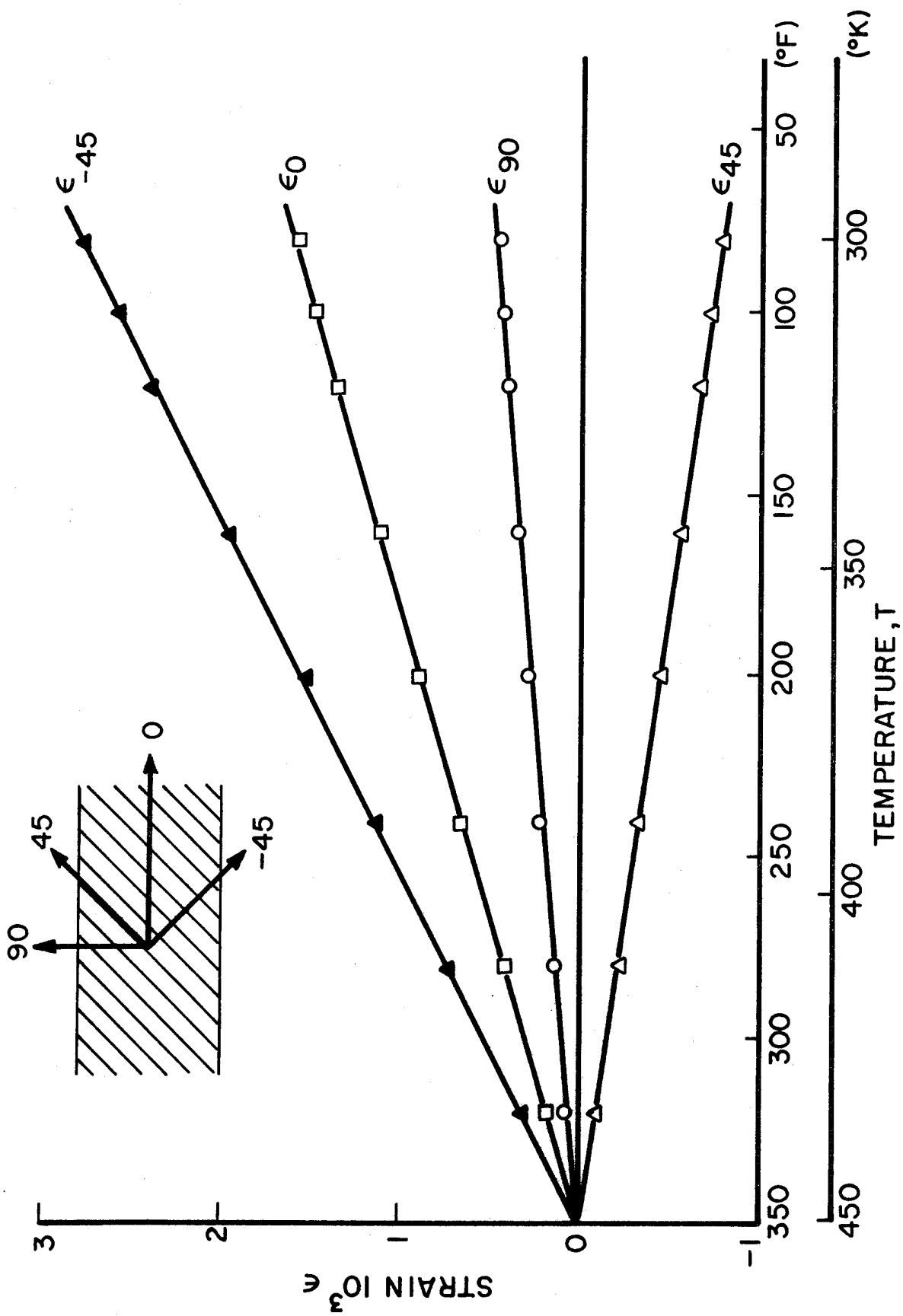
Fig. 3-44 RESIDUAL STRAINS IN 45-DEGREE PLIES OF $\left[0_2/\underline{+}45\right]_s$ BORON/EPOXY SPECIMEN
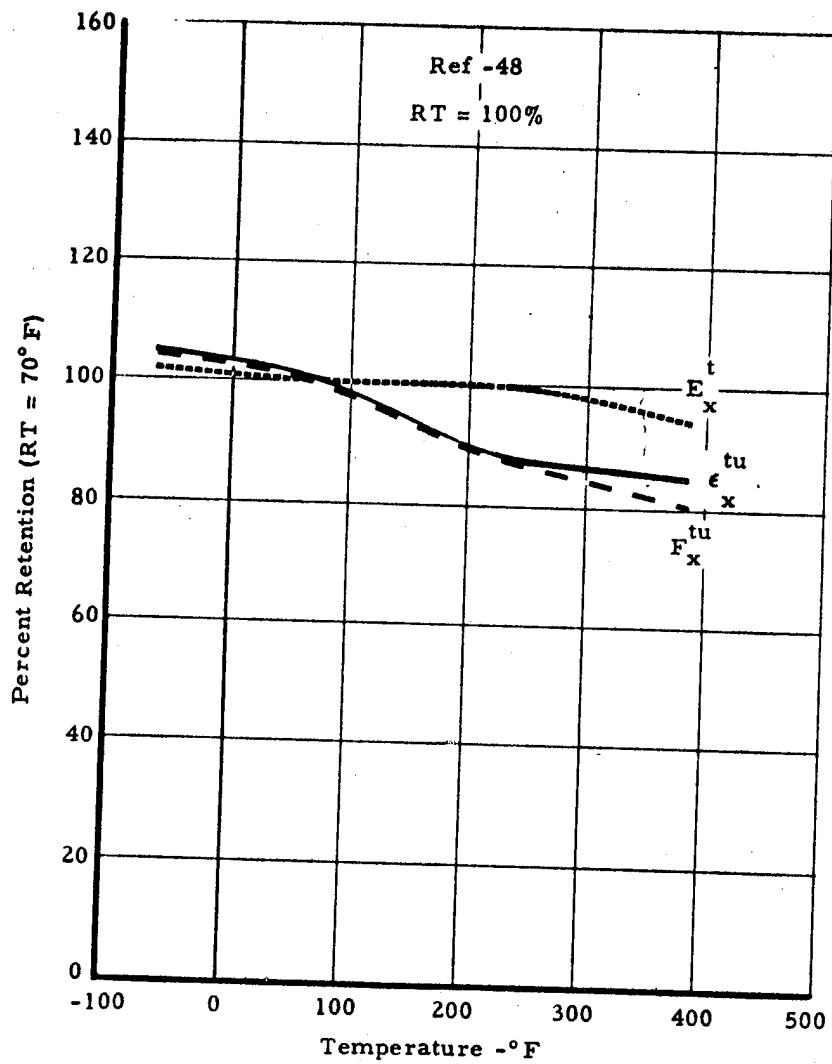
Fig. 3-45 TEMPERATURE VARIATION OF LONGITUDINAL
TENSILE PROPERTIES OF UNIDIRECTIONAL
BORON/EPOXY (Refs. 35, 36)
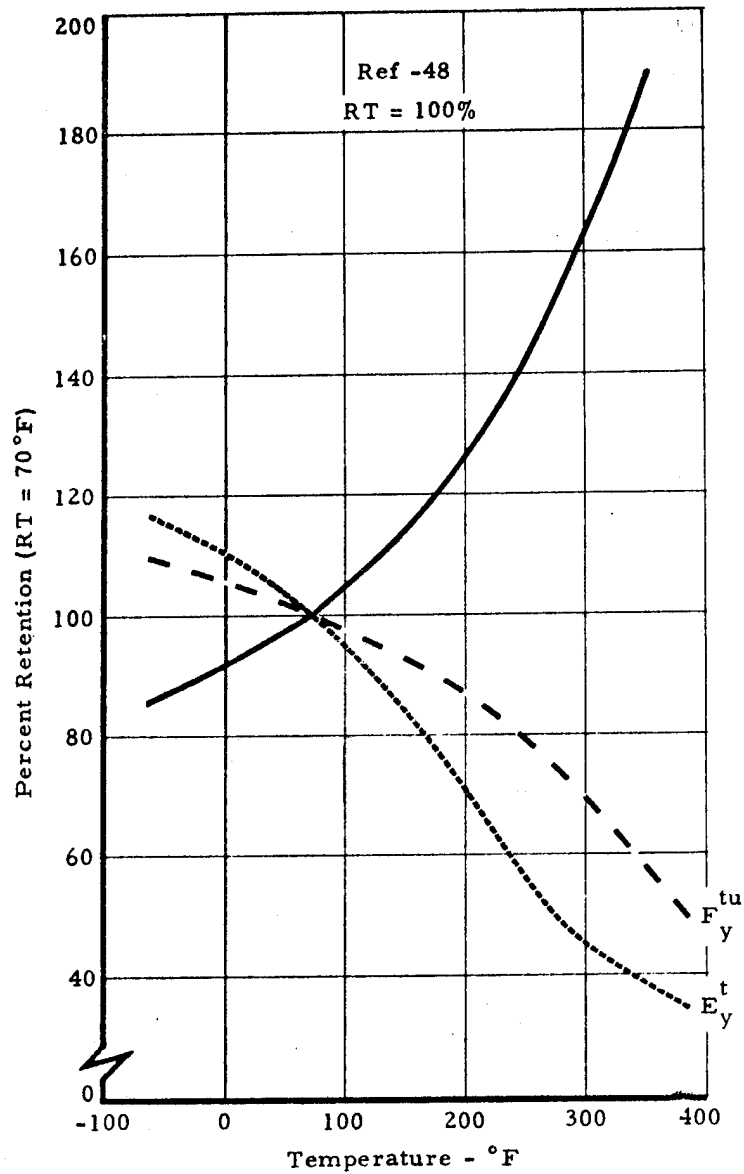
Fig. 3-46 TEMPERATURE VARIATION OF TRANSVERSE
          TENSILE PROPERTIES OF UNIDIRECTIONAL
          BORON/EPOXY (Refs. 35, 36)

3-96
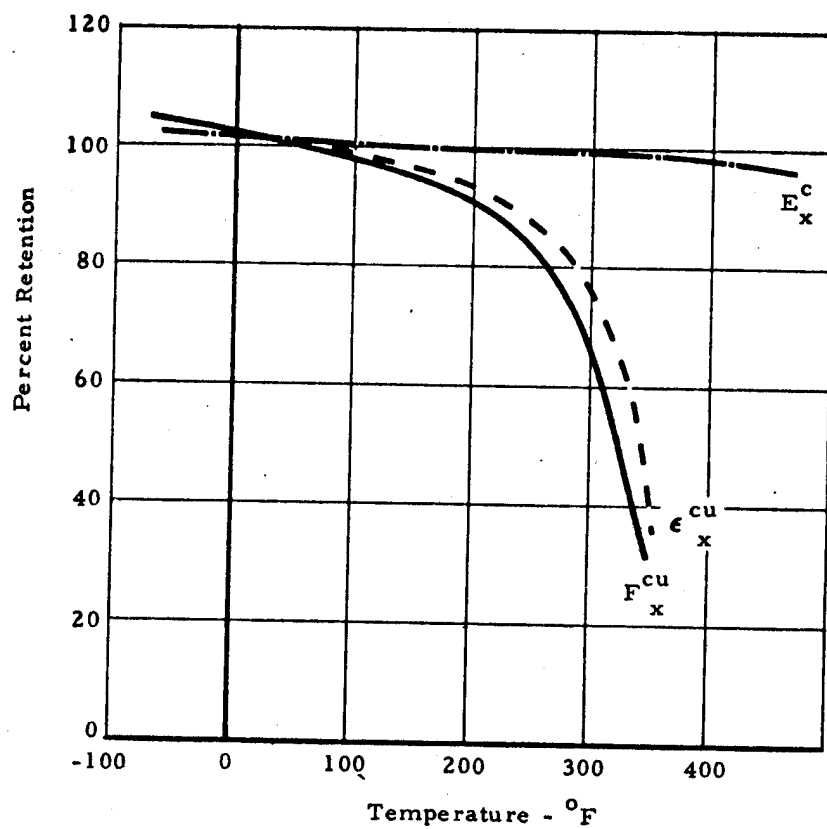
Fig. 3-47   TEMPERATURE VARIATION OF LONGITUDINAL
COMPRESSIVE PROPERTIES OF UNIDIRECTIONAL
BORON/EPOXY   (Refs. 35, 37)
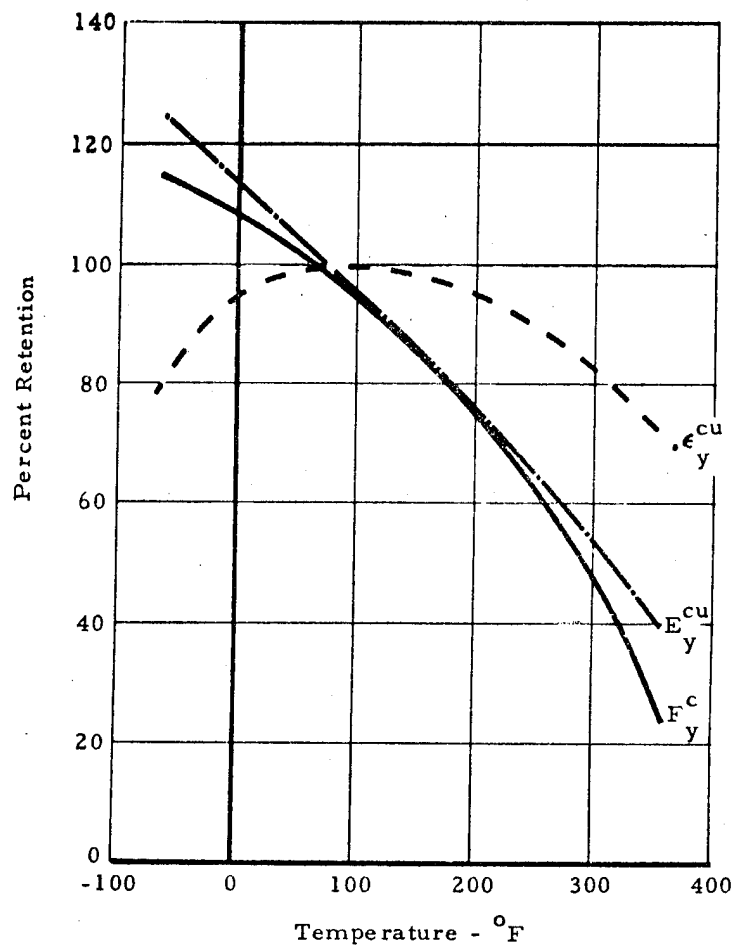
Fig. 3-48   TEMPERATURE VARIATION OF TRANSVERSE COMPRESSIVE
PROPERTIES OF UNIDIRECTIONAL BORON/EPOXY
(Refs. 35, 37)
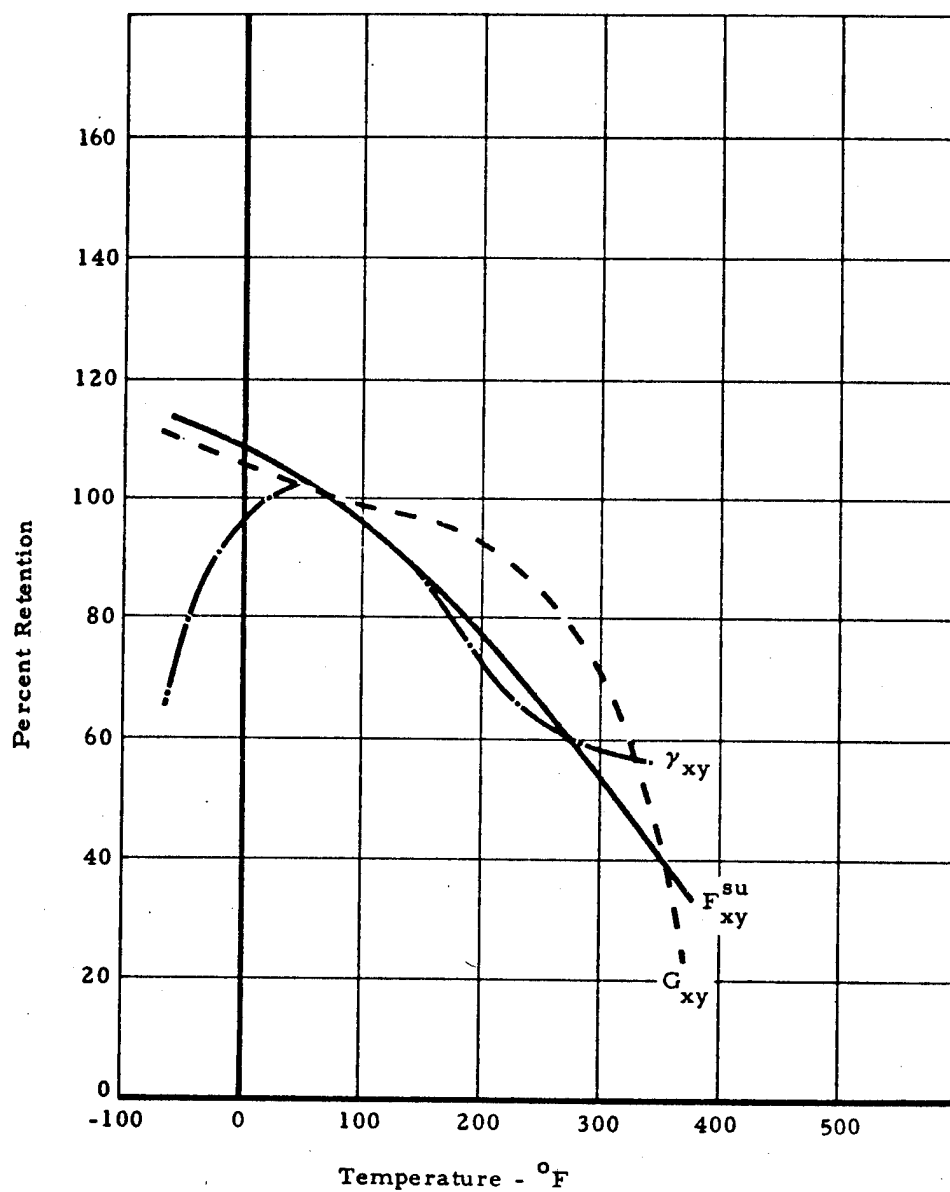
Fig. 3-49   TEMPERATURE VARIATION OF IN-PLANE
SHEAR PROPERTIES OF UNIDIRECTIONAL
BORON/EPOXY   (Refs. 35, 37).
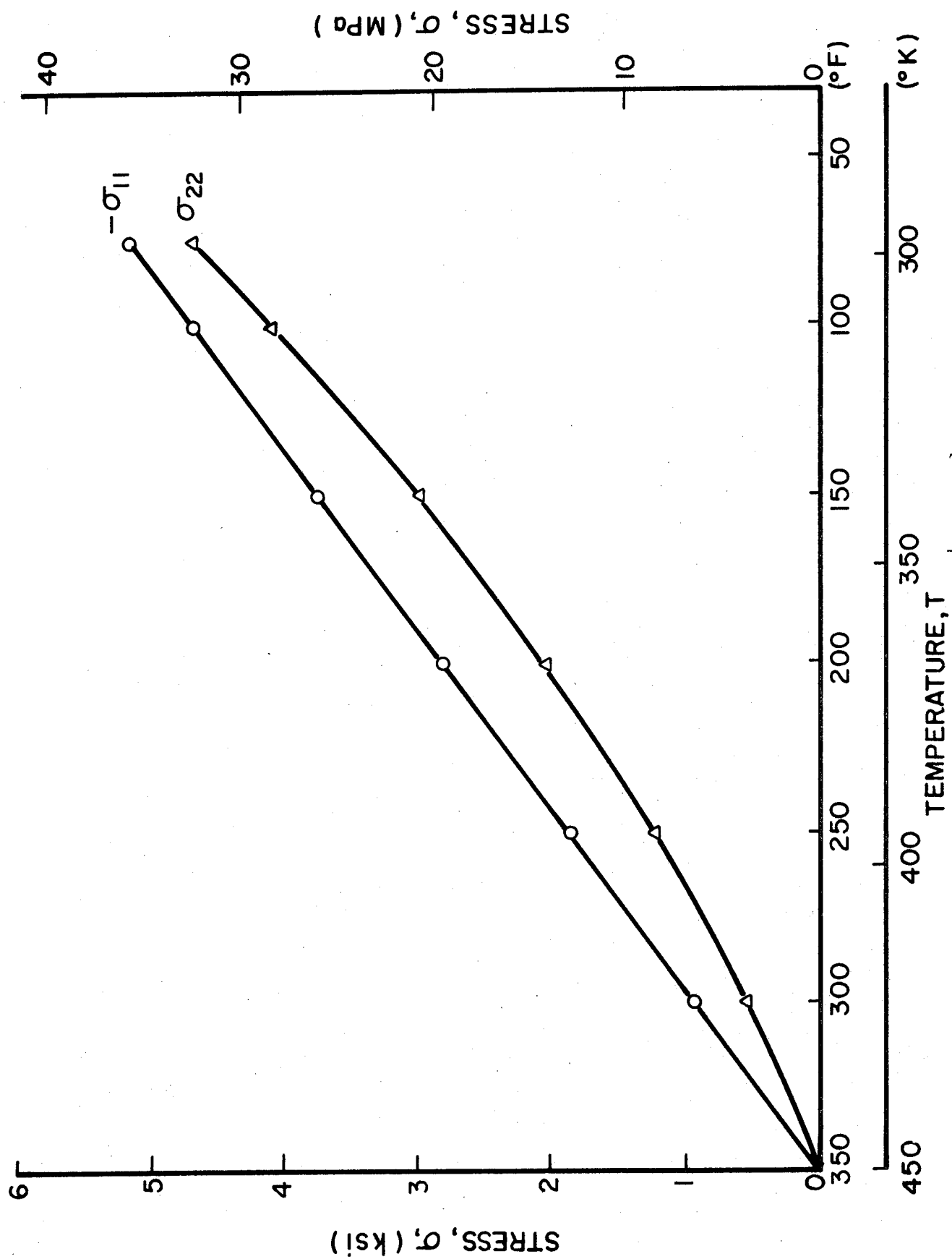
Fig. 3-50 RESIDUAL STRESSES IN 0-DEGREE PLIES OF $\left[0_2/\underline{+45}\right]_s$ BORON/EPOXY SPECIMEN
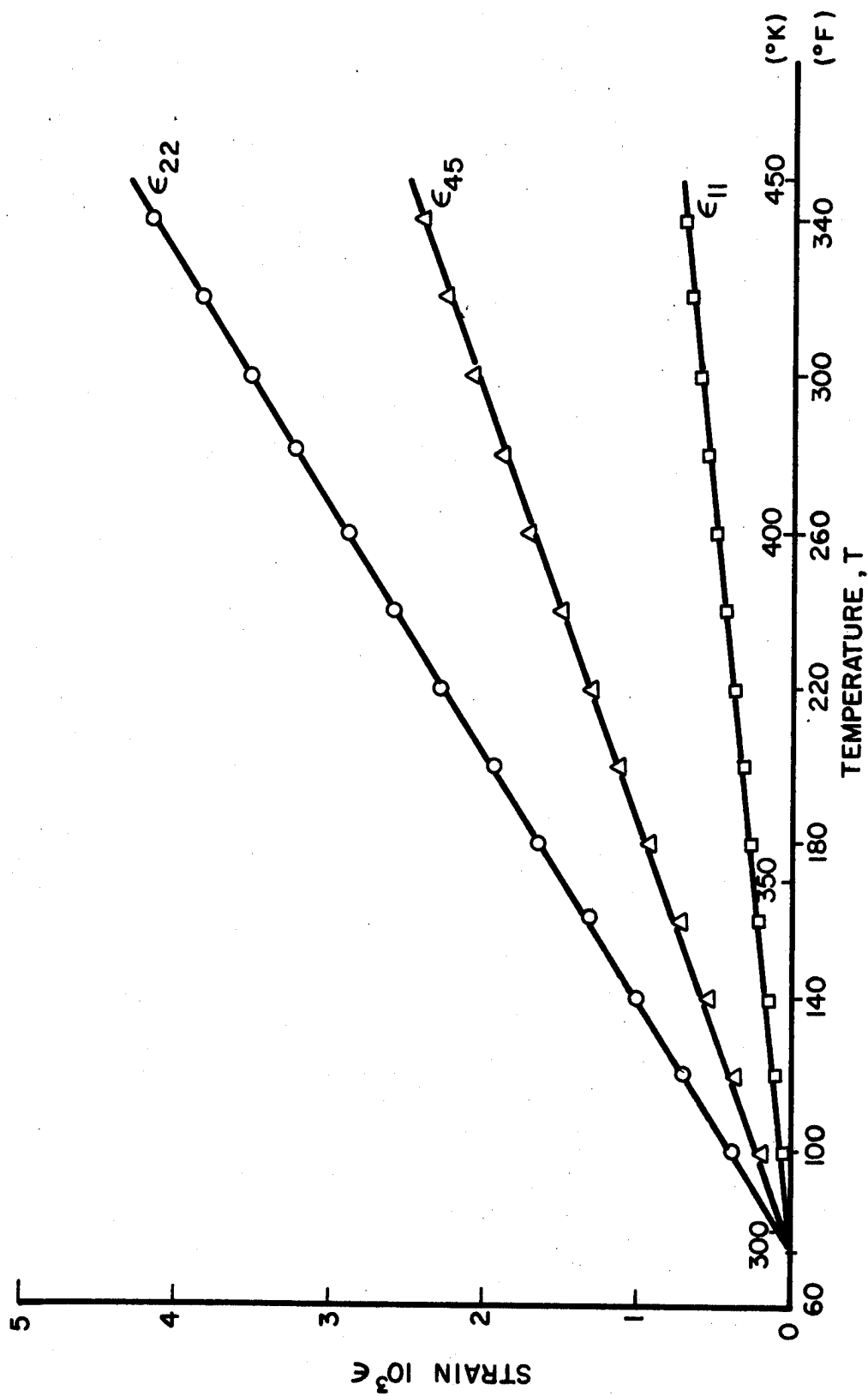
Fig. 3-51 STRAINS IN 0_8 BORON/POLYIMIDE SPECIMEN DURING CURING (Decreasing Temperature)
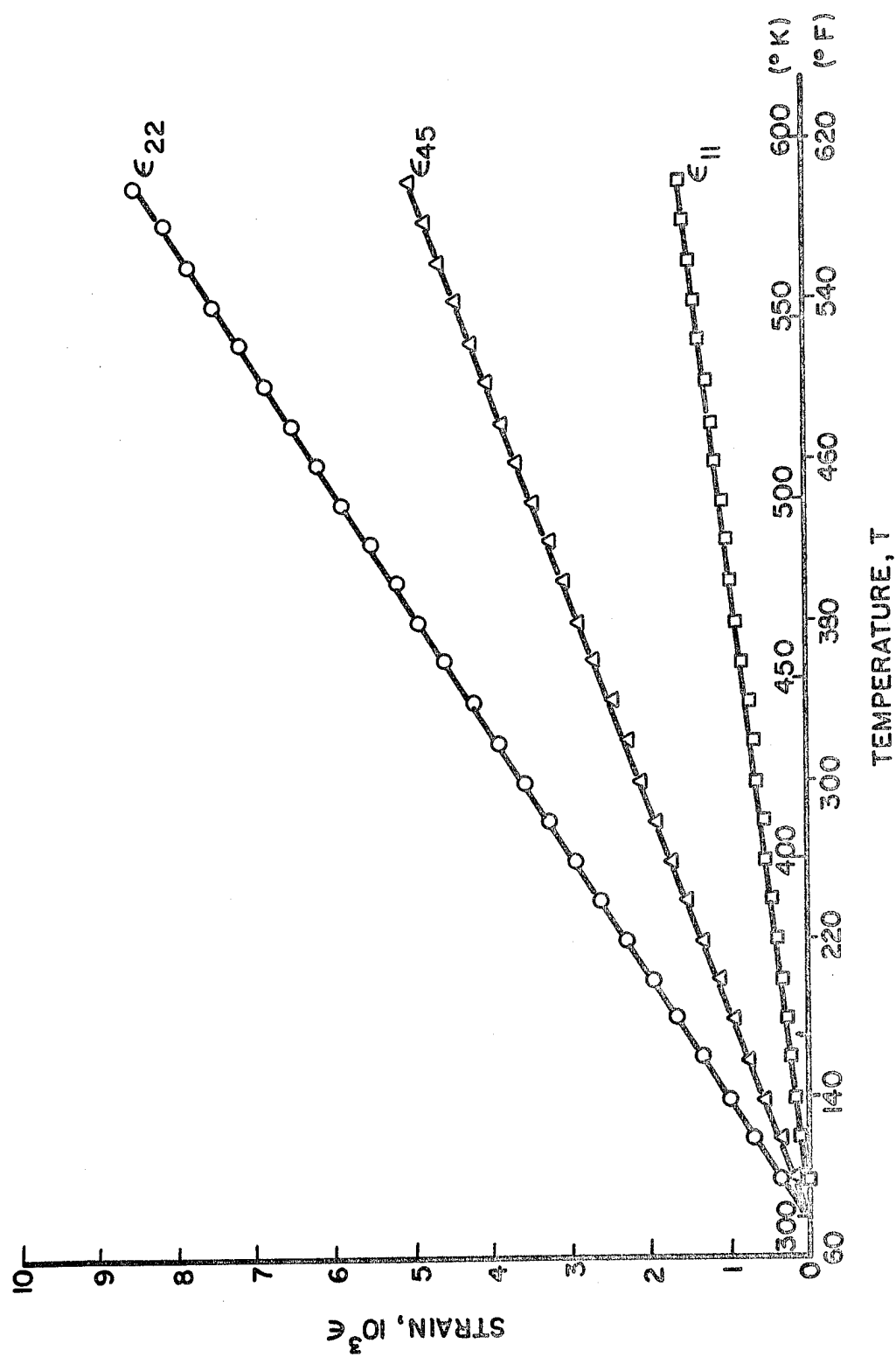
Fig. 3-52 STRAINS IN $[0_8]$ BORON/POLYIMIDE SPECIMEN DURING POSTCURING
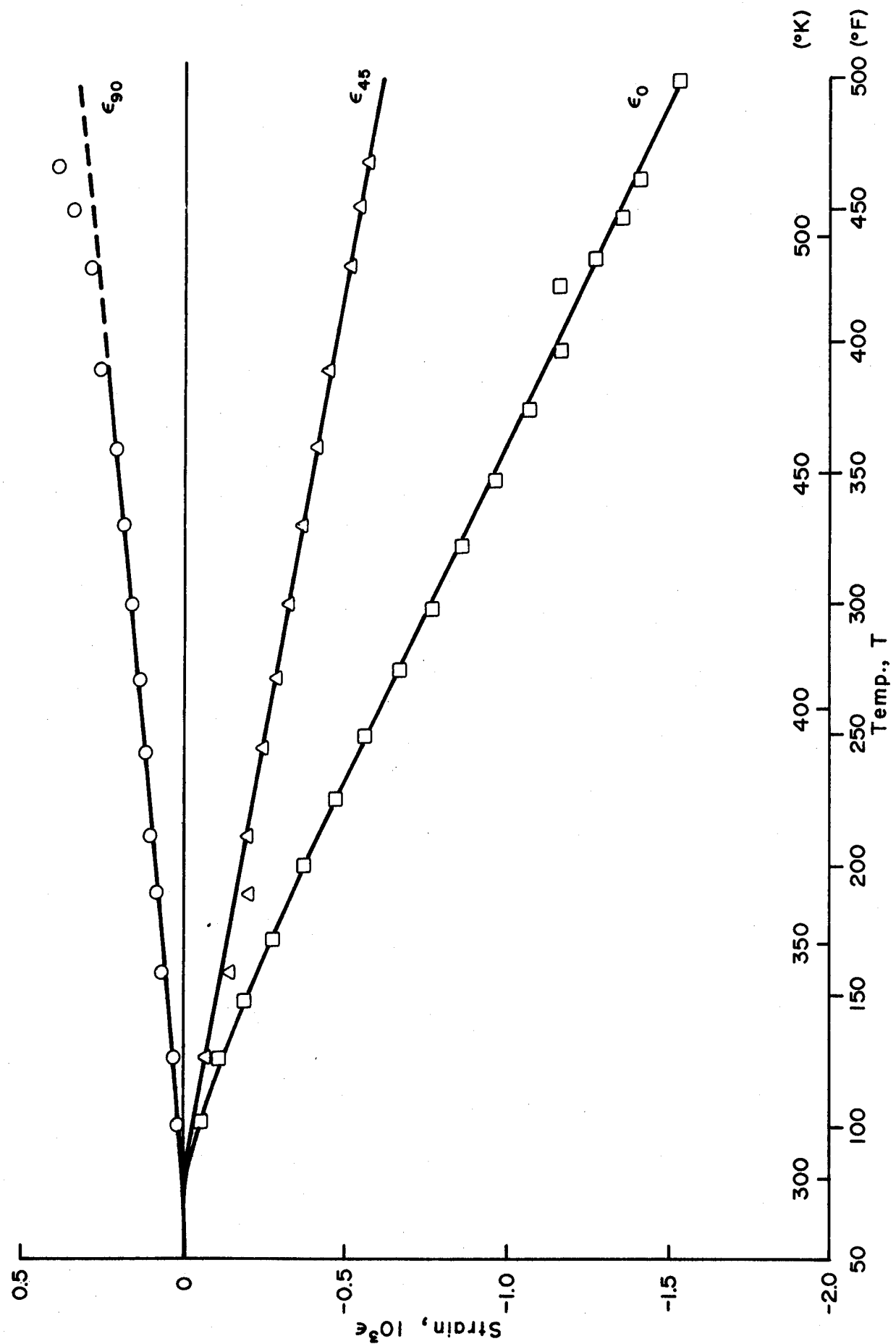
Fig. 3-53 APPARENT STRAINS DURING THERMAL CYCLING IN $\left[0_2/\pm45\right]_s$ BORON/POLYIMIDE SPECIMEN

3-103
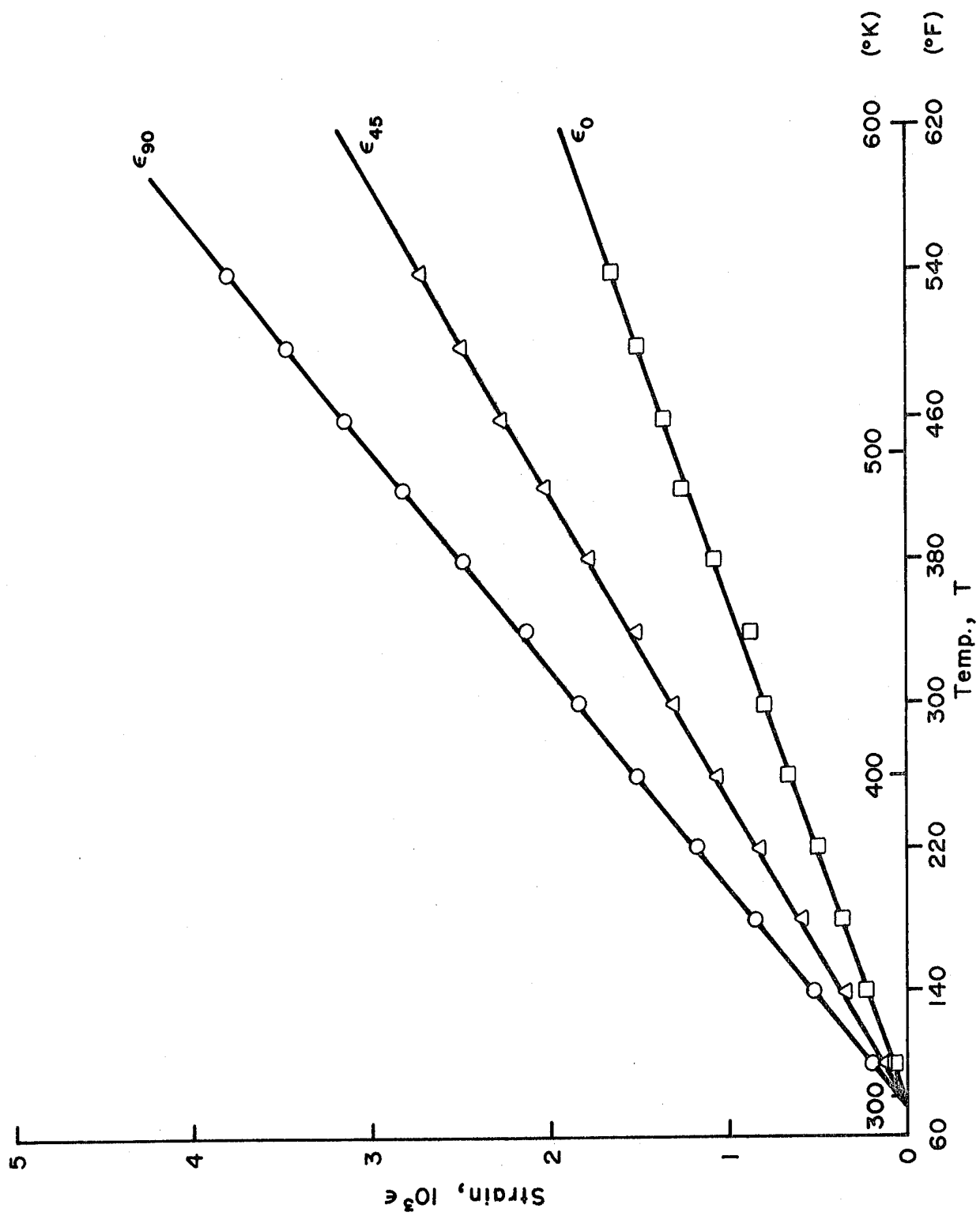
Fig. 3-54 STRAINS IN $\left[0_2/\pm 45\right]_s$ BORON/POLYIMIDE SPECIMEN
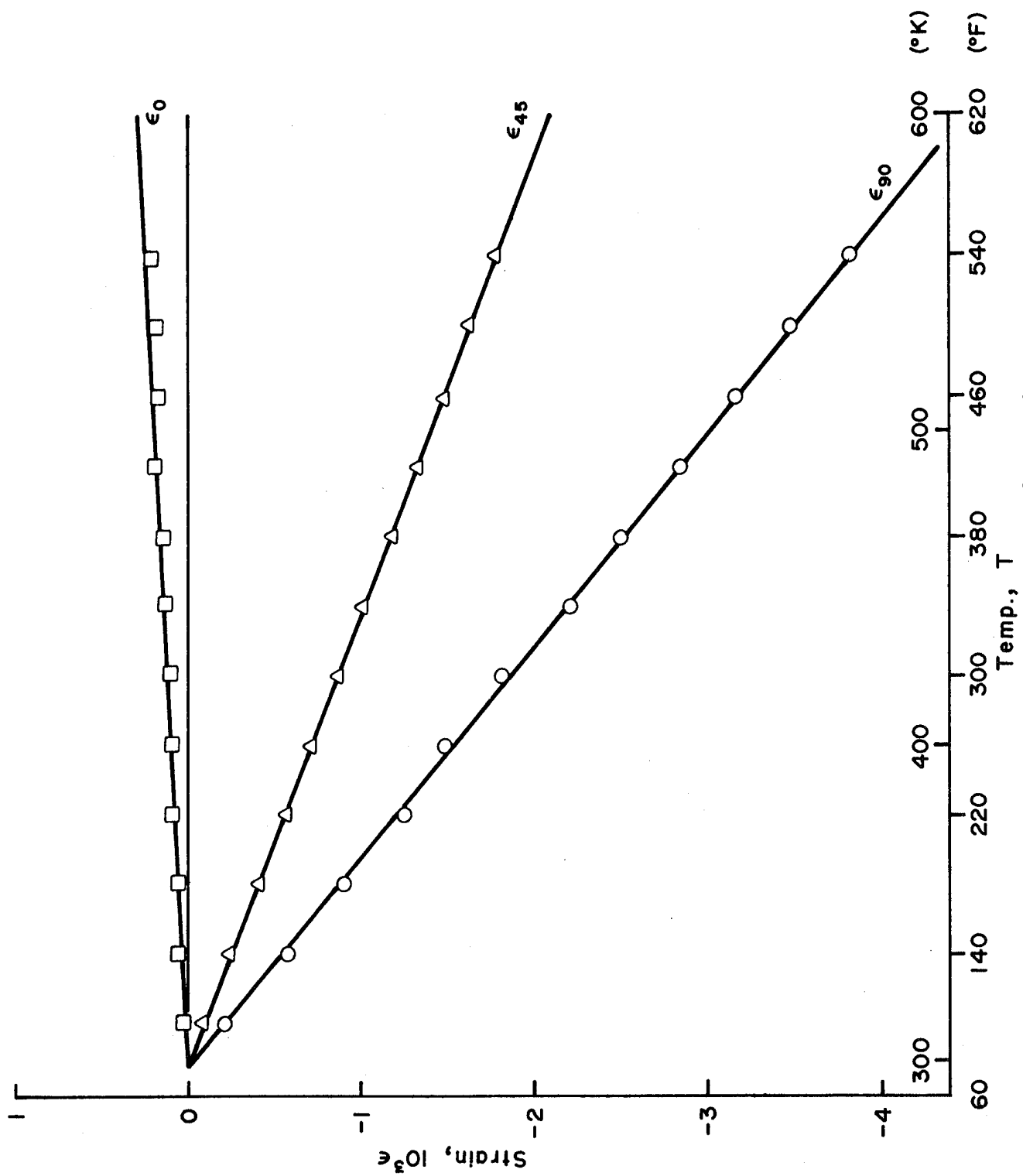
Fig. -55 RESTRAINT STRAINS IN 0-DEGREE PLIES OF $[0_2/\pm45]_s$ BORON/POLYIMIDE SPECIMEN
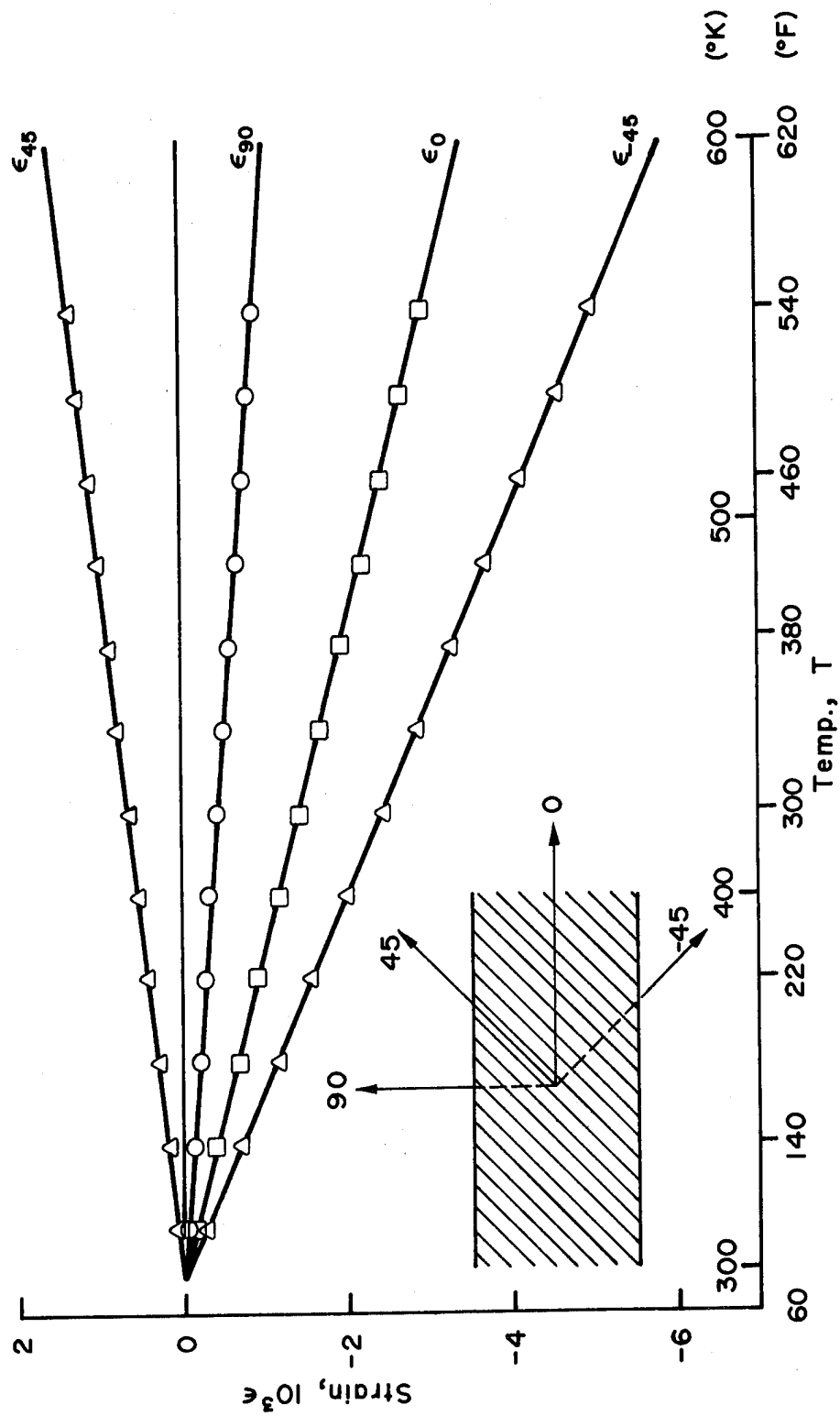
Fig. 3-56 RESTRAINT STRAINS IN 45-DEGREE PLIES OF $[0_2/\pm45]_s$ BORON/
POLYIMIDE SPECIMEN

3-106

Fig. 3-57 STRAINS IN $[0_8]$ GRAPHITE/LOW MODULUS EPOXY SPECIMEN DURING CURING (Decreasing Temperature)
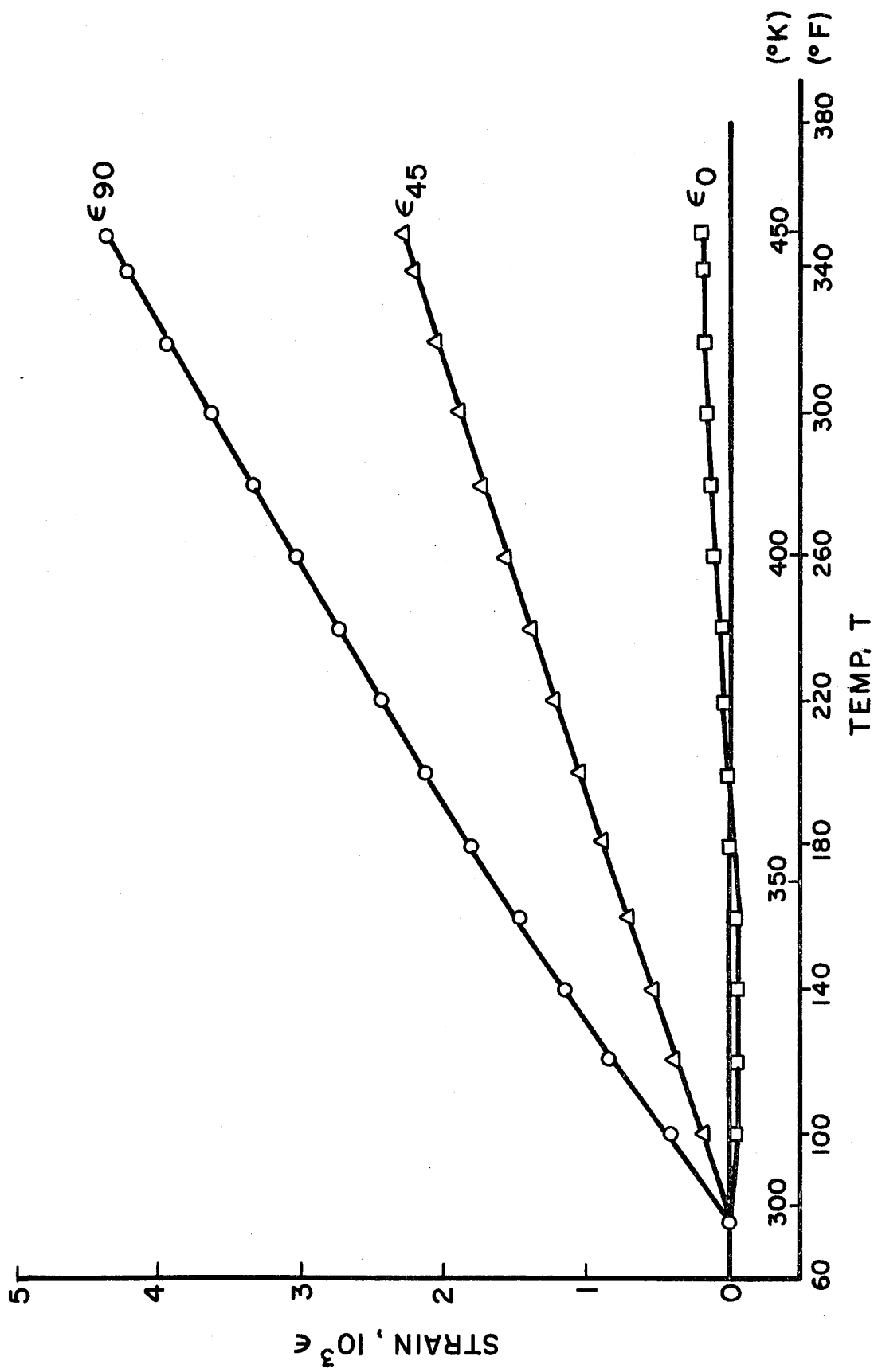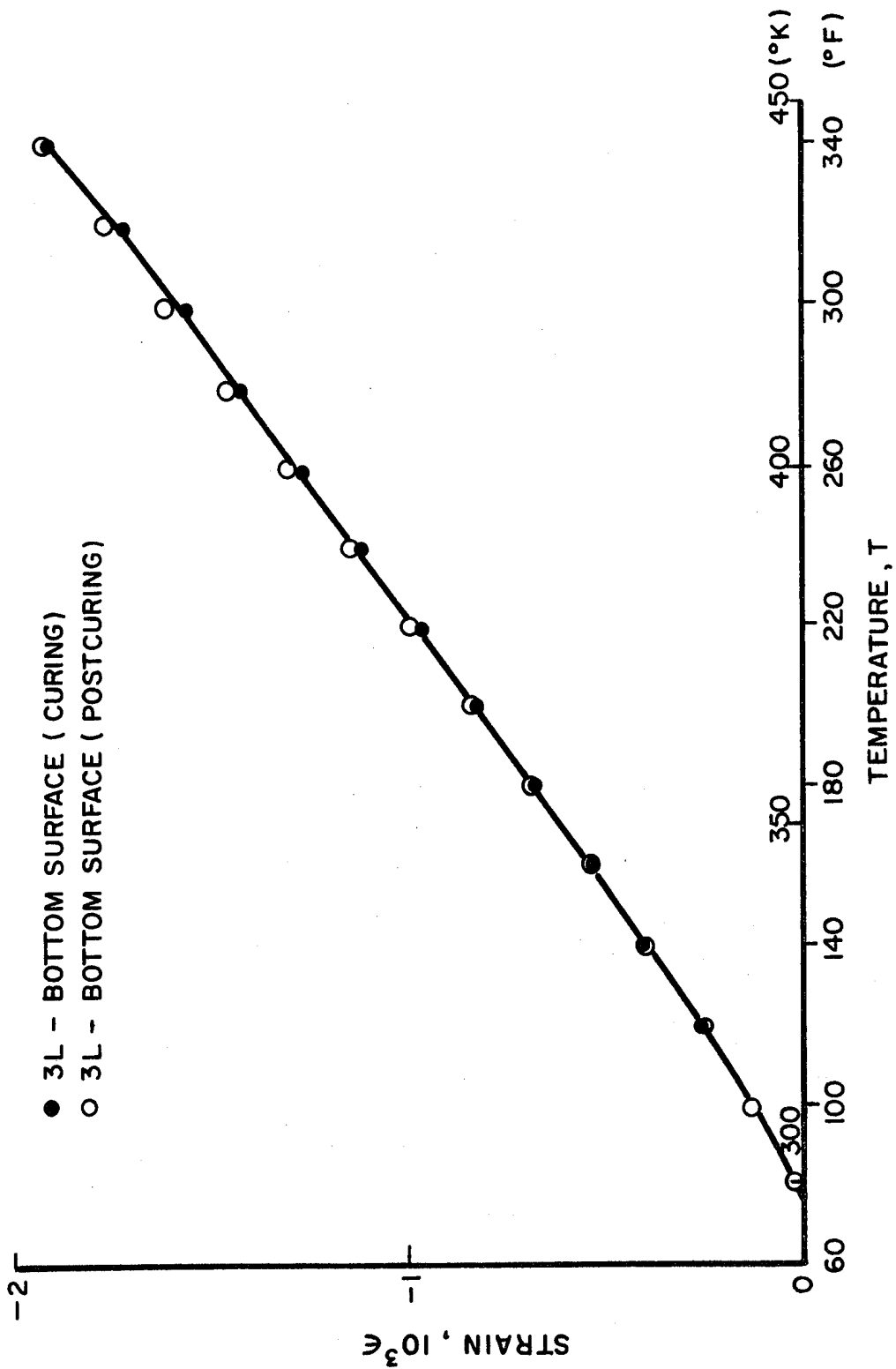
Fig. 3-58   APPARENT LONGITUDINAL STRAINS IN $[0_8]$ UNIDIRECTIONAL GRAPHITE/HIGH MODULUS EPOXY SPECIMEN

3-108
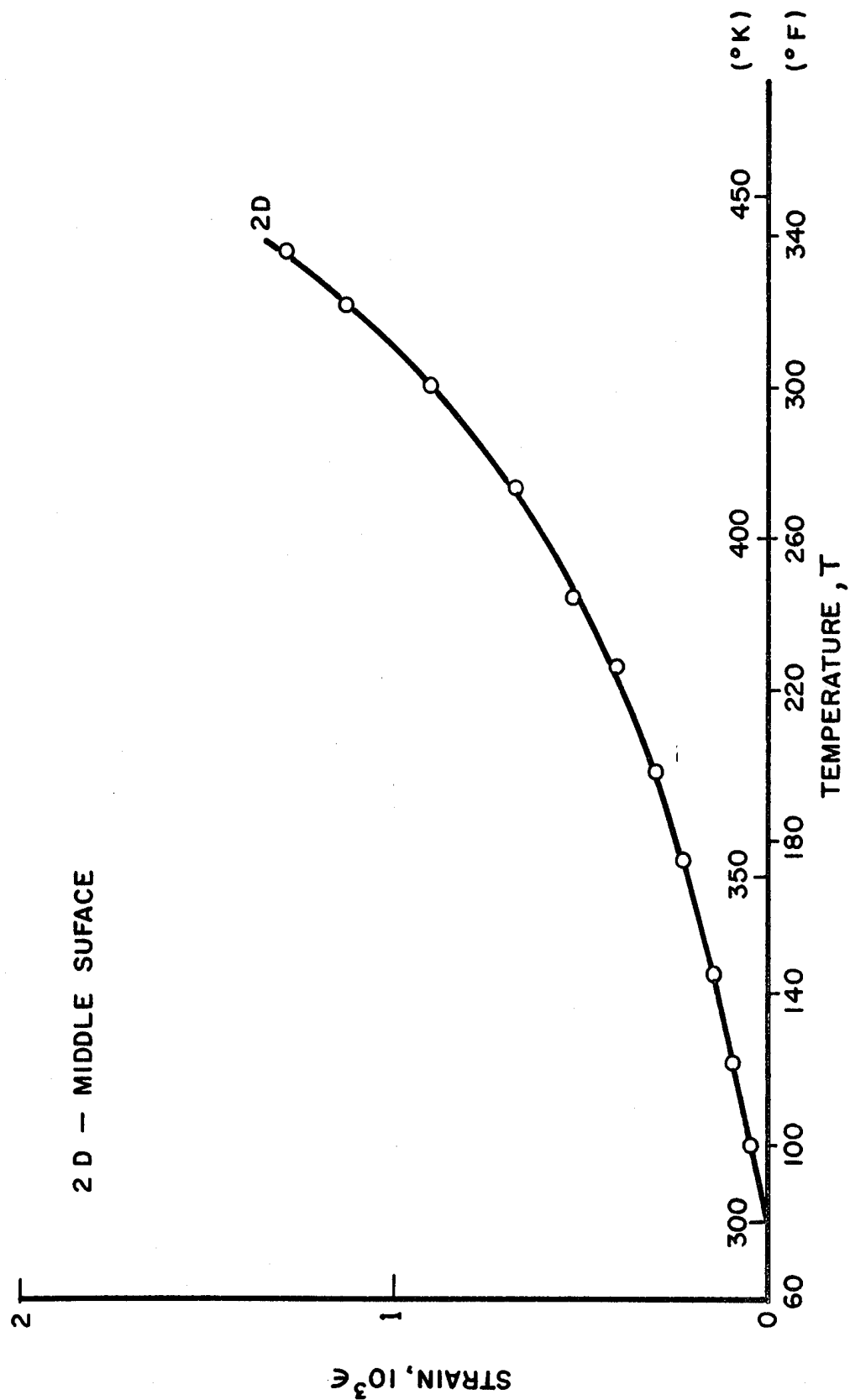
Fig. 3-59 APPARENT 45-DEGREE STRAIN IN $[0_8]$ UNIDIRECTIONAL GRAPHITE/HIGH MODULUS EPOXY SPECIMEN (Postcuring)

3-109
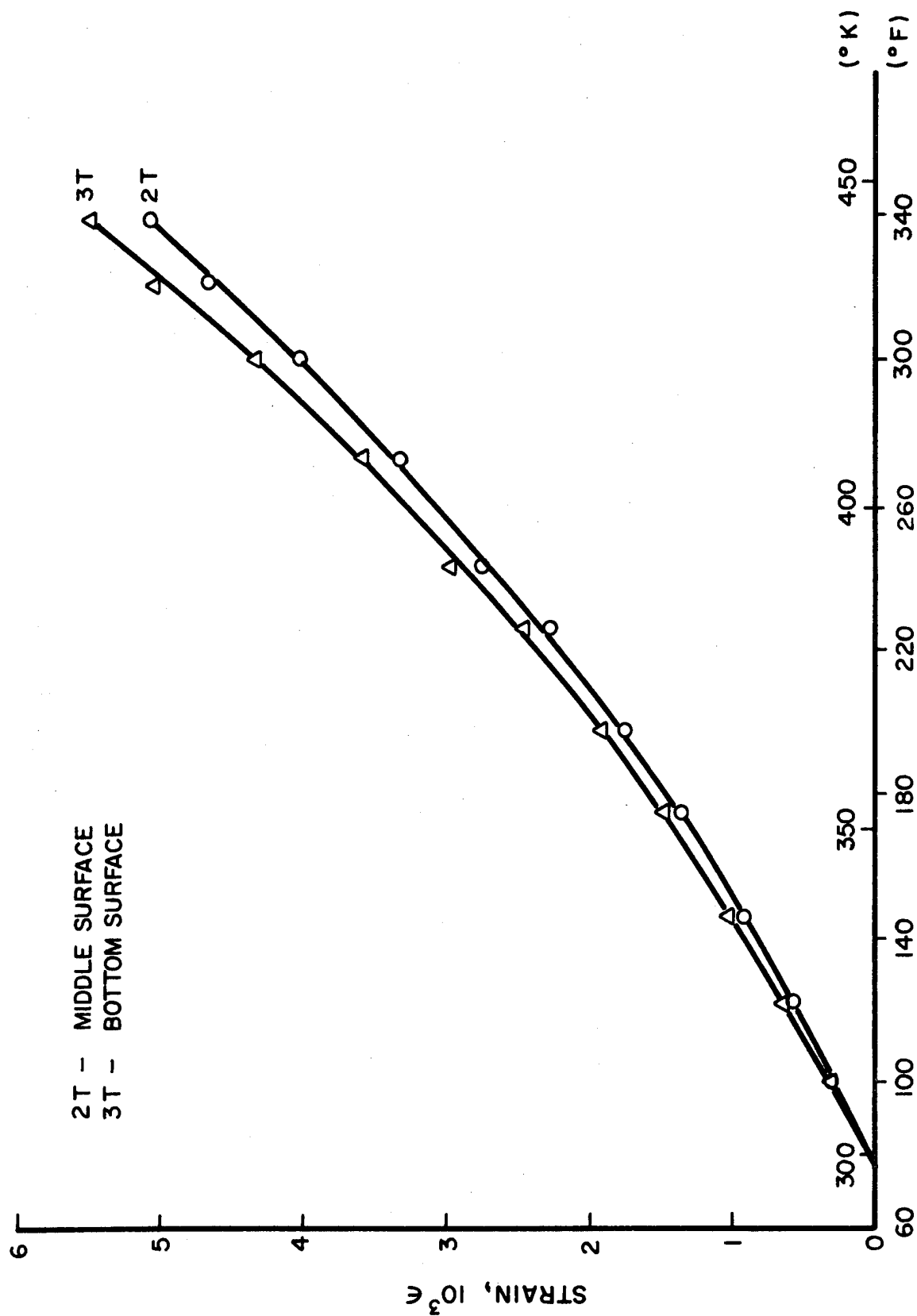
Fig. 3-60 APPARENT TRANSVERSE STRAINS IN 0_8 UNIDIRECTIONAL GRAPHITE/HIGH
MODULUS EPOXY SPECIMEN (Postcuring)
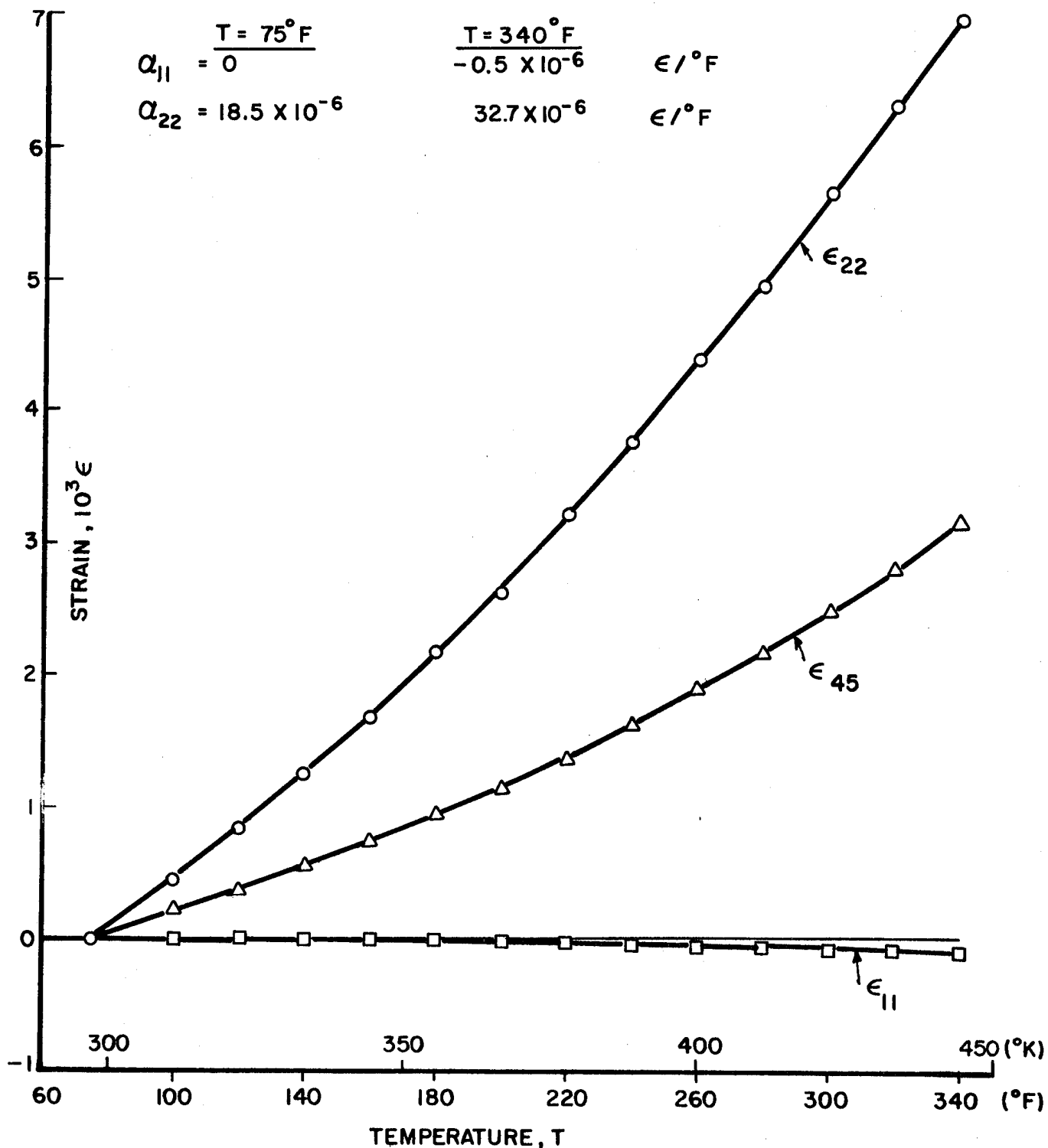
Fig. 3-61 THERMAL STRAINS IN $[0_8]$ UNIDIRECTIONAL GRAPHITE/
HIGH MODULUS EPOXY

3-111
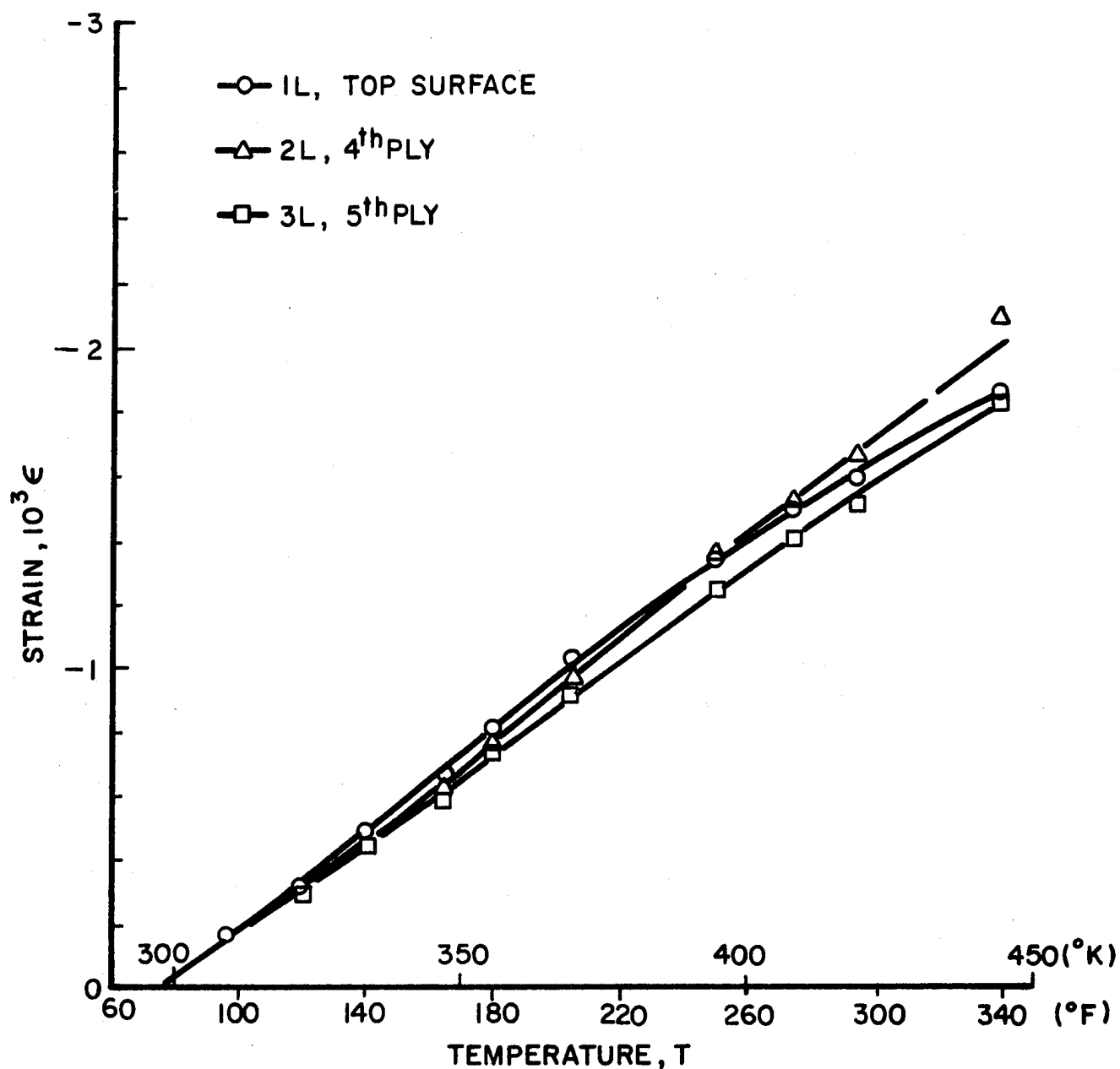
Fig. 3-62 APPARENT LONGITUDINAL STRAINS IN $[0_2/\pm 45]_s$ GRAPHITE/ HIGH MODULUS EPOXY SPECIMEN (Curing Cycle; Decreasing Temperature)
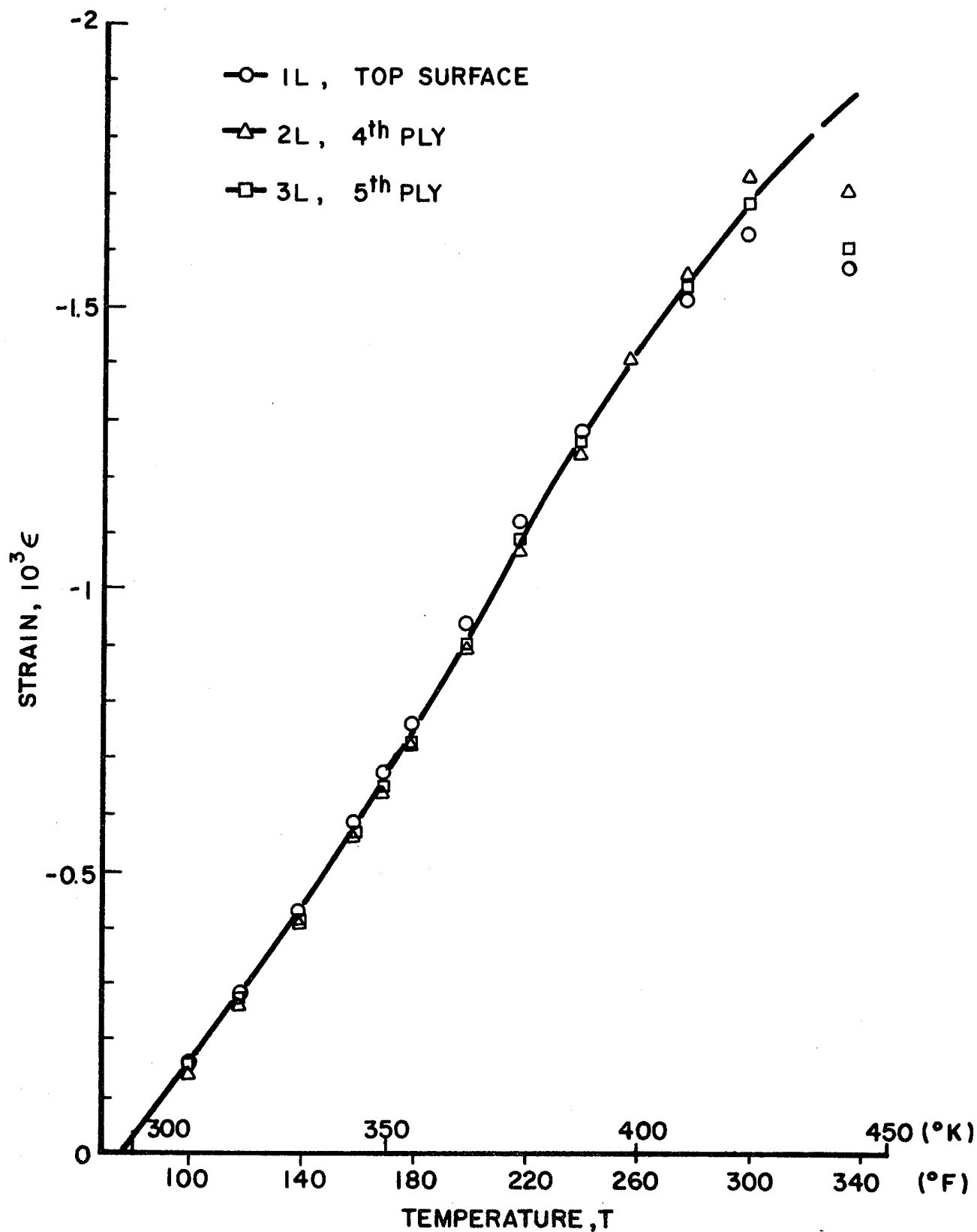
Fig. 3-63 APPARENT LONGITUDINAL STRAINS IN $\left[0_2/\pm45\right]_s$ GRAPHITE/
HIGH MODULUS EPOXY (Postcuring Cycle; Increasing
Temperature)

3-113
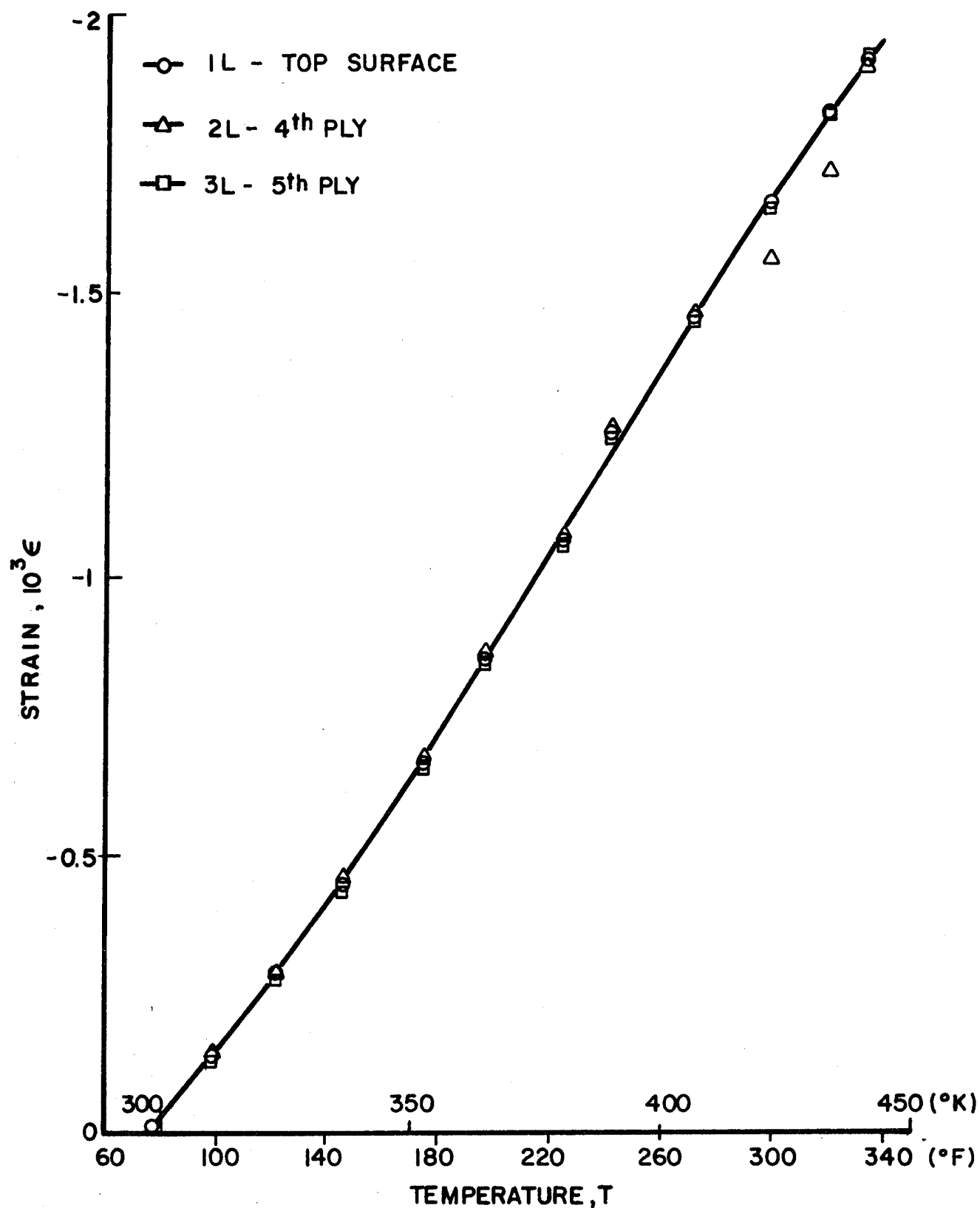
Fig. 3-64 APPARENT LONGITUDINAL STRAINS IN $[0_2/\pm45]_s$ GRAPHITE/HIGH
MODULUS EPOXY SPECIMEN (Postcuring Cycle; Decreasing
Temperature)

3-114
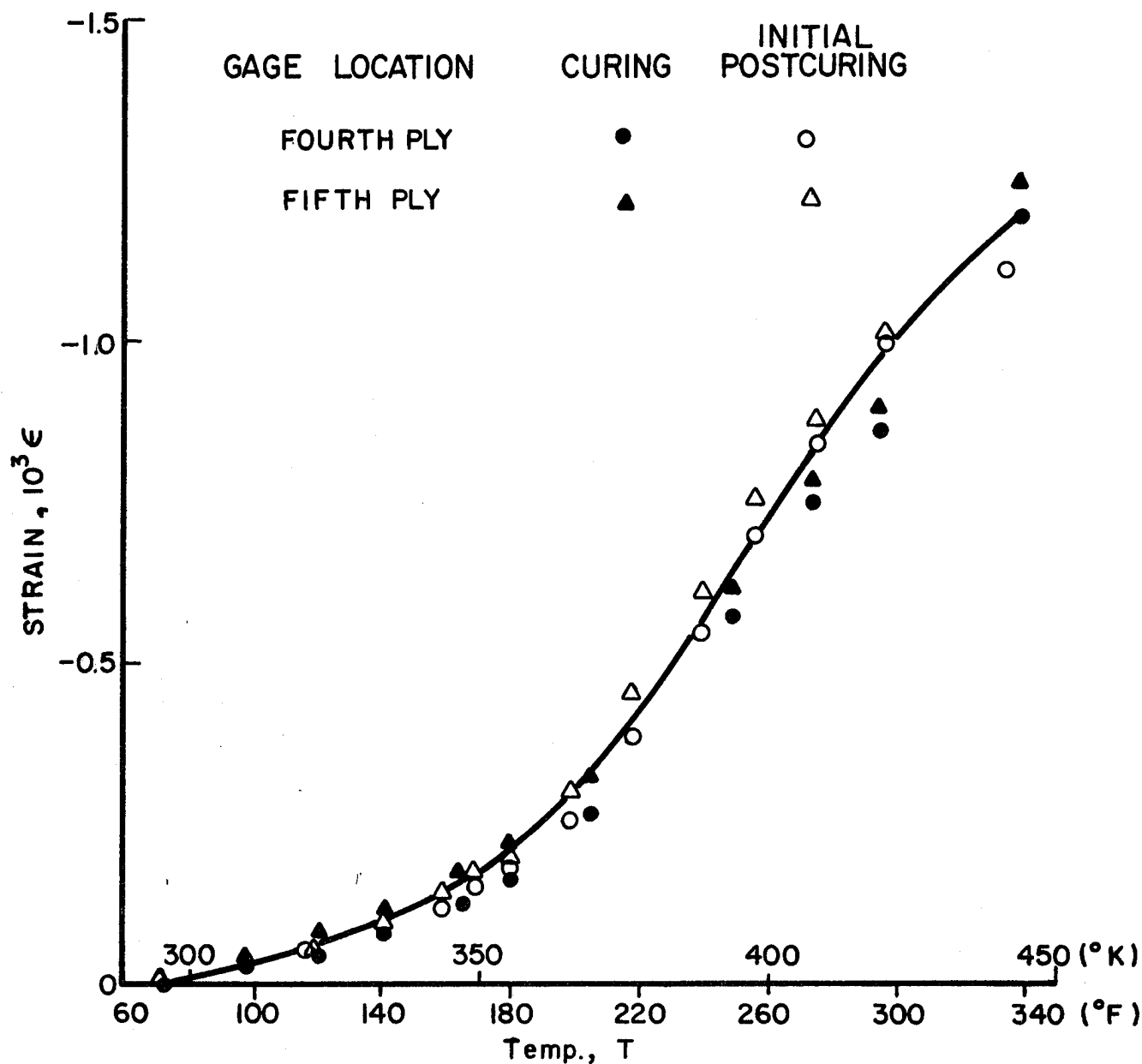
Fig. 3-65   APPARENT TRANSVERSE STRAINS IN $\left[0_2/\pm45\right]_s$ GRAPHITE/
HIGH MODULUS EPOXY SPECIMEN (Curing, Decreasing
Temperature; Postcuring, Increasing Temperature)

3-115
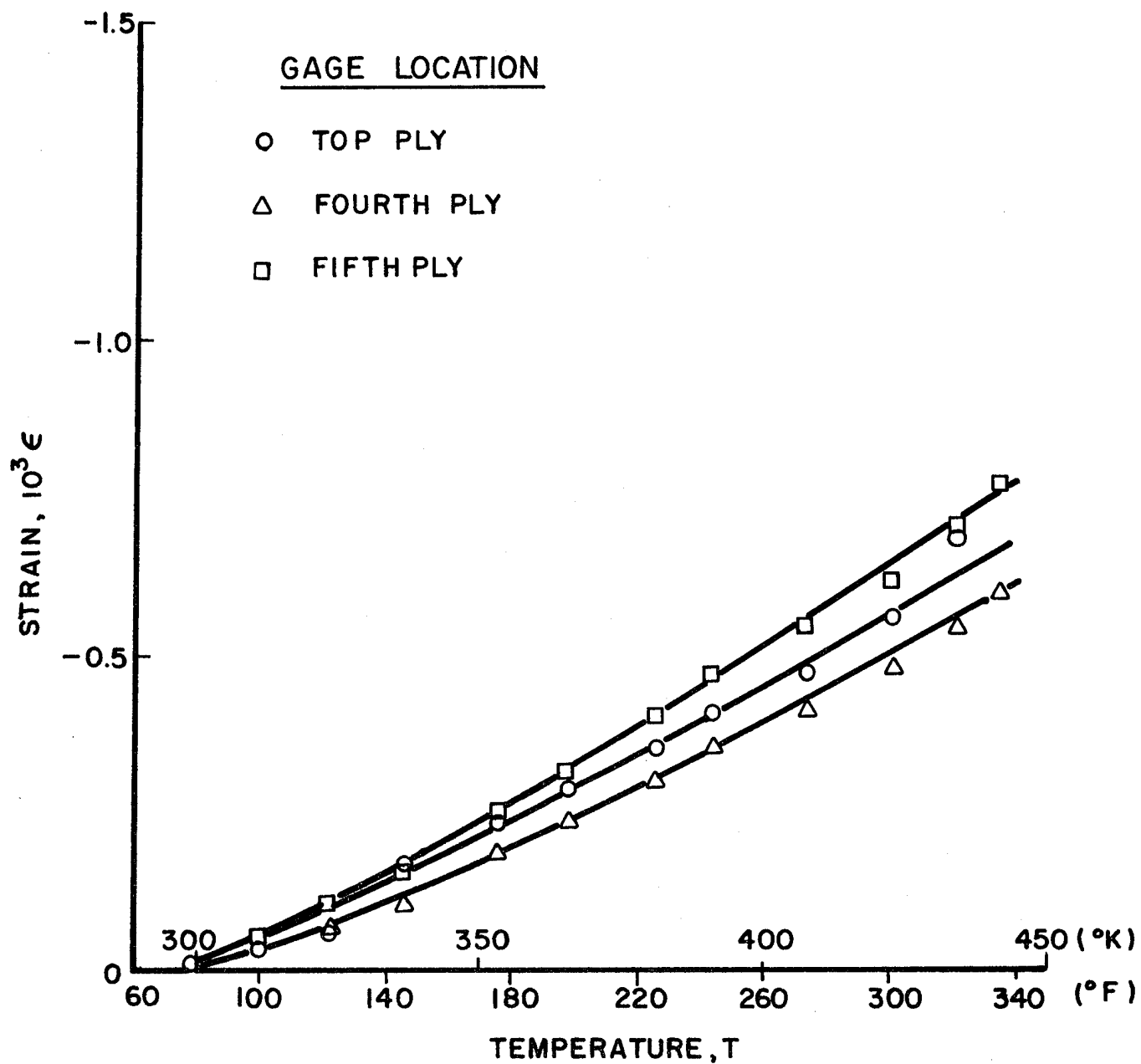
Fig. 3-66   APPARENT TRANSVERSE STRAINS IN $\left[0_2/\pm45\right]_s$ GRAPHITE/ HIGH MODULUS EPOXY SPECIMEN (Postcuring, Decreasing Temperature)
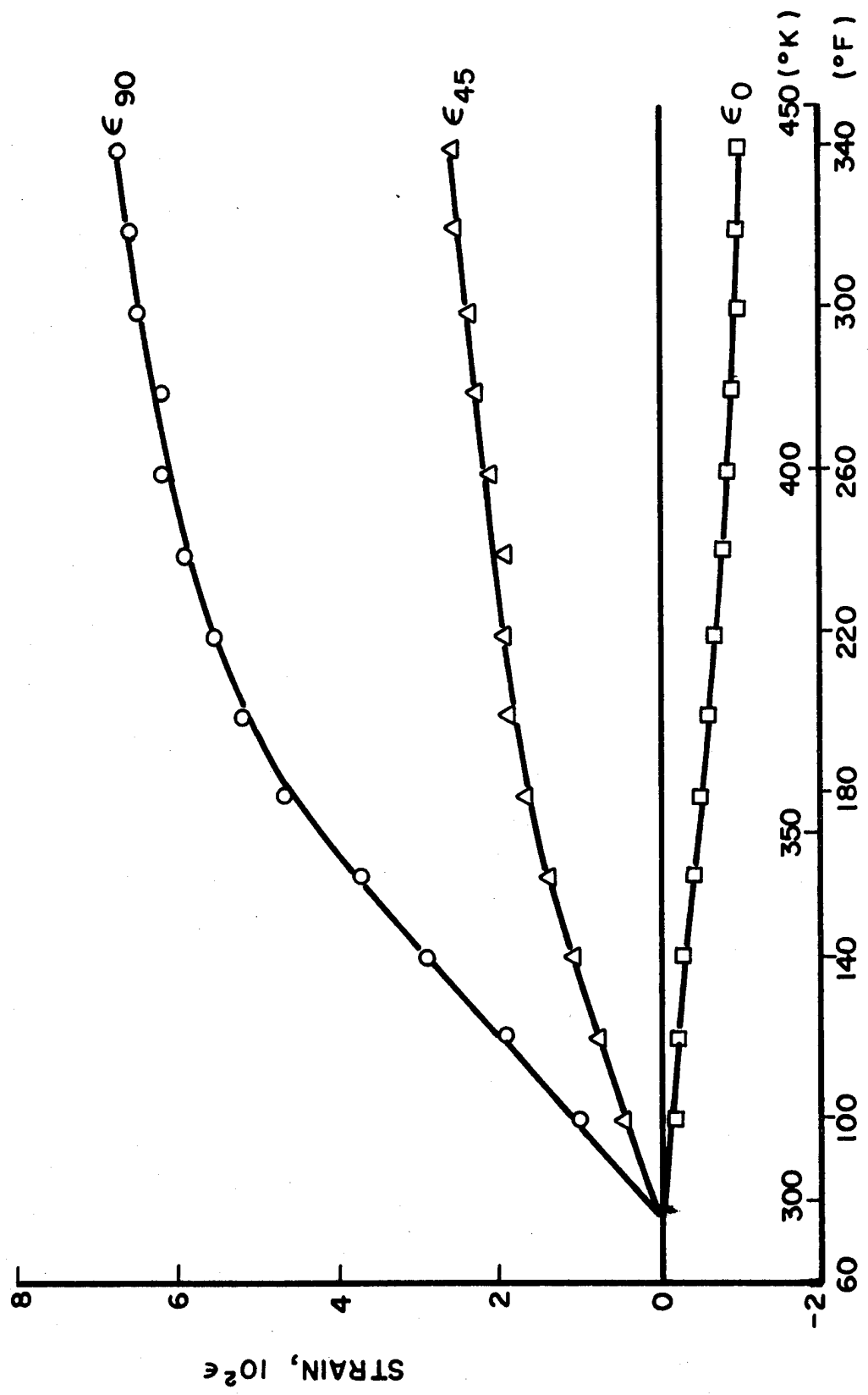
Fig. 3-67 STRAINS IN $\{0_2/\pm 45\}_s$ GRAPHITE/HIGH MODULUS EPOXY SPECIMEN DURING COOLING
STAGE OF CURING AND HEATING STAGE OF POSTCURING

3-117
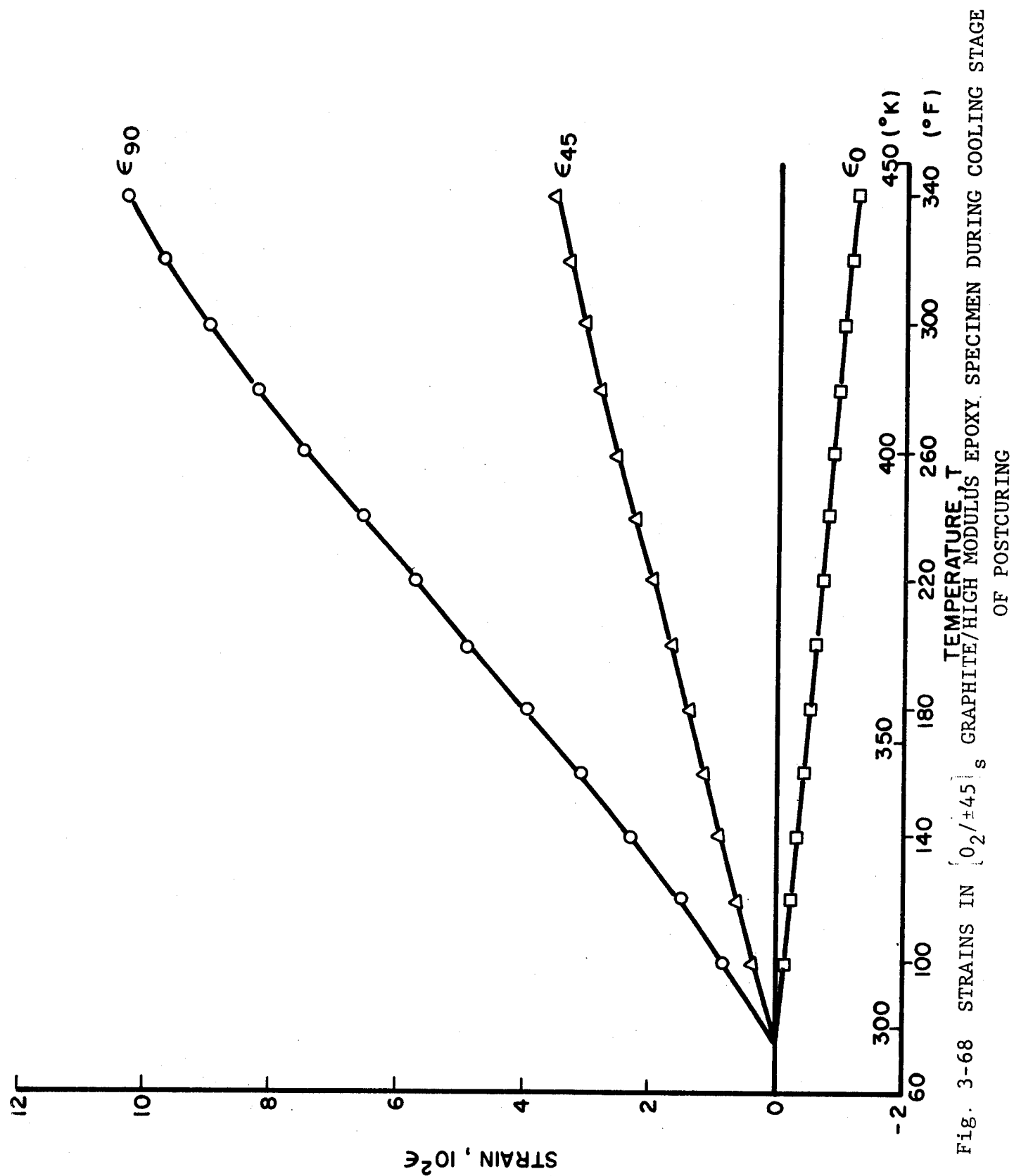
Fig. 3-68 STRAINS IN $[0_2/\pm45]_s$ GRAPHITE/HIGH MODULUS EPOXY SPECIMEN DURING COOLING STAGE OF POSTCURING

3-118
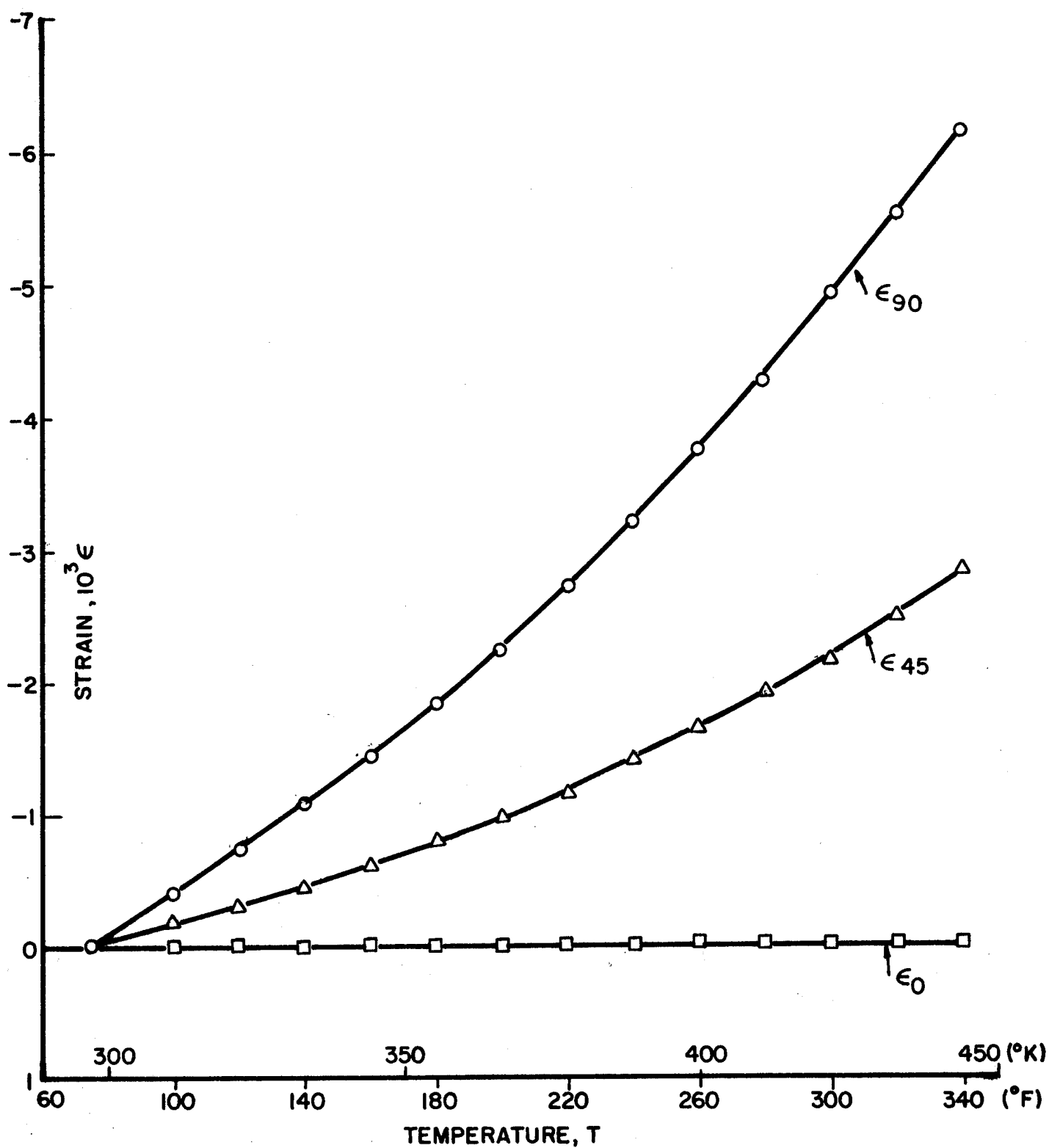
Fig. 3-69   RESTRAINT STRAINS IN 0-DEGREE PLIES OF $[0_2/\pm45]_s$ GRAPHITE/
HIGH MODULUS EPOXY SPECIMEN
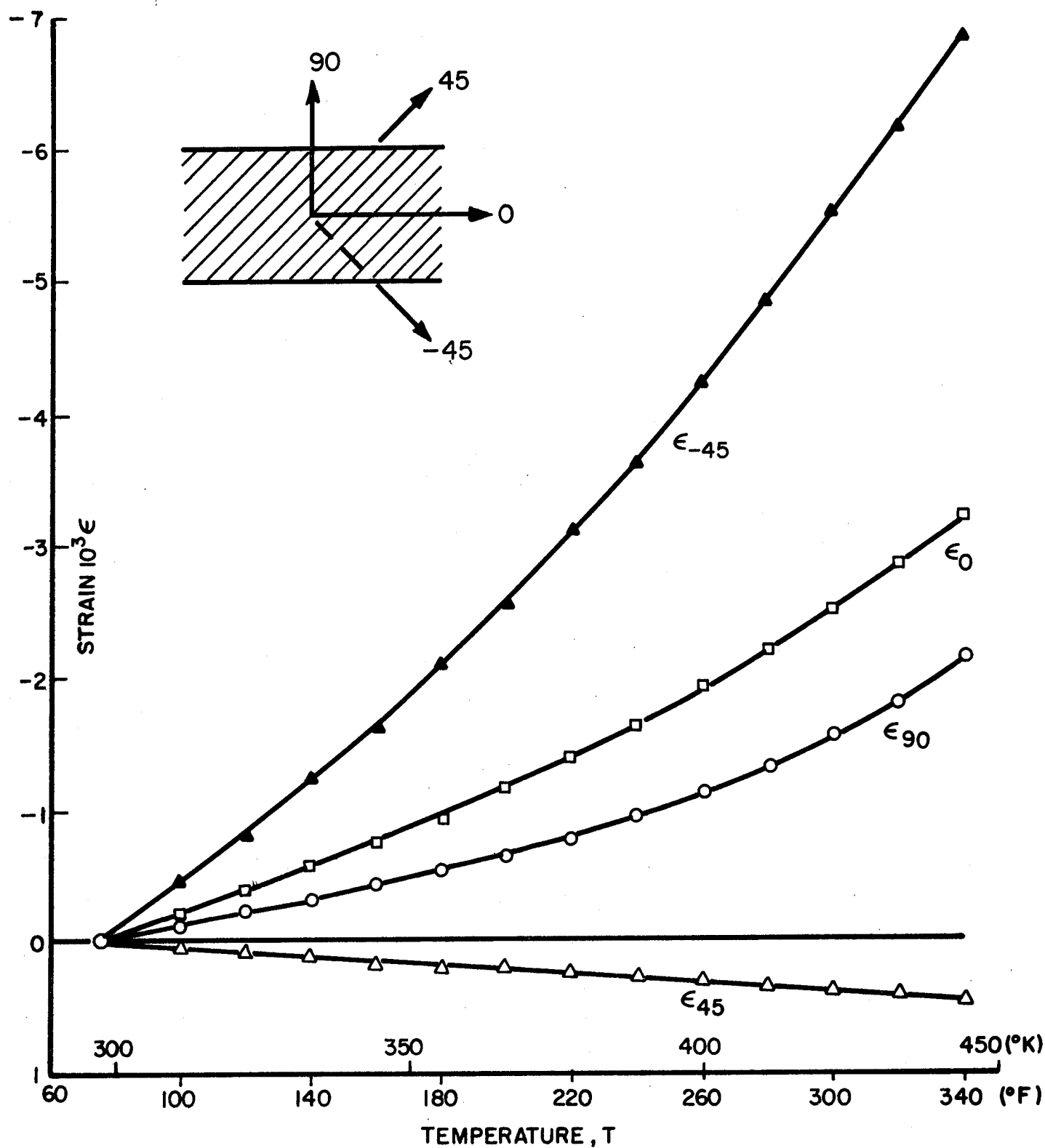
Fig. 3-70   RESTRAINT STRAINS IN 45-DEGREE PLIES OF $\left[0_2/\pm45\right]_s$
GRAPHITE/HIGH MODULUS EPOXY SPECIMEN
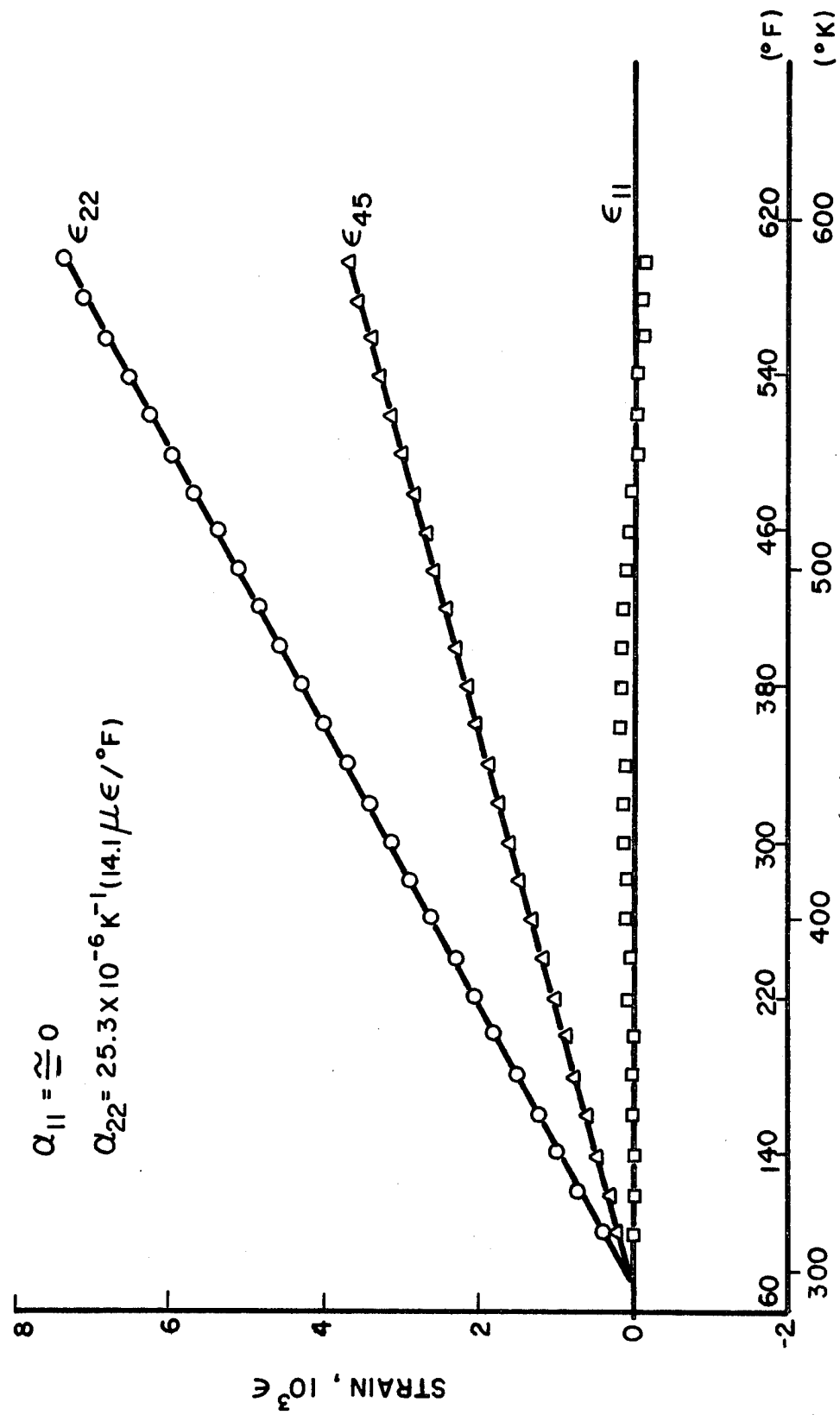
Fig. 3-71   THERMAL STRAINS IN $[0_8]$ GRAPHITE/POLYIMIDE SPECIMEN

3-121
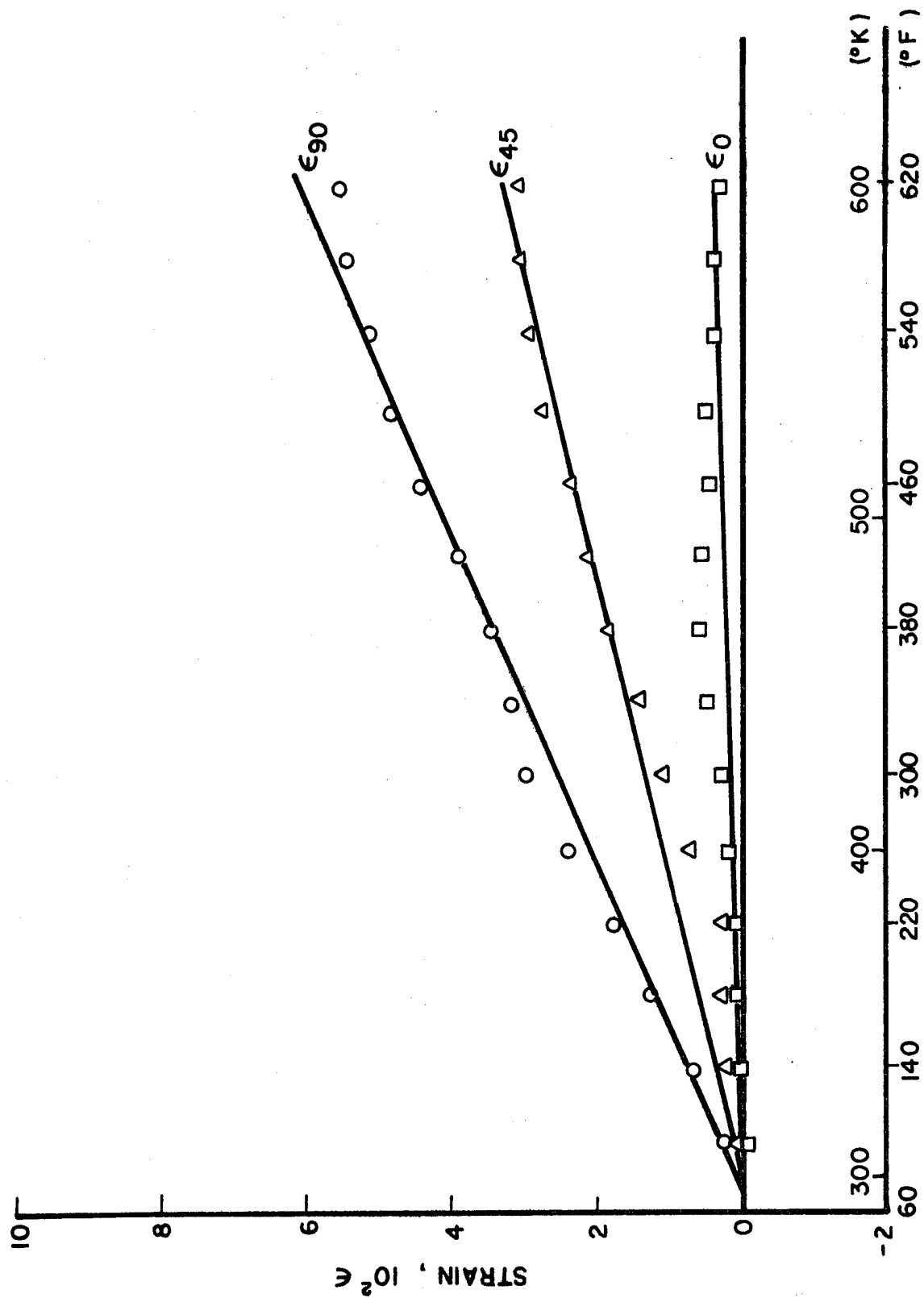
Fig. 3-72 STRAINS IN $[0_2/\pm 45]_s$ GRAPHITE/POLYIMIDE SPECIMEN

3-122
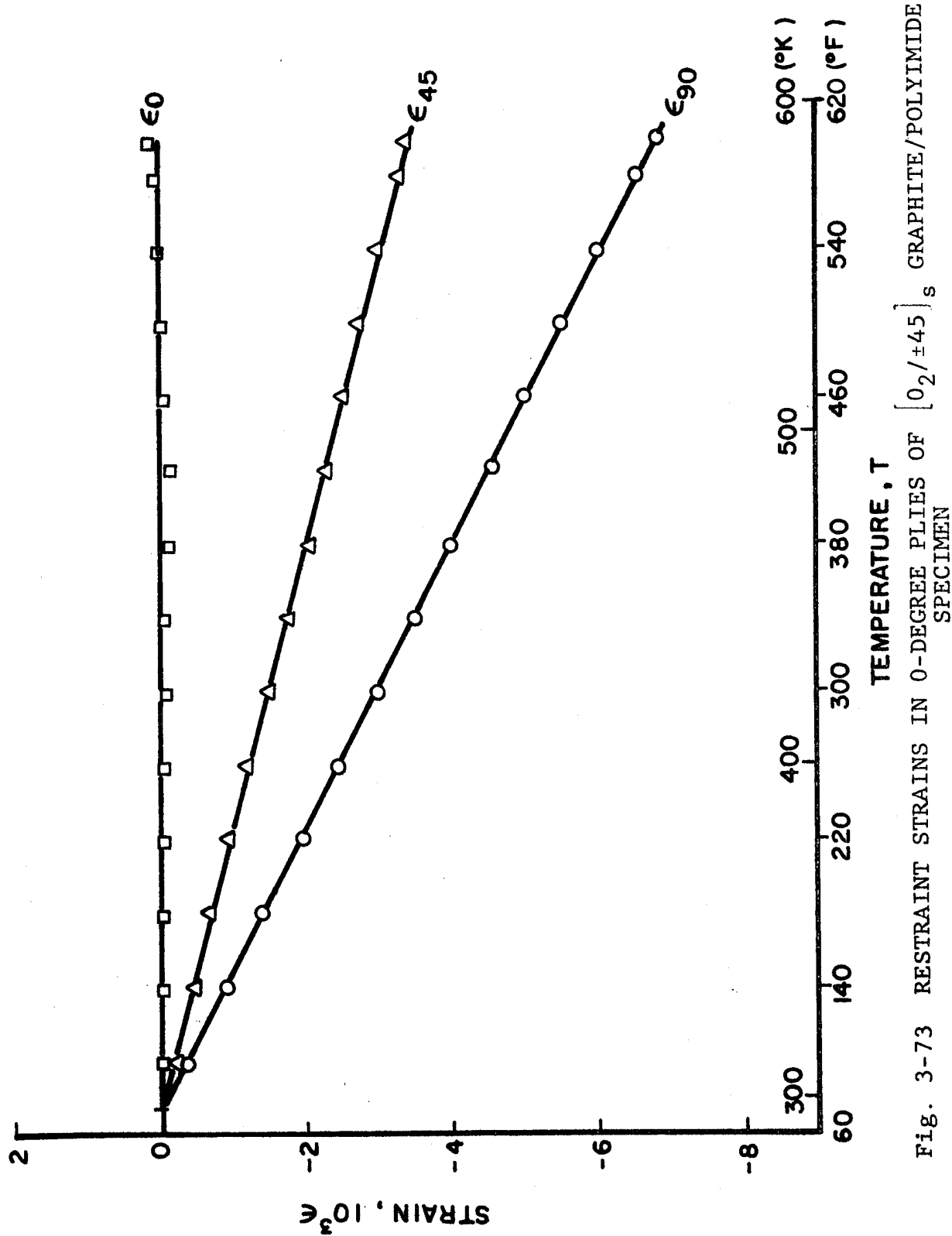
Fig. 3-73 RESTRAINT STRAINS IN 0-DEGREE PLIES OF $\left[0_2/\pm45\right]_s$ GRAPHITE/POLYIMIDE SPECIMEN
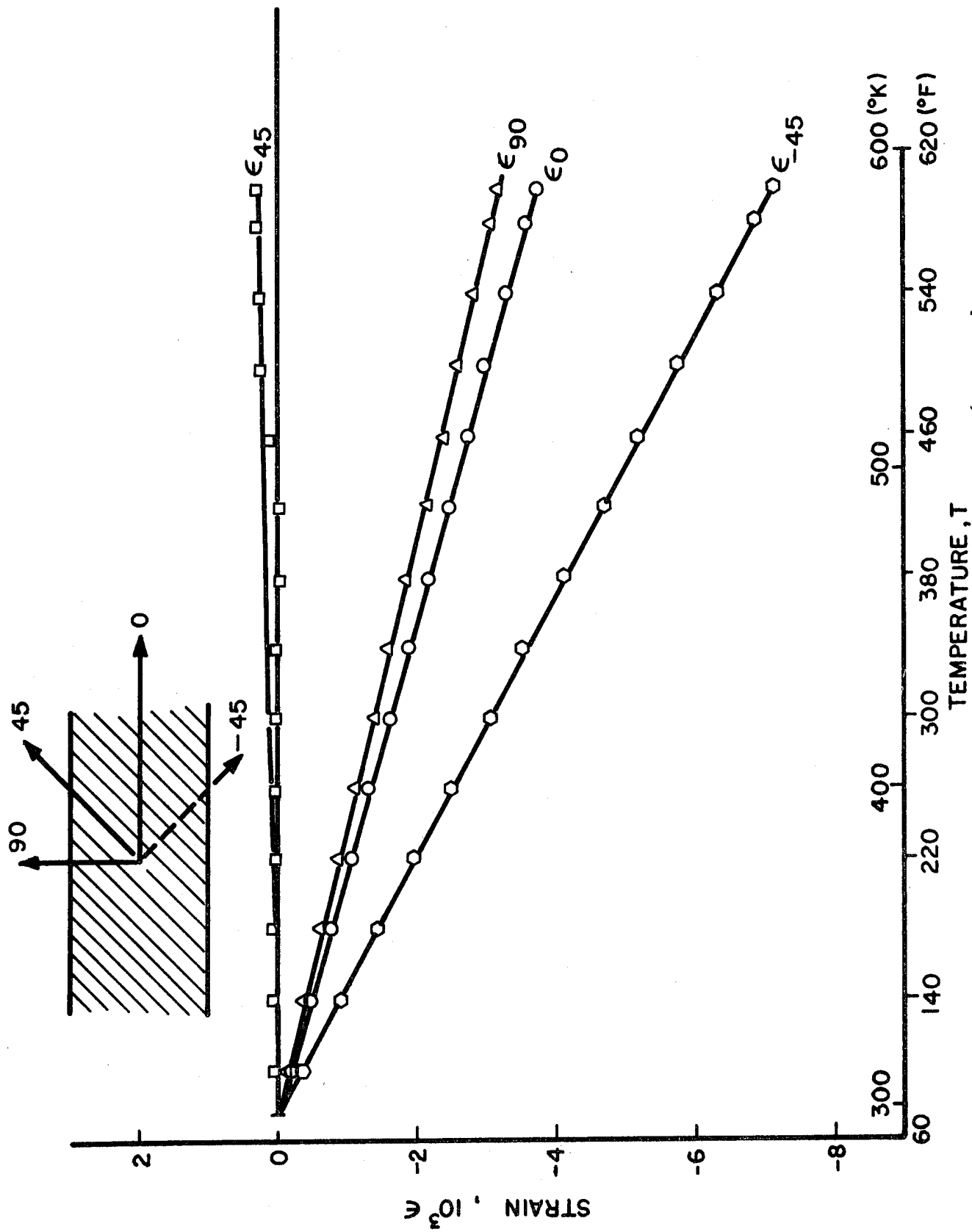
Fig. 3-74 RESTRAINT STRAINS IN 45-DEGREE PLIES OF $\left[0_2/\pm45\right]_s$ GRAPHITE/
POLYIMIDE SPECIMEN

3-124
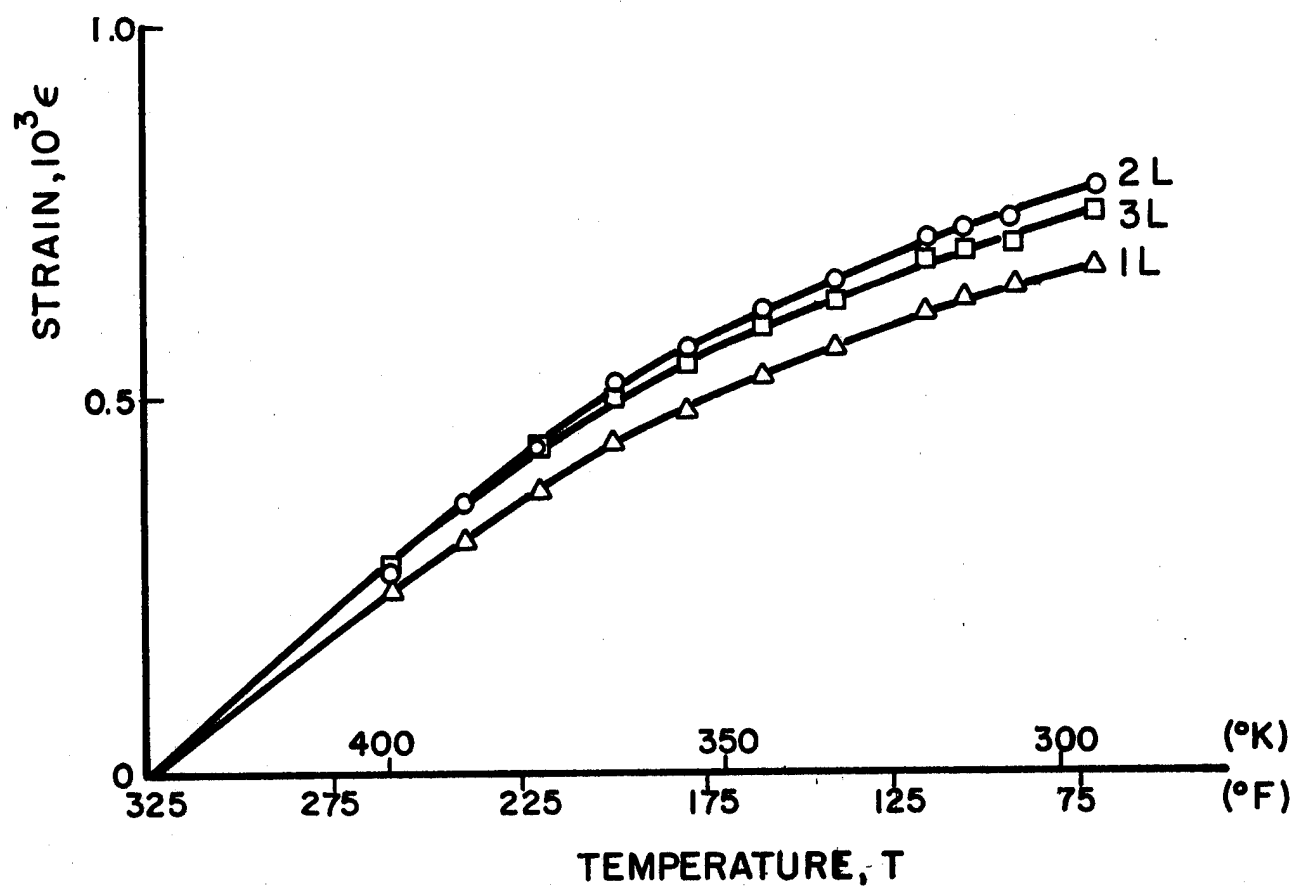
Fig. 3-75   APPARENT LONGITUDINAL STRAINS IN $[0_8]$ S-GLASS/EPOXY
SPECIMEN DURING CURING (Decreasing Temperature)
(1L, 2L, 3L: Top, Middle, and Bottom Surface,
Respectively)

3-125
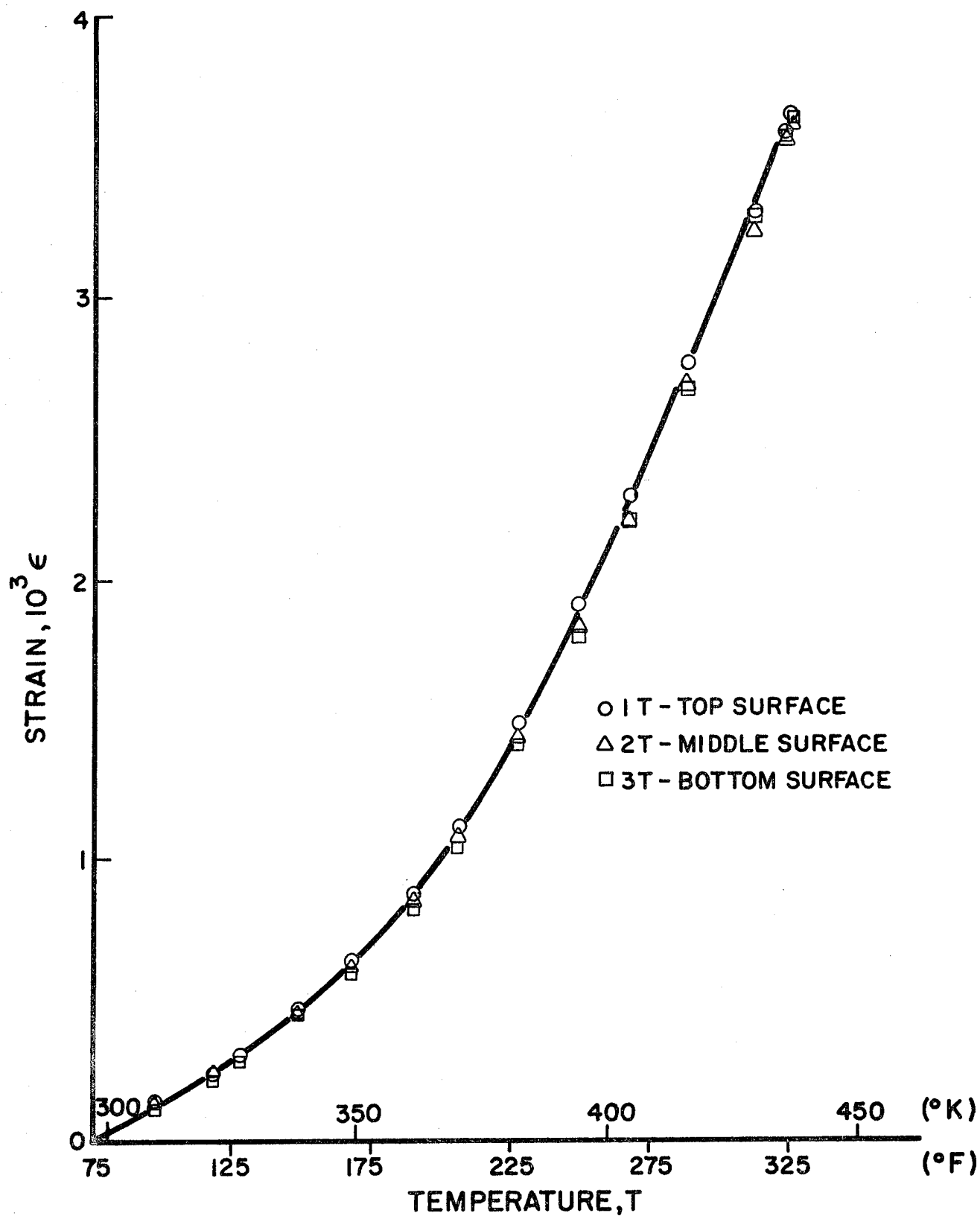
Fig. 3-76 APPARENT TRANSVERSE STRAINS IN $[0_8]$ GLASS/EPOXY SPECIMEN DURING THERMAL CYCLING (Increasing Temperature)
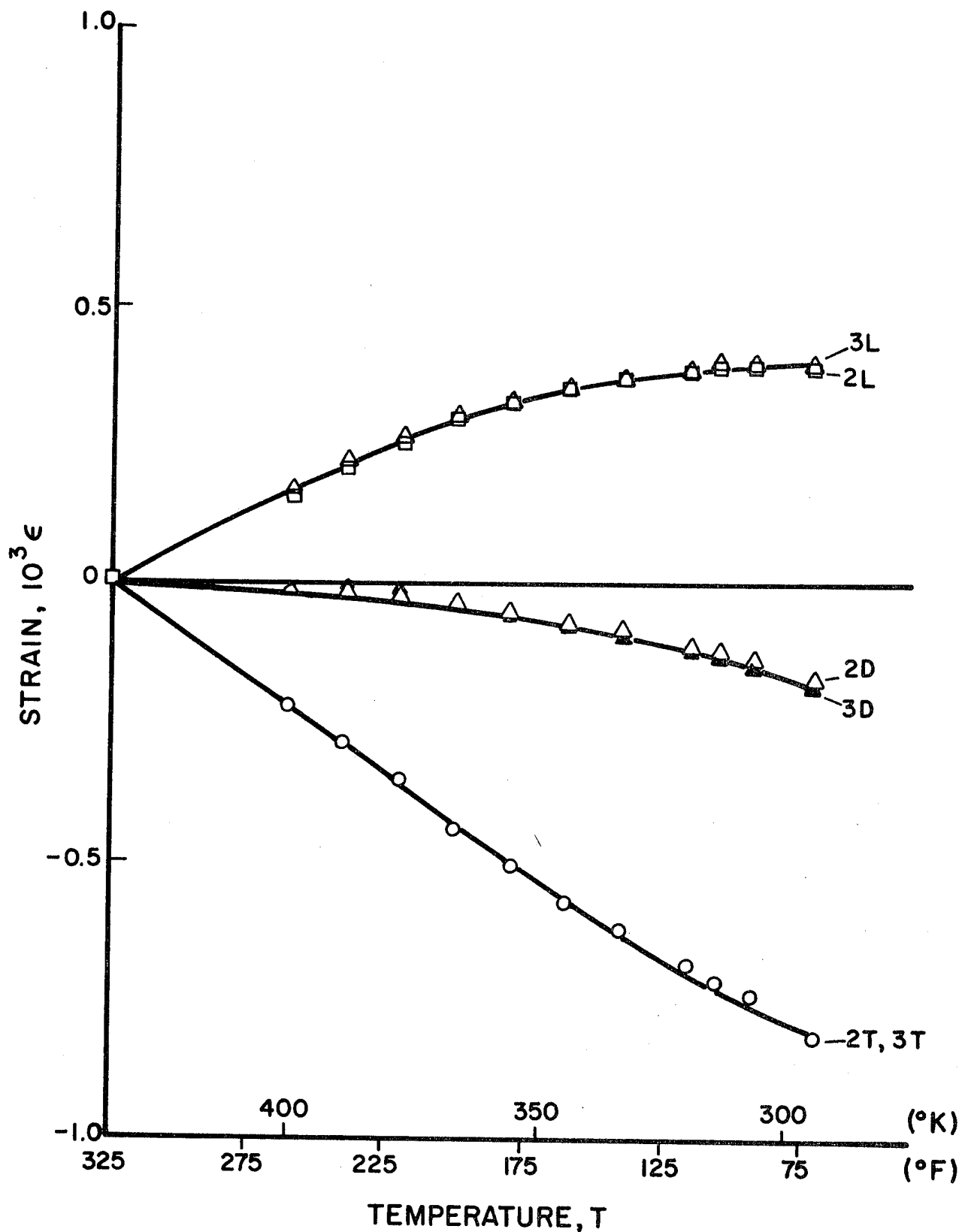
Fig. 3-77   APPARENT STRAINS IN $\left[0_2/\pm45\right]_s$ S-GLASS/EPOXY SPECIMEN
DURING CURING (Decreasing Temperature) (Gages L,T,D,:
Longitudinal, Transverse, 45-degree; Locations 2,3:
4th and 5th Ply, Respectively)

3-127
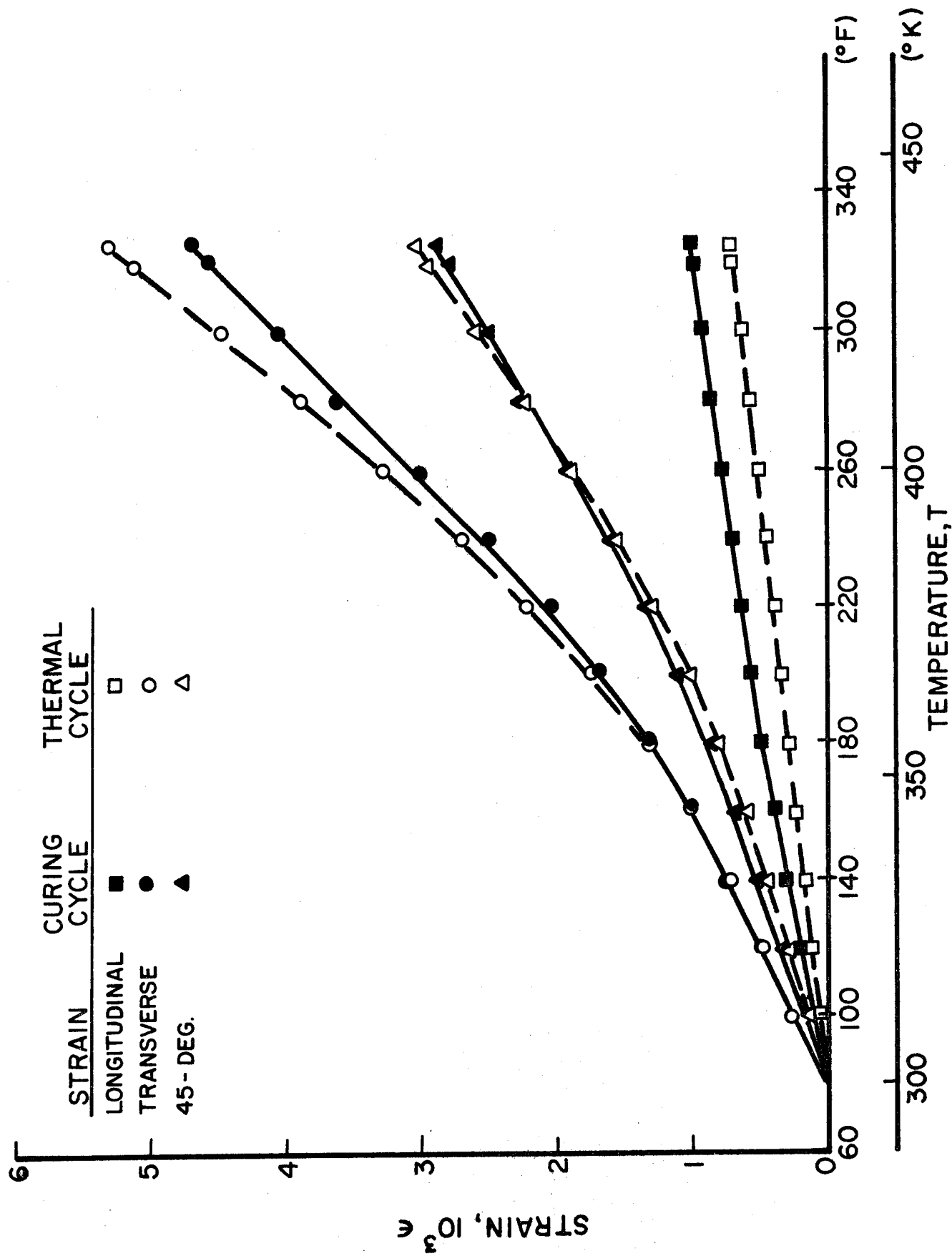
Fig. 3-78 STRAINS IN $[0_8]$ S-GLASS/EPOXY SPECIMEN DURING CURING AND THERMAL CYCLE

3-128
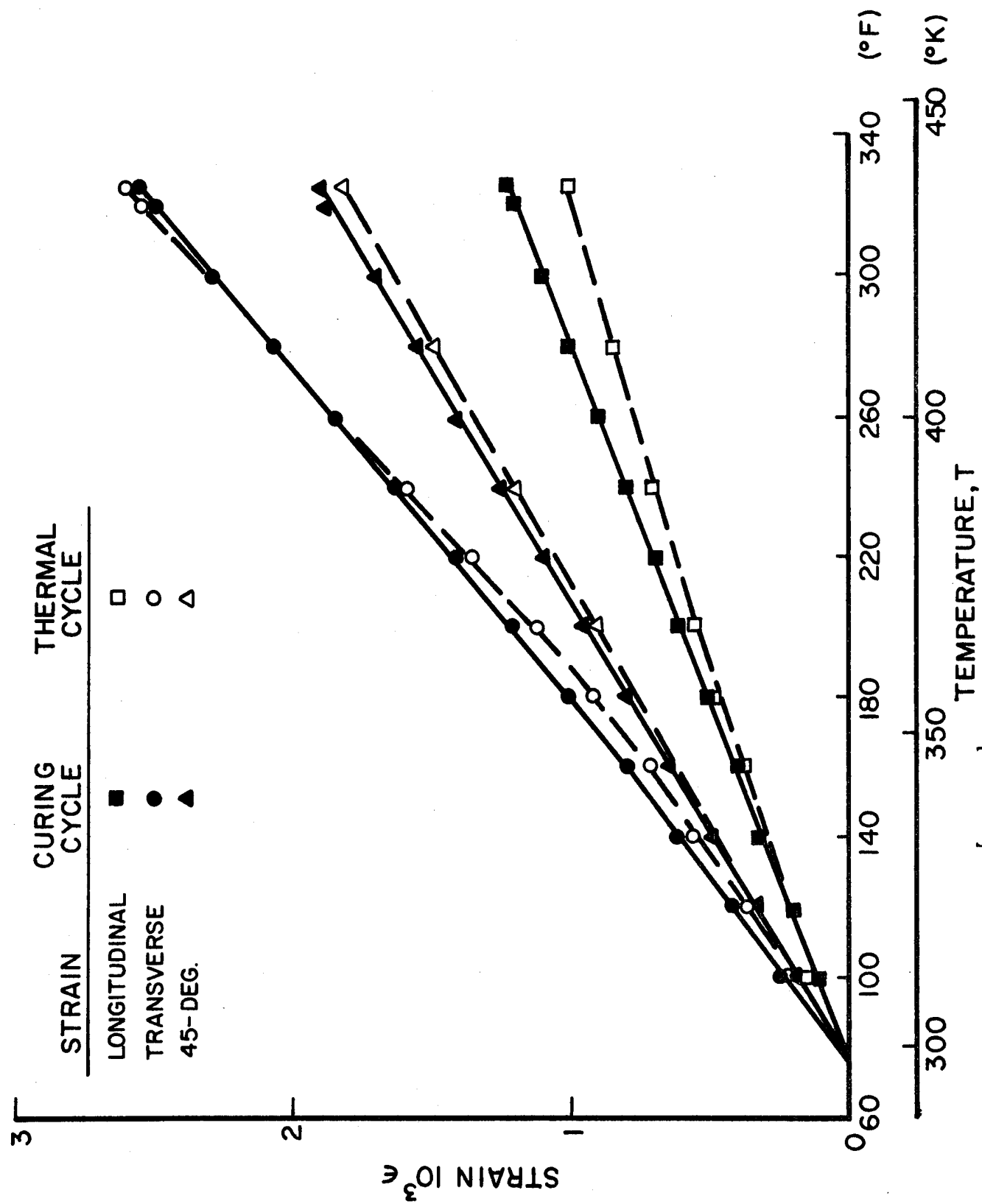
Fig. 3-79 STRAINS IN $[0_2/\pm45]_s$ S-GLASS/EPOXY SPECIMEN DURING CURING AND THERMAL CYCLE
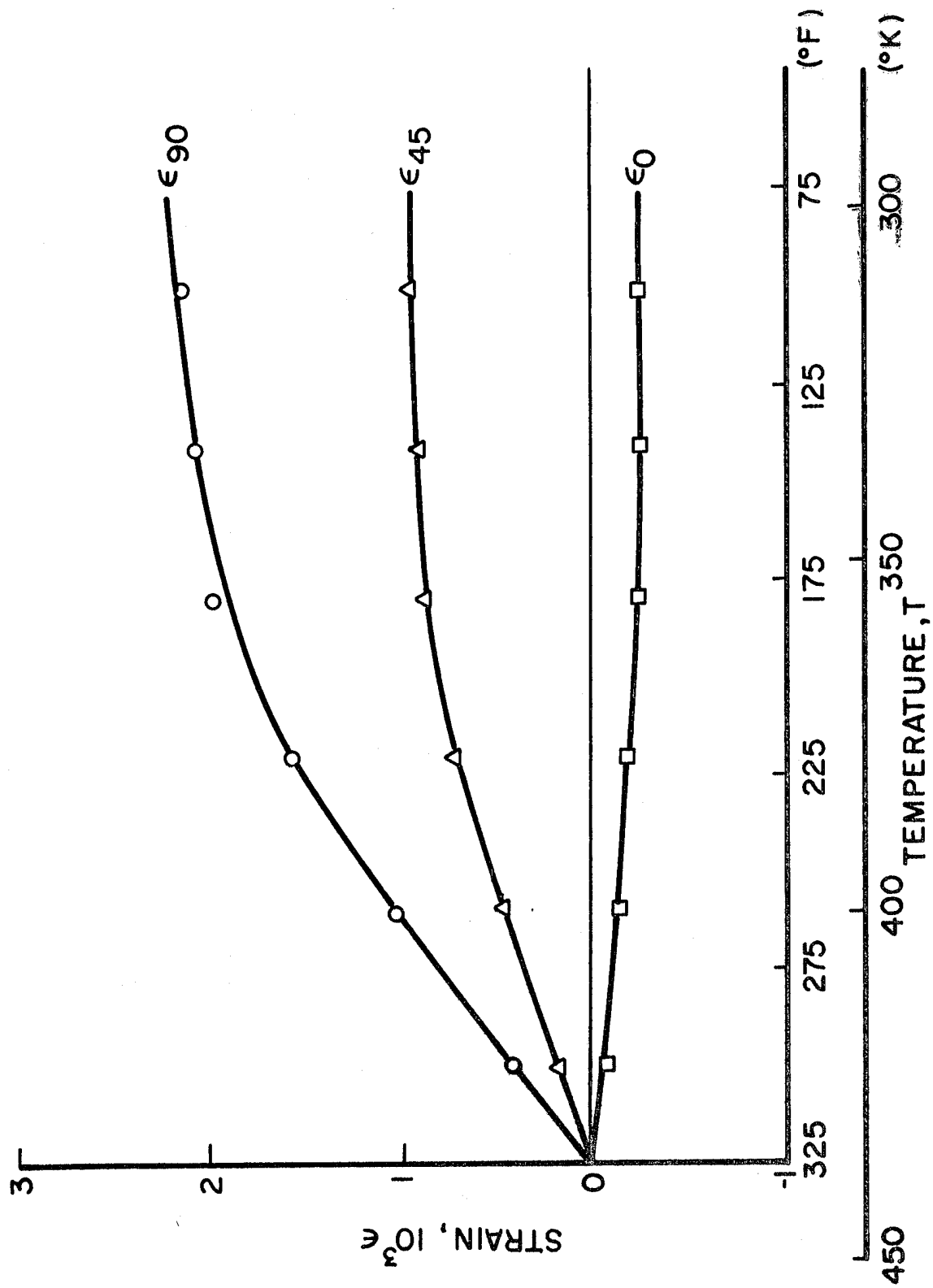
Fig. 3-80   RESIDUAL STRAINS IN 0-DEGREE PLIES OF $[0_2/\pm45]_s$ S-GLASS/EPOXY SPECIMEN
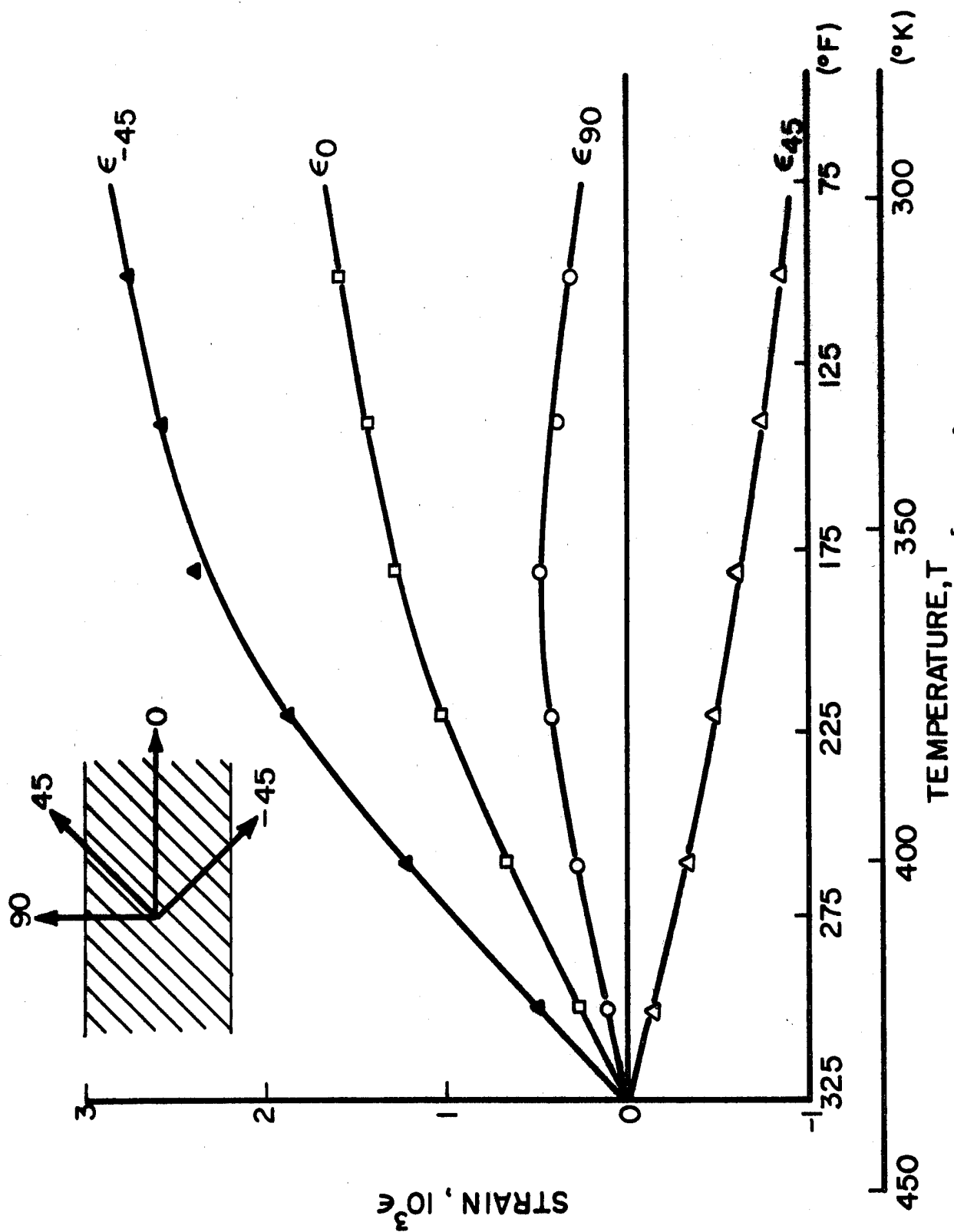
Fig. 3-81 RESIDUAL STRAINS IN 45-DEGREE PLIES OF $[0_2/\underline{\pm}45]_s$ S-GLASS/EPOXY SPECIMEN
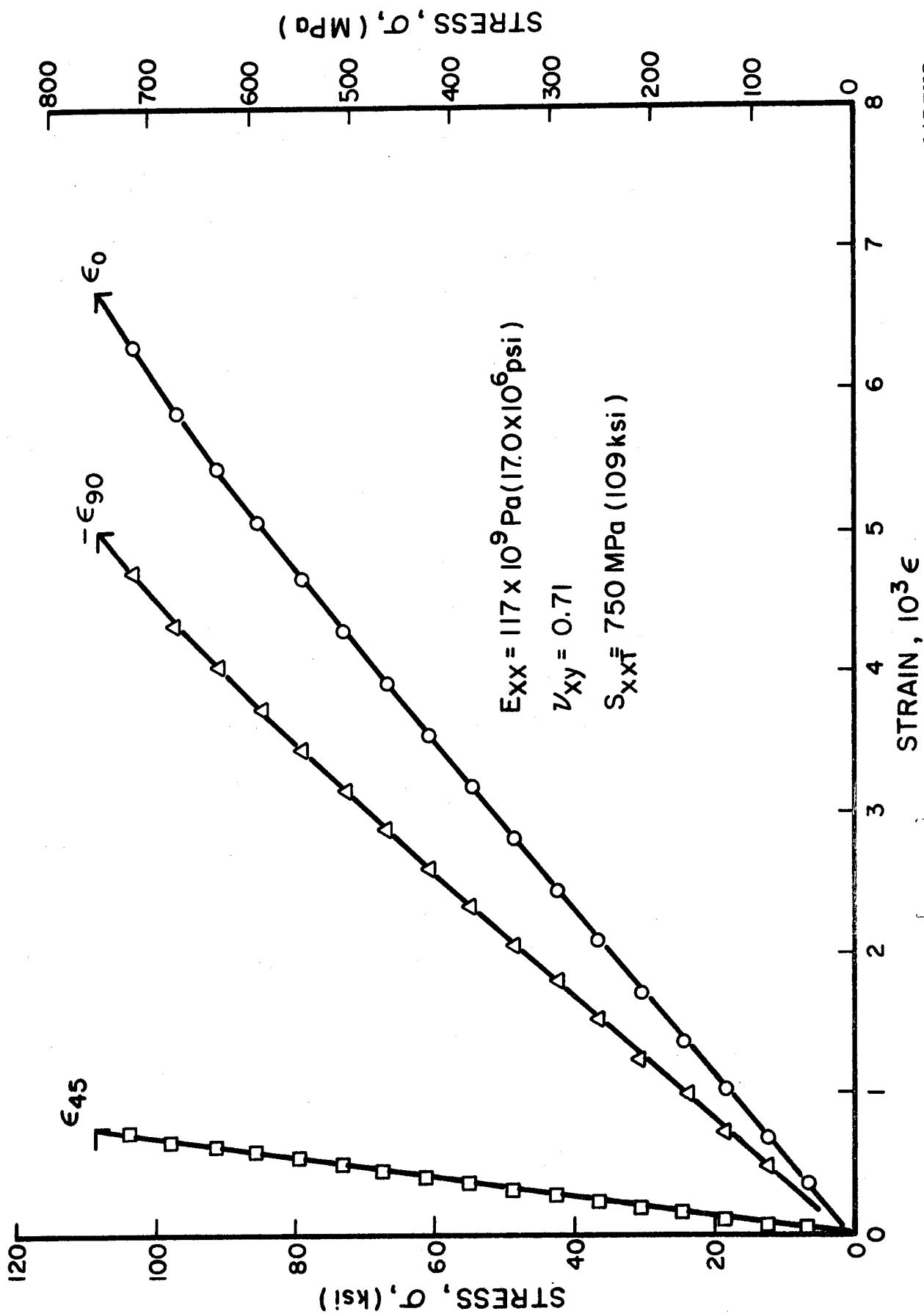
Fig. 3-82 STRAINS IN $[0_2/\pm 45]_s$ BORON/EPOXY SPECIMEN UNDER UNIAXIAL TENSILE LOADING

$E_{xx} = 117 \times 10^9 Pa (17.0 \times 10^6 psi)$

$\nu_{xy} = 0.71$

$S_{xxt} = 750 MPa (109 ksi)$
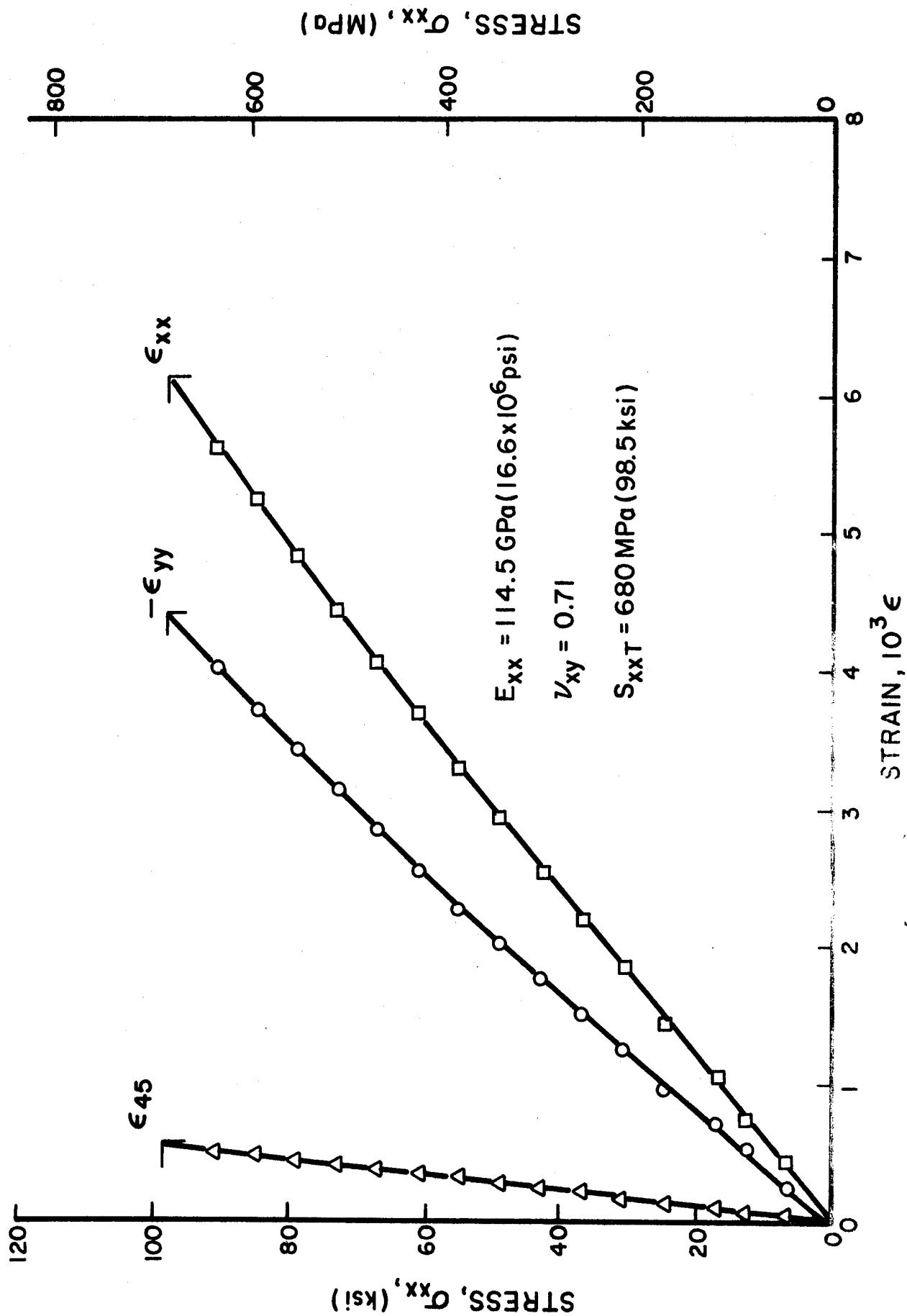
Fig. 3-83 STRAINS IN $[0_2/+45]_s$ BORON/EPOXY SPECIMEN UNDER UNIAXIAL TENSILE LOADING

$E_{xx} = 114.5\,GPa(16.6 \times 10^6\,psi)$

$\nu_{xy} = 0.71$

$S_{xxT} = 680\,MPa(98.5\,ksi)$

Fig. 3-84 STRAINS IN $[0_2/\pm45]_s$ BORON/EPOXY SPECIMEN UNDER UNIAXIAL TENSILE LOADING

$E_{xx} = 114 \times 10^9$ Pa $(16.5 \times 10^6$ psi$)$

$\nu_{xy} = 0.67$

$S_{xxT} = 745$ MPa $(108$ ksi$)$

ϵ_{xx}

$-\epsilon_{yy}$

STRAIN, $10^3 \epsilon$

STRESS, σ_{xx} (MPa)

STRESS, σ_{xx} (ksi)
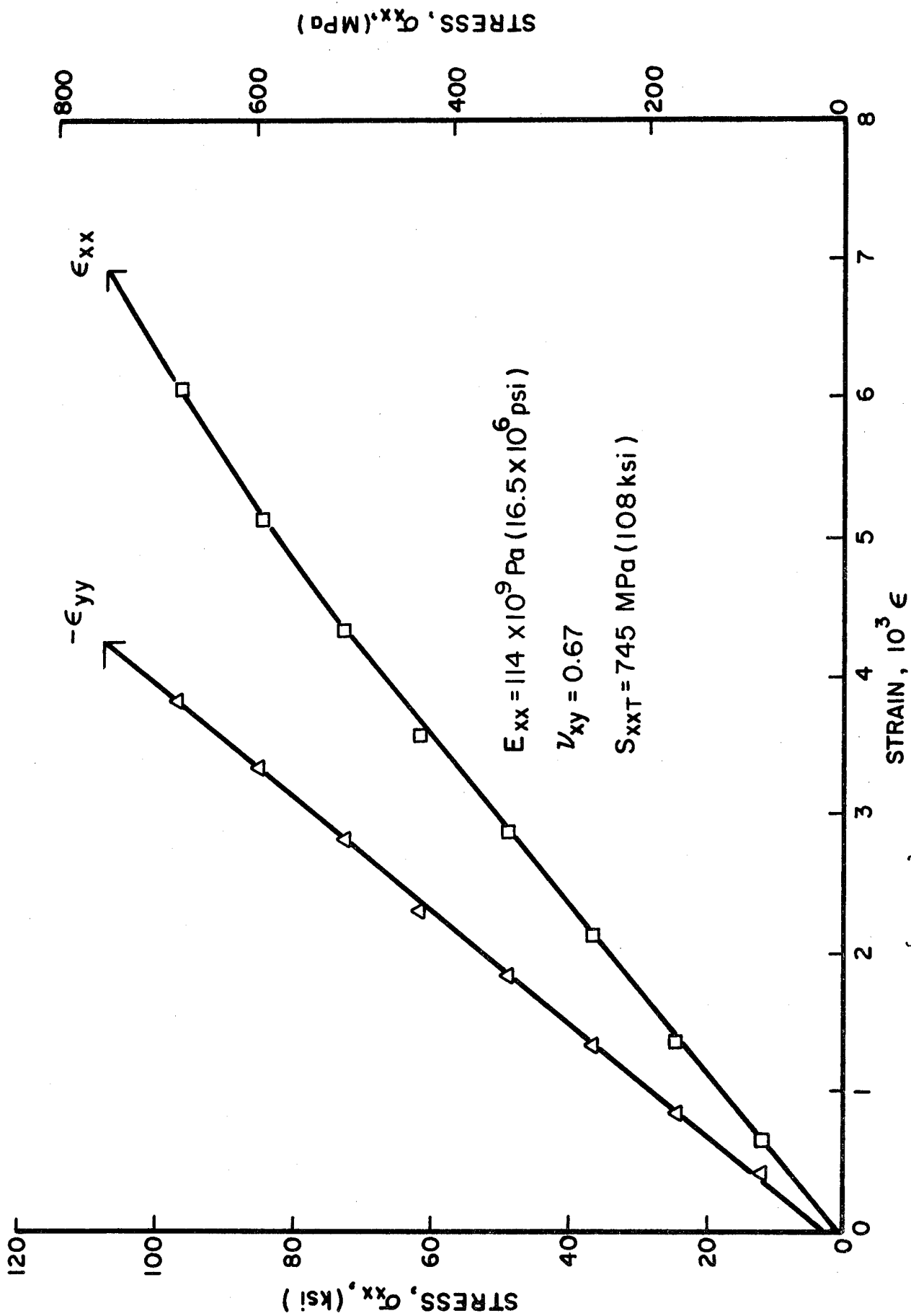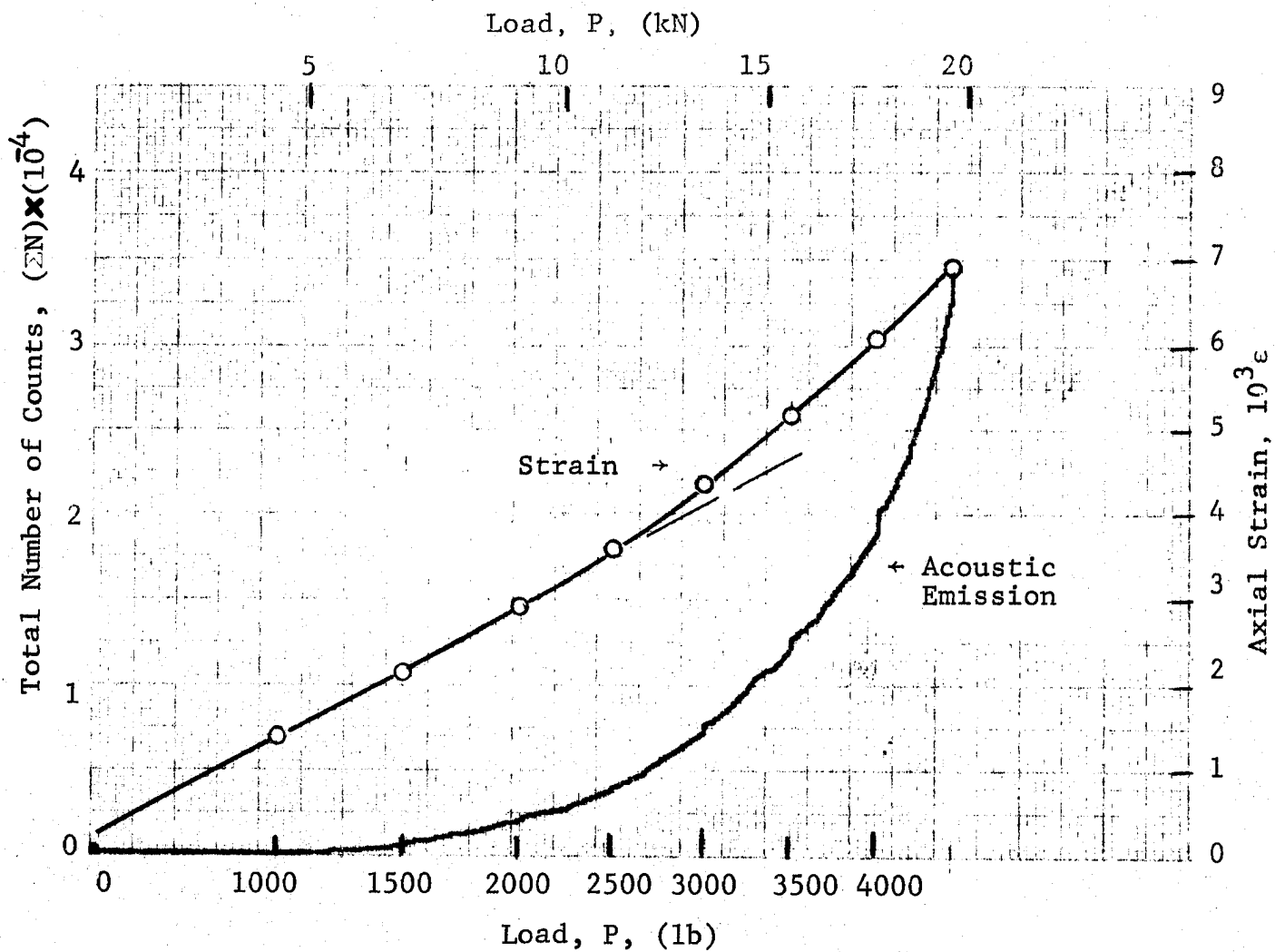
Fig. 3-85 ACOUSTIC EMISSION FROM $\left[0_2/\pm45\right]_s$ BORON/EPOXY SPECIMEN UNDER UNIAXIAL TENSILE LOADING
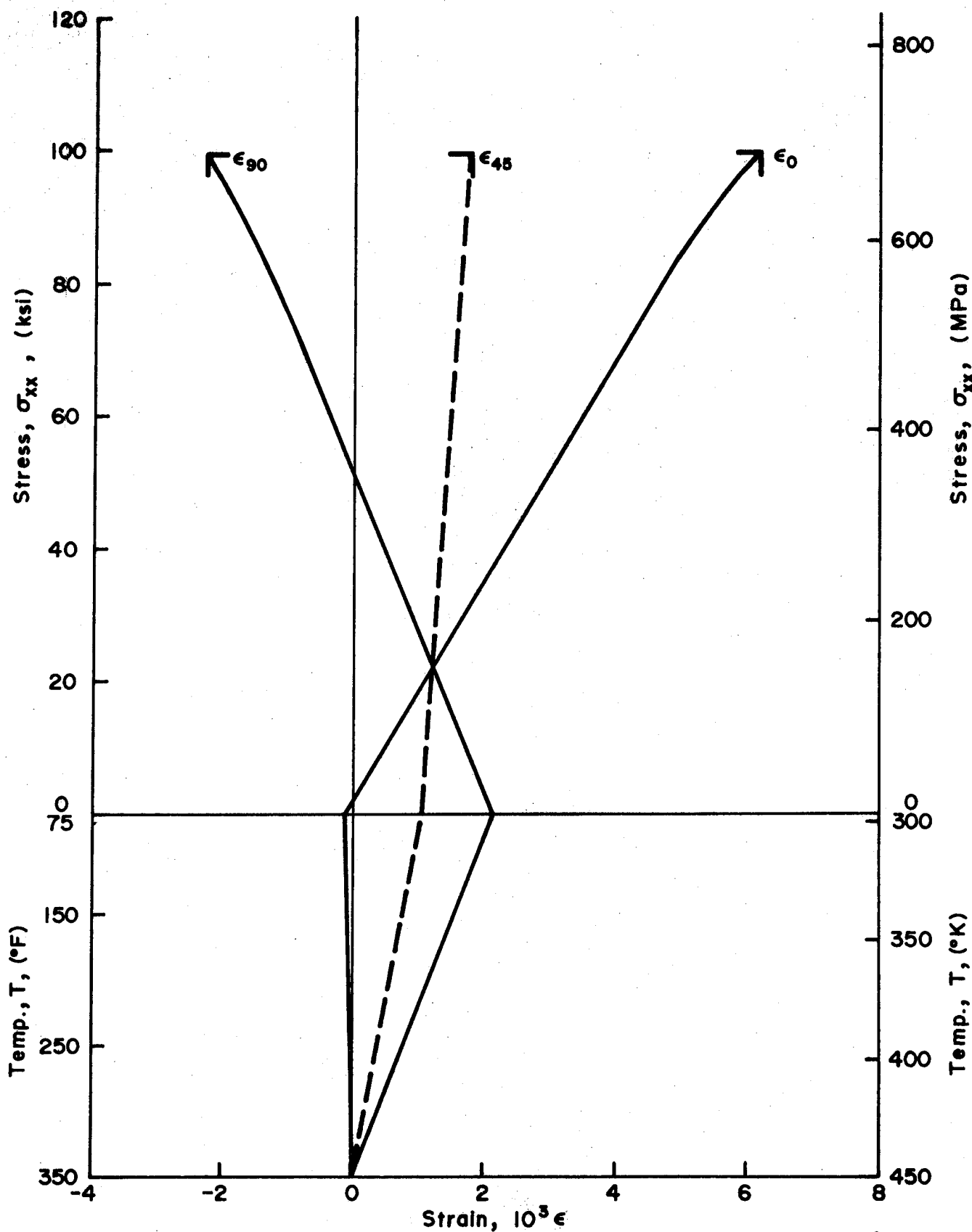
Fig. 3-86 TOTAL STRAIN HISTORY IN 0-DEGREE PLIES OF $[0_2/\pm45]_s$
BORON/EPOXY LAMINATE FROM CURING TO FAILURE UNDER
UNIAXIAL TENSION
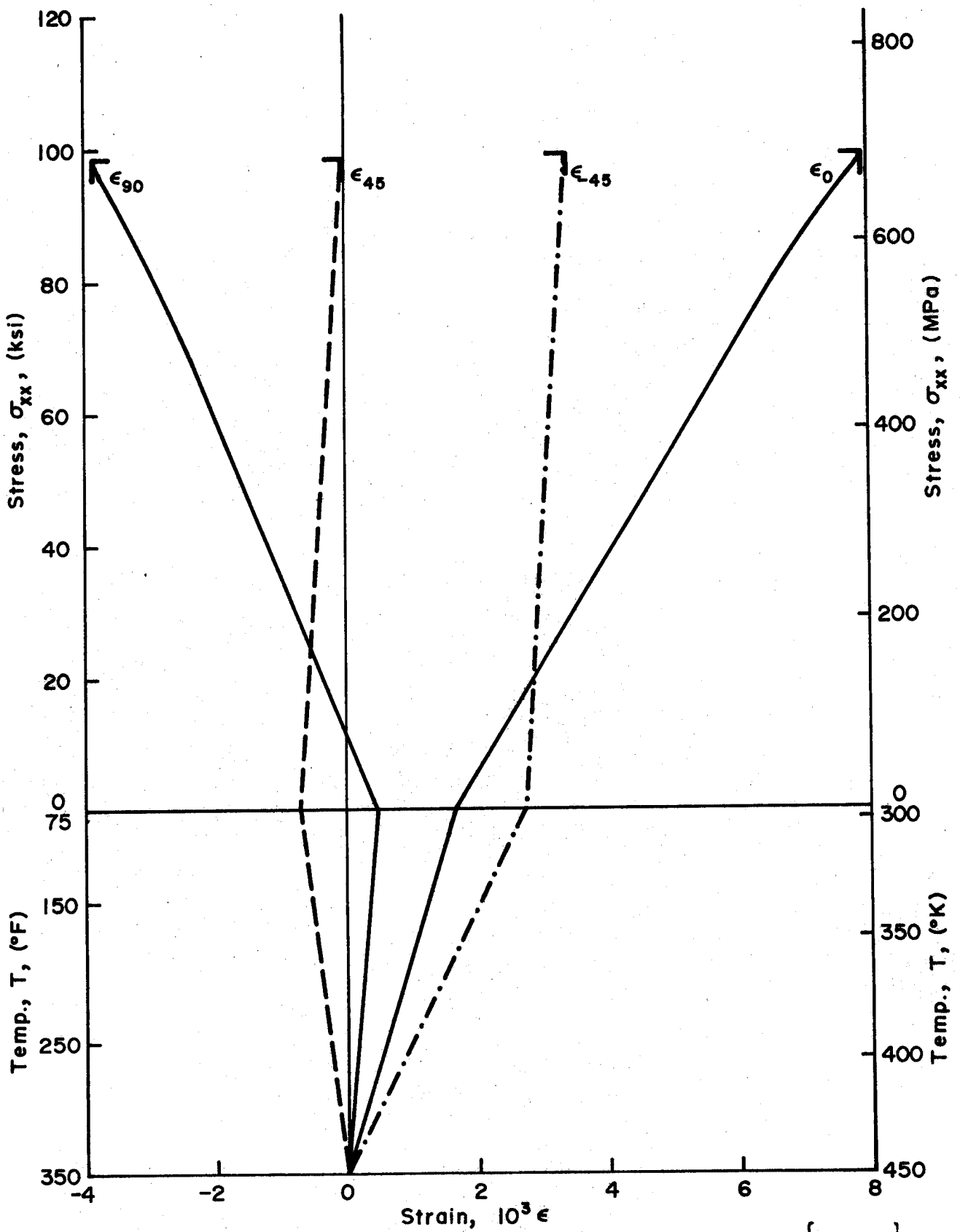
Fig. 3-87 TOTAL STRAIN HISTORY IN 45-DEGREE PLIES OF $\begin{bmatrix} 0_2/\pm45 \end{bmatrix}_s$ BORON/EPOXY LAMINATE FROM CURING TO FAILURE UNDER UNIAXIAL TENSION

3-137

Fig. 3-88 STRAINS IN $[0_2/\pm45]_s$ BORON/POLYIMIDE SPECIMEN UNDER UNIAXIAL TENSILE LOADING

Within the figure:

STRESS, σ_{xx}, (MPa)

STRESS, σ_{xx}, (ksi)

STRAIN, $10^3\epsilon$

ϵ_{xx}

$-\epsilon_{yy}$

$E_{xx} = 117 \times 10^9$ Pa $(17.0 \times 10^6$ psi$)$

$\nu_{xy} = 0.72$

$S_{xxT} = 564$ MPa $(82$ ksi$)$
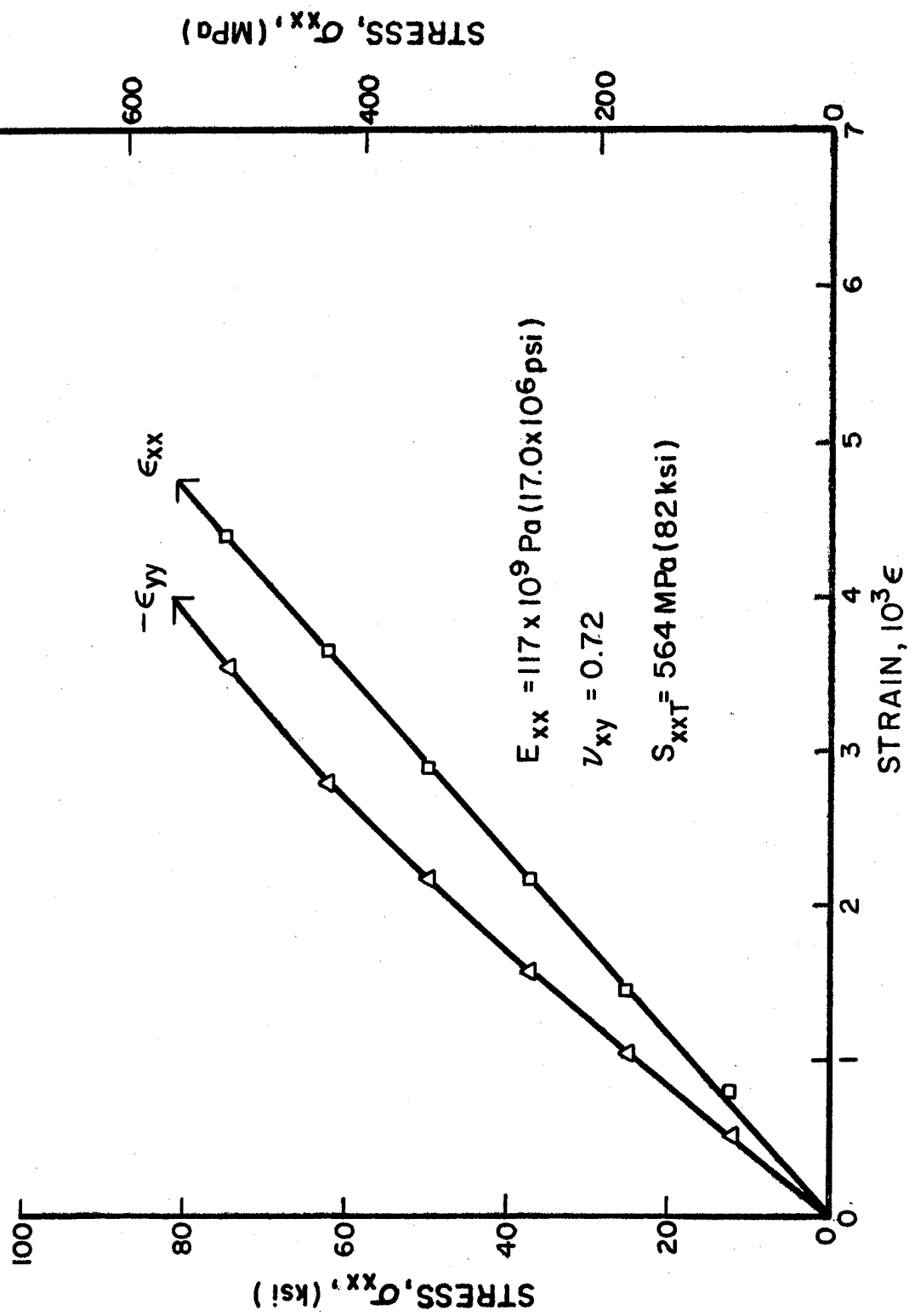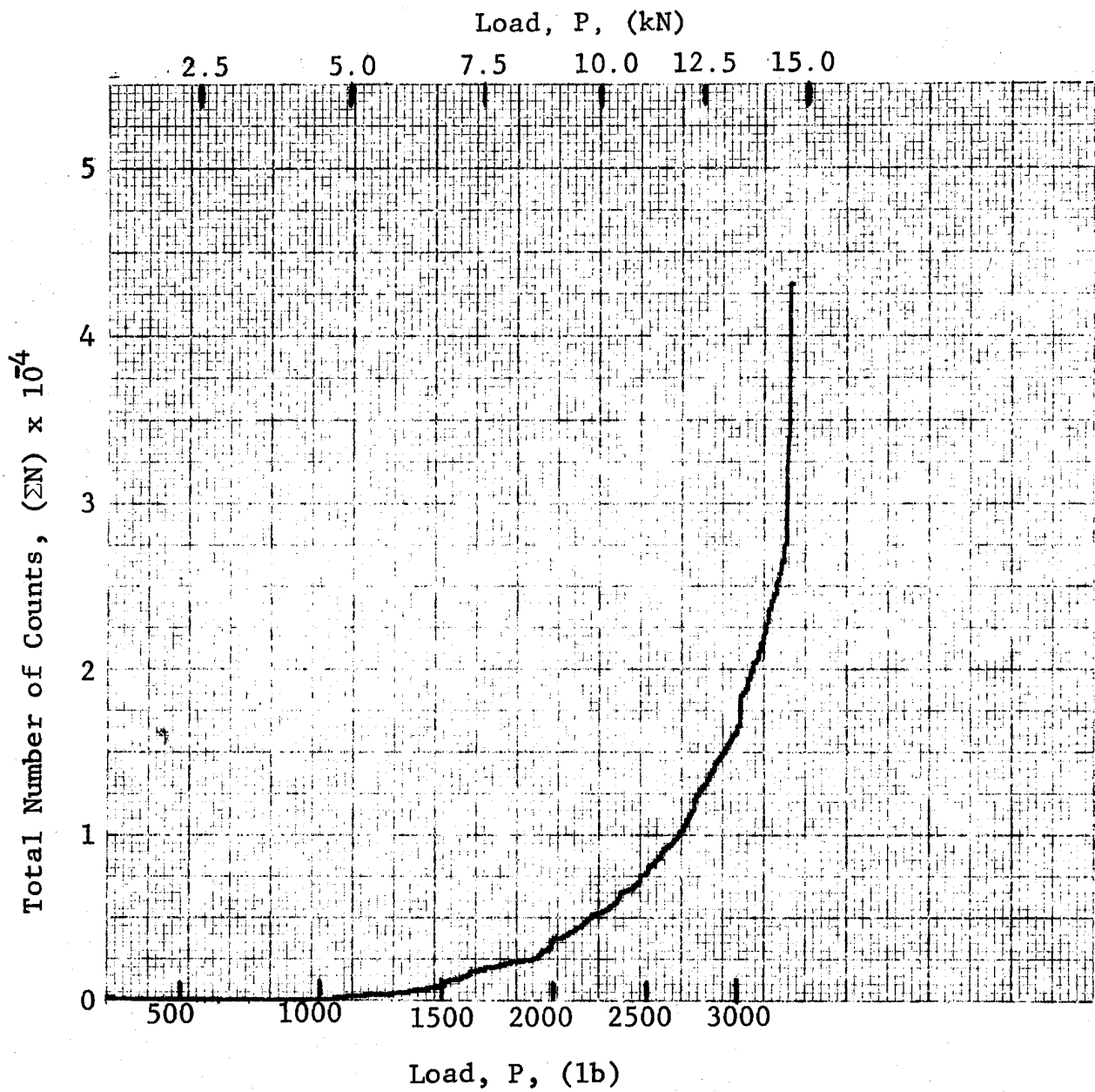
Fig. 3-89 ACOUSTIC EMISSION FROM $\left[0_2/\pm45\right]_s$ BORON/POLYIMIDE SPECIMEN UNDER UNIAXIAL LOADING
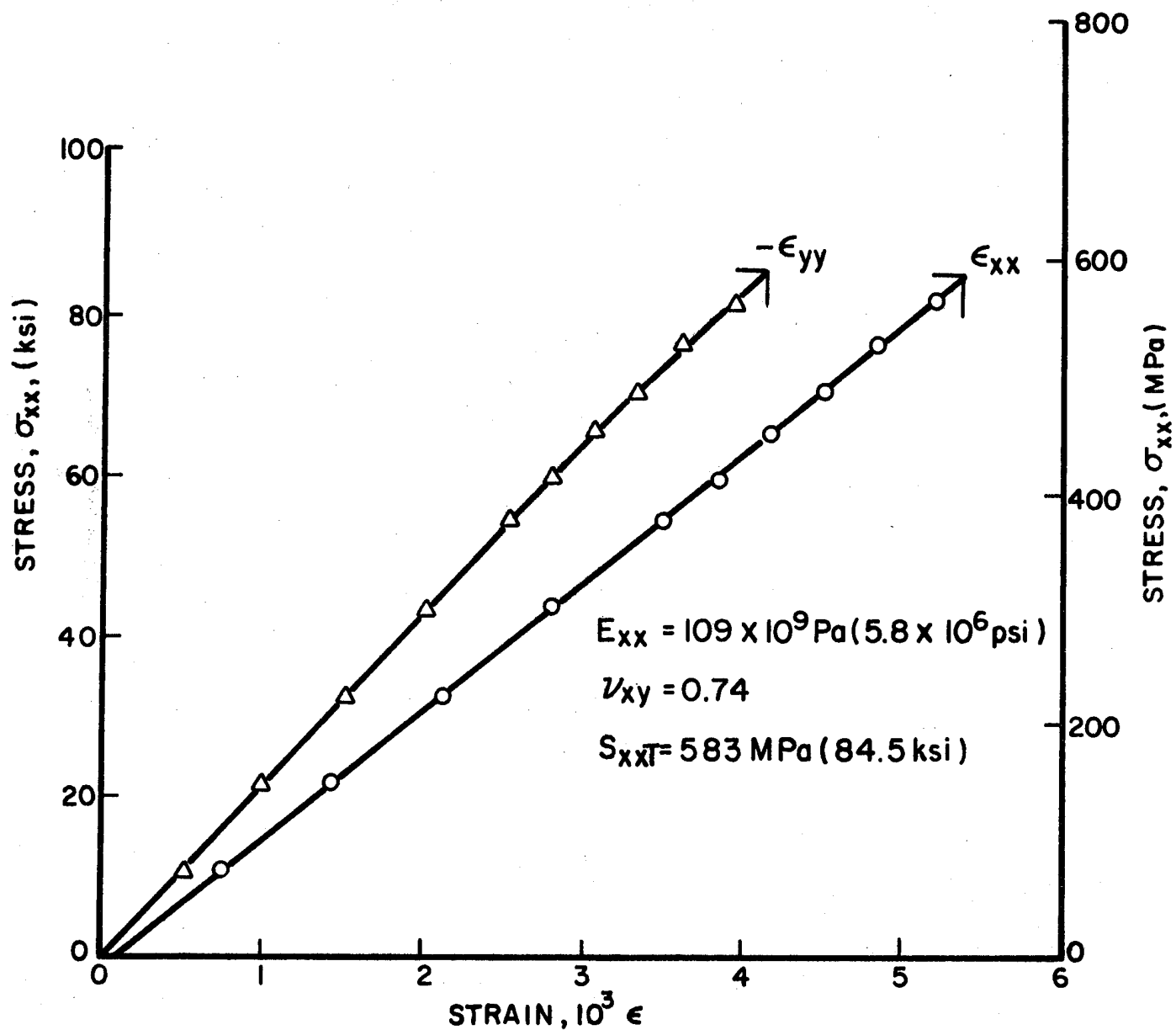
3-139

Fig. 3-90 STRAINS IN $\left[0_2/\pm 45\right]_s$ GRAPHITE/LOW MODULUS EPOXY
SPECIMEN UNDER UNIAXIAL TENSILE LOADING
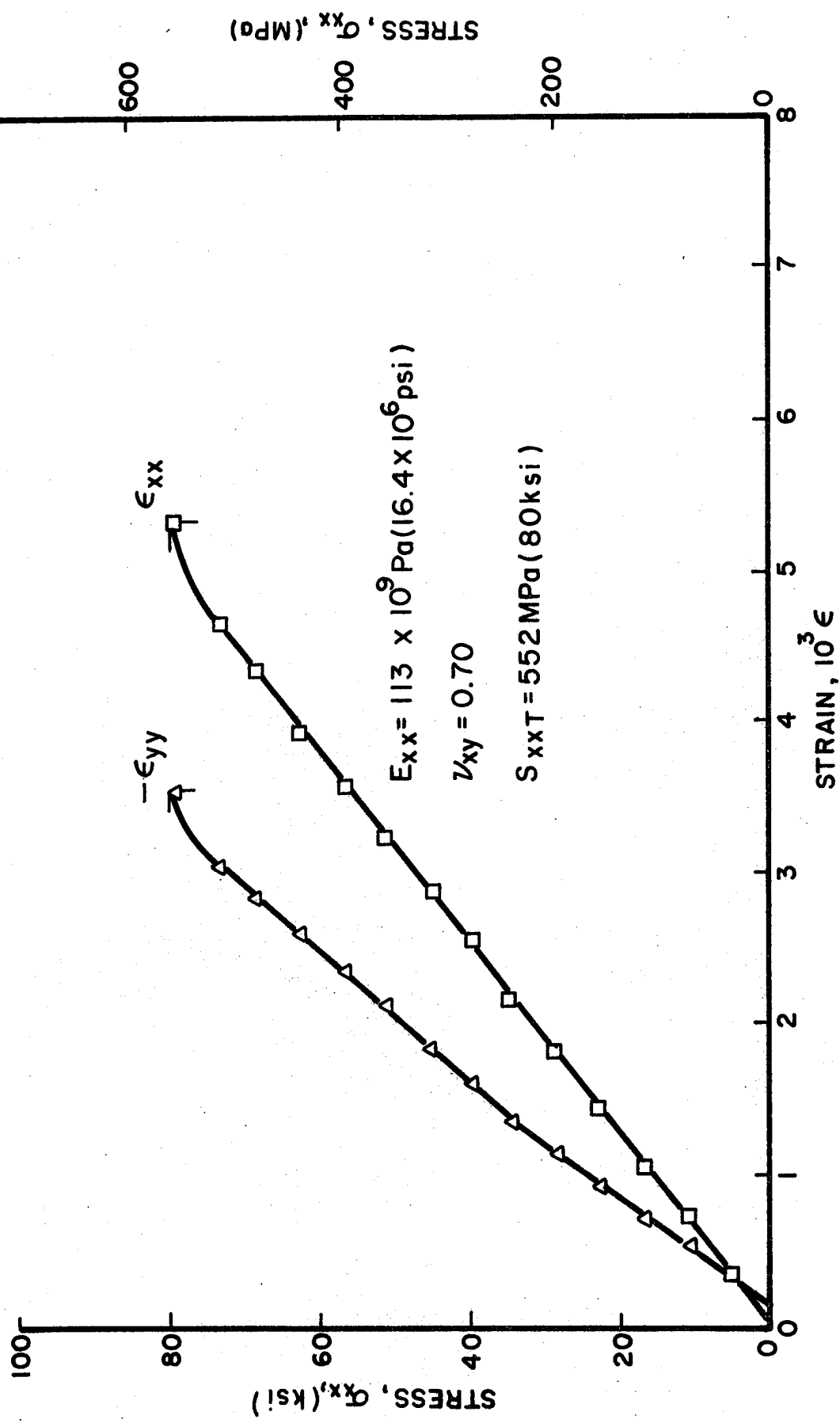
$E_{xx} = 109 \times 10^9 \, Pa \, (5.8 \times 10^6 \, psi)$

$\nu_{xy} = 0.74$

$S_{xxT} = 583 \, MPa \, (84.5 \, ksi)$

Fig. 3-91 STRAINS IN $\left[0_2/\pm45\right]_s$ GRAPHITE/LOW MODULUS EPOXY SPECIMEN UNDER UNIAXIAL TENSILE LOADING

$E_{xx} = 113 \times 10^9 Pa(16.4 \times 10^6 psi)$

$\nu_{xy} = 0.70$

$S_{xxT} = 552 MPa(80 ksi)$
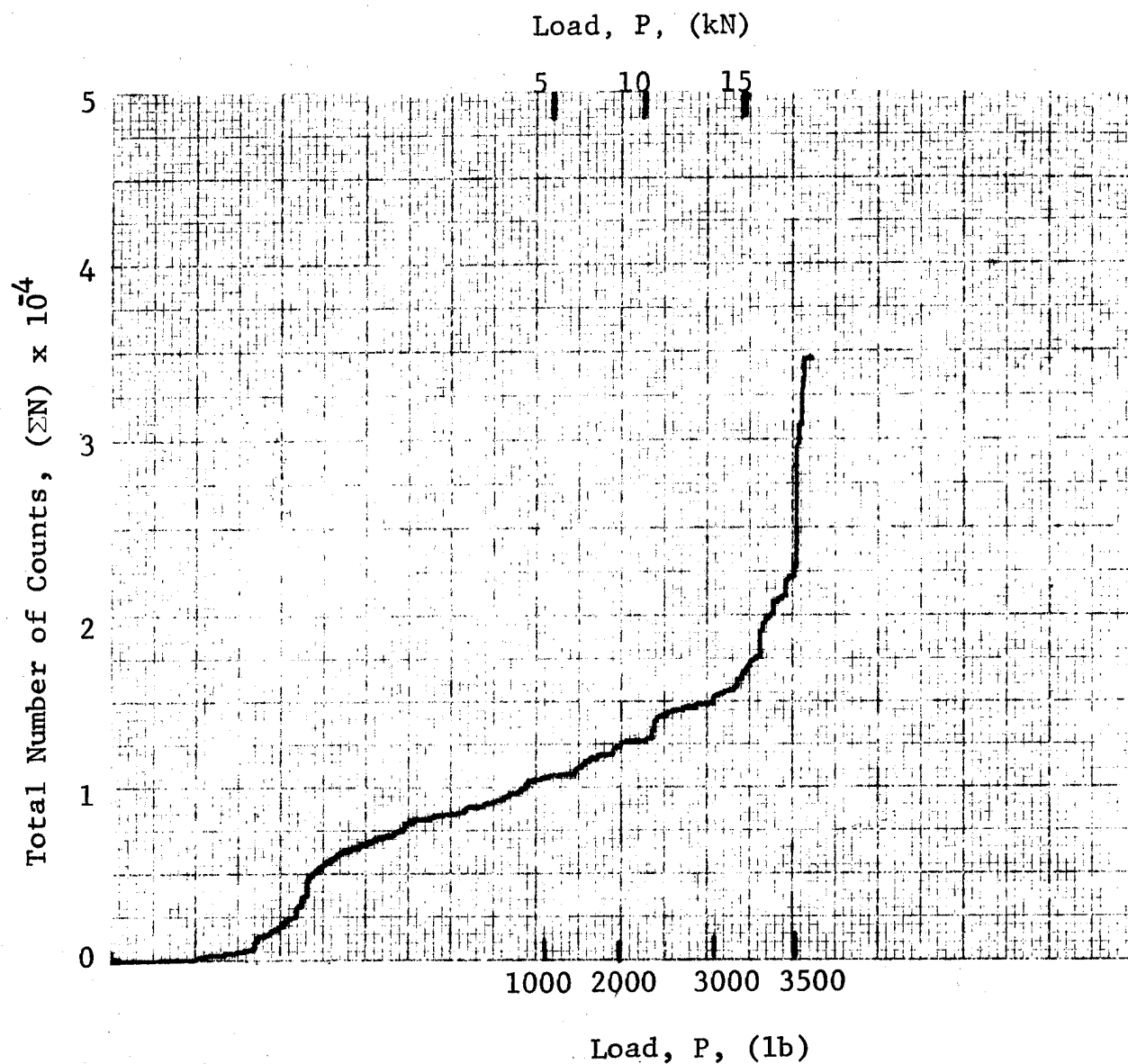
Fig. 3-92 ACOUSTIC EMISSION FROM $[0_2/\pm45]_s$ GRAPHITE/LOW-MODULUS-EPOXY SPECIMEN UNDER UNIAXIAL LOADING
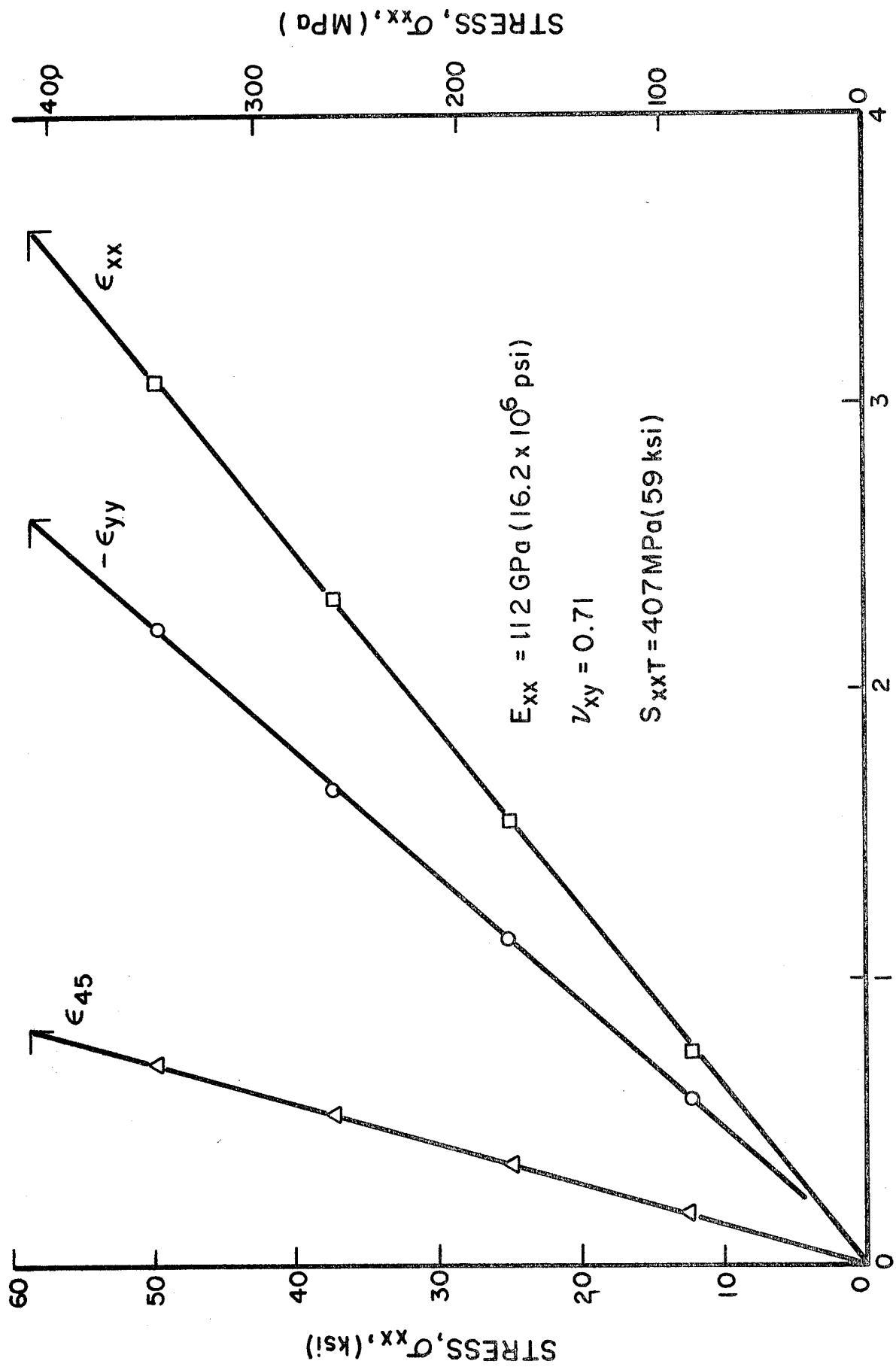
Fig. 3-93   STRAINS IN $[0_2/\pm 45]_s$ GRAPHITE/HIGH MODULUS EPOXY SPECIMEN UNDER UNIAXIAL
TENSILE LOADING

$E_{xx} = 112 \, GPa \, (16.2 \times 10^6 \, psi)$

$\nu_{xy} = 0.71$

$S_{xxT} = 407 \, MPa \, (59 \, ksi)$
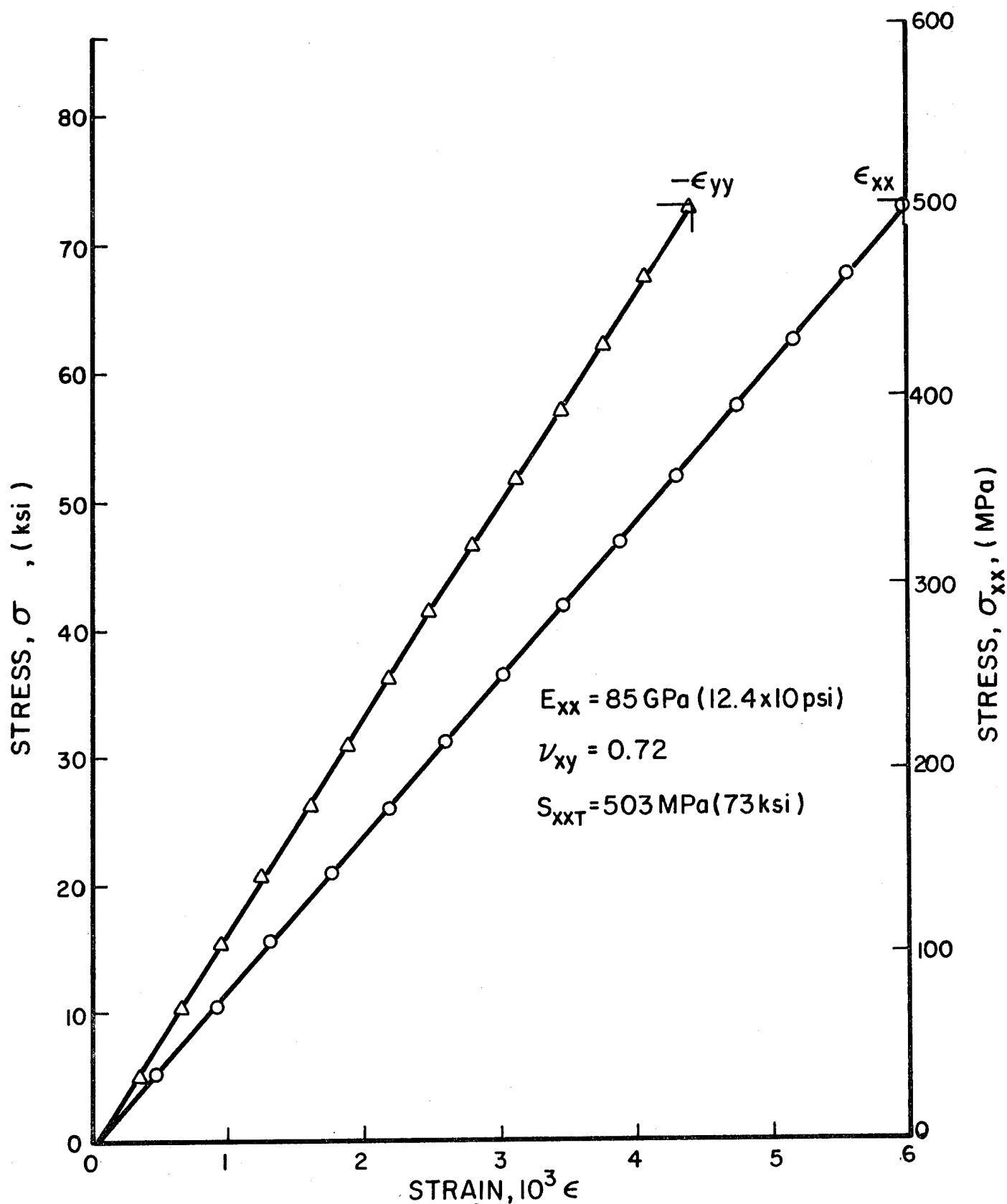
Fig. 3-94 STRAINS IN $\left[0_2/\pm45\right]_s$ GRAPHITE/HIGH MODULUS EPOXY
SPECIMEN UNDER UNIAXIAL TENSILE LOADING
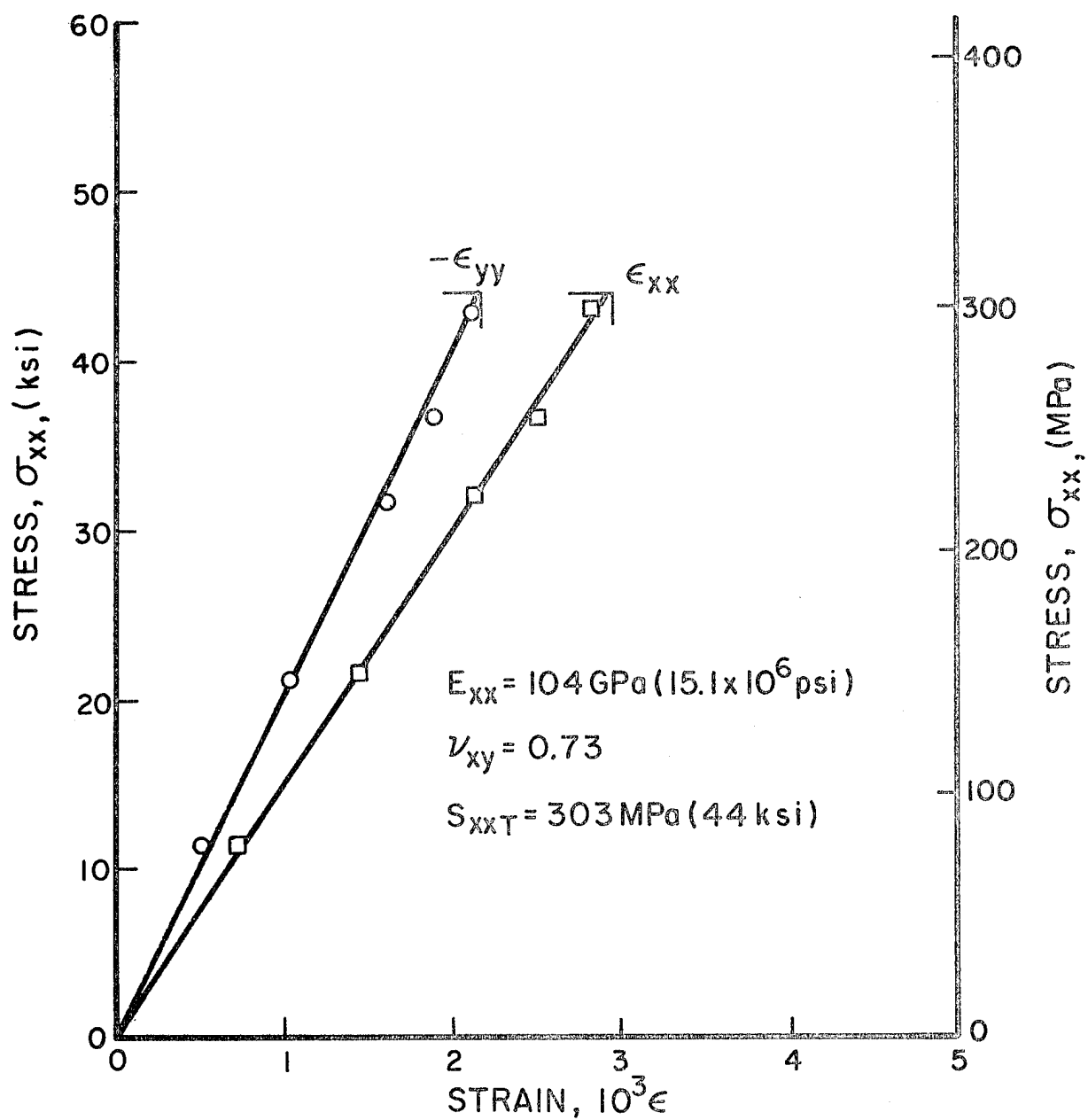
Fig. 3-95 STRAINS IN $\left[0_2/\pm45\right]_s$ GRAPHITE/POLYIMIDE
SPECIMEN UNDER UNIAXIAL TENSILE LOADING

3-145
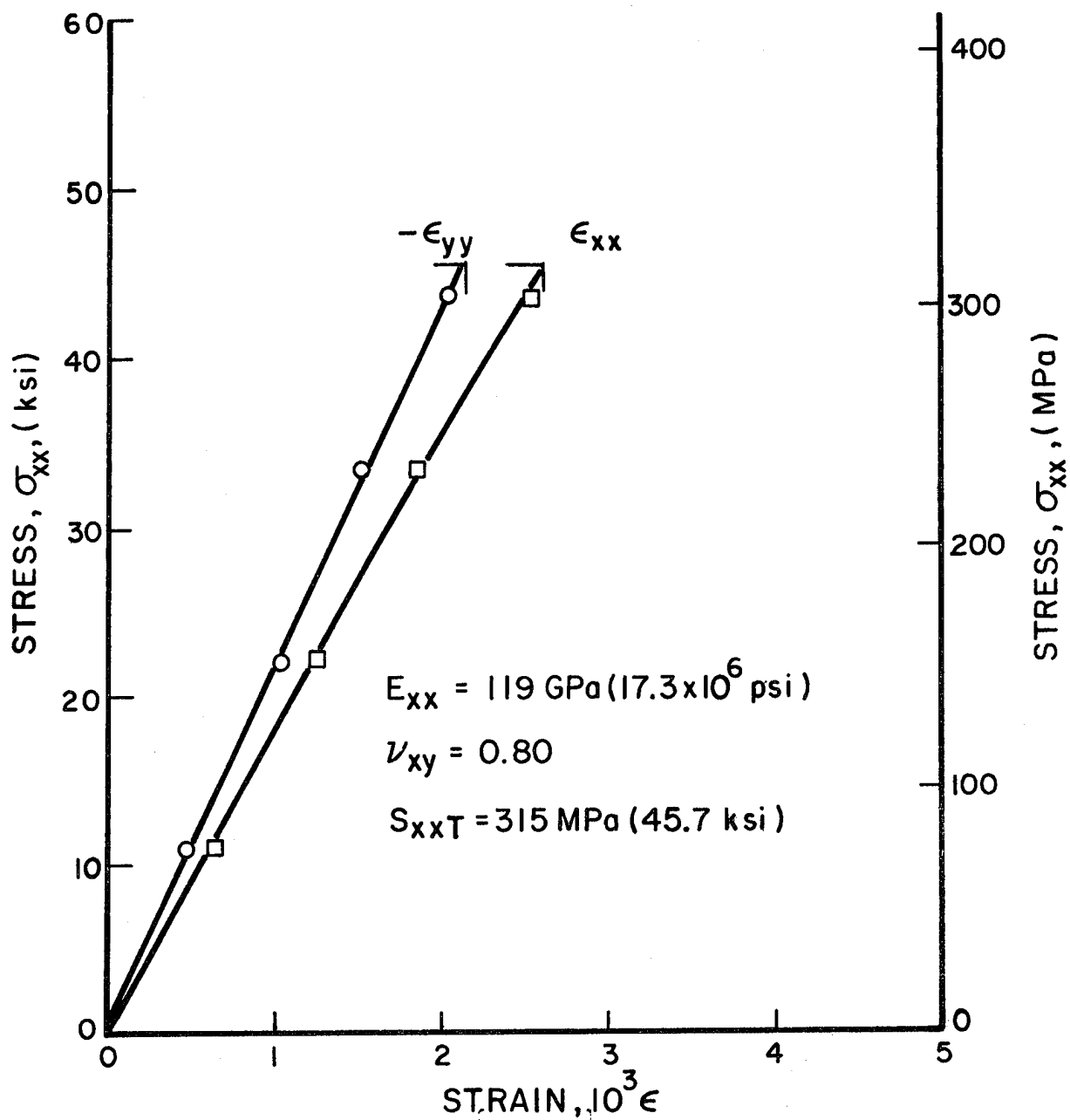
Fig. 3-96   STRAINS IN $[0_2/\pm45]_s$ GRAPHITE/POLYIMIDE
SPECIMEN UNDER UNIAXIAL TENSILE LOADING
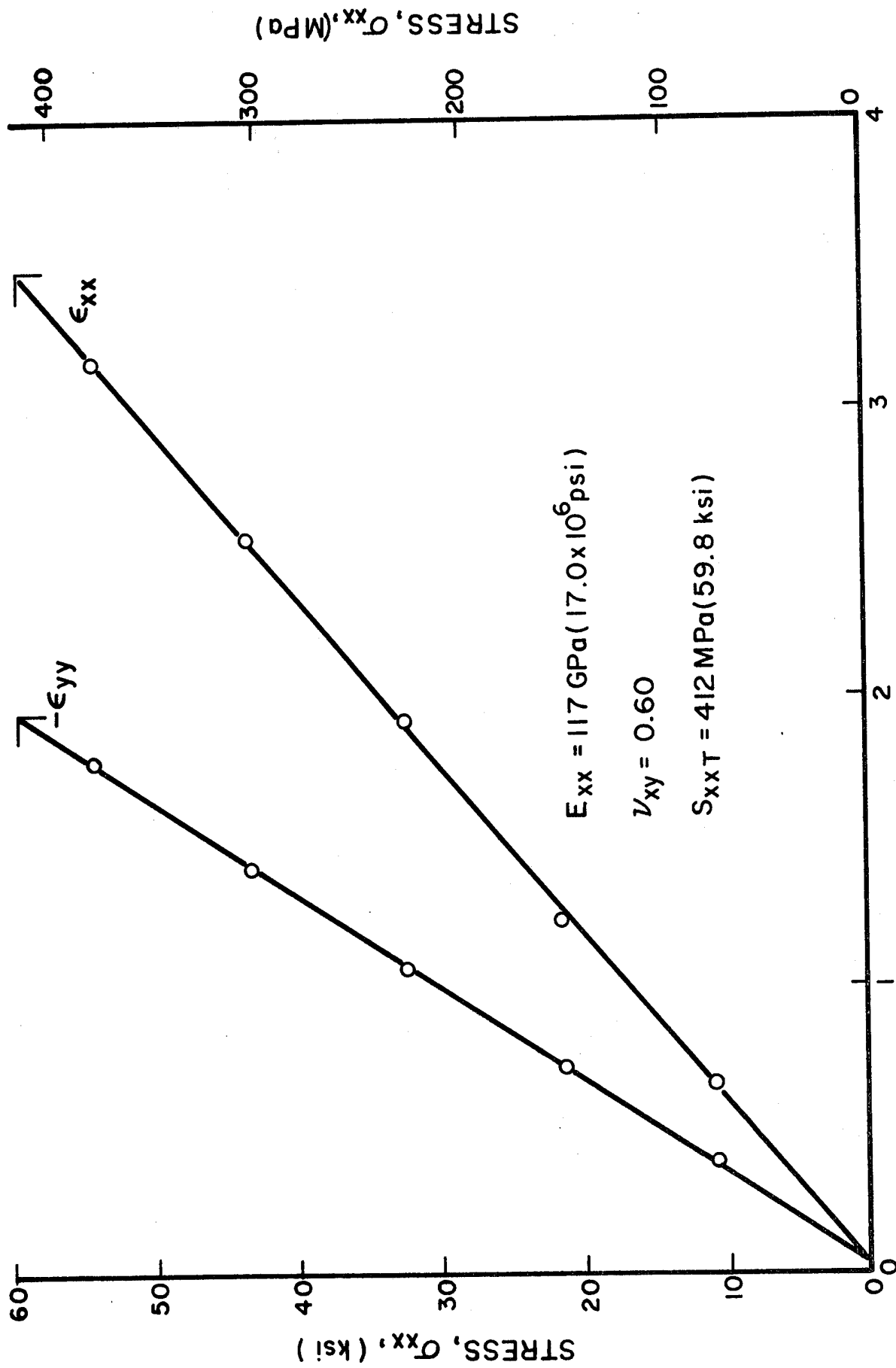
3-146

FIG. 3-97 STRAINS IN $[0_2/\pm45]_s$ GRAPHITE/POLYIMIDE SPECIMEN UNDER UNIAXIAL TENSILE LOADING

$E_{xx} = 117\,GPa\,(17.0 \times 10^6\,psi)$

$\nu_{xy} = 0.60$

$S_{xxT} = 412\,MPa\,(59.8\,ksi)$
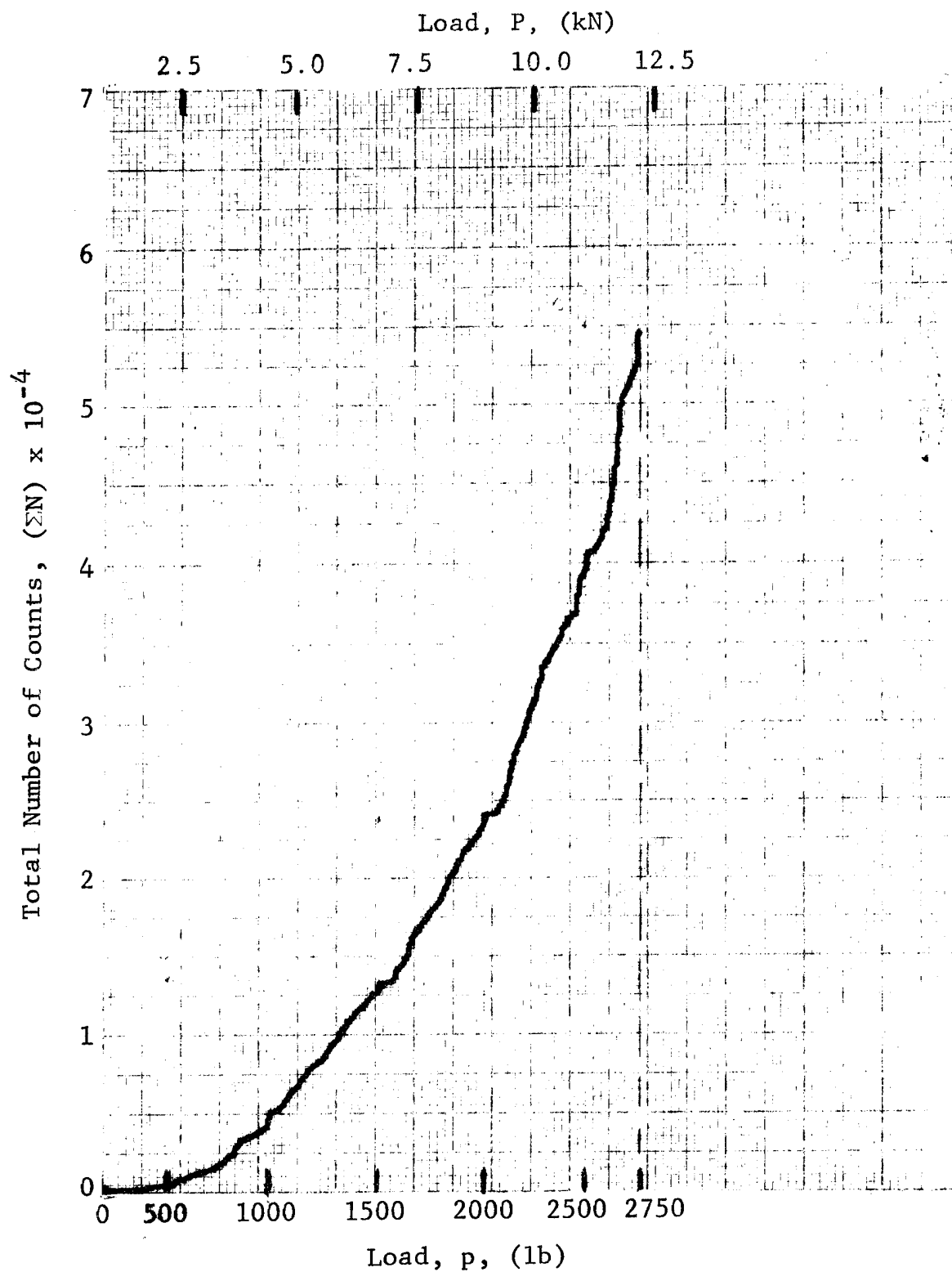
Fig. 3-98 ACOUSTIC EMISSION FOR $[0_2/\underline{+}45]_s$ GRAPHITE/POLYIMIDE SPECIMEN UNDER TENSILE LOADING
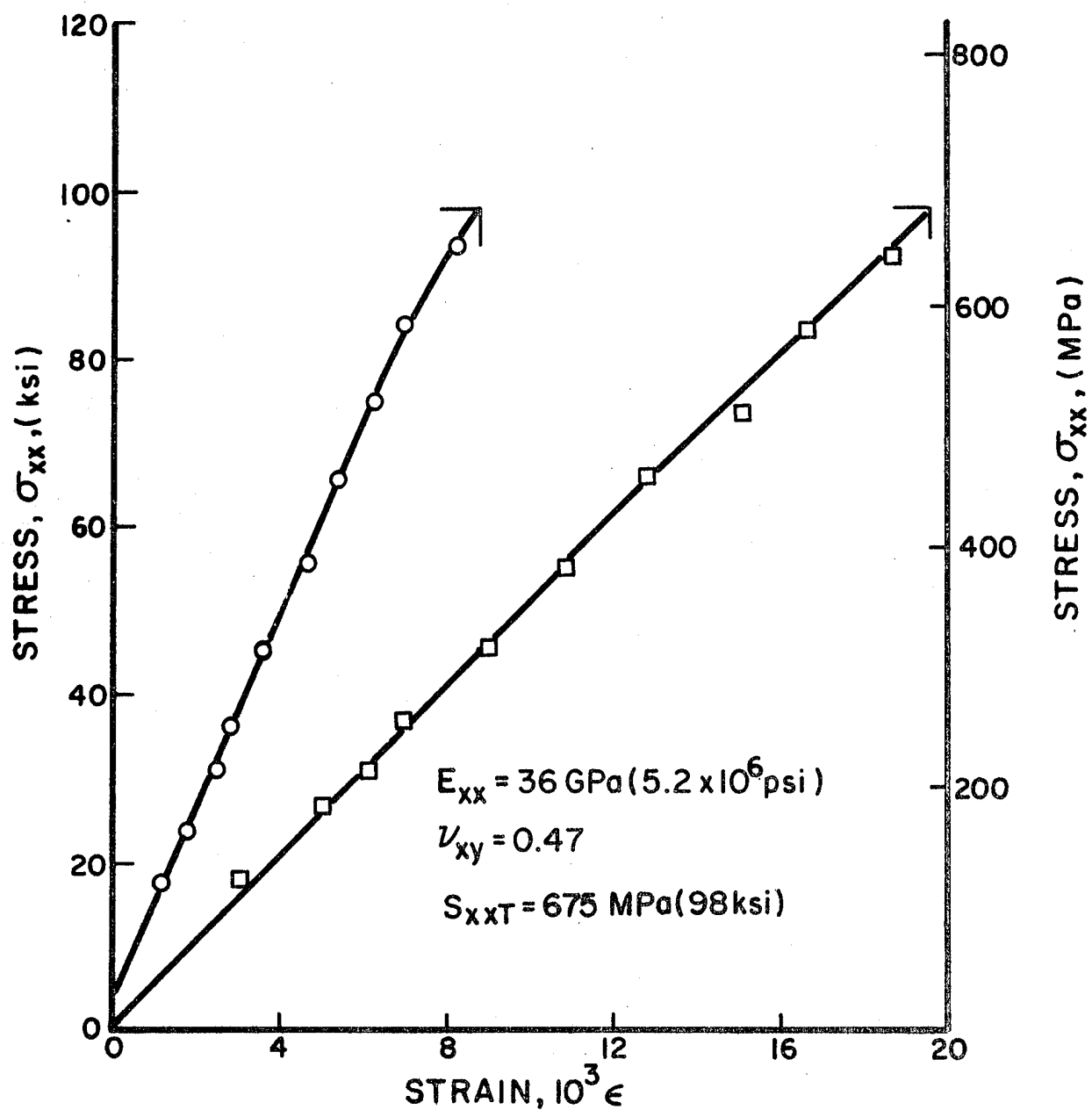
Fig. 3-99 STRAINS IN $\left[0_2/\pm45\right]_s$ S-GLASS/EPOXY SPECIMEN
UNDER UNIAXIAL TENSILE LOADING
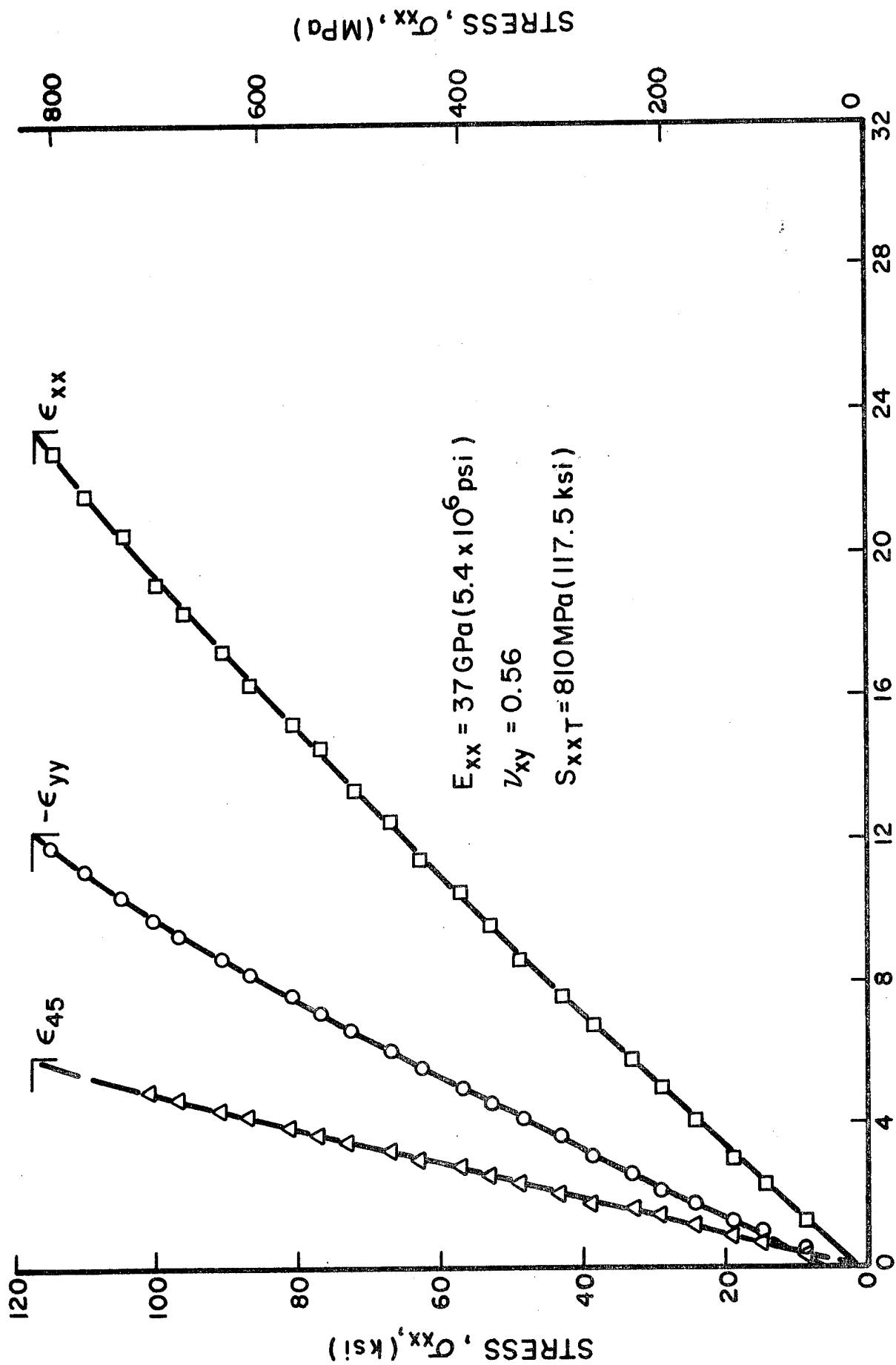
Fig. 3-100 STRAINS IN $[0_2/\pm45]_s$ S-GLASS/EPOXY SPECIMEN UNDER UNIAXIAL TENSILE LOADING

$E_{xx} = 37\,GPa\,(5.4 \times 10^6\,psi)$

$\nu_{xy} = 0.56$

$S_{xxT} = 810\,MPa\,(117.5\,ksi)$

3-150

4.0 TASK III - STRESS RELAXATION EVALUATION

4.1 Introduction

The objective of this task is to investigate the extent
of stress relaxation that the lamination residual stresses undergo.
The various plies of the laminate are cured under conditions
restraining their stress-free thermal deformation. The induced
restraint is directly related to the residual stresses. The
restraint strains remain relatively fixed, allowing only the
possibility of relaxation of the residual stresses. Stress
relaxation is a matrix-controlled property and, therefore, it would
be most pronounced in the transverse to the fiber direction.

Several means of evaluation of residual stress relaxation
were attempted: (1) Direct measurement of strain changes with
time in angle-ply laminates, (2) Stress relaxation determination in
90-degree unidirectional laminates, and (3) Elastic and strength
properties of angle-ply laminates as a function of time after curing.
Results of these three approaches are discussed below.

4.2 Strain Variation in Angle-Ply Laminates

Three 2.54 cm x 22.9 cm $[0_2/\pm45]_s$ S-Glass Epoxy specimens
were prepared with embedded strain gages. Embedded three-gage
rosettes in these specimens were monitored, starting after curing,
over periods up to five months. To maintain gage stability, the
gage voltage was maintained constant throughout the period of
monitoring. At the end of three months, one of the specimens was
removed for static testing to failure.

The average longitudinal and transverse strain variation
for the three specimens is shown in Fig. 4-1. The variations
are very small as expected. Stress relaxation in a given ply in the
transverse to the fiber direction is not accompanied by an
appreciable strain change, since such a deformation is restrained
by the other plies of the laminate. Thus, the small strain

variations that might accompany stress relaxation are not a good measure of this relaxation.

4.3 Stress Relaxation in 90-Degree Unidirectional Laminates

Stress relaxation in composites is a matrix controlled property and as such it is most pronounced in the transverse to the fiber direction. A good measure of the amount of residual stress relaxation occurring in a laminate can be obtained by evaluating the relaxation characteristics of a 90-degree uni-directional laminate under tension. The specimens were 2.54 cm x 22.9 cm (1 in. x 9 in.) $[90_8]$ coupons. They were loaded in the fixture of Fig. 4-2 by applying a certain fixed elongation in a short time. The applied strain corresponded to approximately 70 percent of the static strength of the 90-degree laminate. The change in load with time was monitored with a Schaevitz semi-conductor load cell and also with an aluminum link instrumented with strain gages. The strain in the specimen which is supposed to remain constant throughout the test was checked before every load reading. Some very small adjustments to the load were necessary from time to time to correct for small changes in the specimen strain due to the changing load and the finite compliance of the load cells.

The Boron/Epoxy specimen was loaded with a strain of $2,260 \times 10^{-6}$ corresponding to a stress of 33.8 MPa (4,900 psi). The load variation with time is plotted on a semilogarithmic scale in Fig. 4-3. Most of the relaxation takes place in the first 24 hours and the load (stress) levels off after that time. The maximum amount of relaxation observed was approximately 20 percent.

The Boron/Polyimide specimen was loaded with a strain of 800×10^{-6} producing an instantaneous stress of 6.9 MPa (1000 psi). The load variation with time is plotted on a semilogarithmic scale in Fig. 4-4. Two mechanisms of load relaxation are evident. One, predominant up to approximately 500 minutes, must correspond to stress relaxation in the matrix. The other mechanism related to

a sharp decrease in load comes into effect after 1000 minutes and is probably related to some failure or degradation taking place in the specimen under load.

The relaxation test for Graphite/Low Modulus Epoxy was not successful because of the high fragility of the 90-degree material.

The Graphite/High Modulus Epoxy specimen was loaded with a strain of $4,476 \times 10^{-6}$ producing an instantaneous stress of 31.4 MPa (4,545 psi). The load variation with time is plotted in Fig. 4-5. Stress relaxation was continuing after 25 days of loading.

The Graphite/Polyimide specimen was loaded with a strain of $2,080 \times 10^{-6}$ producing an instantaneous stress of 10.5 MPa (1,520 psi), approximately 71 percent of the ultimate stress. The load variation with time is plotted in Fig. 4-6. The load seems to stabilize at 90 percent of its initial value after approximately 35 days.

The S-Glass/Epoxy specimen was loaded with a strain of $1,560 \times 10^{-6}$ producing an instantaneous stress of 39.7 MPa (5750 psi). The load variation with time is plotted in Fig. 4-7. The load (stress) seems to level off at 86 percent of its initial value after 25 days.

The following Table 4-1 summarizes the results of the relaxation tests described above.

Table 4-1

TENSILE STRESS RELAXATION IN 90-DEGREE UNIDIRECTIONAL SPECIMENS

Material	Applied Stress, σ_{22} MPa (psi)	Percent Relaxation In 30 Days
Boron/Epoxy	33.8 (4,900)	22.5
Boron/Polyimide	6.9 (1,000)	62.0
Graphite/High Modulus Epoxy	31.4 (4,545)	24.5
Graphite/Polyimide	10.5 (1,520)	9.5
S-Glass/Epoxy	39.7 (5,750)	13.0

The Graphite/Polyimide displays the lowest stress relaxation, and the Boron/Polyimide the highest, although both have the same matrix. It is conjectured, however, that the apparent relaxation in the latter is related to microfailure rather than to purely viscoelastic properties of the matrix. Further testing at different stress levels would explain the phenomenon. Of the epoxy matrix composites, the S-Glass/Epoxy displayed the lowest relaxation. This is probably due to the much higher fiber volume ratio of this material (FVR = 0.72).

The results above serve only as indications of the order of magnitude of residual stress relaxation that may occur in an angle-ply laminate. The actual conditions in the laminate are more complicated as each ply is subjected to an in-plane biaxial state of stress and interlaminar shear stress. More extensive testing would be required to evaluate stress relaxation under these more complex conditions.

4.4 Static Properties of Laminates as a Function of Time After Curing

Two specimens of each material system of $\left[0_2/\pm45\right]_s$ layup were tested statically at various times to determine any possible effects of residual stress relaxation on elastic and strength properties. Stress-strain curves for the various specimens tested at various times after curing of the laminates are shown in Figs. 4-8 through 4-33.

Figures 4-8 to 4-10 show stress-strain curves for Boron/ Epoxy specimens tested nine and twelve and one-half months after curing. Both the elastic modulus and strength values are very close to those obtained a short time after curing.

Figures 4-11 through 4-15 show stress-strain curves for Boron/Polyimide specimens tested four and one-half, eight and seventeen months after curing. No significant variation with time in modulus or strength is apparent.

Figures 4-16 and 4-17 show stress-strain curves for Graphite/Low Modulus Epoxy specimens tested three and six and one-half months after curing. An additional specimen was tested sixteen months after curing. The fluctuations in the modulus values are not significant. The strength values at times beyond three months are all the same 350 MPa (51 ksi) but appreciably lower than the initial value of 562 MPa (82 ksi). This may be related to the fact that the initial values for the strength were obtained from 2.54 cm (1 in.) wide specimens, whereas all subsequent tests were performed with 1.27 cm (0.5 in.) wide specimens. The heat produced in cutting the specimens tends to soften the matrix and cause delaminations near the edge which are more serious in the narrower specimens.

Figures 4-18 through 4-21 show stress-strain curves for Graphite/High Modulus Epoxy specimens tested six, nine and one-half and nineteen months after curing. The fluctuations in modulus are larger than in other materials but no trend is apparent. The fluctuations in strength are very small with deviations from the mean of three percent or lower.

Figures 4-22 through 4-26 show stress-strain curves for Graphite/Polyimide specimens tested four, eight and seventeen months after curing. No significant changes with time are seen in the modulus, but the strength values are somewhat lower than initial values. This difference again may be related to the fact that all long-time tests were performed with narrower (1.27 cm; 0.5 in.) specimens than the initially used 2.54 cm (1 in.) wide specimens.

Figures 4-28 through 4-33 show stress-strain curves for S-Glass/Epoxy specimens tested three, six, nine, twelve and one-half and twenty-two months after curing. No significant variations in either modulus or strength exist. The apparent variations in strength are due to the fact that two batches of material are represented. The individually prepared 2.54 cm (1 in.) wide

coupons with embedded strain gages showed consistantly high strength values, 807 MPa (117 ksi), 820 (119 ksi), and 789 MPa (114 ksi) initially, three months and six months after curing, respectively. The strength values at nine, twelve and one-half and twenty-two months obtained from specimens cut from a plate are in closer agreement with the initial value of 675 MPa (98 ksi) obtained from a similar specimen.

The results above are summarized in Table 4-2 where the modulus, Poisson's ratio, strength and age of the specimens are given. In most cases where two or more specimens were tested at one time, the average values are shown. Initial values, or values obtained within one to three months after curing were obtained from Table 3-19.

4.5 Summary and Conclusions

Three approaches were investigated for evaluation of residual stress relaxation in angle-ply laminates: (1) Direct measurement of strain changes with time, (2) Stress relaxation determination in 90-degree unidirectional specimens, and (3) Elastic and strength properties of laminates as a function of time after curing.

Measurement of strain variation is a very insensitive means. Strain variations are very small, sometimes of the order of experimental variability, as they represent a second order effect of stress relaxation.

A better measure of the degree of residual stress relaxation was obtained by means of direct relaxation tests of 90-degree unidirectional laminates. The amount of relaxation in thirty days in most cases ranged between 9.5 and 24.5 percent, except for the Boron/Polyimide where a fracture mechanism was possibly operating. This amount of relaxation represents an upper bound to the actual stress relaxation taking place in an angle-ply laminate. It can be concluded, therefore, that the amount of residual stress relaxation in an angle-ply laminate is small.

Table 4-2
STATIC PROPERTIES OF $\left[0_2/\pm45\right]_s$ AT VARIOUS
TIMES AFTER CURING

Material	Modulus, E_{xx} GPA (10^6 psi)	Poisson's Ratio, ν_{xy}	Strength S_{xxT} MPa (ksi)	Age (Months)
Boron/Epoxy	115 (16.7)	0.70	725 (105)	1-3
	115 (16.7)	0.60	754 (109)	9
	116 (16.8)	0.71	725 (105)	12.5
Boron/Polyimide	117 (17.0)	0.72	562 (82)	1
	114 (16.5)	0.76	522 (76)	4.5
	112 (16.3)	0.77	519 (75)	8
	126 (18.2)	0.69	578 (84)	17
Graphite/Low Modulus Epoxy	111 (16.1)	0.72	562 (82)	1
	110 (15.9)	0.71	350 (51)	3
	105 (15.3)	0.52	350 (51)	6.5
	115 (16.7)	0.80	350 (51)	16
Graphite/High Modulus Epoxy	99 (14.3)	0.72	485 (70)	1-2
	94 (13.6)	0.74	515 (75)	6
	107 (15.6)	0.69	510 (74)	9.5
	112 (16.2)	0.72	497 (72)	19
Graphite/ Polyimide	114 (16.5)	0.71	345 (50)	1
	121 (17.6)	0.67	314 (46)	4
	107 (15.6)	0.72	290 (42)	8
	115 (16.7)	0.65	317 (46)	17
S-Glass/Epoxy	37 (5.3)	0.52	742 (108)	1
	40 (5.8)	0.50	820 (119)	3
	44 (6.4)	0.43	789 (114)	6
	37 (5.3)	0.55	618 (90)	9
	36 (5.2)	0.53	649 (94)	12.5
	37 (5.3)	0.52	696 (101)	22

Indirect measurements were made of the effects of stress relaxation on elastic modulus and strength of angle-ply laminates. No significant variations in modulus or strength were observed in specimens tested over periods from one to twenty-two months after curing.
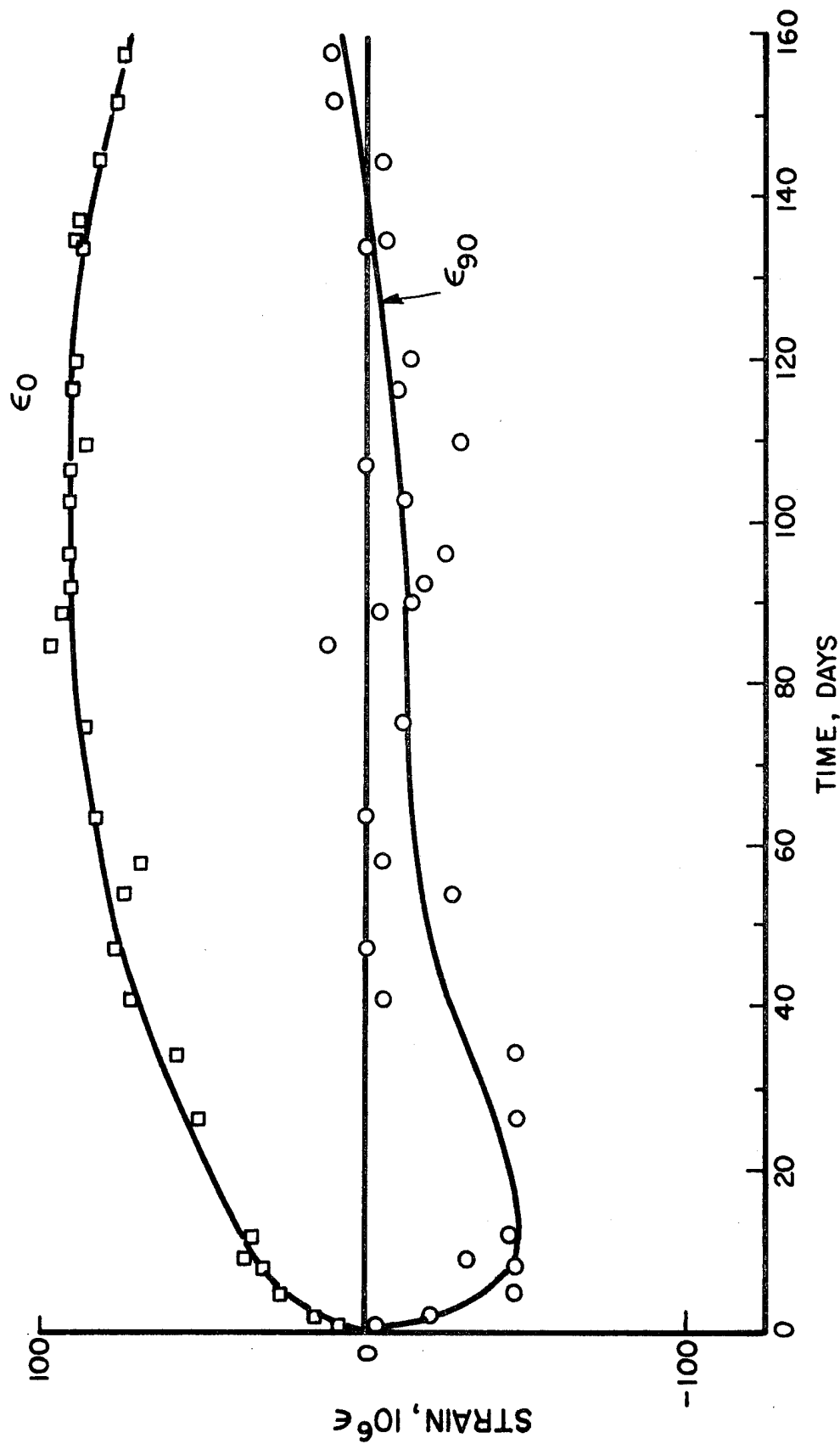
Fig. 4-1 STRAIN VARIATION IN $[0_2/\pm 45]_s$ S-GLASS/EPOXY SPECIMENS AS A FUNCTION OF TIME AFTER CURING (STRAIN GAGES EMBEDDED BETWEEN FOURTH AND FIFTH PLY)

4-9
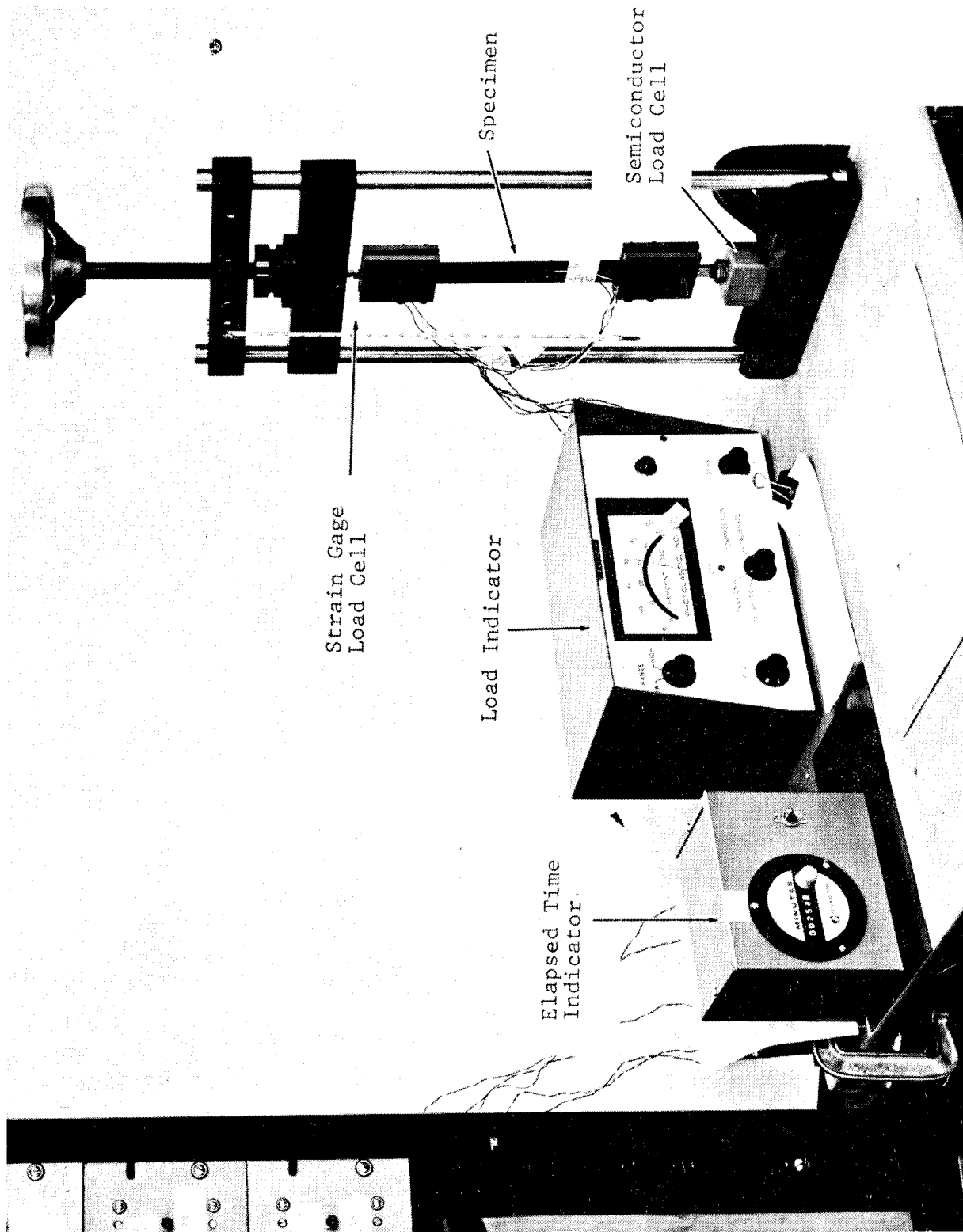
Fig. 4-2 EXPERIMENTAL SETUP FOR MEASURING STRESS RELAXATION IN COMPOSITE SPECIMENS
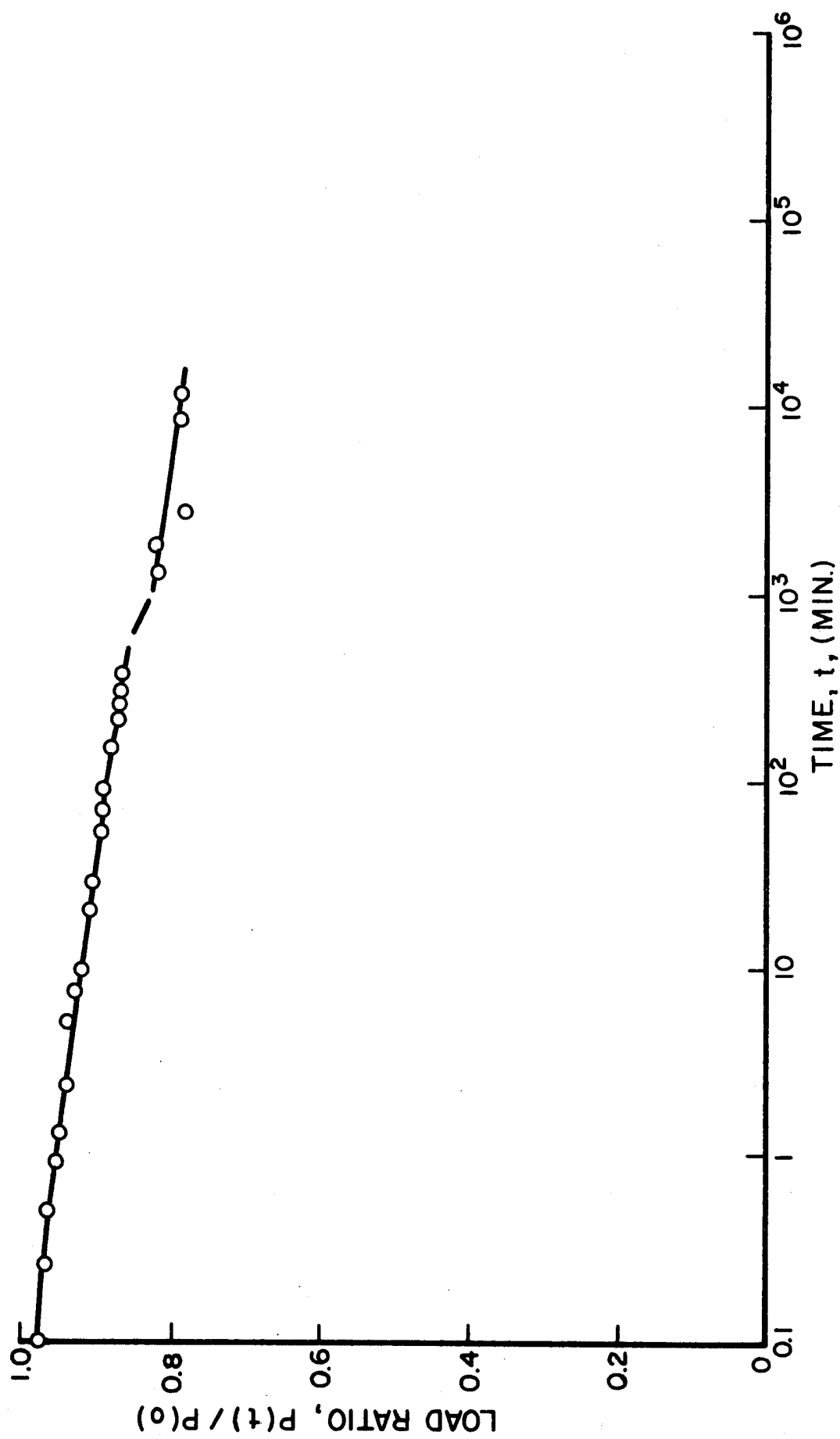
Fig. 4-3 STRESS RELAXATION IN 90-DEGREE UNIDIRECTIONAL BORON/EPOXY SPECIMEN
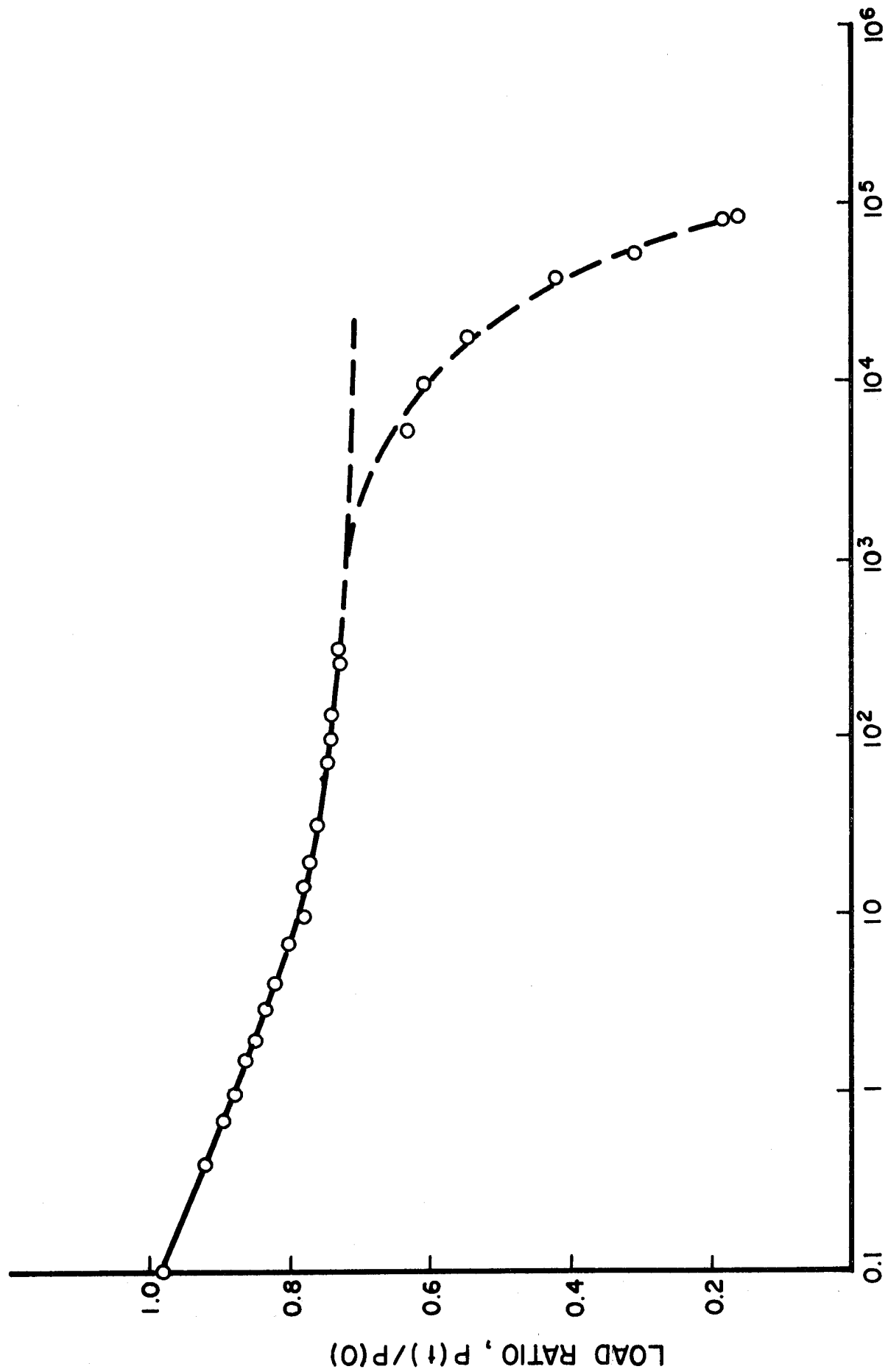
Fig. 4-4 STRESS RELAXATION IN 90-DEGREE UNIDIRECTIONAL BORON/POLYIMIDE SPECIMEN
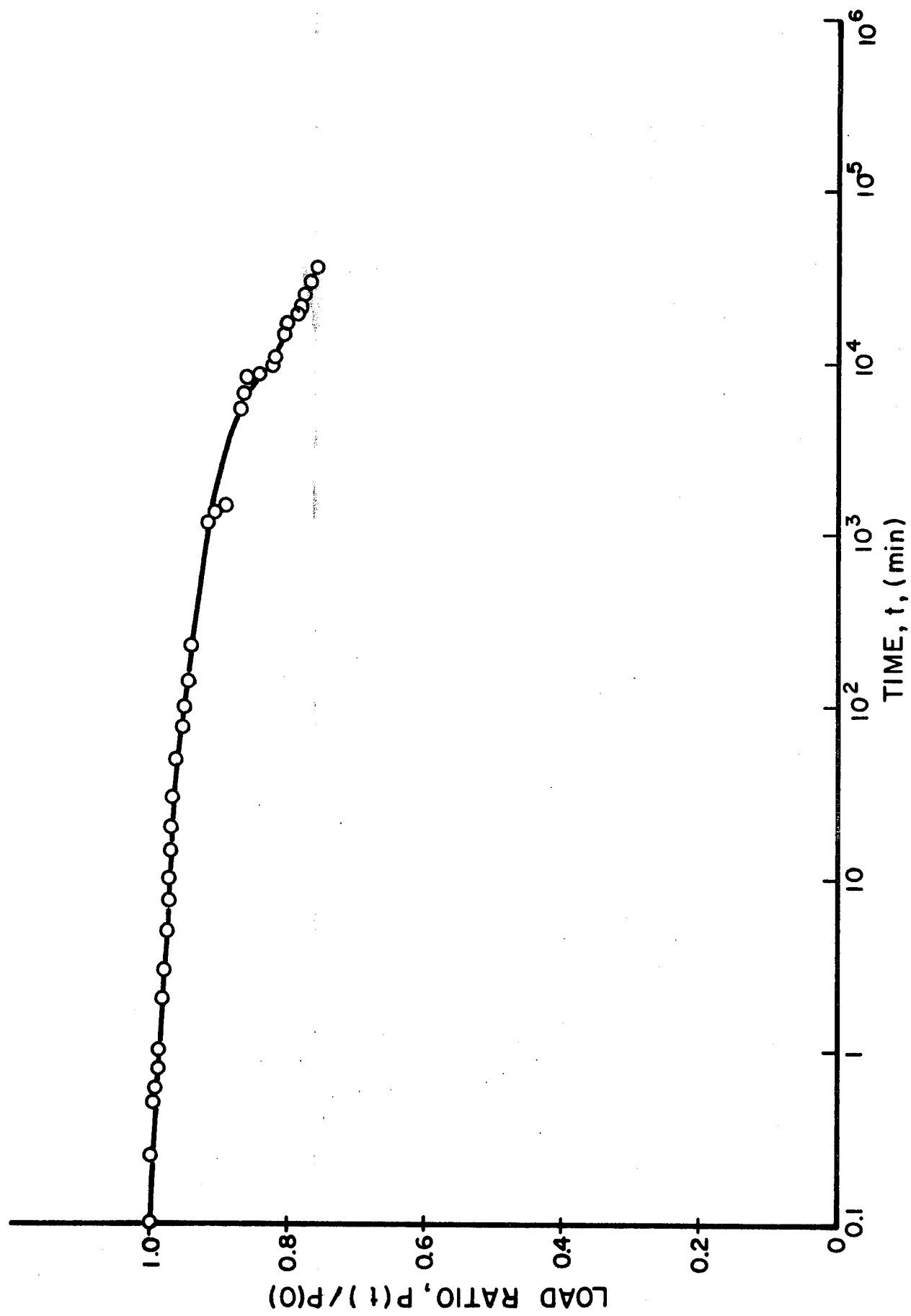
4-12

Fig. 4-5 STRESS RELAXATION IN 90-DEGREE UNIDIRECTIONAL GRAPHITE/HIGH MODULUS EPOXY SPECIMEN
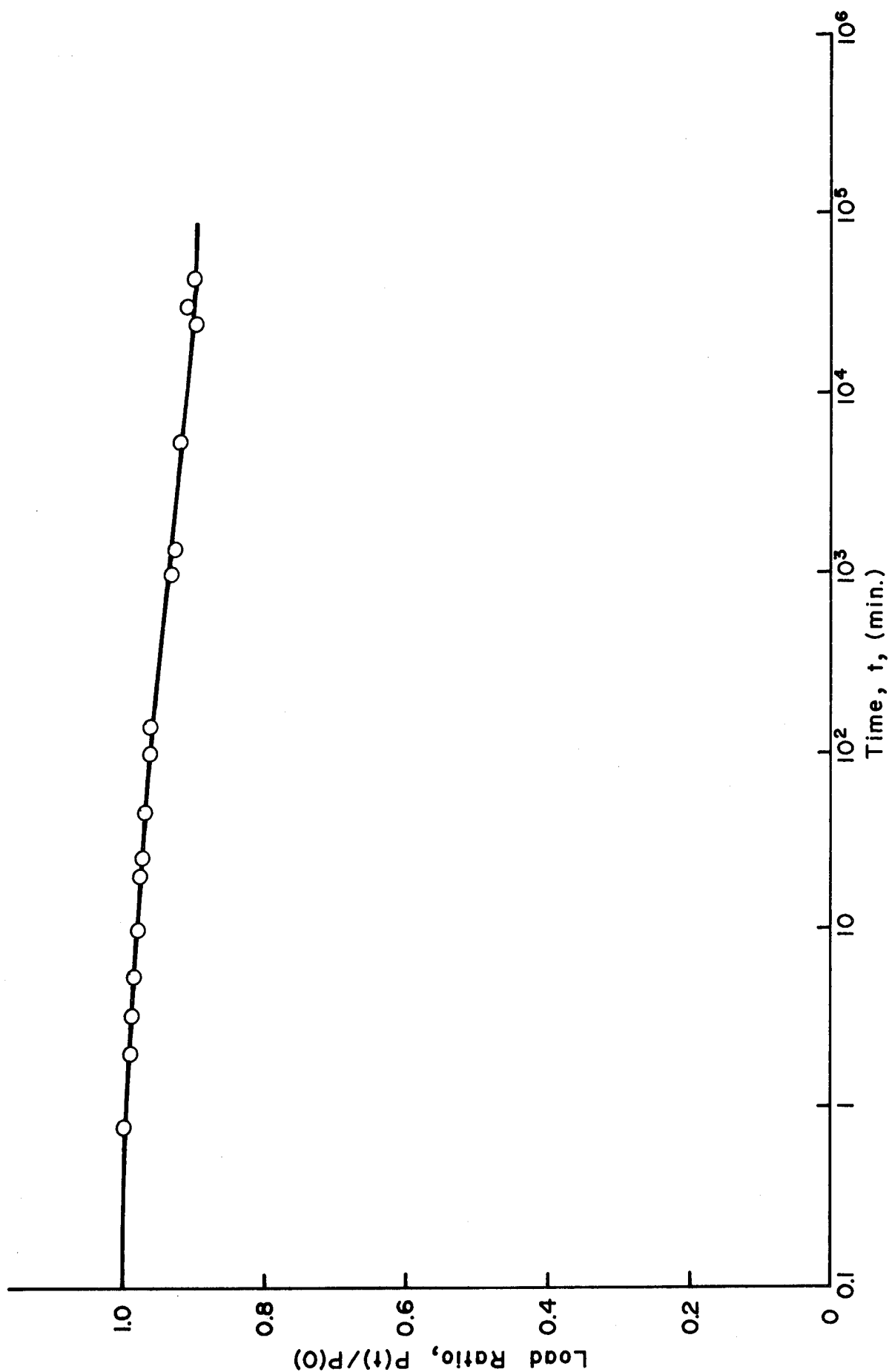
Fig. 4-6   STRESS RELAXATION IN 90-DEGREE UNIDIRECTIONAL GRAPHITE/POLYIMIDE SPECIMEN
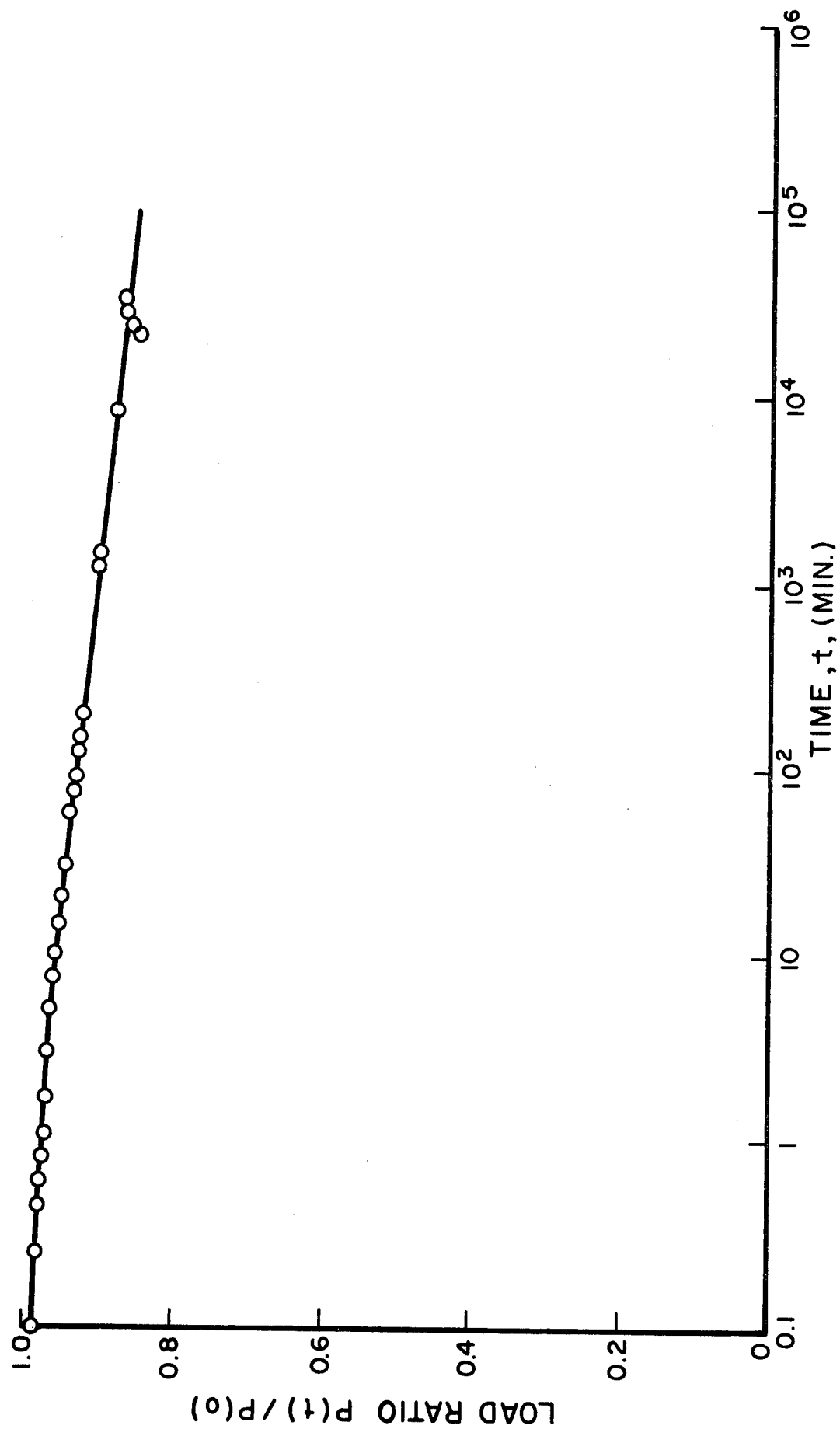
Fig. 4-7 STRESS RELAXATION IN 90-DEGREE UNIDIRECTIONAL S-GLASS/EPOXY SPECIMEN

4-15
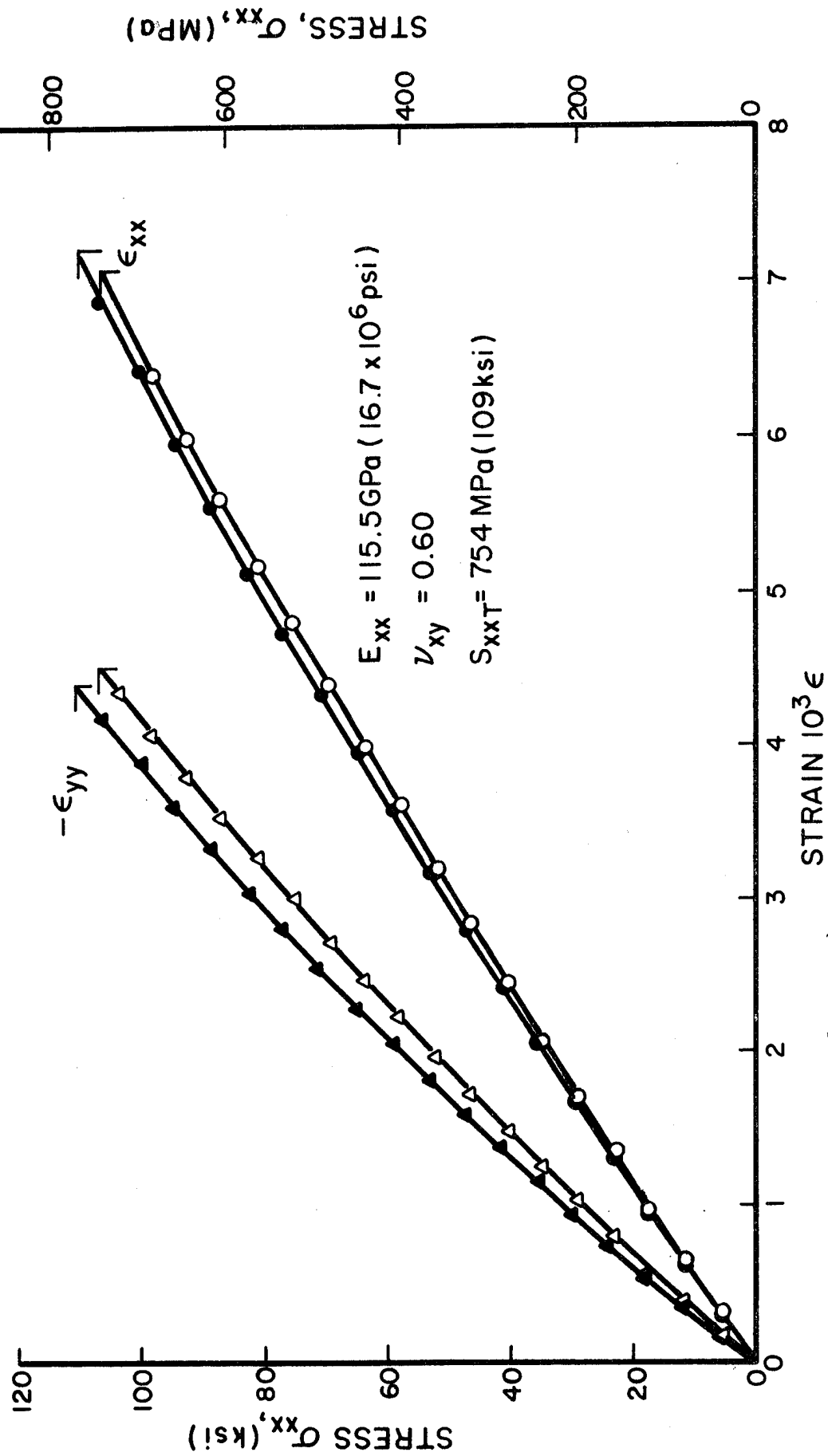
Fig. 4-8 STRAINS IN $[0_2/\pm45]_s$ BORON/EPOXY SPECIMENS UNDER UNIAXIAL TENSILE LOADING NINE MONTHS AFTER CURING (OPEN AND FILLED SYMBOLS REPRESENT TWO DIFFERENT SPECIMENS)
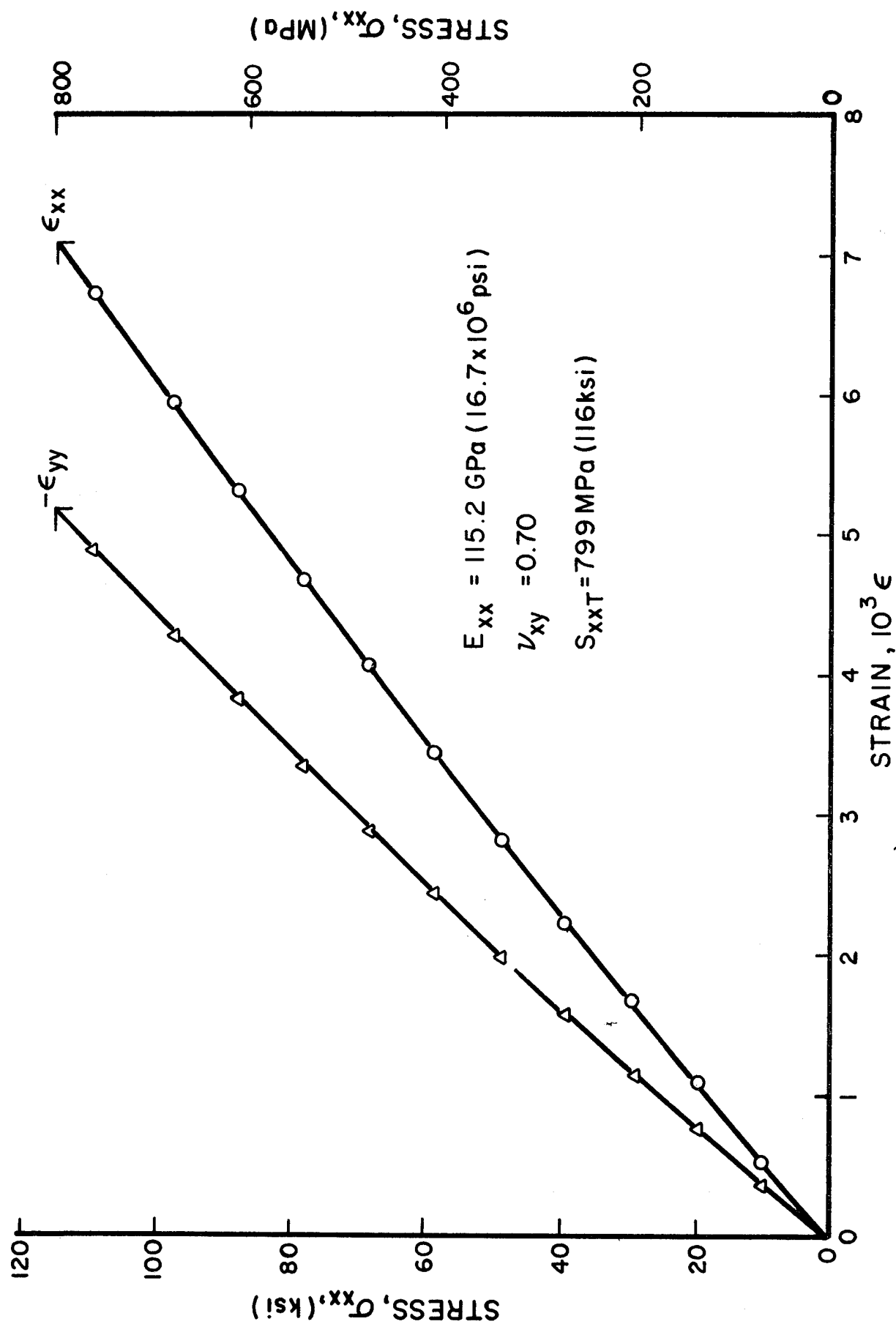
$E_{xx} = 115.5\,GPa\,(16.7 \times 10^6\,psi)$
$\nu_{xy} = 0.60$
$S_{xxT} = 754\,MPa\,(109\,ksi)$

ϵ_{xx}

$-\epsilon_{yy}$

STRESS, σ_{xx}, (MPa)

STRESS σ_{xx}, (ksi)

STRAIN $10^3\,\epsilon$

Fig. 4-9 STRAINS IN $[0_2/\pm45]_s$ BORON/EPOXY SPECIMENS UNDER UNIAXIAL TENSILE
LOADING TWELVE AND ONE-HALF MONTHS AFTER CURING

The figure shows a stress-strain plot with:

STRESS, σ_{xx}, (MPa) on one axis (0, 200, 400, 600, 800)

STRAIN, $10^3 \epsilon$ on horizontal axis (0, 1, 2, 3, 4, 5, 6, 7, 8)

STRESS, σ_{xx}, (ksi) (0, 20, 40, 60, 80, 100, 120)

$E_{xx} = 115.2$ GPa $(16.7 \times 10^6$ psi$)$

$\nu_{xy} = 0.70$

$S_{xxT} = 799$ MPa $(116$ ksi$)$

ϵ_{xx}

$-\epsilon_{yy}$

Fig. 4-10 STRAINS IN $[0_2/\pm45]_s$ BORON/EPOXY SPECIMENS UNDER UNIAXIAL TENSILE LOADING TWELVE AND ONE-HALF MONTHS AFTER CURING

$E_{XX} = 116.6$ GPa $(16.9 \times 10^6$ PSI$)$
$\nu_{XX} = 0.73$
$S_{XXT} = 647$ MPA $(94$ KSI$)$
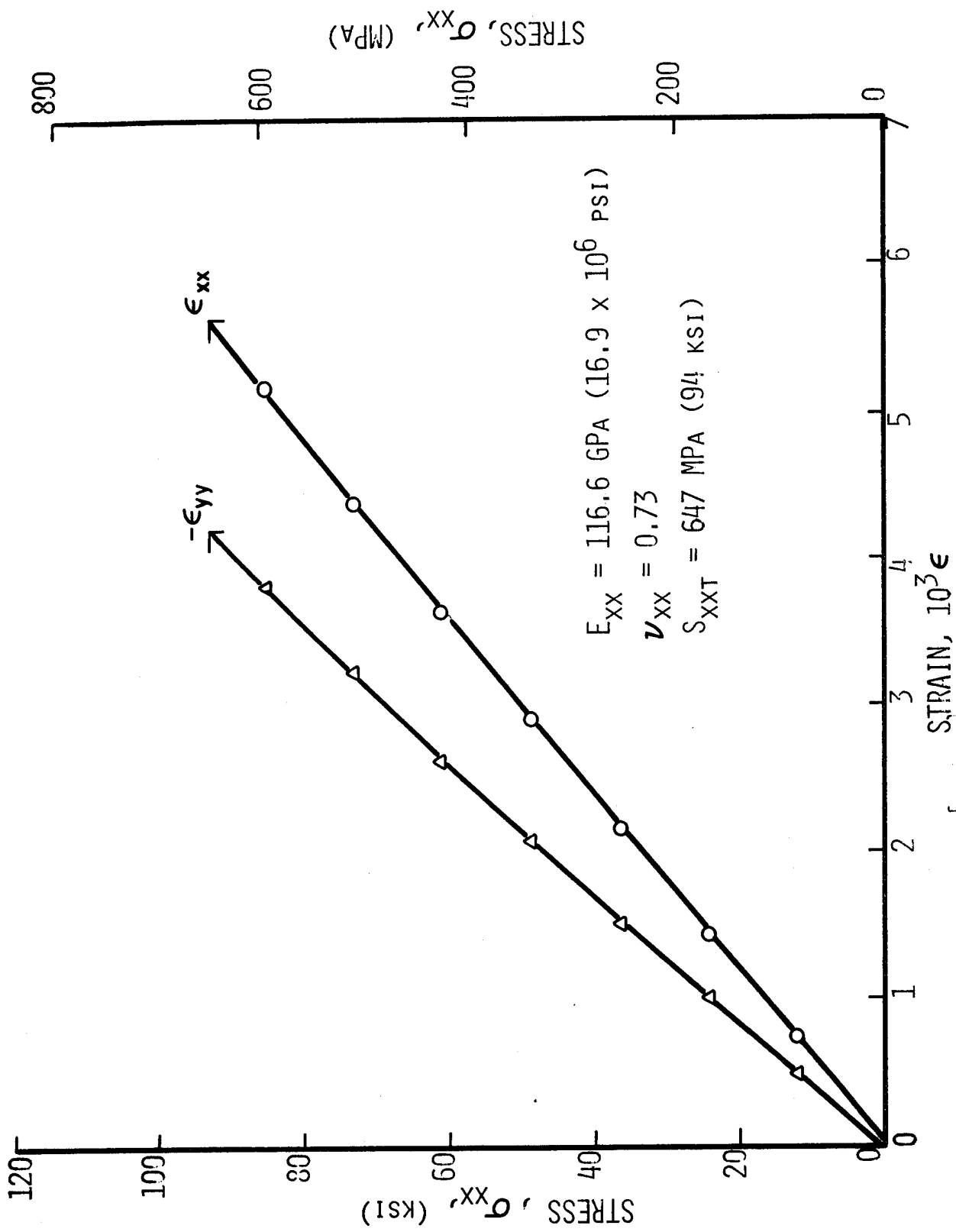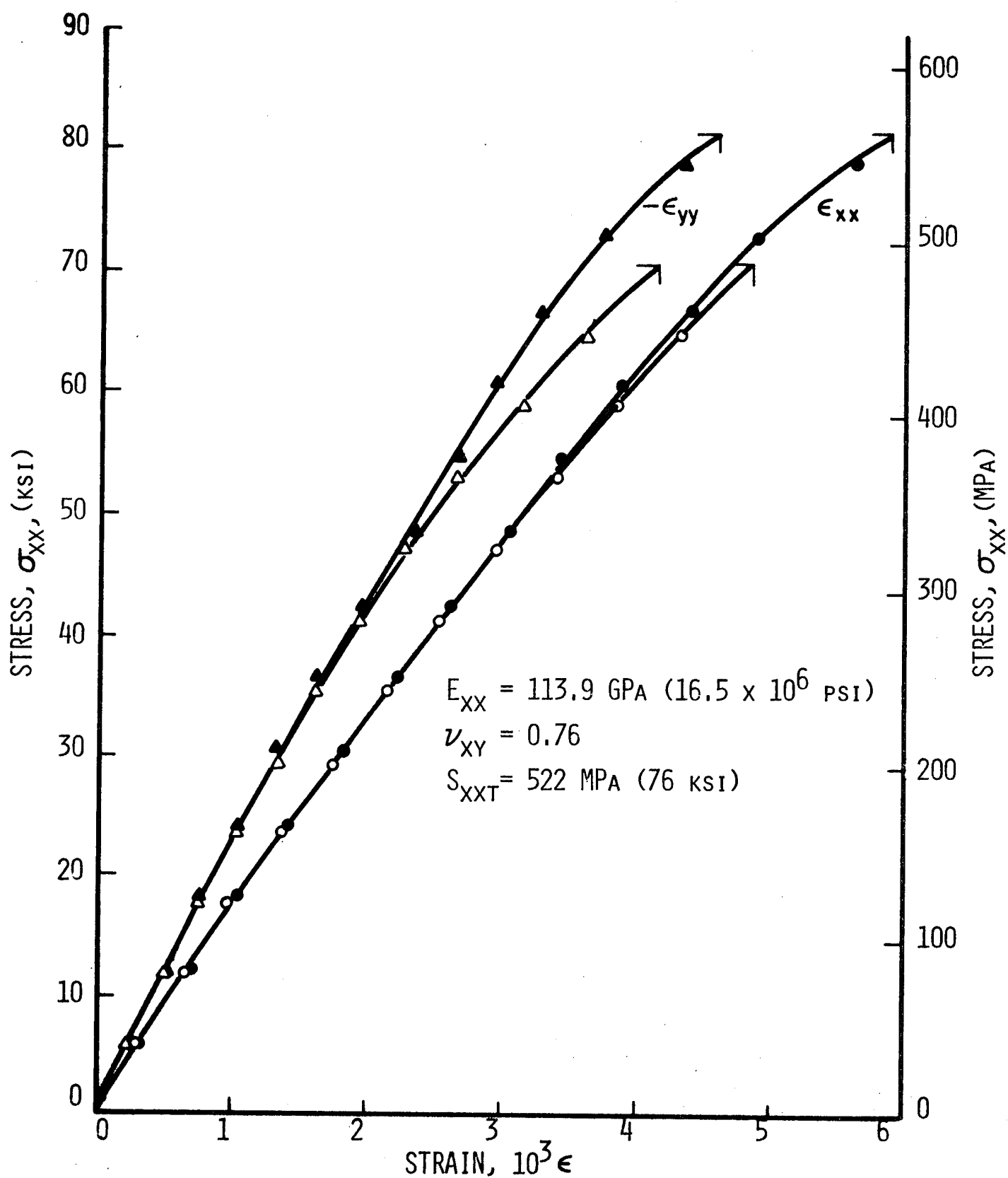
Fig. 4-11   STRAINS IN $\left[0_2/\pm45\right]_s$ BORON/POLYIMIDE SPECIMENS UNDER UNIAXIAL TENSILE LOADING FOUR AND ONE-HALF MONTHS AFTER CURING
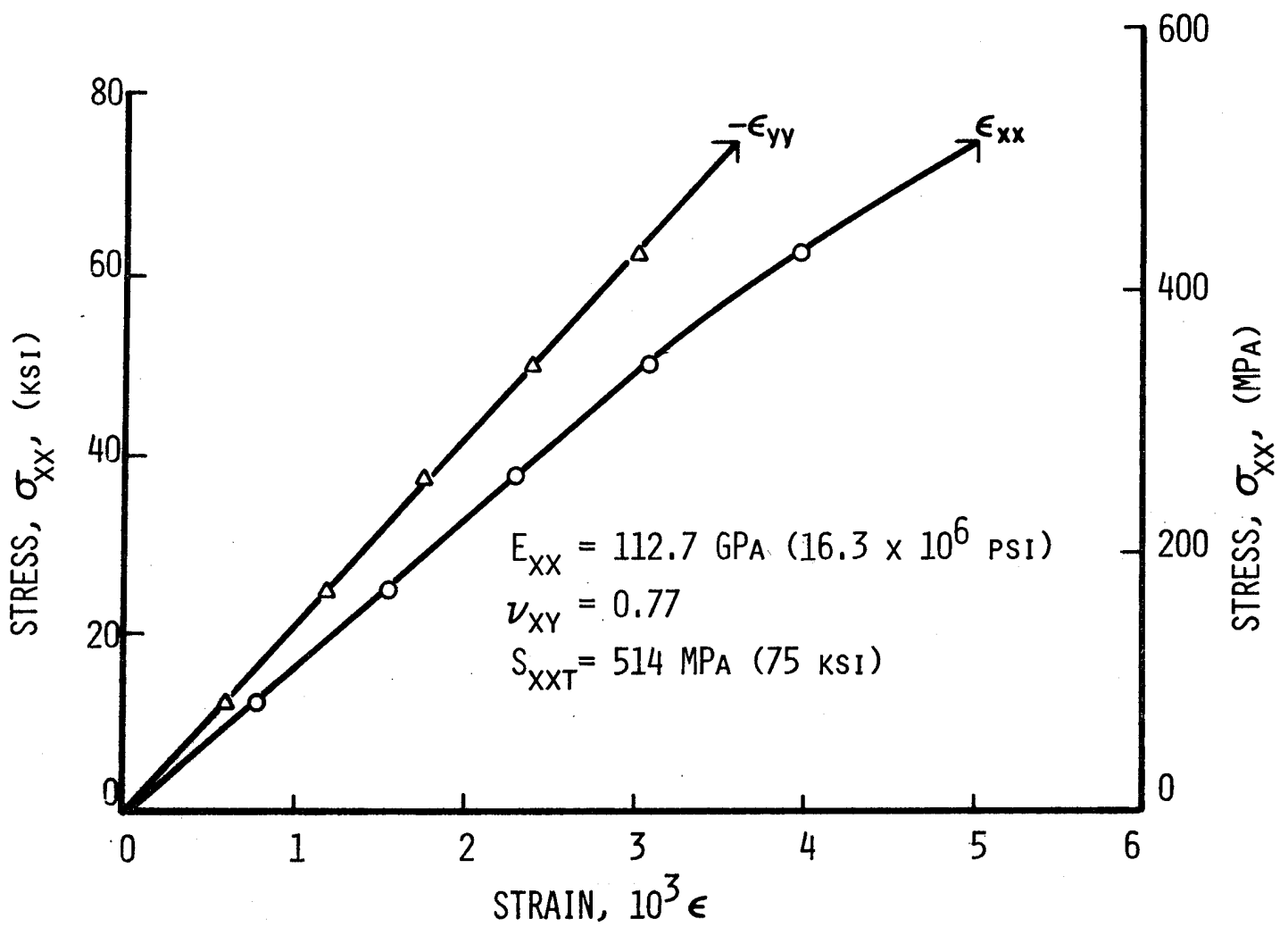
The figure contains the following annotations:

E_{XX} = 113.9 GPa (16.5 x 10^6 PSI)

ν_{XY} = 0.76

S_{XXT} = 522 MPa (76 KSI)

Axis labels: STRESS, σ_{XX}, (KSI); STRESS, σ_{XX}, (MPA); STRAIN, $10^3 \epsilon$

Curve labels: $-\epsilon_{yy}$, ϵ_{xx}

Fig. 4-12 STRAINS IN $[0_2/\pm45]_s$ BORON/POLYIMIDE SPECIMENS UNDER UNIAXIAL TENSILE LOADING EIGHT MONTHS AFTER CURING

The figure contains the following annotations:

$-\epsilon_{yy}$

ϵ_{xx}

$E_{XX} = 112.7$ GPa $(16.3 \times 10^6$ PSI$)$

$\nu_{XY} = 0.77$

$S_{XXT} = 514$ MPa $(75$ KSI$)$

Axis labels: STRESS, σ_{XX}, (KSI); STRESS, σ_{XX}, (MPA); STRAIN, $10^3\epsilon$

Fig. 4-13 STRAINS IN $[0_2/\pm 45]_s$ BORON/POLYIMIDE SPECIMENS UNDER UNIAXIAL TENSILE LOADING EIGHT MONTHS AFTER CURING

The figure plots STRAIN, σ_{xx}, (KSI) and STRAIN, σ_{xx}, (MPA) versus STRAIN, $10^3\epsilon$, showing curves for ϵ_{xx} and $-\epsilon_{yy}$.

$E_{xx} = 112.1$ GPA (16.2 $\times 10^6$ PSI)

$\nu_{XY} = 0.78$

$S_{XXT} = 524$ MPA (76 KSI)

Fig. 4-14 STRAINS IN $\left[0_2/\pm 45\right]_s$ BORON/POLYIMIDE SPECIMENS UNDER UNIAXIAL TENSILE LOADING SEVENTEEN MONTHS AFTER CURING

$E_{xx} = 120.8$ GPa $(17.5 \times 10^6$ PSI)

$\nu_{xy} = 0.70$

$S_{xxT} = 563$ MPA $(82$ KSI$)$

STRESS, σ_{XX}, (MPA)

ϵ_{xx}

$-\epsilon_{yy}$

E_{XX} = 131.1 GPA (19.0 × 10^6 PSI)

ν_{XY} = 0.67

S_{XXT} = 593 MPA (86 KSI)

STRAIN, $10^3 \epsilon$

STRESS, σ_{XX}, (KSI)
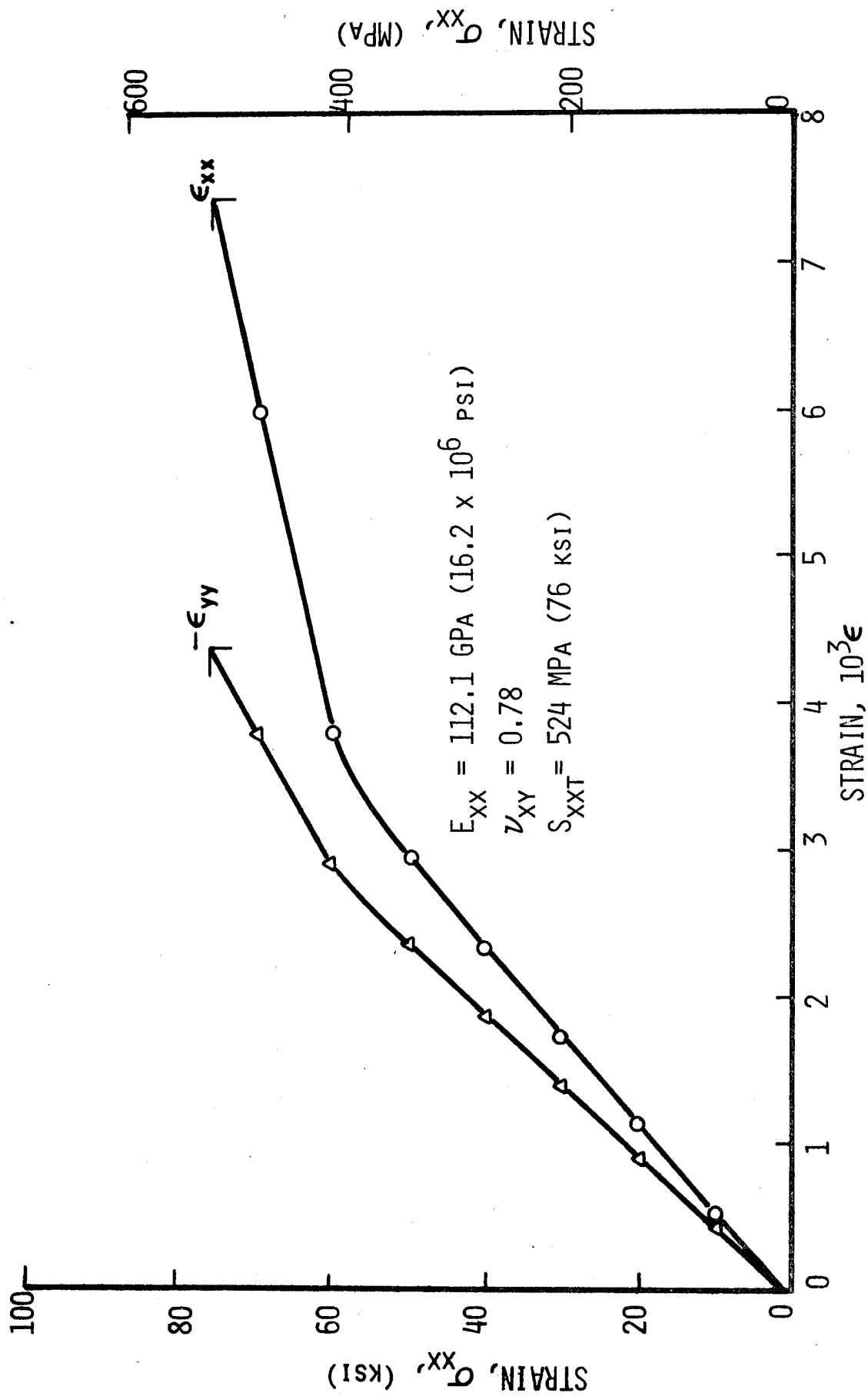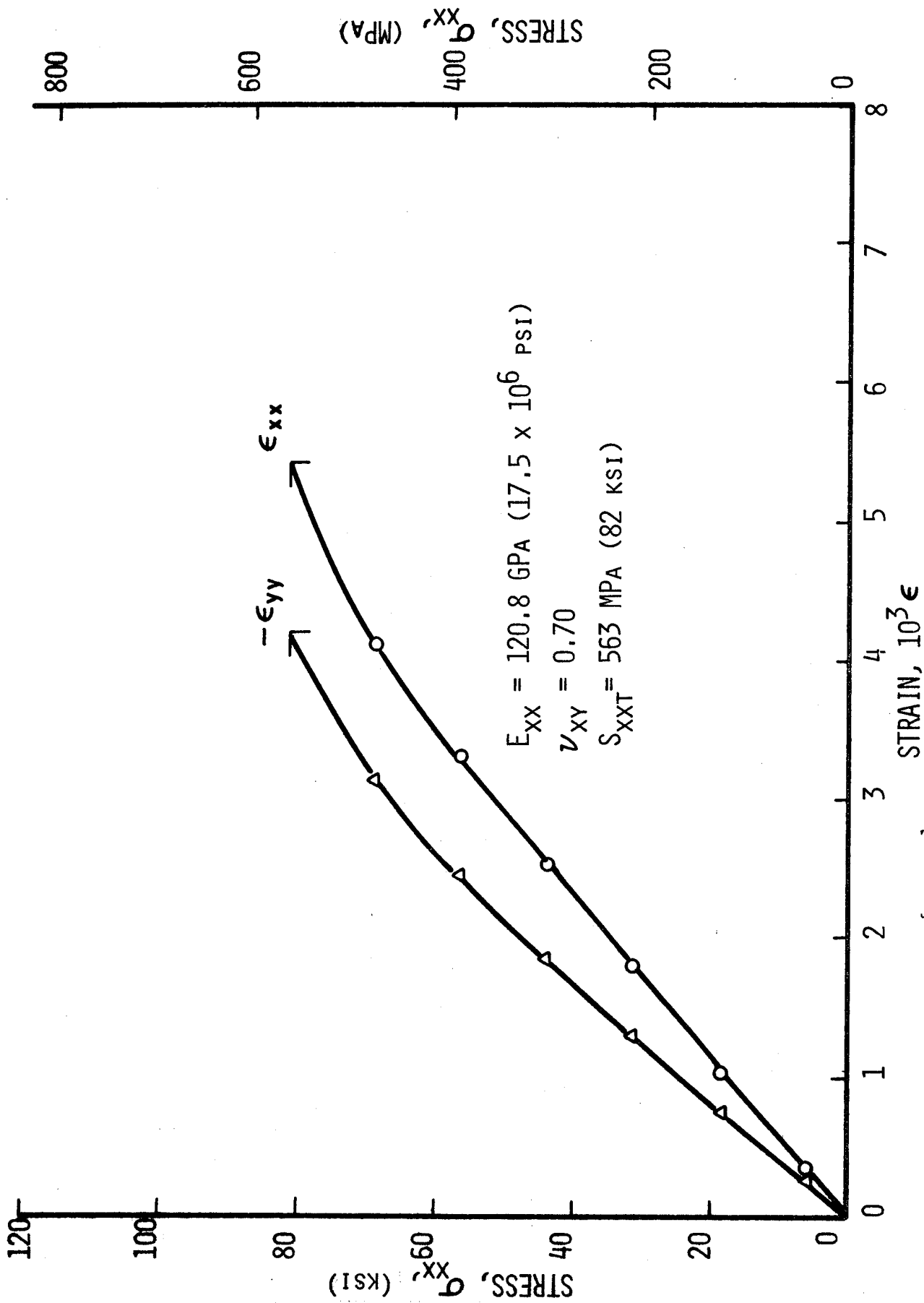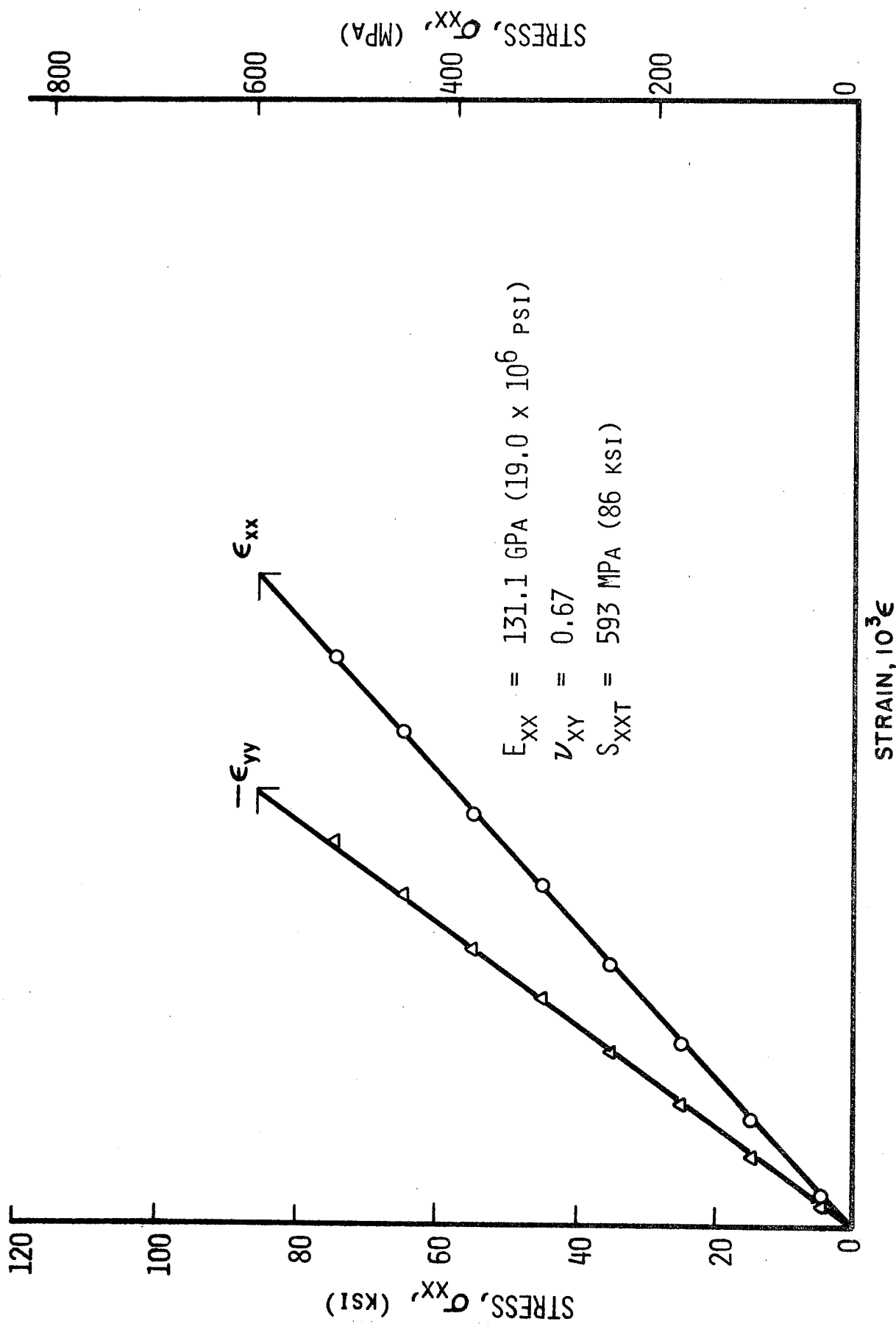
Fig. 4-15 STRAINS IN $[0_2/\pm45]_s$ BORON/POLYIMIDE SPECIMENS UNDER UNIAXIAL TENSILE LOADING SEVENTEEN MONTHS AFTER CURING
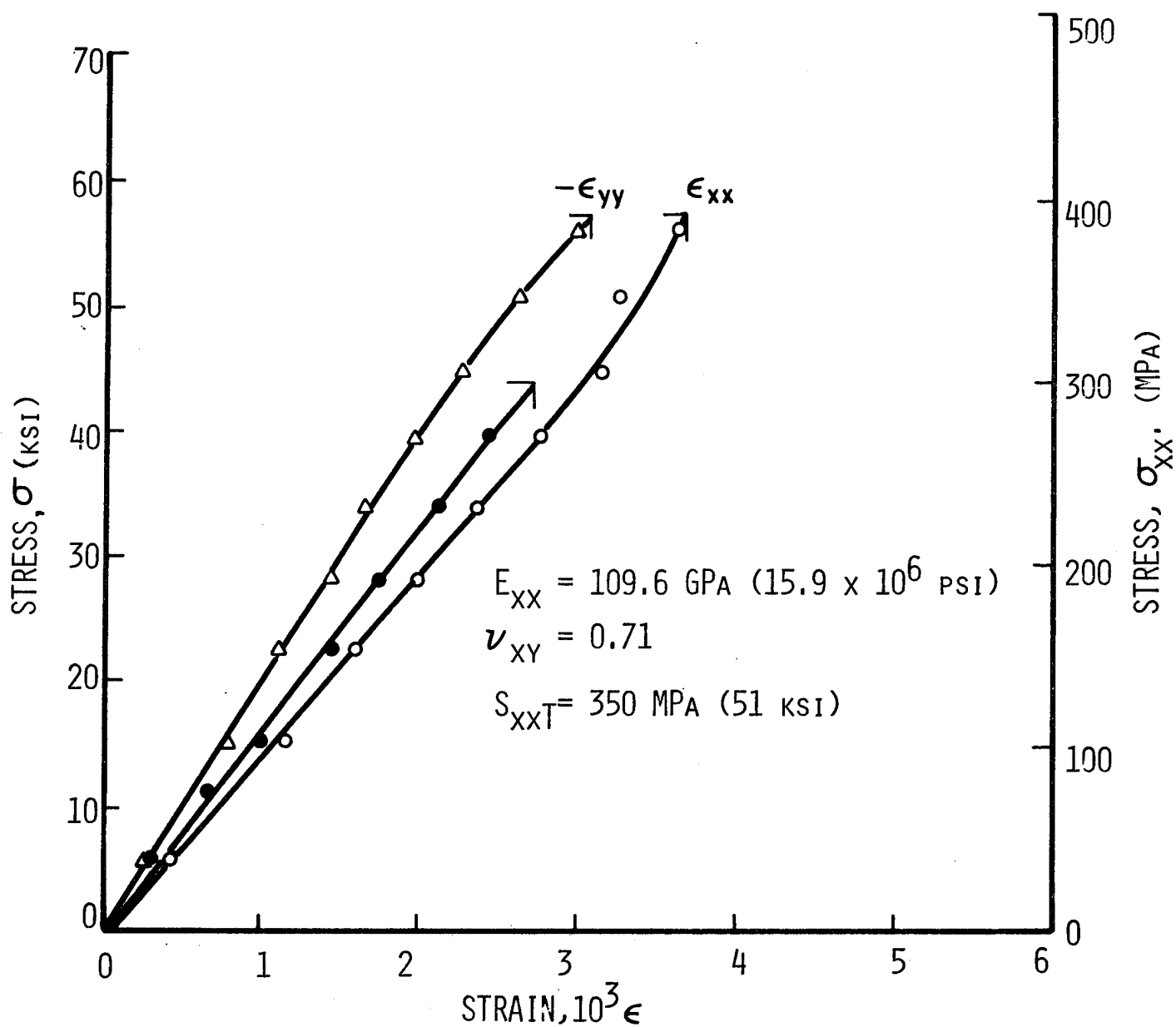
Fig. 4-16 STRAINS IN GRAPHITE/LOW MODULUS EPOXY SPECIMENS
UNDER UNIAXIAL TENSILE LOADING THREE MONTHS
AFTER CURING
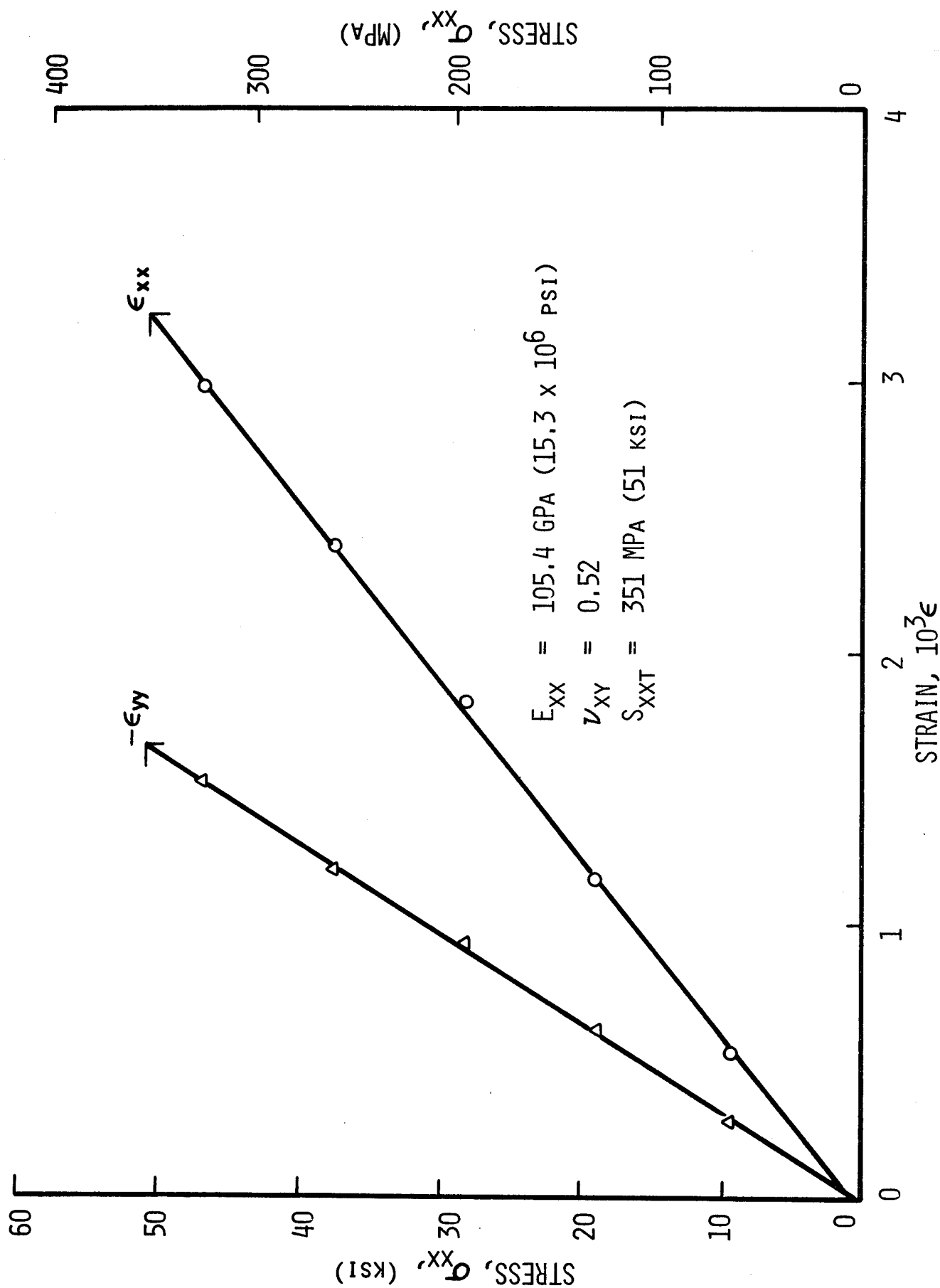
Fig. 4-17 STRAINS IN GRAPHITE/LOW MODULUS EPOXY SPECIMENS UNDER UNIAXIAL TENSILE LOADING SIX AND ONE-HALF MONTHS AFTER CURING
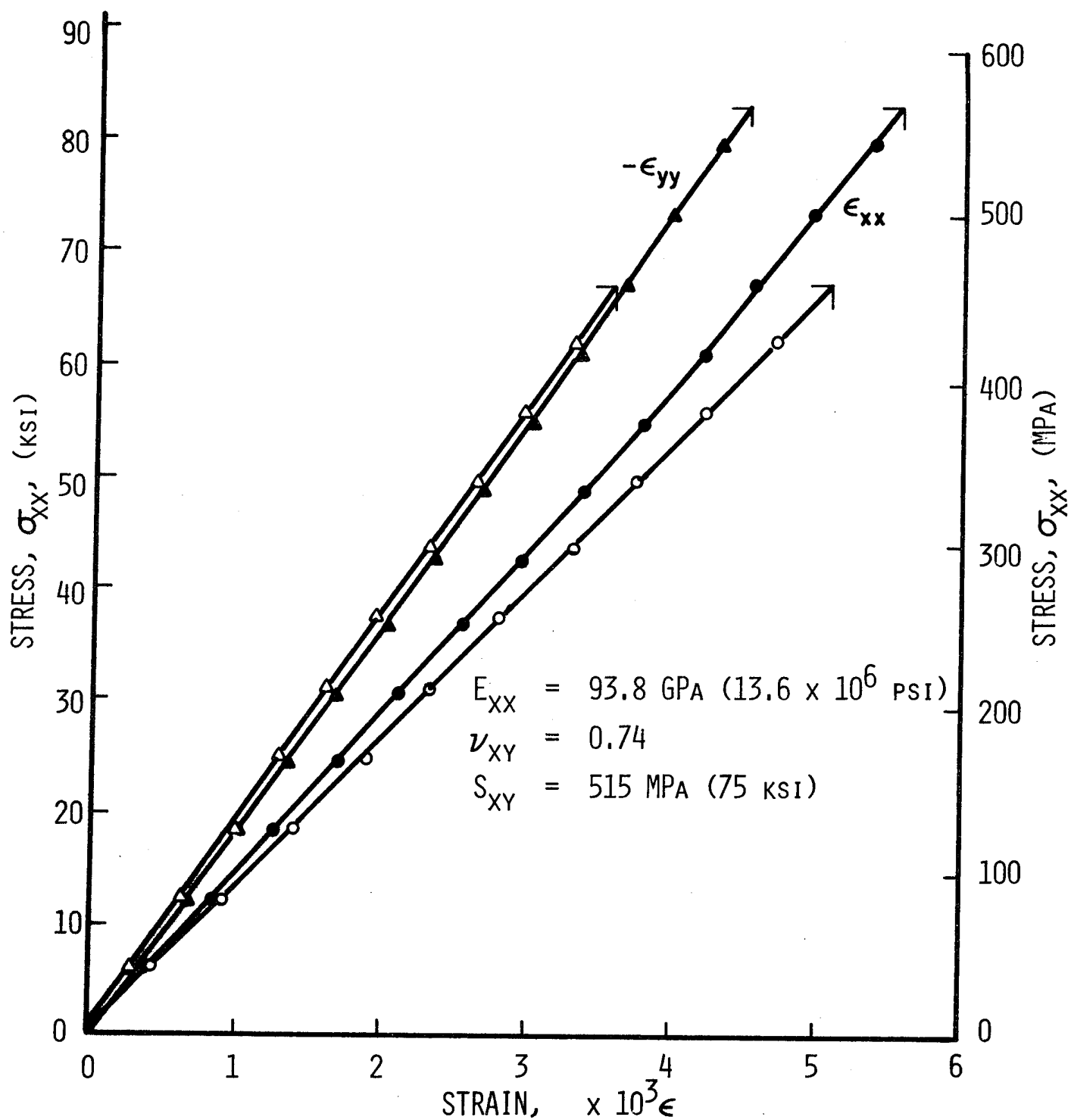
Fig. 4-18 STRAINS IN $[0_2/\pm 45]_s$ GRAPHITE/HIGH MODULUS EPOXY SPECIMENS UNDER UNIAXIAL TENSILE LOADING SIX MONTHS AFTER CURING

4-26

Fig. 4-19 STRAINS IN $\left[0_2/\pm45\right]_s$ GRAPHITE/HIGH MODULUS EPOXY
SPECIMENS UNDER UNIAXIAL TENSILE LOADING NINE
AND ONE-HALF MONTHS AFTER CURING

E_{XX} = 104 GPa (15.1 x 10^6 PSI)

ν_{XY} = 0.74

S_{XXT} = 444 MPa (64 KSI)
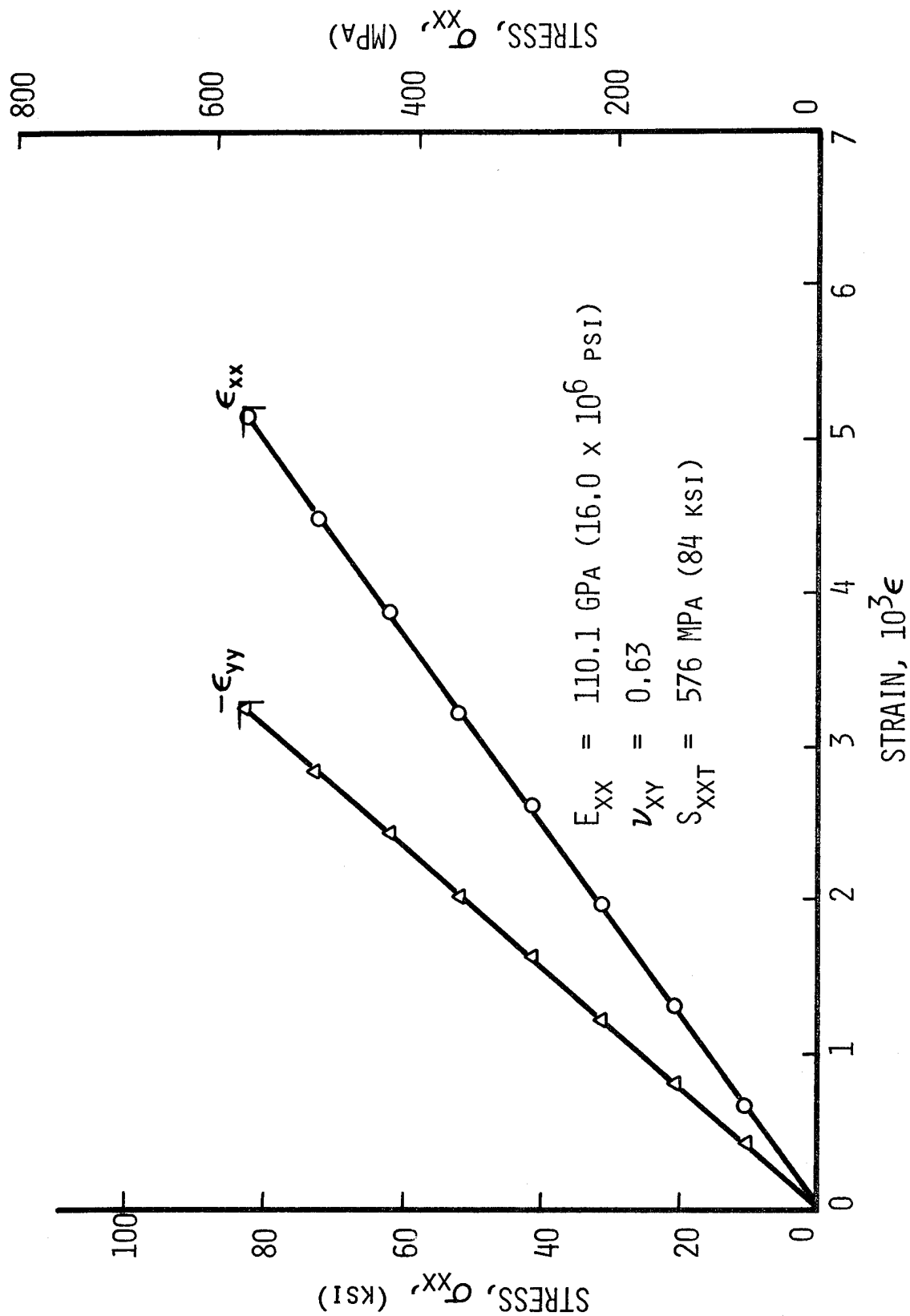
Fig. 4-20 STRAINS IN $[0_2/\pm45]_s$ GRAPHITE/HIGH MODULUS EPOXY SPECIMENS UNDER UNIAXIAL TENSILE LOADING NINE AND ONE-HALF MONTHS AFTER CURING

E_{XX} = 110.1 GPA (16.0 x 10^6 PSI)

ν_{XY} = 0.63

S_{XXT} = 576 MPA (84 KSI)
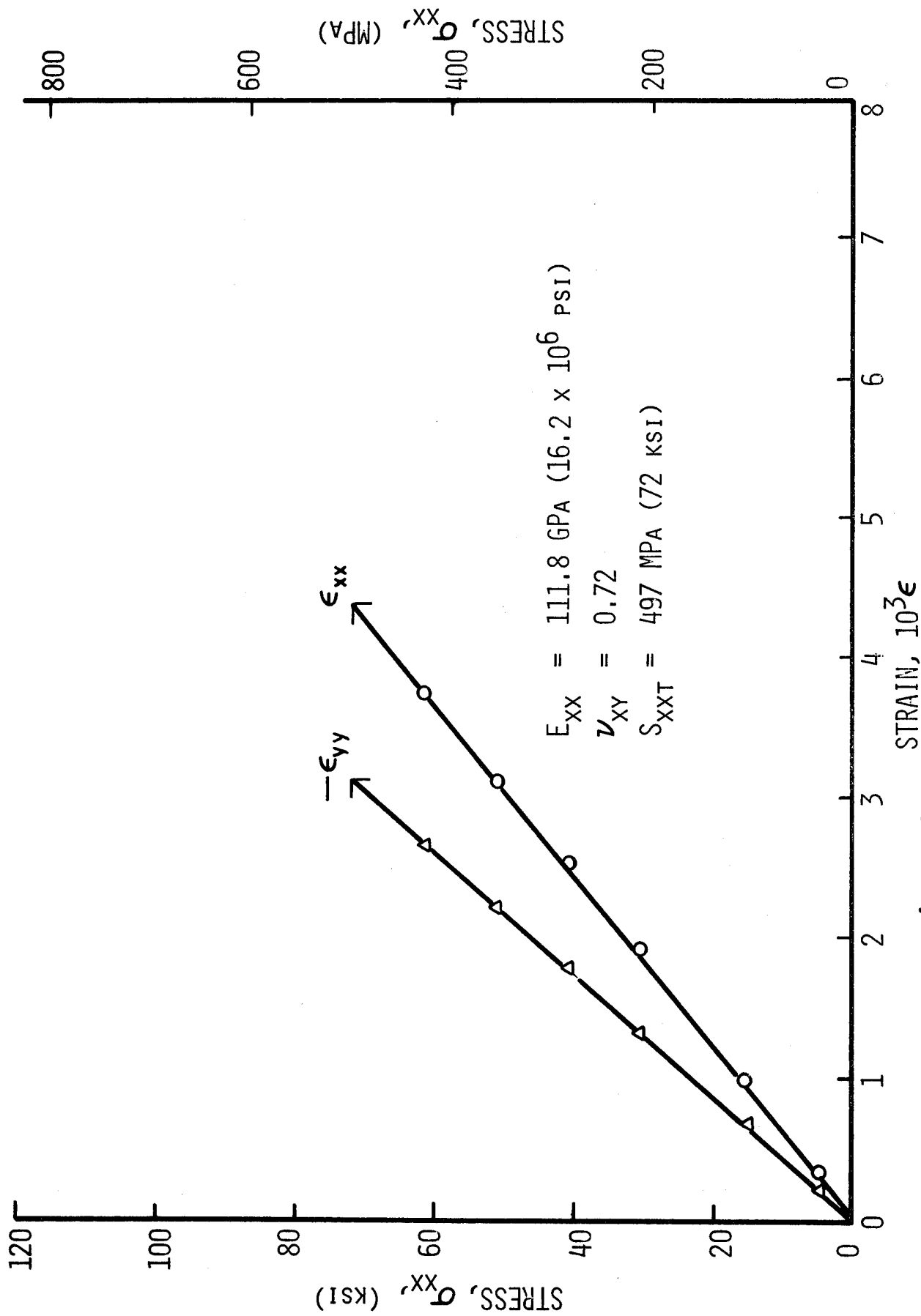
Fig. 4-21 STRAINS IN $[0_2/\pm45]_s$ GRAPHITE/HIGH MODULUS EPOXY SPECIMENS UNDER UNIAXIAL TENSILE LOADING NINETEEN MONTHS AFTER CURING

$E_{XX} = 111.8$ GPA (16.2 x 10^6 PSI)

$\nu_{XY} = 0.72$

$S_{XXT} = 497$ MPA (72 KSI)
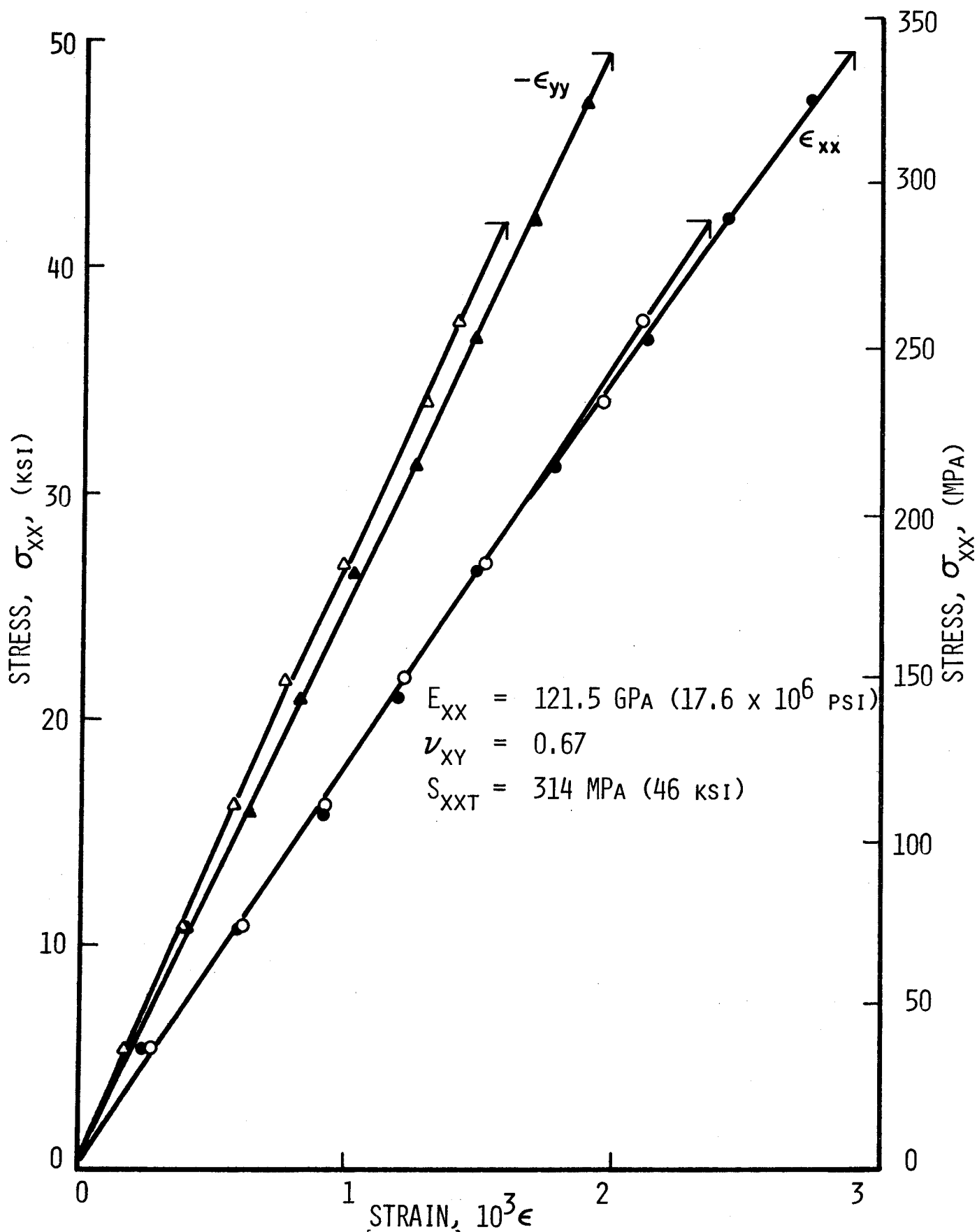
Fig. 4-22   STRAINS IN $[0_2/\pm45]_s$ IN GRAPHITE/POLYIMIDE SPECIMENS
UNDER UNIAXIAL TENSILE LOADING FOUR MONTHS AFTER
CURING
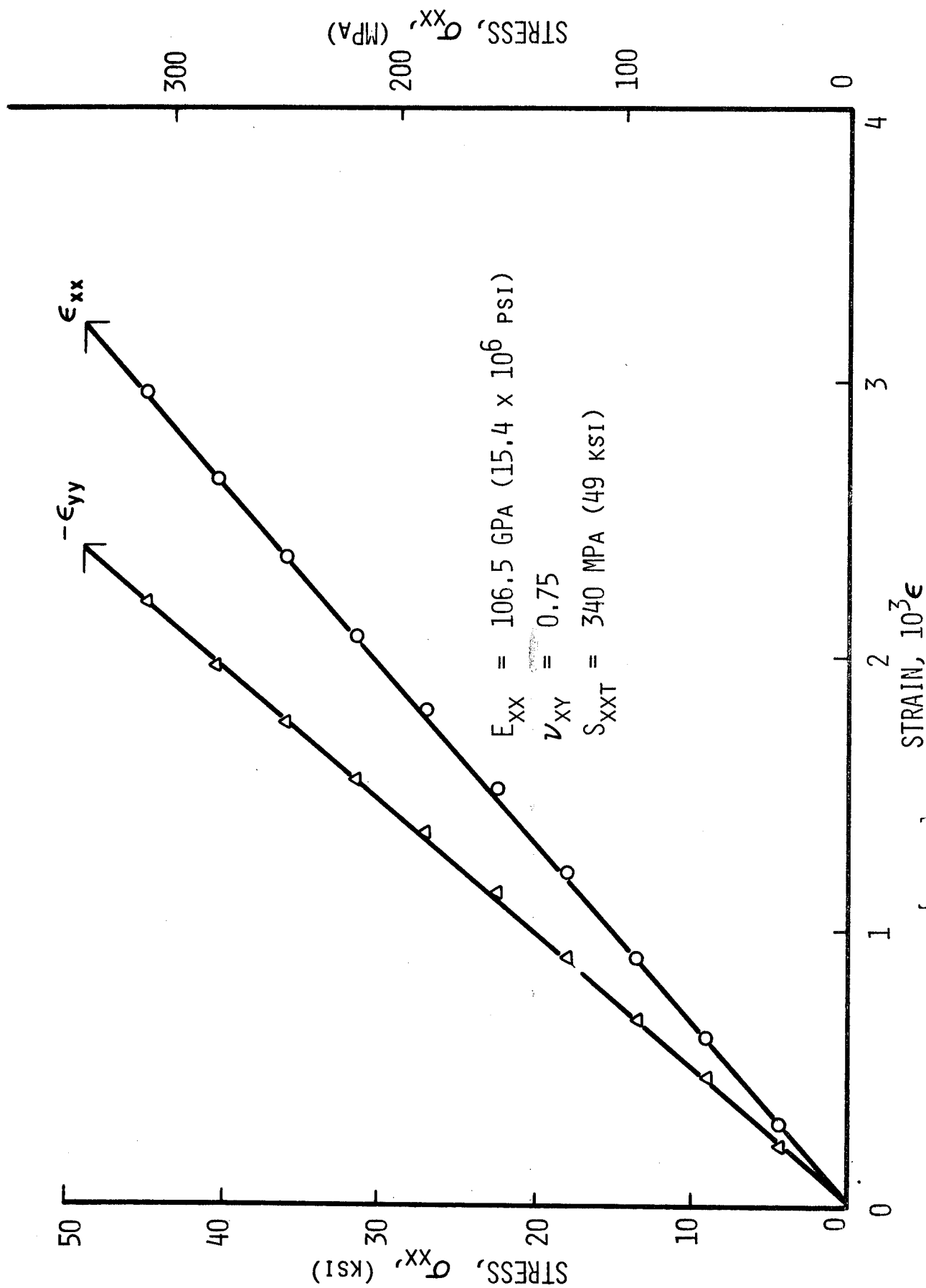
Fig. 4-23 STRAINS IN $[0_2/\pm45]_s$ GRAPHITE/POLYIMIDE SPECIMEN UNDER UNIAXIAL TENSILE LOADING EIGHT MONTHS AFTER CURING

E_{XX} = 106.5 GPa (15.4 × 10⁶ PSI)

ν_{XY} = 0.75

S_{XXT} = 340 MPa (49 KSI)

Axis labels: STRESS, σ_{XX}, (MPA); STRESS, σ_{XX}, (KSI); STRAIN, $10^3 \epsilon$

Curve labels: ϵ_{xx}, $-\epsilon_{yy}$

Fig. 4-24 STRAINS IN $\left[0_2/\pm45\right]_s$ GRAPHITE/POLYIMIDE SPECIMEN UNDER UNIAXIAL TENSILE LOADING EIGHT MONTHS AFTER CURING

E_{XX} = 108.2 GPa (15.7 x 10^6 PSI)
ν_{XY} = 0.70
S_{XXT} = 239 MPa (35 KSI)

Fig. 4-25 STRAINS IN $[0_2/\pm45]_s$ GRAPHITE/POLYIMIDE SPECIMEN UNDER UNIAXIAL TENSILE LOADING SEVENTEEN MONTHS AFTER CURING

E_{XX} = 125.6 GPa (18.2 x 10⁶ PSI)
ν_{XY} = 0.62
S_{XXT} = 373 MPa (54 KSI)

Fig. 4-26 STRAINS IN $[0_2/\pm45]_s$ GRAPHITE/POLYIMIDE SPECIMEN UNDER UNIAXIAL TENSILE LOADING SEVENTEEN MONTHS AFTER CURING

E_{XX} = 104.2 GPA (15.1 × 10⁶ PSI)

ν_{XY} = 0.68

S_{XXT} = 260 MPA (38 KSI)
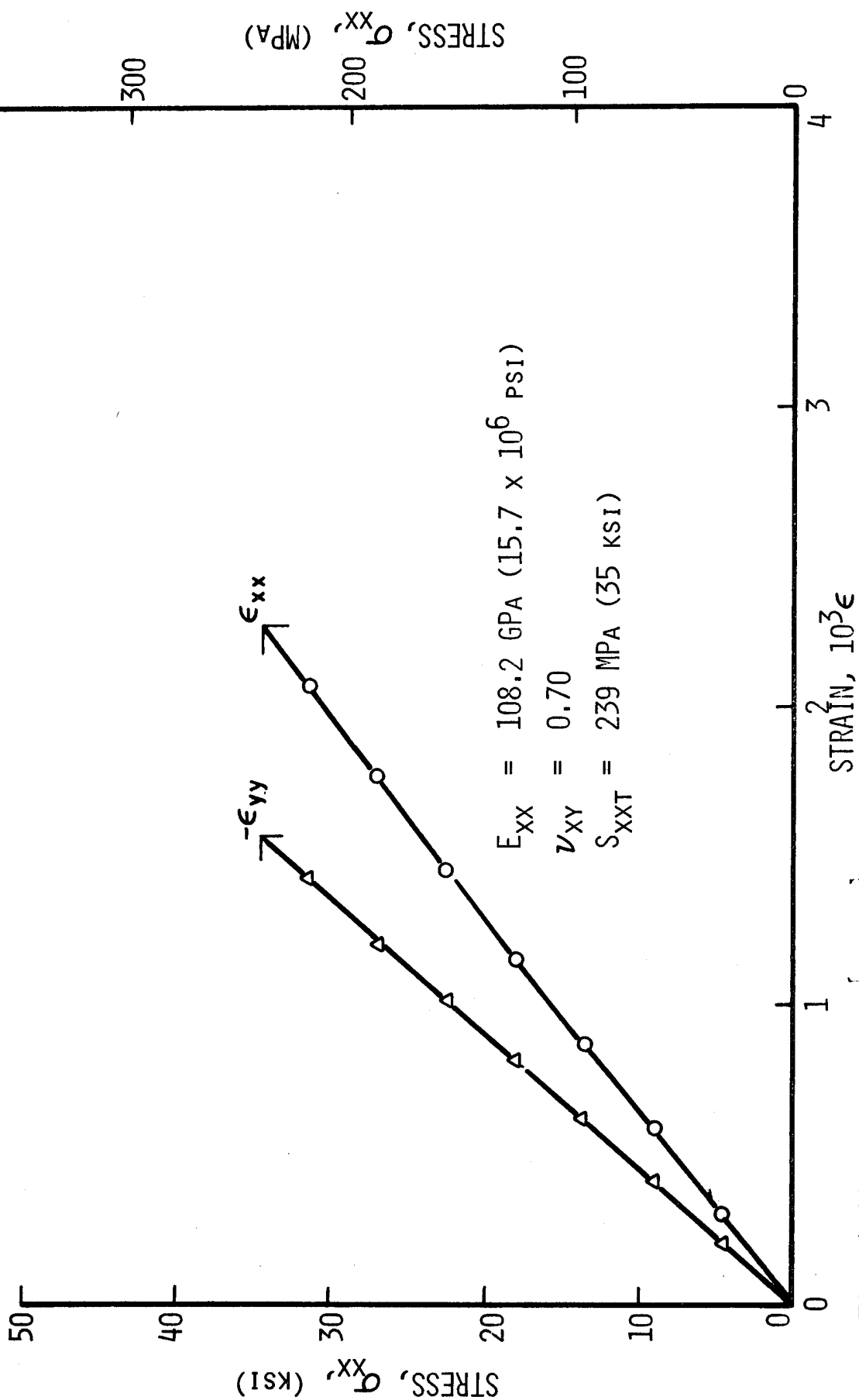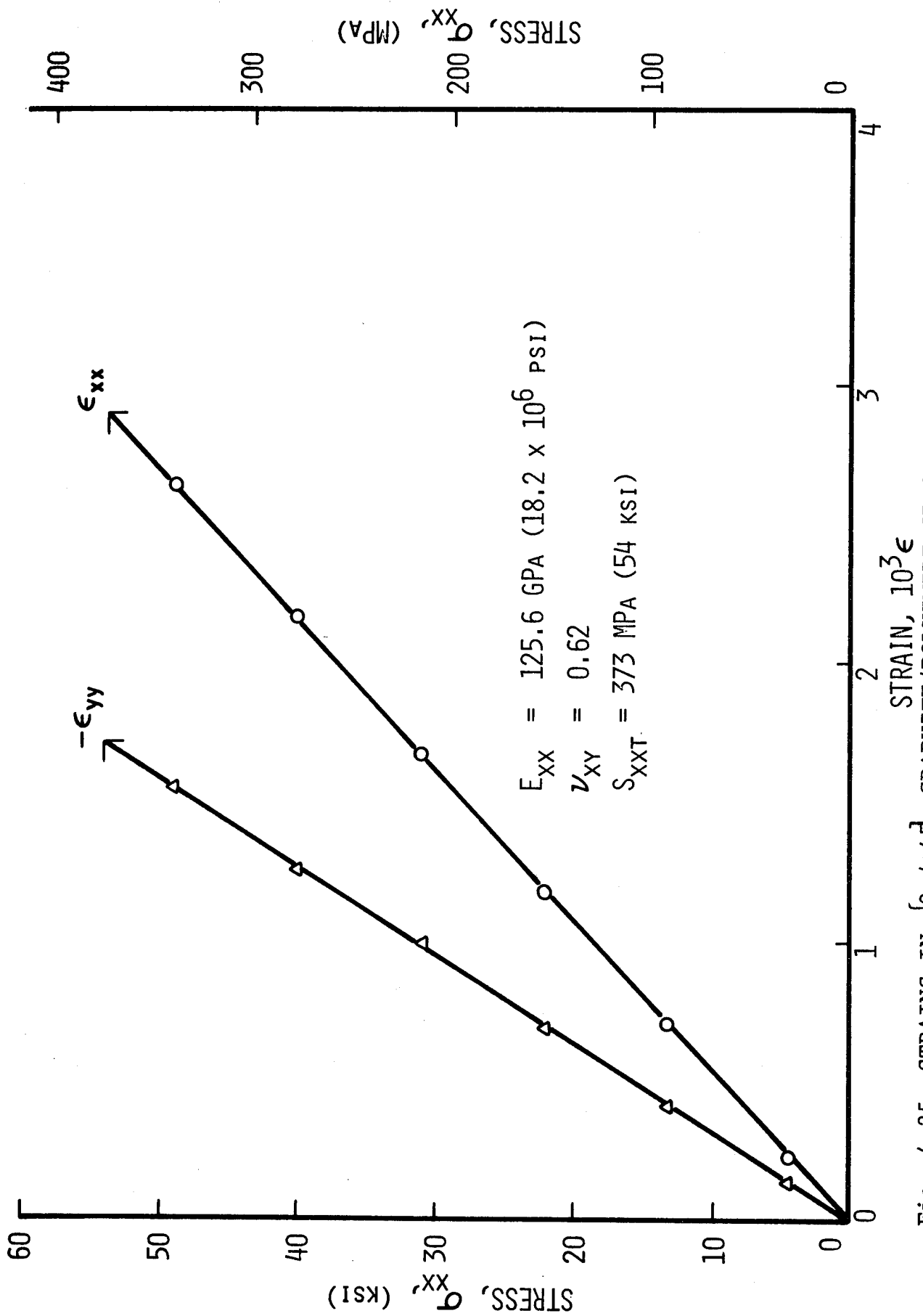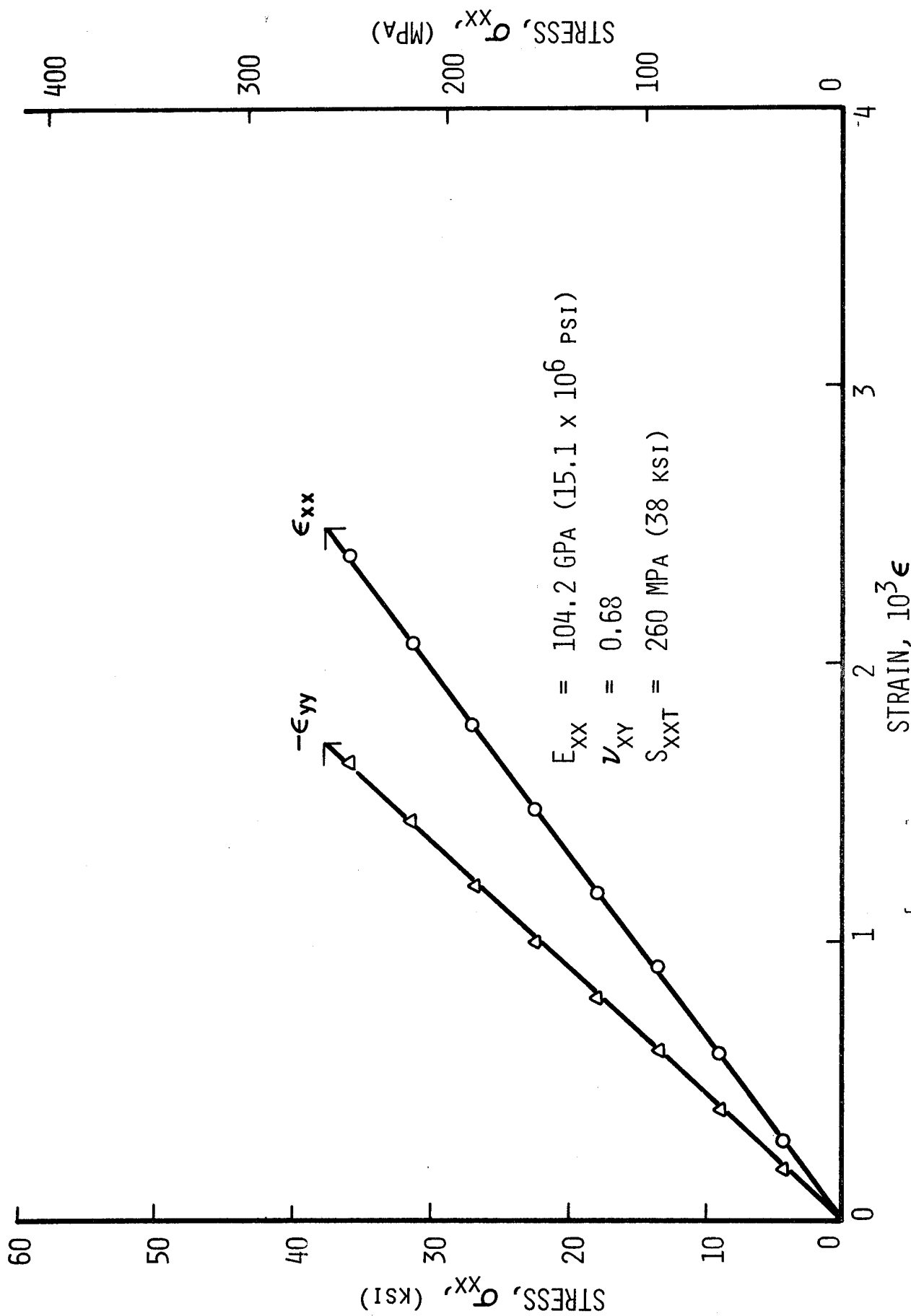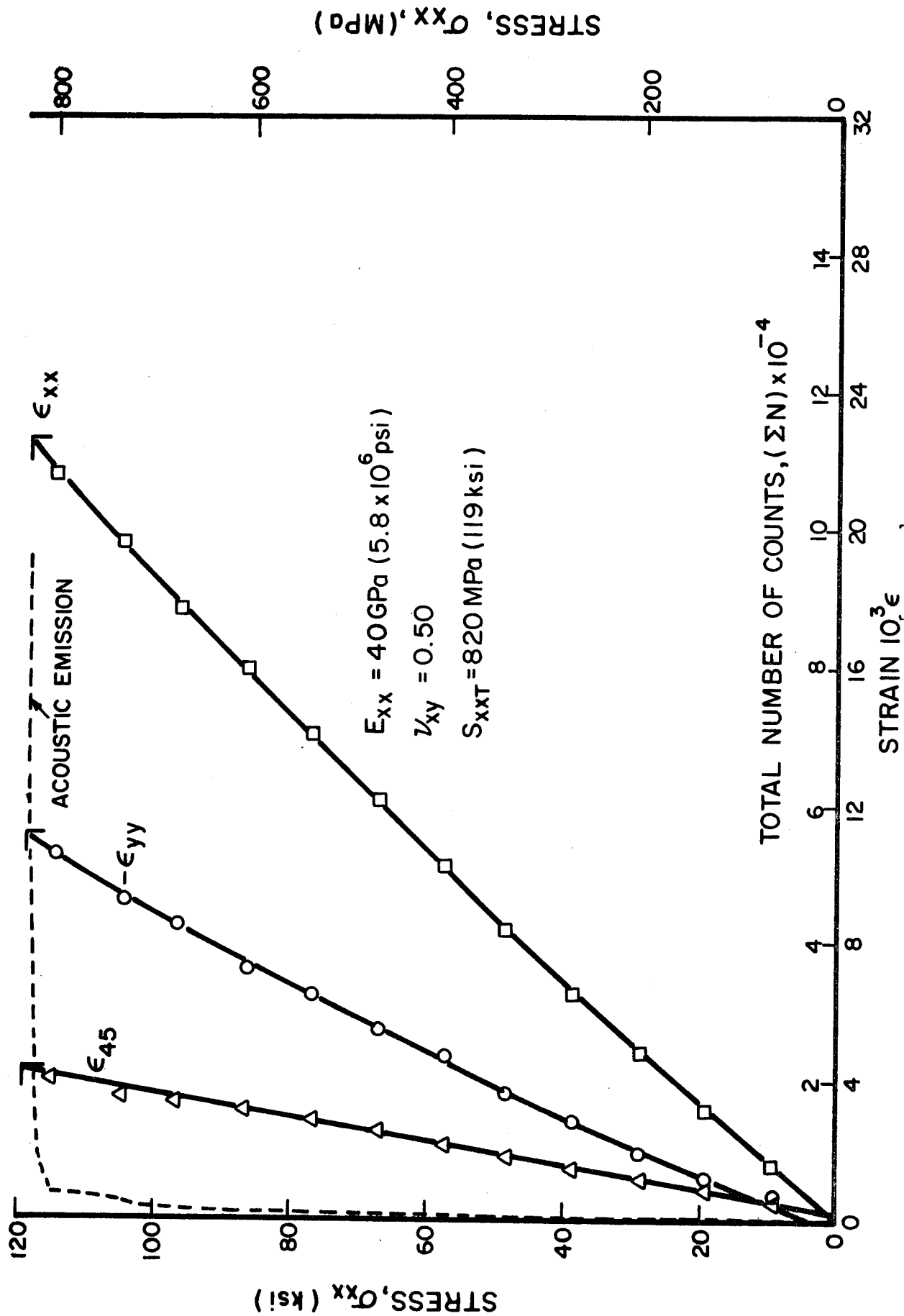
Fig. 4-27 STRAINS AND ACOUSTIC EMISSION IN $[0_2/\pm 45]_s$ S-GLASS/EPOXY SPECIMEN LOADED UNIAXIALLY THREE MONTHS AFTER CURING
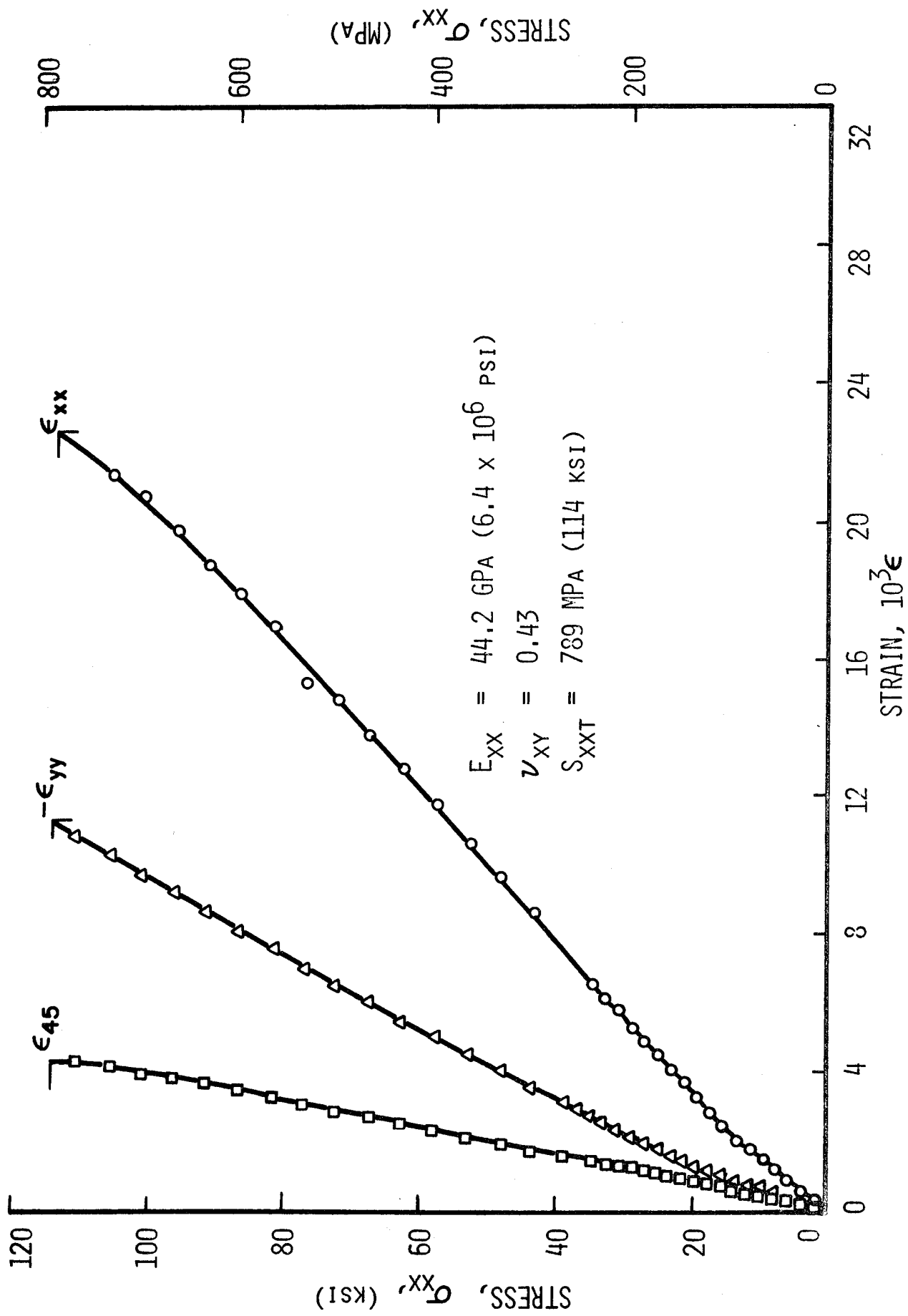
$E_{xx} = 40\,GPa\,(5.8 \times 10^6\,psi)$

$\nu_{xy} = 0.50$

$S_{xxT} = 820\,MPa\,(119\,ksi)$

Fig. 4-28 STRAINS IN $[0_2/\pm 45]_s$ S-GLASS/EPOXY SPECIMEN UNDER UNIAXIAL TENSILE LOADING SIX MONTHS AFTER CURING

E_{XX} = 44.2 GPa (6.4 × 10⁶ PSI)

ν_{XY} = 0.43

S_{XXT} = 789 MPa (114 KSI)

Fig. 4-29 STRAINS IN $[0_2/\pm45]_s$ S-GLASS/EPOXY SPECIMEN UNDER UNIAXIAL TENSILE LOADING NINE
MONTHS AFTER CURING

E_{xx} = 36.6 GPa (5.3 x 10^6 PSI)
ν_{XY} = 0.55
S_{XXT} = 618 MPa (90 KSI)

STRAIN, $10^3 \epsilon$

STRESS, σ_{xx}, (KSI)

ϵ_{xx}

$-\epsilon_{yy}$

Fig. 4-30 STRAINS IN $[0_2/\pm 45]_s$ S-GLASS/EPOXY SPECIMEN UNDER UNIAXIAL TENSILE LOADING TWELVE AND ONE-HALF MONTHS AFTER CURING

E_{XX} = 36.6 GPA (5.3 x 10^6 PSI)
ν_{XY} = 0.52
S_{XXT} = 622 MPA (90 KSI)

Fig. 4-31 STRAINS IN $[0_2/\pm45]_s$ S-GLASS/EPOXY SPECIMEN UNDER UNIAXIAL TENSILE LOADING
TWELVE AND ONE-HALF MONTHS AFTER CURING

$E_{XX} = 35.2$ GPa $(5.1 \times 10^6$ PSI$)$
$\nu_{XY} = 0.54$
$S_{XXT} = 676$ MPa $(98$ KSI$)$

Fig. 4-32 STRAINS IN $\left[0_2/\pm 45\right]_s$ S-GLASS/EPOXY SPECIMEN UNDER UNIAXIAL TENSILE LOADING TWENTY-TWO MONTHS AFTER CURING

E_{xx} = 35.9 GPA (5.2 x 10^6 PSI)

ν_{XY} = 0.55

S_{XXT} = 685 MPA (99 KSI)
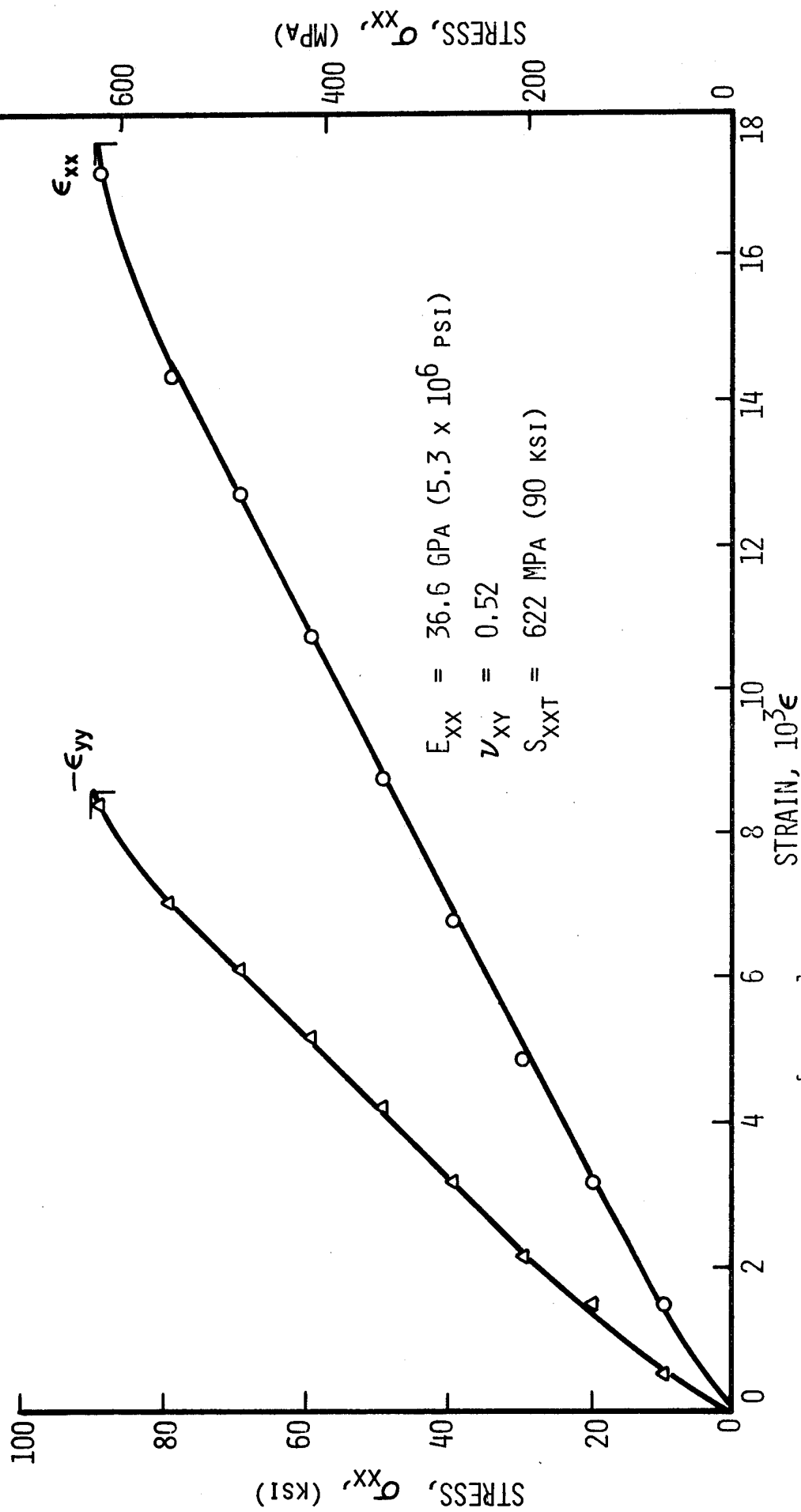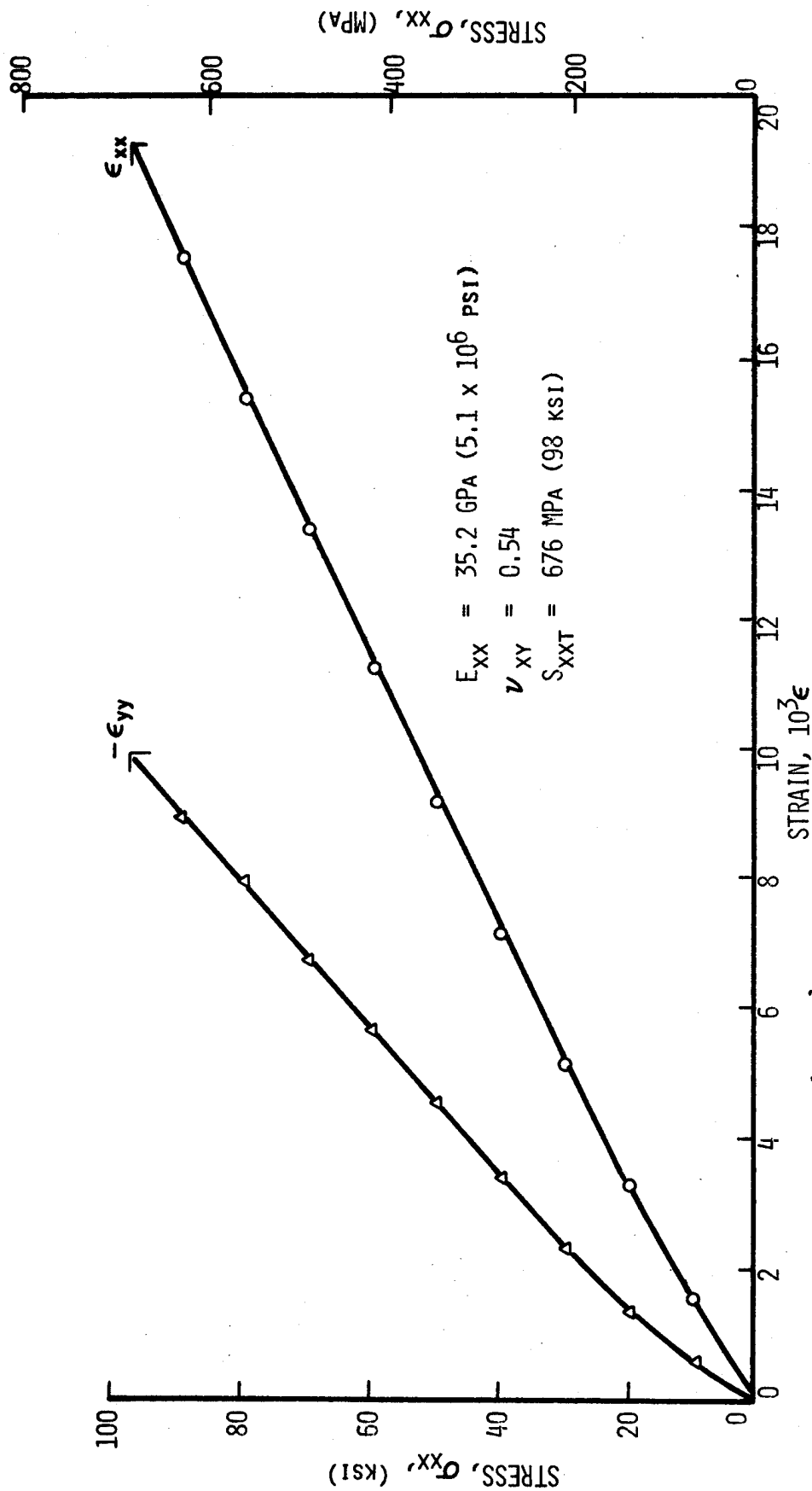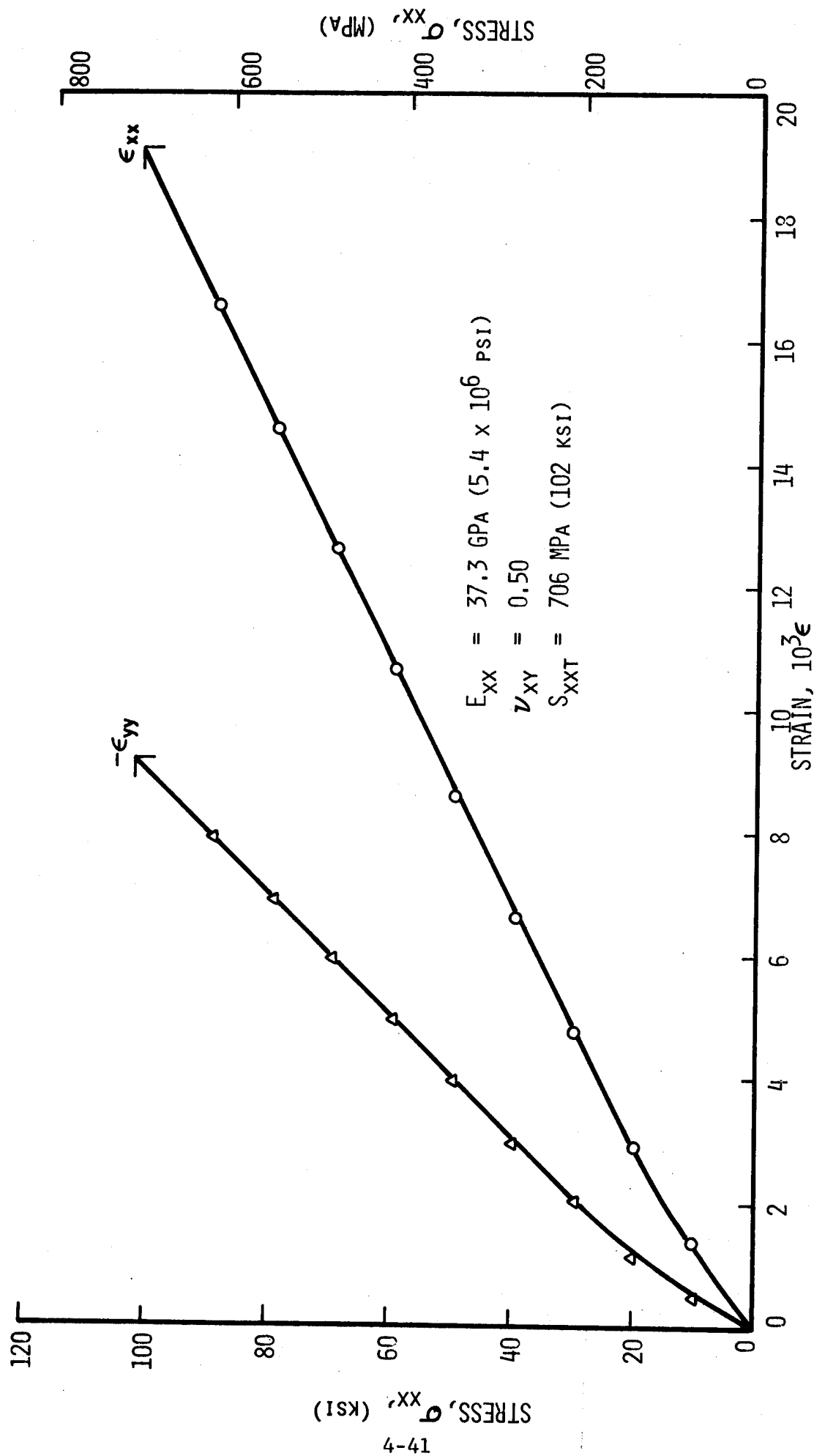
Fig. 4-33 STRAINS IN $[0_2/\pm 45]_s$ S-GLASS/EPOXY SPECIMEN UNDER UNIAXIAL TENSILE LOADING TWENTY-TWO MONTHS AFTER CURING

E_{xx} = 37.3 GPa (5.4 x 10^6 PSI)
ν_{XY} = 0.50
S_{xxT} = 706 MPa (102 KSI)

5.0 TASK IV - CYCLIC LOADING AND RESIDUAL STRENGTH

5.1 Introduction

The objectives of this task are to investigate the behavior of angle-ply laminates during load cycling, thermal cycling and thermal cycling under load and to determine the effects of these cycling programs on residual properties. The laminates were Boron/Epoxy, Boron/Polyimide, Graphite/Low Modulus Epoxy, Graphite/High Modulus Epoxy, Graphite/Polyimide and S-glass/Epoxy of $[0_2/\pm45]_s$ layup.

These laminates are subjected to significant residual stresses built up during fabrication as shown in Section 3. Mechanical or thermal cycling may produce relaxation of some of these stresses and thereby influence the residual strength. Such cycling may also cause degradation in the form of microcracks and thereby affect the residual stiffness and strength of the laminate.

Strains during mechanical and thermal cycling were monitored to determine any possible changes in stiffness or thermal properties caused by internal degradation. The final effects of cycling were determined by comparing the residual modulus, Poisson's ratio and strength with initial values of these properties for uncycled specimens.

5.2 Specimen Fabrication and Strain Monitoring

Two sets of $[0_2/\pm45]_s$ specimens were prepared. Seven specimens of each material, 1.27 cm (0.5 in.) wide and 22.9 cm (9 in.) long, were prepared for testing with surface instrumentation. Seven specimens of each material, 2.54 cm (1 in.) wide and 22.9 cm (9 in.) long, were prepared with embedded instrumentation. For each material the surface instrumentation specimens were cut from a single $[0_2/\pm45]_s$ plate and the embedded instrumentation specimens were layed up individually. In both cases the fabrication procedures were those described in Section 3.0. The embedded instrumentation

specimens were selectively monitored for strain variation with temperature during curing, especially where there were questions on the residual strains measured in Task II. Results obtained were averaged in and incorporated with results obtained in Task II, reported in Section 3.4.

For each material, each of the two sets of specimens was divided into three groups: Two specimens to be used for thermal cycling tests, three specimens for tensile load cycling tests, and two for tensile load with thermal cycling tests.

5.3   Thermal Cycling

The thermal cycling tests consisted of subjecting the specimens of that test group to 100 thermal cycles at a rate of about 30 minutes per cycle in two temperature ranges; room temperature to approximately 80 percent of cure temperature and room temperature to 200 degK (-100°F). Specimen strains in the instrumented specimens were monitored during selected cycles and the specimens were examined periodically for degradation during cycling.

5.3.1   Thermal Cycling of Epoxy Matrix Specimens Between Room Temperature and 411 degK (280°F)

The elevated-temperature thermal cycling of all epoxy matrix specimens was performed by cycling between room temperature and 411 degK (280°F). The specimens were subject to 100 cycles of 35-minute duration. Each cycle consisted of temperature increase and decrease without a dwell period. It was done in a Blue M "Power-O-Matic-60" oven equipped with a temperature cycling control apparatus, air circulation and controlled air exhaust system for cool down control.

Two $[0_2/\pm45]_s$ specimens, one with embedded instrumentation, from each epoxy matrix system were cycled. The specimens were examined visually at intervals for degradation due to cycling. None

was noted. Specimen strains as a function of temperature were monitored during the beginning, middle and end of cycling. Figure 5-1 shows measured strains in Graphite/High Modulus Epoxy in the beginning and end of thermal cycling. No significant differences exist. The situation was similar for the other epoxy-matrix laminates.

5.3.2 Thermal Cycling of Polyimide Matrix Specimens Between Room Temperature and 533 degK (500°F)

The elevated-temperature thermal cycling of the polyimide matrix specimens was performed by cycling them between room temperature and 533 degK (500°F). The large temperature span necessary for this cycling required an excessive cycle length with the existing oven system. Therefore, to accomplish the required 30-minute cycle duration, the oven and the method of cycling had to be modified.

The cycling modification consisted of keeping the oven at the peak temperature while leaving the specimens in the oven for half the cycle and removing them from the oven for the other half cycle. Thus, the specimens were exposed for 15 minutes to peak temperature and for 15 minutes to room temperature in each cycle. To accomplish this, the existing oven door had to be replaced with an apparatus to move the specimens in and out of the oven automatically. To maintain the temperature a new set of oven closures were provided to keep the oven closed with the specimens in or out of it. This system will be described in greater detail in Section 5.5 dealing with thermal cycling under tensile load.

Two $[0_2/\pm45]_s$ specimens of each of the Boron/Polyimide and Graphite Polyimide materials were subjected to 100 thermal cycles of 30-minute duration with the modified cycling method described above. The specimens were examined visually at intervals for degradation due to cycling. None was noted. One specimen of each material was instrumented with embedded strain gages which were used

5-3

to monitor strains as a function of temperature in the third, thirtieth and ninety-ninth cycles. Figure 5-2 shows measured apparent strains in the Boron/Polyimide specimen in the beginning and at the end of cycling. No significant differences exist in the axial and transverse strains, but the 45-degree strain is lower at the end of cycling. This obviously is in error since the 45-degree strain must always equal the mean of the other two strains. The situation was similar in the Graphite/Polyimide specimen where no differences were observed in the measured strains between the beginning and end of cycling.

5.3.3 Thermal Cycling Between Room Temperature and 200 degK (-100°F)

Two $[0_2/\pm45]_s$ specimens, including one with embedded instrumentation, of each of the six material systems studied were subjected to 100 thermal cycles of 30-minute duration between room temperature and 200 degK (-100°F). This cold cycling was done in a large environmental chamber (Thermovac) of over $5.7m^3$ (200 ft^3) capacity capable of controlling temperature from ambient to 200 degK (-100°F).

The cycling method was the same as that used for the elevated temperature cycling of the polyimide matrix specimens. The chamber was kept at 200 degK (-100°F) while the specimens were moved in and out of it at 15 minute intervals. Thus, the specimens were exposed to a 200 degK (-100°F) environment for 15 minutes and room temperature for another 15 minutes during each cycle.

To prevent undesirable effects due to moisture condensation during this cycling special procedures were instituted. The exposed gage leads of all the instrumented specimens were coated with a silicon rubber coating (3140 RTV, Micro-Measurements). After wiring the strain gages, all instrumented and uninstrumented specimens were completely coated with another silicon rubber coating (M-coat C, Micro-Measurements).

During cycling the specimens were examined visually periodically for degradation. None was observed. Strains as a function of temperature were monitored at the beginning and the end of this cycling program. Apparent strains at the beginning and end of the thermal cycling for unloaded Graphite/High Modulus Epoxy and S-Glass/Epoxy specimens are shown in Figs. 5-3 and 5-4. It can be seen that thermal strains do not change as a result of the cycling program.

5.4 Tensile Load Cycling

5.4.1 General Considerations

The tensile load cycling tests required two specimens for each material system, for each of three loading ranges, to be subjected to a cyclic tensile loading of 10^7 cycles or failure, whichever occurred first. Of the two specimens for each load range, one had embedded instrumentation. The three loading ranges, based on the static strength results reported in Table 3-19, were 0 to 40 percent, 0 to 70 percent, and 0 to 90 percent of the corresponding static strength.

Two cycling frequencies were considered. Preliminary tests were conducted to establish whether there is a significant difference in results of cyclic loading at 30 and 100 cycles per second. Specimens 1.27 cm x 1.27 cm (0.5 in. x 0.5 in.) of $[0_2/\pm45]_s$ layup were prepared from the stiffest and least stiff of the six materials, i.e., Boron/Epoxy and S-Glass/Epoxy. Two specimens of each material were tested at each of the cyclic rates above and at each of two load ranges. The load ranges were 70 and 90 percent of the static strength. No significant differences in cycles to failure were observed. The 30 cps rate was then chosen as more convenient, as it allows testing of longer and easier to instrument and monitor specimens.

5.4.2 Experimental Procedure

Two types of $[0_2/\pm45]_s$ specimens were used in these tests: Three specimens 1.27 cm (0.5 in.) wide and 22.9 cm (9 in.) long with surface strain gages and three specimens 2.54 cm (1 in.) wide and 22.9 cm (9 in.) long with embedded strain gages. Thermocouples were bonded to the specimen surfaces for temperature monitoring during cyclic loading. Two specimens of each material, including one with embedded gages, were cycled between 0 and 40 percent of the static ultimate, two specimens between 0 and 70 percent of ultimate and two between 0 and 90 percent of ultimate.

The tensile load cycling was done on a Sontag Universal Fatigue Test Machine. A constant load amplitude was maintained with an R factor of 0.1. Specimens were cycled to failure or to runout at approximately 10^7 cycles. Investigation of progressive degradation at frequent intervals was done by (1) monitoring all strain gages, (2) recording temperature rise on specimen and (3) inspecting surfaces and edges of the specimen for visible signs of degradation.

An eight-channel recording oscillograph (Bell and Howell Type 5-135) with associated signal conditioning instrumentation was utilized for monitoring the specimen gages and thermocouple during cyclic loading. The recorded data and the applied load were used to determine the longitudinal modulus, major Poisson's ratio and temperature as a function of number of load cycles.

5.4.3 Results

A summary of load cycles to failure for the surface-instrumented specimens is shown in Table 5-1. The variation in longitudinal modulus, major Poisson's ratio and temperature with number of loading cycles for these specimens is shown in Figures 5-5 through 5-18.

Table 5-1

SUMMARY OF CYCLIC TENSILE TESTS IN $[0_2/\pm 45]_s$ SPECIMENS
WITH SURFACE INSTRUMENTATION

Material	Nominal Width cm (in.)	Maximum Stress Level (% σ_{ult})	Cycles to Failure
Boron/Epoxy	1.27(0.5)	90	30×10^3
	1.27(0.5)	70	460×10^3
	1.27(0.5)	40	10^7 Runout
Boron/Polyimide	1.27(0.5)	90	10^3
	1.27(0.5)	70	$5,971 \times 10^3$
	1.27(0.5)	40	1.025×10^7 Runout
Graphite/Low Modulus Epoxy	1.27(0.5)	90	10^3
	1.27(0.5)	70	847×10^3
	1.27(0.5)	40	1.015×10^7 Runout
Graphite/High Modulus Epoxy	1.27(0.5)	90	Immediate Tab Failure
	1.27(0.5)	80	512×10^3
	1.27(0.5)	70	10^7 Runout
Graphite/Polyimide	1.27(0.5)	90	440×10^3
	1.27(0.5)	80	1.553×10^6
	1.27(0.5)	70	1.047×10^7 Runout
S-Glass/Epoxy	1.27(0.5)	70	10^3
	1.27(0.5)	40	14×10^3
	1.27(0.5)	25	419×10^3

Of the three Boron/Epoxy specimens tested, the one cycled to 90 percent of ultimate strength failed at 30,000 cycles, the one cycled to 70 percent of ultimate failed at 460,000 cycles and the one cycled at 40 percent of ultimate survived 10 million cycles. The variation of modulus, Poisson's ratio, and temperature with number of cycles for these three specimens is shown in Figures 5-5, 5-6, 5-7. Some interesting characteristics noticed are the early but moderate rise in temperature and the seemingly stepwise drops in modulus. In the case of the lowest load (Fig. 5-7) the rather abrupt increase in specimen compliance was preceded by a gradual rise in temperature. Most of the changes seem to take place in the range between 10^4 and 10^5 cycles with plateaus on either side of this range.

Results for the Boron/Polyimide material are comparable to those of Boron/Epoxy, with 1000 cycles to failure for cycling to 90 percent of ultimate strength, 5,971,000 cycles to failure for cycling to 70 percent of ultimate and runout at 10 million cycles for cycling to 40 percent of ultimate. The variation of longitudinal modulus, Poisson's ratio and temperature with number of loading cycles is shown in Figs. 5-8 and 5-9. In the case of loading at 40 percent of ultimate a gradual increase in temperature between 10^4 and 3×10^6 cycles corresponds to a rather abrupt increase in compliance between 10^5 and 2×10^5 cycles.

Results for Graphite/Low Modulus Epoxy are plotted in Figs. 5-10, 5-11 and 5-12 for the three specimens tested at 90, 70 and 40 percent of ultimate strength. The first two failed at 1000 and 847,000 cycles, respectively. The third specimen was cycled to a 1.015×10^7 cycle runout. All but one longitudinal gage failed after 2×10^5 cycles. Indications are that the modulus remained constant to 10 million cycles, although there was a gradual rise in temperature to 83°F.

The Graphite/High Modulus Epoxy specimens were cycled to 90, 80 and 70 percent of the ultimate static stress, respectively. The 80 percent level was selected after a runout was observed at 70 percent. The specimen cycled to 90 percent of ultimate strength failed immediately at the tab and no strain or temperature data were obtained. Results for the other two specimens are shown in Figs. 5-13 and 5-14. For the specimen tested to 80 percent of ultimate an abrupt change in modulus and Poisson's ratio occurred at 30,000 cycles in the region of gradual temperature rise. The specimen failed at 512,000 cycles. For the specimen cycled to 70 percent of ultimate all gages failed after 204,000 cycles but the specimen did not fail at runout of 10 million cycles. Small changes in modulus and Poisson's ratio are observed in the first 5000 cycles. A small but gradual increase in temperature is also observed, reaching a plateau at 100,000 cycles.

The Graphite/Polyimide specimens were subjected to cyclic loading corresponding to 90, 80 and 70 percent of the ultimate static strength, respectively. As before, the 80 percent level was selected after a runout was observed at 70 percent. The 90 percent of ultimate specimen failed at 440,000 cycles. No variation in modulus, but a gradual rise in temperature from 297 to 298.6 degK (75 to 78°F) was measured between 0 and 50,000 cycles (Fig. 5-15). For the specimen cycled to 80 percent of ultimate strength (Fig. 5-16) the modulus and Poisson's ratio remained constant whereas the temperature showed a gradual rise to a plateau of 298.4 degK (77.7°F) starting at 60,000 cycles. The specimen cycled to 70 percent of ultimate strength survived a runout of 1.047×10^7 cycles. The modulus and Poisson's ratio did not change throughout this cyclic loading (Fig. 5-17). A temperature record was not obtained due to thermocouple failure.

The S-Glass/Epoxy specimens were subjected to maximum cyclic stresses corresponding to 70, 40 and 25 percent of ultimate static strength. The reason for the 25 percent level was that both the 70 and 40 percent levels produced failure after a small number of cycles, namely 1000 and 14,000 cycles respectively. The 25 percent of ultimate

specimen failed at 419,000 cycles. An abrupt drop in modulus occurred between 20,000 and 30,000 cycles (Fig. 5-18). No temperature data were obtained due to thermocouple failure.

A summary of load cycles to failure for the specimens with embedded instrumentation is given in Table 5-2. The variations in longitudinal modulus, major Poisson's ratio and temperature with number of loading cycles are shown in Figures 5-19 through 5-32.

The Boron/Epoxy specimen cycled to 90 percent of ultimate strength failed at 100 cycles. The specimen cycled to 70 percent of ultimate failed at 430,000 cycles. This specimen exhibits an abrupt drop in modulus between 10,000 and 20,000 cycles (Fig. 5-19). Poisson's ratio remains fairly constant. The temperature rises to a plateau of approximately 303 degK (87°F) and then it increases again just before failure. A runout of 10^7 cycles was obtained at a load of 40 percent of ultimate, with small variations in modulus, Poisson's ratio and temperature (Fig. 5-20).

The Boron/Polyimide specimens were cycled to 90, 80 and 70 percent of ultimate strength. The 80 percent level was chosen in place of 40 percent, because a runout was obtained at 70 percent of ultimate. The 90 percent of ultimate test produced immediate failure. At 80 percent of ultimate the specimen failed at 1000 cycles. It exhibited a constant modulus, Poisson's ratio and temperature behavior up to about 300 cycles. Thereafter, it showed a fast dropoff in modulus with an accompanying increase in Poisson's ratio and small temperature increase up to failure at 1,000 cycles (Fig. 5-21). The specimen tested to 70 percent of ultimate strength survived a runout of 1.290 x 10^7 cycles. It showed a constant modulus, and an abrupt but slight change (3 percent) in Poisson's ratio at 50,000 cycles. The temperature remained constant up to 10^6 cycles and dropped by 2.8 degK (5°F) thereafter to runout (Fig. 5-22).

Table 5-2

SUMMARY OF CYCLIC TENSILE TESTS IN $[0_2/\pm45]_s$ SPECIMENS
WITH EMBEDDED INSTRUMENTATION

Material	Nominal Width cm (in.)	Maximum Stress Level (% σ_{ult})	Cycles to Failure
Boron/Epoxy	2.54 (1.0)	90	100
	2.54 (1.0)	70	430×10^3
	2.54 (1.0)	40	10^7 Runout
Boron/Polyimide	2.54 (1.0)	90	Immediate Failure
	2.54 (1.0)	80	1000
	2.54 (1.0)	70	1.290×10^7 Runout
Graphite/Low Modulus Epoxy	2.54 (1.0)	90	Immediate Failure
	2.54 (1.0)	70	Immediate Failure
	2.54 (1.0)	40	10^7 Runout
Graphite/High Modulus Epoxy	2.54 (1.0)	90	18×10^3
	2.54 (1.0)	90	13×10^3
	2.54 (1.0)	80	28×10^3
	2.54 (1.0)	70	1.016×10^7 Runout
Graphite/ Polyimide	2.54 (1.0)	90	1.023×10^7 Runout
	2.54 (1.0)	80	1.005×10^7 Runout
	2.54 (1.0)	70	10^7 Runout
S-Glass/Epoxy	2.54 (1.0)	70	Tab Failure
	2.54 (1.0)	40	77×10^3
	2.54 (1.0)	40	44×10^3
	2.54 (1.0)	25	1.436×10^6

The Graphite/Low Modulus Epoxy specimens were cycled to 90, 70 and 40 percent of ultimate strength. The specimens tested at 90 and 70 percent of ultimate failed after a few cycles. The specimen tested at 40 percent of ultimate survived 10^7 cycles. However, the gages failed early producing no strain record. The temperature was recorded and was essentially constant up to 1.5 x 10^6 cycles, showed a gradual increase up to 3 x 10^6 cycles and a gradual decrease thereafter. The rise was 2.2 degK (4°F) and the drop 1.7 degK (3°F) from the top temperature of 295 degK (71°F).

The Graphite/High Modulus Epoxy specimens were cycled to 90, 80 and 70 percent of ultimate strength. Following previous procedures, the 80 percent level was chosen after a runout of 10 million cycles was obtained for the 70 percent level. The Graphite/ High Modulus Epoxy exhibited small variations in modulus, Poisson's ratio and temperature at all stress levels applied, (Figs. 5-23 through 5-26). The specimens failed at 18,000 to 28,000 cycles under stresses between 90 and 80 percent of ultimate.

The Graphite/Polyimide specimens were cycled to 90, 80 and 70 percent of ultimate. They all survived the runout of 10 million cycles. They all exhibited a very nearly constant modulus through runout. The temperature remained constant up to about 500,000 cycles. Thereafter, all three specimens showed a gradual increase in temperature in the range of 2 x 10^6 to 3 x 10^6 cycles and then a gradual temperature decrease to runout. The temperature variations were within ±2.8 degK (±5°F), (Figs. 5-27, 5-28, 5-29).

The S-Glass/Epoxy specimens were tested at 70, 40 and 25 percent of ultimate strength. At 70 percent the specimen failed at the tab very early. Two specimens tested at 40 percent of ultimate failed at 44,000 and 77,000 cycles. The variation in modulus and

Poisson's ratio was small, however, the temperature rise was drastic, (Figs. 5-30 and 5-31). In one case the temperature rose to a plateau of approximately 329 degK (133°F) at 20,000 cycles, it dipped to 318 degK (113°F) at 50,000 cycles and then rose sharply to 358 degK (185°F) just prior to failure at 77,000 cycles (Fig. 5-30). The dip, also noticeable in Fig. 5-31, is attributed to some heat dissipation associated with the "brooming" mode of failure. The specimen tested at 25 percent of ultimate failed at 1.436×10^6 cycles with relatively small variations in modulus and Poisson's ratio and a not so drastic temperature rise (Fig. 5-32).

5.5   Tensile Load with Thermal Cycling

5.5.1   Experimental Procedure

Tensile load with thermal cycling testing consisted of subjecting the specimens of this test group to a static tensile load and simultaneously to thermal cycling in two temperature ranges; room temperature to 80 percent of cure temperature and room temperature to 200 degK (-100°F). The static tensile load selected for each material was approximately 70 percent of the average static strength at room temperature. The loaded specimens were subjected to 100 thermal cycles of 30 minute duration. Strains as a function of temperature were monitored at selected cycles. Specimens were examined periodically to detect visually possible degradation during cycling.

The application of tensile load during thermal cycling required the design and fabrication of special loading fixtures unique to this task. The loads required for the individual specimens ranged from 4450N to 17800N (1000 lb to 4000 lb). These were too large for direct dead weight loading and loading by means of a lever arm system was found to be too cumbersome and impractical. Hydraulic loading is feasible but is not very versatile and requires expensive fixturing. A suitable solution was found by means of a spring loading fixture.

Figure 5-33 shows the construction and dimensions of such a typical fixture. Each fixture is used to load a single specimen and consists basically of a load support frame, screw-clamped serrated gripping jaws, loading coil spring, spring load plate and a threaded loading rod with a clevis link. Mounting and loading of the specimen required a careful procedure. To insure the alignment of the specimen axis with the central pivot holes of the jaws, the specimen was clamped in the jaws in an aligning jig outside the loading fixture. The specimen with the clamped jaws was then mounted in the load support frame, the clevis and loading rod attached and the coil spring and spring load plate slipped over the rod. Next, the spring was compressed in a testing machine to a pre-determined calibrated length and the load nut on the rod tightened against the spring load plate. Release of the test machine load transferred the spring load to the desired tensile load in the specimen. The loading spring for each specimen was selected with a sufficiently large deflection, to insure that the thermal expansion during cycling did not significantly change the specimen load. To prevent twisting of the specimen during spring loading, the clamping jaws were arranged to fit closely between the vertical bars of the loading fixture. Eight fixtures of this type were built to perform the required tests.

To achieve a 30-minute thermal cycle duration in the presence of the large fixture masses, the modified cycling method, briefly described in Section 5.3.2, was adopted. As indicated in that section, in the modified cycling method the chamber temperature is kept constant while the specimens are moved in and out of the chamber. The specimens are thereby exposed for half the cycle to chamber temperature and half the cycle to room temperature. This approach required the design and fabrication of a cycling apparatus and modification of the existing chamber closures.

Figures 5-34, 5-35, and 5-36 show this cycling apparatus, the modified oven closures for the Blue M "Power-O-Matic-60" oven, the loading fixtures and the specimens. Figure 5-34 also shows the data acquisition system used to monitor the strain gages and thermocouples. The cycling apparatus consists of a fixed support frame, a cycling lever, a reciprocating frame, a cycle counter and an actuation system operated by a compressed air actuator controlled by a solenoid valve. The valve is timed by an electric timer set to the desired cycling rate. The reciprocating frame carries the specimens in their loading fixtures in front and back of which there is a separate oven closure. The oven is therefore kept closed both when the specimens are in and out of the oven.

Cycling between room temperature and 200 degK (-100°F), was done in the large environmental chamber (Thermovac) mentioned earlier. A similar cycling apparatus and chamber closure system was built for this purpose and is shown in Figures 5-37 and 5-38. Cold cycling produces moisture condensation on the specimens with alternating freezing and thawing. To prevent specimen and instrumentation damage the specimens and gage and thermocouple leads exiting from the specimens were completely coated with silicon rubber (RTV) coatings as described earlier (Section 5.3.3).

5.5.2 Tensile Load with Thermal Cycling of Epoxy Matrix Specimens Between Room Temperature and 411 degK (280°F)

Two $[0_2/\pm45]_s$ specimens, including one with embedded instrumentation, of each of Boron/Epoxy, Graphite/Low Modulus Epoxy, Graphite/High Modulus Epoxy and S-Glass/Epoxy were subjected to a static load equal to 70 percent of the ultimate and simultaneously to 100 thermal cycles of 30 minute duration between room temperature and 411 degK (280°F). The applied tensile loads were 497 MPA (72 ksi) for the Boron/Epoxy, 310 MPa (45 ksi) for the Graphite/Low Modulus

5-15

Epoxy, 331 MPa (48 ksi) for the Graphite/High Modulus Epoxy and 524 MPa (76 ksi) for the S-Glass/Epoxy specimens. Of the eight specimens, the Graphite/Low Modulus Epoxy and the S-Glass/Epoxy specimens failed during the first thermal cycle. This is not surprising since the strength of S-Glass/Epoxy decreases rapidly with increasing temperature and the low modulus epoxy has a heat distortion temperature of 316 degK (109°F). The surviving Boron/Epoxy and Graphite/High Modulus Epoxy specimens were visually inspected during intervals of the cycling but showed no apparent degradation. Their embedded gages were monitored as a function of temperature during the twelfth, sixtieth and hundredth cycles. No significant differences were observed in the recorded strains throughout the thermal cycling. Apparent strains for the Graphite/High Modulus Epoxy are shown in Figure 5-39 for the sixtieth and hundredth thermal cycles.

5.5.3 Tensile Load with Thermal Cycling of Polyimide Matrix Specimens Between Room Temperature and 533 degK (500°F)

Two $[0_2/\pm45]_s$ specimens, including one with embedded instrumentation, of each of Boron/Polyimide and Graphite/Polyimide were subjected to a static load equal to 70 percent of the ultimate load and simultaneously to 100 thermal cycles of 30 minute duration between room temperature and 533 degK (500°F). The tensile load applied to the Boron/Polyimide specimens was 414 MPa (60 ksi) and that applied to the Graphite/Polyimide specimens was 242 MPa (35 ksi). Of the specimens cycled, the 1.27 cm (0.5 in.) wide Graphite/Polyimide specimen failed under load during the first thermal cycle. The 2.54 cm (1 in.) wide specimen survived the cycling without apparent degradation or deterioration of residual properties when subsequently tested for residual strength. In view of this, the failure of the 1.27 cm (0.5 in.) wide specimen does not represent typical behavior of Graphite/Polyimide under tensile load with thermal cycling. The Boron/Polyimide specimens showed no apparent degradation due to cycling.

Specimen strains of the instrumented specimens were monitored as a function of temperature during the third, thirtieth and ninety-ninth cycles. Apparent strains in the Graphite/Polyimide during these cycles are shown in Figure 5-40. It is seen that these strains are essentially the same throughout the 100 thermal cycles and nearly the same as the strains recorded in the similarly cycled unloaded specimen.

5.5.4 Tensile Load with Thermal Cycling Between Room Temperature and 200 degK (-100°F)

Two $[0_2/\pm45]_s$ specimens, including one with embedded instrumentation, of each of the six material systems studied were loaded in tension to 70 percent of the ultimate load and thermally cycled for 100 cycles of 30 minute duration, between room temperature and 200 degK (-100°F). The applied loads were 497 MPa (72 ksi) for the Boron/Epoxy, 310 MPa (45 ksi) for the Graphite/Low Modulus Epoxy, 331 MPa (48 ksi) for the Graphite/High Modulus Epoxy, 524 MPa (76 ksi) for the S-Glass/Epoxy, 414 MPa (60 ksi) for the Boron/Polyimide and 242 MPa (35 ksi) for the Graphite/Polyimide specimens. Inspection before cycling revealed that the Graphite/Low Modulus Epoxy specimen with embedded instrumentation was defective. It was replaced by a 1.27 cm (0.5 in.) wide specimen cut from a $[0_2/\pm45]_s$ plate.

Periodic inspection during cycling revealed a delamination crack in the 1.27 cm (0.5 in.) wide Glass/Epoxy Specimen, (Fig. 5-41). The specimen, however, held the load and survived the thermal cycling. Subsequent testing revealed a reduction in strength but no change of longitudinal modulus and an insignificant change in Poisson's ratio (see Section 5.6.3).

When the specimens were unloaded at the end of the thermal cycling it was noted that the two Graphite/Low Modulus Epoxy specimens were bowing (Fig. 5-42). Closer examination revealed that the two

0-degree top plies on one side of each specimen were delaminated from the remaining plies (Fig. 5-43). Subsequent testing of these specimens (Section 5.6.3) showed a reduction in strength, modulus and Poisson's ratio. It should be noted that the Graphite/Low Modulus Epoxy and the S-Glass/Epoxy materials did not survive the tensile load with thermal cycling to 411 degK (280°F).

Specimen strains as a function of temperature of the instrumented specimens were monitored at the beginning and end of the thermal cycling. The apparent strains in the Graphite/High Modulus Epoxy specimen are shown in Figure 5-44. There is no evidence of change due to cycling. Comparing this with the results obtained for the similarly cold-cycled specimen without load, (Fig. 5-3), it can be concluded that the thermal strains for this material do not change after 100 cycles between room temperature and 200 degK (-100°F).

5.6 Residual Strength

All specimens which survived the thermal cycling, tensile load cycling and tensile load with thermal cycling tests were tested statically to failure in tension. Those specimens which were uninstrumented were provided with surface strain gages so that stress-strain data could be recorded for all specimens during the tensile tests. The data were used to determine the residual longitudinal strength S_{xxT}, the residual longitudinal modulus E_{xx} and the residual major Poisson's ratio ν_{xy}. The residual property results are presented in Tables 5-3 to 5-7, and the stress-strain curves are given in Figures 5-45 through 5-98. Presented in the tables for comparison are values of initial static room temperature properties for similar uncycled specimens. These are averages obtained from Table 3-19. All results presented here are based on nominal specimen thicknesses.

Table 5-3

RESIDUAL PROPERTIES OF $[0_2/\pm45]_s$ SPECIMENS AFTER 100 THERMAL CYCLES BETWEEN ROOM TEMPERATURE AND 411 degK (280°F) FOR THE EPOXY MATRIX AND 533 degK (500°F) FOR THE POLYIMIDE MATRIX SPECIMENS. COMPARISON WITH INITIAL PROPERTIES

Specimen Material	Initial Properties			Residual Properties		
	Strength S_{xx} MPa (ksi)	Modulus E_{xx} GPa (ksi)	Poisson's Ratio ν_{xy}	Strength S_{xx} MPa (ksi)	Modulus E_{xx} GPa (ksi)	Poisson's Ratio ν_{xy}
Boron/Epoxy	725 (105)	115 (16.7)	0.70	773 (112)	116 (16.8)	0.72
Graphite/Low Modulus Epoxy	566 (82)	111 (16.1)	0.72	614 (89)	117 (16.9)	0.67
Graphite/High Modulus Epoxy	483 (70)	99 (14.3)	0.72	518 (75)	106 (15.4)	0.77
S-Glass/Epoxy	745 (108)	37 (5.3)	0.52	773 (112)	37 (5.4)	0.50
Boron/Polyimide	566 (82)	117 (17.0)	0.72	518 (75)	123 (17.8)	0.74
Graphite/Polyimide	345 (50)	114 (16.5)	0.71	384 (56)	116 (16.8)	0.81

Table 5-4

RESIDUAL PROPERTIES OF $[0_2/\pm45]_s$ SPECIMENS AFTER 100 THERMAL CYCLES BETWEEN ROOM TEMPERATURE AND 200 degK (-100°F). COMPARISON WITH INITIAL PROPERTIES.

Specimen Material	Initial Properties			Residual Properties		
	Strength S_{xx} MPa (ksi)	Modulus E_{xx} GPa (ksi)	Poisson's Ratio ν_{xy}	Strength S_{xx} MPa (ksi)	Modulus E_{xx} GPa (ksi)	Poisson's Ratio ν_{xy}
Boron/Epoxy	725 (105)	115 (16.7)	0.70	759 (110)	111 (16.1)	0.71
Graphite/Low Modulus Epoxy	566 (82)	111 (16.1)	0.72	366 (53)	82 (11.9)	0.57
Graphite/High Modulus Epoxy	483 (70)	99 (14.3)	0.72	511 (74)	104 (15.1)	0.73
S-Glass/Epoxy	745 (108)	37 (5.3)	0.52	731 (106)	36 (5.2)	0.52
Boron/Polyimide	566 (82)	117 (17.0)	0.72	511 (74)	117 (16.9)	0.79
Graphite/Polyimide	345 (50)	114 (16.5)	0.71	373 (54)	115 (16.7)	0.82

Table 5-5

RESIDUAL STRENGTH OF CYCLIC TENSILE SPECIMENS $[0_2/\pm45]_s$

Specimen Material	Initial Properties			Maximum Cyclic Stress (% σ_{ult})	Specimen Nominal Width cm (in.)	Residual Properties		
	Strength S_{xx} MPa (ksi)	Modulus E_{xx} GPa (ksi)	Poisson's Ratio ν_{xy}			Strength S_{xx} MPa (ksi)	Modulus E_{xx} GPa (ksi)	Poisson's Ratio ν_{xy}
Boron/Epoxy	725 (105)	115 (16.7)	0.70	40 40	1.27 (0.5) 2.54 (1.0)	752 (109) 710 (103)	120 (17.4) 119 (17.2)	0.78 0.74
Boron/Polyimide	566 (82)	117 (17.0)	0.72	40 70	1.27 (0.5) 2.54 (1.0)	587 (85) 470 (68)	113 (16.3) 102 (14.8)	0.82 0.70
Graphite/Low Modulus Epoxy	566 (82)	111 (16.1)	0.72	40 40	1.27 (0.5) 2.54 (1.0)	570 (83) 352 (51)	114 (16.5) -	0.84 -
Graphite/High Modulus Epoxy	483 (70)	99 (14.3)	0.72	70 70	1.27 (0.5) 2.54 (1.0)	497 (72) 483 (70)	100 (14.5) 107 (15.5)	0.68 0.75
Graphite/Polyimide	345 (50)	114 (16.5)	0.71	70 70 80 90	1.27 (0.5) 2.54 (1.0) 2.54 (1.0) 2.54 (1.0)	438 (63) 338 (49) 387 (56) 328 (48)	93 (13.5) 119 (17.2) 117 (17.0) 116 (16.8)	0.71 0.82 0.80 0.54

Table 5-6

RESIDUAL PROPERTIES OF $[0_2/\pm 45]_s$ SPECIMENS AFTER 100 THERMAL CYCLES BETWEEN ROOM TEMPERATURE AND 411 degK (280°F) FOR THE EPOXY MATRIX AND 533 degK (500°F) FOR THE POLYIMIDE MATRIX SPECIMENS UNDER TENSILE LOAD. COMPARISON WITH INITIAL PROPERTIES.

Specimen Material	Initial Properties			Tensile Preload MPa (ksi)	Residual Properties		
	Strength S_{xx} MPa (ksi)	Modulus E_{xx} GPA (ksi)	Poisson's Ratio ν_{xy}		Strength S_{xx} MPa (ksi)	Modulus E_{xx} GPa (ksi)	Poisson's Ratio ν_{xy}
Boron/Epoxy	725 (105)	115 (16.7)	0.70	497 (72)	745 (108)	116 (16.8)	0.73
Graphite/High Modulus Epoxy	483 (70)	99 (14.3)	0.72	331 (48)	497 (72)	110 (15.9)	0.65
Boron/Polyimide	566 (82)	117 (17.0)	0.72	414 (60)	570 (83)	119 (17.2)	0.80
Graphite/Polyimide	345 (50)	114 (16.5)	0.71	242 (35)	359 (52)	119 (17.2)	0.79

Table 5-7

RESIDUAL PROPERTIES OF $[0_2/\pm45]_s$ SPECIMENS AFTER 100 THERMAL CYCLES BETWEEN ROOM TEMPERATURE AND 200 degK (-100°F) UNDER TENSILE LOAD. COMPARISON WITH INITIAL PROPERTIES.

Specimen Material	Initial Properties			Tensile Preload MPa (ksi)	Residual Properties		
	Strength S_{xx} MPa (ksi)	Modulus E_{xx} GPa (ksi)	Poisson's Ratio ν_{xy}		Strength S_{xx} MPa (ksi)	Modulus E_{xx} GPa (ksi)	Poisson's Ratio ν_{xy}
Boron/Epoxy	725 (105)	115 (16.7)	0.70	497 (72)	759 (110)	114 (16.4)	0.71
Graphite/Low Modulus Epoxy	566 (82)	111 (16.1)	0.72	396 (57)	449 (65)	91 (13.3)	0.65
Graphite/High Modulus Epoxy	483 (70)	99 (14.3)	0.72	331 (48)	545 (79)	107 (15.5)	0.73
S-Glass/Epoxy	745 (108)	37 (5.3)	0.52	524 (76)	714 (104)	37 (5.3)	0.54
Boron/Polyimide	566 (82)	117 (17.0)	0.72	414 (60)	490 (71)	115 (16.7)	0.78
Graphite/Polyimide	345 (50)	114 (16.5)	0.71	242 (35)	331 (48)	118 (17.0)	0.82

5.6.1 Residual Properties of Unloaded Specimens Subjected to Thermal Cycling

All epoxy matrix specimens which were cycled between room temperature and 411 degK (280°F) and polyimide matrix specimens which were cycled between room temperature and 533 degK (500°F) were tested statically in tension to failure. Stress-strain curves for these tests are shown in Figs. 5-45 through 5-55. In the case of the Boron/Polyimide specimen of Fig. 5-53 a rather abrupt change in slope is observed, accompanied by an increasing discrepancy between the strains on the two sides of the specimen. This is attributed to failure of at least three of the outer 0-degree plies and partial damage of the remaining 0-degree ply. This is further corroborated by the fact that the modulus drops to less than a quarter of its initial value. The values of longitudinal modulus and Poisson's ratio obtained from these curves and the measured strength values are tabulated in Table 5-3 where they are compared with the corresponding initial properties of uncycled specimens.

The residual moduli seem to be very close to the initial values. Any possible relaxation of residual stresses or even some matrix degradation during cycling would not influence the longitudinal modulus. Changes in Poisson's ratio are not regarded as significant, since they fall within the variability of this value from specimen to specimen. The residual strengths, with the exception of that of the Boron/Polyimide, are slightly higher than the initial strengths. The differences are small to be taken as significant in view of the small numbers of specimens tested, however, they could be attributed to some residual stress relaxation.

All specimens which were cycled between room temperature and 200 degK (-100°F) were tested statically in tension to failure. Stress-strain curves for these tests are shown in Figs. 5-56 through 5-66. The average values of modulus, Poisson's ratio and strength are tabulated in Table 5-4 where they are compared with corresponding initial properties of uncycled specimens.

The residual moduli remained virtually unchanged, except for the Graphite/Low Modulus Epoxy. In the latter case the significant drop in modulus and Poisson's ratio is attributed to degradation during cycling. The lower modulus results primarily from degradation of at least one 0-degree ply. The lower Poisson's ratio would result from some delamination which would remove some of the transverse effects of the ±45-degree plies. The abrupt change in the slopes of the stress-strain curves (Fig. 5-58) indicates further degradation of 0-degree plies during static loading. The residual strength values in general are not significantly different from the initial values except for the Graphite/Low Modulus Epoxy. The appreciable strength reduction in the latter, approximately 35 percent, is due to laminate degradation during cycling.

5.6.2   Residual Properties of Specimens Subjected to Tensile Load Cycling

All specimens which survived 10 million cycles of tensile load at 40 to 90 percent of the ultimate load were subsequently tested statically in tension to failure. Stress-strain curves for these tests are shown in Figs. 5-67 through 5-77. The values of longitudinal modulus and Poisson's ratio obtained from these curves and the measured strength values are tabulated in Table 5-5.

Most of the specimens showed insignificant changes in residual strength and residual modulus. The exceptions include the 2.54 cm (1 in.) wide Boron/Polyimide specimen cycled to 70 percent of ultimate which showed reduced residual strength and modulus, a Graphite/Low Modulus Epoxy which showed lower residual strength and the 1.27 cm (0.5 in.) wide Graphite/Polyimide which had a lower residual modulus. Changes in Poisson's ratio do not appear significant although, in general, a trend for higher residual values is apparent.

5.6.3 Residual Properties of Specimens Subjected to Tensile Load with Thermal Cycling

Of the specimens subjected to tensile load and elevated temperature thermal cycling, the Graphite/Low Modulus Epoxy and the S-Glass/Epoxy specimens failed during the first cycle. The surviving specimens were tested statically in tension to failure. Stress-strain curves for these tests are shown in Figs. 5-78 through 5-86. The values of longitudinal modulus and Poisson's ratio obtained from these curves and the measured strength values are tabulated in Table 5-6 where they are compared with the corresponding initial properties of uncycled specimens.

The residual moduli and strengths seem to be very close to the initial values. The changes in Poisson's ratio are not consistent and are not considered significant. Ultrasonic C-scans of the Boron/Polyimide specimen of Fig. 5-84 before and after thermal cycling under load did not reveal any conclusive differences.

All specimens which were cycled between room temperature and 200 degK (-100°F) under tensile loading survived and were subsequently tested statically in tension to failure. Stress-strain curves for these tests are shown in Figs. 5-87 through 5-98. The Boron/Epoxy and Boron/Polyimide specimens show some nonlinear behavior which was not evident in the original tests or other residual strength tests. The Graphite/Low Modulus Epoxy specimens warped and delaminated under cold cycling with tensile load as mentioned earlier and shown in Figs. 5-42 and 5-43. The stress-strain curves of Fig. 5-91 are perfectly linear to failure whereas those of Fig. 5-92 are concave upwards near failure. The latter corresponds to the badly warped and delaminated specimen. The stress-strain curves of Fig. 5-98 for the S-Glass/Epoxy correspond to the slightly delaminated specimen shown in Figs. 5-41 and 5-43. The values of longitudinal modulus and Poisson's ratio obtained from these

curves and the measured strength values are tabulated in Table 5-7 where they are compared with the corresponding initial properties of uncycled specimens.

The residual moduli remained relatively unchanged except for the Graphite/Low Modulus Epoxy which showed a marked decrease due to the observed structural degradation. The reduction in residual strength for this material is also due to degradation. A similar strength reduction was observed in the slightly damaged S-Glass/Epoxy specimen of Fig. 5-98. The apparent decrease in strength for the Boron/Polyimide and increase for the Graphite/High Modulus Epoxy cannot be explained and may not be significant. In all cases, except for that of the structurally degraded Graphite/Low Modulus Epoxy, Poisson's ratio remained nearly the same or increased.

5.7 Summary and Conclusions

The behavior of angle-ply laminates subjected to thermal cycling, tensile load cycling and thermal cycling with tensile load was investigated. The laminates investigated were Boron/Epoxy, Boron/Polyimide, Graphite/Low Modulus Epoxy, Graphite/Polyimide and S-Glass/Epoxy of $[0_2/\pm45]_s$ layup.

Two specimens of each material were subjected to 100 thermal cycles between room temperature and 411 degK (280°F) for the epoxy-matrix composites and between room temperature and 511 degK (500°K) for the polyimide-matrix composites. No visual degradation was evident due to the cycling. Strain gages monitored during cycling showed no significant differences between the beginning and end of cycling. All cycled specimens were subsequently tested statically to failure and the residual properties were compared with the corresponding initial properties of uncycled specimens. The residual moduli are very close to the initial values. Any possible relaxation of residual stresses or even some matrix degradation during cycling would not influence the

longitudinal modulus. Changes in Poisson's ratio were not significant. The residual strength, with the exception of the Boron/Polyimide, are slightly higher than the initial strengths. The differences are small to be considered significant in view of the small number of specimens tested, however, they could be attributed to some residual stress relaxation.

Two specimens of each material were subjected to 100 thermal cycles between room temperature and 200 degK (-100°F). Periodic visual inspection during cycling did not reveal any apparent degradation. Strains monitored in the beginning and at the end of cycling did not show any change. All cycled specimens were subsequently tested statically to failure. The residual moduli remained virtually unchanged, except for the Graphite/Low Modulus Epoxy which showed a significant reduction due to some degradation. The residual strengths are not significantly different from the initial values, except for the Graphite/Low Modulus Epoxy which showed a significant (approximately 35 percent) reduction due to laminate degradation during cycling.

Six specimens of each material were subjected to tensile load cycling between 0 and 25 to 90 percent of the static strength. The specimens were inspected visually at intervals for signs of degradation. Specimen temperature and strains were monitored at frequent intervals. The Boron/Epoxy specimens cycled to 70 and 90 percent of ultimate failed, but those cycled to 40 percent of ultimate survived 10 million cycles. In most cases a stepwise reduction in modulus concomitant with a gradual rise in temperature was noticed. The Boron/Polyimide specimens showed similar behavior with slightly better endurance to cycling loading. Runouts at 10 million cycles were observed at the 40 and 70 percent of ultimate levels. The Graphite/Low Modulus Epoxy specimens cycled to 70 and 90 percent of ultimate failed early but those cycled to 40 percent of ultimate survived. The latter showed a small gradual temperature rise. The Graphite/High Modulus Epoxy specimens cycled to 80 and 90 percent of

ultimate failed whereas those cycled to 70 percent survived 10 million cycles. Small changes in modulus, Poisson's ratio and temperature were observed. The Graphite/Polyimide specimens showed the highest endurance to cycling loading with consistent runouts at 70 and 80 percent of ultimate and in one case even at 90 percent of ultimate. They all exhibited nearly constant modulus through runout with very moderate temperature variation. The S-Glass/Epoxy specimens cycled to 40 and 70 percent of ultimate failed early and even those tested to 25 percent of ultimate did not survive to runout. The variations in modulus and Poisson's ratio were not large. The temperature variation showed a sharp rise, then a characteristic dip just prior to failure (Figs. 5-30, 5-31). This dip is attributed to some heat dissipation associated with the "brooming" mode of failure.

All specimens which survived 10 million cycles of tensile load to 40 to 90 percent of ultimate were tested statically to failure. As in the case of thermal cycling, no significant changes in residual strength and modulus were observed. The same appears true for Poisson's ratios, although some trend for slightly higher values is noticed.

Two specimens of each material were subjected to a static tensile load equal to 70 percent of the ultimate and simultaneously to 100 thermal cycles between room temperature and 411 degK (280°F) for the epoxy-matrix and between room temperature and 533 degK (500°F) for the polyimide matrix specimens. No visible degradation was observed during cycling and the strains monitored in the beginning and at the end of the cycling did not show any changes. The Graphite/Low Modulus Epoxy and the S-Glass/Epoxy specimens did not survive. The remaining specimens were tested statically to failure. The residual stiffness and strength were very close to the initial values.

A similar group of specimens was subjected to a static tensile load of 70 percent of the ultimate and simultaneously to 100 thermal cycles between room temperature and 200 degK (-100°F). The

Graphite/Low Modulus Epoxy and the S-Glass/Epoxy showed visible de-
gradation. Subsequent static testing showed significant reductions
in strength and modulus in the Graphite/Low Modulus Epoxy and some
strength reduction in the S-Glass/Epoxy. The residual stiffnesses
and strengths for the remaining specimens remained relatively unchanged.
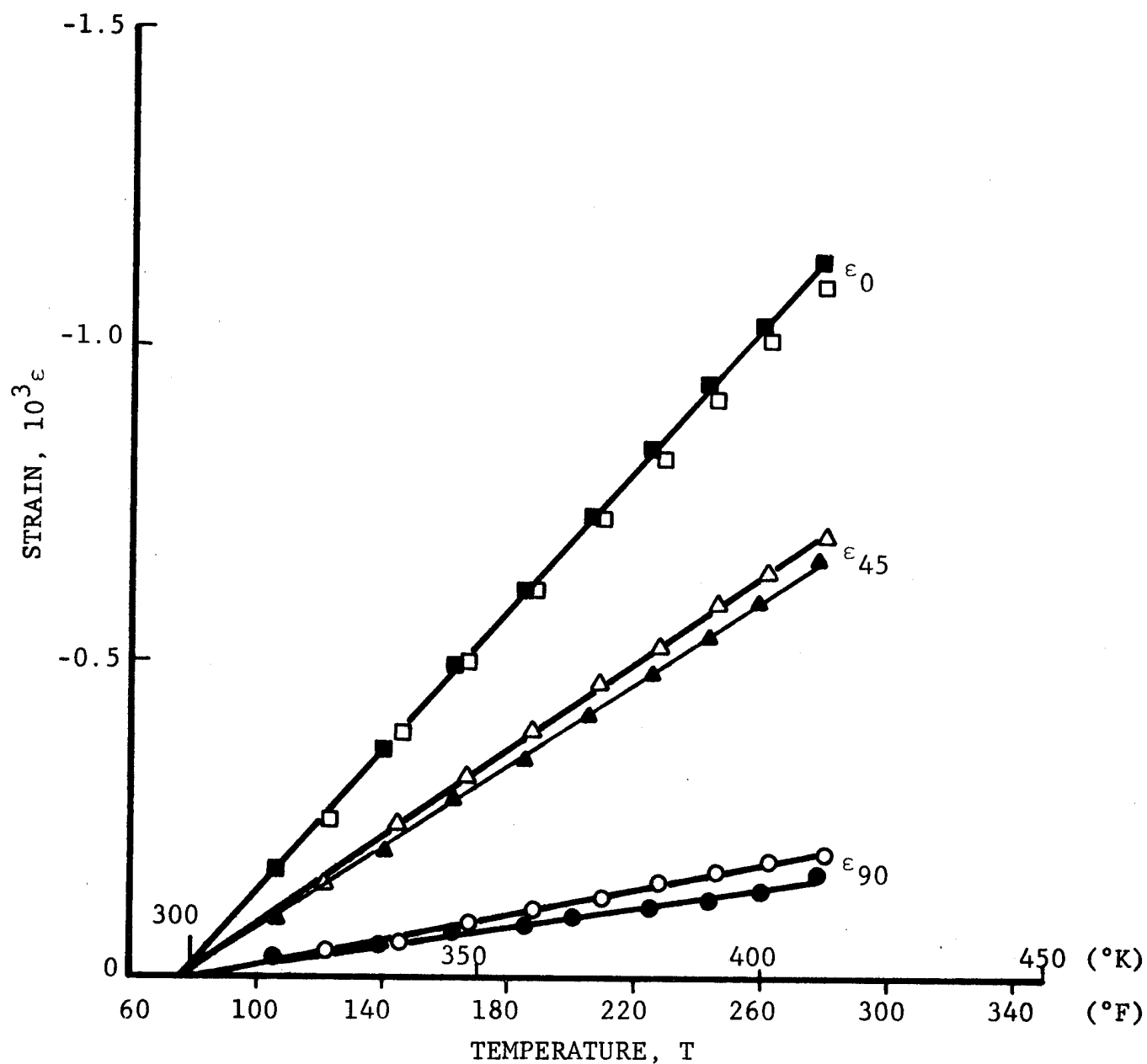
Fig. 5-1 APPARENT STRAINS IN UNLOADED $[0_2/\pm45]_s$ GRAPHITE/HIGH
MODULUS EPOXY SPECIMEN DURING THERMAL CYCLING (FILLED
SYMBOLS: BEGINNING OF CYCLING; OPEN SYMBOLS: END OF
CYCLING).
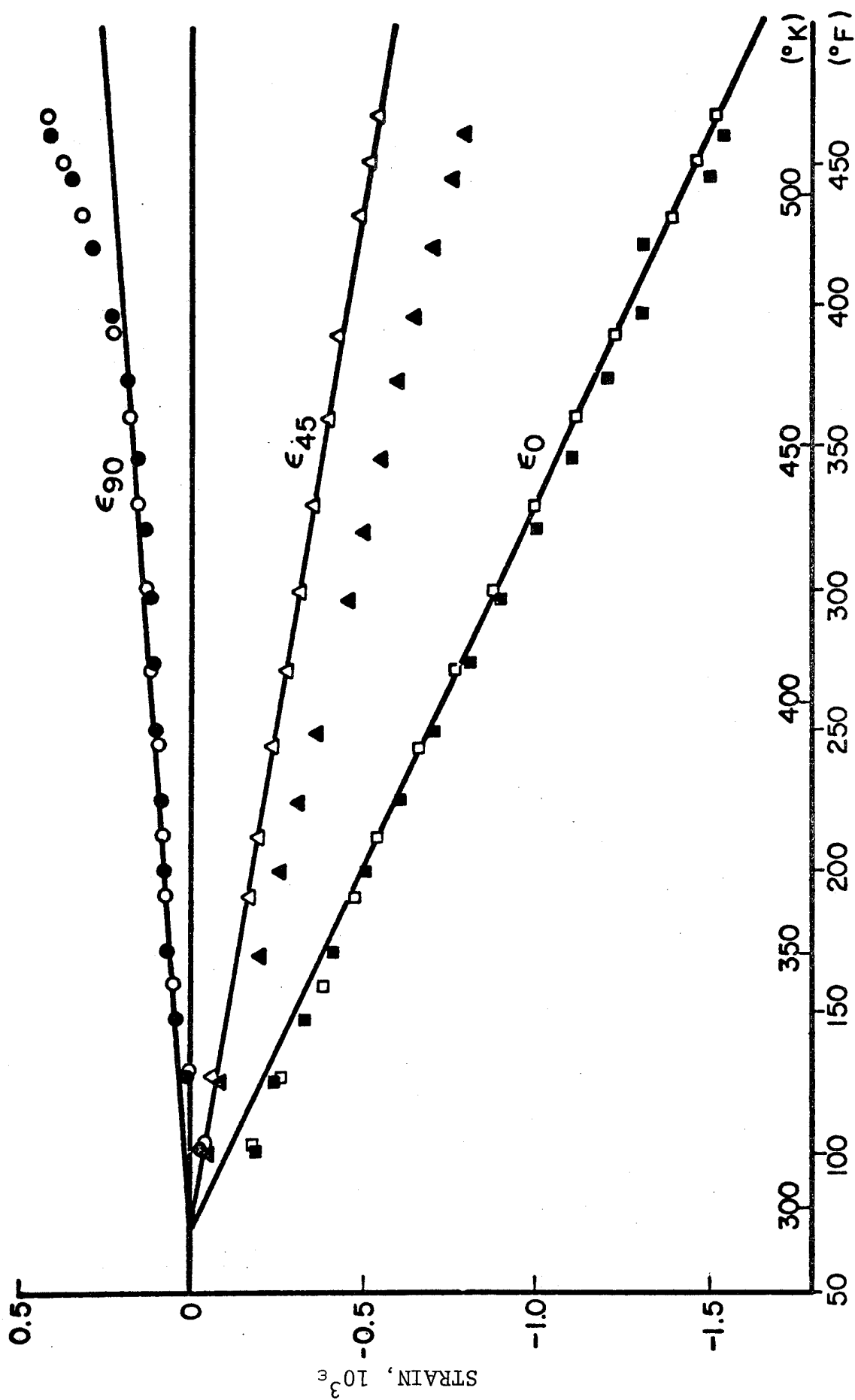
Fig. 5-2 APPARENT STRAINS IN UNLOADED $[0_2/\pm 45]_s$ BORON/POLYIMIDE SPECIMEN DURING THERMAL CYCLING (FILLED SYMBOLS: BEGINNING OF CYCLING; OPEN SYMBOLS: END OF CYCLING)

5-5
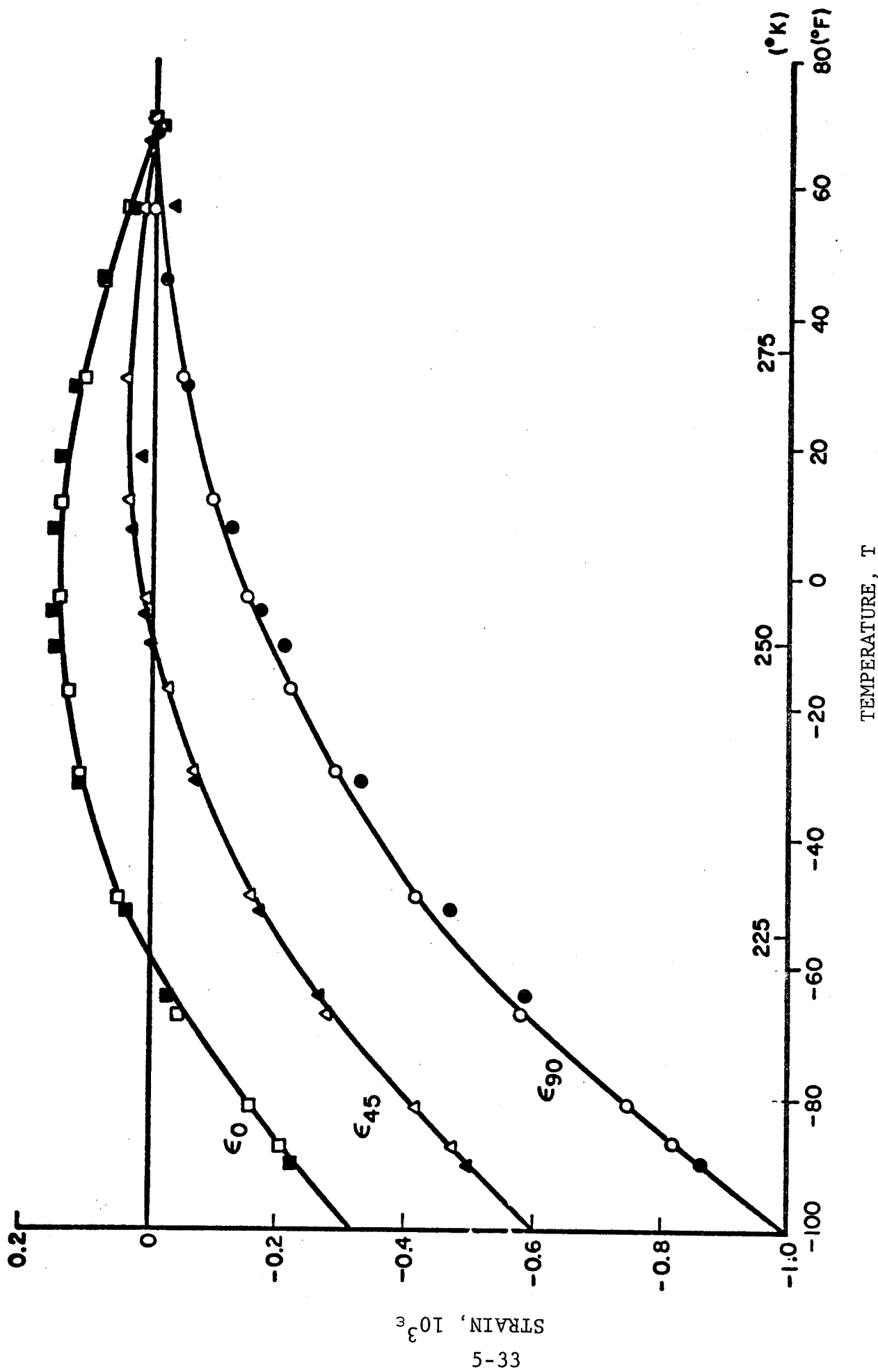
Fig. 5-3 APPARENT STRAINS IN UNLOADED $[0_2/\pm45]_s$ GRAPHITE/HIGH MODULUS EPOXY SPECIMEN DURING THERMAL CYCLING (FILLED SYMBOLS: BEGINNING OF CYCLING; OPEN SYMBOLS: END OF CYCLING)

5-33
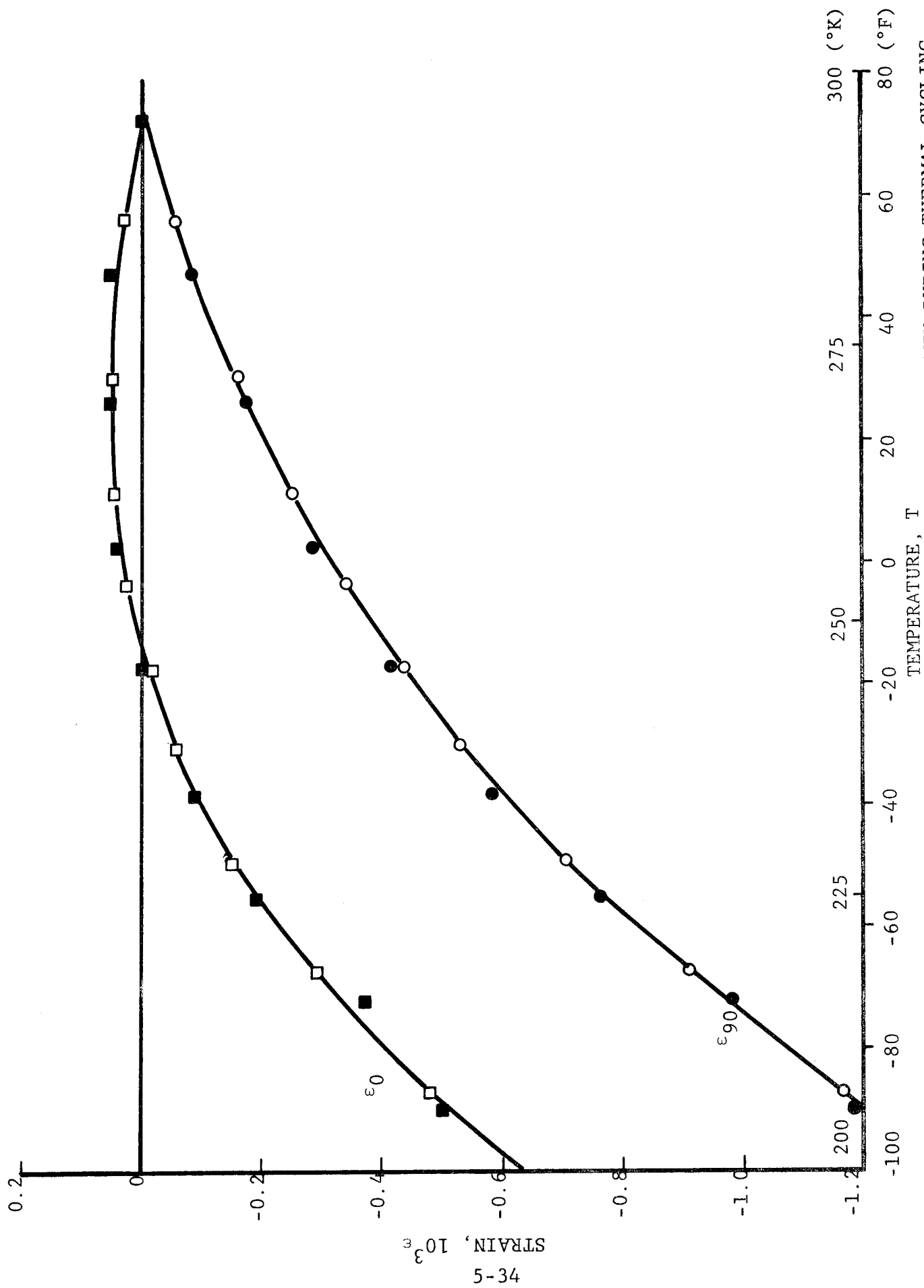
Fig. 5-4 APPARENT STRAINS IN UNLOADED $[0_2/\pm 45]_s$ S-GLASS/EPOXY SPECIMEN DURING THERMAL CYCLING (FILLED SYMBOLS: BEGINNING OF CYCLING; OPEN SYMBOLS: END OF CYCLING)

5-5

5-34

Fig. 5-5 VARIATION OF MODULUS, POISSON'S RATIO AND TEMPERATURE WITH NUMBER OF CYCLES ($[0_2/\pm45]_s$ BORON/EPOXY; $\sigma_{max} = 90\%$ σ_{ult}; CYCLES TO FAILURE:30×10^3)
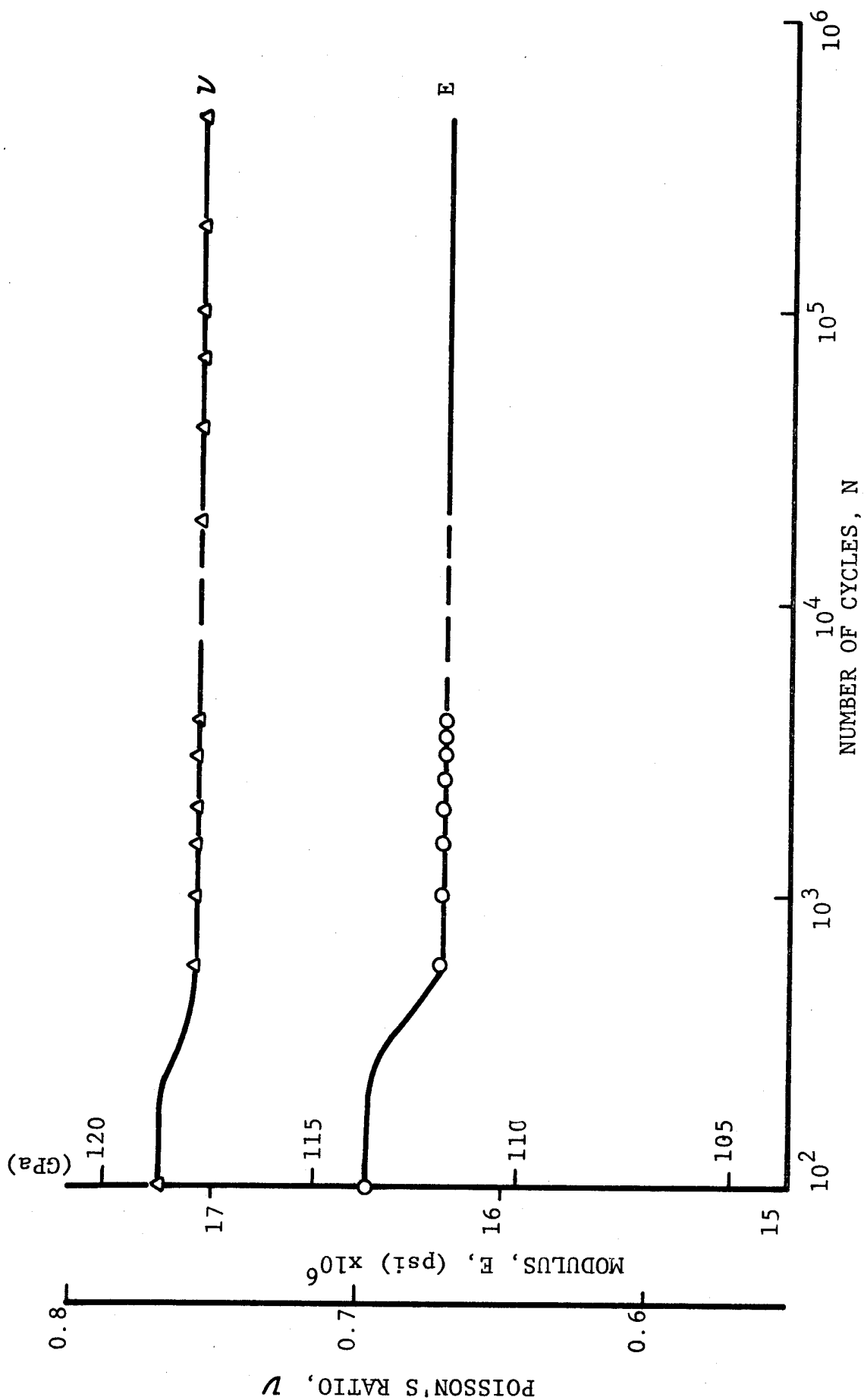
Fig. 5-6   VARIATION OF MODULUS AND POISSON'S RATIO WITH NUMBER OF CYCLES $([0_2/\pm 45]_s$
BORON/EPOXY; $\sigma_{max} = 70\%$ σ_{ult}; CYCLES TO FAILURE: 460×10^3)

Fig. 5-7 VARIATION OF MODULUS, POISSON'S RATIO AND TEMPERATURE WITH NUMBER OF CYCLES ($[0_2/\pm45]_s$ BORON EPOXY; σ_{max} = 40% σ_{ult}; RUNOUT AT 10^7 CYCLES)

Fig. 5-8 VARIATION OF MODULUS, POISSON'S RATIO AND TEMPERATURE WITH NUMBER OF CYCLES ($[0_2/\pm45]_s$ BORON/POLYIMIDE; σ_{max} = 70% σ_{ult}; CYCLES TO FAILURE: 5.97 x 10^6)

Fig. 5-9   VARIATION OF MODULUS, POISSON'S RATIO AND TEMPERATURE WITH NUMBER OF CYCLES ($[0_2/\pm45]_s$ BORON/POLYIMIDE; σ_{max} = 40% σ_{ult}; RUNOUT AT 1.025 x 10^7 CYCLES)

5-39
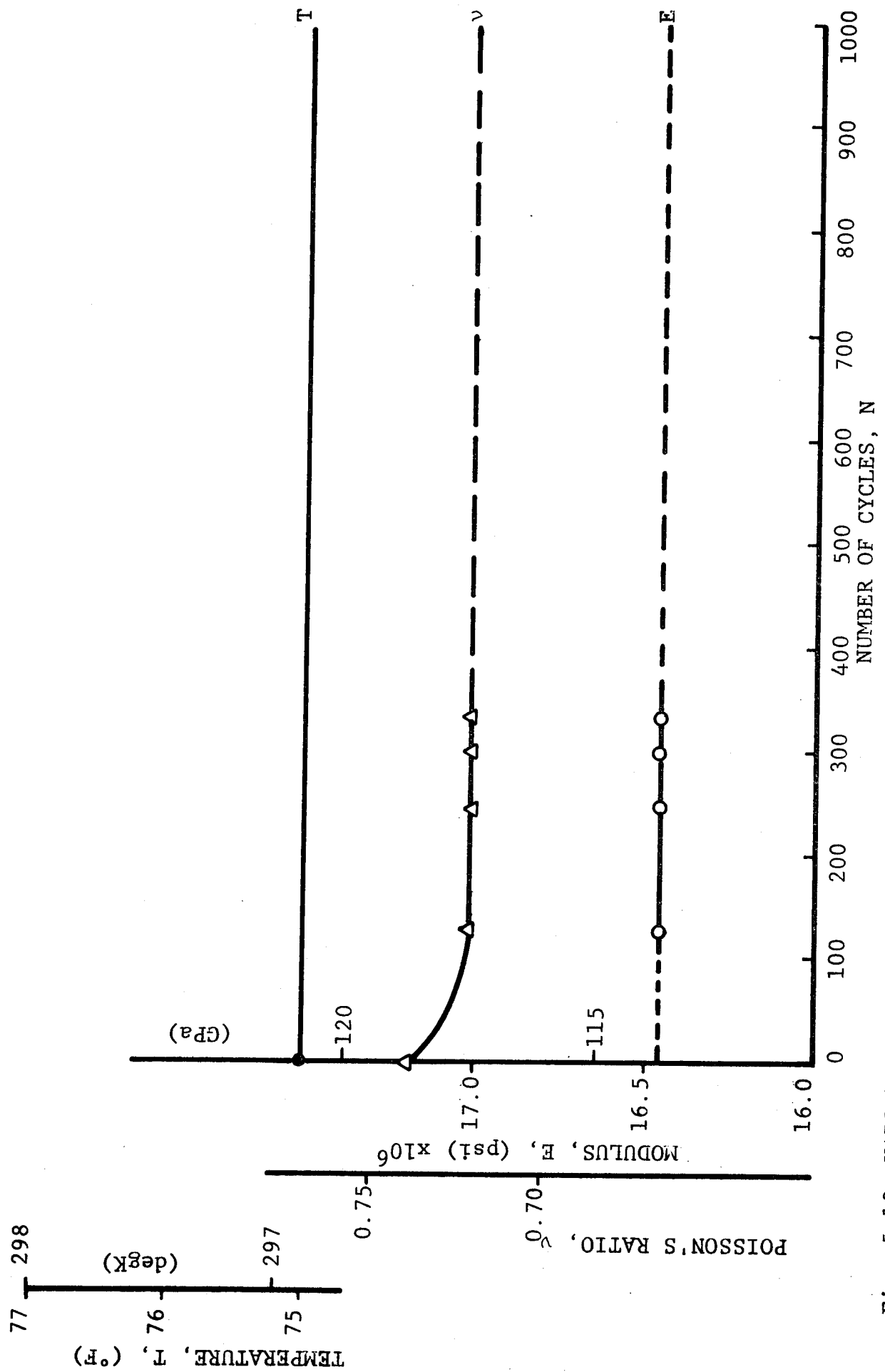
Fig. 5-10 VARIATION OF MODULUS, POISSON'S RATIO AND TEMPERATURE WITH NUMBER OF CYCLES $([0_2/\pm45]_s$ GRAPHITE/LOW MODULUS EPOXY; σ_{max} = 90% σ_{ult}; CYCLES TO FAILURE: 1000)

5-40
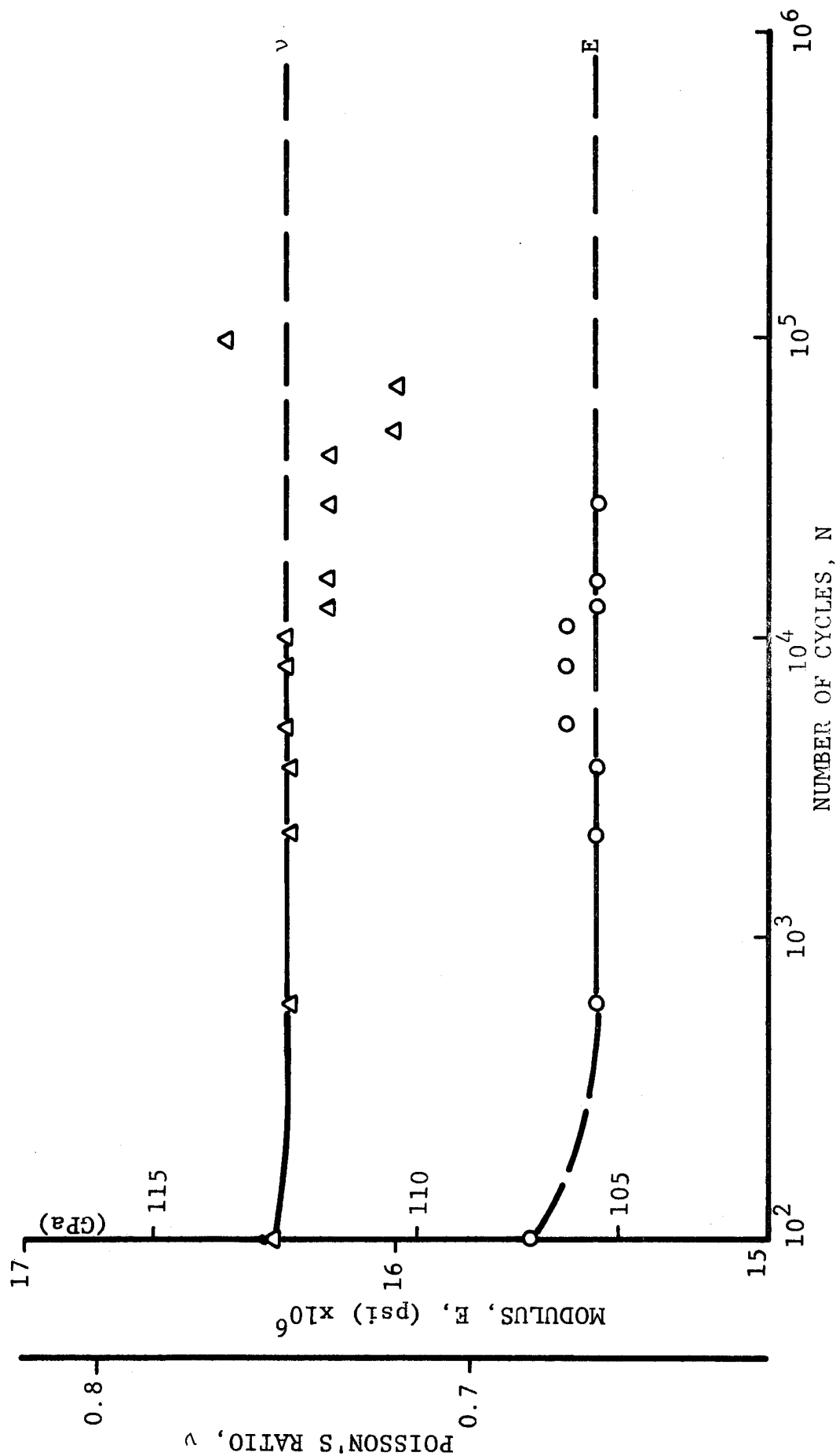
Fig. 5-11 VARIATION OF MODULUS AND POISSON'S RATIO WITH NUMBER OF CYCLES $([0_2/\pm45]_s$ GRAPHITE/LOW MODULUS EPOXY; σ_{max} = 70% σ_{ult}; CYCLES TO FAILURE: 847,000)
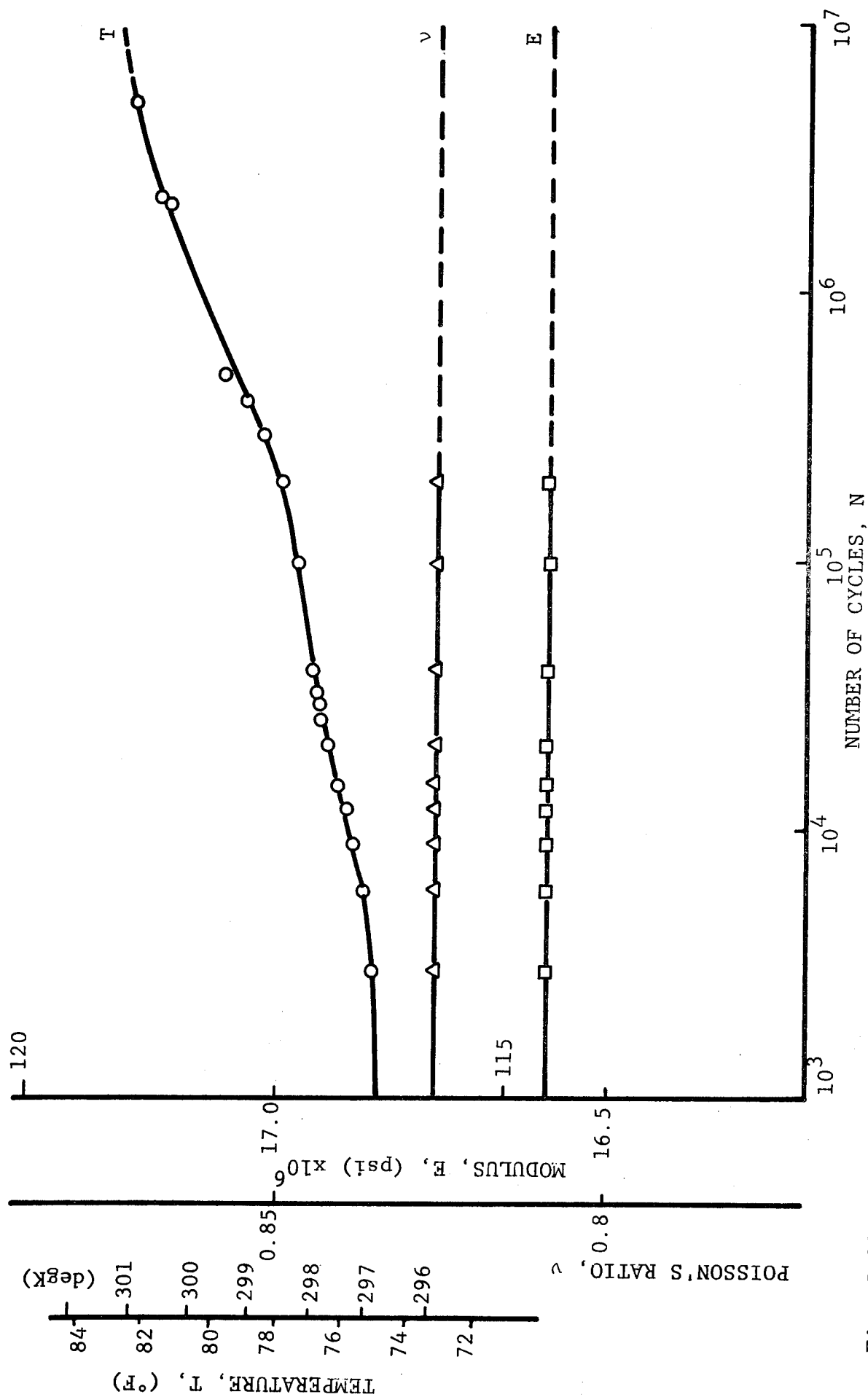
Fig. 5-12 VARIATION OF MODULUS, POISSON'S RATIO AND TEMPERATURE WITH NUMBER OF CYCLES ($[0_2/\pm45]_s$ GRAPHITE/LOW MODULUS EPOXY; $\sigma_{max} = 40\% \ \sigma_{ult}$; RUNOUT AT 1.015×10^7 CYCLES)
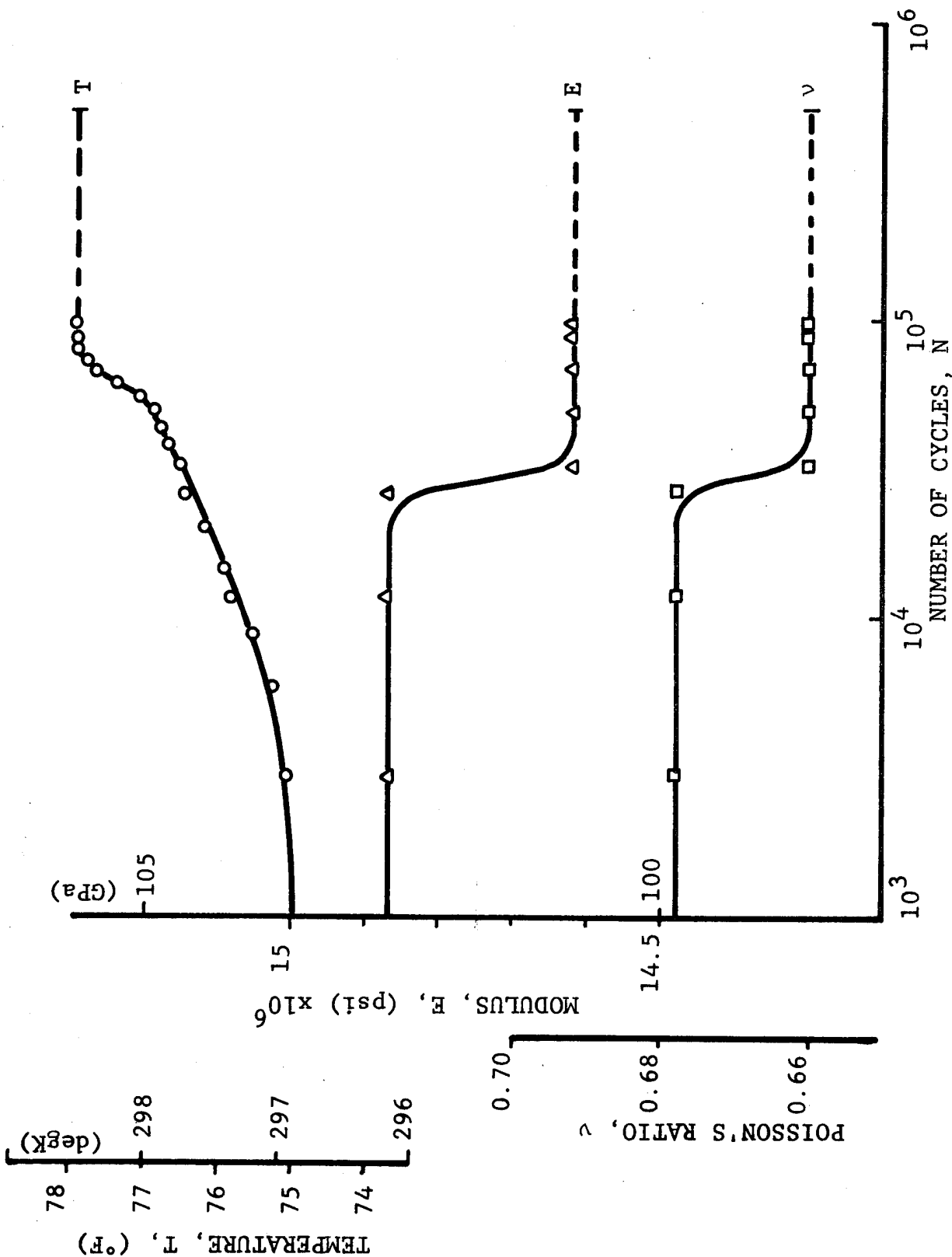
Fig. 5-13 VARIATION OF MODULUS, POISSON'S RATIO AND TEMPERATURE WITH NUMBER OF CYCLES ($[0_2/\pm45]_s$ GRAPHITE/HIGH MODULUS EPOXY; σ_{max} = 80% σ_{ult}; CYCLES AT FAILURE: 512,000)
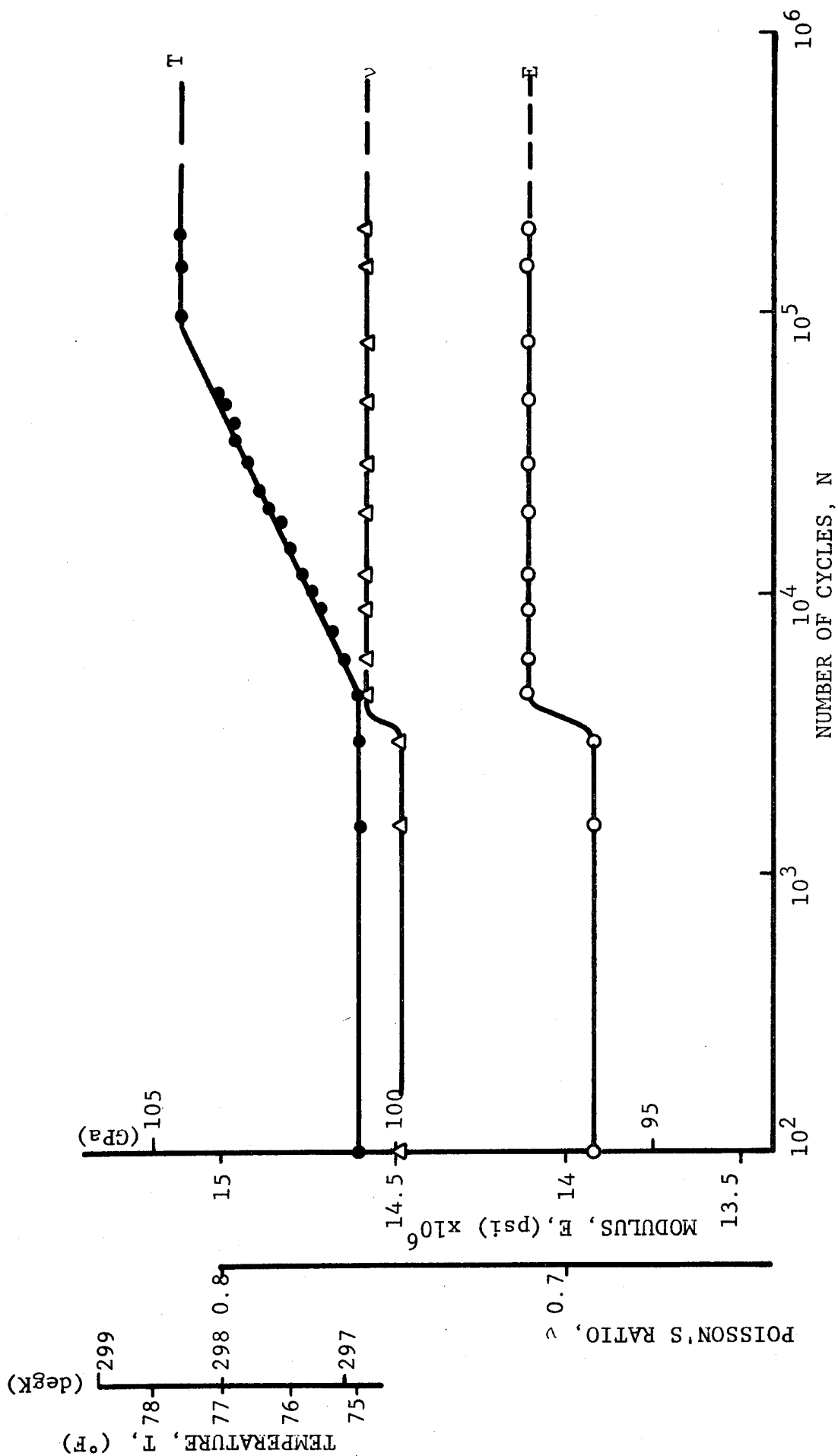
Fig. 5-14 VARIATION OF MODULUS, POISSON'S RATIO AND TEMPERATURE WITH NUMBER OF CYCLES ($[0_2/\pm45]_s$ GRAPHITE/HIGH MODULUS EPOXY; $\sigma_{max} = 70\% \ \sigma_{ult}$; RUNOUT AT 10^7 CYCLES)
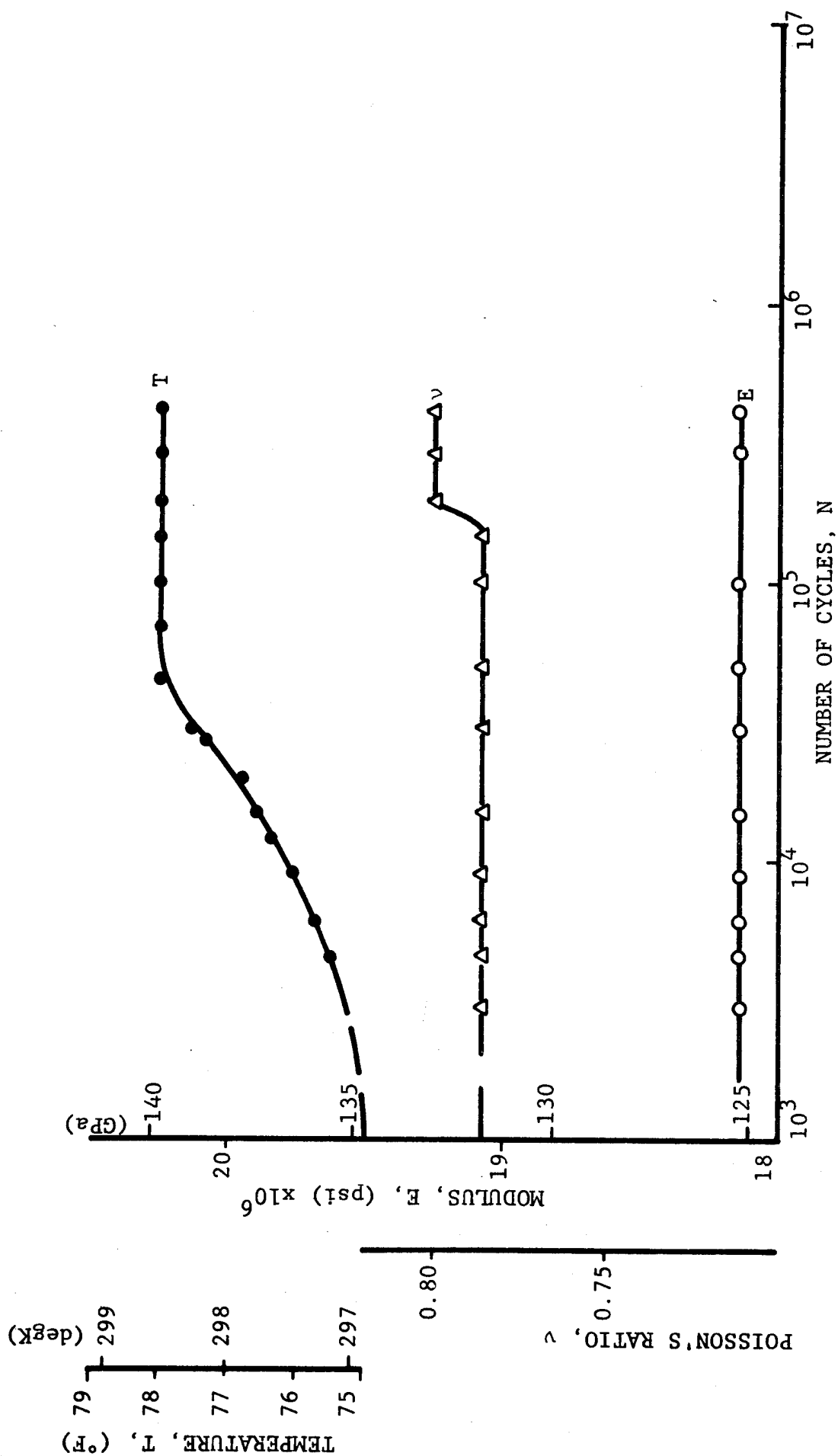
Fig. 5-15 VARIATION OF MODULUS, POISSON'S RATIO AND TEMPERATURE WITH NUMBER OF CYCLES ($[0_2/\pm 45]_s$ GRAPHITE/POLYIMIDE; $\sigma_{max} = 90\%$ σ_{ult}; CYCLES TO FAILURE: 440,000)
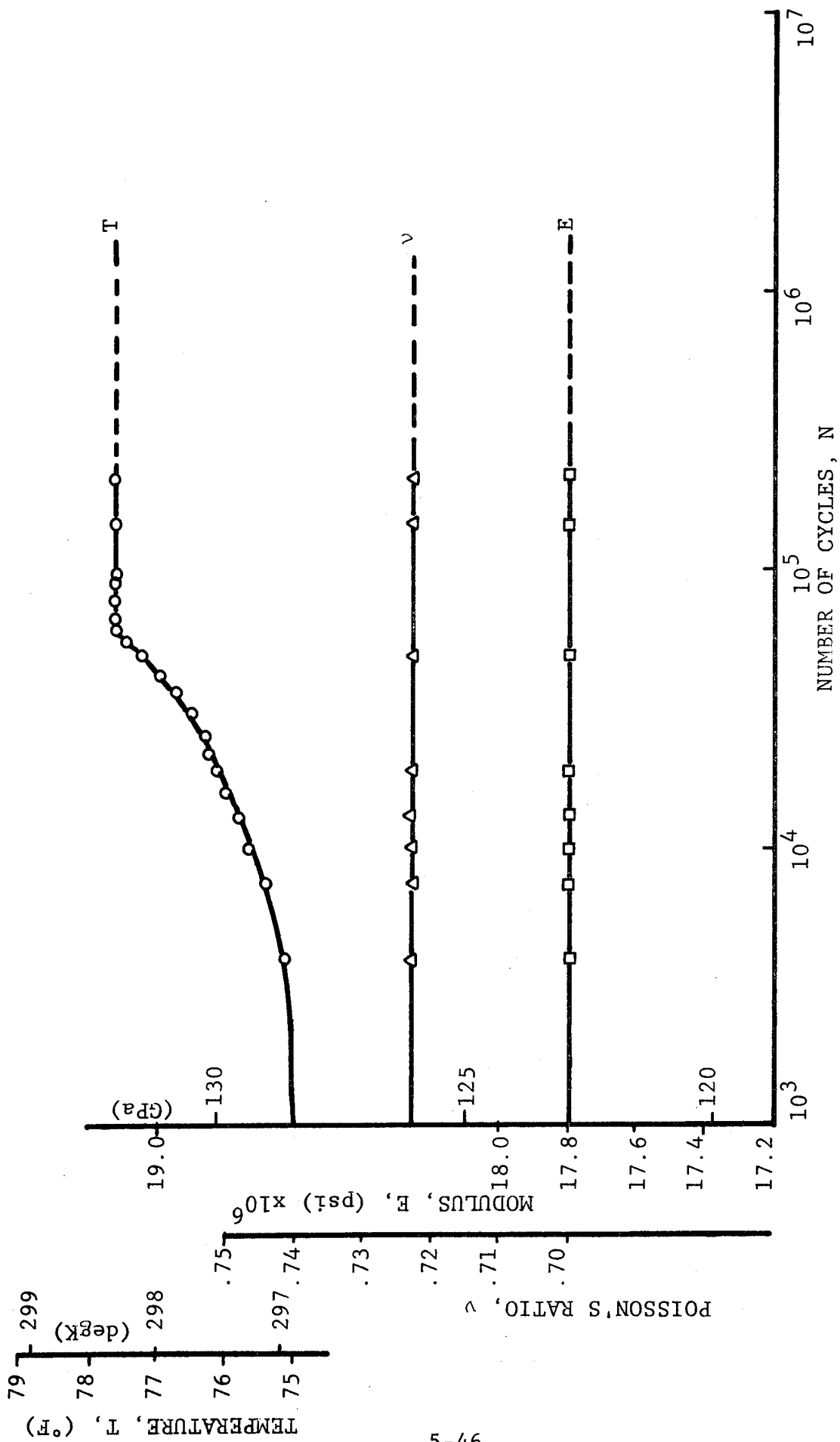
Fig. 5-16 MODULUS, POISSON'S RATIO AND TEMPERATURE AS A FUNCTION OF NUMBER OF CYCLES ($[0_2/\pm45]_s$ GRAPHITE/POLYIMIDE; σ_{max} = 80% σ_{ult}; CYCLES TO FAILURE: 1.553 x 10^6)
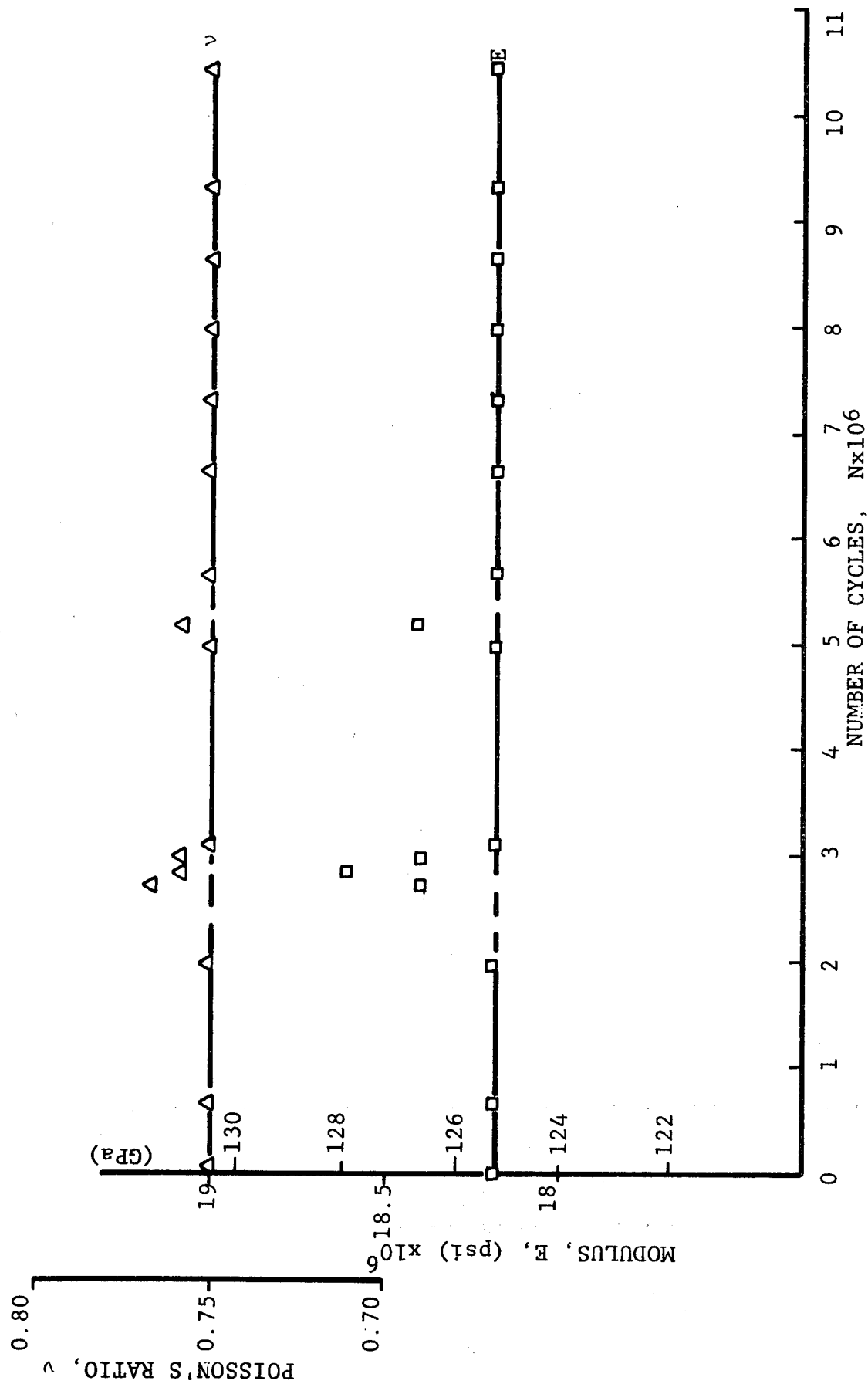
Fig. 5-17 MODULUS AND POISSON'S RATIO AS A FUNCTION OF NUMBER OF LOADING CYCLES ($[0_2/\pm 45]_s$ GRAPHITE/POLYIMIDE; σ_{max} = 70% σ_{ult}; RUNOUT AT 1.047 x 10^7 CYCLES)
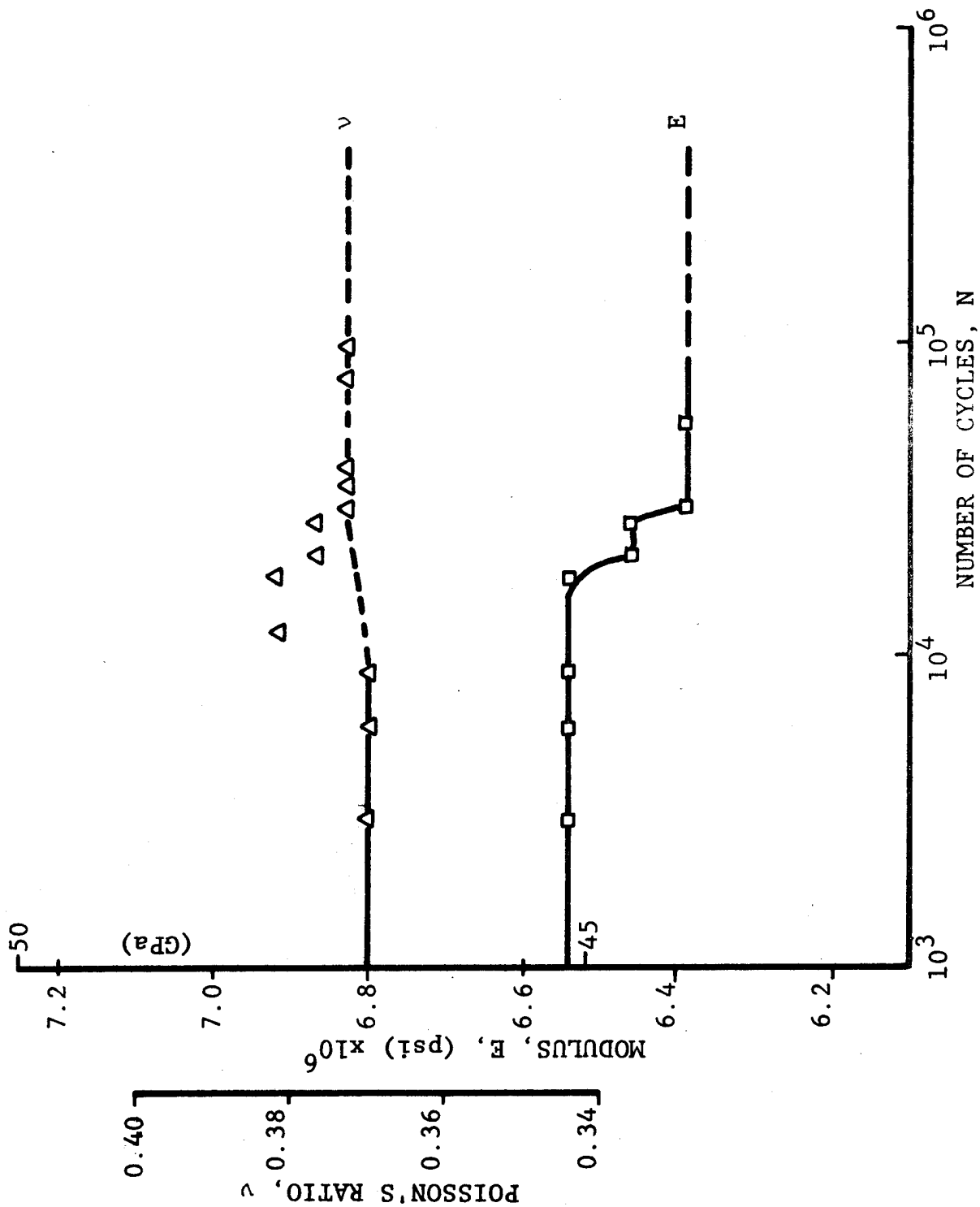
Fig. 5-18 MODULUS AND POISSON'S RATIO AS A FUNCTION OF NUMBER OF CYCLES ($[0_2/\pm45]_s$ S-GLASS EPOXY; σ_{max} = 25% σ_{ult}; CYCLES TO FAILURE: 419,000)
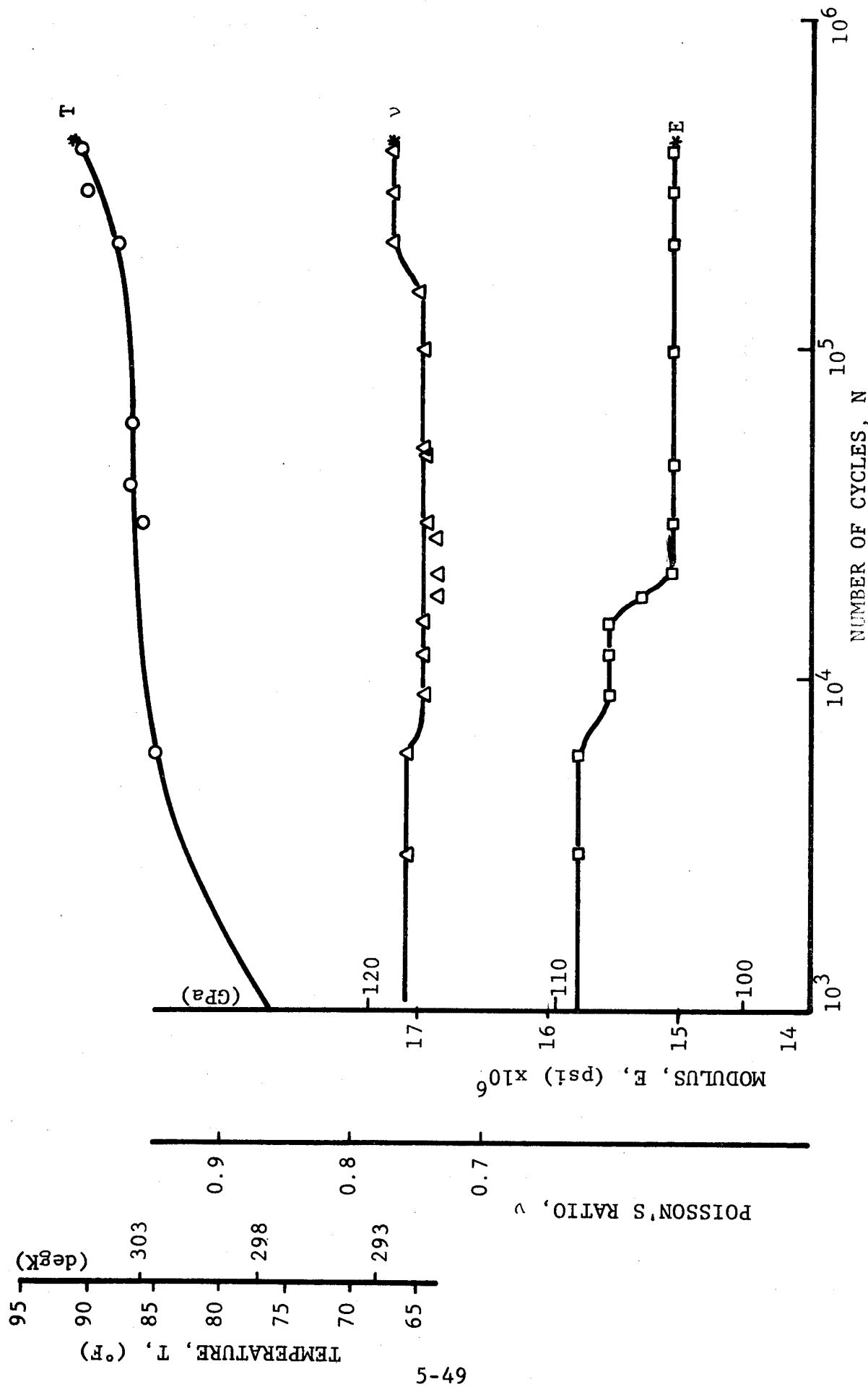
Fig. 5-19   VARIATION OF MODULUS, POISSON'S RATIO AND TEMPERATURE WITH NUMBER OF CYCLES ($[0_2/\pm45]_s$ BORON/EPOXY; $\sigma_{max} = 70\%~\sigma_{ult}$; CYCLES TO FAILURE: 43,000)
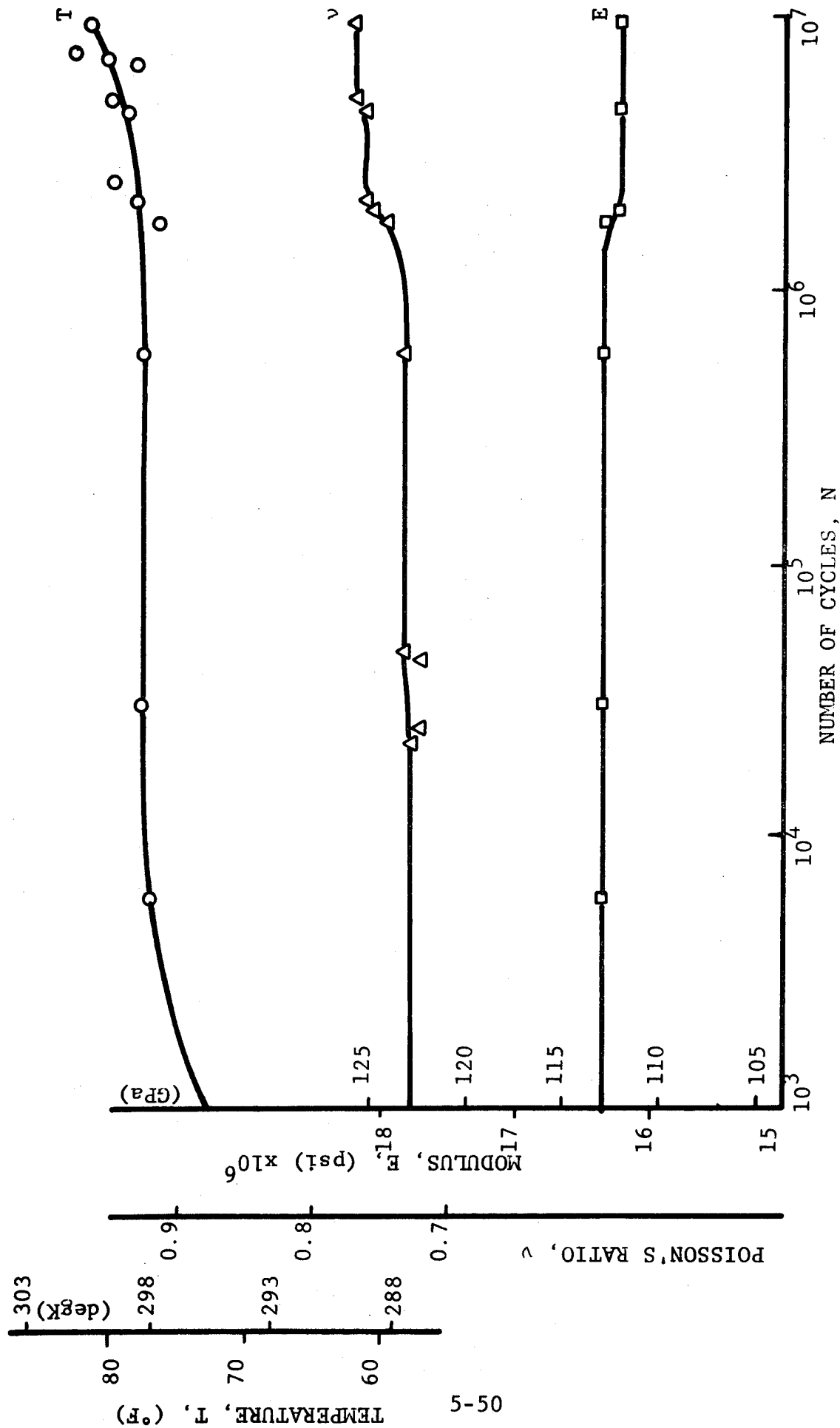
Fig. 5-20 VARIATION OF MODULUS, POISSON'S RATIO AND TEMPERATURE WITH NUMBER OF CYCLES ($[0_2/\pm45]_s$ BORON/EPOXY: $\sigma_{max} = 40\% \ \sigma_{ult}$; RUNOUT AT 10^7 CYCLES)

5-50
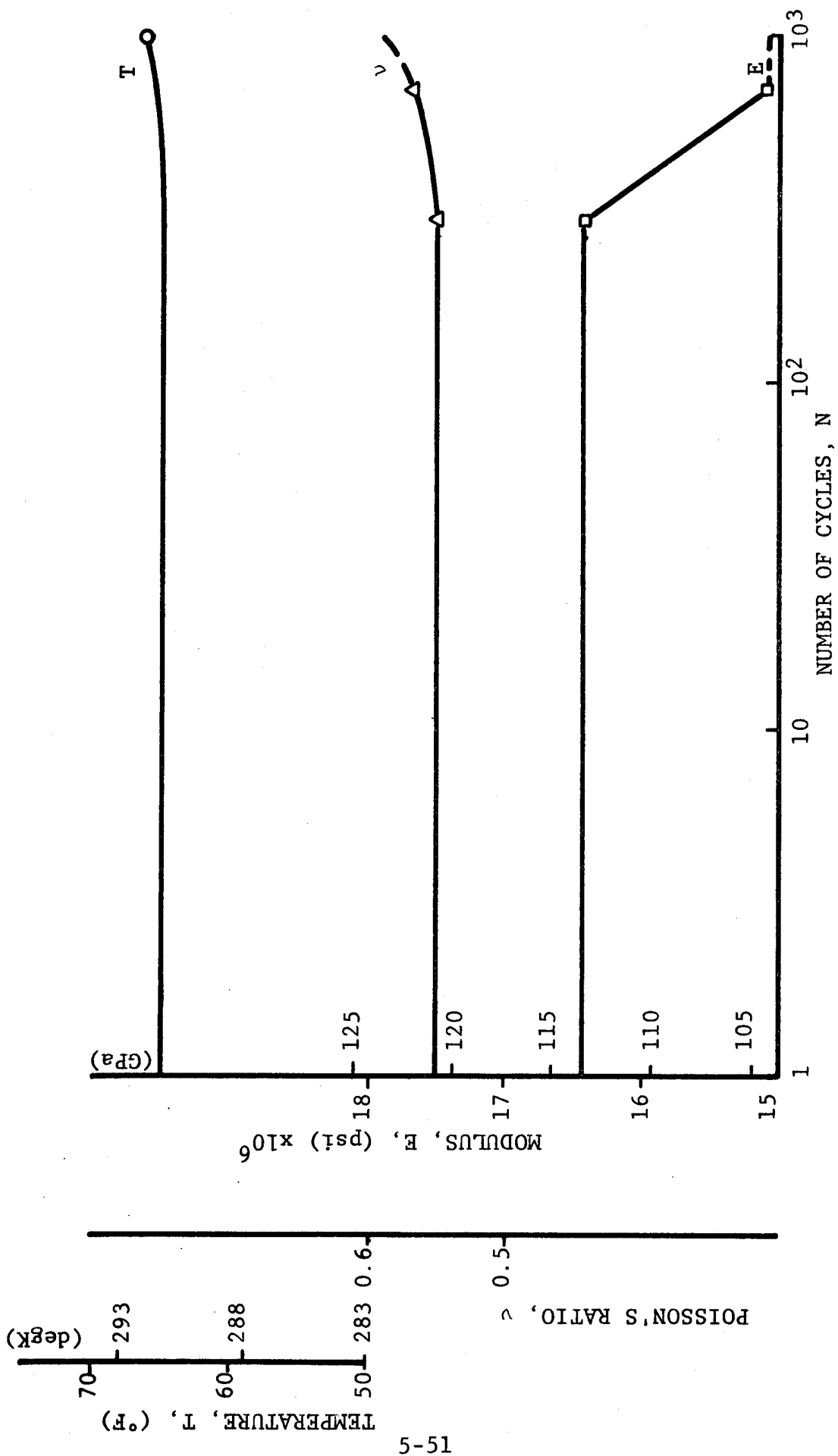
Fig. 5-21 VARIATION OF MODULUS, POISSON'S RATIO AND TEMPERATURE WITH NUMBER OF CYCLES, $([0_2/\pm 45]_s$ BORON/POLYIMIDE; σ_{max} = 80% σ_{ult}; CYCLES TO FAILURE: 1000)
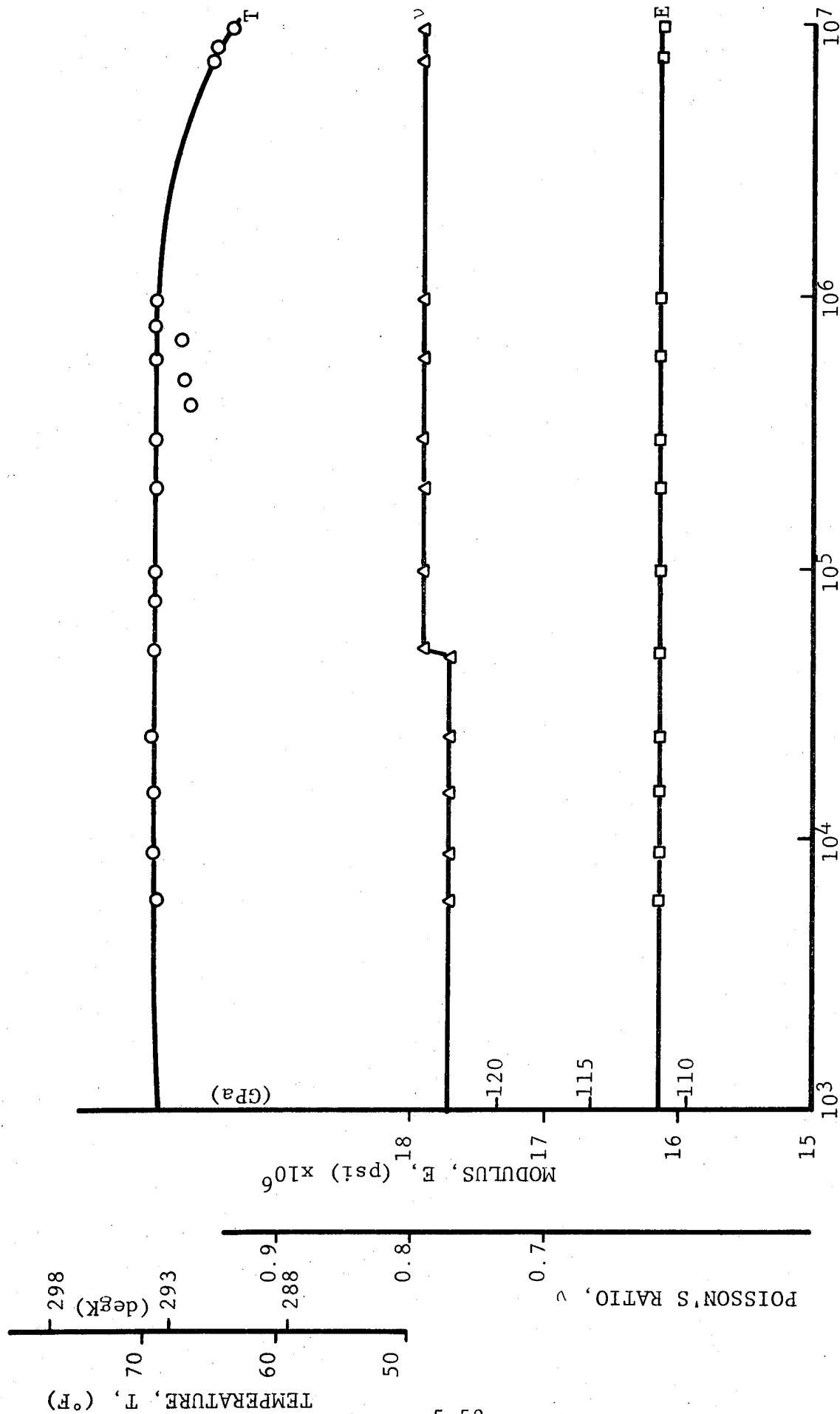
Fig. 5-22 VARIATION OF MODULUS, POISSON'S RATIO AND TEMPERATURE WITH NUMBER OF CYCLES ($[0_2/\pm45]_s$ BORON/POLYIMIDE: $\sigma_{max} = 70\%\ \sigma_{ult}$; RUNOUT AT 1.29×10^7 CYCLES)
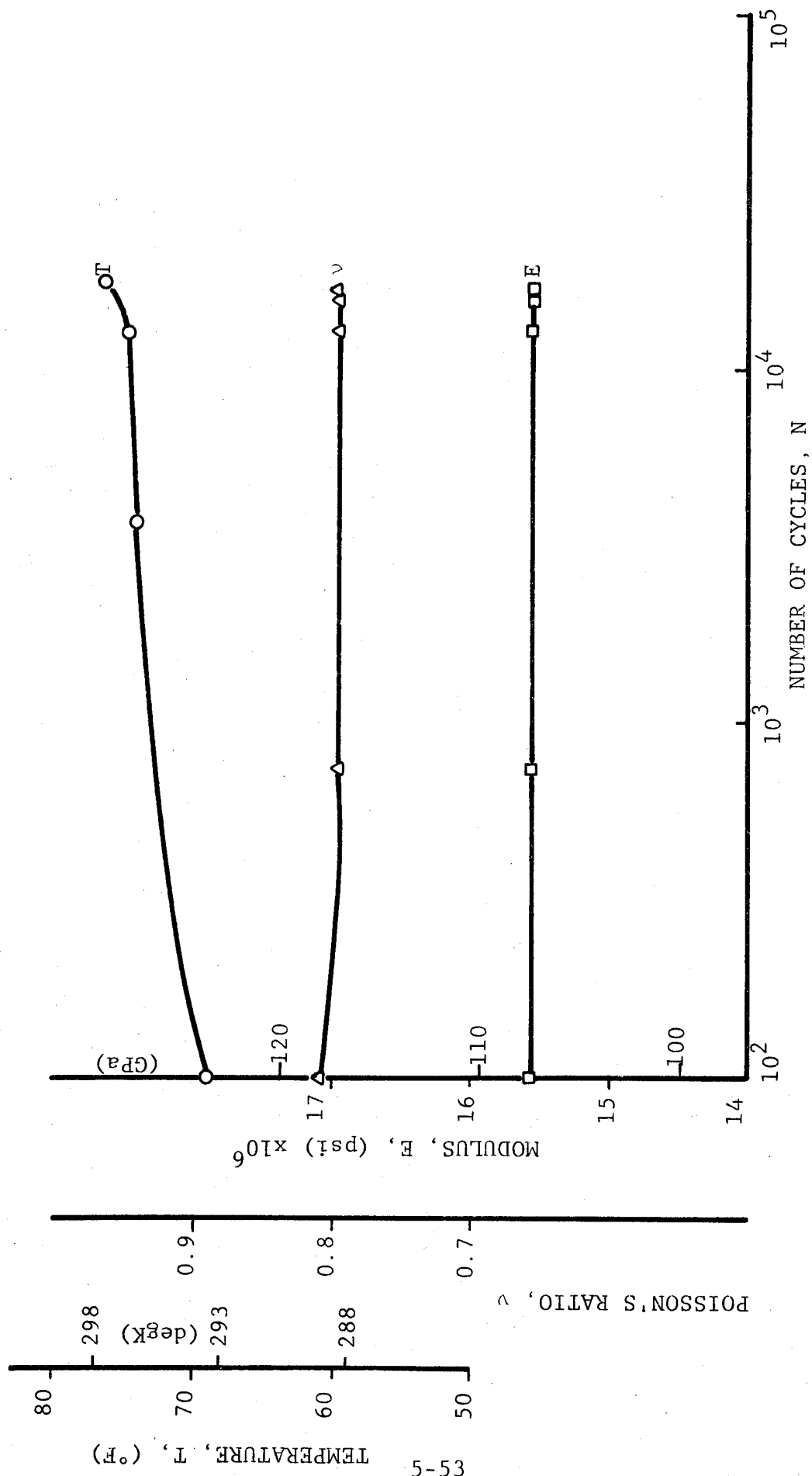
Fig. 5-23   VARIATION IN MODULUS, POISSON'S RATIO AND TEMPERATURE WITH NUMBER OF CYCLES ($[0_2/\pm45]_s$ GRAPHITE/HIGH MODULUS EPOXY; σ_{max} = 90% σ_{ult}; CYCLES TO FAILURE: 18,000)
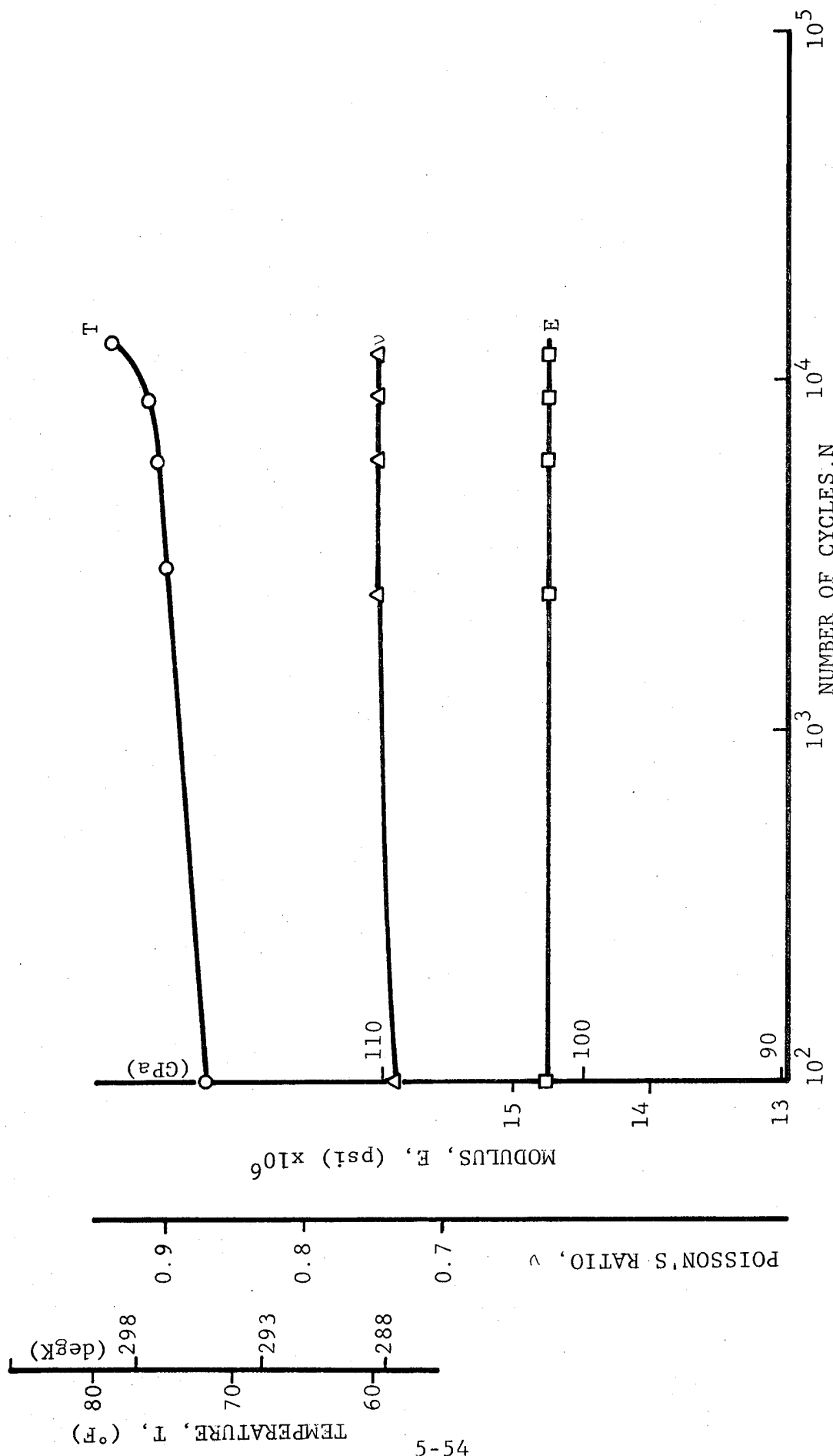
Fig. 5-24 VARIATION OF MODULUS, POISSON'S RATIO AND TEMPERATURE WITH NUMBER OF CYCLES ($[0_2/\pm45]_s$ GRAPHITE/HIGH MODULUS EPOXY; σ_{max} = 90% σ_{ult}; CYCLES TO FAILURE: 13,000)

5-54
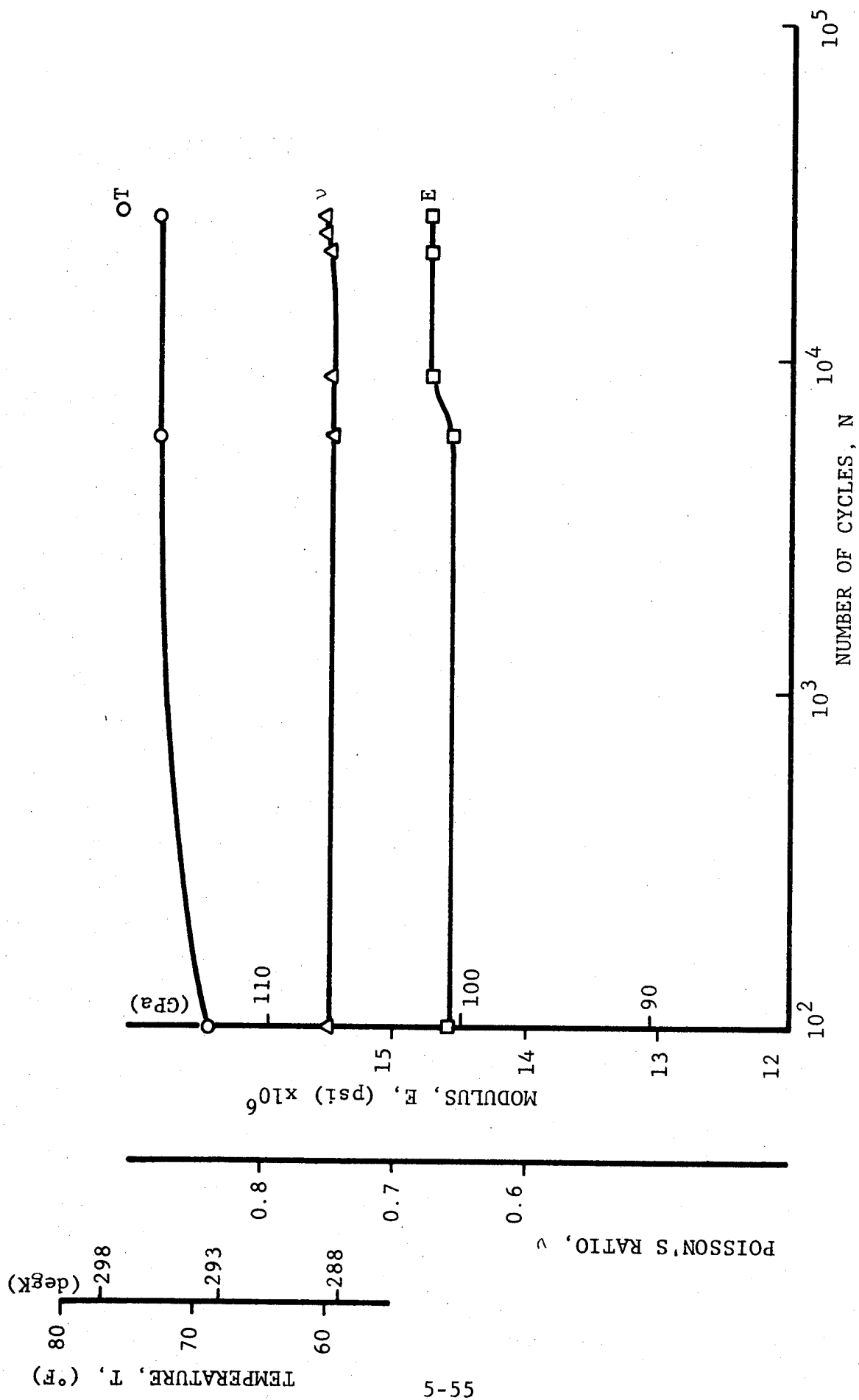
Fig. 5-25 VARIATION OF MODULUS, POISSON'S RATIO AND TEMPERATURE WITH NUMBER OF CYCLES ($[0_2/\pm 45]_s$ GRAPHITE/HIGH MODULUS EPOXY; σ_{max} = 80% σ_{ult}; CYCLES TO FAILURE: 28,000)

Fig. 5-26 VARIATION OF MODULUS, POISSON'S RATIO AND TEMPERATURE WITH NUMBER OF CYCLES $([0_2/\pm45]_s$ GRAPHITE/HIGH MODULUS EPOXY; $\sigma_{max} = 70\%\ \sigma_{ult}$; RUNOUT AT 1.016×10^7 CYCLES)
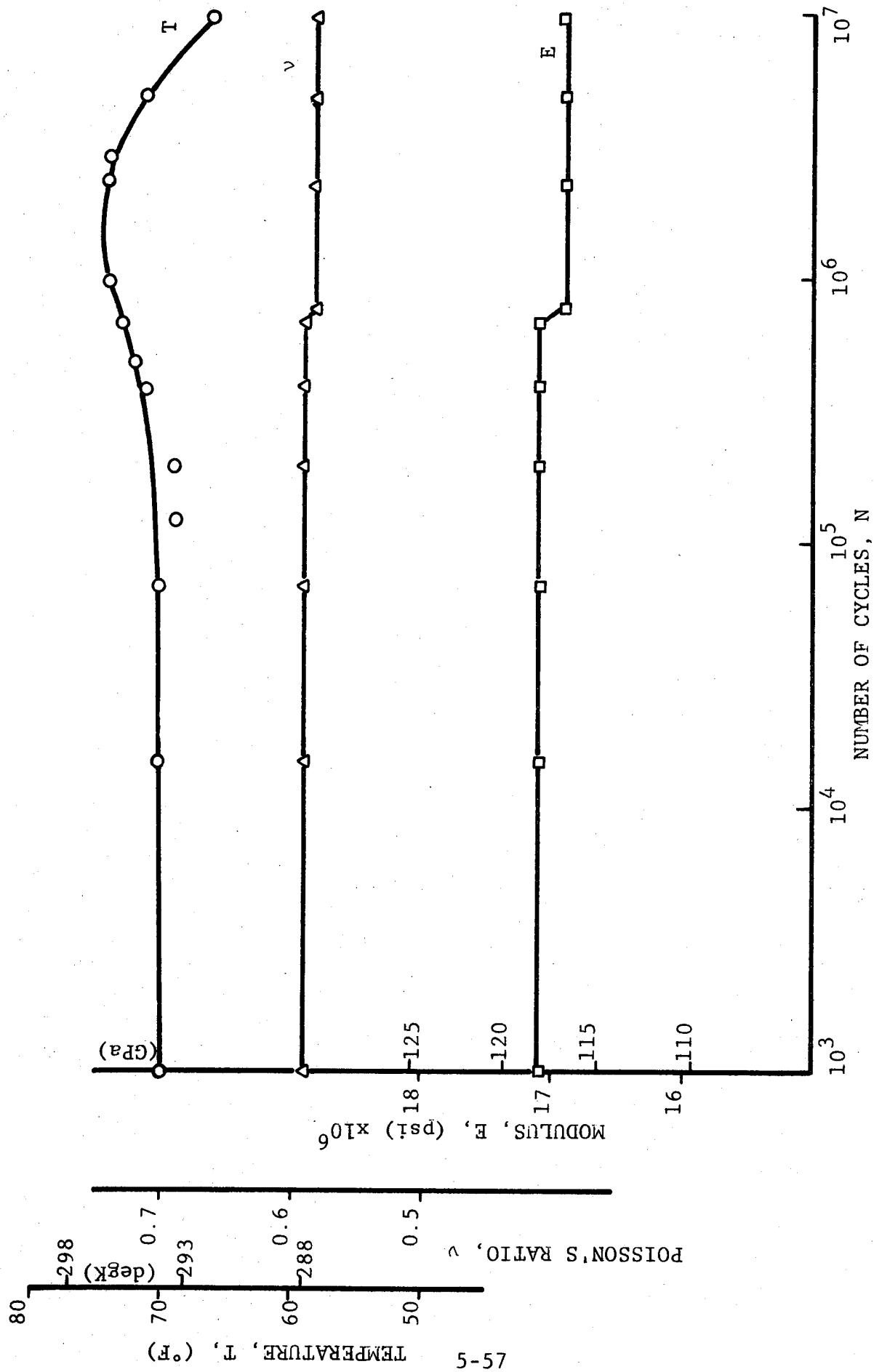
Fig. 5-27 VARIATION OF MODULUS, POISSON'S RATIO AND TEMPERATURE WITH NUMBER OF CYCLES ($[0_2/\pm45]_s$ GRAPHITE/POLYIMIDE; σ_{max} = 90% σ_{ult}; RUNOUT AT 1.023 x 10^7 CYCLES)

5-57
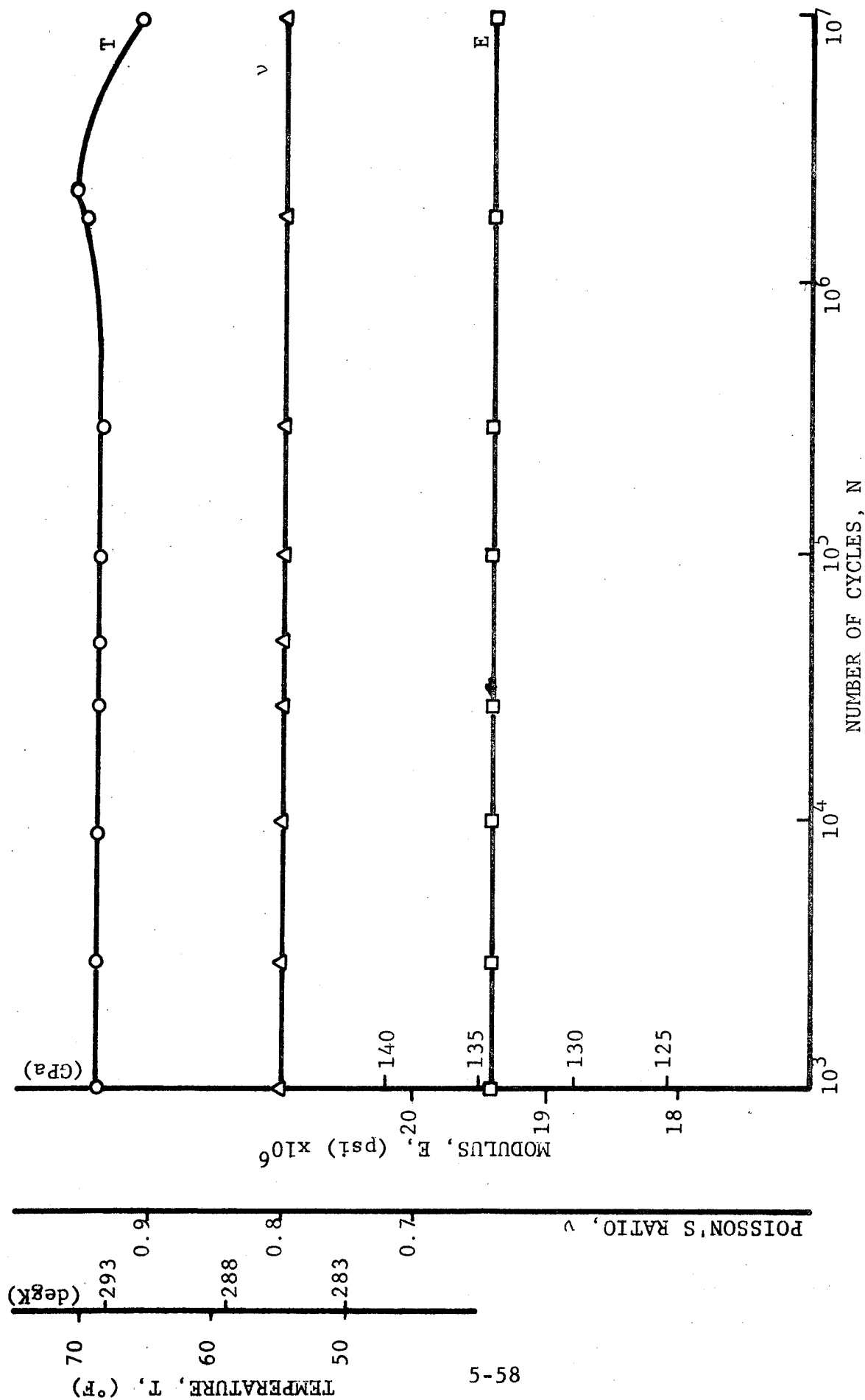
Fig. 5-28 VARIATION OF MODULUS, POISSON'S RATIO AND TEMPERATURE WITH NUMBER OF CYCLES ($[0_2/\pm45]_s$ GRAPHITE/POLYIMIDE; σ_{max} = 80% σ_{ult}; RUNOUT AT 1.005 x 10^7 CYCLES)
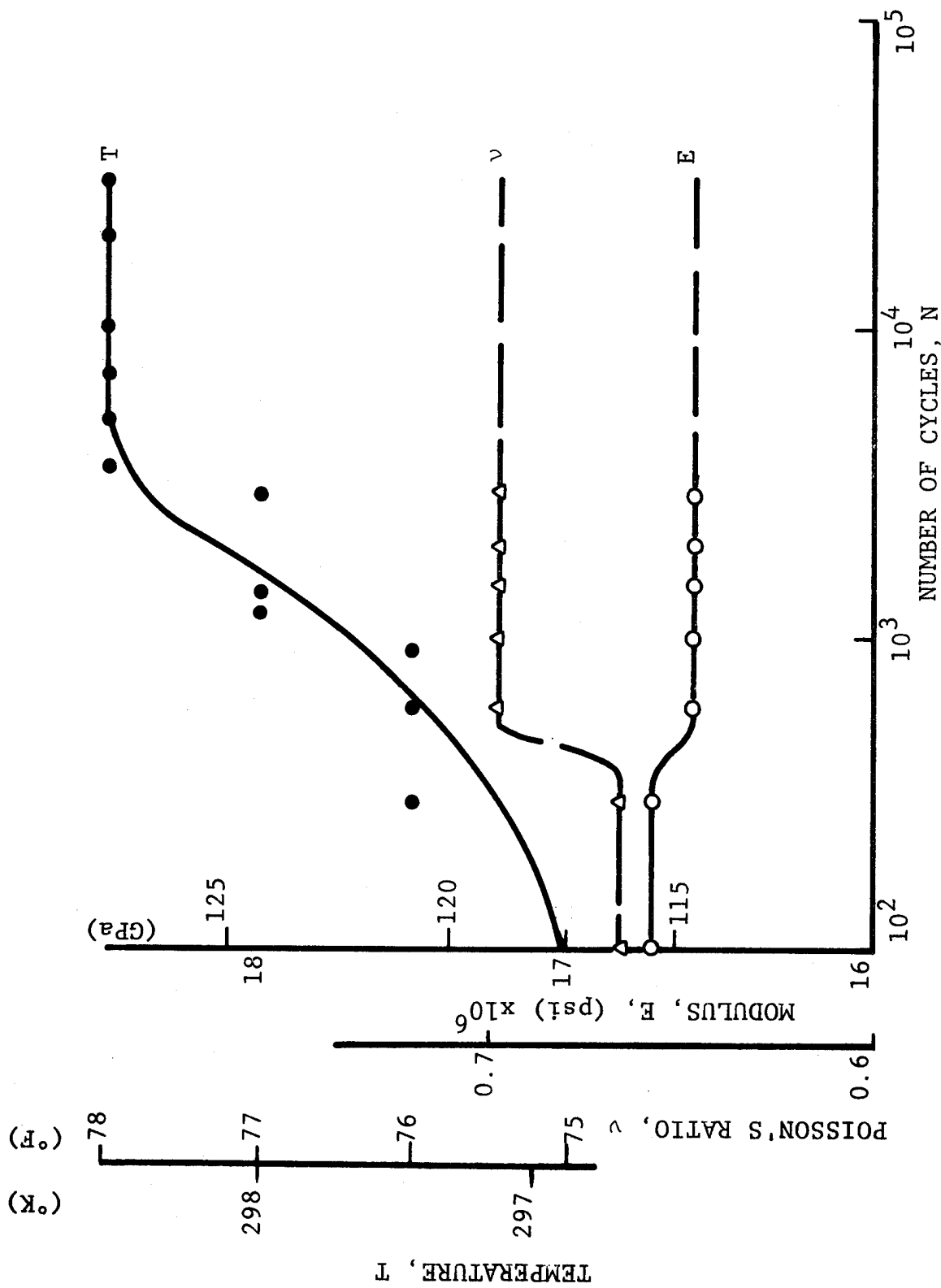
5-58
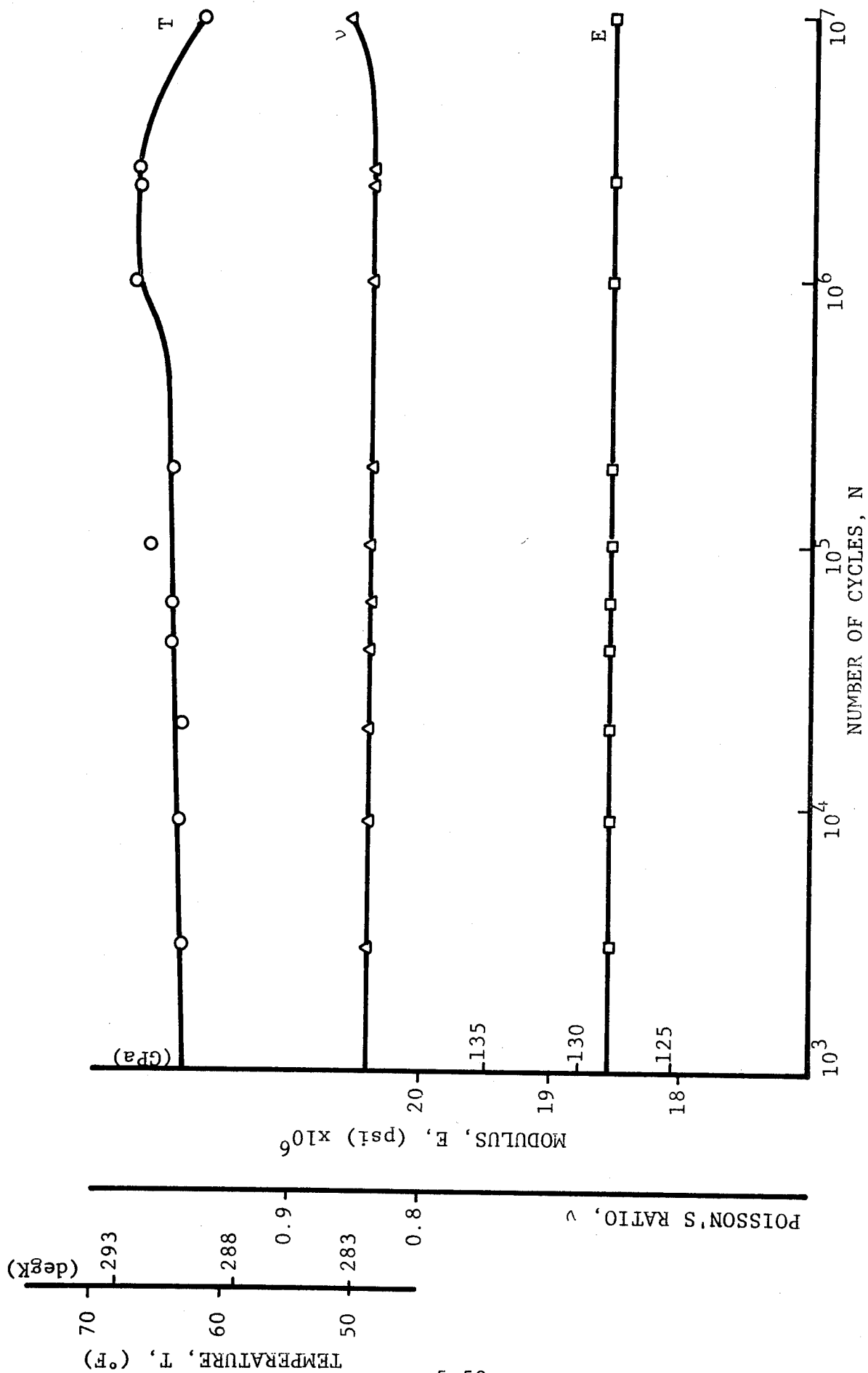
Fig. 5-29   VARIATION OF MODULUS, POISSON'S RATIO AND TEMPERATURE WITH NUMBER OF CYCLES ($[0_2/\pm45]_s$ GRAPHITE/POLYIMIDE; $\sigma_{max} = 70\%$ σ_{ult}; RUNOUT AT 10^7 CYCLES)
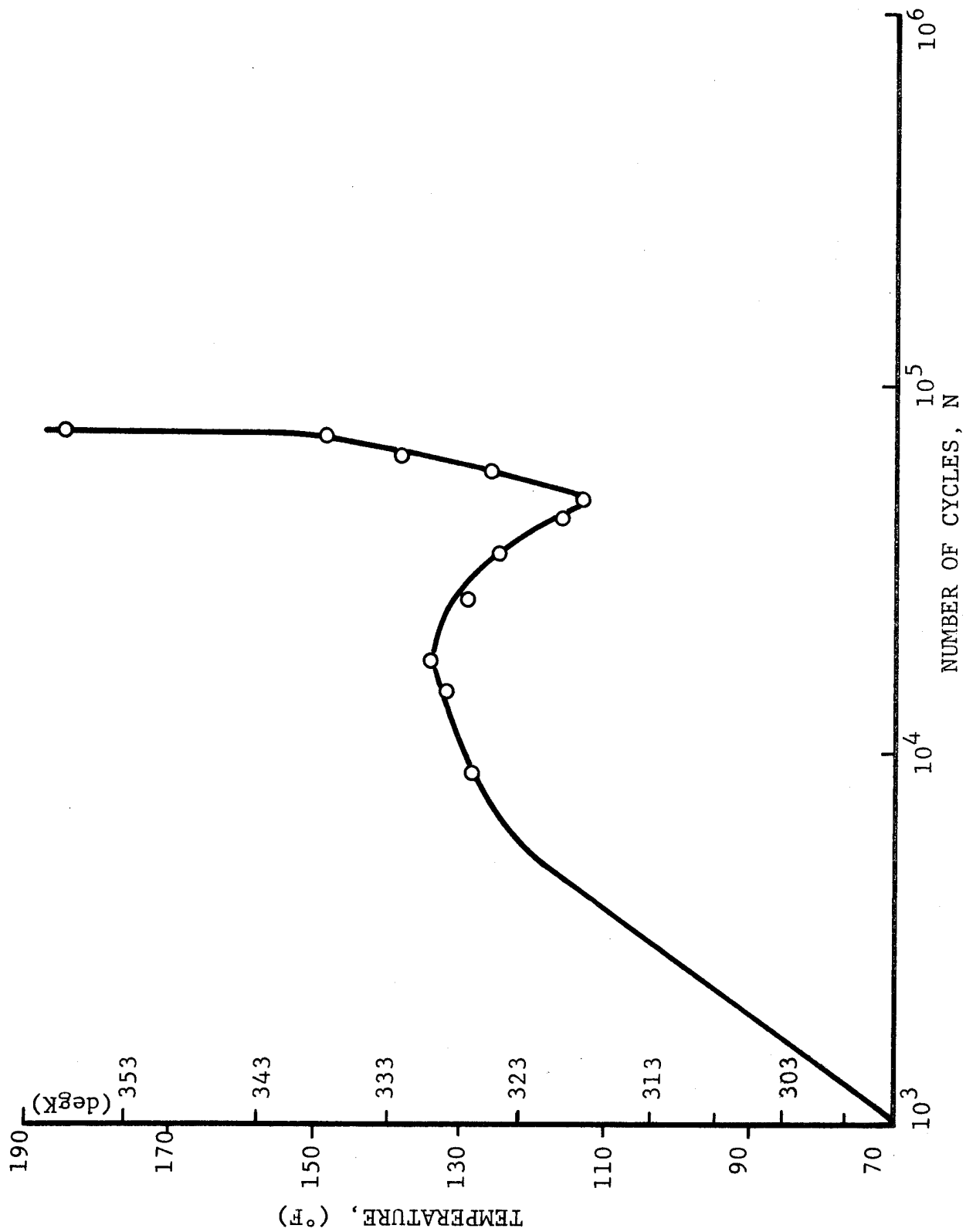
Fig. 5-30   TEMPERATURE VARIATION WITH NUMBER OF CYCLES ($[0_2/\pm45]_s$ S-GLASS/EPOXY: σ_{max} = 40% σ_{ult}; CYCLES TO FAILURE: 77,000)
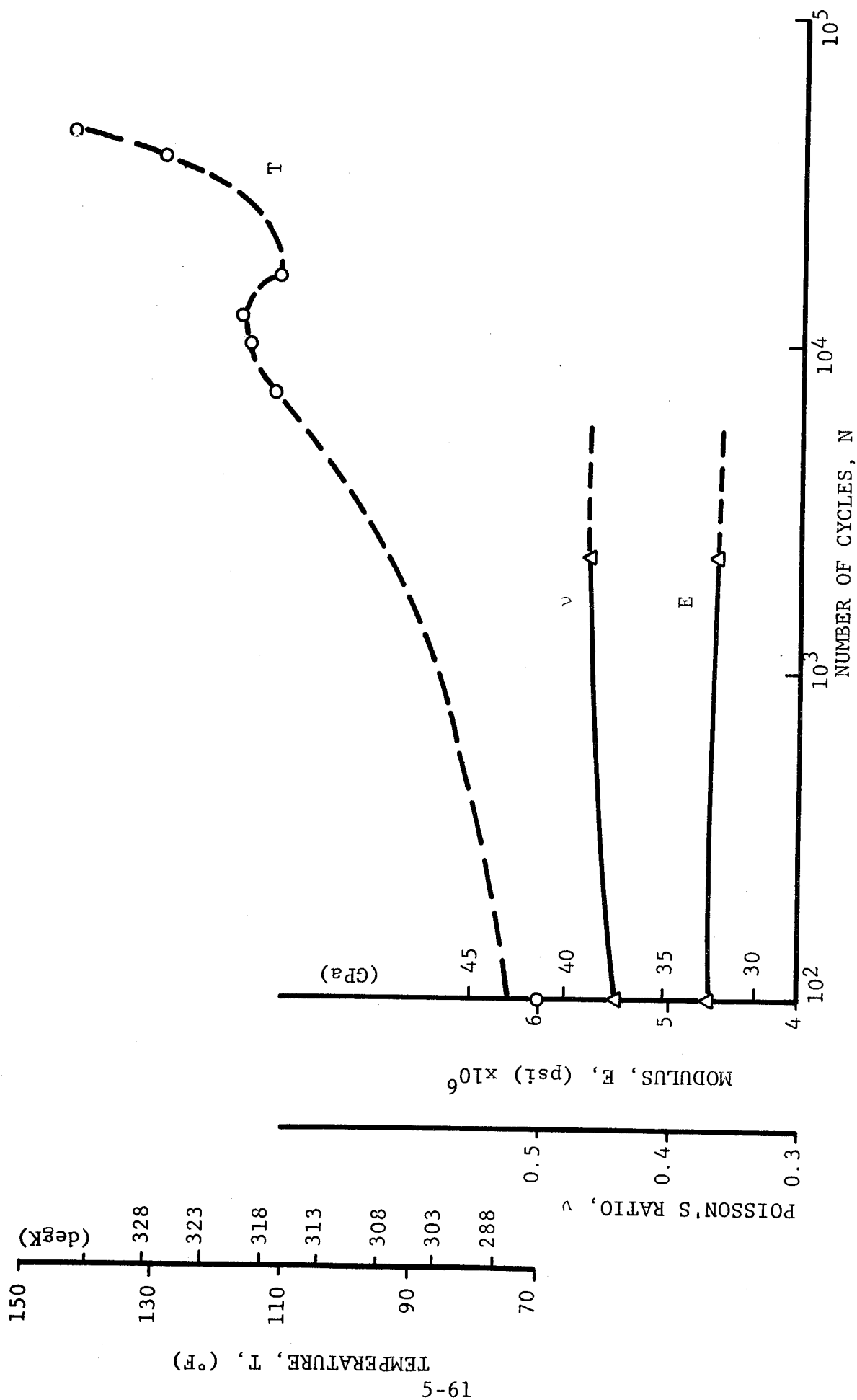
Fig. 5-31 VARIATION OF MODULUS, POISSON'S RATIO AND TEMPERATURE WITH NUMBER OF CYCLES $([0_2/\pm45]_s$ S-GLASS/EPOXY; $\sigma_{max} = 40\%\ \sigma_{ult}$; CYCLES TO FAILURE: 44,000)

5-5
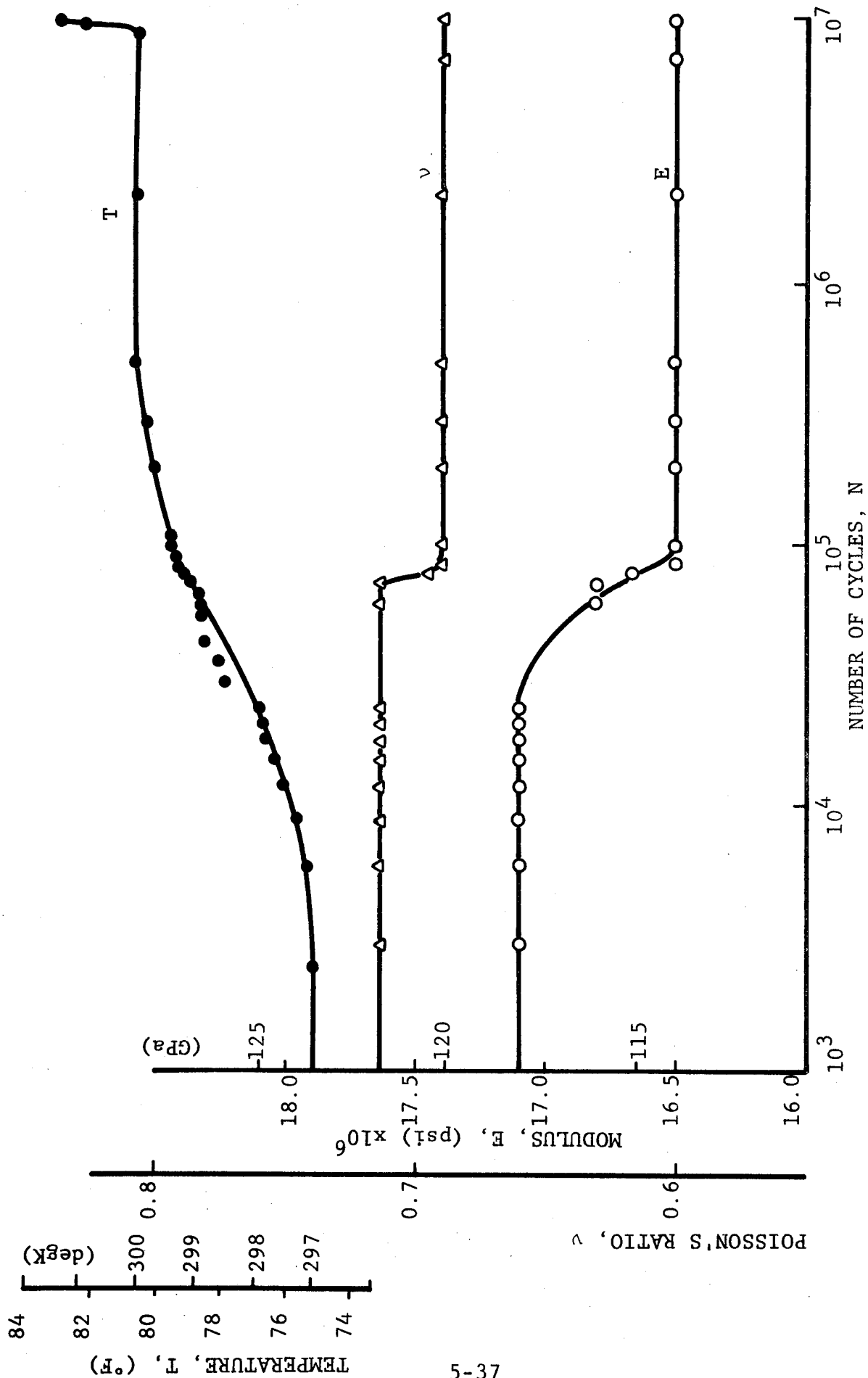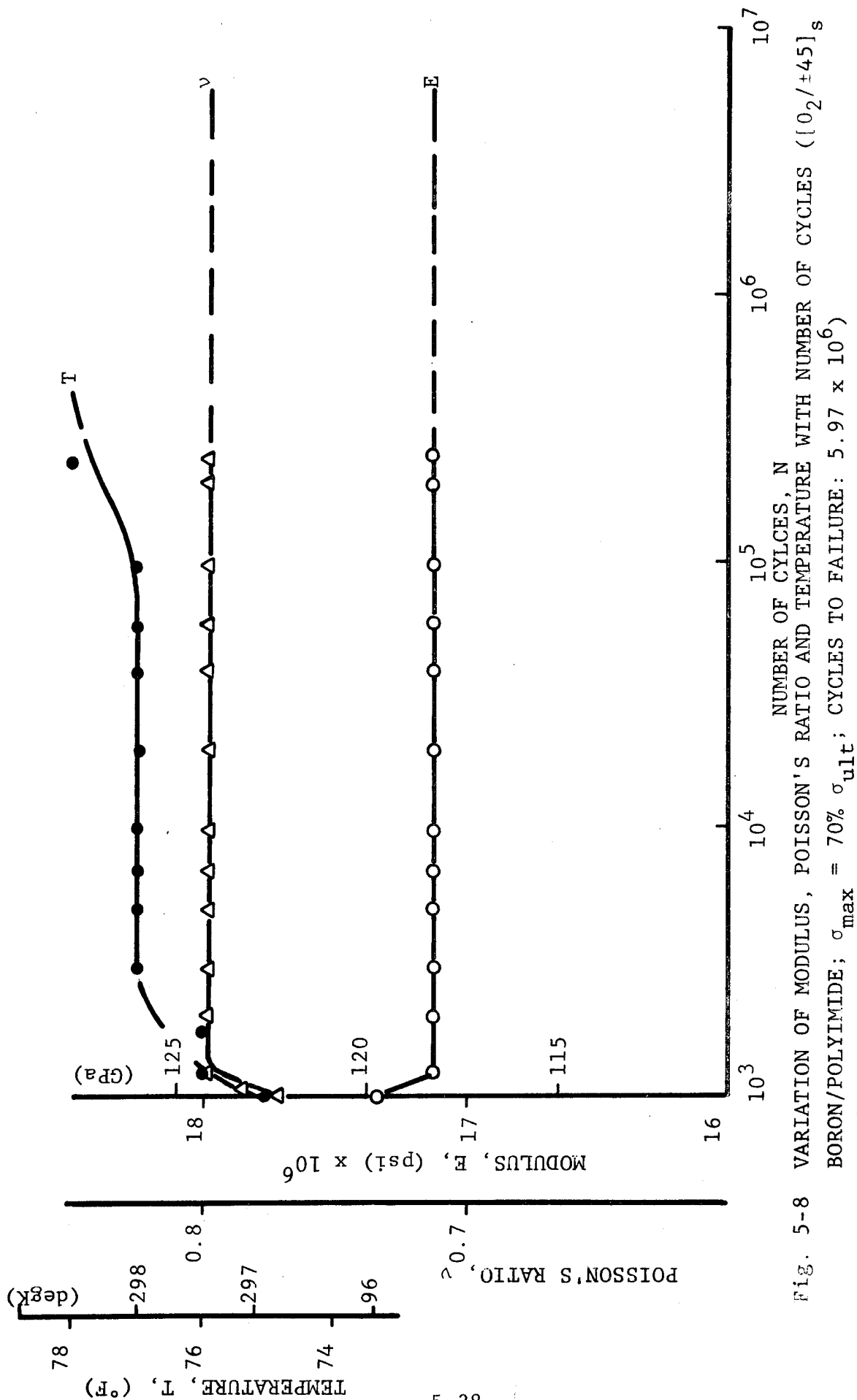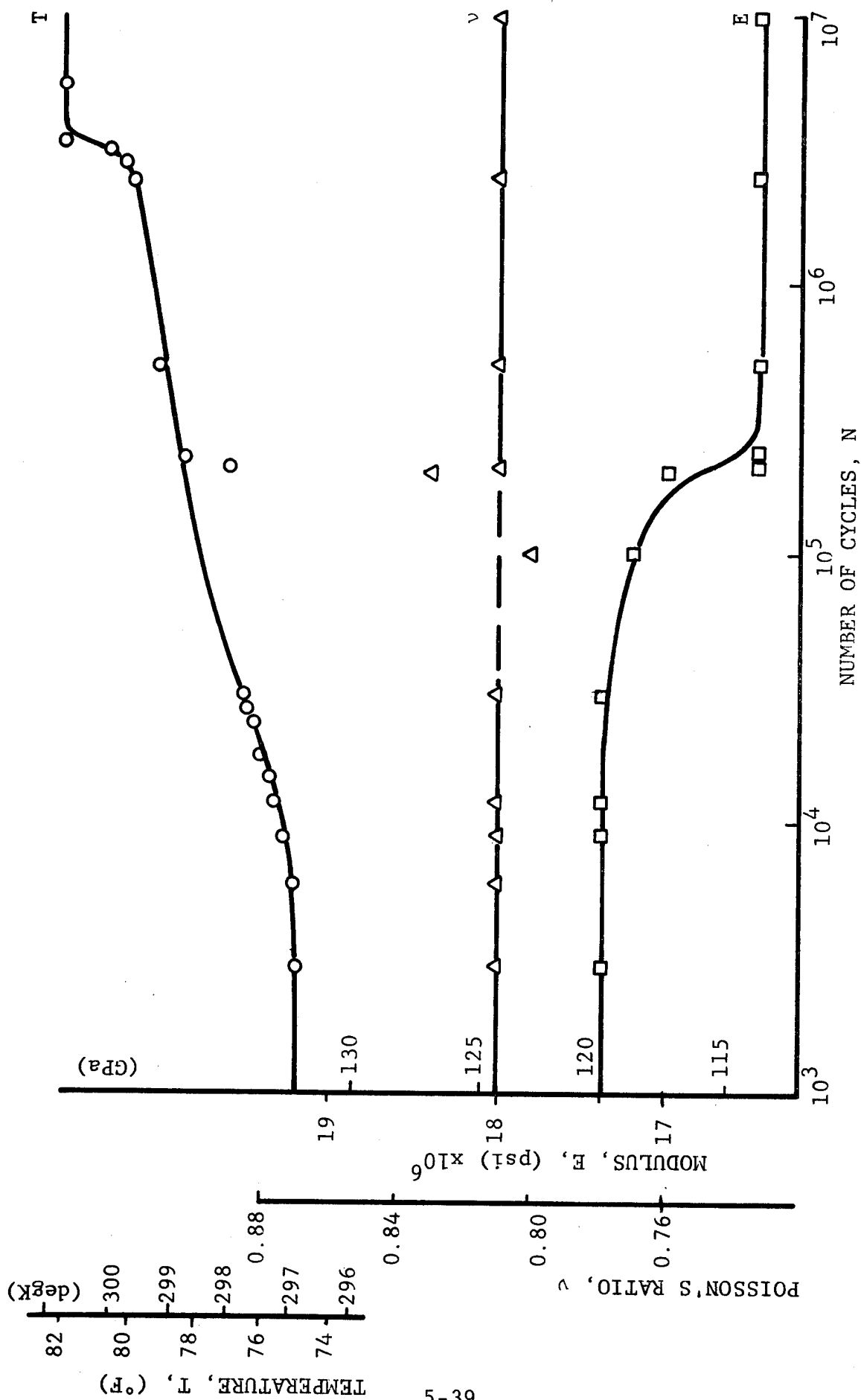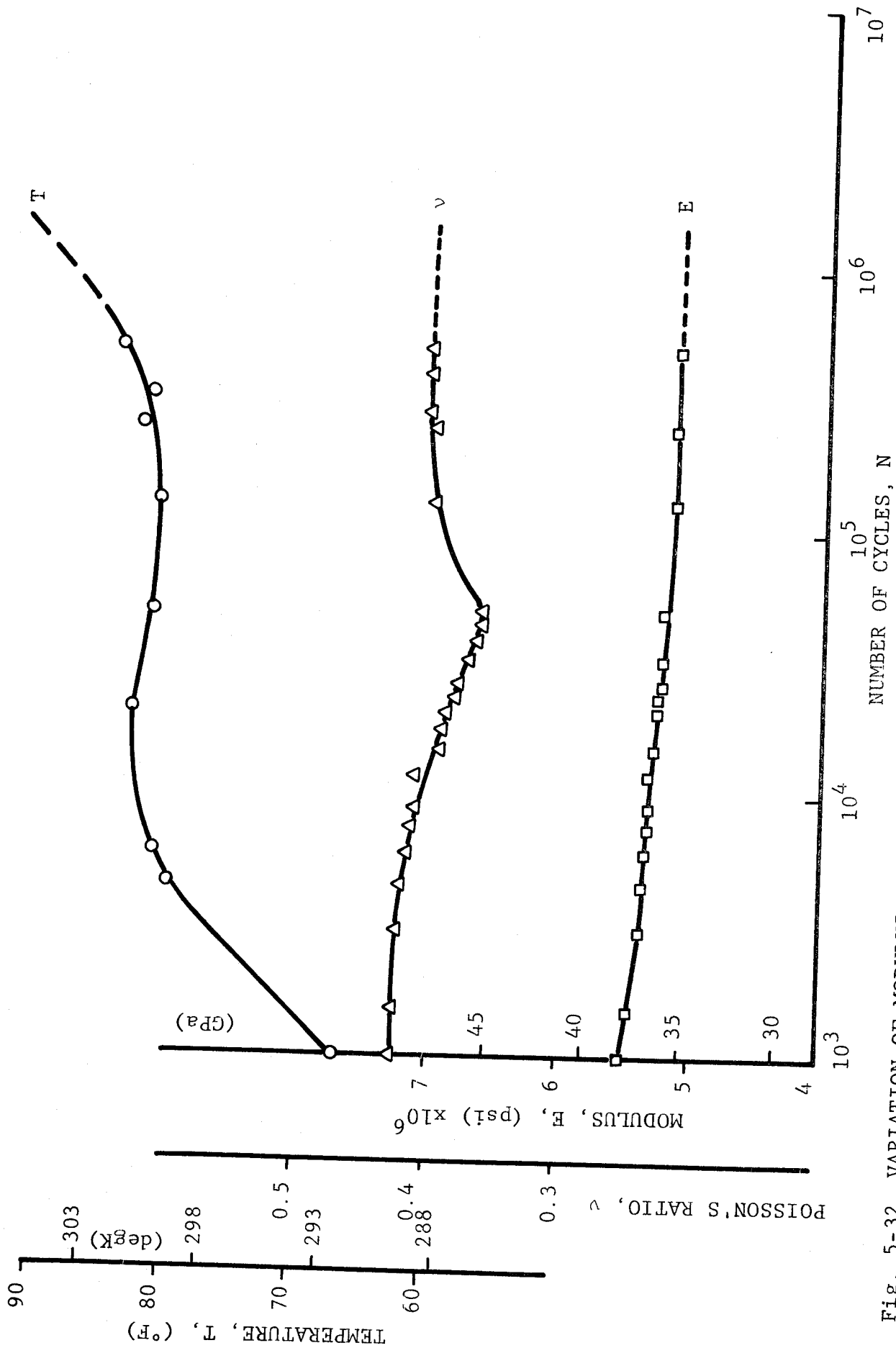
Fig. 5-32 VARIATION OF MODULUS, POISSON'S RATIO AND TEMPERATURE WITH NUMBER OF CYCLES ($[0_2/\pm45]_s$ S-GLASS/EPOXY; $\sigma_{max} = 25\%$ σ_{ult}; CYCLES TO FAILURE: 1.436 x 10^6)

Fig. 5-33 SPRING LOADING FIXTURE FOR PERFORMING THERMAL CYCLING TESTS UNDER TENSILE LOAD
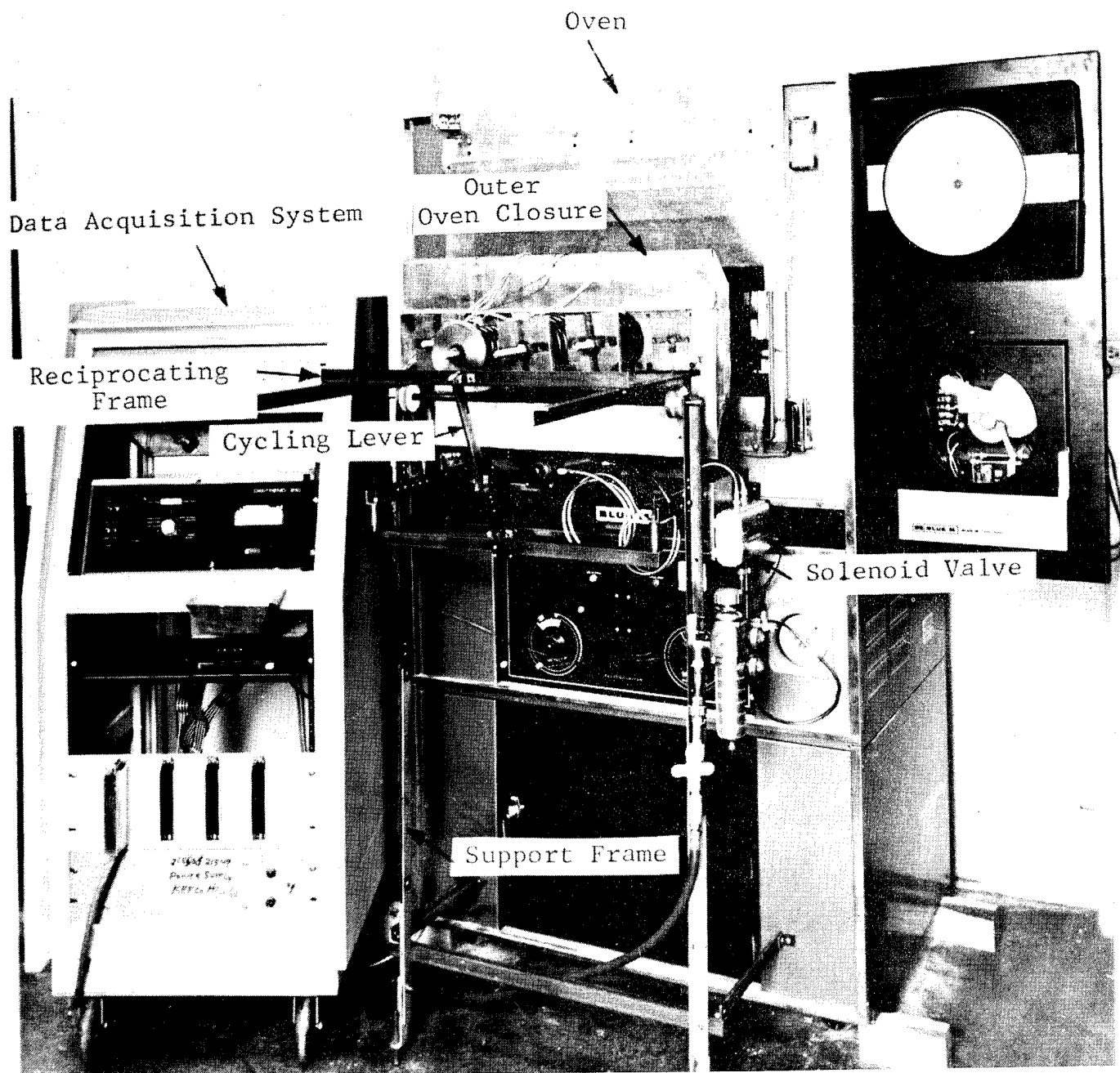
Fig. 5-34 CYCLING APPARATUS AND MODIFIED OVEN CLOSURE FOR THERMAL
CYCLING.   (SPECIMENS OUTSIDE OVEN; OVEN CLOSED BY INNER
CLOSURE, NOT VISIBLE)

Outer Oven Closure

Oven

Specimen Load Springs

Solenoid Valve

Reciprocating Frame

Support Frame

Cycling Lever

Air Actuator
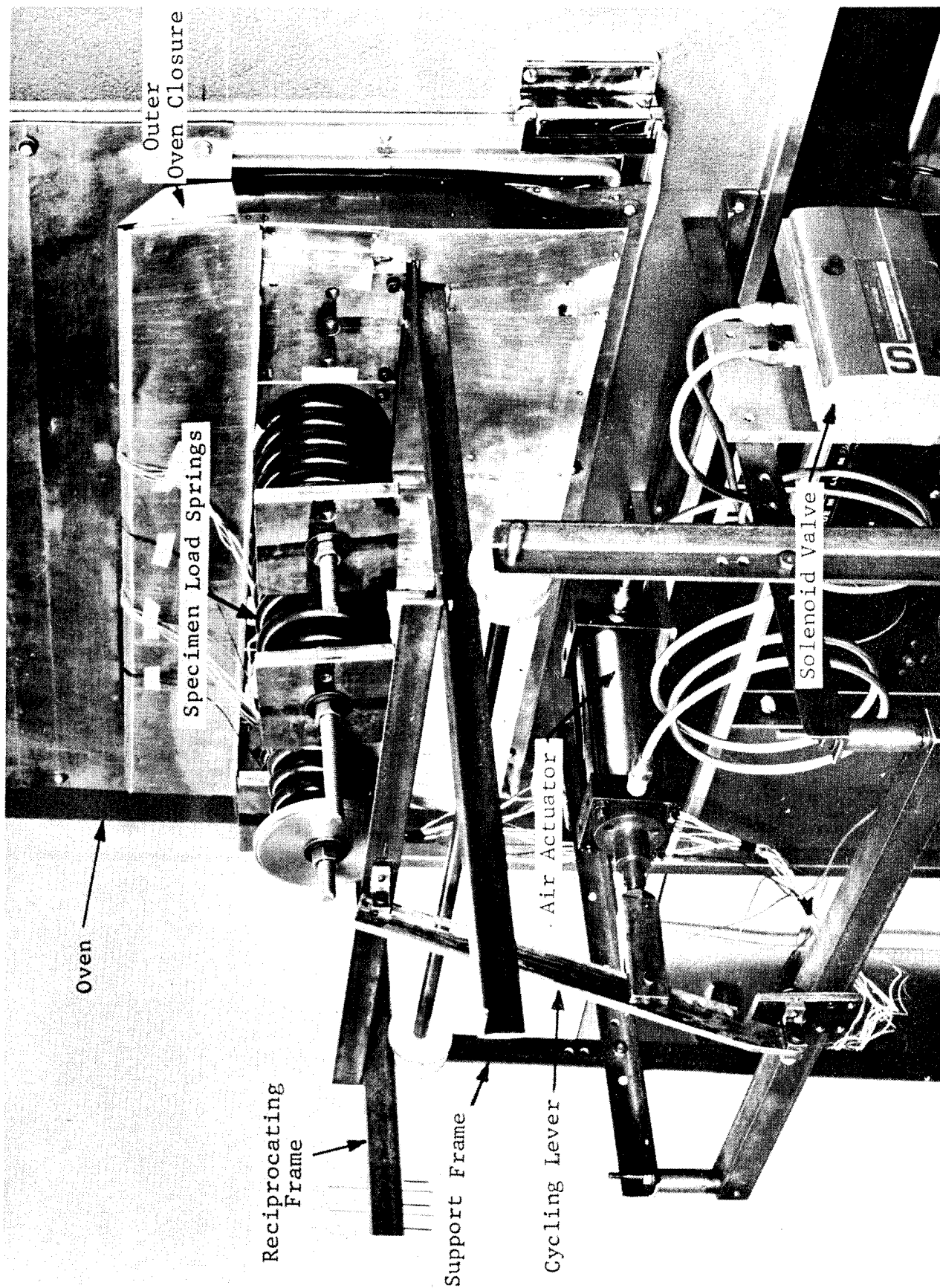
Fig. 5-35 CLOSEUP VIEW OF CYCLING APPARATUS AND MODIFIED OVEN CLOSURE FOR THERMAL CYCLING
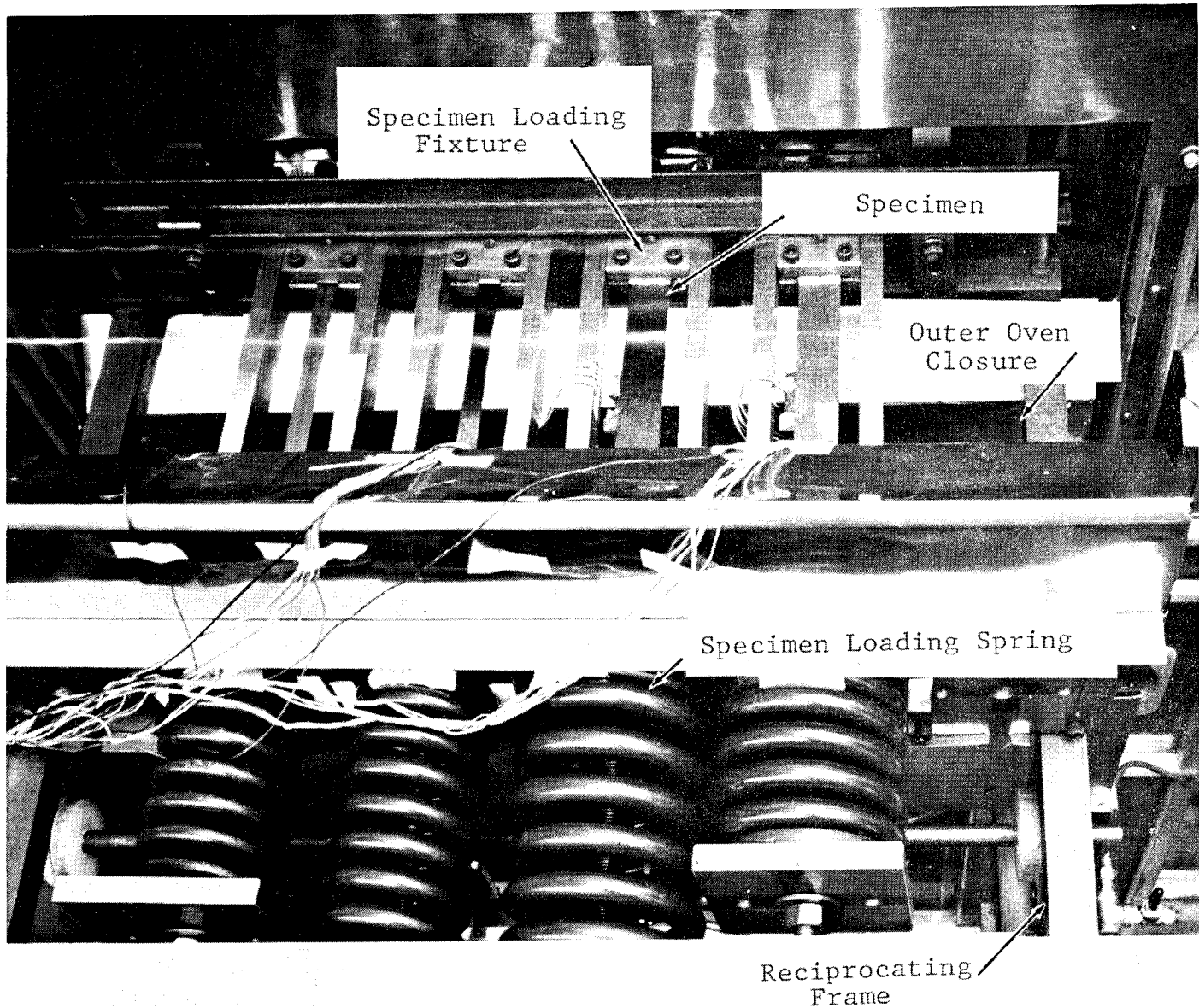
Fig. 5-36 CLOSEUP TOP VIEW OF APPARATUS FOR THERMAL CYCLING
SHOWING LOADING FIXTURES AND SPECIMENS IN POSITION
OUTSIDE OVEN

Fig. 5-37   APPARATUS FOR THERMAL CYCLING OF SPECIMENS
IN COLD CHAMBER
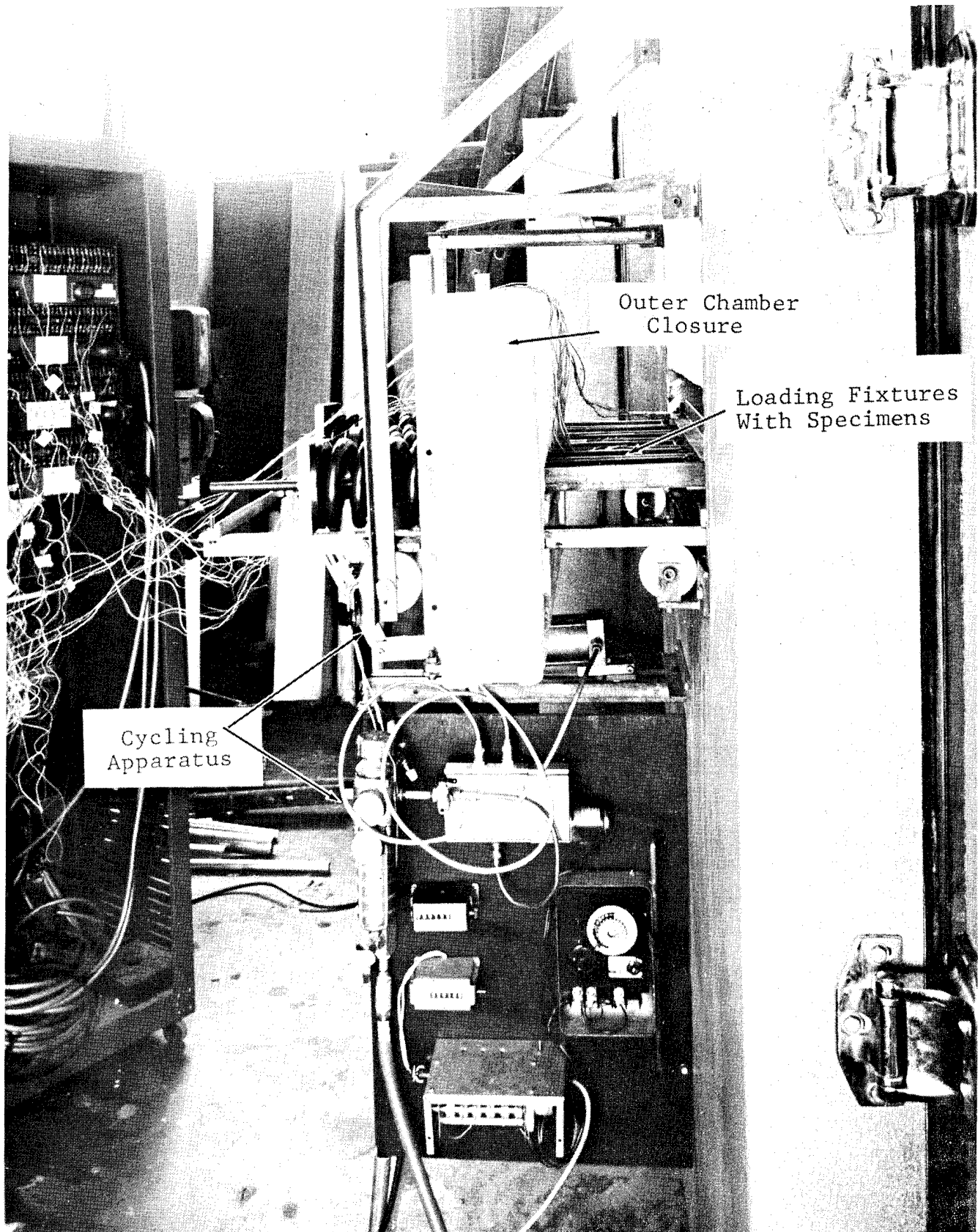
Fig. 5-38   CLOSEUP SIDE VIEW OF APPARATUS FOR THERMAL CYCLING
            OF SPECIMENS IN COLD CHAMBER.   (SPECIMENS OUTSIDE
            CHAMBER; CHAMBER CLOSED BY INNER CLOSURE, NOT VISIBLE)
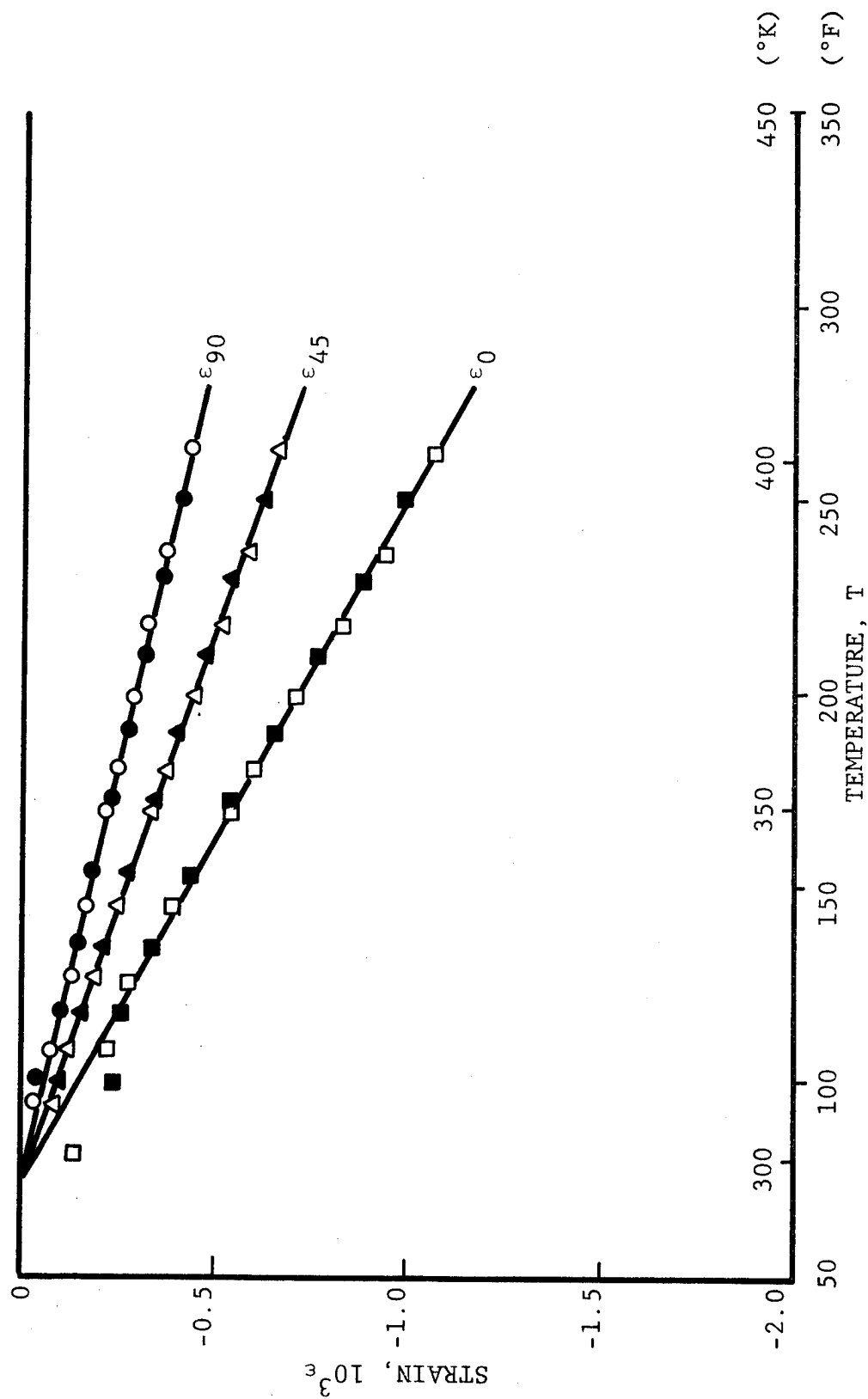
Fig. 5-39   APPARENT STRAINS IN $[0_2/\pm45]_s$ GRAPHITE/HIGH MODULUS EPOXY SPECIMENS DURING THERMAL CYCLING UNDER TENSILE LOAD (FILLED SYMBOLS: SIXTIETH CYCLE; OPEN SYMBOLS: ONE-HUNDREDTH CYCLE)
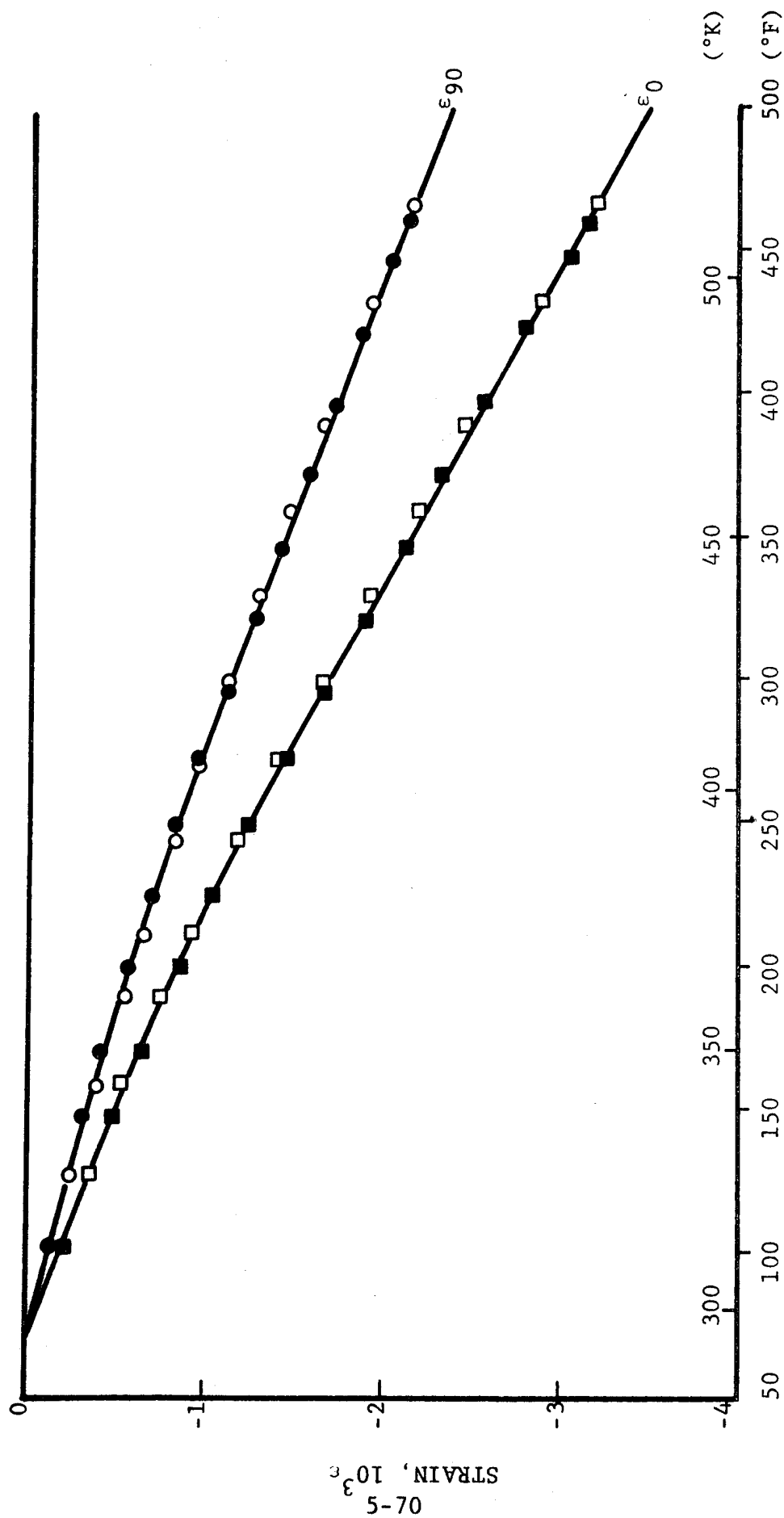
Fig. 5-40 APPARENT STRAINS IN $[0_2/\pm45]_s$ GRAPHITE/POLYIMIDE SPECIMEN DURING THERMAL CYCLING UNDER
TENSILE LOAD (FILLED SYMBOLS: THIRD CYCLE; OPEN SYMBOLS: NINETY-NINTH CYCLE)
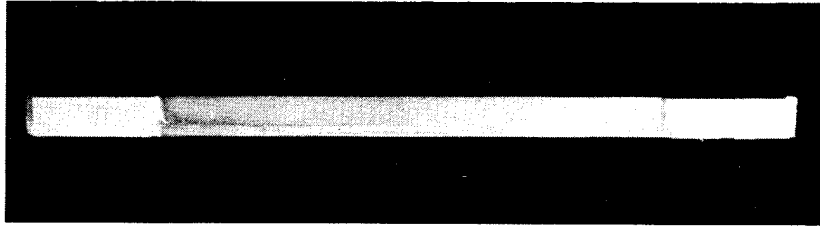
Fig. 5-41   DELAMINATION CRACK IN S-GLASS/EPOXY SPECIMEN
             DEVELOPED DURING COLD CYCLING WITH TENSILE LOAD
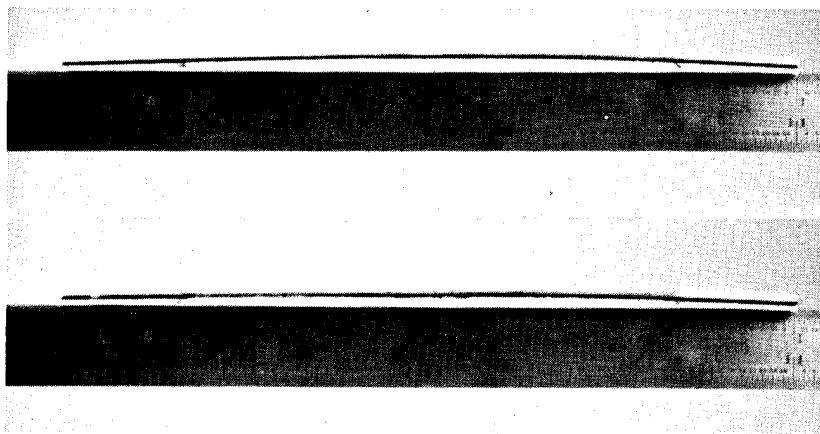
Fig. 5-42   BOWING DUE TO DELAMINATIONS DEVELOPED IN THE
             GRAPHITE/LOW MODULUS EPOXY SPECIMENS DURING
             COLD CYCLING WITH TENSILE LOAD
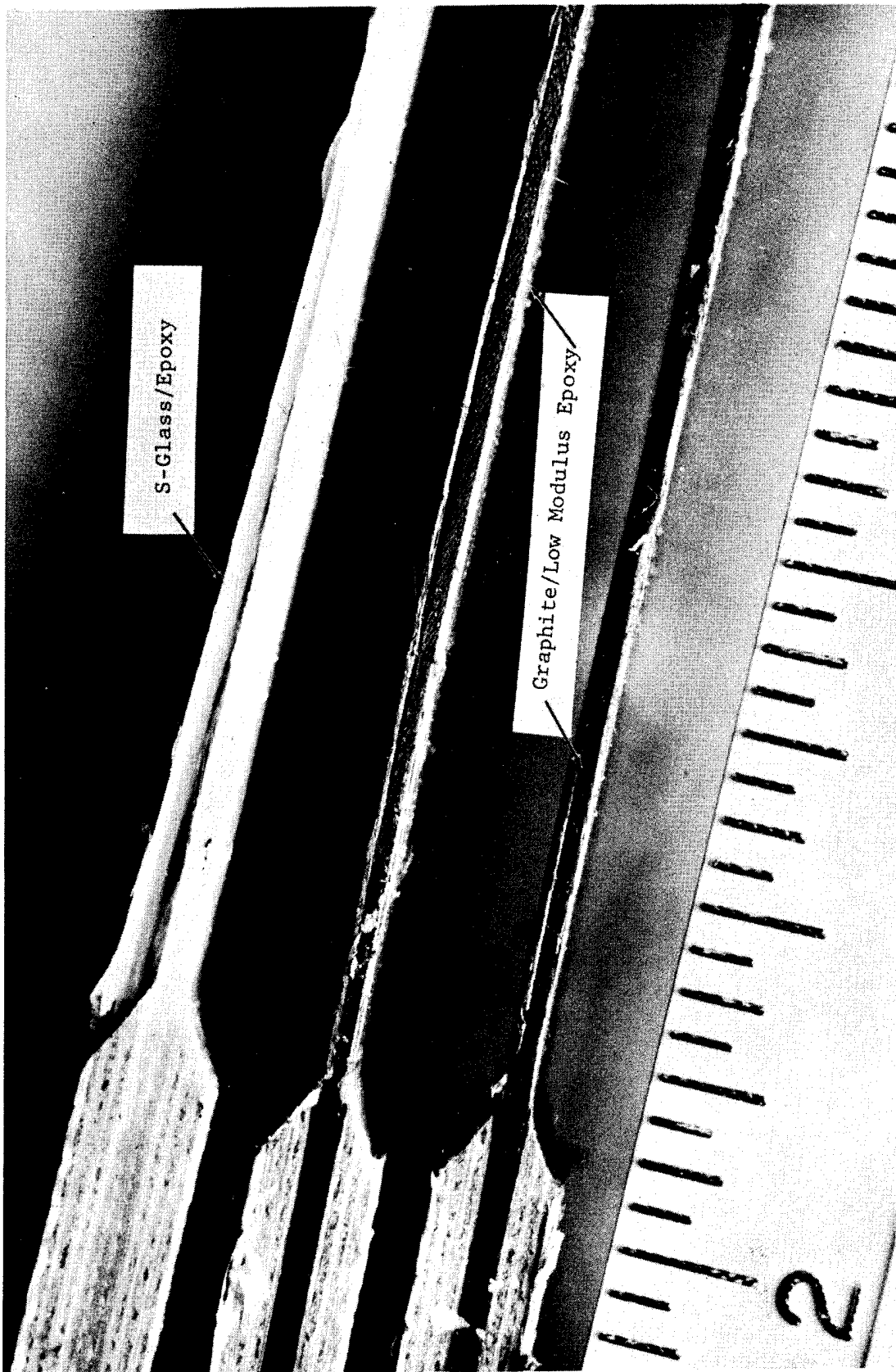
Fig. 5-43   DELAMINATIONS DEVELOPED IN S-GLASS/EPOXY AND GRAPHITE/LOW MODULUS EPOXY SPECIMENS DURING COLD CYCLING WITH TENSILE LOAD.
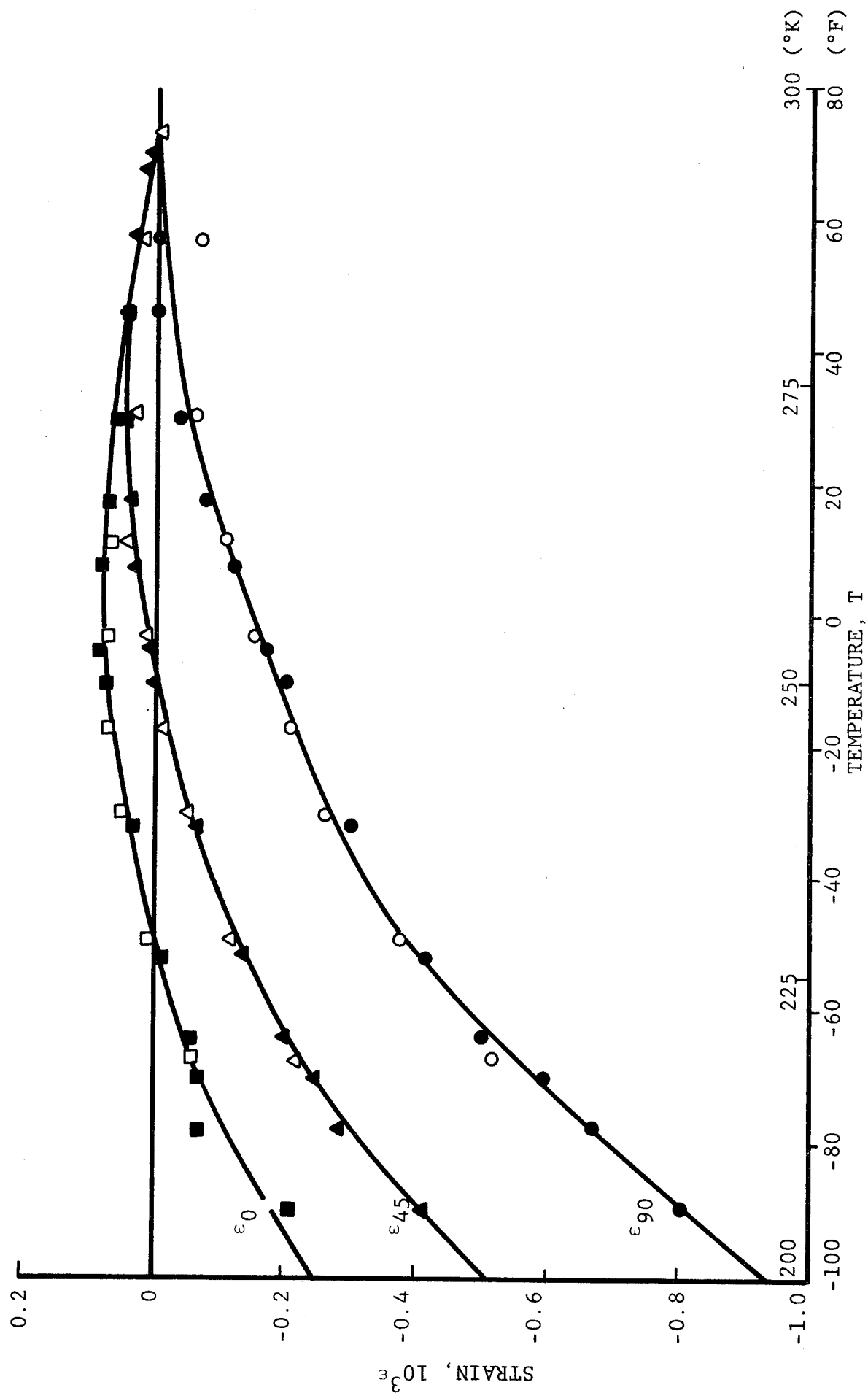
Fig. 5-44 APPARENT STRAINS IN LOADED $[0_2/\pm45]_s$ GRAPHITE/HIGH MODULUS EPOXY SPECIMEN DURING THERMAL CYCLING (FILLED SYMBOLS: BEGINNING OF CYCLING; OPEN SYMBOLS: END OF CYCLING)

5-73

Fig. 5-45 STRAINS IN $[0_2/\pm 45]_s$ BORON/EPOXY SPECIMEN UNDER UNIAXIAL TENSILE LOADING AFTER 100 THERMAL CYCLES BETWEEN ROOM TEMPERATURE AND 411 degK (280°F).

E_{xx} = 112 GPa (16.3 x 10^6 psi)

ν_{xy} = 0.75

S_{xxT} = 745 MPa (108 ksi)

Fig. 5-46 STRAINS IN $[0_2/\pm 45]_s$ GRAPHITE/LOW MODULUS EPOXY SPECIMEN UNDER UNIAXIAL TENSILE LOADING AFTER 100 THERMAL CYCLES BETWEEN ROOM TEMPERATURE AND 411 degK (280°F)

E_{xx} = 121 GPa (17.5 x 10^6 psi)

ν_{xy} = 0.62

S_{xxT} = 662 MPa (96 ksi)

Fig. 5-47 STRAINS IN $[0_2/\pm45]_s$ GRAPHITE/LOW MODULUS EPOXY SPECIMEN UNDER UNIAXIAL TENSILE LOADING AFTER 100 THERMAL CYCLES BETWEEN ROOM TEMPERATURE AND 411 degK (280°F)

E_{xx} = 112 GPa (16.3 x 10^6 psi)

ν_{xy} = 0.75

S_{xxT} = 566 MPa (82 ksi)

Fig. 5-48 STRAINS IN $[0_2/\pm45]_s$ GRAPHITE/HIGH MODULUS EPOXY SPECIMEN UNDER UNIAXIAL
TENSILE LOADING AFTER 100 THERMAL CYCLES BETWEEN ROOM TEMPERATURE AND
411 degK (280°F)

E_{xx} = 108 GPa (15.6 x 10^6 psi)

ν_{xy} = 0.81

S_{xxT} = 600 MPa (87 ksi)

Fig. 5-49 STRAINS IN $[0_2/\pm45]_s$ GRAPHITE/HIGH MODULUS EPOXY SPECIMEN UNDER UNIAXIAL TENSILE LOADING AFTER 100 THERMAL CYCLES BETWEEN ROOM TEMPERATURE AND 411 degK (280°F)

E_{xx} = 105 GPa (15.2 x 10^6 psi)

ν_{xy} = 0.73

S_{xxT} = 435 MPa (63 ksi)

5-78

Fig. 5-50   STRAINS IN $[0_2/\pm45]_s$ S-GLASS/INTERMEDIATE MODULUS
EPOXY SPECIMEN UNDER UNIAXIAL TENSILE LOADING AFTER
100 THERMAL CYCLES BETWEEN ROOM TEMPERATURE AND
411 degK (280°F)

Fig. 5-51 STRESS-STRAIN CURVES FOR $[0_2/\pm45]_s$ S-GLASS/EPOXY
SPECIMEN UNDER UNIAXIAL TENSILE LOADING AFTER 100
THERMAL CYCLES BETWEEN ROOM TEMPERATURE AND 411 degK
(280°F)

5-80

Fig. 5-52 STRAINS IN $[0_2/\pm 45]_s$ BORON/POLYIMIDE SPECIMEN UNDER UNIAXIAL TENSILE LOADING AFTER 100 THERMAL CYCLES BETWEEN ROOM TEMPERATURE AND 533 degK (500°F)

E_{xx} = 126 GPa (18.2 x 10^3 psi)

ν_{xy} = 0.67

S_{xxT} = 504 MPa (73 ksi)

5-5

Fig. 5-53   STRAINS IN $[0_2/\pm 45]_s$ BORON/POLYIMIDE SPECIMEN UNDER
UNIAXIAL TENSILE LOADING AFTER 100 THERMAL CYCLES
BETWEEN ROOM TEMPERATURE AND 533 degK (500°F)

Fig. 5-54 STRAINS IN $[0_2/\pm 45]_s$ GRAPHITE/POLYIMIDE SPECIMEN UNDER UNIAXIAL TENSILE LOADING AFTER 100 THERMAL CYCLES BETWEEN ROOM TEMPERATURE AND 533 degK (500°F)

Fig. 5-55 STRAINS IN $[0_2/\pm45]_s$ GRAPHITE/POLYIMIDE SPECIMEN UNDER UNIAXIAL TENSILE LOADING AFTER 100 THERMAL CYCLES BETWEEN ROOM TEMPERATURE AND 533 degK (500°F)

E_{xx} = 116 GPa (16.8 x 10^6 psi)

ν_{xy} = 0.79

S_{xxT} = 373 MPa (54 ksi)

Fig. 5-56 STRAINS IN $[0_2/\pm45]_s$ BORON/EPOXY SPECIMEN UNDER UNIAXIAL TENSILE LOADING AFTER 100 THERMAL CYCLES BETWEEN ROOM TEMPERATURE AND 200 degK (-100°F)

Fig. 5-57 STRAINS IN $[0_2/\pm 45]_s$ BORON/EPOXY SPECIMEN UNDER UNIAXIAL TENSILE LOADING AFTER 100 THERMAL CYCLES BETWEEN ROOM TEMPERATURE AND 200 degK (-100°F)

E_{xx} = 112 GPa (16.2 x 10^6 psi)

ν_{xy} = 0.67

S_{xxT} = 800 MPa (116 ksi)

Fig. 5-58 STRAINS IN $[0_2/\pm 45]_s$ GRAPHITE/LOW MODULUS EPOXY SPECIMEN UNDER UNIAXIAL TENSILE LOADING AFTER 100 THERMAL CYCLES BETWEEN ROOM TEMPERATURE AND 200 degK (-100°F)

E_{xx} = 83 GPa (12.0 x 10^6 psi)

ν_{xy} = 0.57

S_{xxT} = 357 MPa (52 ksi)

Fig. 5-59 STRAINS IN $[0_2/\pm45]_s$ GRAPHITE/HIGH MODULUS EPOXY SPECIMEN UNDER UNIAXIAL TENSILE LOADING AFTER 100 THERMAL CYCLES BETWEEN ROOM TEMPERATURE AND 200 degK (-100°F)

E_{xx} = 101 GPa (14.7 x 10^6 psi)

ν_{xy} = 0.71

S_{xxT} = 453 MPa (66 ksi)

5-88

Fig. 5-60   STRAINS IN $[0_2/\pm 45]_s$ GRAPHITE/HIGH MODULUS EPOXY SPECIMEN UNDER UNIAXIAL TENSILE LOADING AFTER 100 THERMAL CYCLES BETWEEN ROOM TEMPERATURE AND 200 degK (-100°F)

E_{xx} = 107 GPa (15.5 x 10⁶ psi)

ν_{xy} = 0.74

S_{xxT} = 571 MPa (83 ksi)

Fig. 5-61 STRAINS IN $[0_2/\pm 45]_s$ S-GLASS/EPOXY SPECIMEN UNDER UNIAXIAL
TENSILE LOADING AFTER 100 THERMAL CYCLES BETWEEN ROOM
TEMPERATURE AND 200 degK (-100°F)

Fig. 5-62 STRAINS IN $[0_2/\pm 45]_s$ S-GLASS/EPOXY SPECIMEN UNDER
UNIAXIAL TENSILE LOADING AFTER 100 THERMAL CYCLES
BETWEEN ROOM TEMPERATURE AND 200 degK (-100°F)

Fig. 5-63 STRAINS IN $[0_2/\pm 45]_s$ BORON/POLYIMIDE SPECIMEN UNDER UNIAXIAL TENSILE
LOADING AFTER 100 THERMAL CYCLES BETWEEN ROOM TEMPERATURE AND 200 degK
(-100°F)

E_{xx} = 121 GPa (17.6 x 10^6 psi)

ν_{xy} = 0.80

S_{xxT} = 508 MPa (74 ksi)

Fig. 5-64 STRAINS IN $[0_2/\pm 45]_s$ BORON/POLYIMIDE SPECIMEN UNDER UNIAXIAL TENSILE LOADING AFTER 100 THERMAL CYCLES BETWEEN ROOM TEMPERATURE AND 200 degK (-100°F)

E_{xx} = 112 GPa (16.2 x 10^6 psi)

ν_{xy} = 0.77

S_{xxT} = 513 MPa (74 ksi)

Fig. 5-65   STRAINS IN $[0_2/\pm45]_s$ GRAPHITE/POLYIMIDE SPECIMEN UNDER UNIAXIAL TENSILE LOADING
AFTER 100 THERMAL CYCLES BETWEEN ROOM TEMPERATURE AND 200 degK (-100°F)
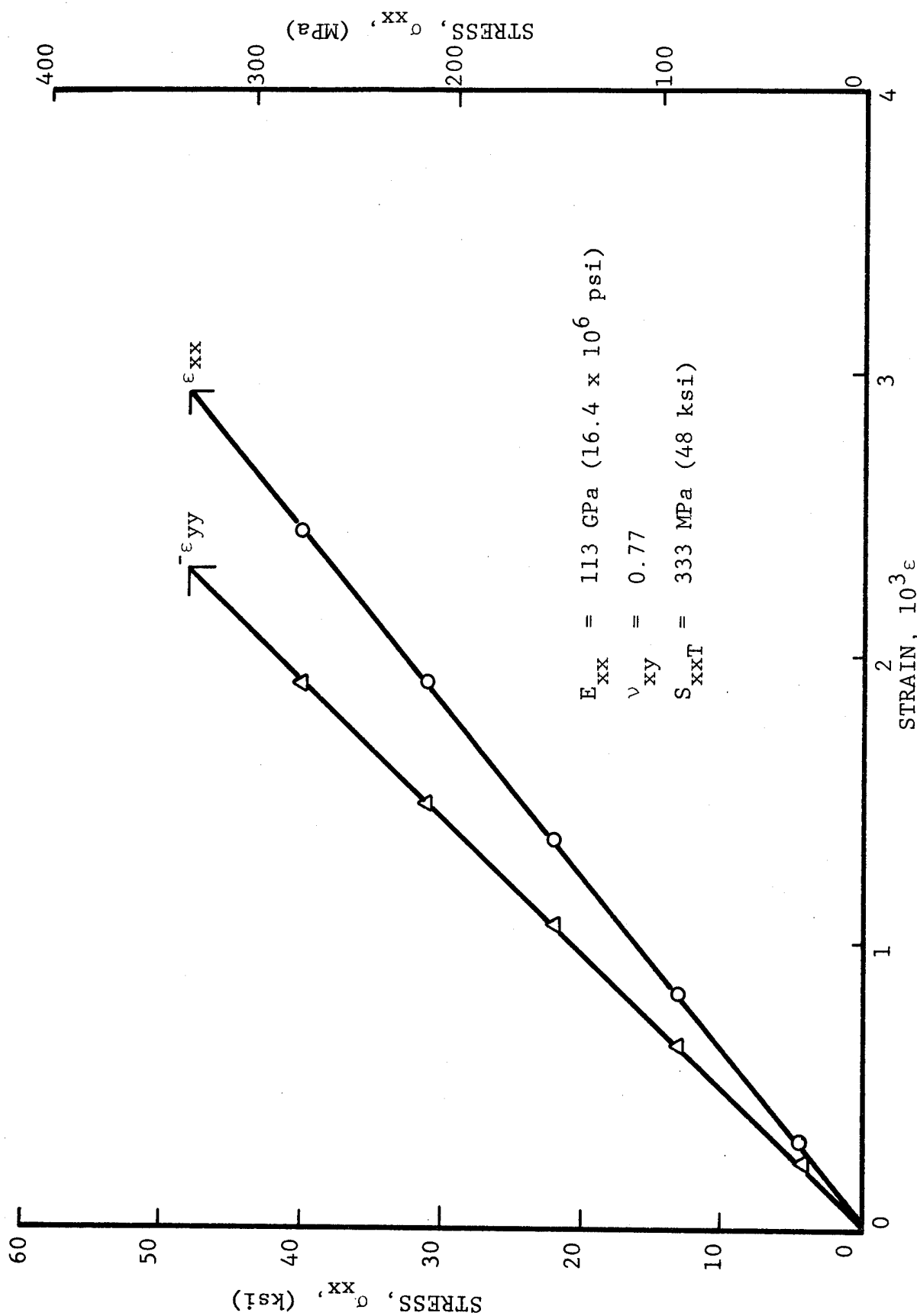
Fig. 5-66 STRAINS IN $[0_2/\pm45]_s$ GRAPHITE/POLYIMIDE SPECIMEN UNDER UNIAXIAL TENSILE LOADING AFTER 100 THERMAL CYCLES BETWEEN ROOM TEMPERATURE AND 200 degK (-100°)

The figure shows STRESS, σ_{xx}, (ksi) and STRESS, σ_{xx}, (MPa) versus STRAIN, $10^3\varepsilon$, with curves labeled ε_{xx} and $-\varepsilon_{yy}$.

E_{xx} = 113 GPa (16.4 x 10^6 psi)

ν_{xy} = 0.77

S_{xxT} = 333 MPa (48 ksi)

Fig. 5-67 STRESS-STRAIN CURVES FOR $[0_2/\pm45]_s$ BORON/EPOXY SPECIMEN UNDER UNIAXIAL TENSION AFTER 10^7 CYCLES TO 40 PERCENT OF ULTIMATE

Fig. 5-68 STRESS-STRAIN CURVES FOR $[0_2/\pm45]_s$ BORON/EPOXY SPECIMEN UNDER UNIAXIAL TENSION AFTER 10^7 CYCLES TO 40 PERCENT OF ULTIMATE

E_{xx} = 119 GPa (17.2 x 10^6 psi)

ν_{xy} = 0.74

S_{xxT} = 710 MPa (103 ksi)

Fig. 5-69   STRESS-STRAIN CURVES FOR $[0_2/\pm45]_s$ BORON/POLYIMIDE SPECIMEN UNDER UNIAXIAL TENSION AFTER 10^7 CYCLES TO 40 PERCENT OF ULTIMATE

E_{xx} = 113 GPa (16.3×10^6 psi)

ν_{xy} = 0.82

S_{xxT} = 587 MPa (85 ksi)

Fig. 5-70 STRESS-STRAIN CURVES FOR $[0_2/\pm45]_s$ BORON/POLYIMIDE SPECIMEN UNDER UNIAXIAL TENSION AFTER 10^7 CYCLES TO 70 PERCENT OF ULTIMATE

The figure shows stress-strain curves with axes labeled:
- STRESS, σ_{xx}, (MPa) — values 0, 200, 400, 600
- STRESS, σ_{xx}, (ksi) — values 0, 20, 40, 60, 80
- STRAIN, $10^3\epsilon$ — values 0, 1, 2, 3, 4, 5, 6

Curves labeled ϵ_{xx} and $-\epsilon_{yy}$

E_{xx} = 102 GPa (14.8 x 10^6 psi)

ν_{xy} = 0.70

S_{xxT} = 470 MPa (68 ksi)

5-99
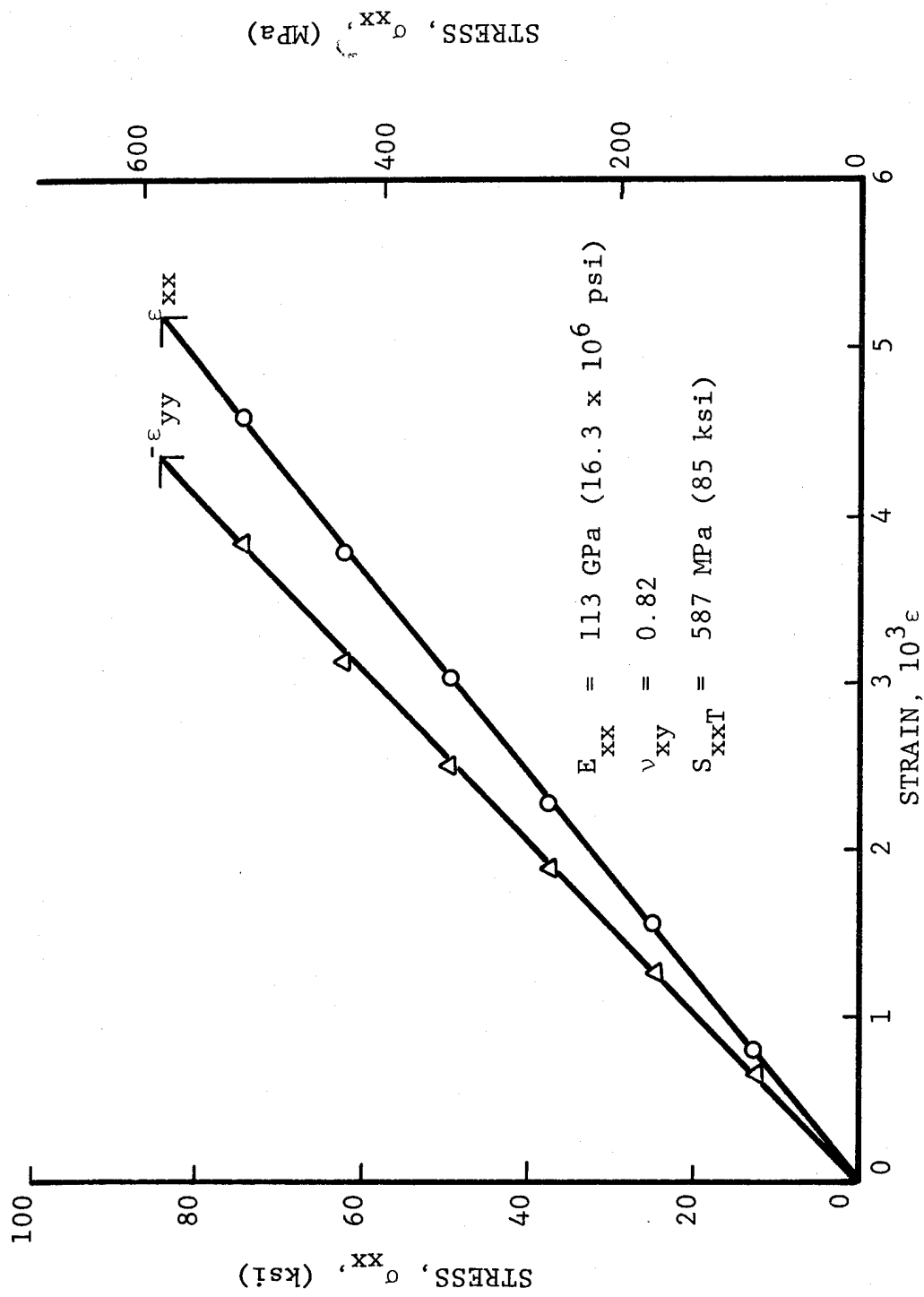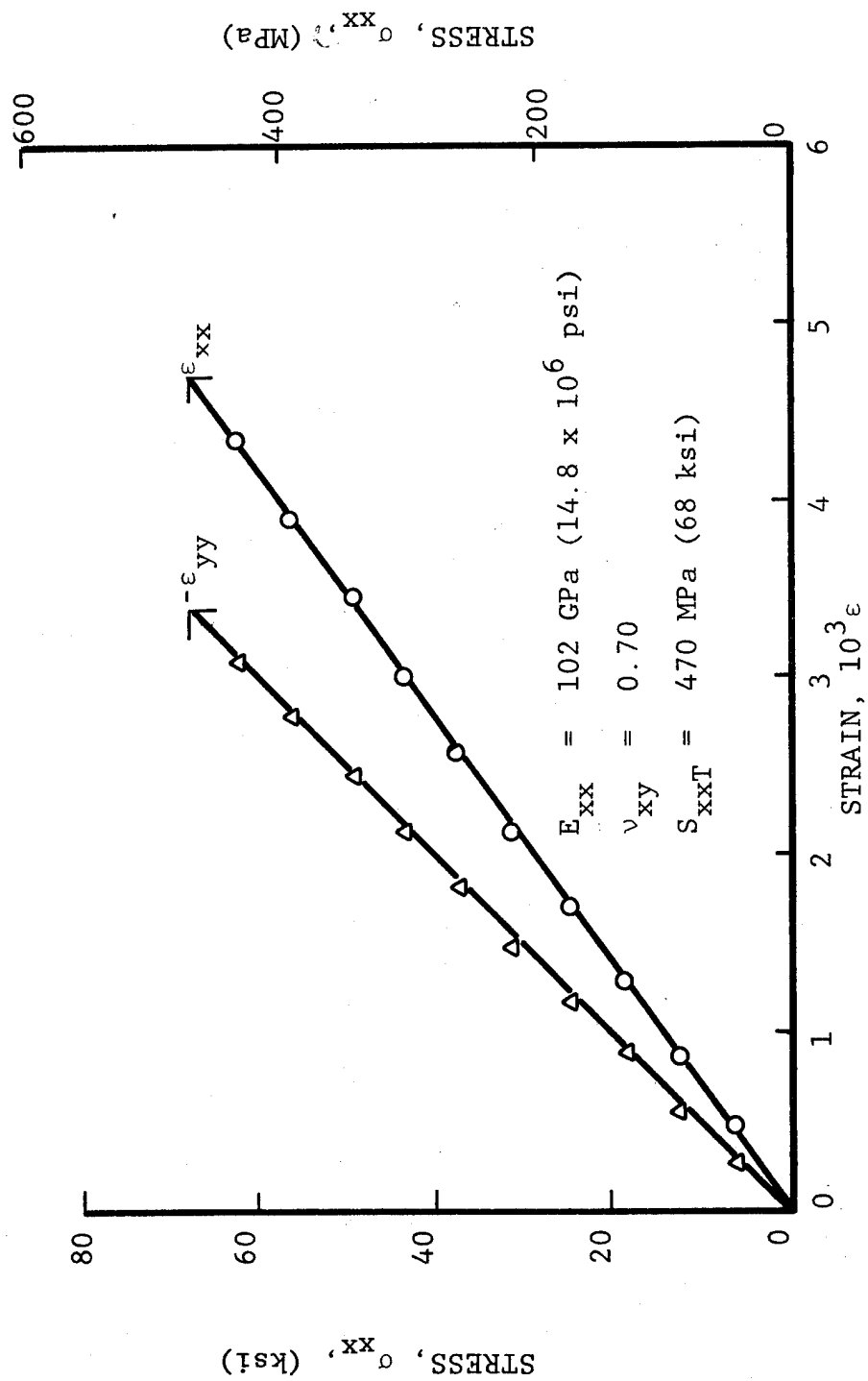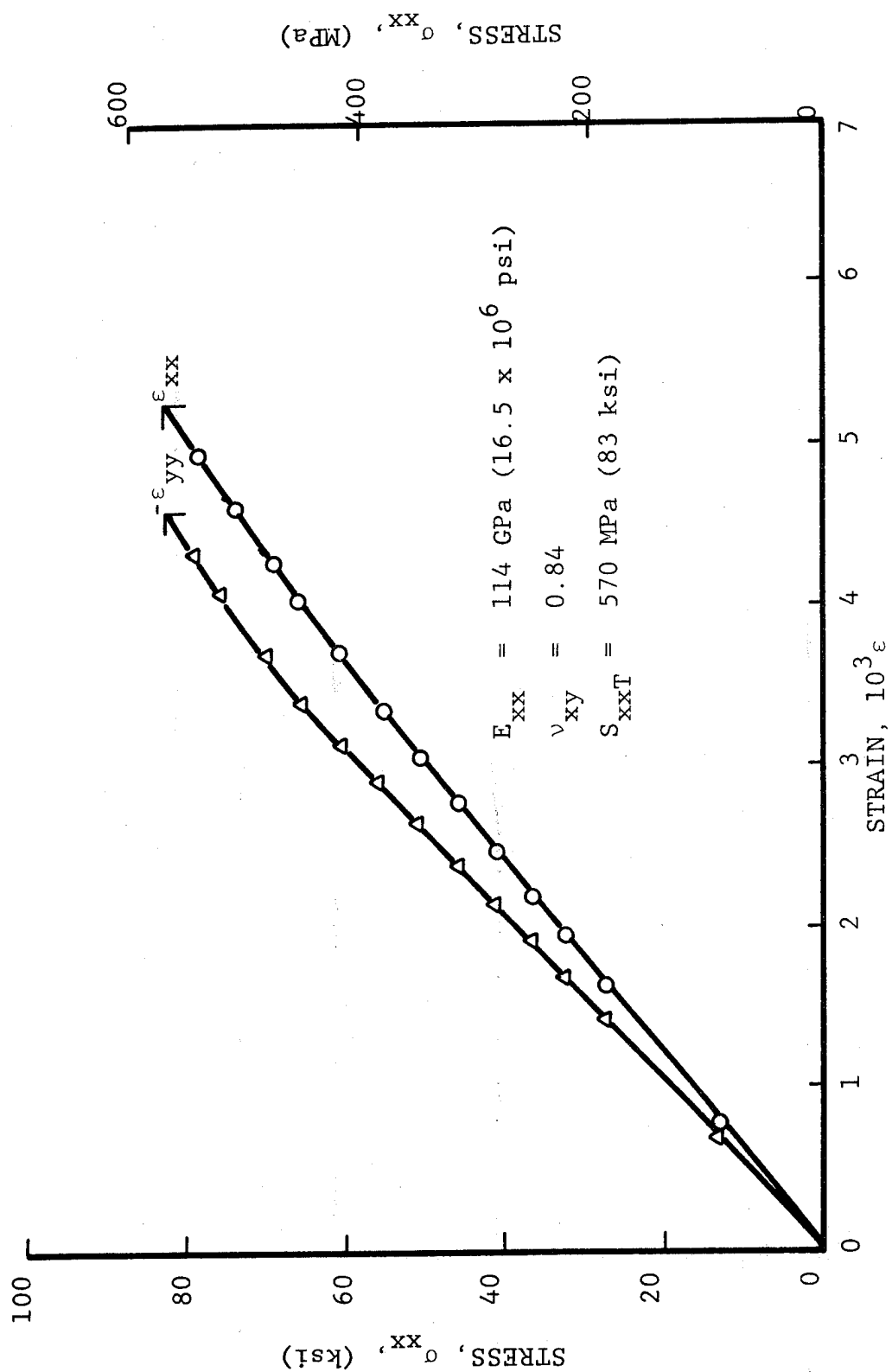
Fig. 5-71 STRESS-STRAIN CURVES FOR $[0_2/\pm 45]_s$ GRAPHITE/LOW MODULUS EPOXY SPECIMEN UNDER UNIAXIAL TENSION AFTER 10^7 CYCLES TO 40 PERCENT OF ULTIMATE

E_{xx} = 114 GPa (16.5 x 10^6 psi)
ν_{xy} = 0.84
S_{xxT} = 570 MPa (83 ksi)

Fig. 5-72 STRESS-STRAIN CURVES FOR $[0_2/\pm45]_s$ GRAPHITE/HIGH
MODULUS EPOXY UNDER UNIAXIAL TENSILE LOADING AFTER
10^7 CYCLES TO 70 PERCENT OF ULTIMATE.

In the figure:

E_{xx} = 100 GPa (14.5 x 10^6 psi)

ν_{xy} = 0.68

S_{xxT} = 497 MPa (72 ksi)

Axis labels: STRESS, σ_{xx}, (ksi); STRESS, σ_{xx}, (MPa); STRAIN, $10^3\varepsilon$

Curve labels: ε_{yy}, ε_{xx}
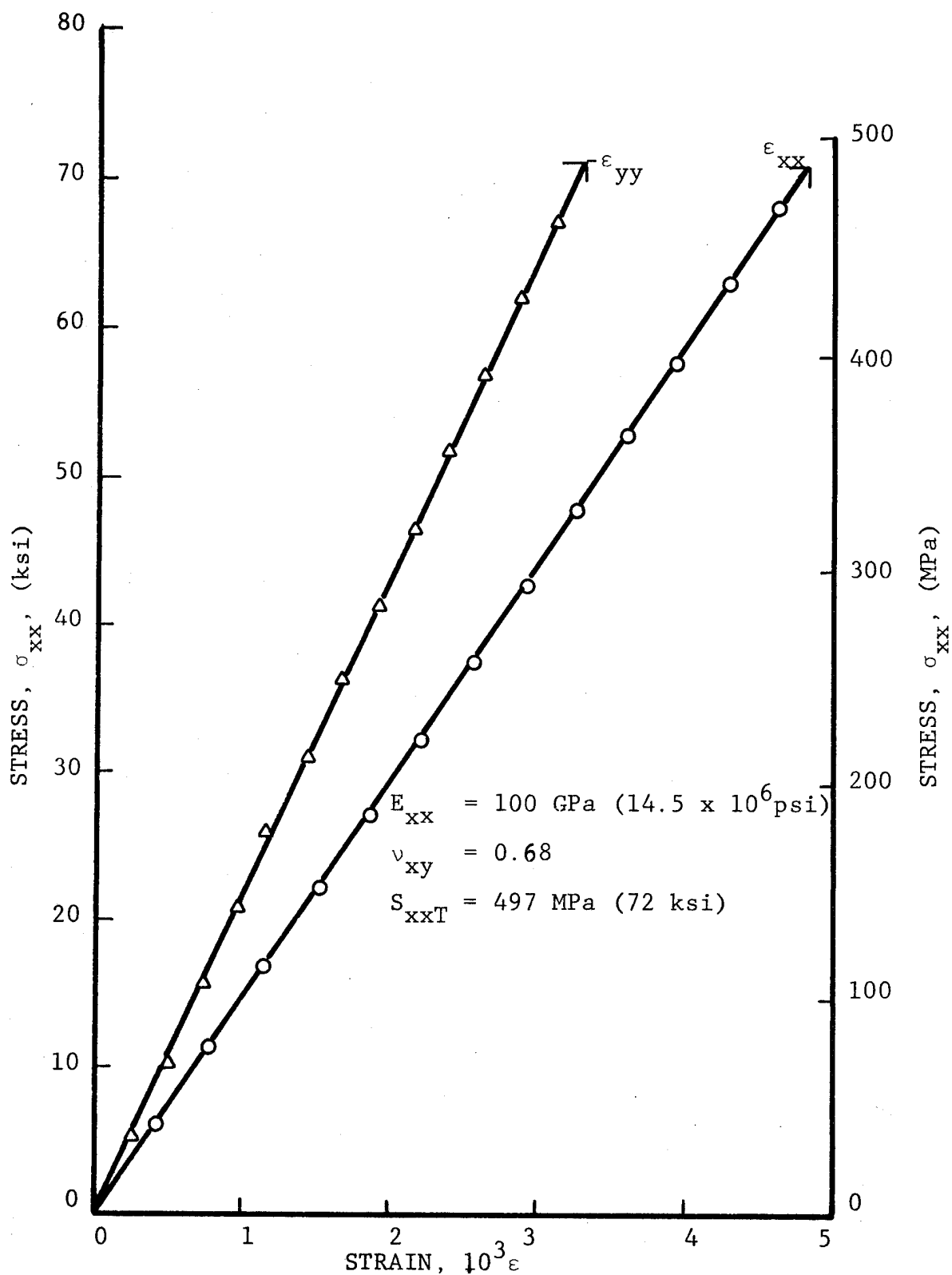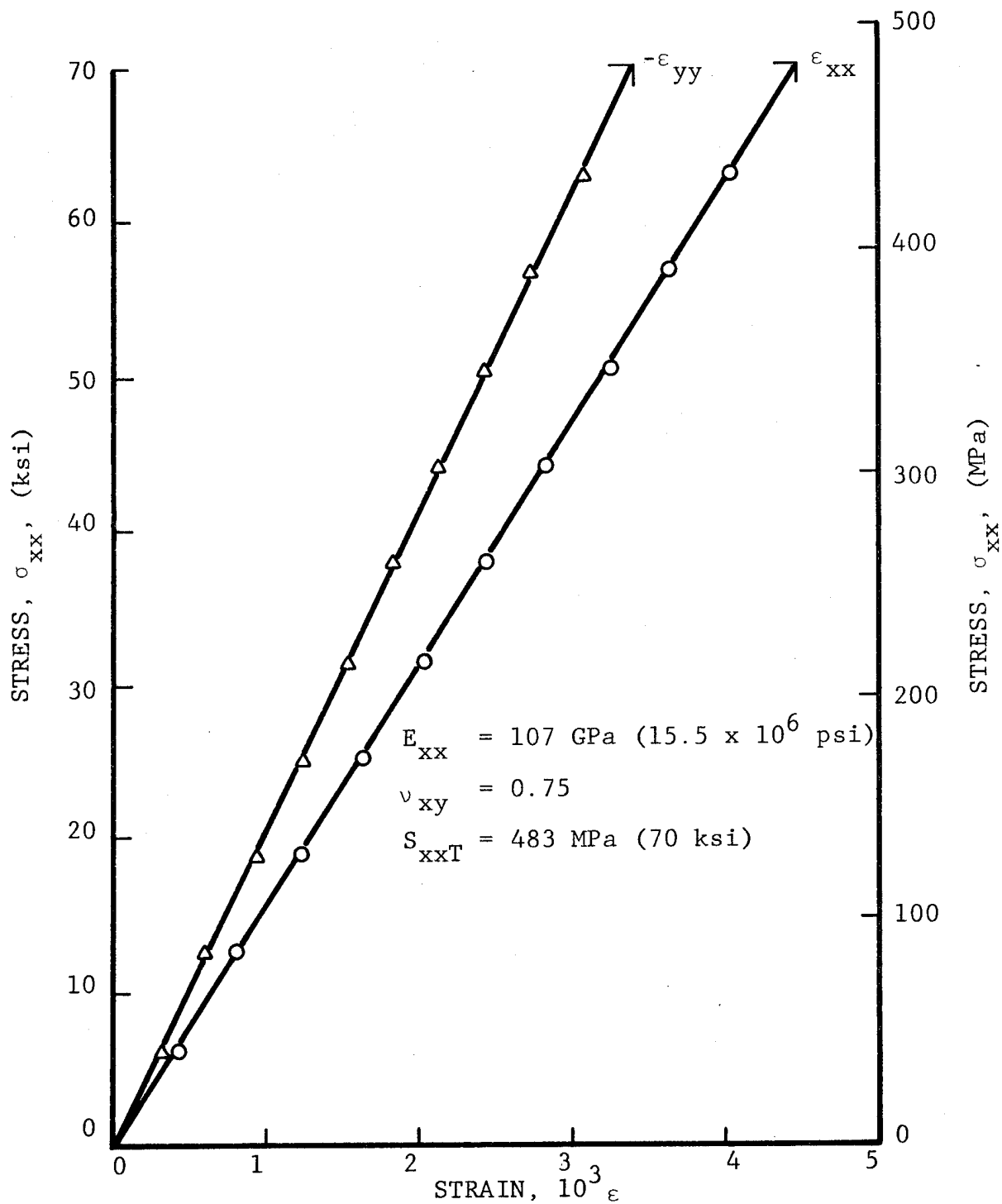
Fig. 5-73 STRESS-STRAIN CURVES FOR $[0_2/\pm 45]_s$ GRAPHITE/HIGH
MODULUS EPOXY UNDER UNIAXIAL TENSILE LOADING AFTER
10^7 CYCLES TO 70 PERCENT OF ULTIMATE
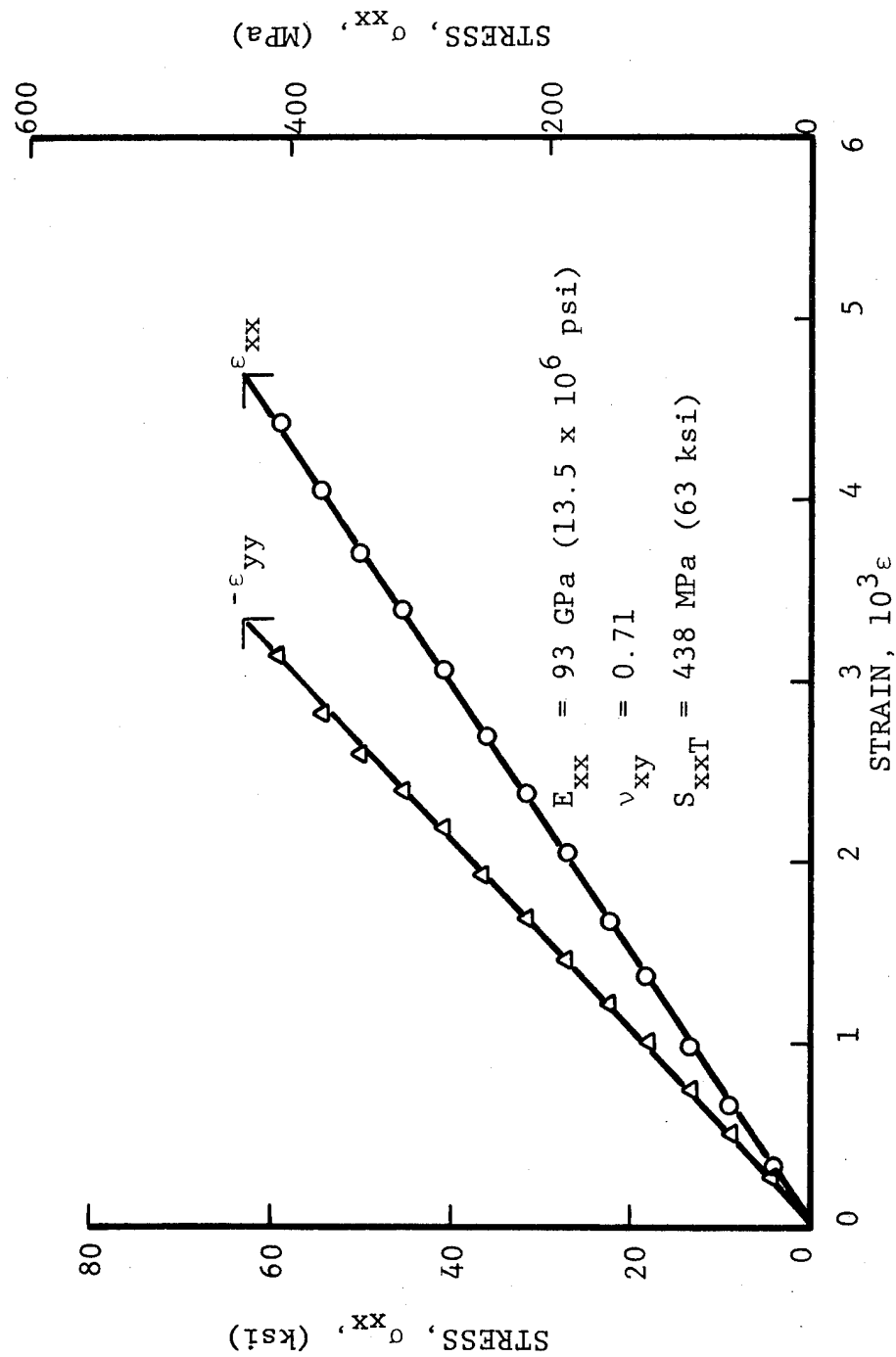
Fig. 5-74 STRESS-STRAIN CURVES FOR $[0_2/\pm45]_s$ GRAPHITE/POLYIMIDE SPECIMEN UNDER UNIAXIAL TENSION AFTER 10^7 CYCLES TO 70 PERCENT OF ULTIMATE
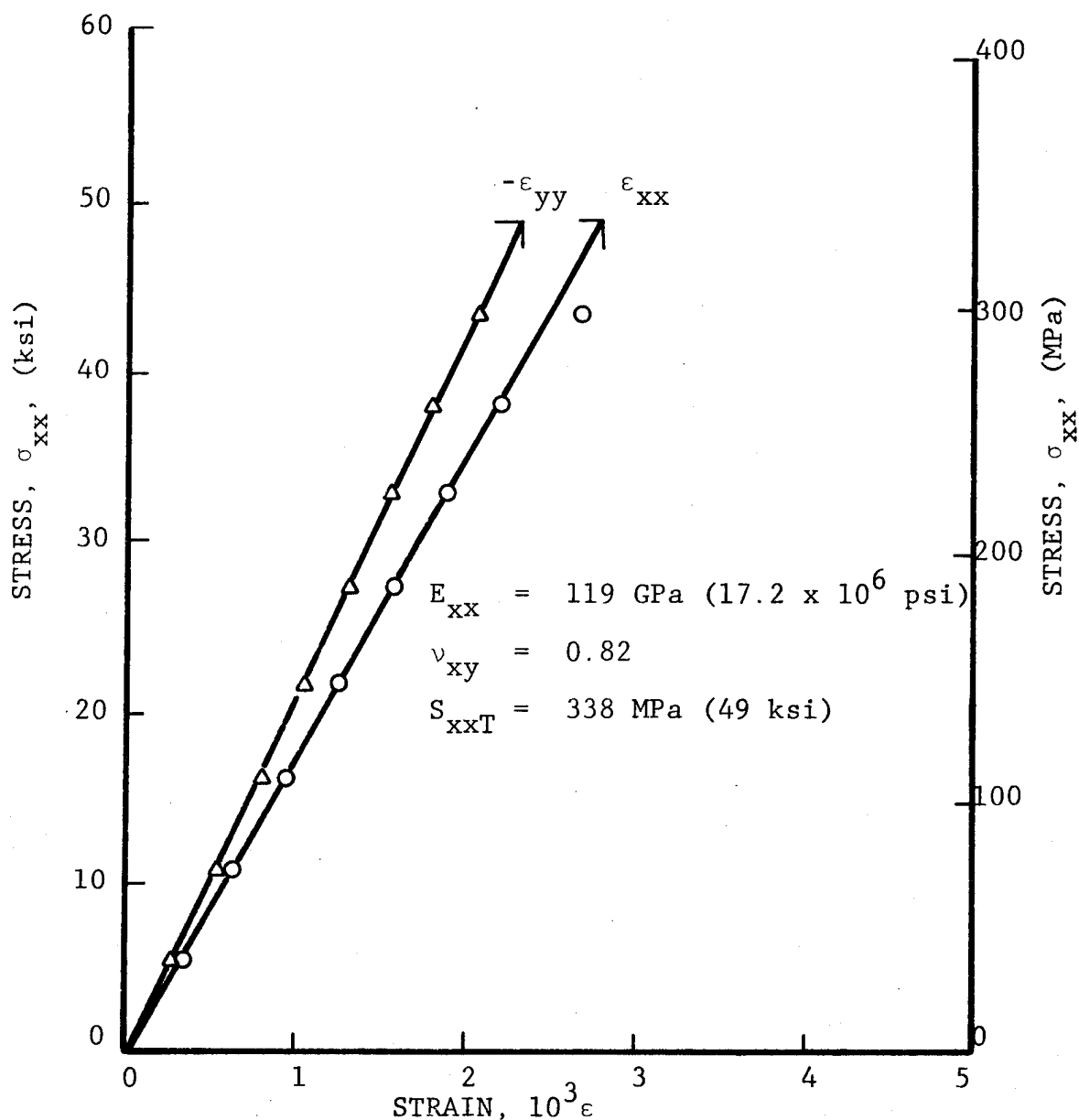
Fig. 5-75 STRESS-STRAIN CURVES FOR $[0_2/\pm45]_s$ GRAPHITE/POLYIMIDE
SPECIMEN UNDER UNIAXIAL TENSION AFTER 10^7 CYCLES TO
70 PERCENT OF ULTIMATE
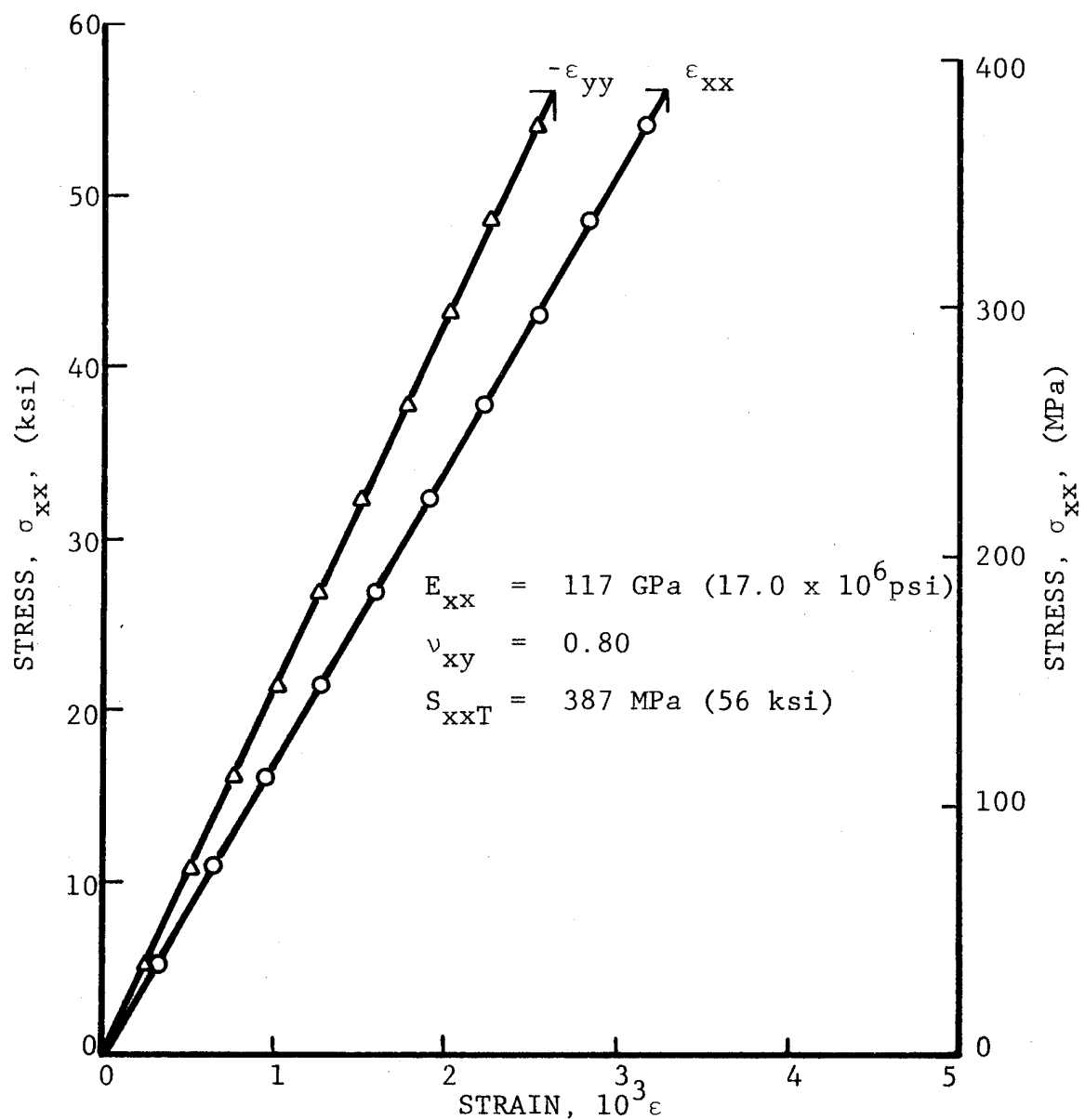
Fig. 5-76 STRESS-STRAIN CURVES FOR $[0_2/\pm45]_s$ GRAPHITE/POLYIMIDE
SPECIMEN UNDER UNIAXIAL TENSION AFTER 10^7 CYCLES TO
80 PERCENT OF ULTIMATE
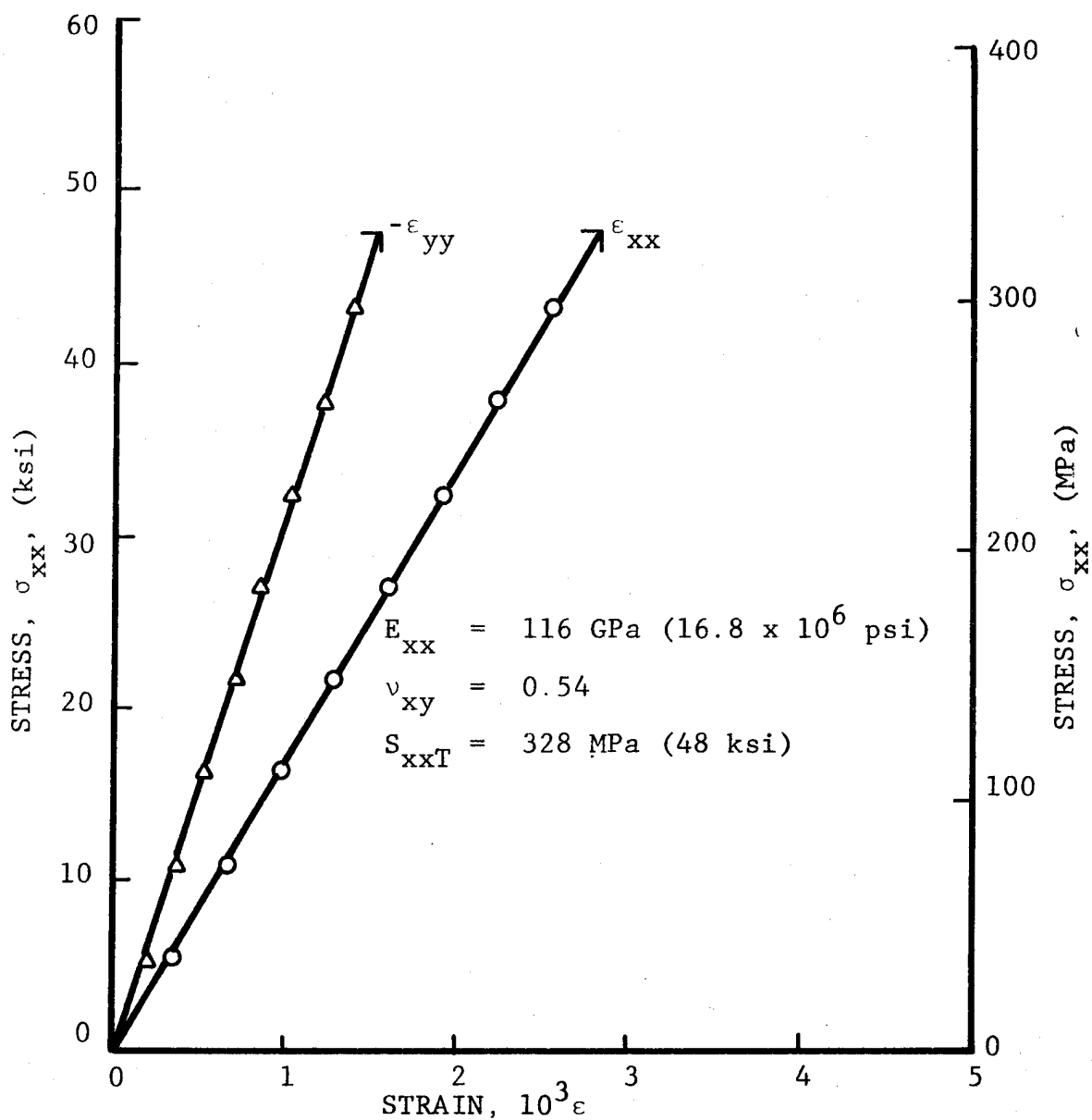
Fig. 5-77   STRESS-STRAIN CURVES FOR $[0_2/\pm 45]_s$ GRAPHITE/POLYIMIDE
SPECIMEN UNDER UNIAXIAL TENSION AFTER 10^7 CYCLES TO
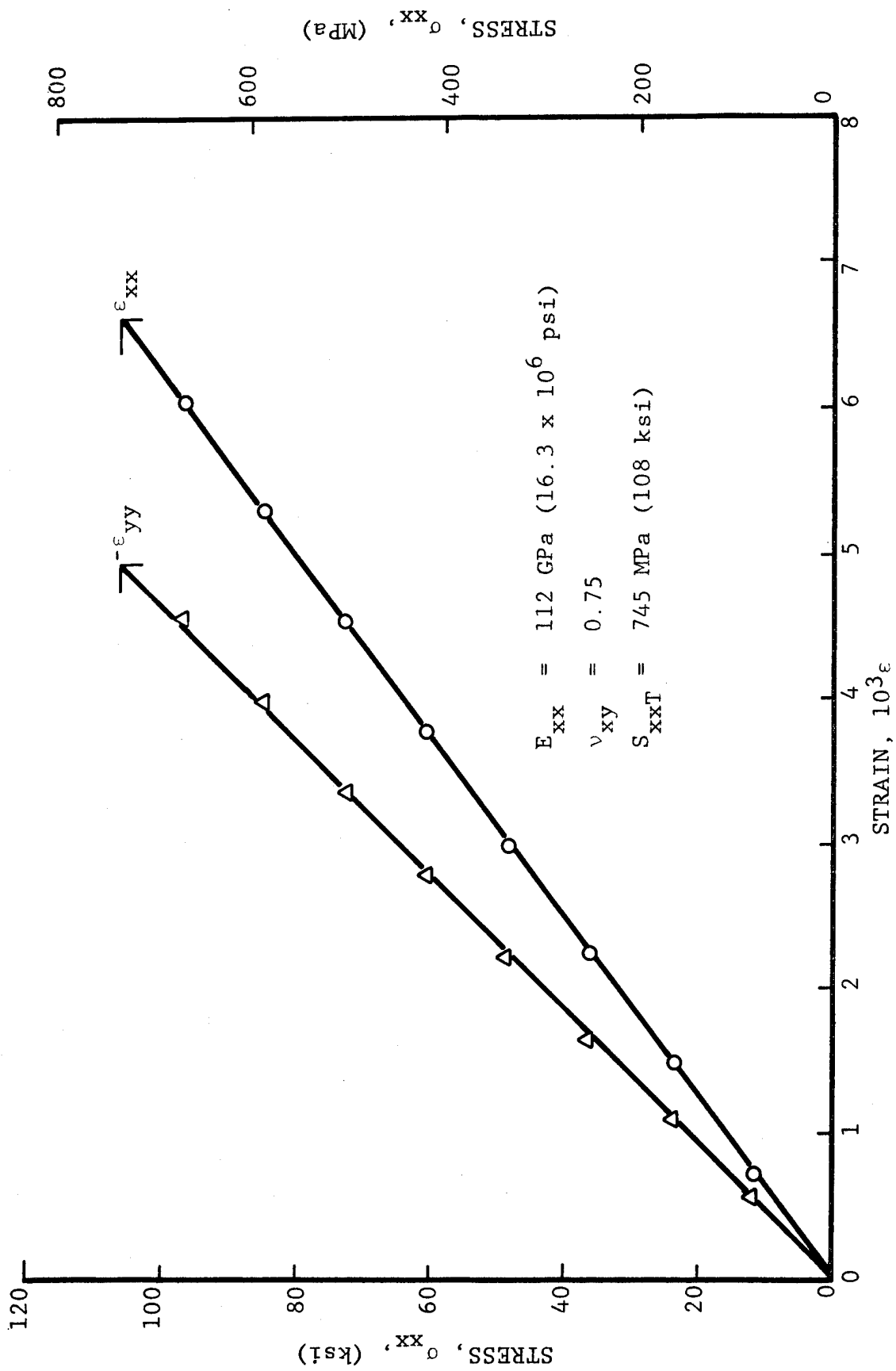90 PERCENT OF ULTIMATE
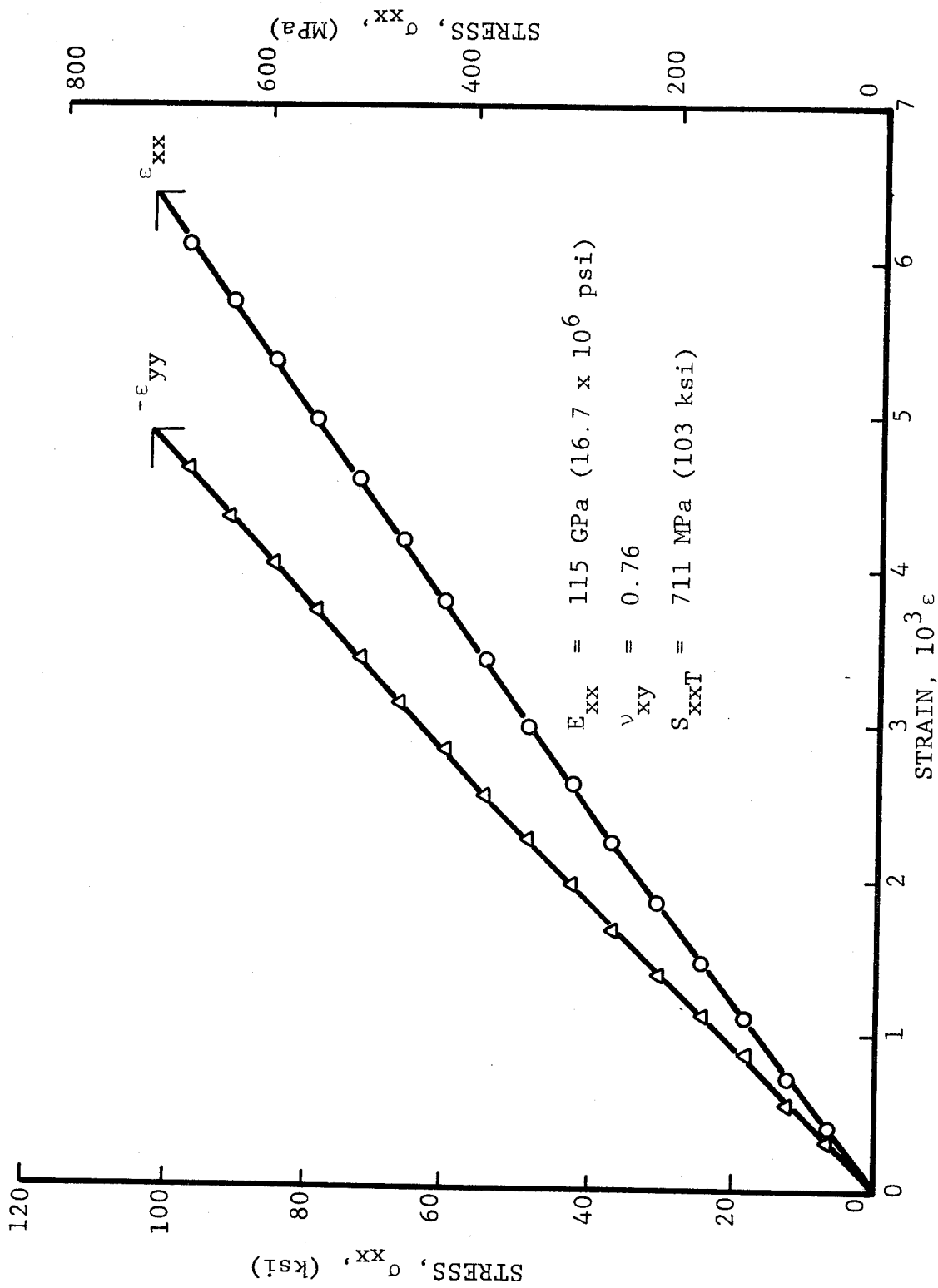
Fig. 5-78 STRESS-STRAIN CURVES FOR $[0_2/\pm 45]_s$ BORON/EPOXY SPECIMEN UNDER UNIAXIAL TENSILE LOADING AFTER 100 THERMAL CYCLES BETWEEN ROOM TEMPERATURE AND 411 degK (280°F) UNDER TENSILE LOADING OF 510 MPa (74 ksi)
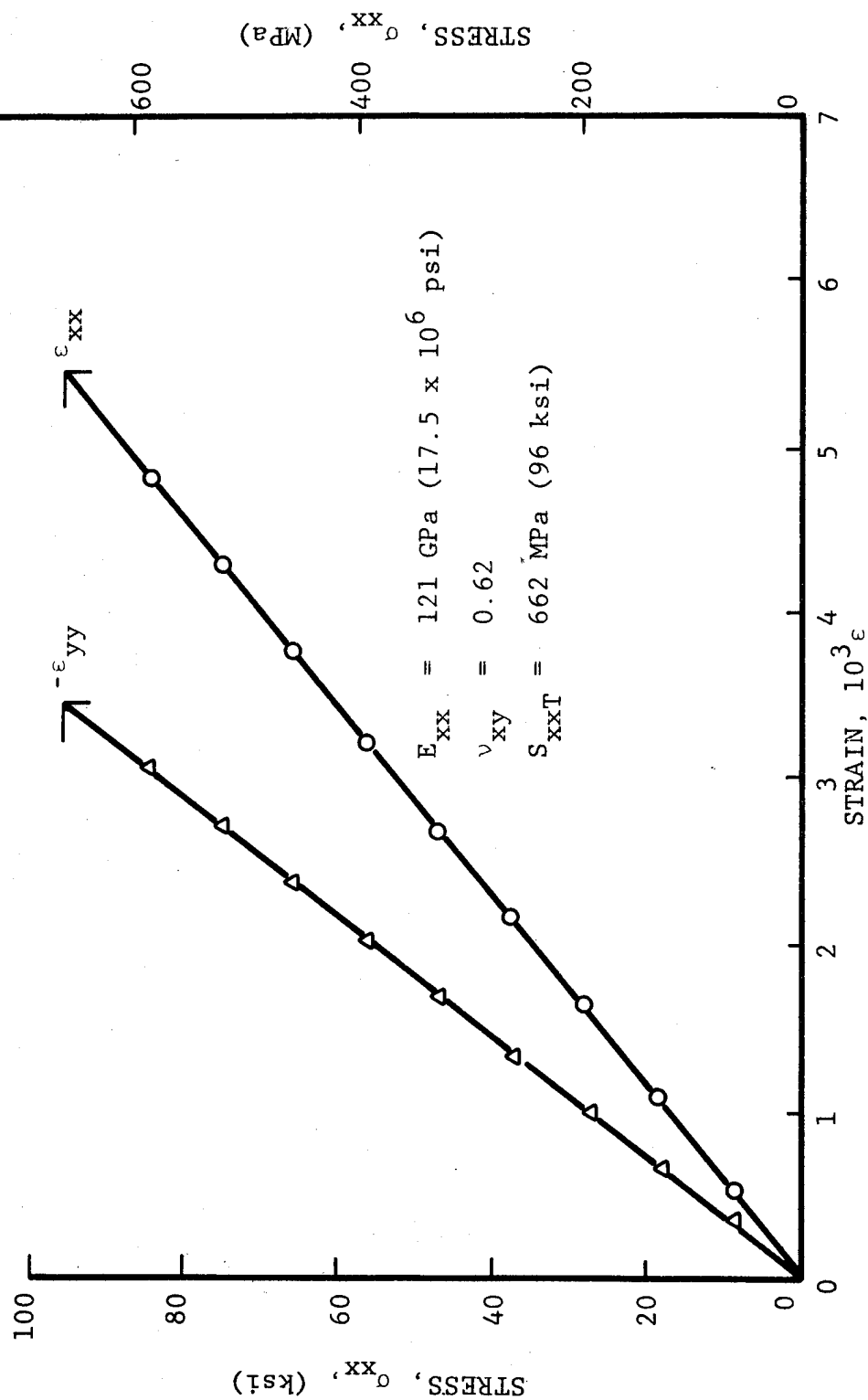
E_{xx} = 115 GPa (16.7 x 10^6 psi)

ν_{xy} = 0.76

S_{xxT} = 711 MPa (103 ksi)

Fig. 5-79 STRESS-STRAIN CURVES FOR $[0_2/\pm45]_s$ BORON/EPOXY SPECIMEN UNDER UNIAXIAL TENSILE LOADING AFTER 100 THERMAL CYCLES BETWEEN ROOM TEMPERATURE AND 411 degK (280°F) UNDER TENSILE LOADING OF 510 MPa (74 ksi)
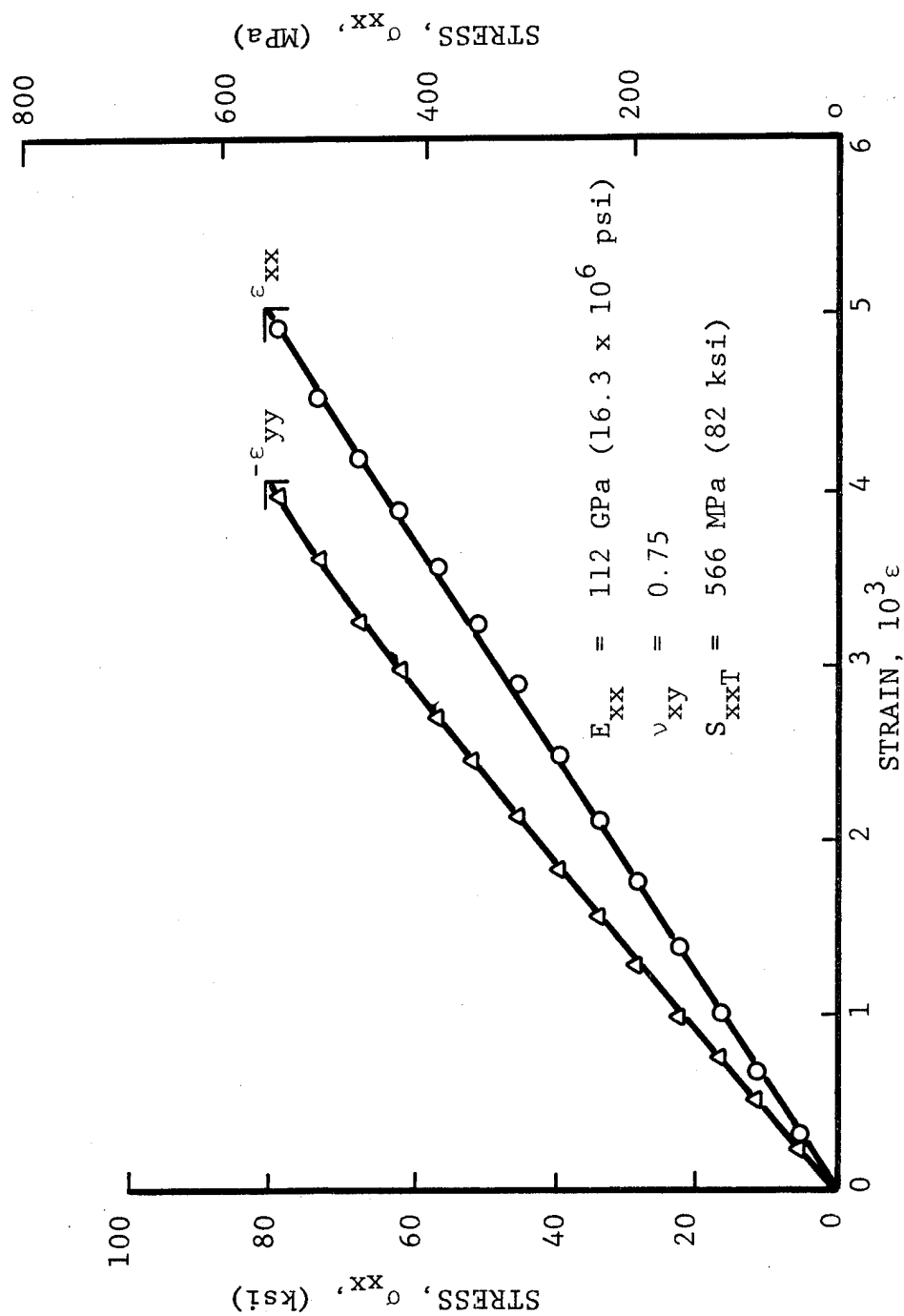
E_{xx} = 117 GPa (16.9 x 10^6 psi)

ν_{xy} = 0.69
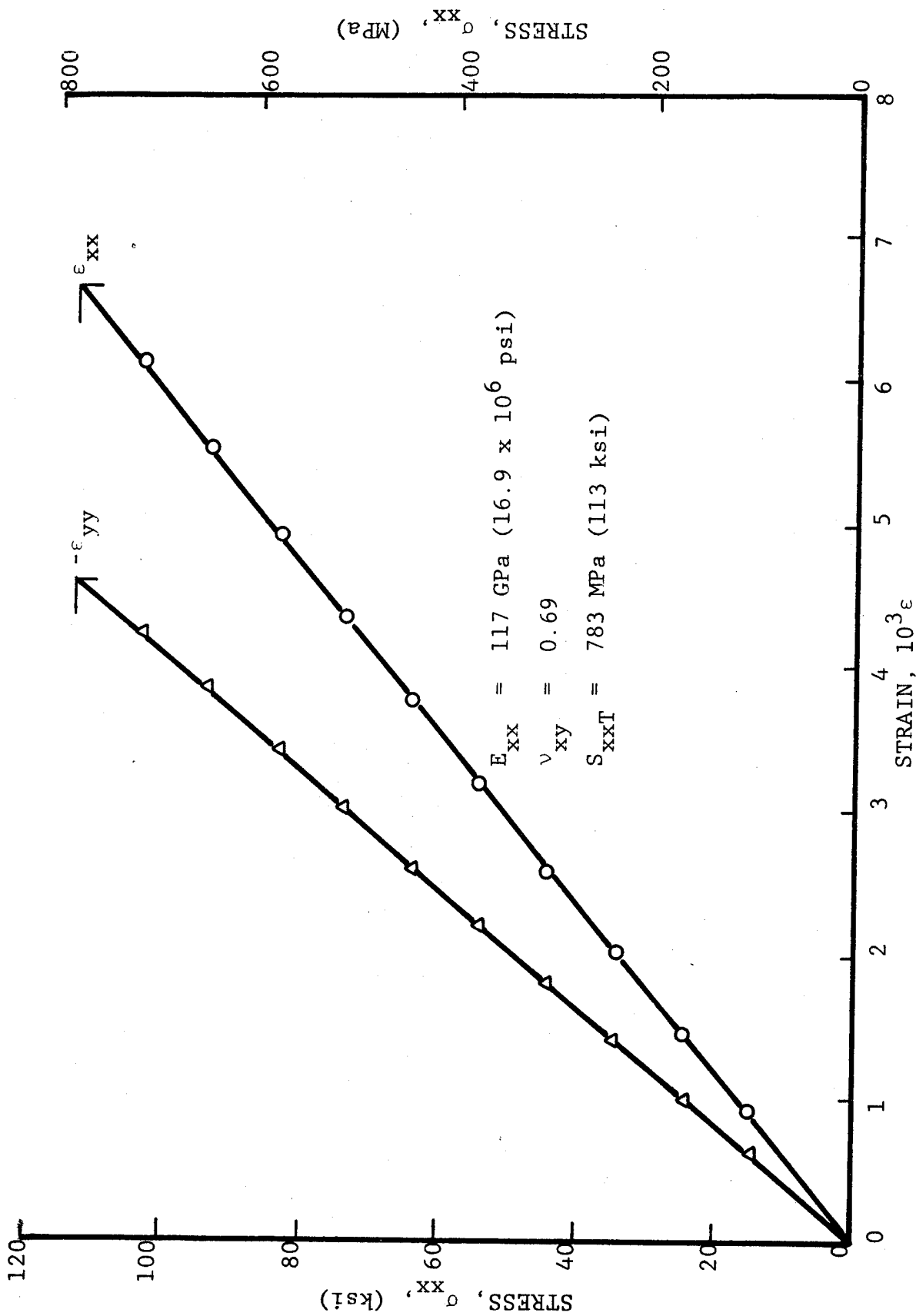
S_{xxT} = 783 MPa (113 ksi)
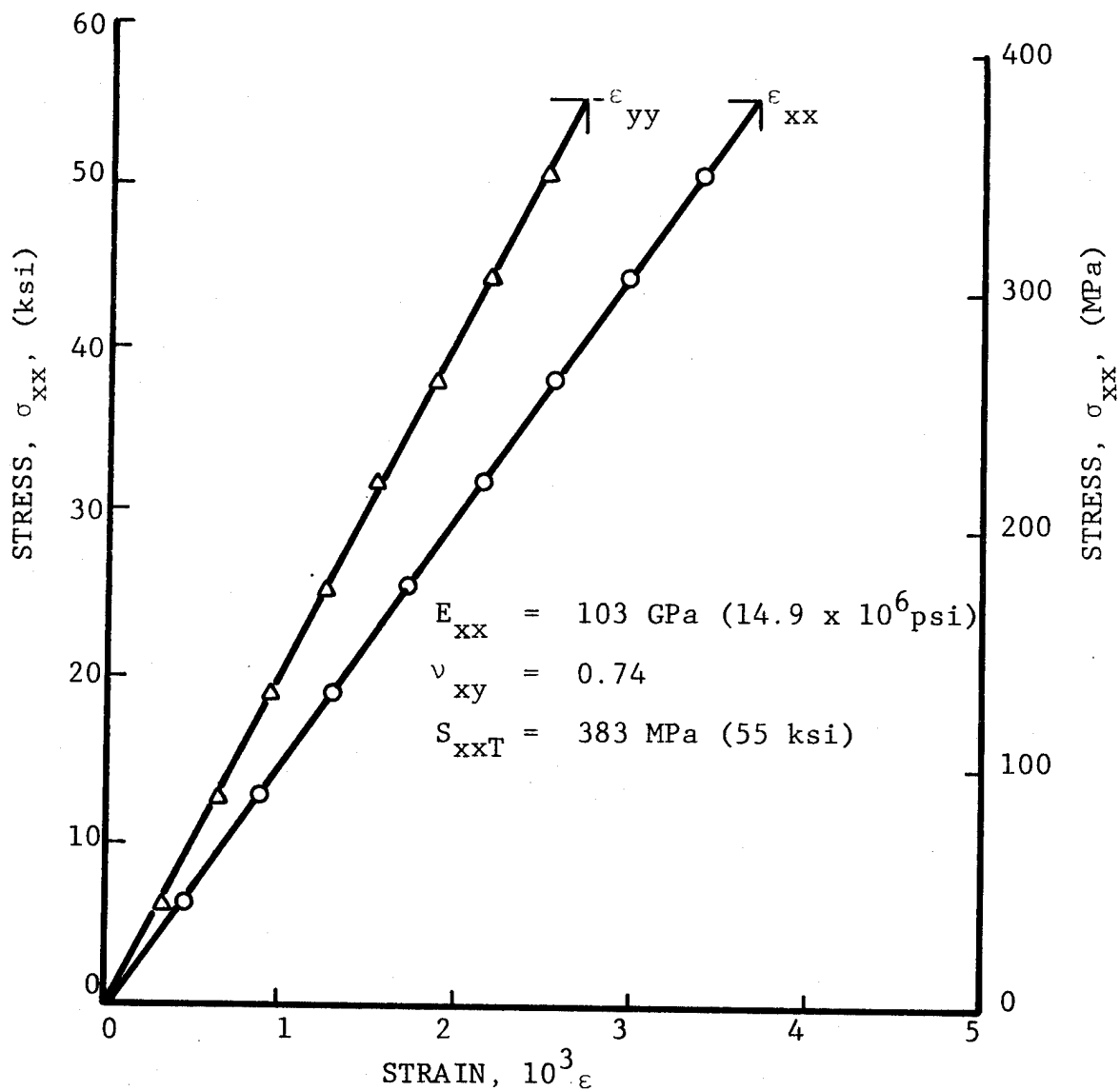
Fig. 5-80   STRESS-STRAIN CURVES FOR $[0_2/\pm 45]_s$ GRAPHITE/HIGH MODULUS
EPOXY SPECIMEN UNDER UNIAXIAL TENSILE LOADING AFTER 100
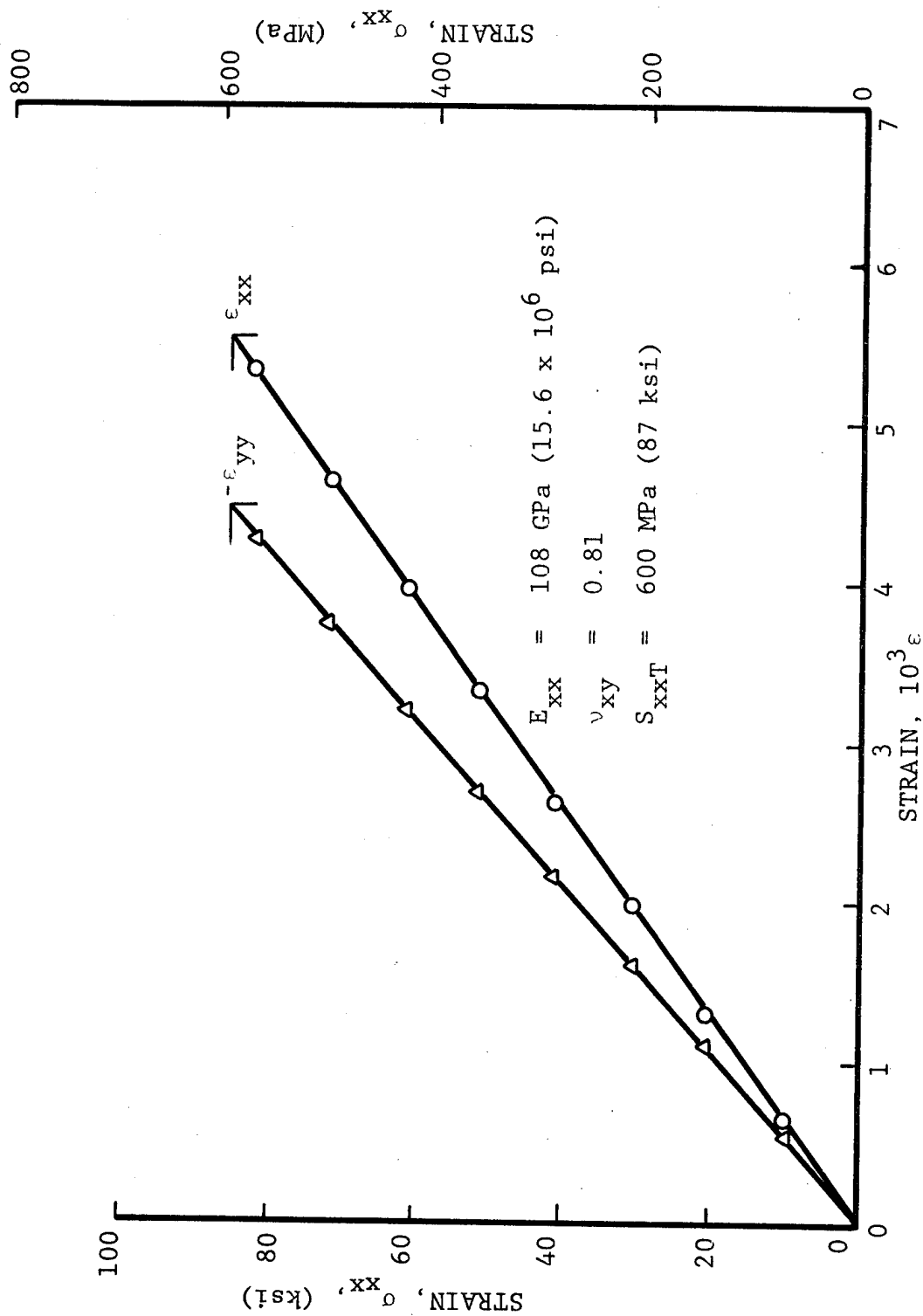THERMAL CYCLES BETWEEN ROOM TEMPERATURE AND 411 degK (280°F)
UNDER TENSILE LOADING OF 340 MPa (49 ksi)
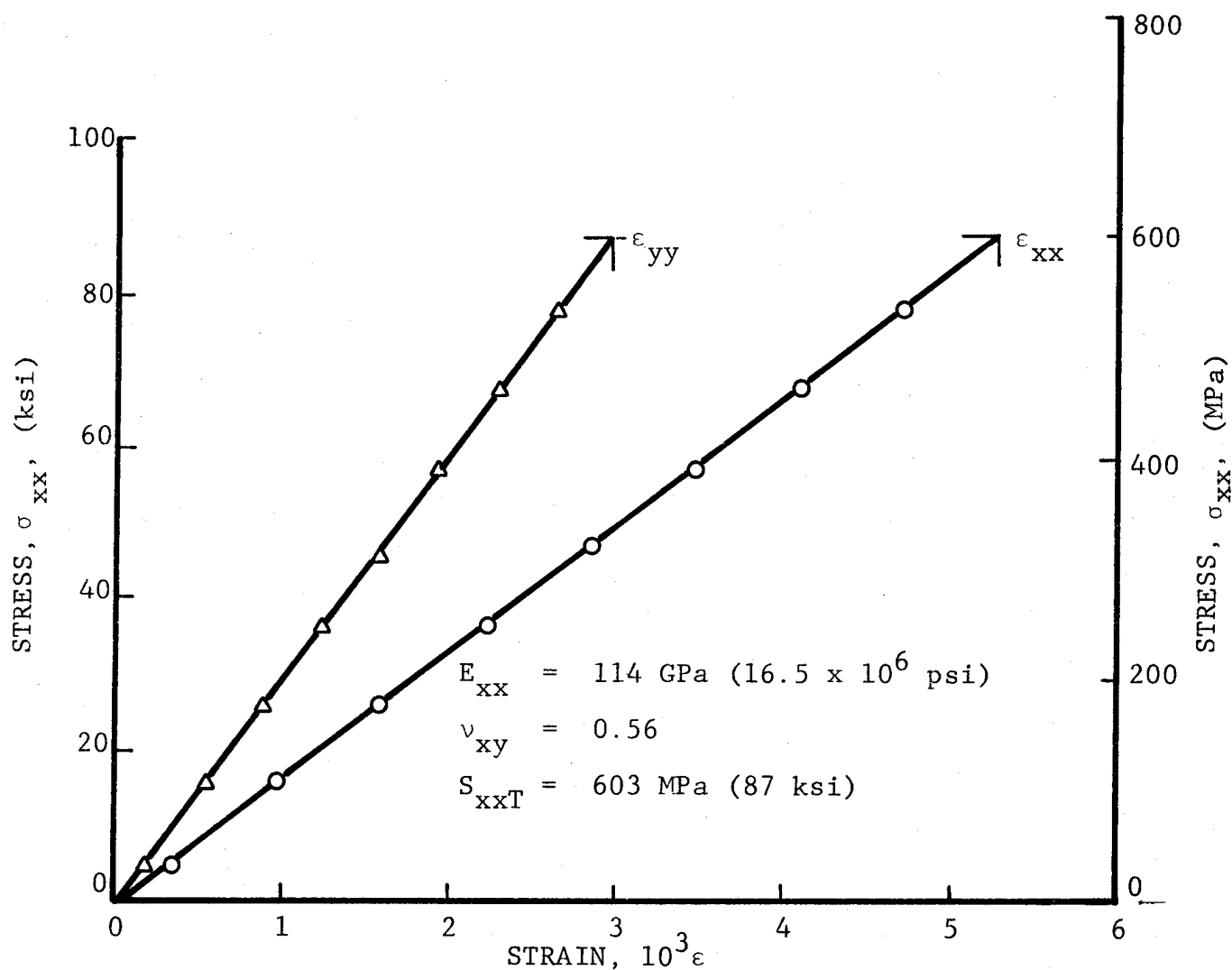
Fig. 5-81   STRESS-STRAIN CURVES FOR $[0_2/\pm45]_s$ GRAPHITE/HIGH MODULUS
EPOXY SPECIMEN UNDER UNIAXIAL TENSILE LOADING AFTER 100
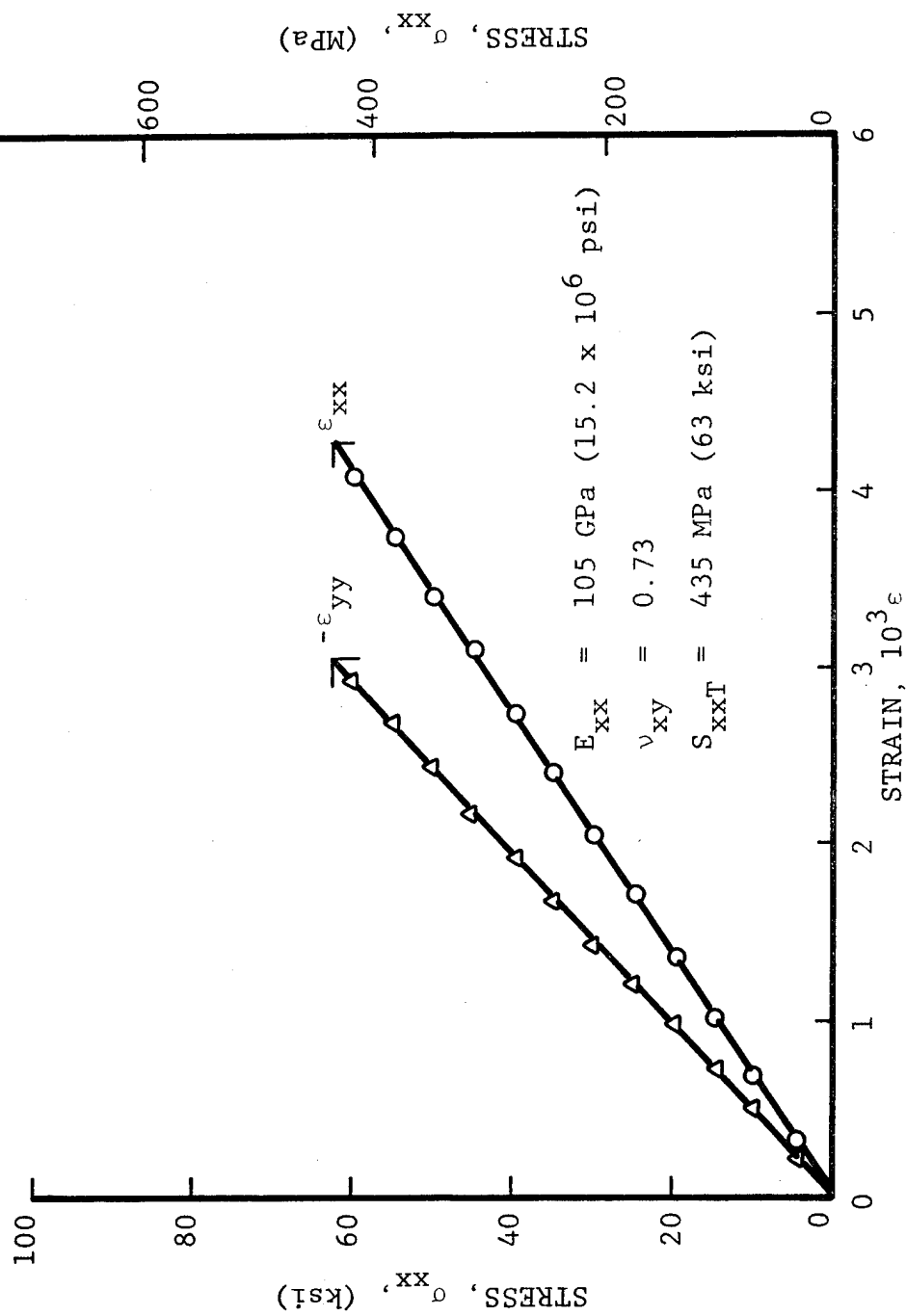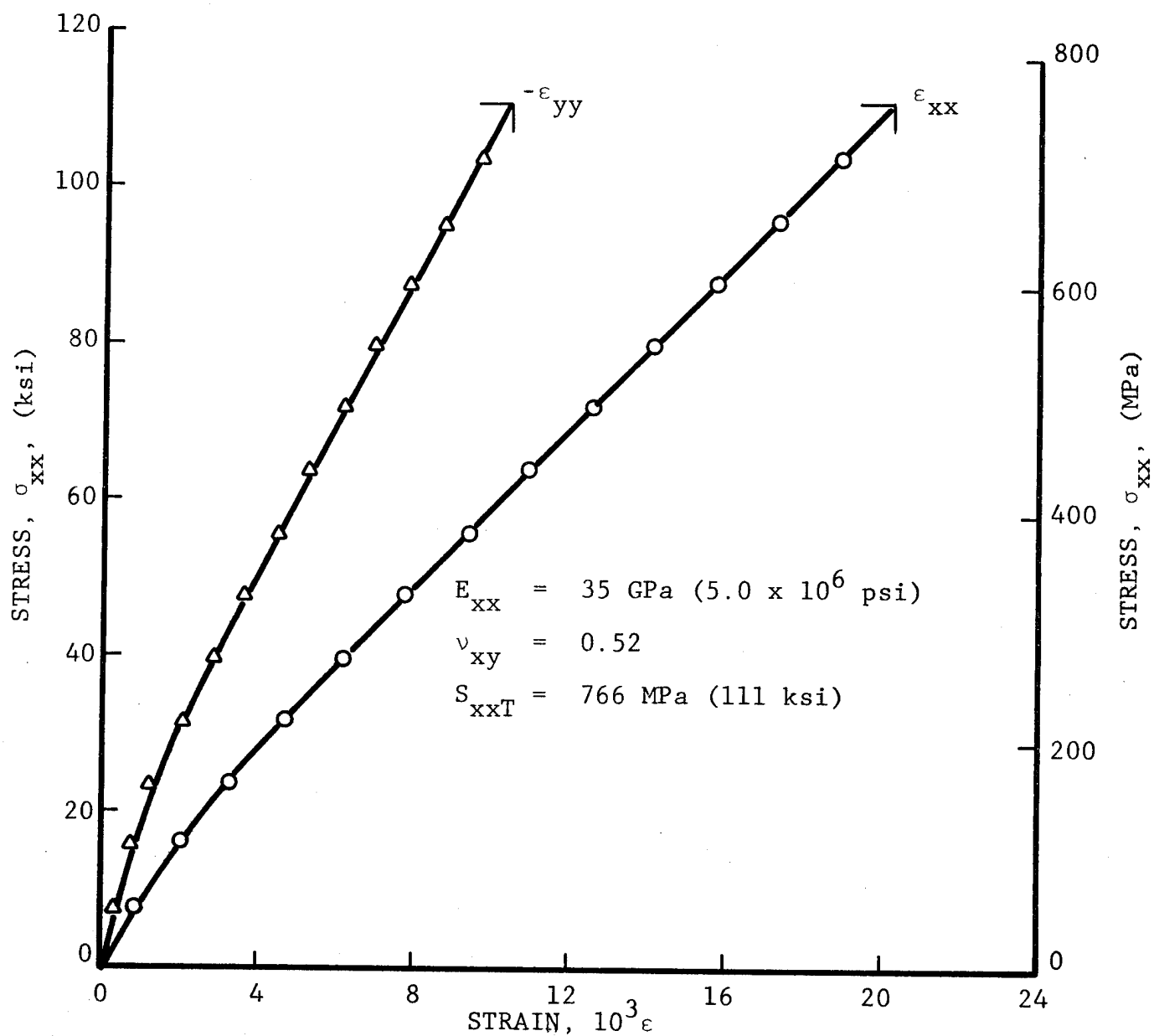THERMAL CYCLES BETWEEN ROOM TEMPERATURE AND 411 degK (280°F)
UNDER TENSILE LOADING OF 340 MPa (49 ksi)

5-110
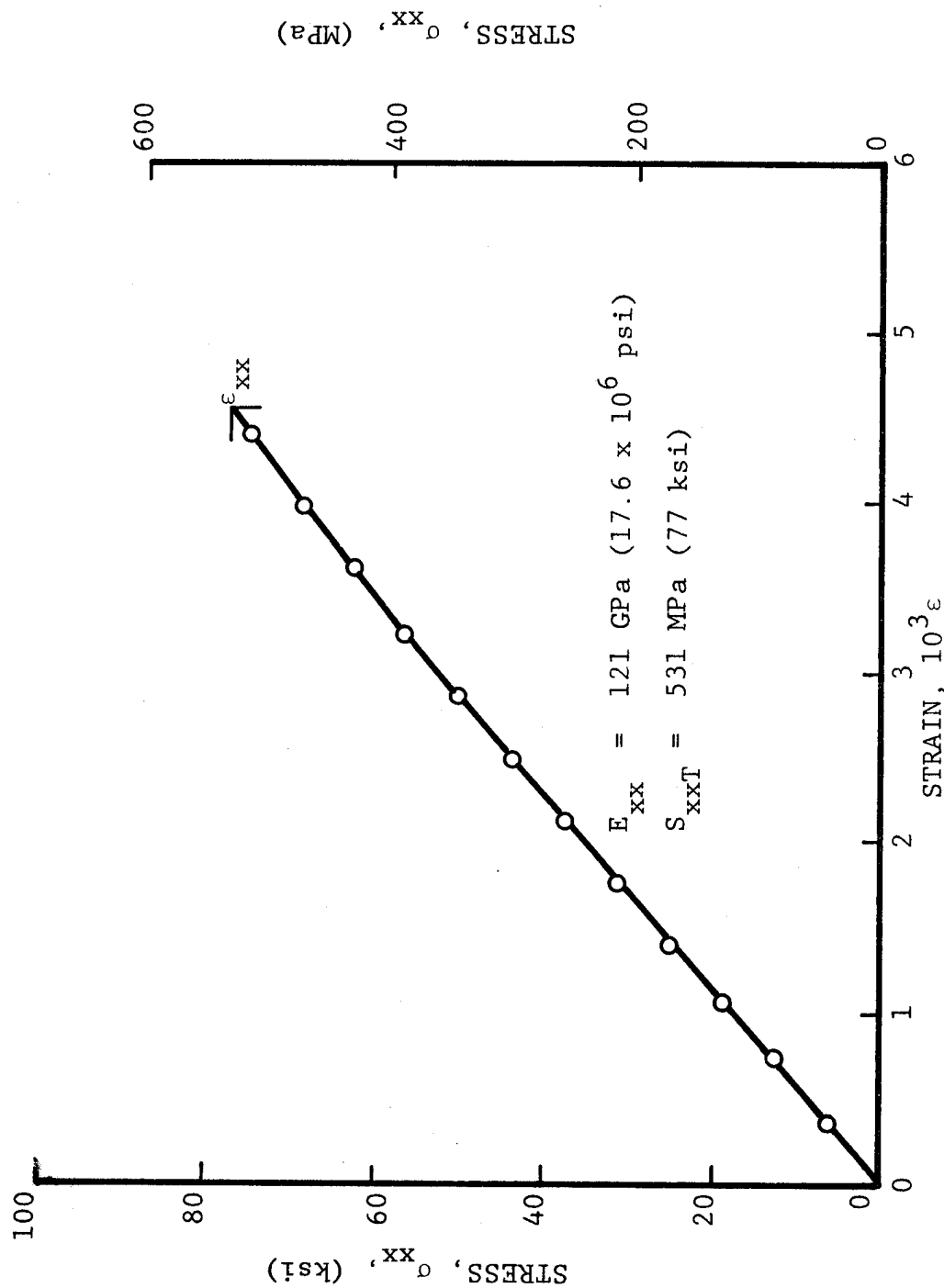
Fig. 5-82 STRESS-STRAIN CURVE FOR $[0_2/\pm45]_s$ BORON/POLYIMIDE SPECIMEN UNDER UNIAXIAL TENSILE LOADING AFTER 100 THERMAL CYCLES BETWEEN ROOM TEMPERATURE AND 533 degK (500°F) UNDER TENSILE LOADING OF 395 MPa (57 ksi)

E_{xx} = 121 GPa (17.6 x 10^6 psi)
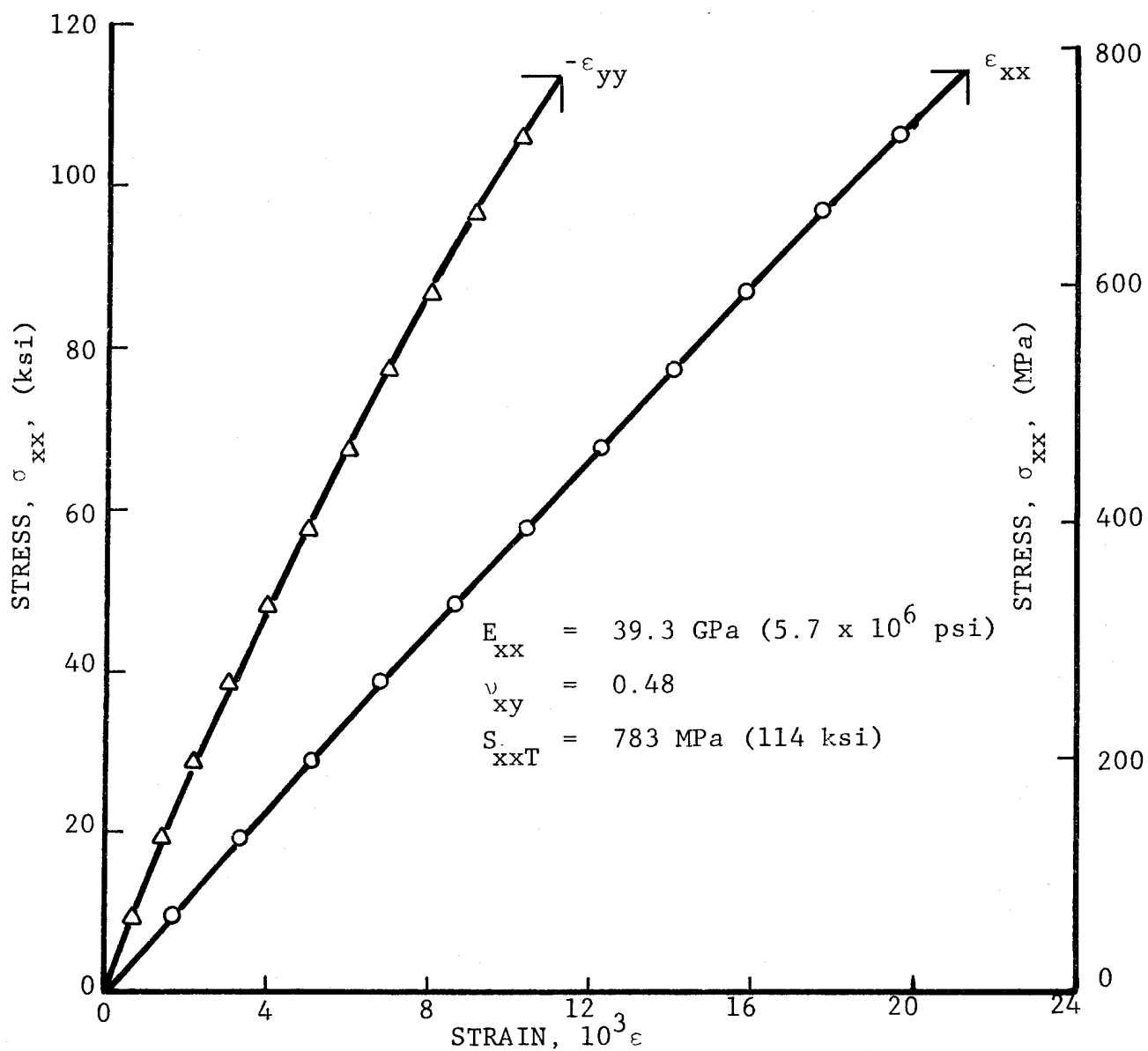
S_{xxT} = 531 MPa (77 ksi)

Fig. 5-83 STRESS-STRAIN CURVES FOR $[0_2/\pm45]_s$ BORON/POLYIMIDE SPECIMEN UNDER UNIAXIAL TENSILE LOADING AFTER 100 THERMAL CYCLES BETWEEN ROOM TEMPERATURE AND 533 degK (500°F) UNDER TENSILE LOADING OF 395 MPa (57 ksi)

E_{xx} = 119 GPa (17.3 x 10^6 psi)

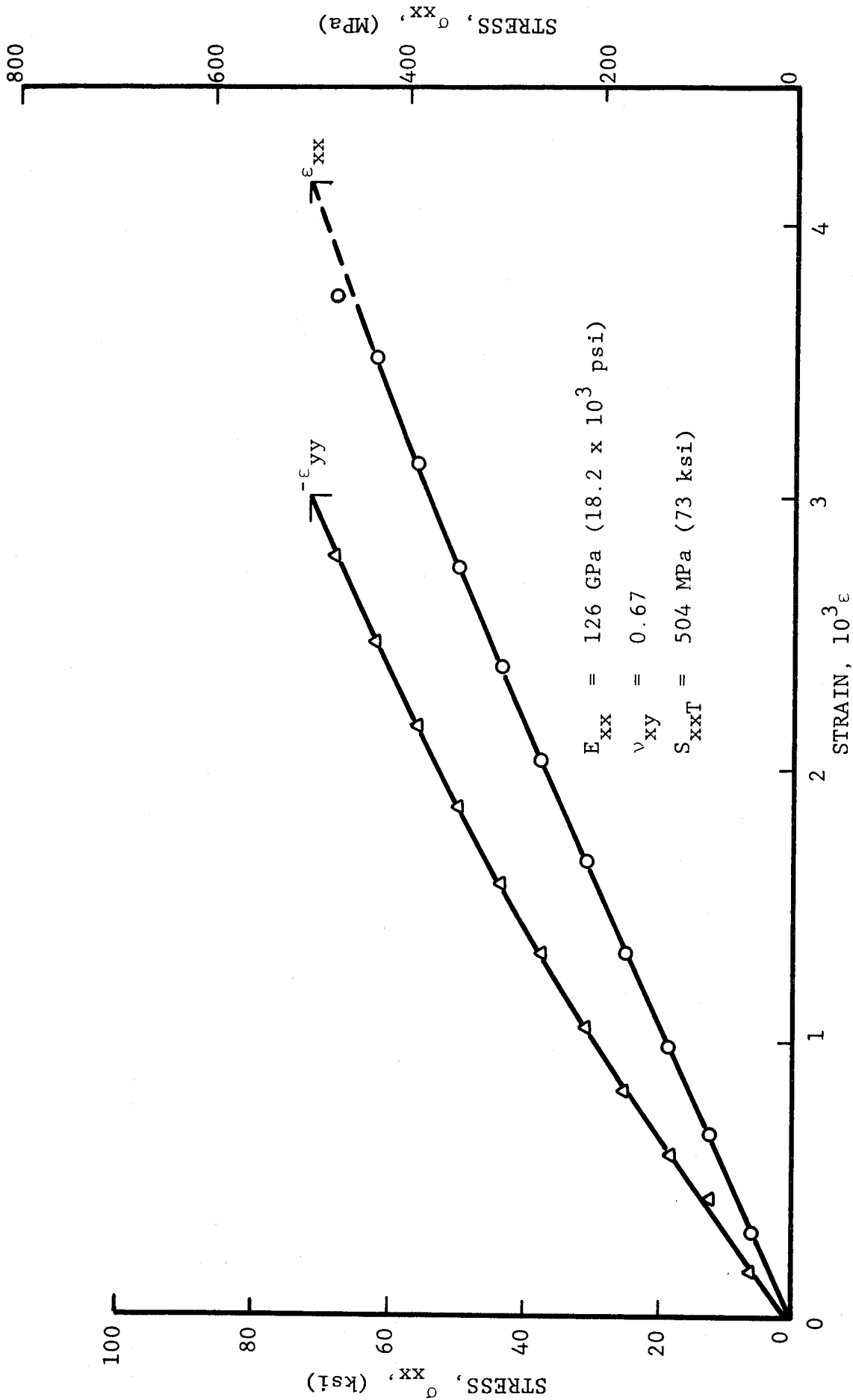ν_{xy} = 0.85
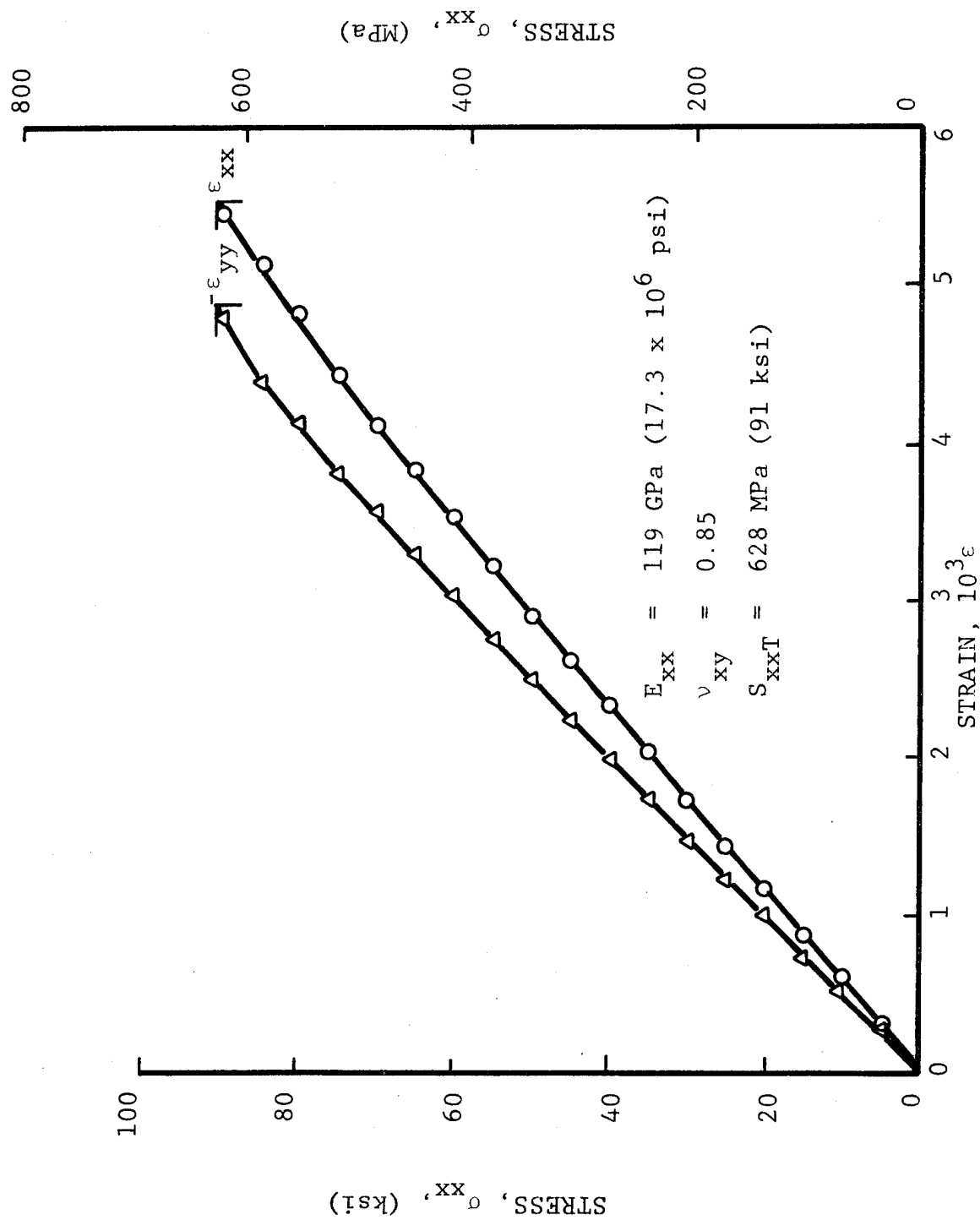
S_{xxT} = 628 MPa (91 ksi)

Fig. 5-84 STRESS-STRAIN CURVES FOR $[0_2/\pm 45]_s$ BORON/POLYIMIDE SPECIMEN UNDER UNIAXIAL TENSILE LOADING AFTER 100 THERMAL CYCLES BETWEEN ROOM TEMPERATURE AND 533 degK (500°F) UNDER TENSILE LOADING OF 395 MPa (57 ksi)

E_{xx} = 115 GPa (16.7 x 10^6 psi)

ν_{xy} = 0.76
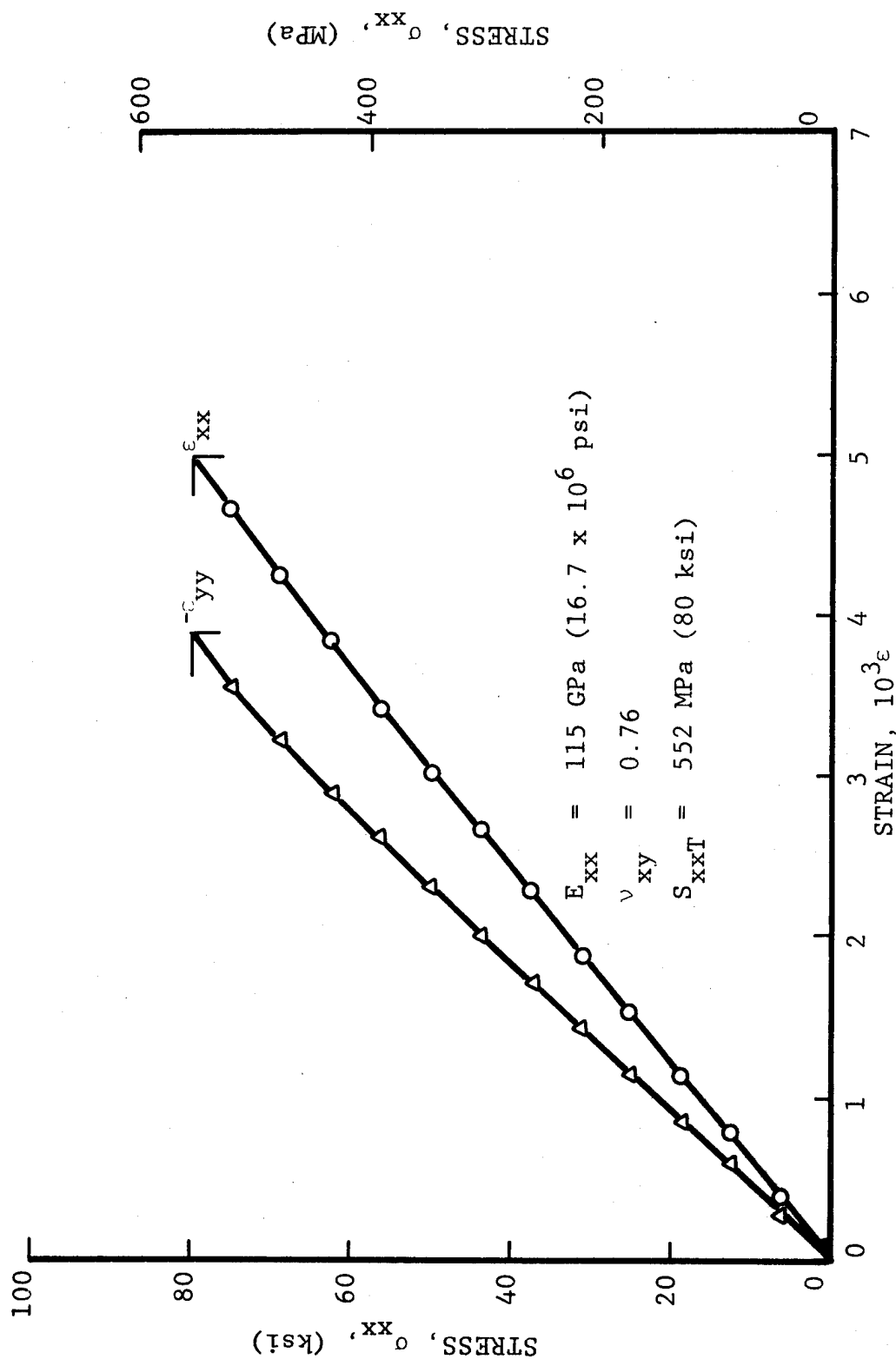
S_{xxT} = 552 MPa (80 ksi)
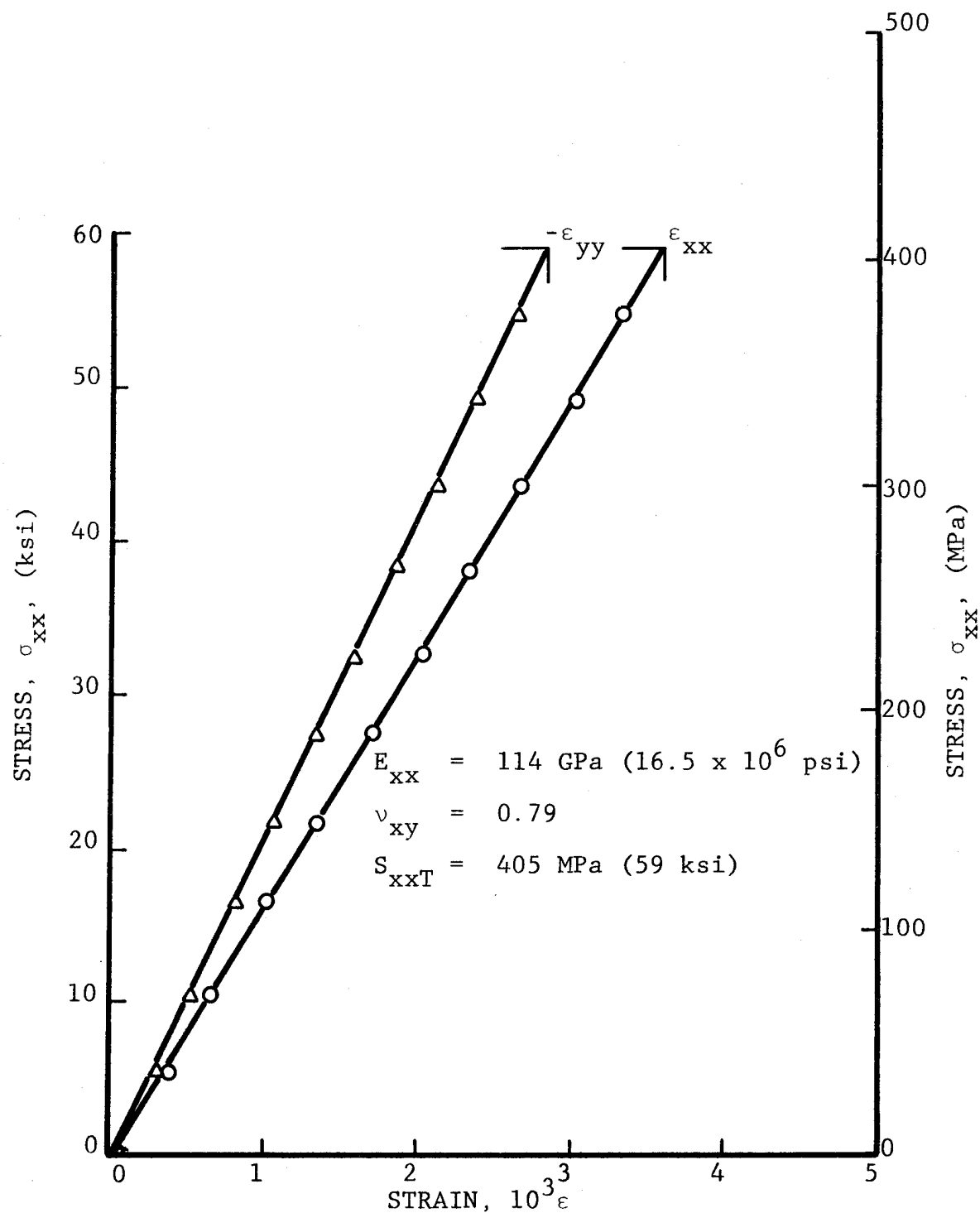
Fig. 5-85 STRESS-STRAIN CURVES FOR $[0_2/\pm45]_s$ GRAPHITE/POLYIMIDE
SPECIMEN UNDER UNIAXIAL TENSILE LOADING AFTER 100
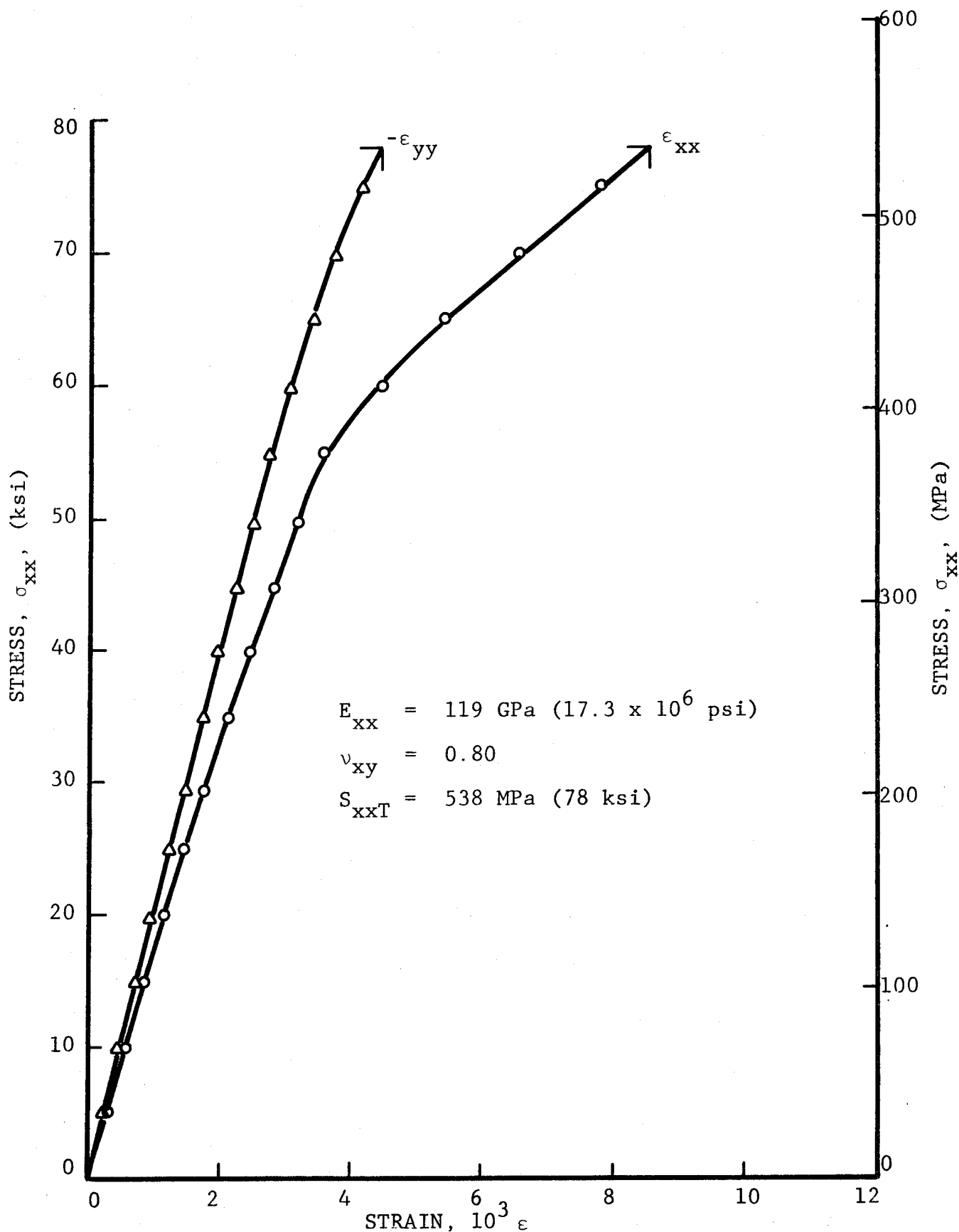THERMAL CYCLES BETWEEN ROOM TEMPERATURE AND 533 degK
(500°F) UNDER TENSILE LOADING OF 240 MPa (35 ksi)
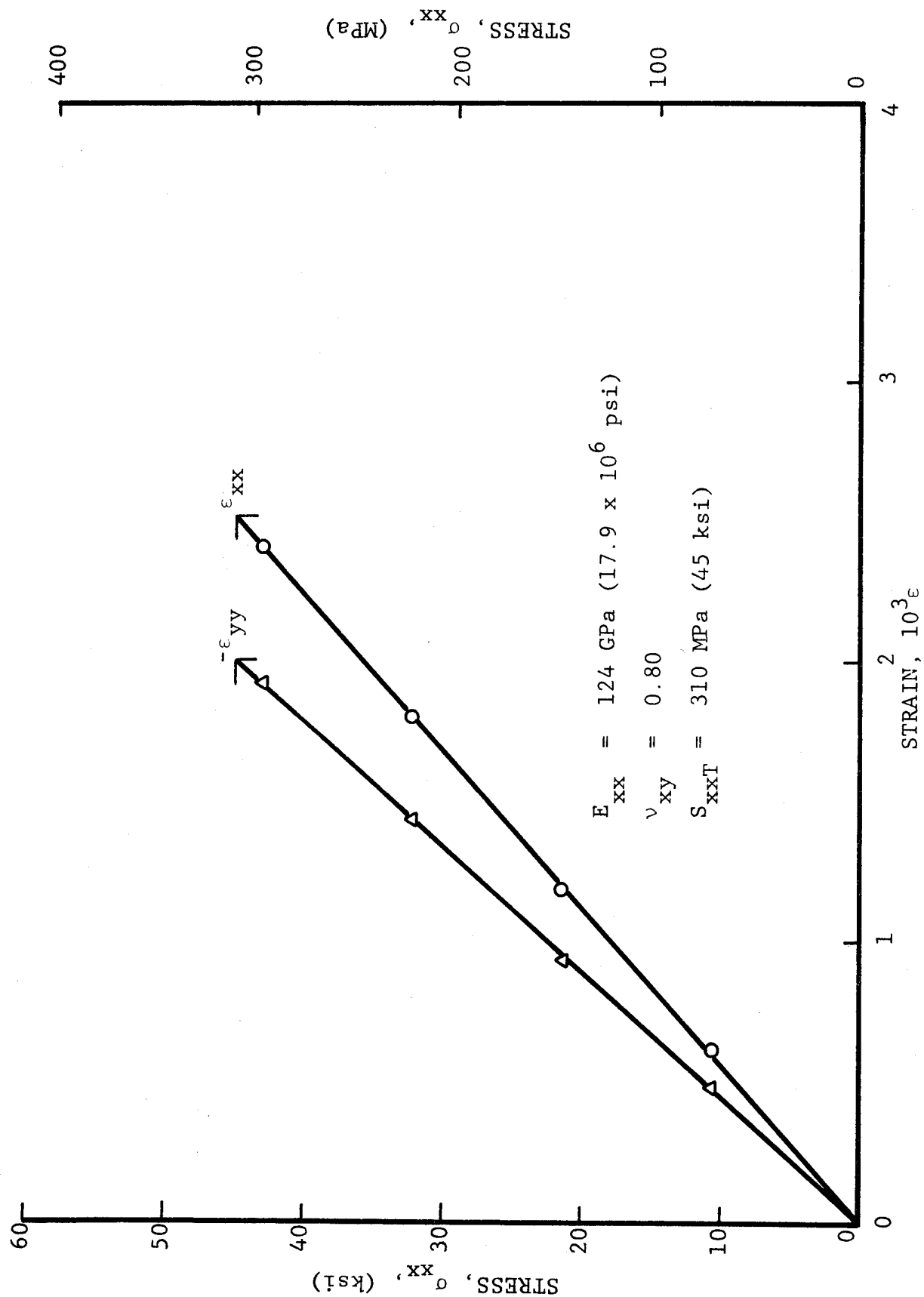
Fig. 5-86 STRESS-STRAIN CURVES FOR $[0_2/\pm 45]_s$ GRAPHITE/POLYIMIDE SPECIMEN UNDER UNIAXIAL TENSILE LOADING AFTER 100 THERMAL CYCLES BETWEEN ROOM TEMPERATURE AND 533 degK (500°F) UNDER UNDER TENSILE LOADING OF 240 MPa (35 ksi)
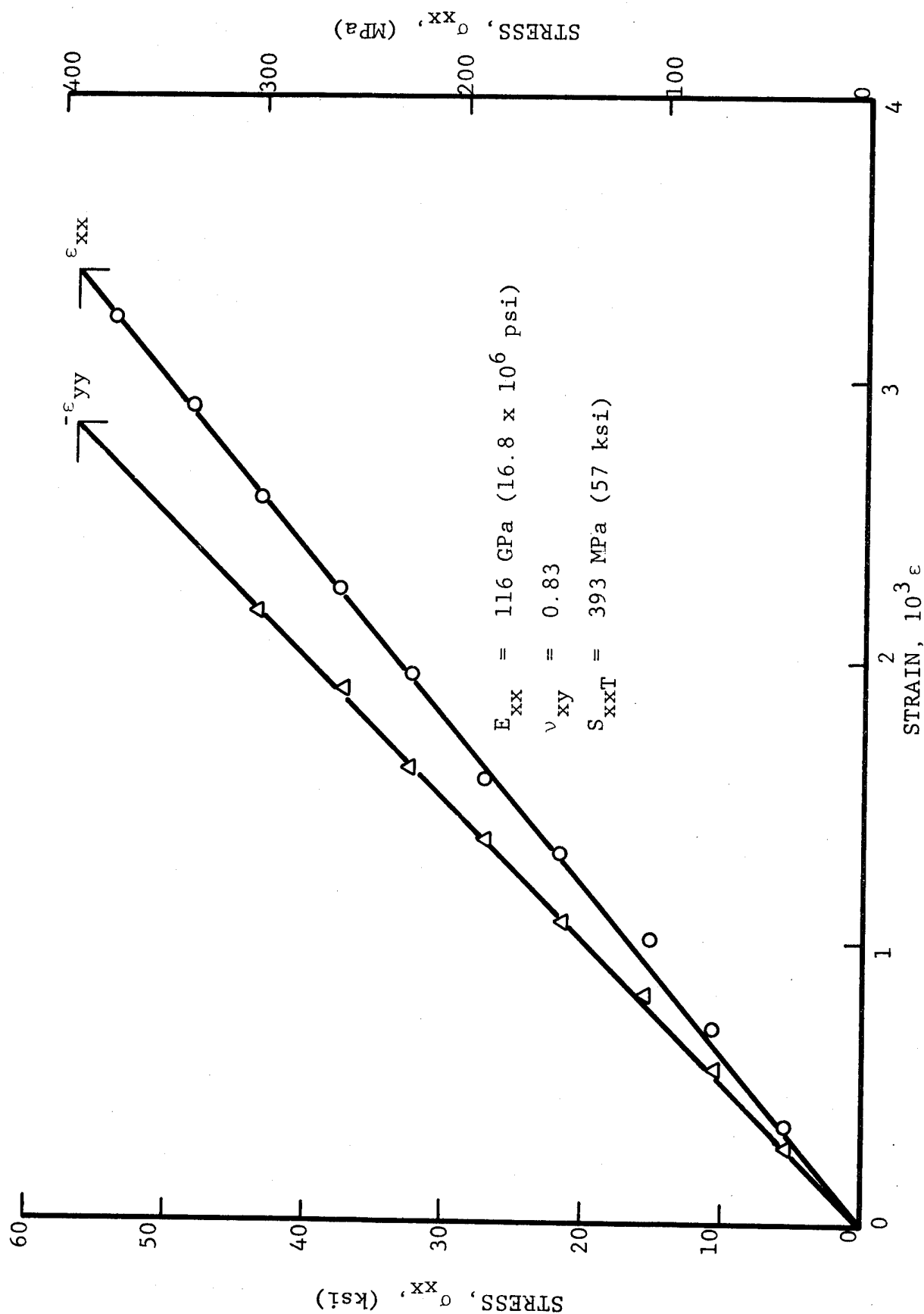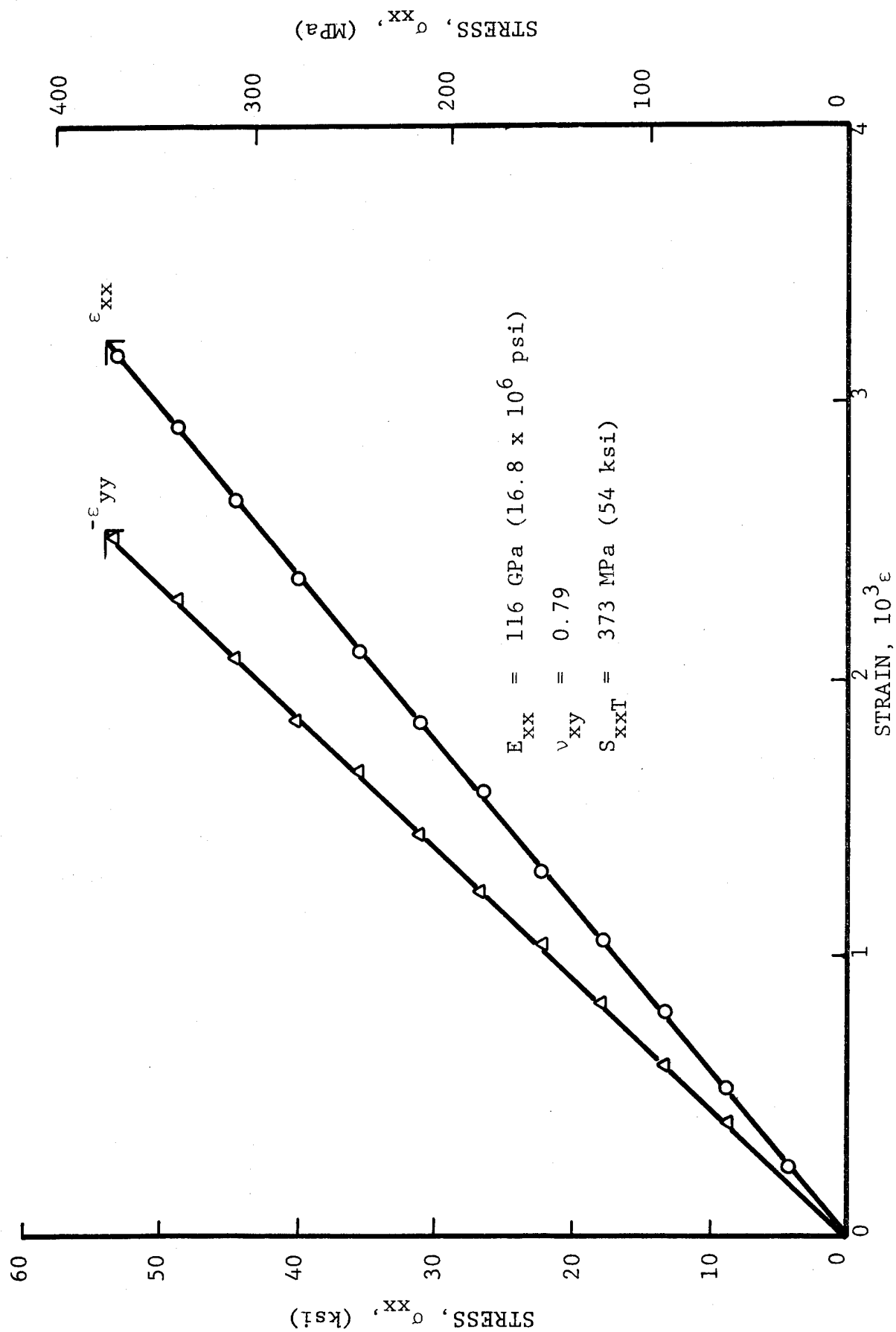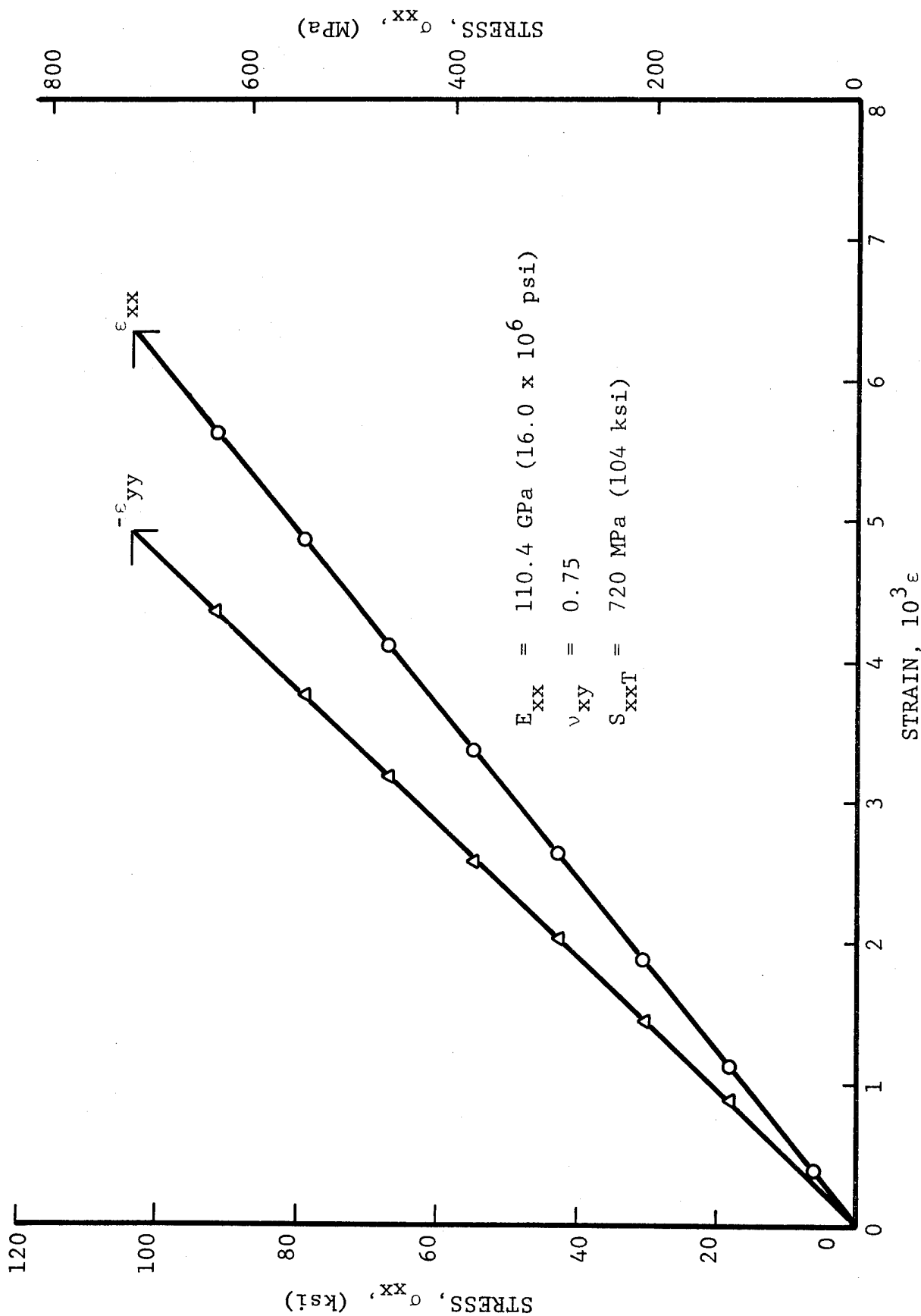
Fig. 5-87 STRAINS IN $[0_2/\pm 45]_s$ BORON/EPOXY SPECIMEN UNDER UNIAXIAL TENSILE LOADING AFTER 100 THERMAL CYCLES BETWEEN ROOM TEMPERATURE AND 200 degK (-100°F) UNDER TENSILE LOADING OF 510 MPa (74 ksi)

The figure contains the following labels and values:

STRESS, σ_{xx}, (MPa)

STRESS, σ_{xx}, (ksi)

STRAIN, $10^3 \varepsilon$

ε_{xx}

$-\varepsilon_{yy}$

E_{xx} = 115 GPa (16.6 x 10^6 psi)

ν_{xy} = 0.70
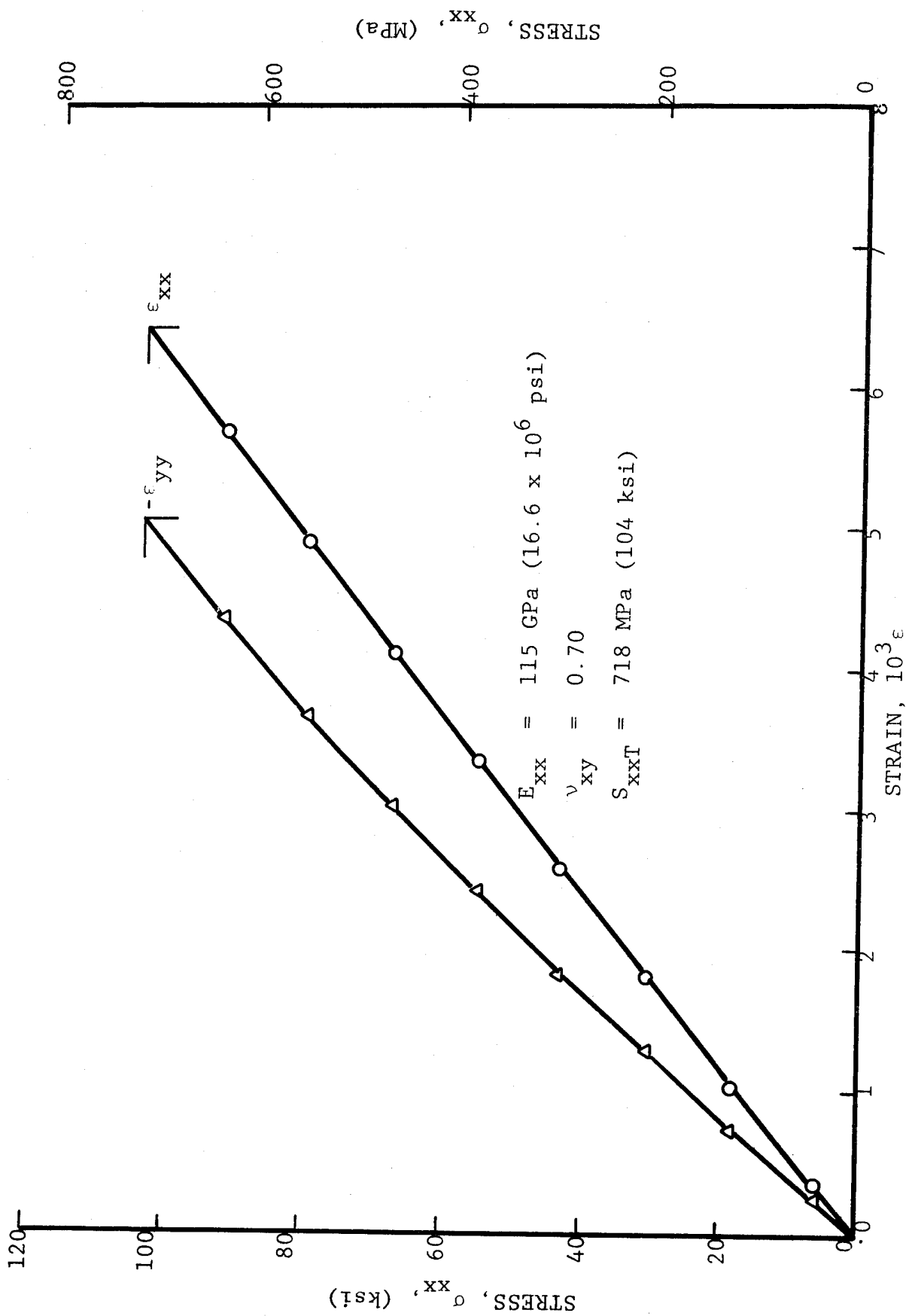
S_{xxT} = 718 MPa (104 ksi)

Fig. 5-88 STRAINS IN $[0_2/\pm 45]_s$ BORON/EPOXY SPECIMEN UNDER UNIAXIAL TENSILE LOADING AFTER 100 THERMAL CYCLES BETWEEN ROOM TEMPERATURE AND 200 degK (-100°F) UNDER TENSILE LOADING OF 510 MPa (74 ksi)
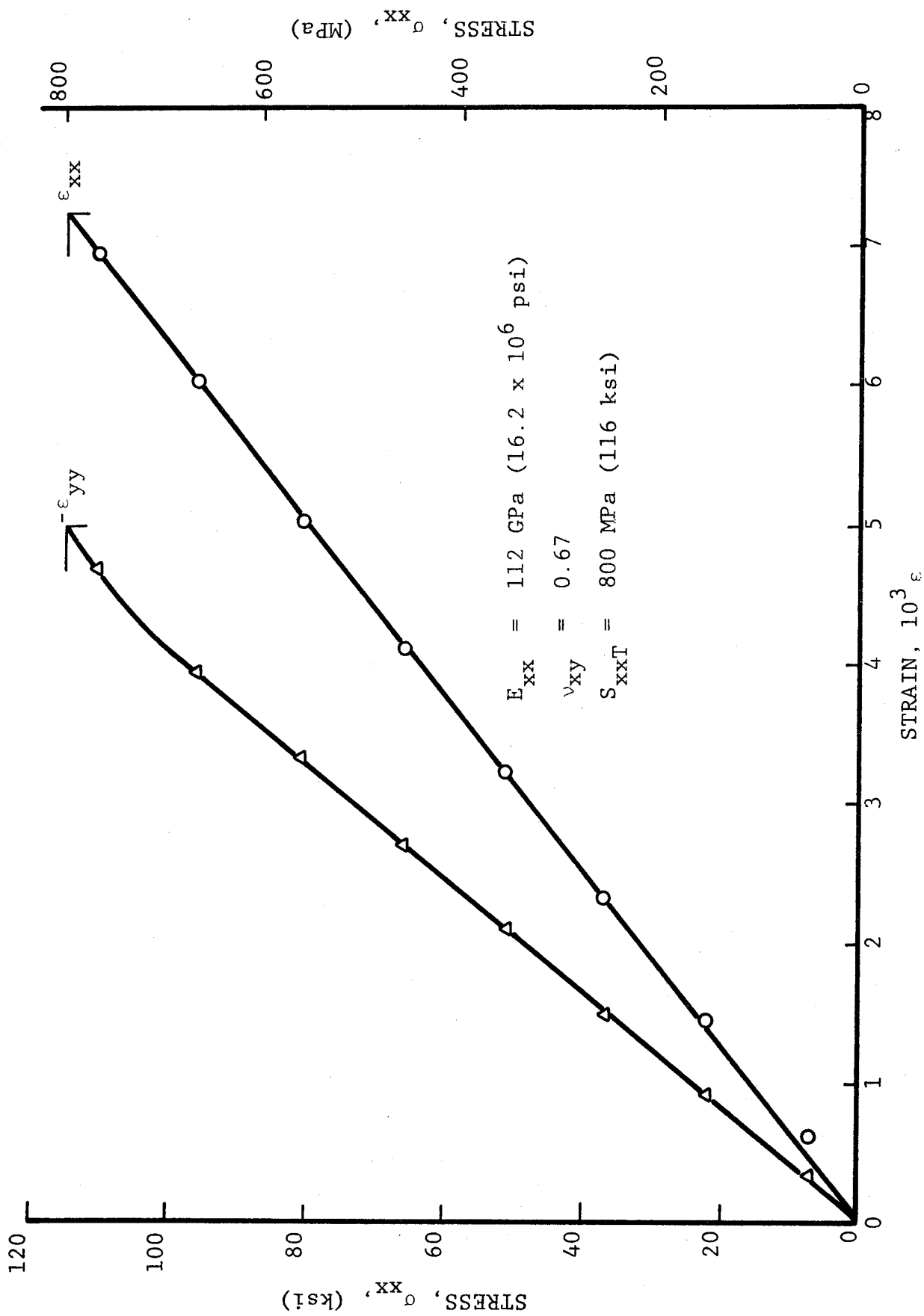
E_{xx} = 112 GPa (16.2 x 10^6 psi)
ν_{xy} = 0.73
S_{xxT} = 798 MPa (116 ksi)

Fig. 5-89 STRAINS IN $[0_2/\pm 45]_s$ BORON/POLYIMIDE SPECIMEN UNDER UNIAXIAL TENSILE LOADING AFTER 100 THERMAL CYCLES BETWEEN ROOM TEMPERATURE AND 200 degK (-100°F) UNDER TENSILE LOADING OF 395 MPa (57 ksi)
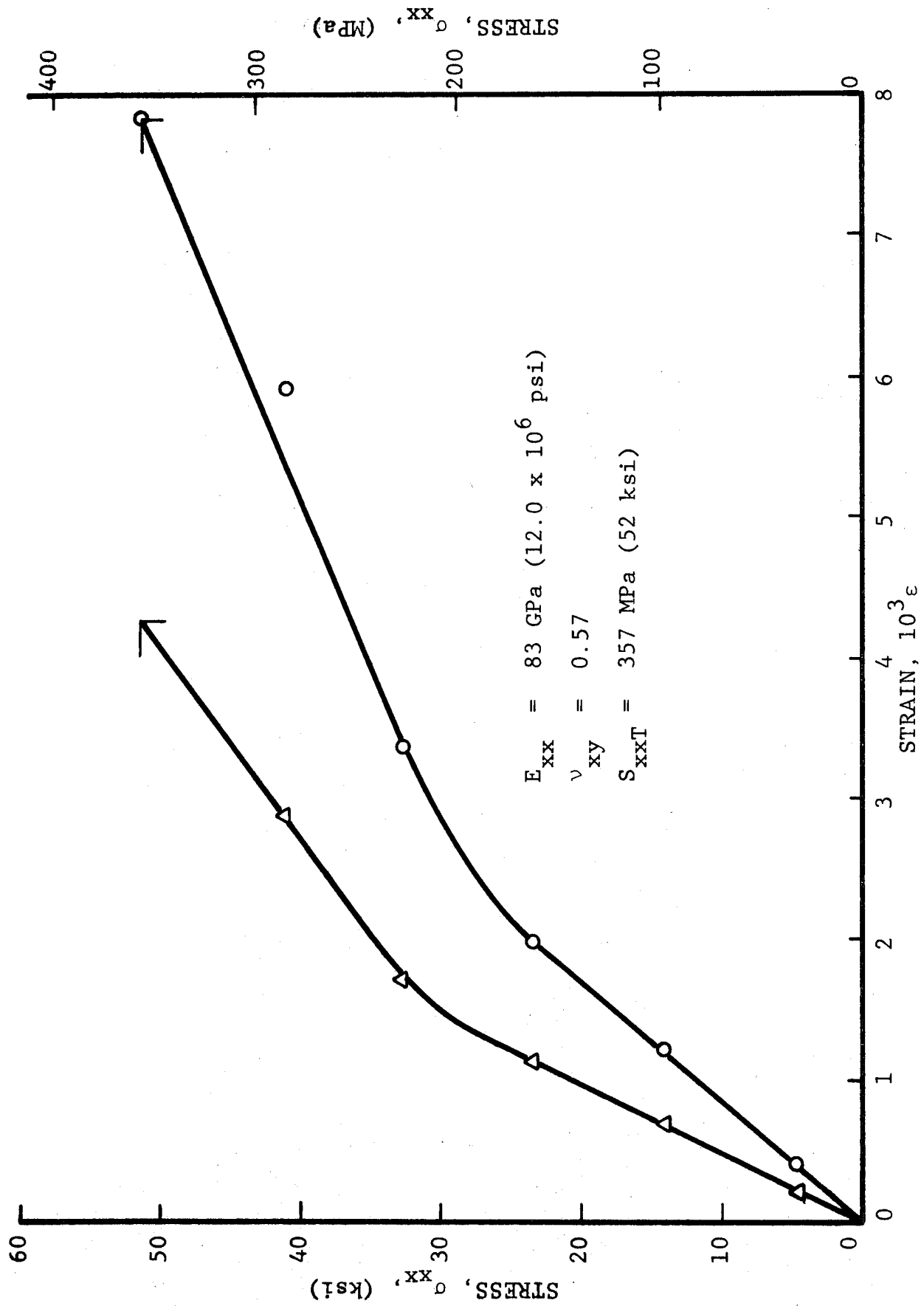
E_{xx} = 113 GPa (16.4 x 10^6 psi)

ν_{xy} = 0.81

S_{xxT} = 489 MPa (71 ksi)

Fig. 5-90 STRAINS IN $[0_2/\pm45]_s$ BORON/POLYIMIDE SPECIMEN UNDER UNIAXIAL TENSILE LOADING AFTER 100 THERMAL CYCLES BETWEEN ROOM TEMPERATURE AND 200 degK (-100°F) UNDER TENSILE LOADING OF 395 MPa (57 ksi)

E_{xx} = 117 GPa (17.0 x 10^6 psi)
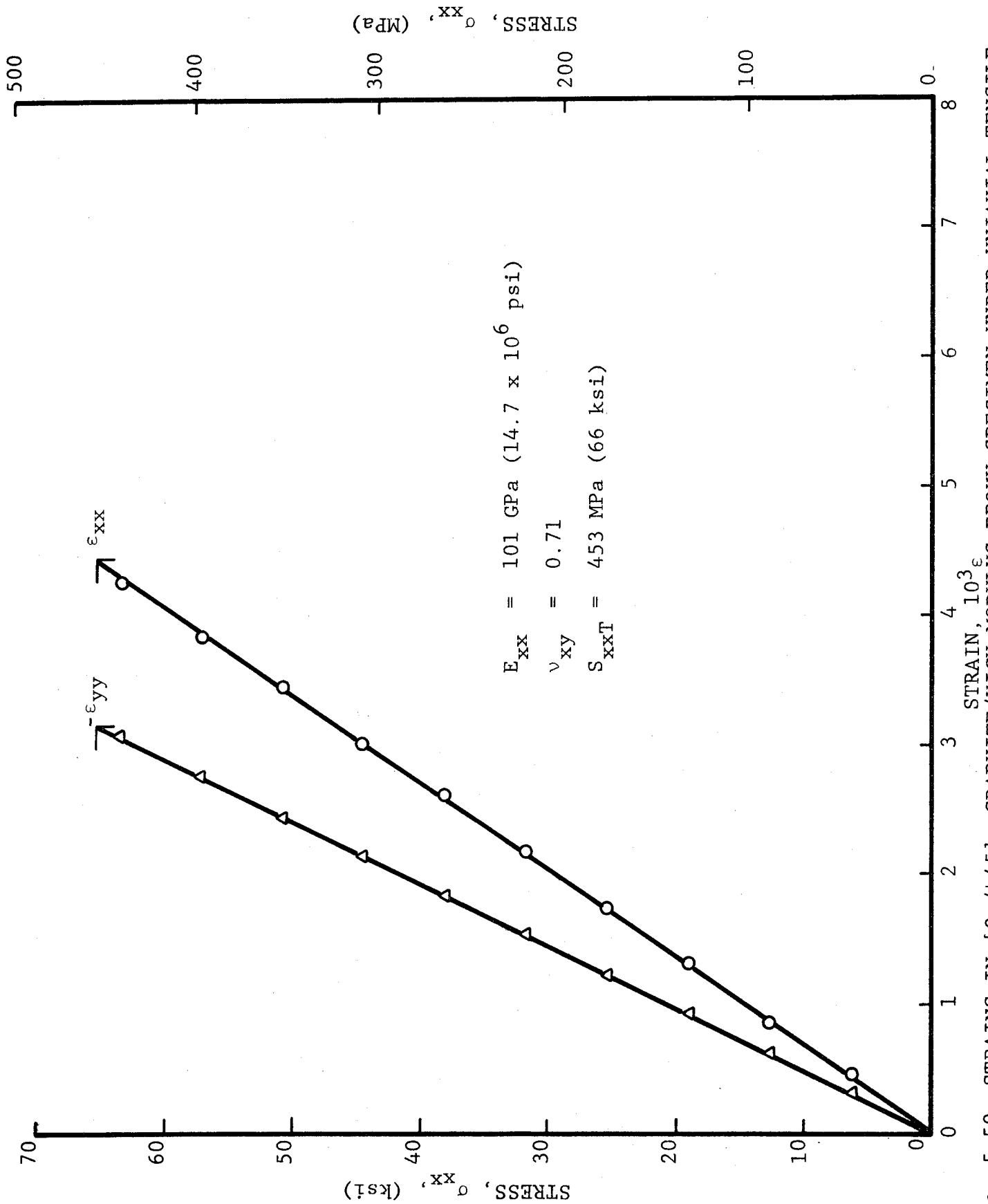
ν_{xy} = 0.74
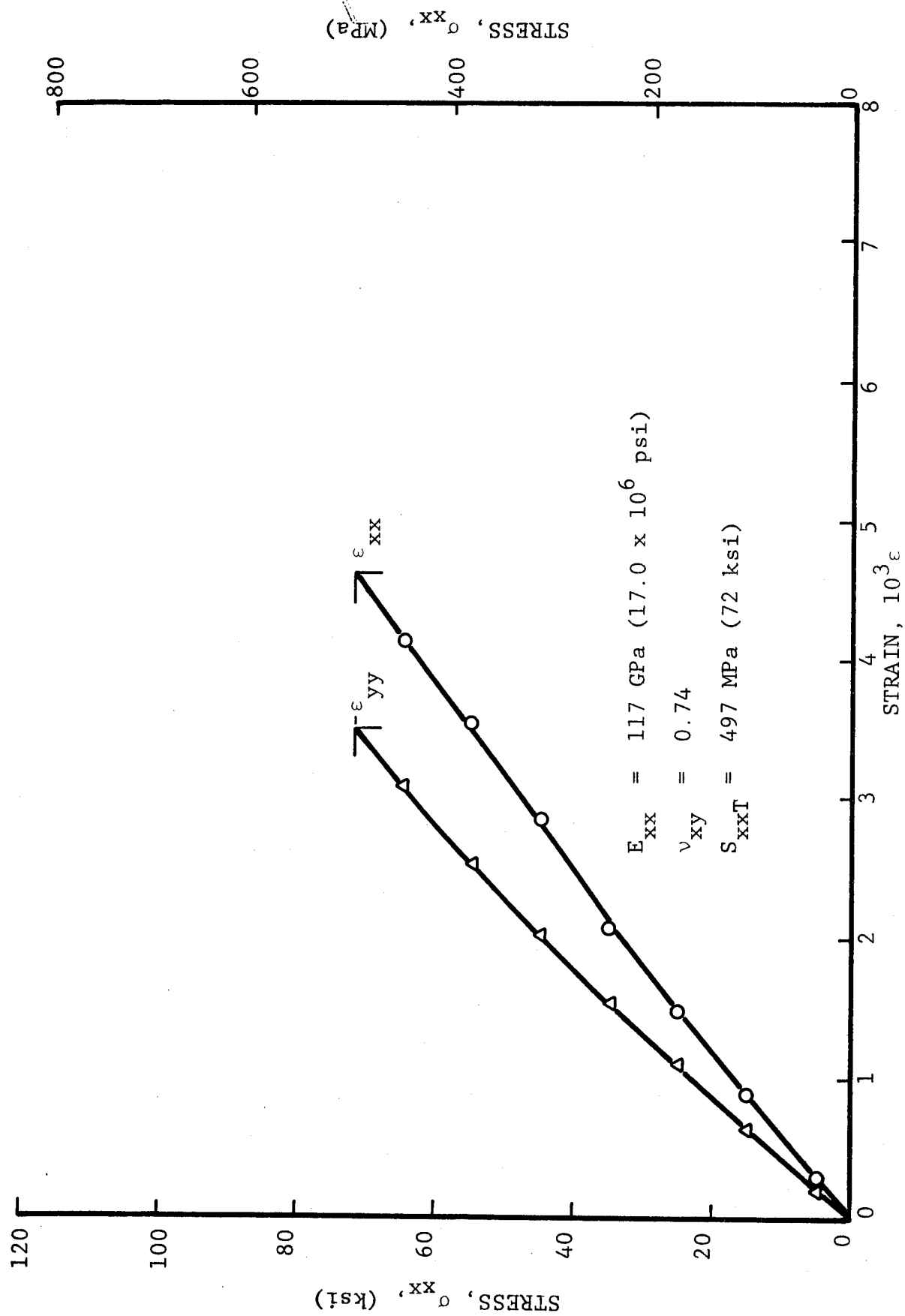
S_{xxT} = 497 MPa (72 ksi)

Fig. 5-91 STRAINS IN [0₂/±45]ₛ GRAPHITE/LOW MODULUS EPOXY SPECIMEN UNDER UNIAXIAL TENSILE LOADING AFTER 100 THERMAL CYCLES BETWEEN ROOM TEMPERATURE AND 200 degK (-100°F) UNDER TENSILE LOADING OF 395 MPa (57 ksi)
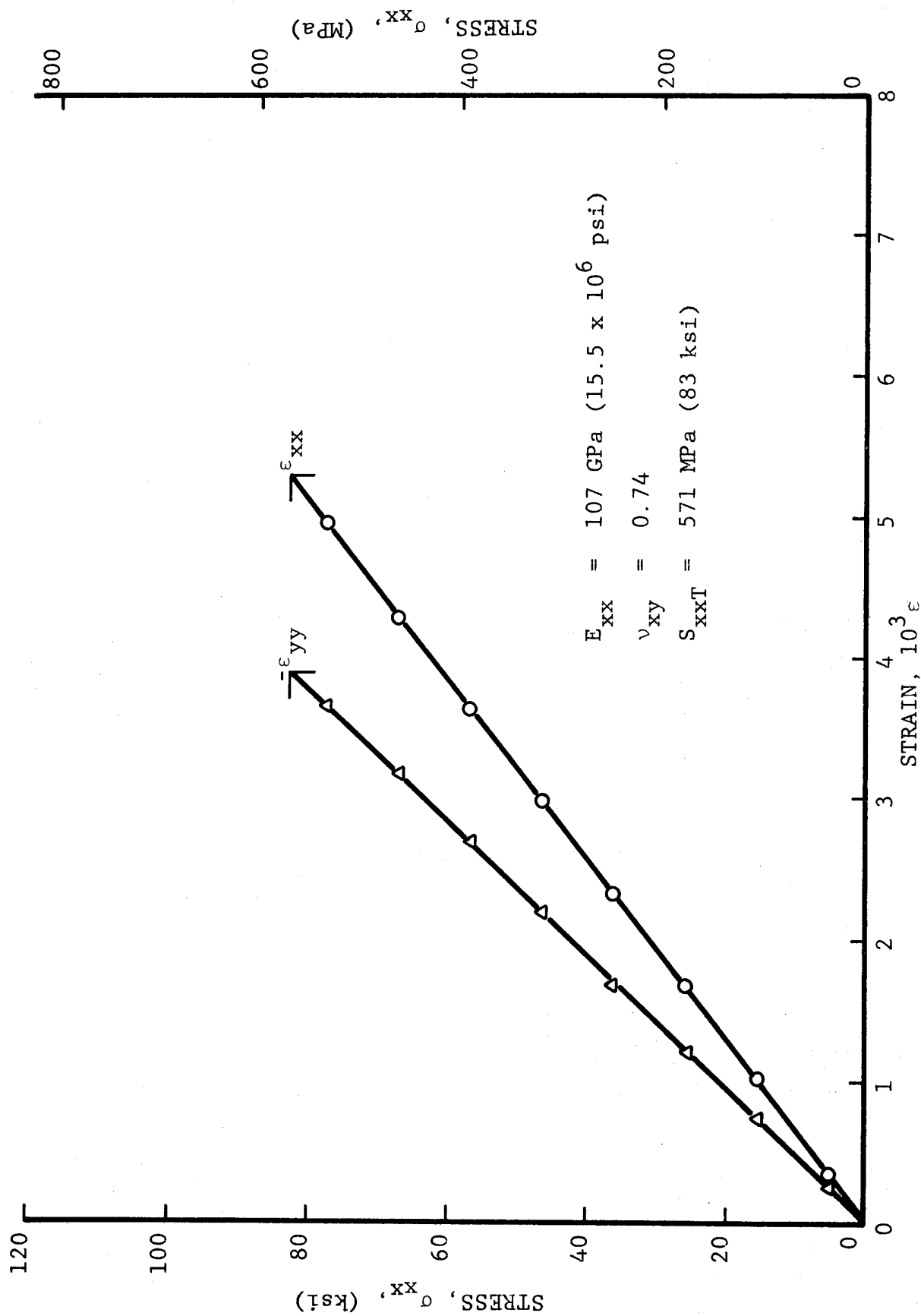
E_{xx} = 91 GPa (13.2 x 10⁶ psi)

ν_{xy} = 0.60

S_{xxT} = 477 MPa (69 ksi)
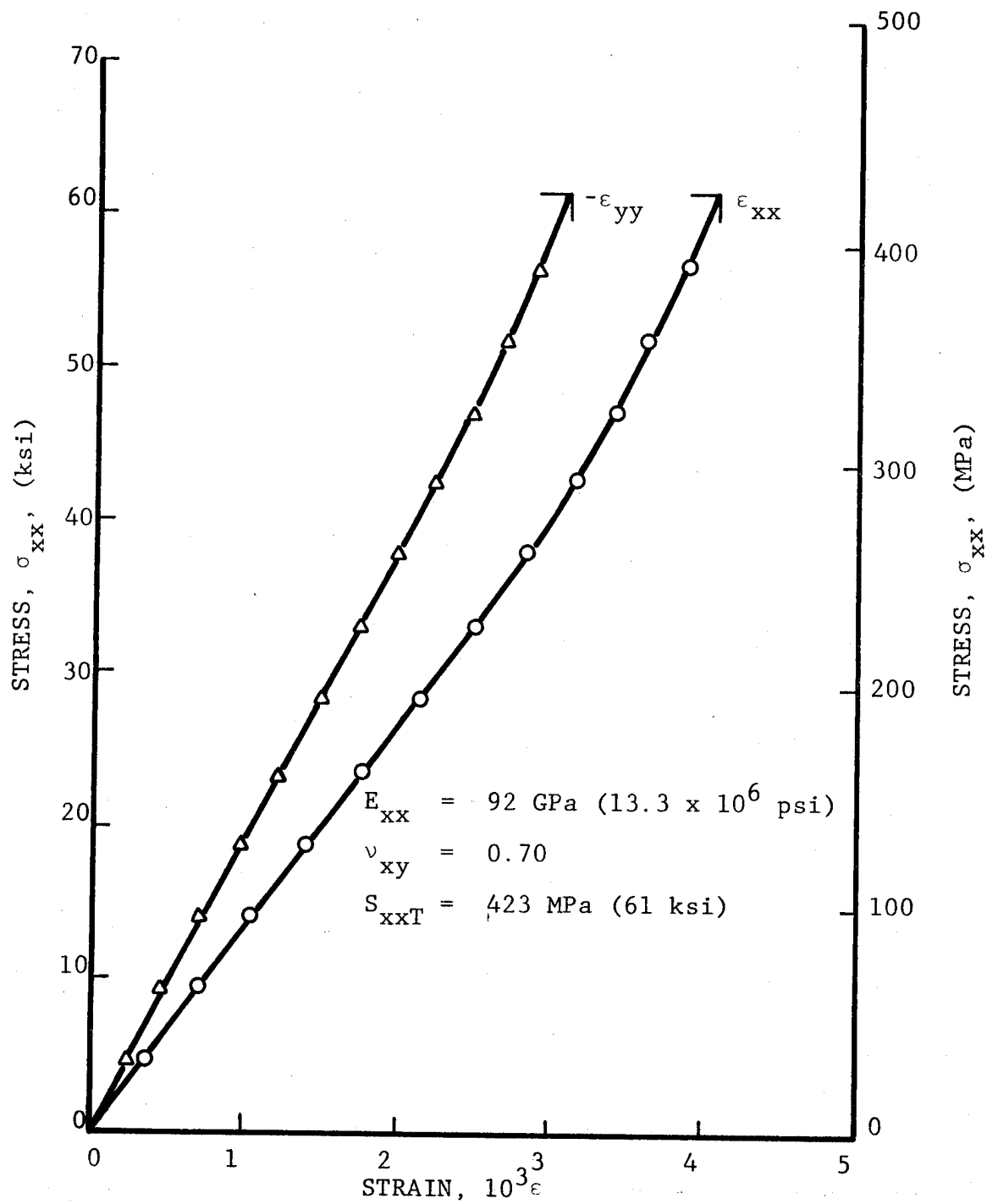
Fig. 5-92 STRAINS IN $[0_2/\pm 45]_s$ GRAPHITE/LOW MODULUS EPOXY SPECIMEN
UNDER UNIAXIAL TENSILE LOADING AFTER 100 THERMAL CYCLES
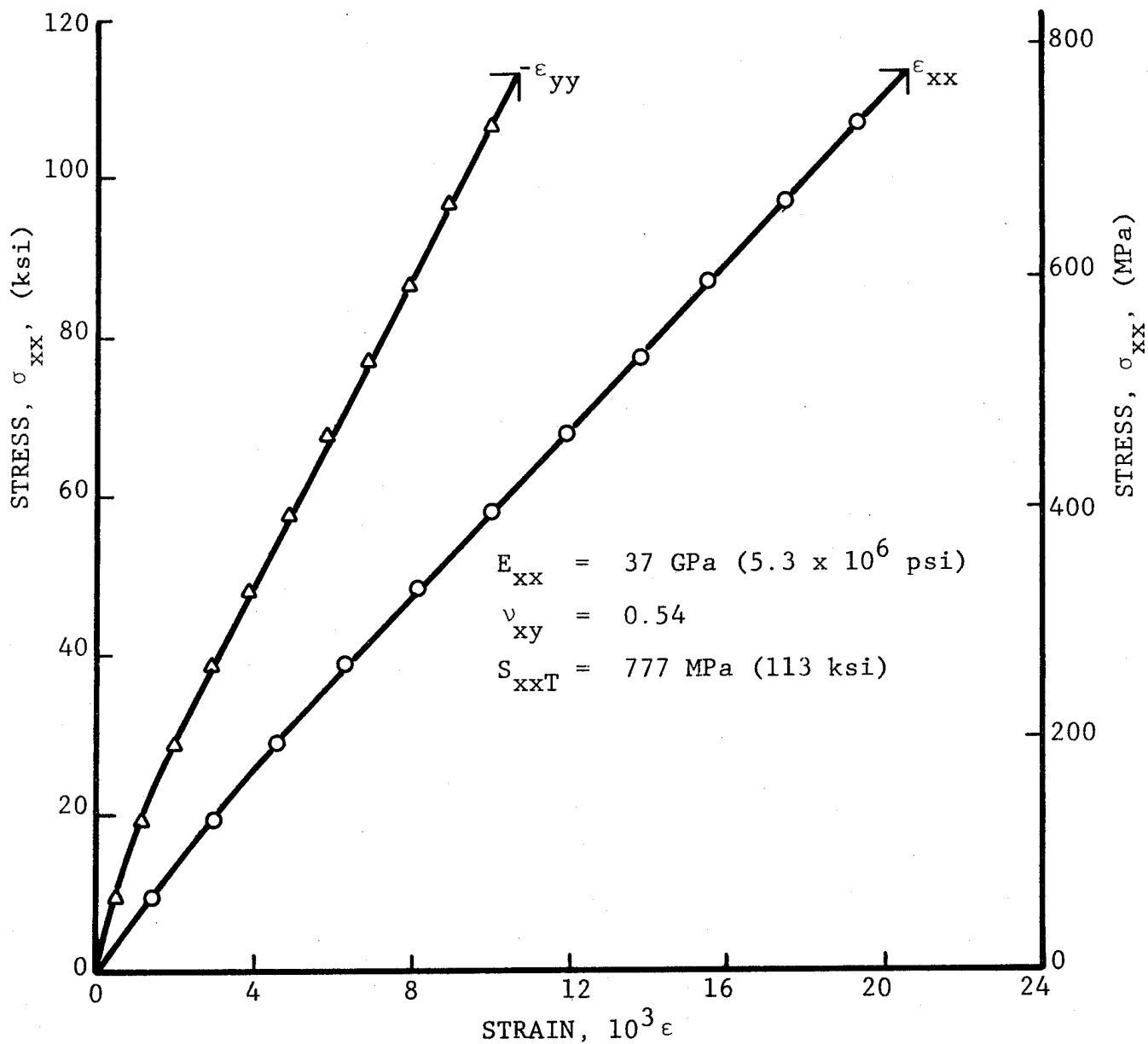BETWEEN ROOM TEMPERATURE AND 200 degK (-100°F) UNDER
TENSILE LOADING OF 395 MPa (57 ksi)

5-121

Fig. 5-93 STRAINS IN $[0_2/\pm45]_s$ GRAPHITE/HIGH MODULUS EPOXY SPECIMEN UNDER UNIAXIAL TENSILE LOADING AFTER 100 THERMAL CYCLES BETWEEN ROOM TEMPERATURE AND 200 degK (-100°F) UNDER TENSILE LOADING OF 340 MPa (49 ksi)
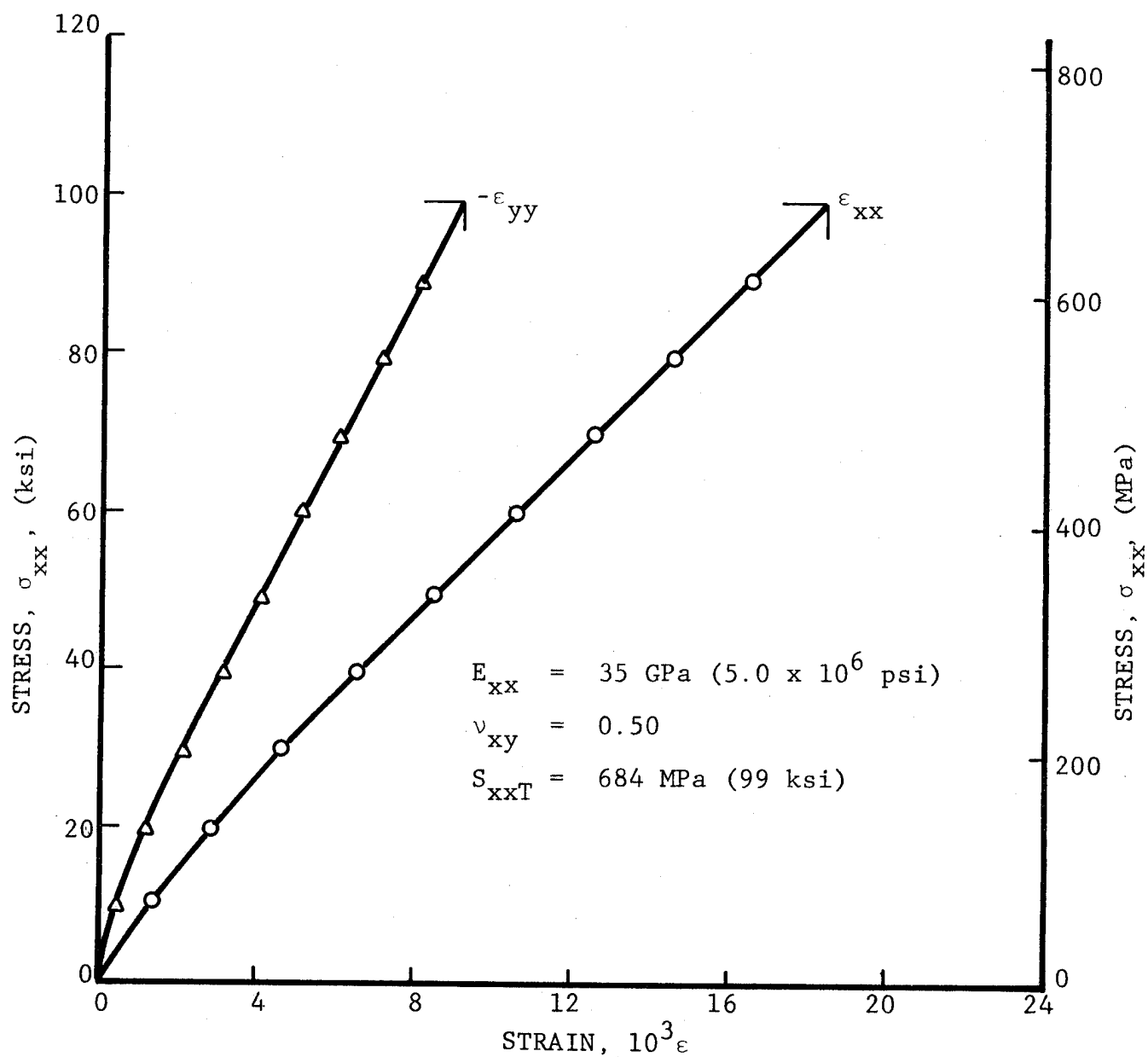
E_{xx} = 108 GPa (15.7 x 10^6 psi)

ν_{xy} = 0.71
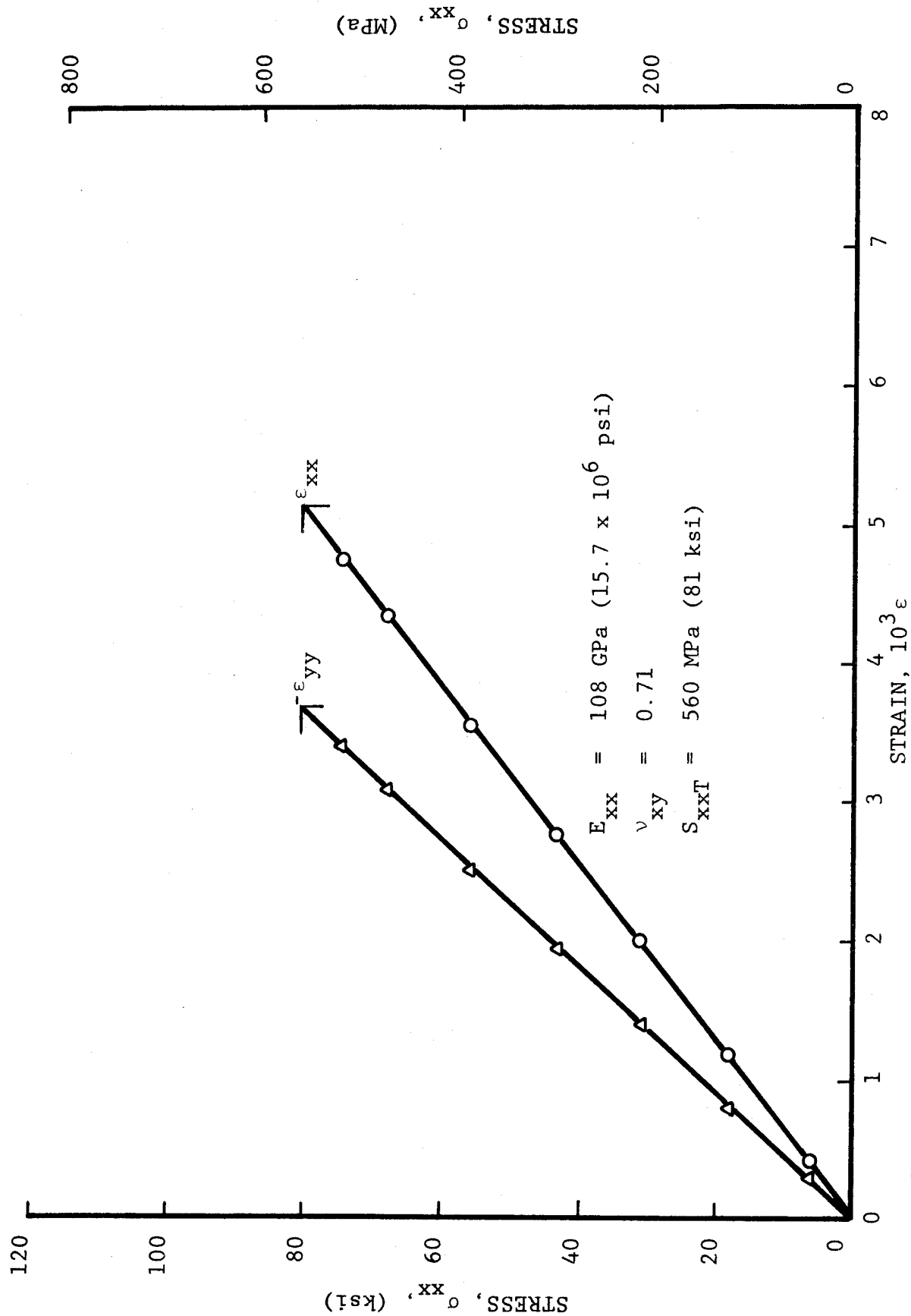
S_{xxT} = 560 MPa (81 ksi)

Fig. 5-94 STRAINS IN $[0_2/\pm45]_s$ GRAPHITE/HIGH MODULUS EPOXY SPECIMEN UNDER UNIAXIAL TENSILE
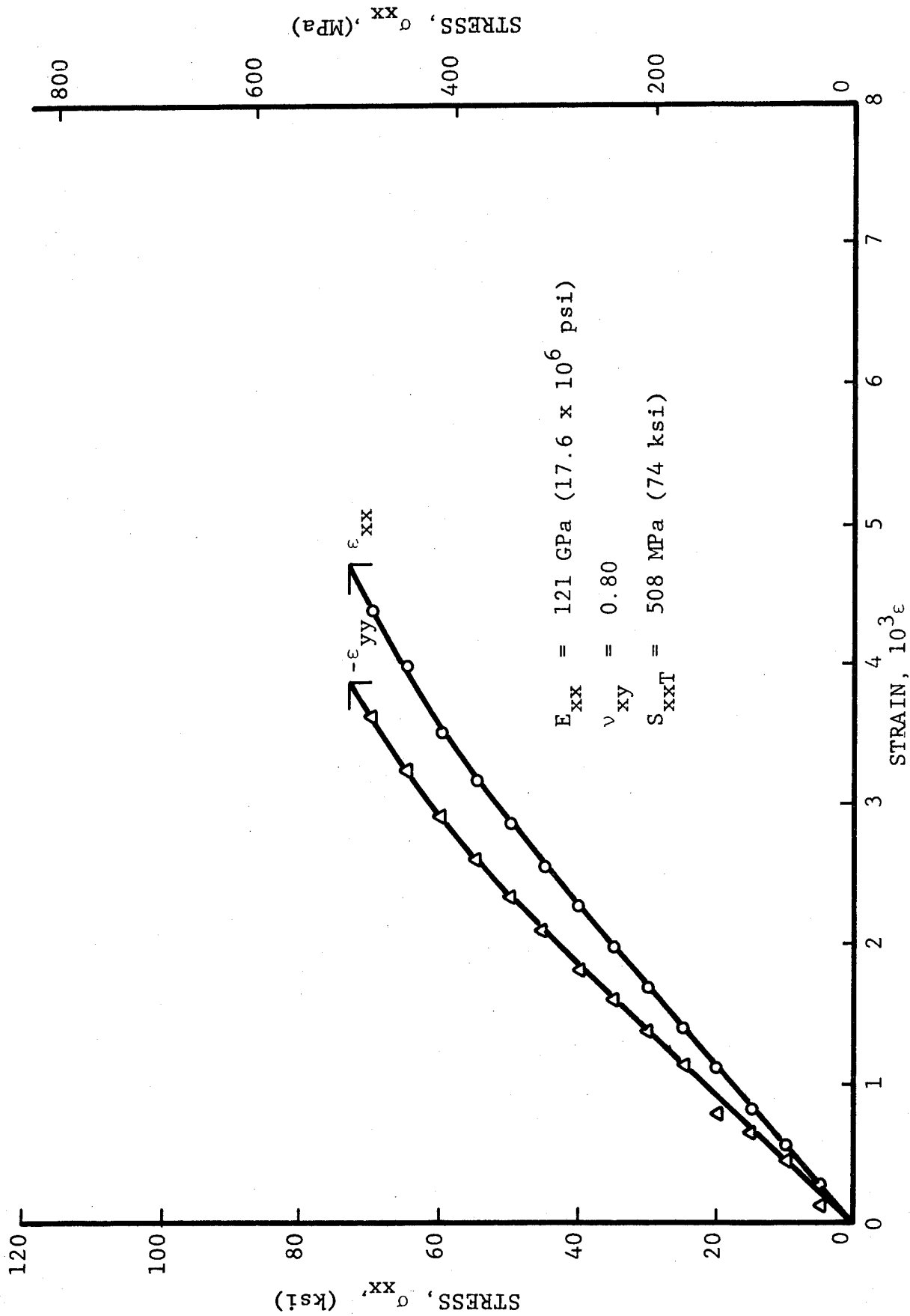LOADING AFTER 100 THERMAL CYCLES BETWEEN ROOM TEMPERATURE AND 200 degK (-100°F)
UNDER TENSILE LOADING OF 340 MPa (49 ksi)

The following values appear within the figure:

E_{xx} = 106 GPa (15.4 x 10^6 psi)

ν_{xy} = 0.74
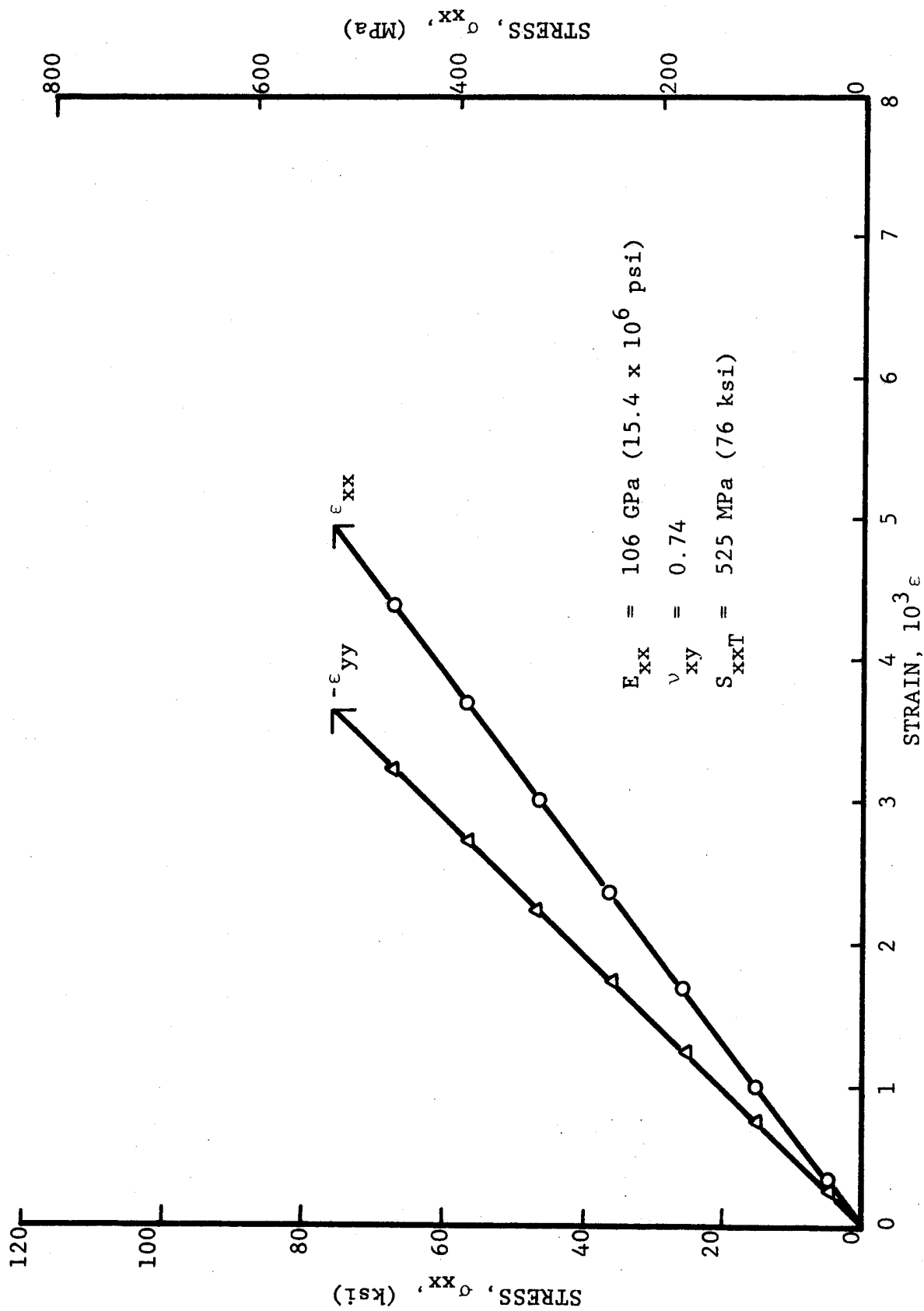
S_{xxT} = 525 MPa (76 ksi)

Fig. 5-95 STRAINS IN $[0_2/\pm45]_s$ GRAPHITE/POLYIMIDE SPECIMEN UNDER UNIAXIAL TENSILE LOADING AFTER 100 THERMAL CYCLES BETWEEN ROOM TEMPERATURE AND 200 degK (-100°F) UNDER TENSILE LOADING OF 240 MPa (35 ksi)
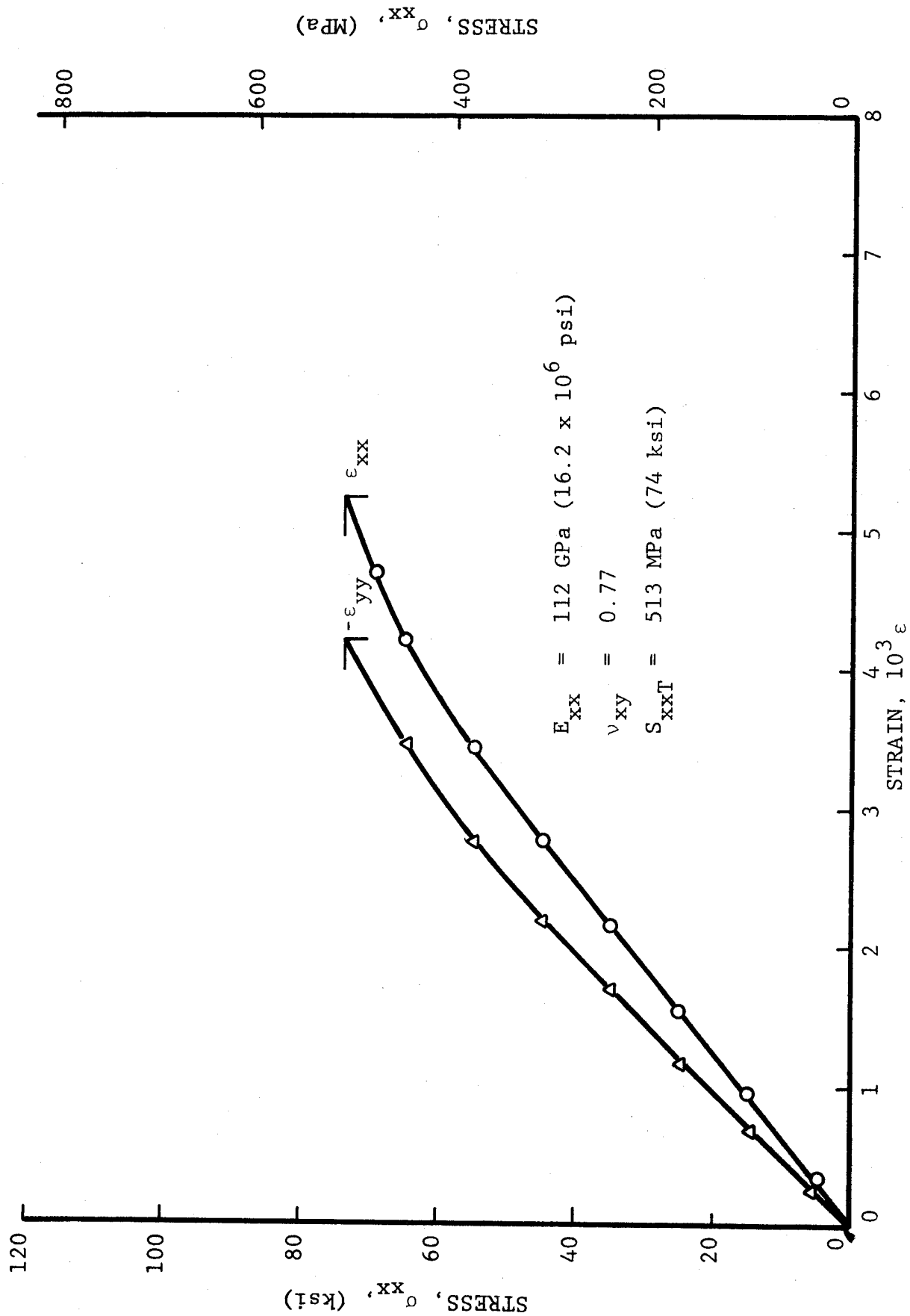
E_{xx} = 111 GPa (16.1 x 10^6 psi)

ν_{xy} = .0.83
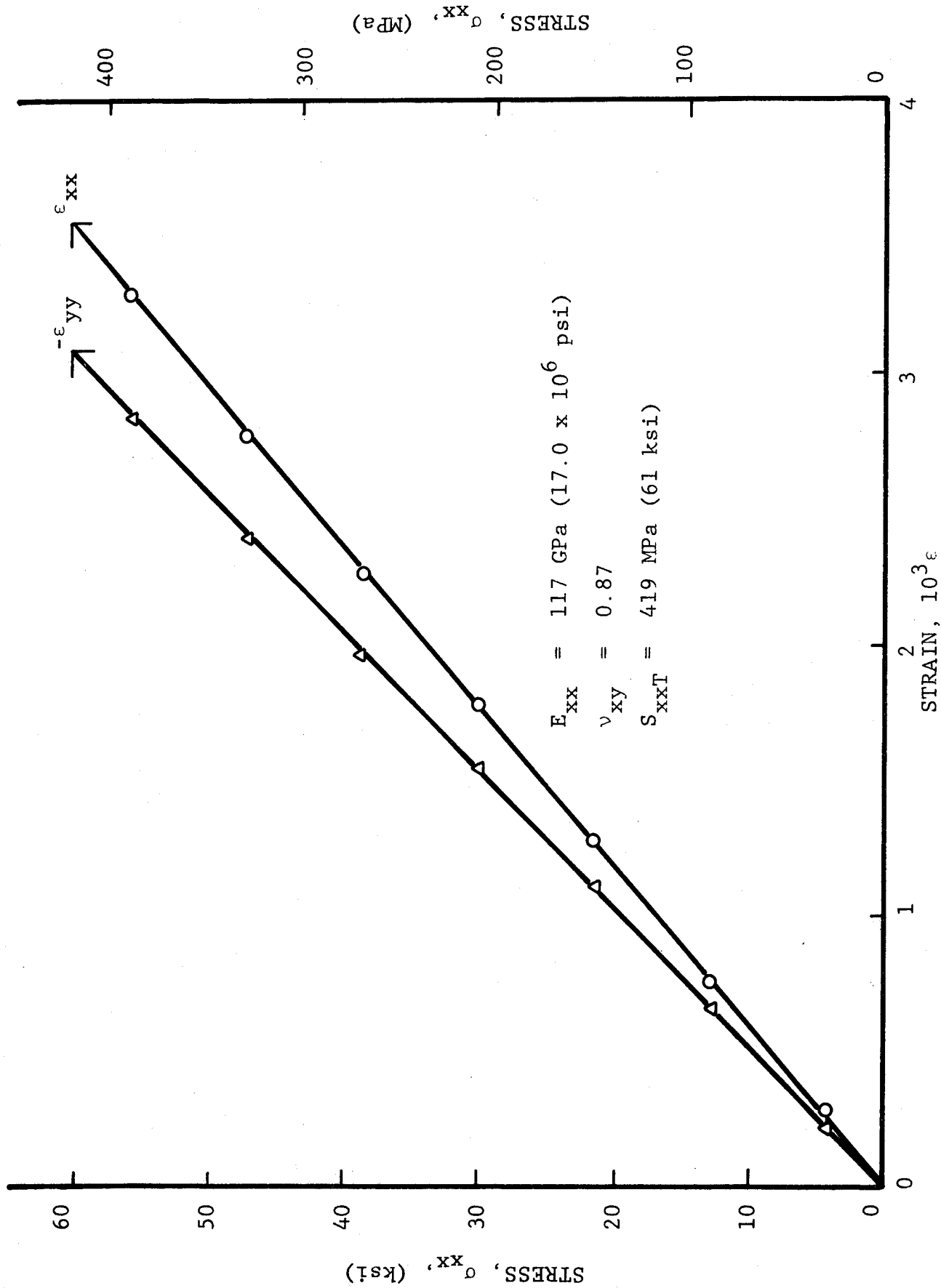
S_{xxT} = 350 MPa (51 ksi)

Fig. 5-96 STRAINS IN $[0_2/\pm 45]_s$ GRAPHITE/POLYIMIDE SPECIMEN UNDER UNIAXIAL TENSILE LOADING AFTER 100 THERMAL CYCLES BETWEEN ROOM TEMPERATURE AND 200 degK (-100°F) UNDER TENSILE LOADING OF 240 MPa (35 ksi)
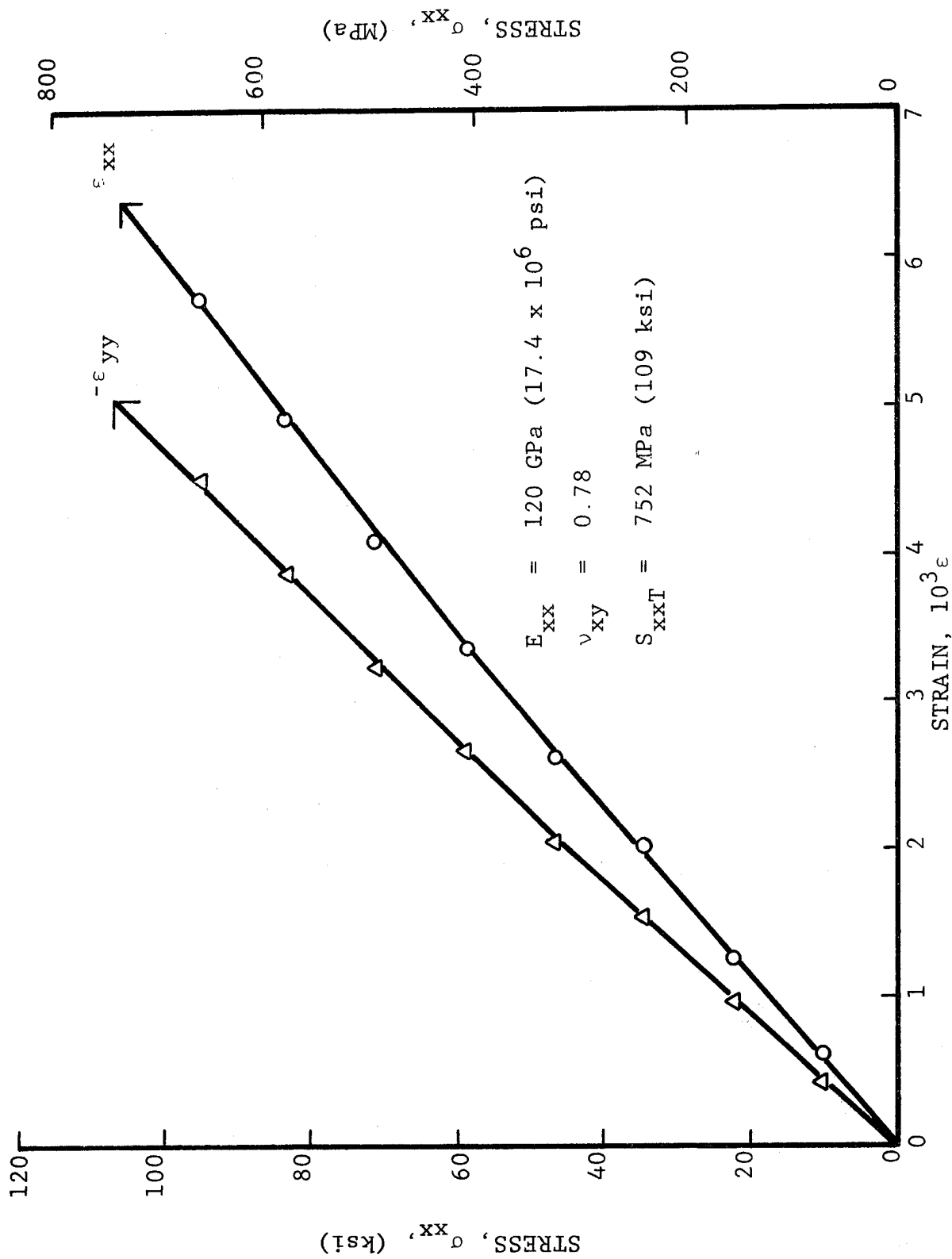
The figure includes the following annotations:

E_{xx} = 124.1 GPa (18.0 x 10^6 psi)

ν_{xy} = 0.82
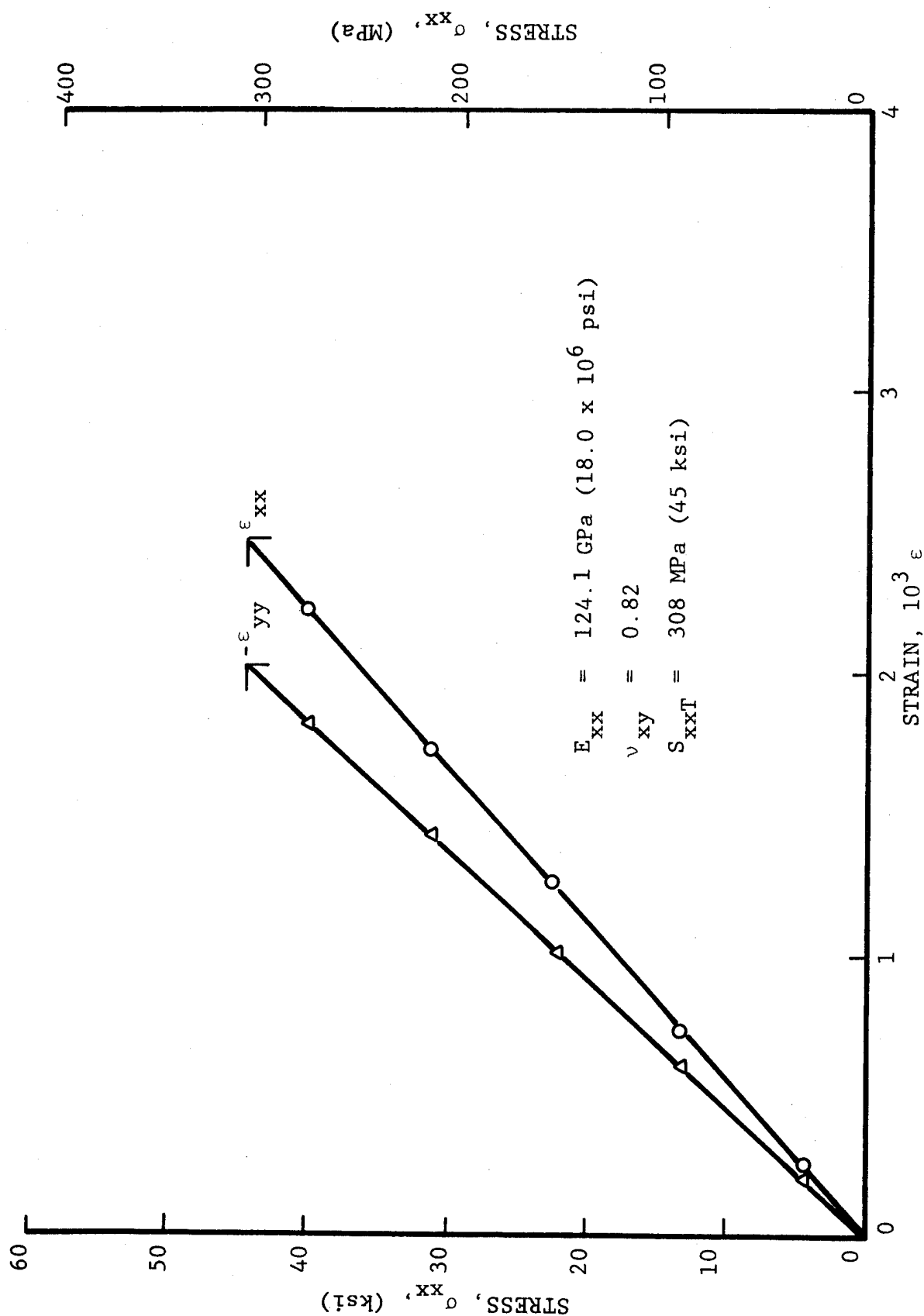
S_{xxT} = 308 MPa (45 ksi)
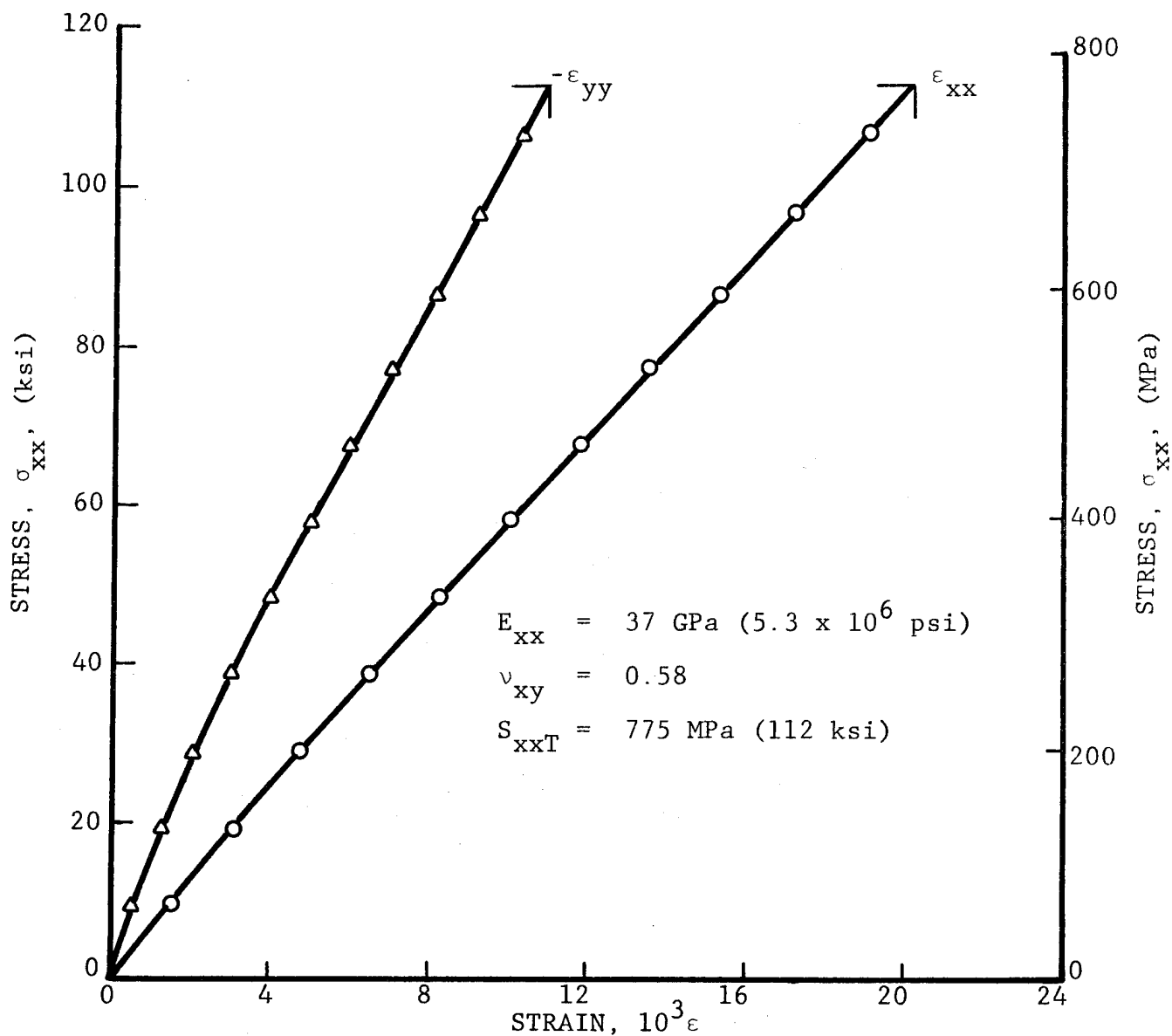
Fig. 5-97 STRAINS IN $[0_2/\pm45]_s$ S-GLASS/EPOXY SPECIMEN UNDER UNIAXIAL
TENSILE LOADING AFTER 100 THERMAL CYCLES BETWEEN ROOM
TEMPERATURE AND 200 degK (-100°F) UNDER TENSILE LOADING
OF 520 MPa (75 ksi)
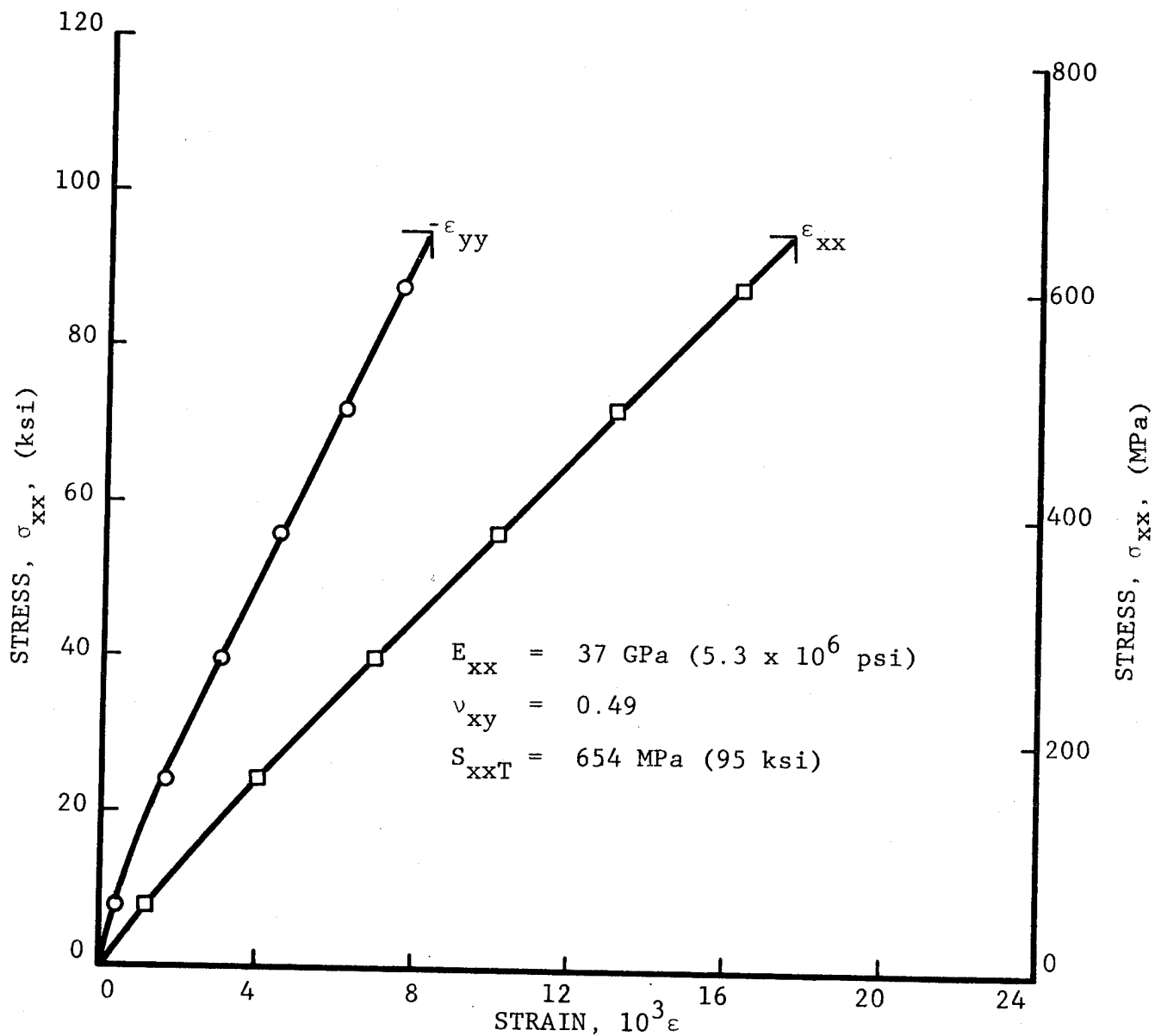
Fig. 5-98   STRAINS IN $[0_2/\pm 45]_s$ S-GLASS/EPOXY SPECIMEN UNDER UNIAXIAL
TENSILE LOADING AFTER 100 THERMAL CYCLES BETWEEN ROOM
TEMPERATURE AND 200 degK (-100°F) UNDER TENSILE LOADING
OF 520 MPa (75 ksi)

6.0   TASK V -- EFFECTS OF LAMINATE CONFIGURATION VARIABLES

6.1   Introduction

The objective of this task was to investigate the effects
on the magnitudes of residual stress and strength of ply stacking
sequence, ply orientation and fiber volume ratio. This investigation
was conducted only on the Graphite/Polyimide material. Specimens
with a lower fiber volume ratio than the one used in Tasks II, III
and IV, were tested to evaluate the effects of this parameter.
The effects of ply configuration (layup) were evaluated with specimens
of $[0_2/\pm15]_s$ and $[0_2/90_2]_s$ in addition to the $[0_2/\pm45]_s$ specimens
used in previous tasks. The effects of ply stacking sequence were
investigated with specimens of $[\pm45/0_2]_s$, $[0/+45/0/-45]_s$ and
$[+45/0_2/-45]_s$ layups. Six specimens, including three with embedded
instrumentation, were tested for each of the configuration variables
above.

6.2   Specimen Fabrication and Strain Monitoring

Preliminary experiments were conducted for the purpose of
producing Graphite/Polyimide specimens with a controlled lower fiber
volume ratio. It was found that reduction of curing pressure alone
does not decrease the fiber volume ratio. Tests with different
degrees of vacuum and various numbers of soak cloth layers were also
conducted. A reduced fiber volume ratio of $v_f = 0.37$ was obtained
by curing the laminates between two pressure plates and using only
one soak glass paper layer on top.

Three 2.54 cm x 22.9 cm (1 in. x 9 in.) specimens with
embedded gages and an 8.9 cm x 22.9 cm (3.5 in. x 9 in.) plate of
$[0_2/\pm45]_s$ layup and a fiber volume ratio of $v_f = 0.37$ were prepared.
In addition to these, a 2.54 cm x 12.7 cm (1 in. x 5 in.) $[0_8]$ control
specimen with embedded gages and an embedded thermocouple, an
8.9 cm x 22.9 cm (3.5 in. x 9 in.) $[0_8]$ plate and an 8.9 cm x 22.9 cm
(3.5 in. x 9 in.) $[90_8]$ plate were prepared. The latter were used
for preparation of specimens for material characterization.

Three 2.54 cm x 22.9 cm (1 in. x 9 in.) $[0_2/\pm15]_s$ specimens
with embedded gages, a 2.54 cm x 12.7 cm (1 in. x 5 in.) $[0_8]$
specimen with embedded gages and a thermocouple and an 8.9 cm x 22.9 cm
(3.5 in. x 9 in.) $[0_2/\pm15]_s$ plate were prepared. These specimens
and plate had the same fiber volume ratio as the material used in
Tasks II, III and IV.

Similar sets of specimens and plates as above were prepared
with $[0_2/90_2]_s$, $[\pm45/0_2]_s$, $[0/+45/0/-45]_s$, and $[+45/0_2/-45]_s$ ply
configurations.

All specimens and plates above were cured and postcured as
before. Strain gages and thermocouples were monitored during post-
curing, since it was shown earlier that the thermal strains in
Graphite/Polyimide are essentially the same during the second part
(cool down) of the curing cycle and the lower temperature part of
the postcuring cycle.

6.3 Effect of Fiber Volume Ratio

6.3.1 Characterization of Unidirectional Laminates

Unidirectional properties of the Graphite/Polyimide material
with the lower fiber volume ratio of $v_f = 0.37$ were determined.
Stress-strain curves for the 0-degree material under uniaxial tension
are shown in Figs. 6-1, 6-2 and 6-3. All strains appear to be
fairly linear to failure. The longitudinal modulus is not
significantly lower than the corresponding modulus for the higher
fiber volume ratio material of Task II. The longitudinal tensile
strength is approximately 8 percent lower than the corresponding
strength for the standard material of Task II. The transverse modulus
is appreciably lower and the transverse tensile strength is less
than half the corresponding value of the standard material. The
latter value of course is very much influenced by initial flaws
and initial curvature of the specimen introduced during manufacturing.

Two unidirectional 10-degree off-axis specimens were tested in tension to determine in-plane shear properties. Shear strain was computed from the readings of two three-gage rosettes used in each specimen. Shear stress versus shear strain curves to failure are shown in Figs. 6-4 and 6-5. The curves are linear up to approximately 16 MPa (2300 psi). The shear strength is higher than the corresponding strength of the standard material with the higher fiber volume ratio.

The measured properties above are summarized in the following Table 6-1. Included in this table are the coefficients of thermal expansion measured during the subsequent task of residual strain determination.

Table 6-1
PROPERTIES OF UNIDIRECTIONAL GRAPHITE/POLYIMIDE
(Modmor I/WRD 9371)

Fiber Volume Ratio	0.37
Longitudinal Thermal Coefficient, α_{11}	-0.4×10^{-6} K^{-1} (-0.2 $\mu\epsilon/°F$)
Transverse Thermal Coefficient, α_{22}	27.1×10^{-6} K^{-1} (15.0 $\mu\epsilon/°F$)
Longitudinal Modulus, E_{11}	207 GPa (30×10^{6} psi)
Transverse Modulus, E_{22}	4.14 GPa (600 ksi)
Shear Modulus, G_{12}	4.11 GPa (595 ksi)
Major Poisson's Ratio, ν_{12}	0.39
Minor Poisson's Ratio, ν_{21}	0.01
Longitudinal Tensile Strength, S_{11T}	744 MPa (107.8 ksi)
Transverse Tensile Strength, S_{22T}	5.9 MPa (850 psi)
Intralaminar Shear Strength, S_{12}	25.0 MPa (3620 psi)

6.3.2 Residual Strain

The embedded strain gages and thermocouples in the $[0_2/\pm45]_s$ and $[0_8]$ specimens of the low fiber volume ratio Graphite/Polyimide were monitored during postcuring. Thermal strains in the unidirectional specimen are shown in Fig. 6-6. They vary linearly with temperature as the standard material described in Section 3. The thermal coefficients of expansion determined from these curves are:

$$\alpha_{11} = -0.4 \times 10^{-6} \ K^{-1} \ (-0.2 \ \mu\varepsilon/°F)$$

$$\alpha_{22} = 27.1 \times 10^{-6} \ K^{-1} \ (15.0 \ \mu\varepsilon/°F)$$

As expected, the transverse thermal expansion coefficient is slightly higher than the corresponding coefficient of the standard material of Task II.

Strains in the angle-ply laminate are plotted in Fig. 6-7. They are approximately one-tenth the corresponding strains in the unidirectional specimens. They are approximately 30 percent higher than the corresponding strains of the standard material.

Restraint strains in the 0-degree and 45-degree plies of the $[0_2/\pm45]_s$ laminate were obtained as before and plotted in Figs. 6-8 and 6-9. They are linear with temperature and they are approximately of the same magnitude as in the standard material (Figs. 3-73 and 3-74).

6.3.3 Static Strength

Two 2.54 cm x 22.9 cm (1 in. x 9 in.) $[0_2/\pm45]_s$ specimens, including one with embedded gages, were tested to failure under static tensile loading. Stress-strain curves are shown in Figs. 6-10 and 6-11. The average modulus, Poisson's ratio and strength determined from these tests are:

6-4

$$E_{xx} = 107.5 \text{ GPa } (15.6 \times 10^6 \text{ psi})$$

$$\nu_{xy} = 0.87$$

$$S_{xxT} = 388 \text{ MPa } (56 \text{ ksi})$$

Results are summarized at the end of this section in Table 6-2.

6.3.4 Tensile Load with Thermal Cycling

Two $[0_2/\pm45]_s$ specimens, including one with embedded gages, were subjected to a static tensile load equal to 70 percent of the ultimate and to 100 thermal cycles between room temperature and 533 degK (500°F). Both specimens failed during this cycling.

Two similar specimens as above were subjected to a static tensile load equal to 70 percent of the ultimate and to 100 thermal cycles between room temperature and 200 degK (-100°F). Strain gages were monitored in the beginning and at the end of this cycling program. The strain gage readings were inconclusive. The specimens were subsequently tested statically to failure. Figures 6-12 and 6-13 show the stress-strain curves obtained.

The resulting values for the elastic properties and strength are:

$$E_{xx} = 100 \text{ GPa } (14.4 \times 10^6 \text{ psi})$$

$$\nu_{xy} = 0.85$$

$$S_{xxT} = 383 \text{ MPa } (55 \text{ ksi})$$

The modulus is somewhat lower than the initial value, but the strength is nearly the same as the initial static strength. These results are summarized at the end of this section in Table 6-4.

6.4 Effect of Ply Orientation

6.4.1 Residual Strain

Embedded strain gages and thermocouples in $[0_2/\pm15]_s$ and $[0_2/90_2]$ Graphite/Polyimide specimens having the standard fiber volume ratio as in Task II were monitored during postcuring.

Strains in the $[0_2/\pm15]_s$ specimen are shown in Fig. 6-14. They vary linearly with temperature and are an order of magnitude higher than the corresponding strains of the $[0_2/\pm45]_s$ specimen (Fig. 3-72). They are of the same order of magnitude as the strains in the unidirectional material (Fig. 3-71) as the $[0_2/\pm15]_s$ layup does not deviate much from the unidirectional construction. Restraint strains in the 0-degree plies were computed as before and shown in Fig. 6-15. Restraint strains in the 15-degree ply were computed as follows:

$$\varepsilon_0^r = \varepsilon_0^a - \varepsilon_{15}^u$$

$$\varepsilon_{90}^r = \varepsilon_{90}^a - \varepsilon_{75}^u$$

$$\varepsilon_{15}^r = \varepsilon_{15}^a - \varepsilon_0^u \qquad \text{(parallel to fibers)}$$

$$\varepsilon_{-75}^r = \varepsilon_{75}^a - \varepsilon_{90}^u \qquad \text{(normal to fibers)}$$

where subscripts refer to angle of direction measured from the longitudinal axis of the specimen (0-axis) and superscripts r, a and u refer to restraint, angle-ply laminate and unidirectional laminate, respectively. The strains in the unidirectional and angle-ply laminates at 15- and 75-deg directions were computed from the measured strains using the strain transformation equation:

$$\varepsilon_\theta = \frac{\varepsilon_0 + \varepsilon_{90}}{2} + \frac{\varepsilon_0 - \varepsilon_{90}}{2}\cos2\theta$$

where θ = 15- and 75-deg. The computed restraint strains are shown in Fig. 6-16.

Thermal strains in the $[0_2/90_2]$ specimen were very small because of the restraint produced by the fibers in two directions. The apparent strains recorded are shown in Fig. 6-17 next to the purely thermal output of the gage. As can be seen, the determination of the true thermal strains involves computation of small differences of large numbers. The resulting strains in the laminate are shown in Fig. 6-18. The scatter appears large because of the enlarged scale and the low magnitude of the strains. It is not known whether the small difference between the 0-deg. and 90-deg strains is significant. Restraint strains in 0- and 90-deg. plies of the laminate are shown in Figs. 6-19 and 6-20. As expected, the restraint strains in the axial and transverse directions of the 0-degree ply (ε_0 and ε_{90}) are equal to the restraint strains in the transverse and axial directions (ε_{90} and ε_0) of the 90-degree ply. Naturally, the 45-degree strains are equal for both plies.

6.4.2 Static Strength

Two 2.54 cm x 22.9 cm (1 in. x 9 in.) specimens of each of the two laminate constructions above were tested to failure under static tensile loading. In each pair of specimens, one specimen was instrumented with embedded gages and the other with surface gages only. Stress-strain curves are shown in Figs. 6-21 through 6-23. The average values for the elastic properties and strength are:

For the $[0_2/\pm15]_s$ specimens,

$$E_{xx} = 201 \text{ GPa } (29.2 \times 10^6 \text{ psi})$$

$$\nu_{xy} = 1.53$$

$$S_{xxT} = 606 \text{ MPa } (88 \text{ ksi})$$

and for the $[0_2/90_2]_s$ specimens,

$$E_{xx} = 131 \text{ GPa } (19.0 \times 10^6 \text{ psi})$$

$$\nu_{xy} = 0.035$$

$$S_{xxT} = 421 \text{ MPa } (61 \text{ ksi})$$

These results are summarized in Table 6-2 at the end of this section.

6.4.3 Tensile Load with Thermal Cycling

Two specimens of each of the two laminate constructions above, including one with embedded gages, were subjected to a static tensile load equal to 70 percent of the static ultimate and to 100 thermal cycles between room temperature and 533 degK (500°F). Strain gages were monitored in the beginning and at the end of this cycling program. Apparent strains monitored during the first and one hundred and first thermal cycles for specimen $[0_2/\pm15]_s$ are shown in Fig. 6-24. The axial strains are identical in the beginning and at the end of cycling, but discrepancies appear in the 45-degree and transverse strains. These discrepancies cannot be attributed to structural degradation, since the strains at the end of thermal cycling are in closer agreement with the thermal strains recorded during curing (Fig. 6-14).

The thermally cycled specimens above were tested statically to failure. Stress-strain curves are shown in Figs. 6-25 through 6-28. The average values for the elastic properties and strength are:

For the $[0_2/\pm15]_s$ specimens,

$$E_{xx} = 203 \text{ GPa } (29.5 \times 10^6 \text{ psi})$$

$$\nu_{xy} = 1.50$$

$$S_{xxT} = 698 \text{ MPa } (101 \text{ ksi})$$

6-8

and for the $[0_2/90_2]_s$ specimens,

$$E_{xx} = 112 \text{ GPa } (16.3 \times 10^6 \text{ psi})$$

$$\nu_{xy} = 0.013$$

$$S_{xxT} = 338 \text{ MPa } (49 \text{ ksi})$$

These results are summarized in Table 6-3 at the end of this section. In the case of $[0_2/\pm15]_s$ specimens the residual strength is somewhat higher than the initial strength whereas the two moduli are approximately the same. In the case of the $[0_2/90_2]_s$ specimens the residual strength and modulus are both lower than the corresponding initial values.

Two additional specimens, including one with embedded instrumentation, of each of the two laminate constructions above were subjected to a static tensile load equal to 70 percent of the ultimate and to 100 thermal cycles between room temperature and 200 degK (-100°F). Strain gages were monitored in the beginning and at the end of this cycling program. Apparent strains recorded during this thermal cycling are shown in Figs. 6-29 and 6-30. No significant differences appear between the strains recorded in the beginning and those recorded at the end of the thermal cycling.

The thermally cycled specimens above were tested statically to failure. Stress-strain curves are shown in Figs. 6-31 through 6-34. The average values for the elastic properties and strength are:

For the $[0_2/\pm15]_s$ specimens,

$$E_{xx} = 201 \text{ GPa } (29.2 \times 10^6 \text{ psi})$$

$$\nu_{xy} = 1.40$$

$$S_{xxT} = 700 \text{ MPa } (101 \text{ ksi})$$

and for the $[0_2/90_2]_s$ specimens,

$$E_{xx} = 123 \text{ GPa } (17.9 \times 10^6 \text{ psi})$$

$$\nu_{xy} = 0.045$$

$$S_{xxT} = 393 \text{ MPa } (57 \text{ ksi})$$

These results are summarized in Table 6-4 at the end of this
section. The residual strength of the $[0_2/\pm15]_s$ specimens is
somewhat higher than the initial strength whereas the reverse is
true in the case of the $[0_2/90_2]_s$ specimens. These differences,
however, may not be significant.

6.5 Effect of Ply Stacking Sequence

6.5.1 Residual Strain

Embedded strain gages and thermocouples in $[\pm45/0_2]_s$,
$[0/+45/0/-45]_s$ and $[+45/0_2/-45]_s$ Graphite/Polyimide specimens
were monitored during postcuring.

Strains in these specimens are shown in Figs. 6-35 through 6-37.
They vary linearly with temperature and they are all approximately
of the same magnitude, within experimental variability, and equal
to the corresponding strains of the standard $[0_2/\pm45]_s$ specimen
(Fig. 3-72). Restraint strains in the 0-degree and 45-degree plies
computed as before are shown in Figs. 6-38 through 6-43. All these
strains vary linearly with temperature and are equal for all ply
stacking sequence variations, including the standard layup $[0_2/\pm45]_s$
(Figs. 3-73 and 3-74).

6.5.2 Static Strength

Two specimens of each of the three layups above, including
one with embedded strain gages, were tested to failure under static
tensile loading. Stress-strain curves are shown in Figs. 6-44 through
6-49. Results are summarized in Table 6-2 at the end of this section.
The average values for the elastic properties and strength are:

For the $[\pm45/0_2]_s$ specimens,

$$E_{xx} = 129 \text{ GPa } (18.6 \times 10^6 \text{ psi})$$

$$\nu_{xy} = 0.81$$

$$S_{xxT} = 506 \text{ MPa } (76 \text{ ksi})$$

for the $[0/+45/0/-45]_s$ specimens,

$$E_{xx} = 129 \text{ GPa } (18.6 \times 10^6 \text{ psi})$$

$$\nu_{xy} = 0.85$$

$$S_{xxT} = 430 \text{ MPa } (62 \text{ ksi})$$

and for the $[+45/0_2/-45]_s$ specimens,

$$E_{xx} = 126 \text{ GPa } (18.3 \times 10^6 \text{ psi})$$

$$\nu_{xy} = 0.76$$

$$S_{xxT} = 497 \text{ MPa } (72 \text{ ksi})$$

Except for the somewhat lower strength of the $[0/+45/0/-45]_s$ layup, all other properties seem to be approximately the same for all three layups. All strengths are appreciably higher than the basic $[0_2/\pm45]_s$ laminate tested under Task II. This difference may be related to the fact that the laminates above were cured in a separate batch at a much later date.

6.5.3 <u>Tensile Load with Thermal Cycling</u>

Two specimens of each of the three laminate constructions above, including one with embedded gages, were subjected to a static tensile load equal to 70 percent of the static ultimate and to 100 thermal cycles between room temperature and 533 degK (500°F). Strain gages were monitored in the beginning and at the end of this cycling program. No significant differences were observed in the recorded strains between the beginning and the end of cycling.

These specimens were subsequently tested statically to failure. Stress-strain curves are shown in Figs. 6-50 through 6-55. The average values for the elastic properties and strength are:

For the $[\pm45/0_2]_s$ specimens,

E_{xx} = 125 GPa (18.1 x 10^6 psi)

ν_{xy} = 0.79

S_{xxT} = 465 MPa (68 ksi)

for the $[0/+45/0/-45]_s$ specimens,

E_{xx} = 131 GPa (19.0 x 10^6 psi)

ν_{xy} = 0.81

S_{xxT} = 440 MPa (64 ksi)

and for the $[+45/0_2/-45]_s$ specimens,

E_{xx} = 128 GPa (18.6 x 10^6 psi)

ν_{xy} = 0.77

S_{xxT} = 462 MPa (67 ksi)

These results are summarized in Table 6-3 at the end of this section. No significant differences exist among the three layups and between residual and initial properties. The largest differences, up to 10 percent, appear in the strength values.

Two additional specimens of each of the three layups above, including one with embedded gages, were subjected to a static tensile load equal to 70 percent of the ultimate and to 100 thermal cycles between room temperature and 200 degK (-100°F). Strain gages were monitored in the beginning and at the end of this cycling program.

These specimens were subsequently tested statically to failure. Stress-strain curves are shown in Figs. 6-56 through 6-61. The average values for the elastic properties and strength are:

For the $[\pm 45/0_2]_s$ specimens,

E_{xx} = 125 GPa (18.1 x 10^6 psi)

ν_{xy} = 0.79

S_{xxT} = 531 MPa (77 ksi)

for the $[0/+45/0/-45]_s$ specimens,

E_{xx} = 122 GPa (17.7 x 10^6 psi)

ν_{xy} = 0.82

S_{xxT} = 431 MPa (62 ksi)

and for the $[+45/0_2/-45]_s$ specimens,

E_{xx} = 128 GPa (18.5 x 10^6 psi)

ν_{xy} = 0.83

S_{xxT} = 458 MPa (66 ksi)

These results are summarized in Table 6-4. No significant differences appear between initial and residual properties and among the three layups. The largest differences, up to 10 percent, appear in the strength values.

6.6   Summary and Conclusions

The effects of fiber volume ratio, ply orientation and ply stacking sequence on the magnitudes of residual stress, stiffness and strength of Graphite/Polyimide laminates were investigated.

Residual strains in the lower fiber volume ratio laminates were approximately the same as those of the standard material. Restraint strains in the 0-degree plies of the $[0_2/\pm15]_s$ are approximately one-fourth of those in the 0-degree plies of the $[0_2/\pm45]_s$ layup. This is because the ±15-degree plies offer less restraint to transversal contraction of the 0-degree plies than do ±45-degree plies. Restraint strains in the 0-degree plies of the $[0_2/90_2]_s$ laminate are higher than corresponding strains in the $[0_2/\pm45]_s$ laminate by approximately 8 percent. Ply stacking sequence was found to have no measureable effect on the magnitude of residual strains. These strains were almost identical for all four variations of ply stacking sequence: $[0_2/\pm45]_s$, $[\pm45/0_2]_s$, $[0/+45/0/-45]_s$ and $[+45/0_2/-45]_s$.

Results of static tensile tests are tabulated in Table 6-2. The modulus and tensile strength of the low fiber-volume-ratio laminate were lower than corresponding properties of the standard material by approximately the same ratio as the corresponding fiber volume ratios. The ratio of FVR's is 0.45/0.37 = 1.22 and compares closely with the ratio of measured moduli of 18.5/15.6 = 1.19 and the strength ratio of 69/56 = 1.23. This means that the stiffness and strength per ply are not affected by moderate changes in the fiber volume ratio. The modulus of the cross-ply laminate $[0_2/90_2]_s$ is only slightly higher than that of the $[0_2/\pm45]_s$ laminate and its stacking sequence variations, but its strength is lower by approximately 12 percent. The $[0_2/\pm15]_s$ layup showed the most dramatic influences of ply orientation. The modulus of 201 GPa (29.2 x 10^6 psi) approaches that of the unidirectional material and the strength is higher than that of the $[0_2/\pm45]_s$ layups by approximately 28 percent. The most pronounced result is the high value of 1.53 for Poisson's ratio. Stacking sequence variations of the basic $[0_2/\pm45]_s$ had no significant effect on measured modulus and strength, although the $[0/+45/0/-45]_s$ layup displayed consistently lower strength values.

Table 6-2

STATIC TENSILE STRENGTH OF GRAPHITE/POLYIMIDE ANGLE-PLY LAMINATES

Laminate	Modulus, E_{xx} GPa (10^6 psi)		Poisson's Ratio, ν_{xy}	Tensile Strength, S_{xxT} MPa (ksi)	
$[0_2/\pm 45]_s$ (Lower FVR)	108	(15.6)	0.87	388	(56)
$[0_2/\pm 15]_s$	201	(29.2)	1.53	606	(88)
$[0_2/90_2]_s$	131	(19.0)	0.035	421	(61)
$[\pm 45/0_2]_s$	129	(18.6)	0.81	506	(73)
$[0/+45/0/-45]_s$	129	(18.6)	0.85	430	(62)
$[+45/0_2/-45]_s$	126	(18.3)	0.76	497	(72)

The effects of fiber volume ratio and ply orientation and stacking sequence were also evaluated by subjecting specimens to a tensile preload and to 100 thermal cycles between room temperature and 533 degK (500°F). The low fiber volume ratio specimens failed during thermal cycling under a tensile preload equal to 70 percent of the static ultimate. All other specimens survived the cycling under a similar preload. Strains monitored during thermal cycling did not disclose any significant changes between the beginning and end of cycling. Residual properties of all surviving specimens were determined by testing them statically to failure after thermal cycling. Results are tabulated in Table 6-3. The $[0_2/\pm15]_s$ specimens show somewhat higher residual strength and unchanged modulus. The $[0_2/90_2]_s$ laminate, having the highest residual stresses, showed a reduction in both strength and stiffness. No significant changes between initial and residual properties were observed in the three stacking sequence variations of the basic $[0_2/\pm45]_s$ laminate.

The effects of the same parameters above were evaluated for thermal cycling between room temperature and 200 degK (-100°F) under tensile preload. Strains monitored during this cycling did not disclose any significant differences between the beginning and end of cycling. Results on residual properties of all cycled specimens are tabulated in Table 6-4. The strength in the low fiber-volume-ratio specimens remained unchanged, but the modulus showed some reduction. The $[0_2/\pm15]_s$ specimens showed higher residual strength and unchanged modulus. The $[0_2/90_2]_s$ laminate, having the highest residual stresses, showed a reduction in both strength and modulus, as above. The stacking sequence variations of the basic $[0_2/\pm45]_s$ laminate showed no significant changes between initial and residual properties. Again, as in the case of initial static properties and residual properties after elevated temperature cycling, the $[0/+45/0/-45]_s$ layup showed a somewhat lower strength than the other stacking sequence variations.

Table 6-3

RESIDUAL PROPERTIES OF GRAPHITE/POLYIMIDE SPECIMENS AFTER

100 THERMAL CYCLES BETWEEN ROOM TEMPERATURE AND 533 degK

(500°F) UNDER TENSILE LOAD

Laminate	Initial Properties				Residual Properties		
	Strength, S_{xxT} MPa (ksi)	Modulus, E_{xx} GPa (10^6psi)	Poisson's Ratio, ν_{xy}	Tensile Stress MPa (ksi)	Strength, S_{xxT} MPa (ksi)	Modulus, E_{xx} GPa (10^6psi)	Poisson's Ratio, ν_{xy}
$[0_2/\pm15]_s$	606 (88)	201 (29.2)	1.53	425 (62)	698 (101)	203 (29.5)	1.50
$[0_2/90_2]_s$	421 (61)	131 (19.0)	0.035	290 (42)	338 (49)	112 (16.3)	0.013
$[\pm45/0_2]_s$	506 (73)	129 (18.6)	0.81	352 (51)	465 (68)	125 (18.1)	0.79
$[0/+45/0/-45]_s$	430 (62)	129 (18.6)	0.85	297 (43)	440 (64)	131 (19.0)	0.81
$[+45/0_2/-45]_s$	497 (72)	126 (18.3)	0.76	345 (50)	462 (67)	128 (18.6)	0.77

Table 6-4

RESIDUAL PROPERTIES OF GRAPHITE/POLYIMIDE SPECIMENS AFTER
100 THERMAL CYCLES BETWEEN ROOM TEMPERATURE AND 200 degK
(-100°F) UNDER TENSILE LOAD

Laminate	Initial Properties			Tensile Stress, MPa (ksi)	Residual Properties		
	Strength, S_{xxT} MPa (ksi)	Modulus, E_{xx} GPa (10^6 psi)	Poisson's Ratio, ν_{xy}		Strength, S_{xxT} MPa (ksi)	Modulus, E_{xx} GPa (10^6 psi)	Poisson's Ratio ν_{xy}
$[0_2/\pm45]_s$ (Low FVR)	388 (56)	107 (15.6)	0.87	270 (39)	383 (55)	100 (14.4)	0.85
$[0_2/\pm15]_s$	606 (88)	201 (29.2)	1.53	425 (62)	700 (101)	201 (29.2)	1.40
$[0_2/90_2]_s$	421 (61)	131 (19.0)	0.035	290 (42)	393 (57)	123 (17.9)	0.045
$[\pm45/0_2]_s$	506 (73)	129 (18.6)	0.81	352 (51)	531 (77)	125 (18.1)	0.79
$[0/+45/0/-45]_s$	430 (62)	129 (18.6)	0.85	297 (43)	431 (62)	122 (17.7)	0.82
$[+45/0_2/-45]_s$	497 (72)	126 (18.3)	0.76	345 (50)	458 (66)	128 (18.5)	0.83
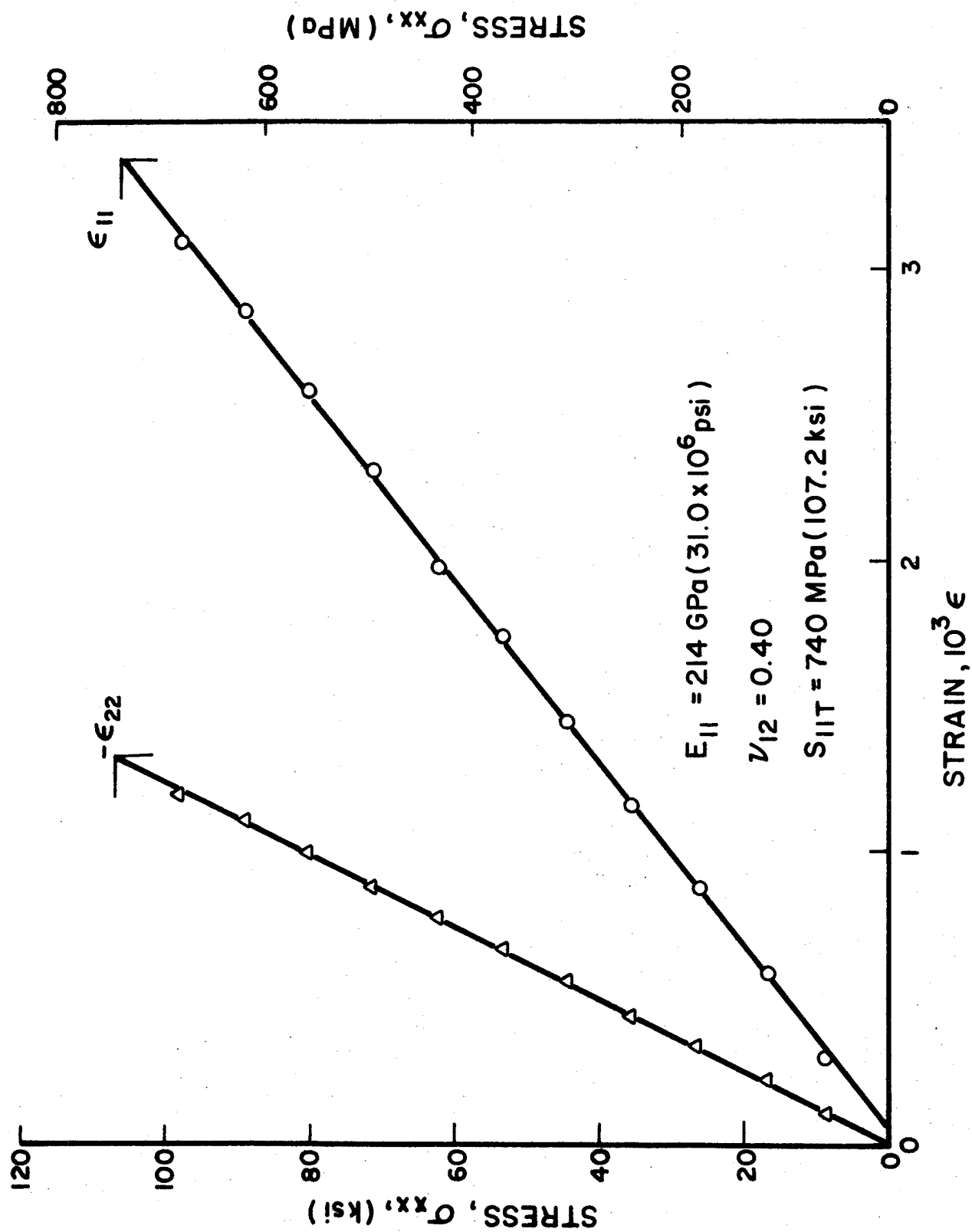
Fig. 6-1 STRAINS IN [0₈] GRAPHITE/POLYIMIDE SPECIMEN WITH LOW FIBER VOLUME RATIO UNDER TENSILE LOADING

Fig. 6-2 STRAINS IN [0₈] GRAPHITE/POLYIMIDE SPECIMEN WITH LOW FIBER VOLUME RATIO UNDER TENSILE LOADING

The figure shows stress-strain curves with the following labeled parameters:

$E_{11} = 200\, GPa\, (29.0 \times 10^6\, psi)$

$\nu_{12} = 0.38$

$S_{11T} = 748\, MPa\, (108.4\, ksi)$

Axes:
- Top: STRESS, σ_{xx}, (MPa), scale 0 to 800
- Bottom: STRESS, σ_{xx}, (ksi), scale 0 to 120
- STRAIN, $10^3\, \epsilon$, scale 0 to 4

Curves labeled ϵ_{11} and $-\epsilon_{22}$
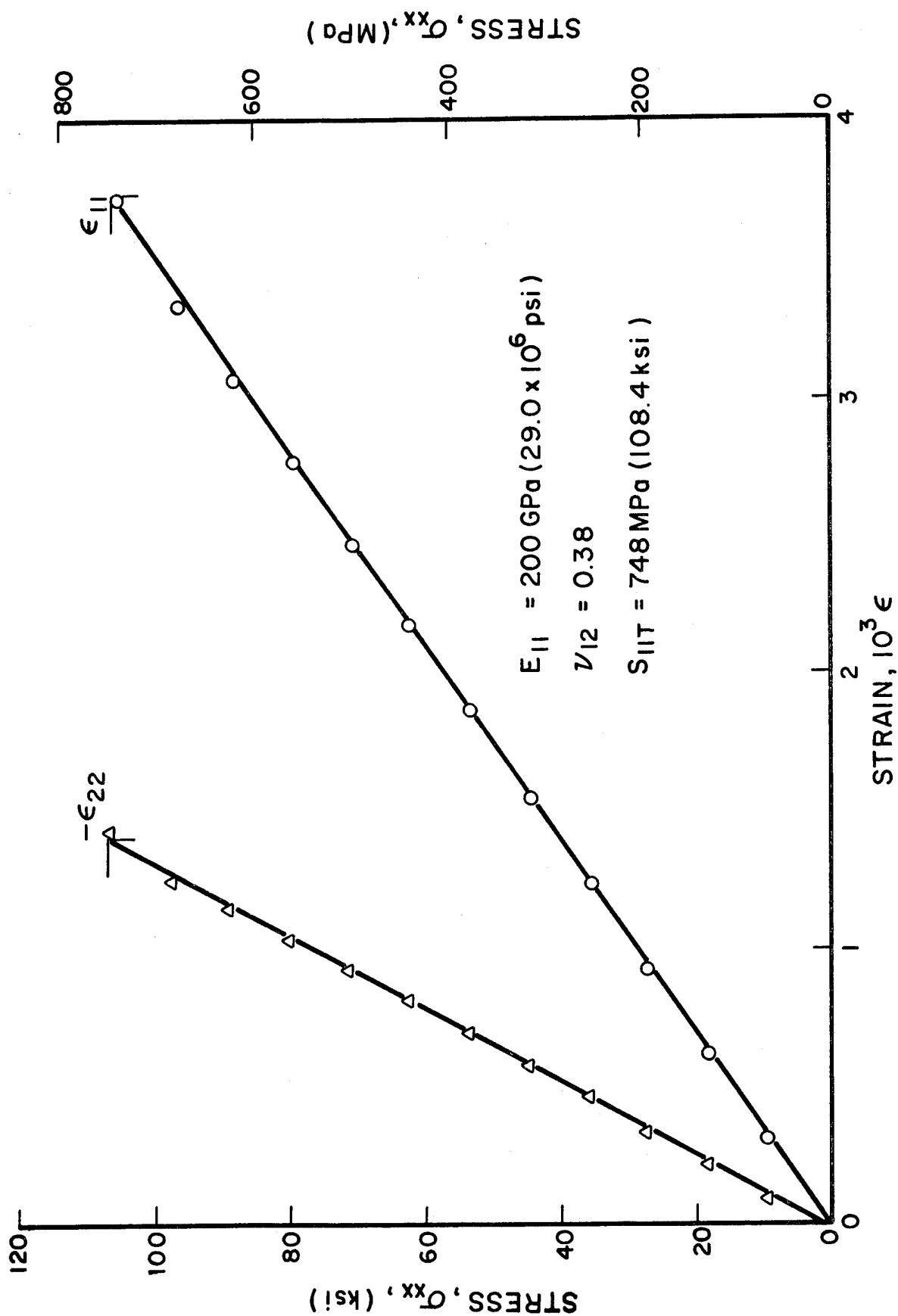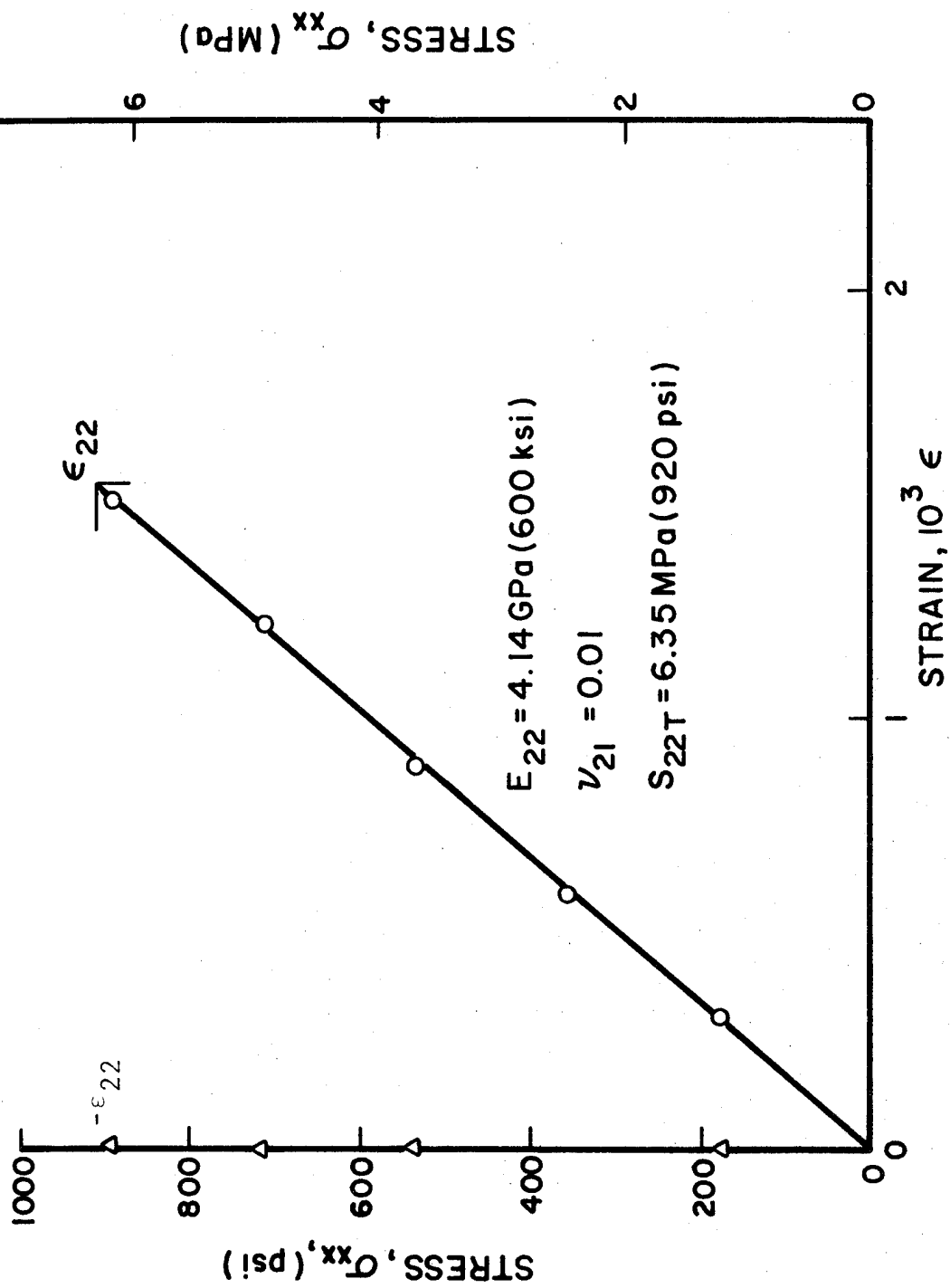
Fig. 6-3 STRAINS IN [90₈] GRAPHITE/POLYIMIDE SPECIMEN WITH LOW FIBER VOLUME RATIO UNDER TENSILE LOADING
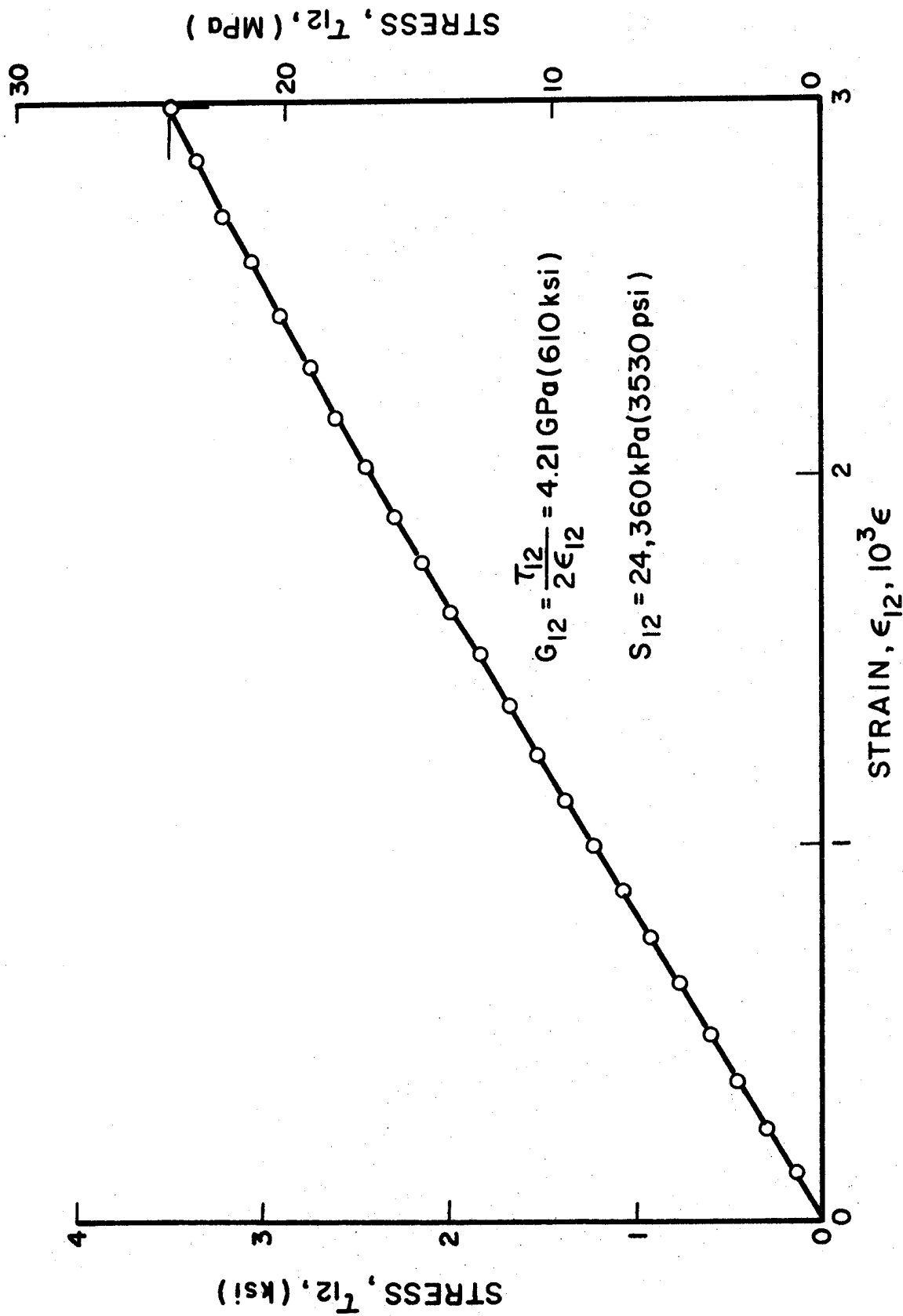
Fig. 6-4 SHEAR STRESS VERSUS SHEAR STRAIN IN 10-DEGREE OFF-AXIS UNIDIRECTIONAL GRAPHITE/POLYIMIDE SPECIMEN

Fig. 6-5 SHEAR STRESS VERSUS SHEAR STRAIN IN 10-DEGREE OFF-AXIS UNIDIRECTIONAL GRAPHITE/ POLYIMIDE SPECIMEN

$$G_{12} = \frac{\tau_{12}}{2\epsilon_{12}} = 4.02\,GPa\,(580\,ksi\,)$$

$$S_{12} = 25,670\,kPa\,(3,720\,psi\,)$$
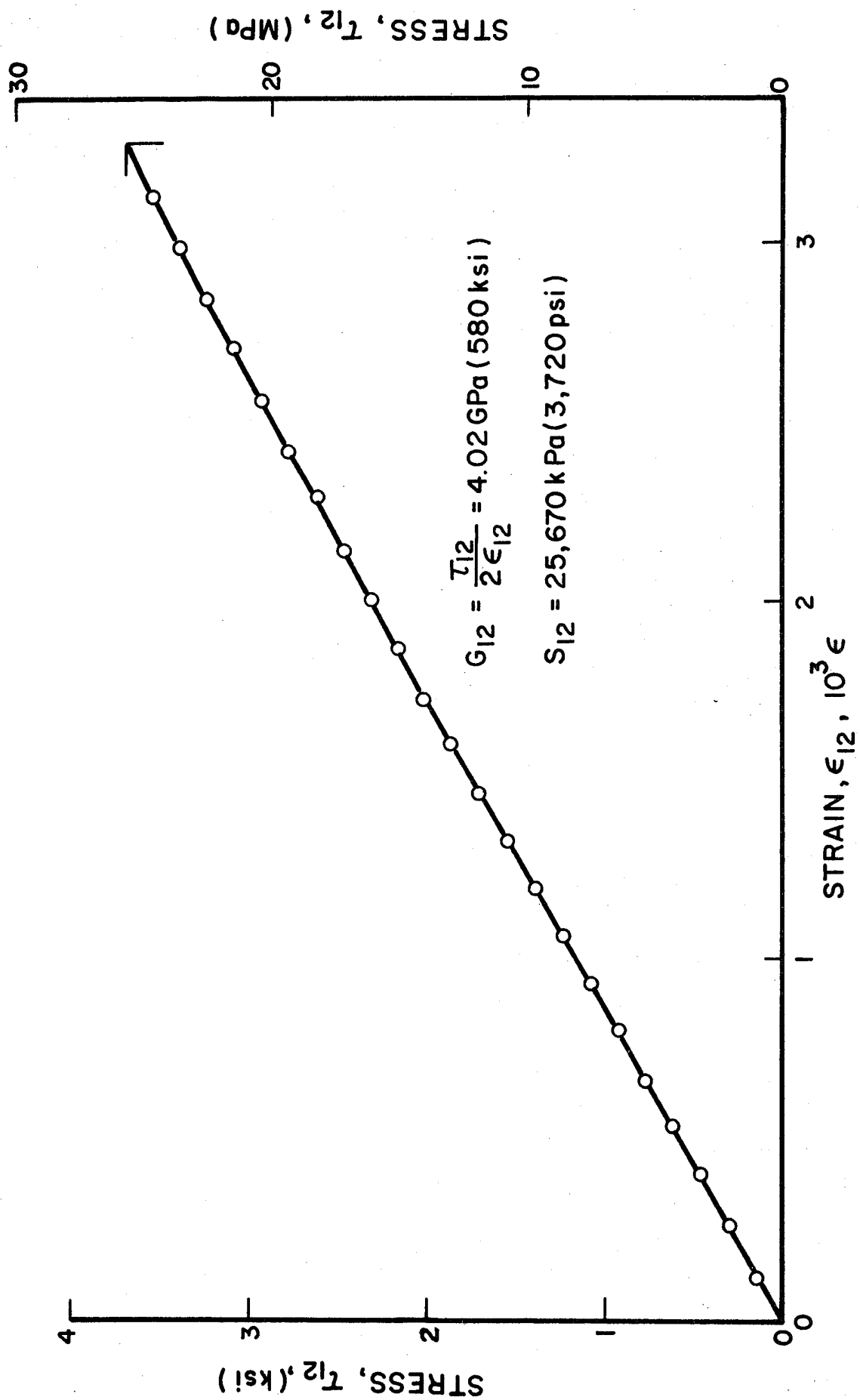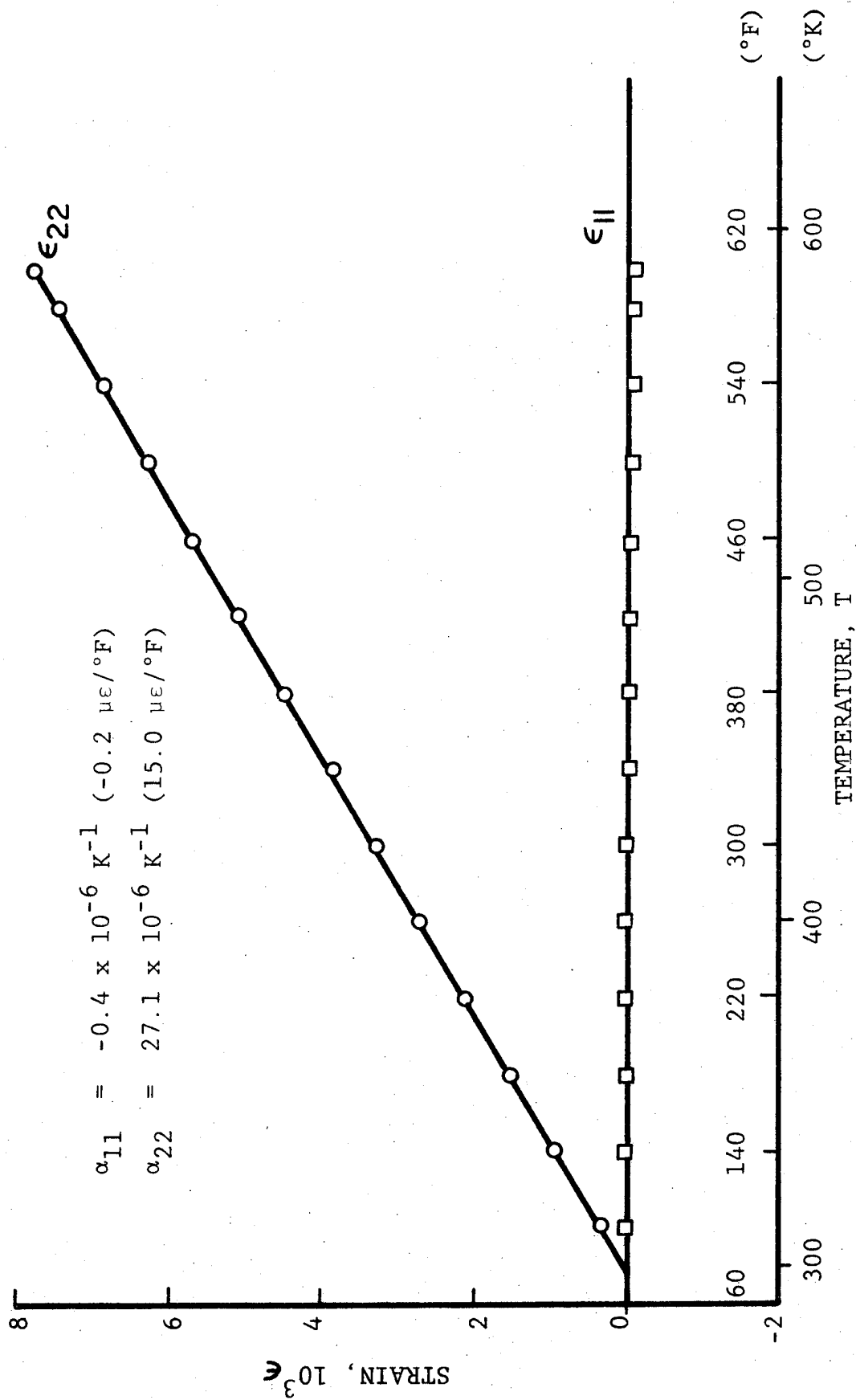
Fig. 6-6 THERMAL STRAINS IN $[0_8]$ LOW FIBER VOLUME RATIO GRAPHITE/POLYIMIDE SPECIMEN

$$\alpha_{11} = -0.4 \times 10^{-6} \ K^{-1} \ (-0.2 \ \mu\epsilon/^\circ F)$$
$$\alpha_{22} = 27.1 \times 10^{-6} \ K^{-1} \ (15.0 \ \mu\epsilon/^\circ F)$$

6-9
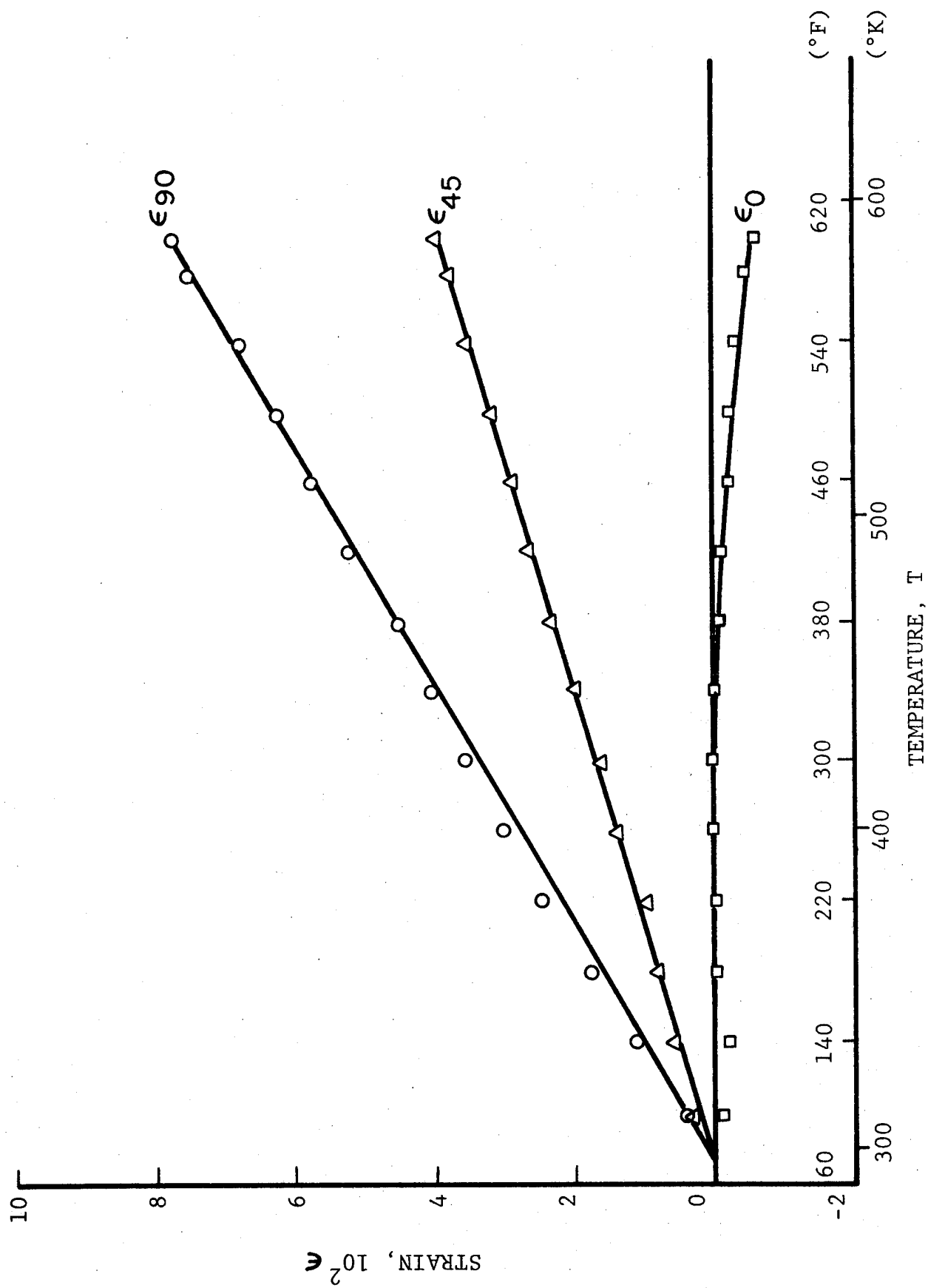
Fig. 6-7   THERMAL STRAINS IN $[0_2/\pm45]_s$ LOW FIBER VOLUME RATIO GRAPHITE/POLYIMIDE
SPECIMEN

6-25
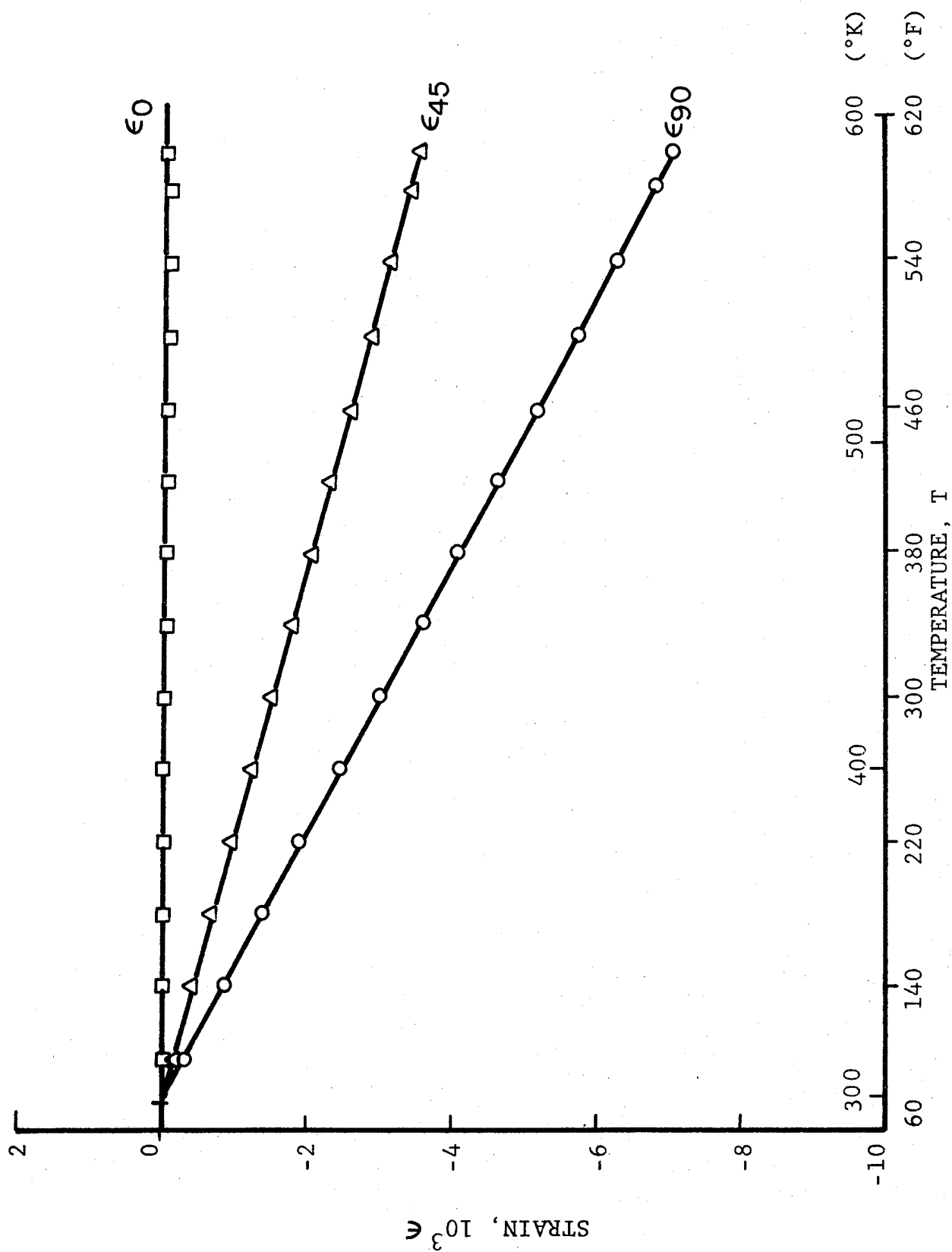
Fig. 6-8   RESTRAINT STRAINS IN 0-DEGREE PLIES OF $[0_2/\pm45]_s$ LOW FIBER VOLUME
RATIO GRAPHITE/POLYIMIDE SPECIMEN
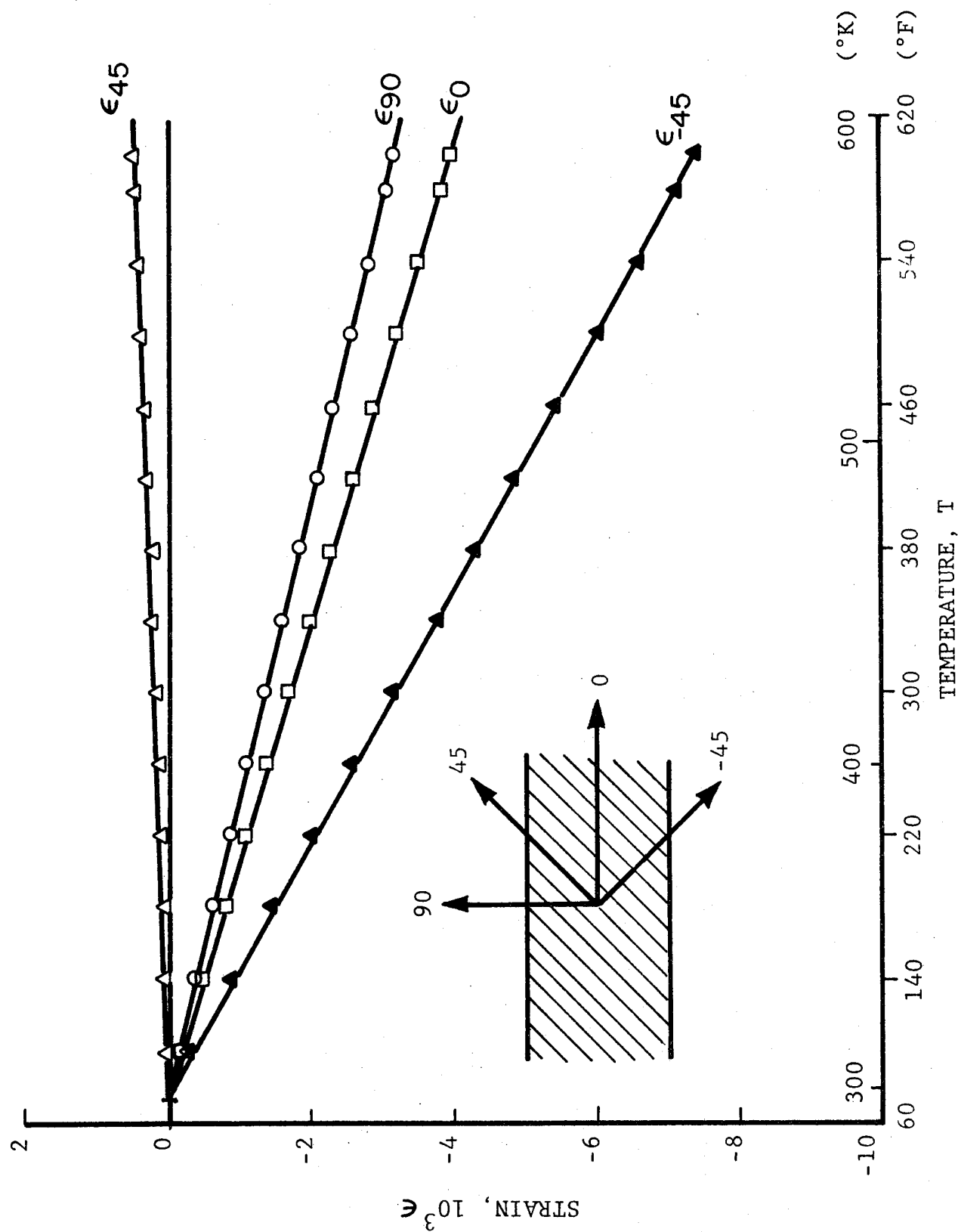
Fig. 6-9 RESTRAINT STRAINS IN 45-DEGREE PLIES OF $[0_2/\pm45]_s$ LOW FIBER VOLUME RATIO GRAPHITE/POLYIMIDE SPECIMEN

6-27
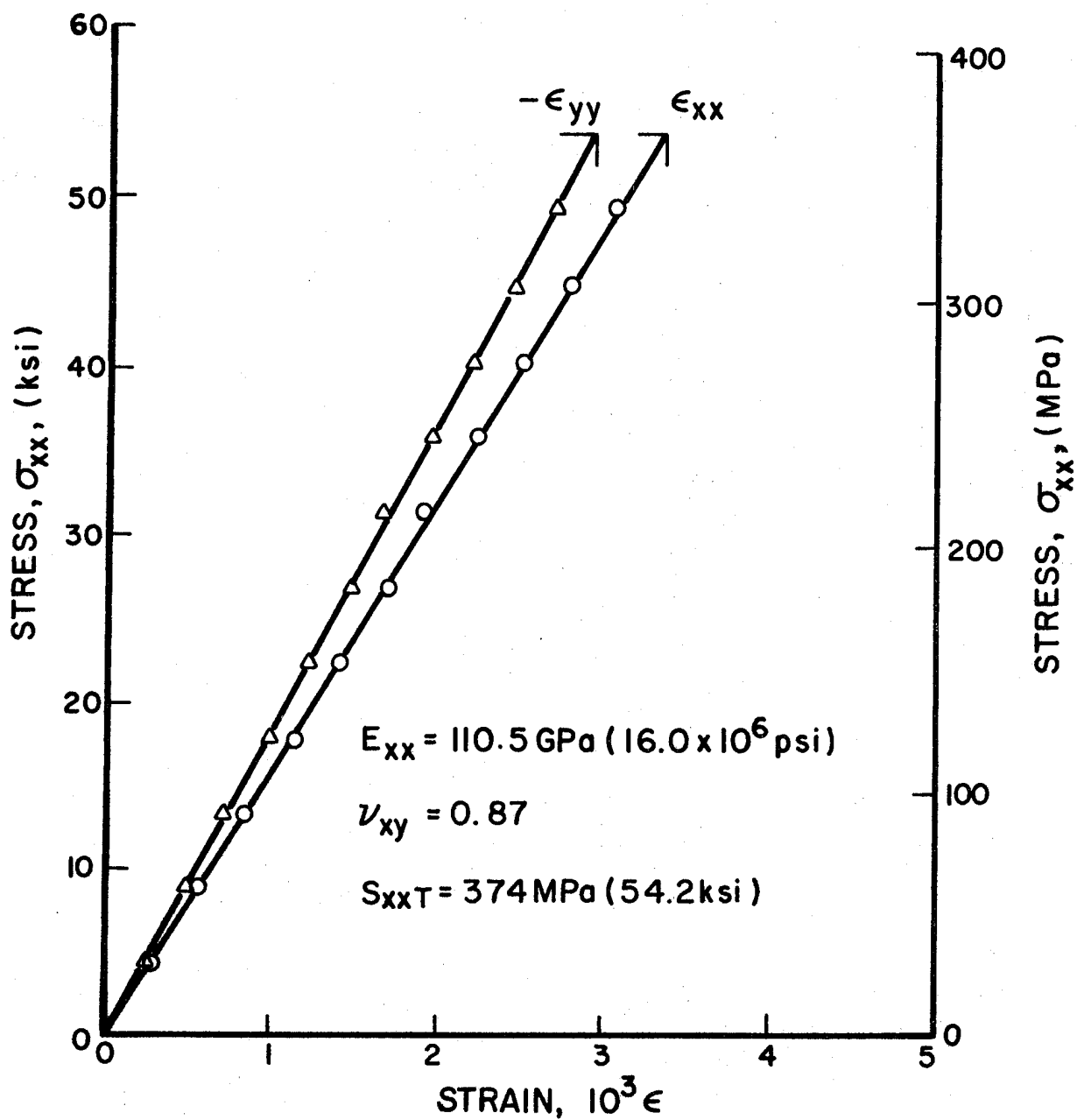
Fig. 6-10 STRAINS IN $[0_2/\pm45]_s$ GRAPHITE/POLYIMIDE
SPECIMEN WITH LOW FIBER VOLUME RATIO
UNDER TENSILE LOADING
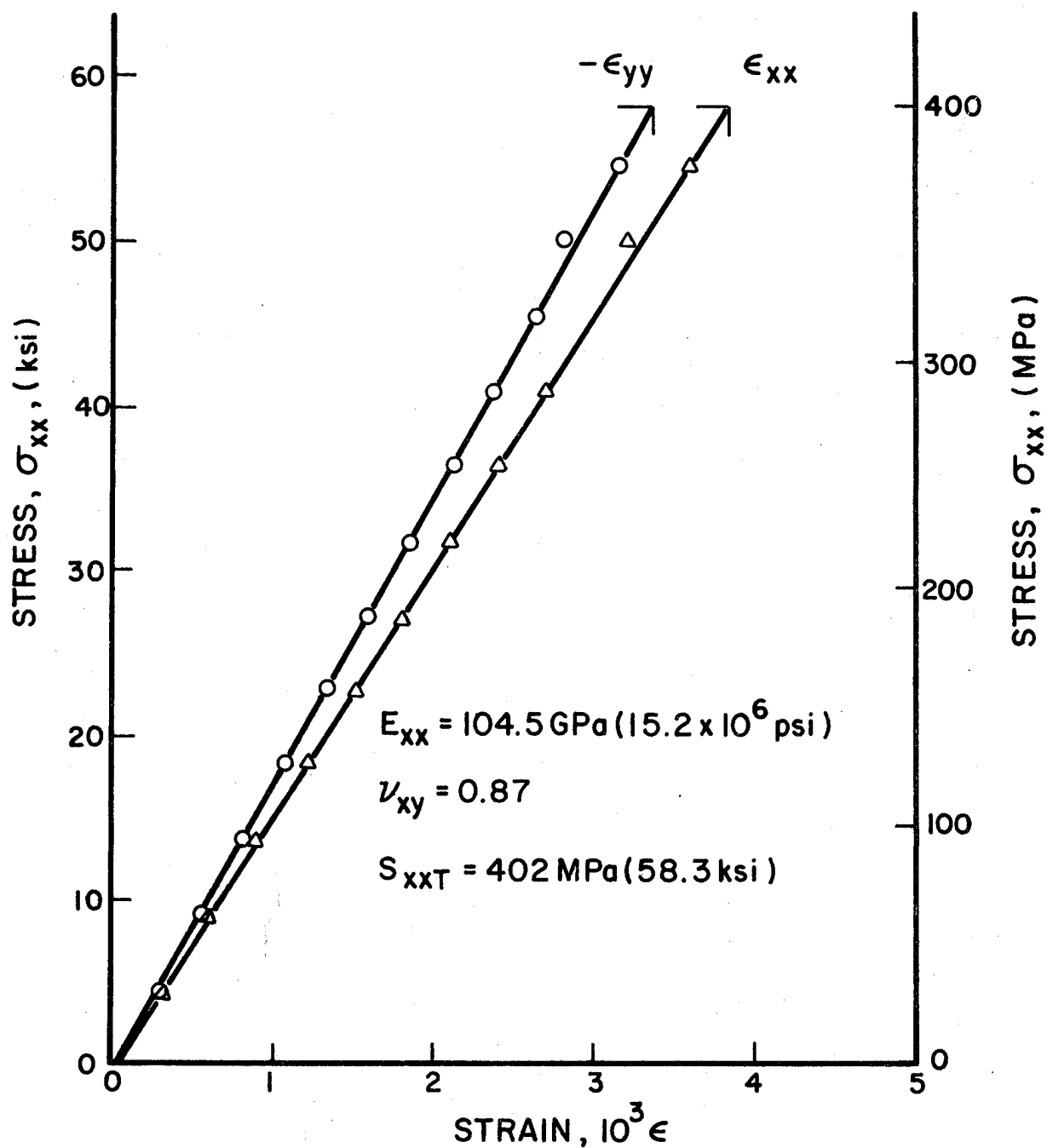
Fig. 6-11 STRAINS IN $[0_2/\pm 45]_s$ GRAPHITE/POLYIMIDE SPECIMEN WITH LOW FIBER VOLUME RATIO UNDER TENSILE LOADING

Fig. 6-12 STRAINS IN $[0_2/\pm45]_s$ LOW FIBER VOLUME RATIO GRAPHITE/POLYIMIDE SPECIMEN UNDER UNIAXIAL TENSILE LOADING AFTER 100 THERMAL CYCLES BETWEEN ROOM TEMPERATURE AND 200 degK (-100°F) UNDER TENSILE LOADING

$E_{xx} = 98$ GPa (14.2 x 10^6 psi)

$\nu_{xy} = 0.87$

$S_{xxT} = 400$ MPa (58 ksi)

Fig. 6-13 STRAINS IN $[0_2/\pm 45]_s$ LOW FIBER VOLUME RATIO GRAPHITE/POLYIMIDE SPECIMEN UNDER UNIAXIAL TENSILE LOADING AFTER 100 THERMAL CYCLES BETWEEN ROOM TEMPERATURE AND 200 degK (-100°F) UNDER TENSILE LOADING
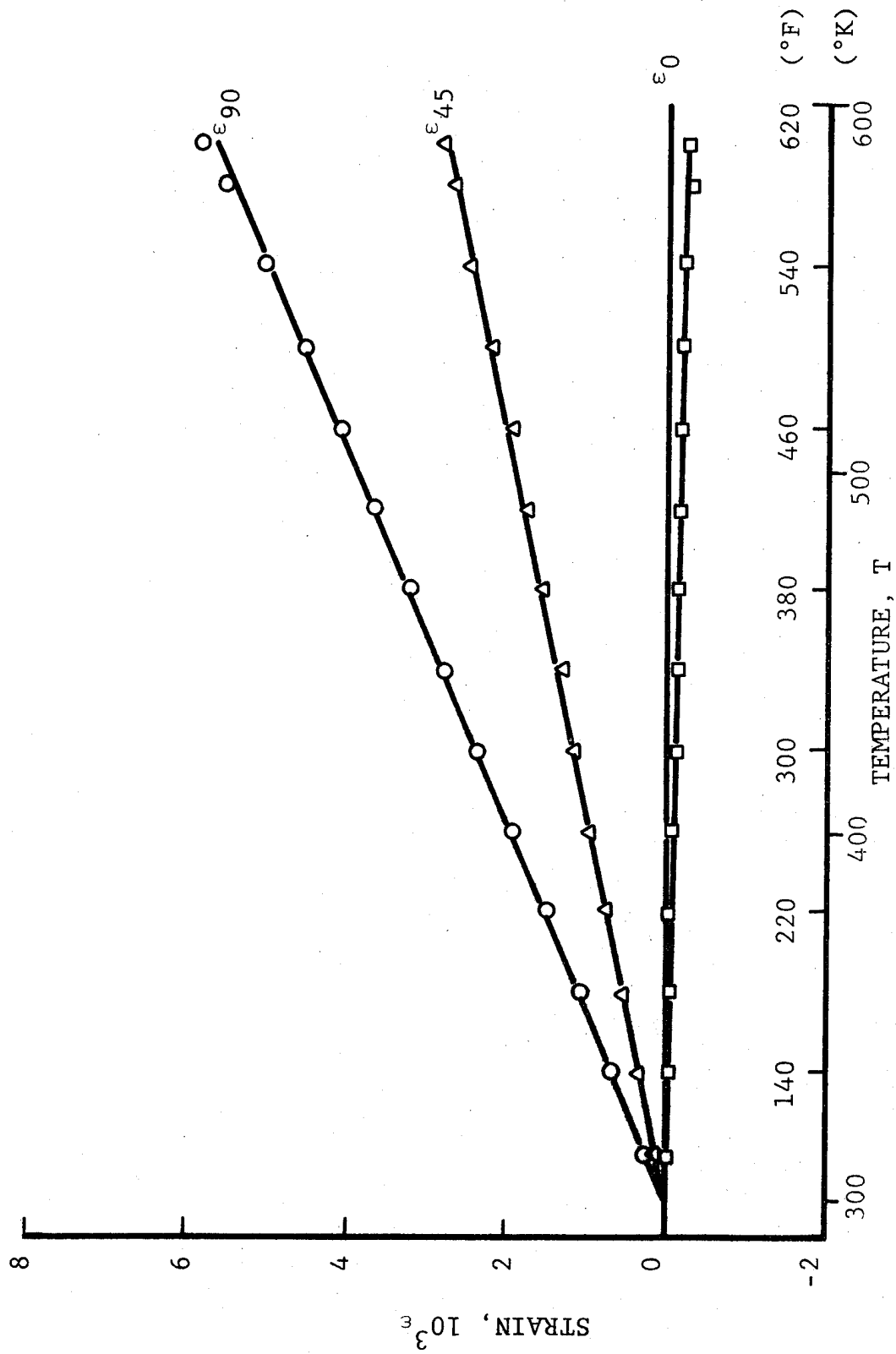
Fig. 6-14 THERMAL STRAINS IN $[0_2/\pm15]_s$ GRAPHITE/POLYIMIDE SPECIMEN

Fig. 6-15 RESTRAINT STRAINS IN 0-DEGREE PLIES OF $[0_2/\pm15]_s$ GRAPHITE/POLYIMIDE SPECIMEN

6-9

Fig. 6-16 RESTRAINT STRAINS IN 15-DEGREE PLIES OF $[0_2/\pm15]_s$ GRAPHITE/ POLYIMIDE SPECIMEN

6-9

Fig. 6-17 APPARENT STRAINS IN $[0_2/90_2]_s$ GRAPHITE/POLYIMIDE SPECIMEN AS A FUNCTION OF TEMPERATURE

Fig. 6-18 STRAINS IN $[0_2/90_2]_s$ GRAPHITE/POLYIMIDE SPECIMEN

6-36
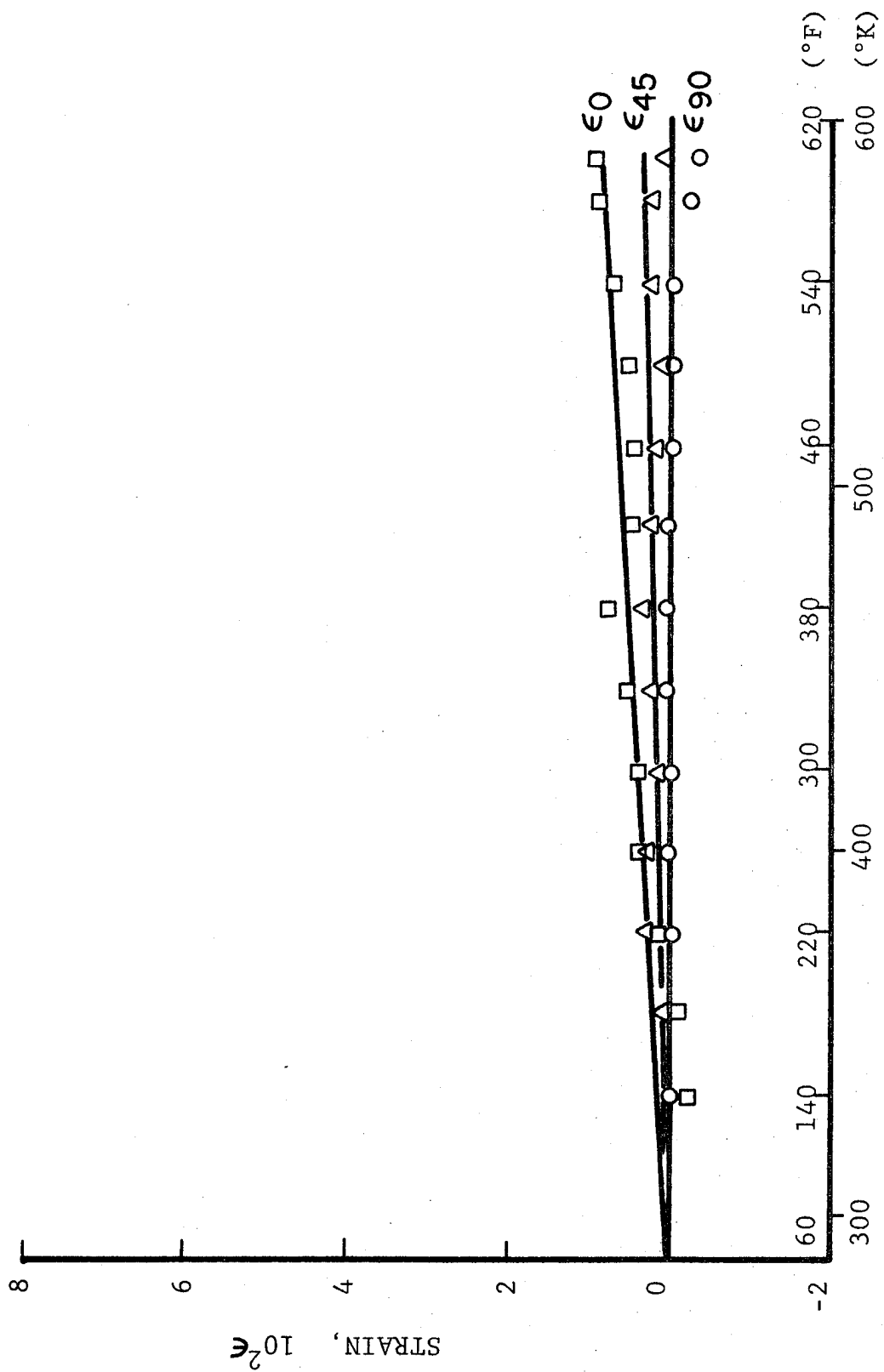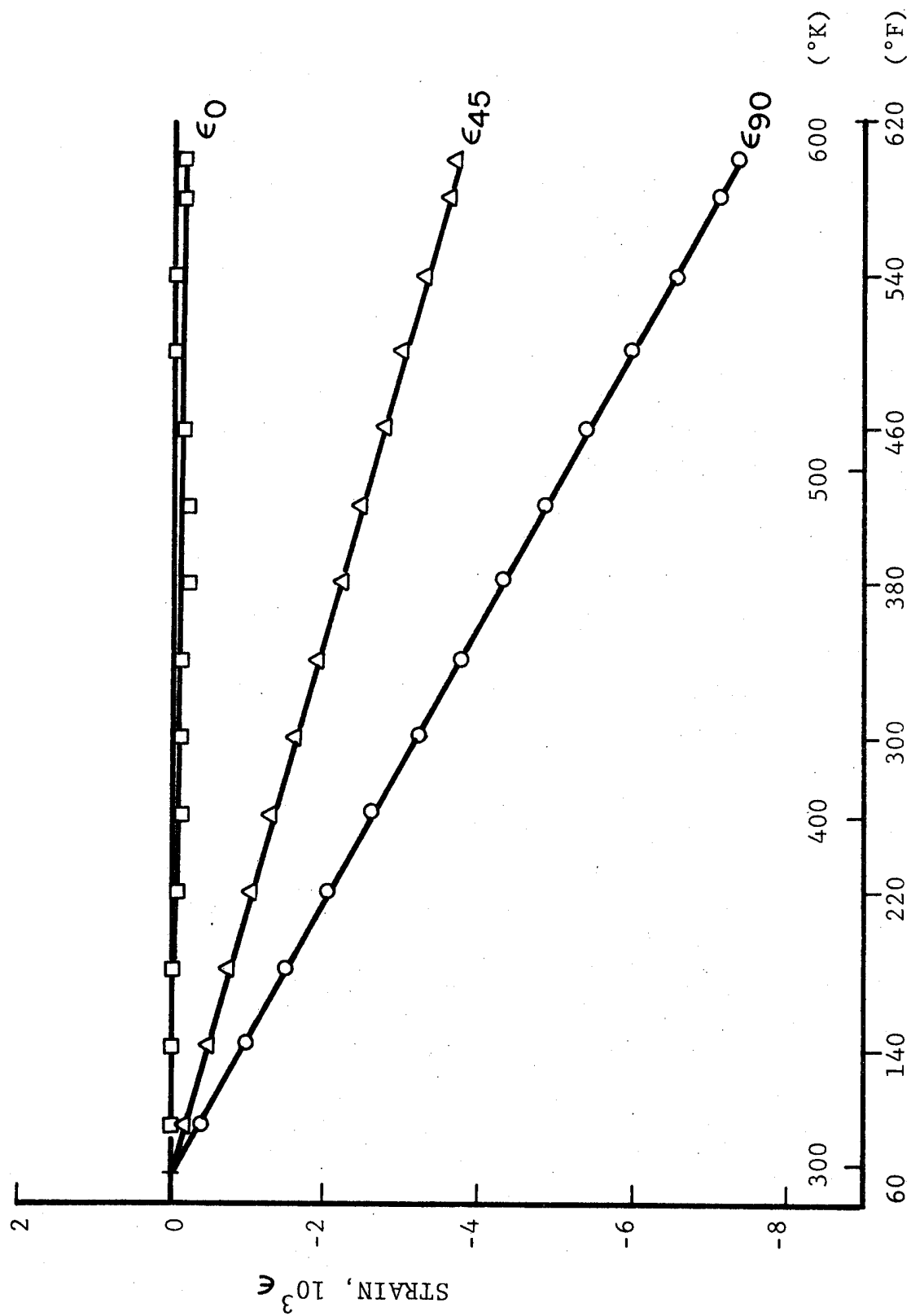
Fig. 6-19 RESTRAINT STRAINS IN 0-DEG PLIES OF $[0_2/90_2]_s$ GRAPHITE/POLYIMIDE SPECIMEN

6-37

6-9
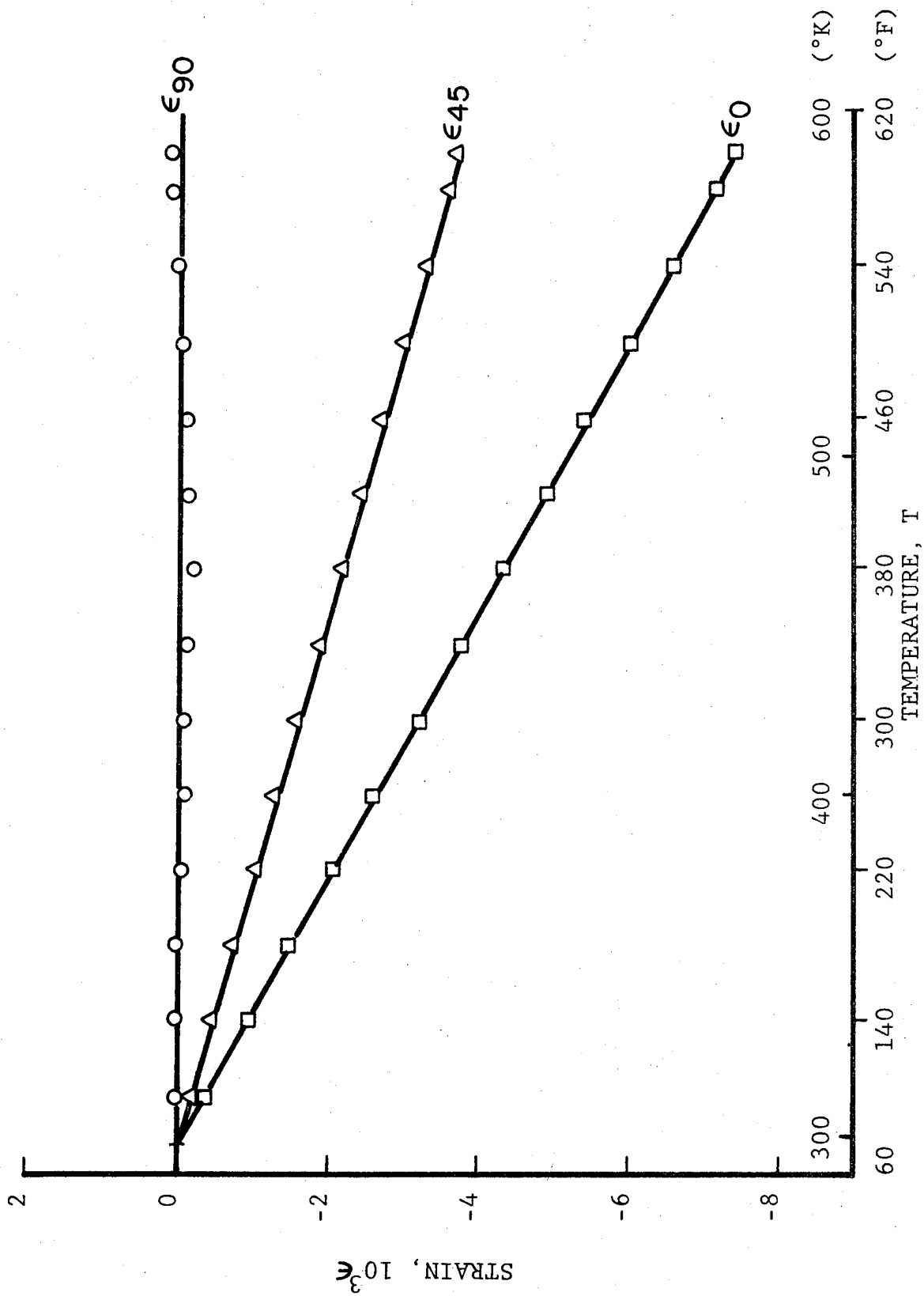
Fig. 6-20 RESTRAINT STRAINS IN 90-DEG PLIES OF $[0_2/90_2]_s$ GRAPHITE/POLYIMIDE SPECIMEN

6-38

Fig. 6-21 STRAINS IN $[0_2/\pm15]_s$ GRAPHITE/POLYIMIDE SPECIMEN UNDER TENSILE LOADING

$E_{xx} = 186.$ GPa $(27.0 \times 10^6$ psi$)$

$\nu_{xy} = 1.50$

$S_{xxT} = 590$ MPa $(85.5$ ksi$)$

STRESS, σ_{xx}, (MPa)

STRAIN, $10^3 \epsilon$

STRESS, σ_{xx}, (ksi)

$-\epsilon_{yy}$

ϵ_{xx}

Fig. 6-22 STRAINS IN $[0_2/\pm15]_s$ GRAPHITE/POLYIMIDE SPECIMEN UNDER UNIAXIAL LOADING

$E_{xx} = 217$ GPa (31.5×10^6 psi)

$\nu_{xy} = 1.57$

$S_{xxT} = 622$ MPa (90.2 ksi)

Fig. 6-23   STRAINS IN $[0_2/90_2]_s$ GRAPHITE/POLYIMIDE
SPECIMEN UNDER TENSILE LOADING

Fig. 6-24   APPARENT STRAINS IN $[0_2/\pm 15]_s$ GRAPHITE/POLYIMIDE SPECIMEN DURING THERMAL CYCLING WITH
TENSILE LOAD (FILLED SYMBOLS: BEGINNING OF CYCLING; OPEN SYMBOLS: END OF CYCLING).

6-42

6-9

Fig. 6-25 STRAINS IN $[0_2/\pm 15]_s$ GRAPHITE/POLYIMIDE SPECIMEN UNDER UNIAXIAL
TENSILE LOADING AFTER 100 THERMAL CYCLES BETWEEN ROOM TEMPERATURE
AND 533 degK (500°F) UNDER TENSILE LOADING

E_{xx} = 208 GPa (30.2 x 10^6 psi)

ν_{xy} = 1.37

S_{xxT} = 720 MPa (104 ksi)

Fig. 6-26 STRAINS IN $[0_2/\pm15]_s$ GRAPHITE/POLYIMIDE SPECIMEN UNDER UNIAXIAL TENSILE LOADING AFTER 100 THERMAL CYCLES BETWEEN ROOM TEMPERATURE AND 533 degK (500°F) UNDER TENSILE LOADING

E_{xx} = 199 GPa (28.8 x 10^6 psi)

ν_{xy} = 1.62

S_{xxT} = 676 MPa (98 ksi)

Fig. 6-27 STRAINS IN $[0_2/90_2]_s$ GRAPHITE/POLYIMIDE SPECIMEN UNDER UNIAXIAL TENSILE LOADING AFTER 100 THERMAL CYCLES BETWEEN ROOM TEMPERATURE AND 533 degK (500°F) UNDER TENSILE LOADING

E_{xx} = 117 GPa (17.0 x 10^6 psi)

ν_{xy} = 0.012

S_{xxT} = 342 MPa (50 ksi)

Fig. 6-28 STRAINS IN $[0_2/90_2]_s$ GRAPHITE/POLYIMIDE SPECIMEN UNDER UNIAXIAL TENSILE LOADING AFTER 100 THERMAL CYCLES BETWEEN ROOM TEMPERATURE AND 533 degK (500°F) UNDER TENSILE LOADING

E_{xx} = 107 GPa (15.5 x 10^6 psi)

ν_{xy} = 0.015

S_{xxT} = 333 MPa (48 ksi)

Fig. 6-29 APPARENT STRAINS IN $[0_2/\pm15]_s$ GRAPHITE/POLYIMIDE
SPECIMEN DURING THERMAL CYCLING WITH TENSILE
LOAD (FILLED SYMBOLS: BEGINNING OF CYCLING; OPEN
SYMBOLS: END OF CYCLING).
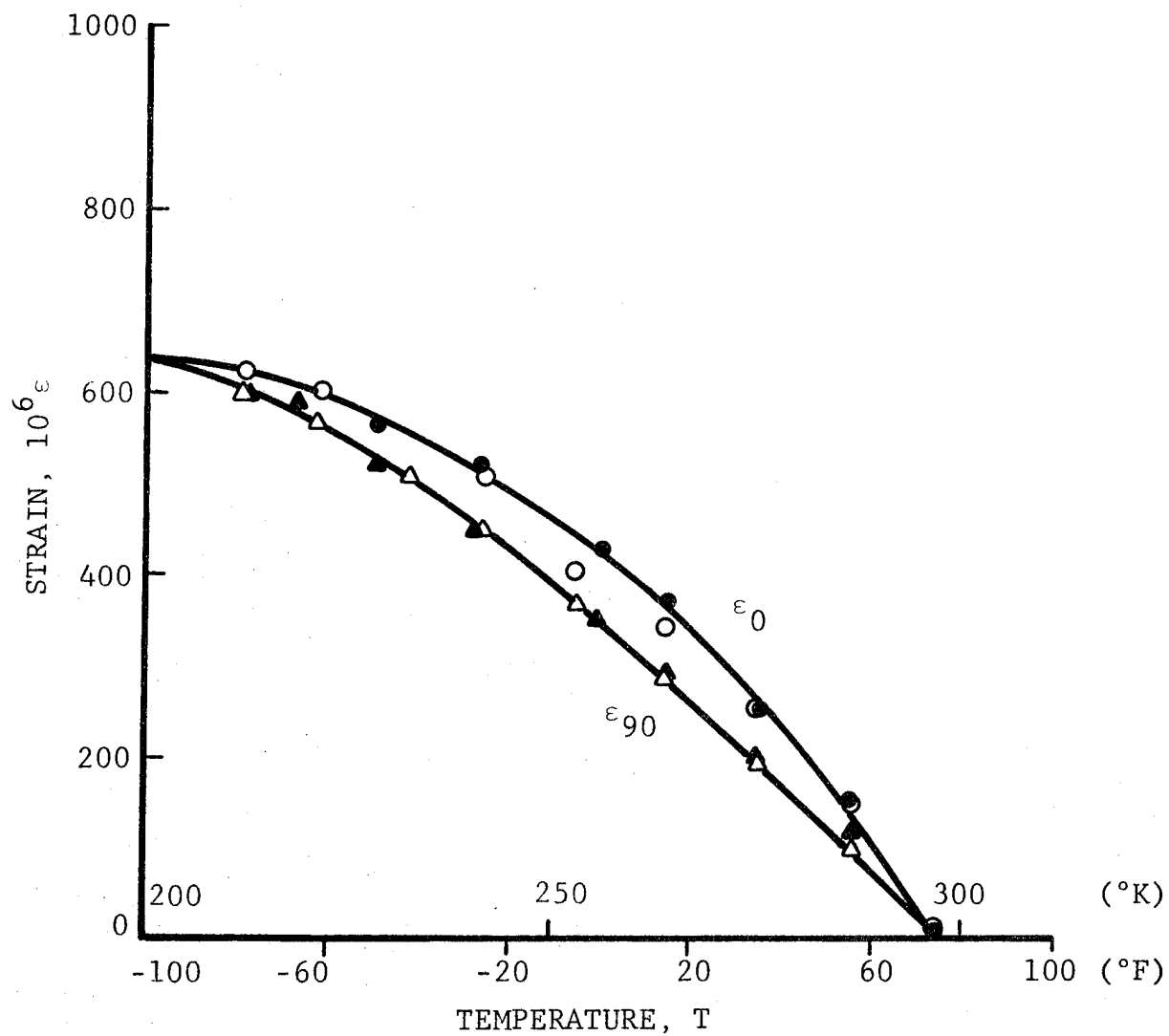
Fig. 6-30 APPARENT STRAINS IN $[0_2/90_2]_s$ GRAPHITE/
POLYIMIDE SPECIMEN DURING THERMAL CYCLING
WITH TENSILE LOAD (FILLED SYMBOLS: BEGINNING
OF CYCLING; OPEN SYMBOLS: END OF CYCLING)

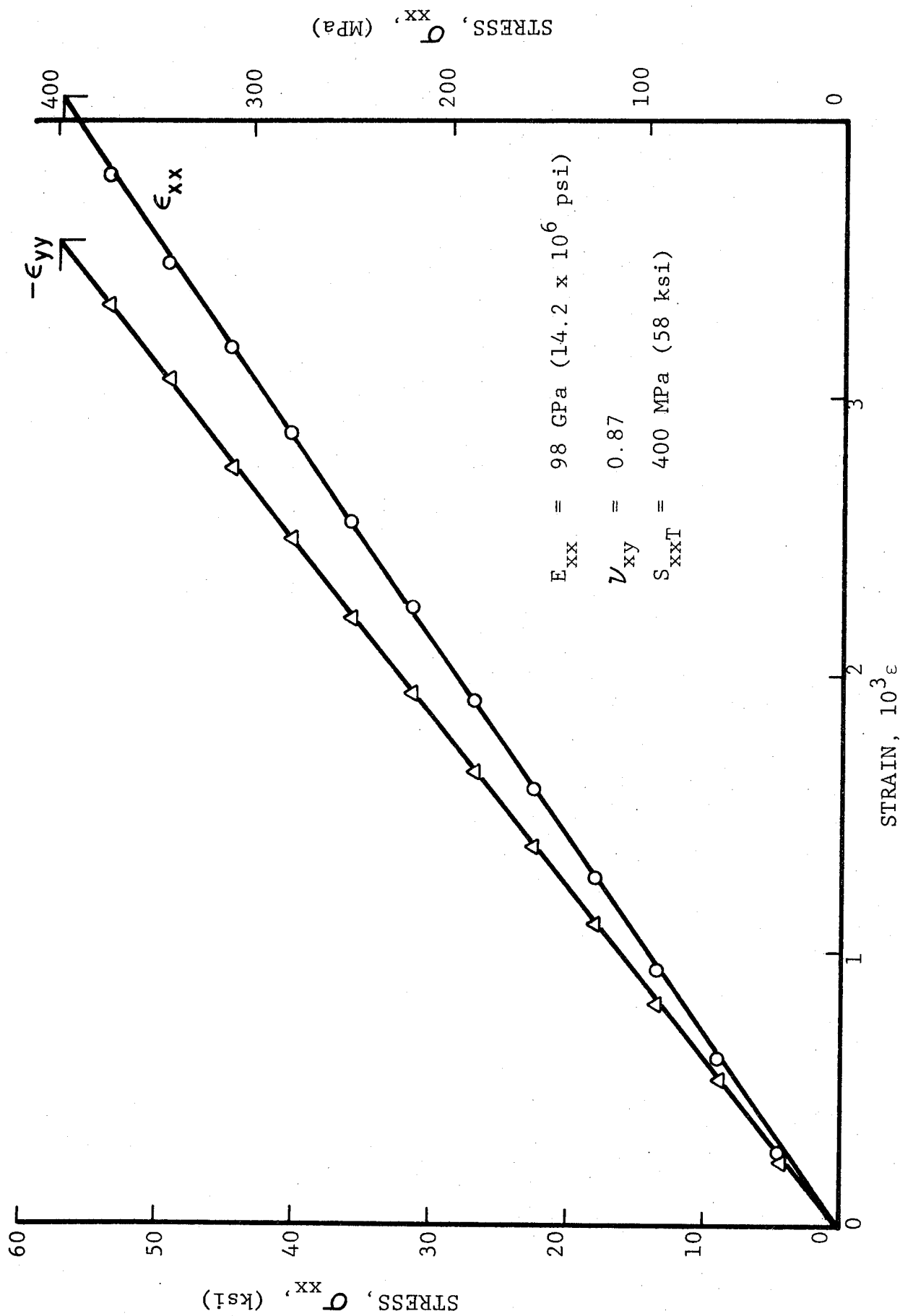Fig. 6-31 STRAINS IN $[0_2/\pm 15]_s$ GRAPHITE/POLYIMIDE SPECIMEN UNDER UNIAXIAL TENSILE LOADING AFTER 100 THERMAL CYCLES BETWEEN ROOM TEMPERATURE AND 200 degK (-100°F) UNDER TENSILE LOADING

E_{xx} = 206 GPa (29.8 x 10^6 psi)

ν_{xy} = 1.30

S_{xxT} = 809 MPa (117 ksi)

Fig. 6-32 STRAINS IN $[0_2/\pm15]_s$ GRAPHITE/POLYIMIDE SPECIMEN UNDER UNIAXIAL TENSILE LOADING AFTER 100 THERMAL CYCLES BETWEEN ROOM TEMPERATURE AND 200 degK (-100°F) UNDER TENSILE LOADING
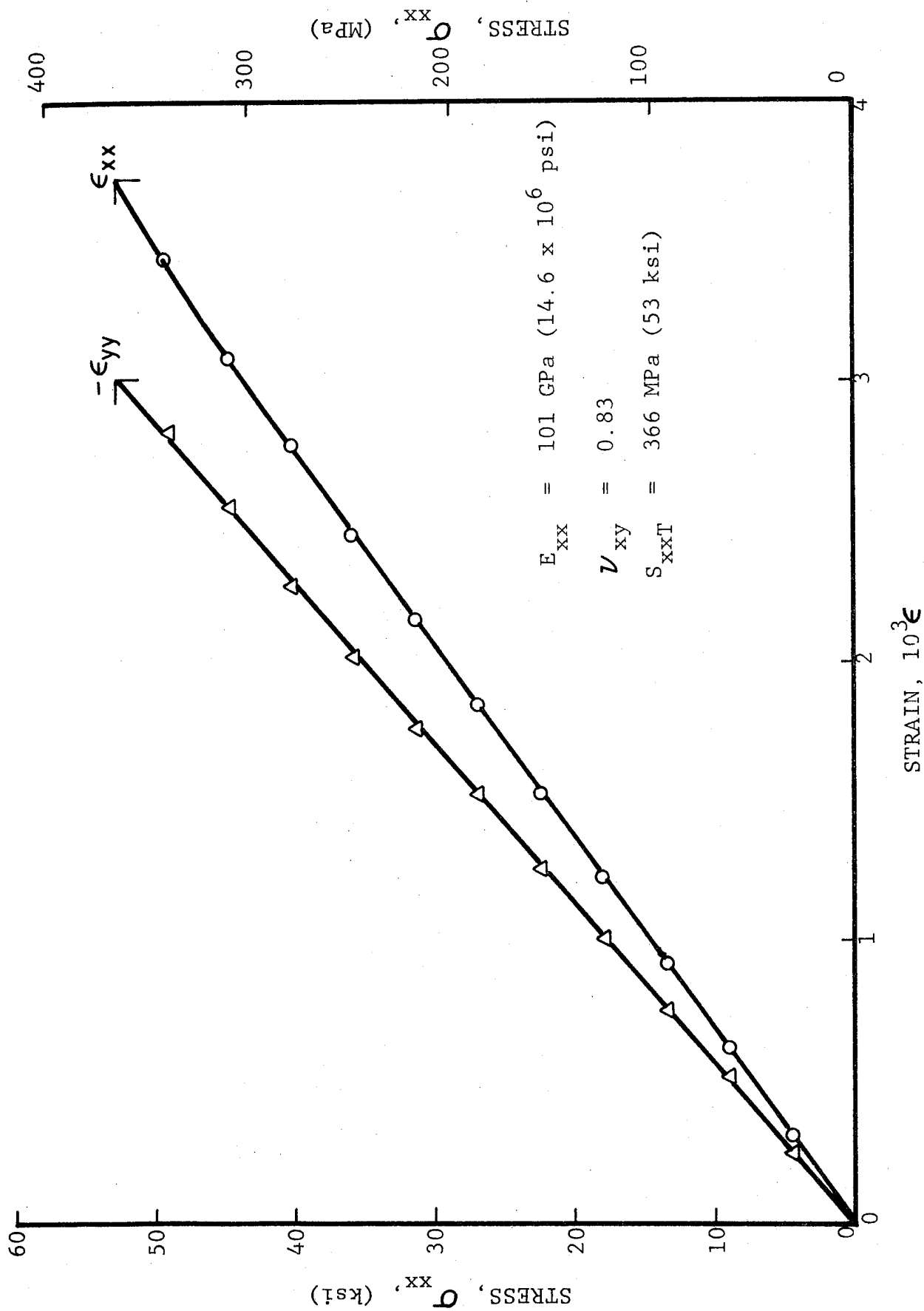
E_{xx} = 197 GPa (28.5 x 10^6 psi)

ν_{xy} = 1.50

S_{xxT} = 591 MPa (86 ksi)

Fig. 6-33   STRAINS IN $[0_2/90_2]_s$ GRAPHITE/POLYIMIDE SPECIMEN UNDER UNIAXIAL TENSILE LOADING AFTER 100 THERMAL CYCLES BETWEEN ROOM TEMPERATURE AND 200 degK (-100°F) UNDER TENSILE LOADING

E_{xx} = 122 GPa (17.7 x 10^6 psi)

ν_{xy} = 0.06

S_{xxT} = 328 MPa (48 ksi)
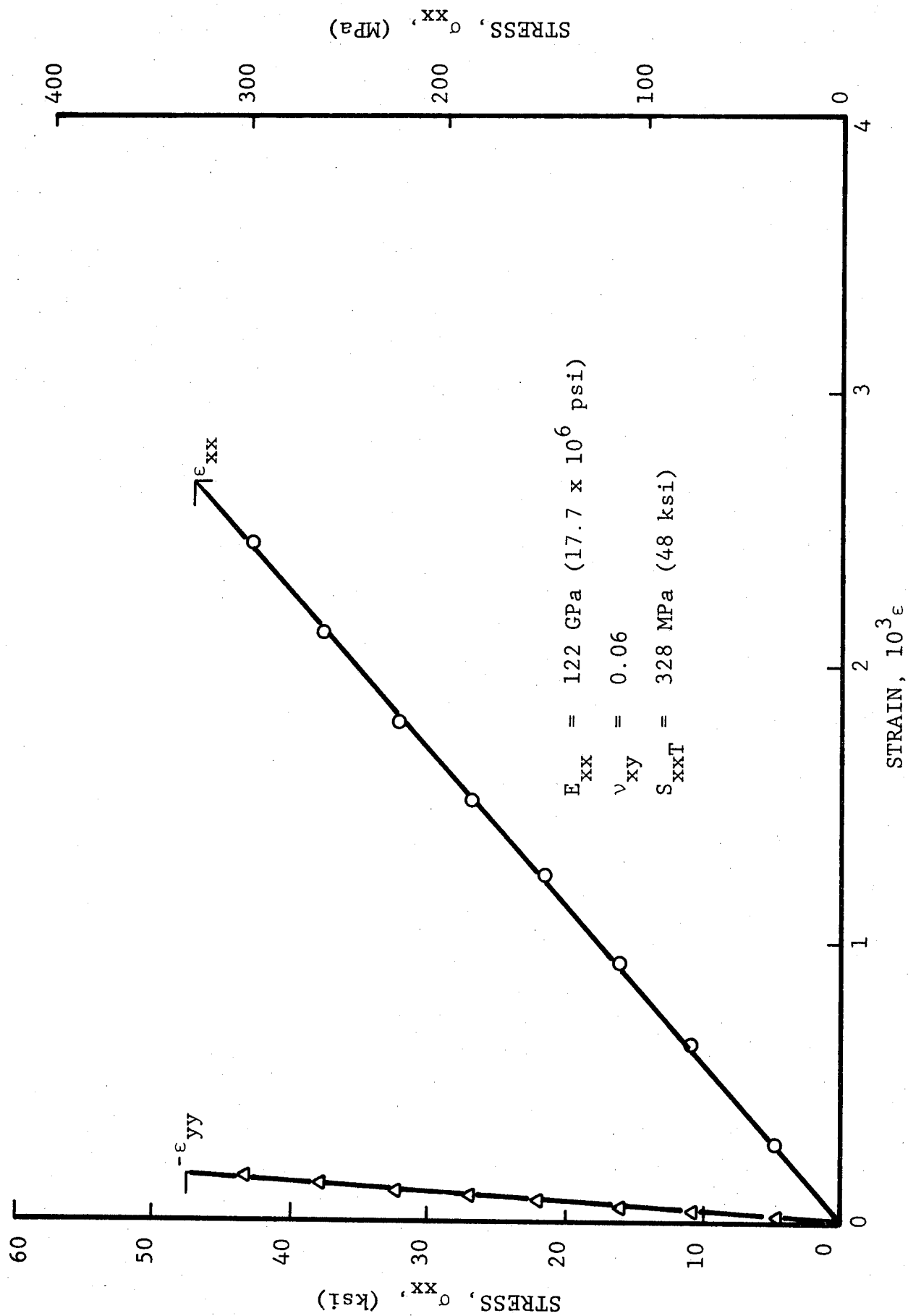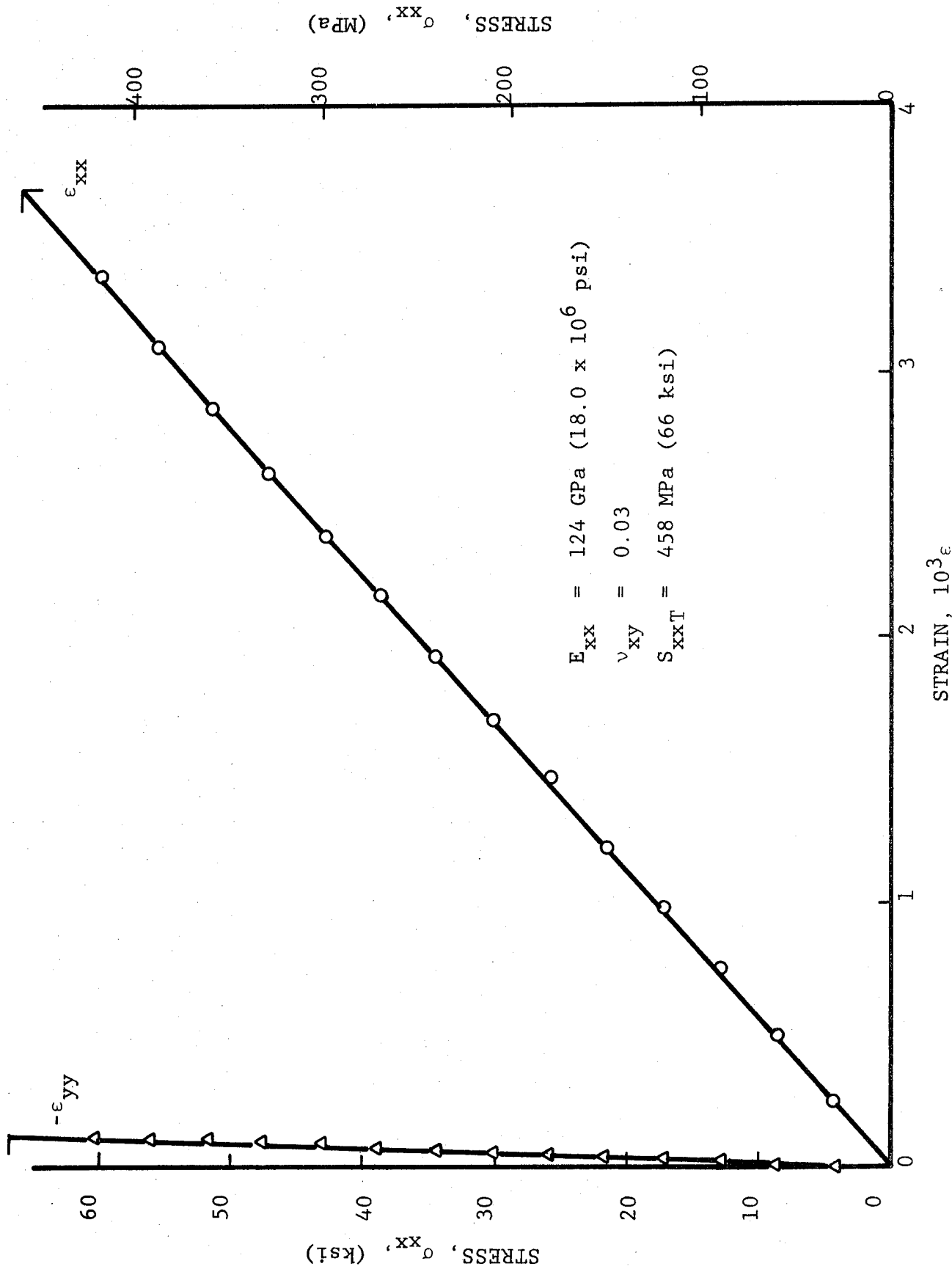
Fig. 6-34 STRAINS IN $[0_2/90_2]_s$ GRAPHITE/POLYIMIDE SPECIMEN UNDER UNIAXIAL TENSILE LOADING AFTER 100 THERMAL CYCLES BETWEEN ROOM TEMPERATURE AND 200 degK (-100°F) UNDER TENSILE LOADING

E_{xx} = 124 GPa (18.0 x 10^6 psi)

ν_{xy} = 0.03

S_{xxT} = 458 MPa (66 ksi)
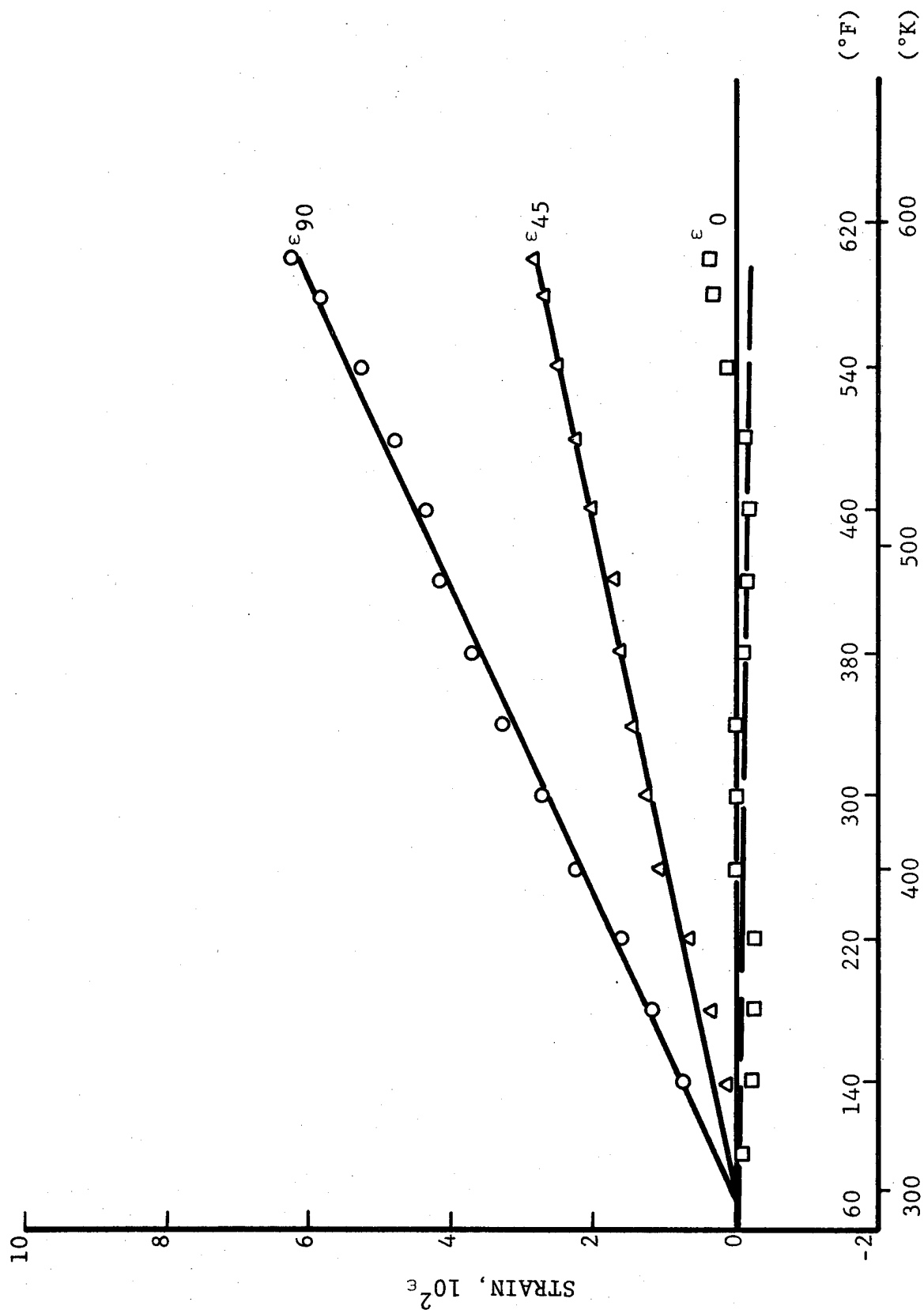
Fig. 6-35 STRAINS IN $[\pm 45/0_2]_s$ GRAPHITE/POLYIMIDE SPECIMEN
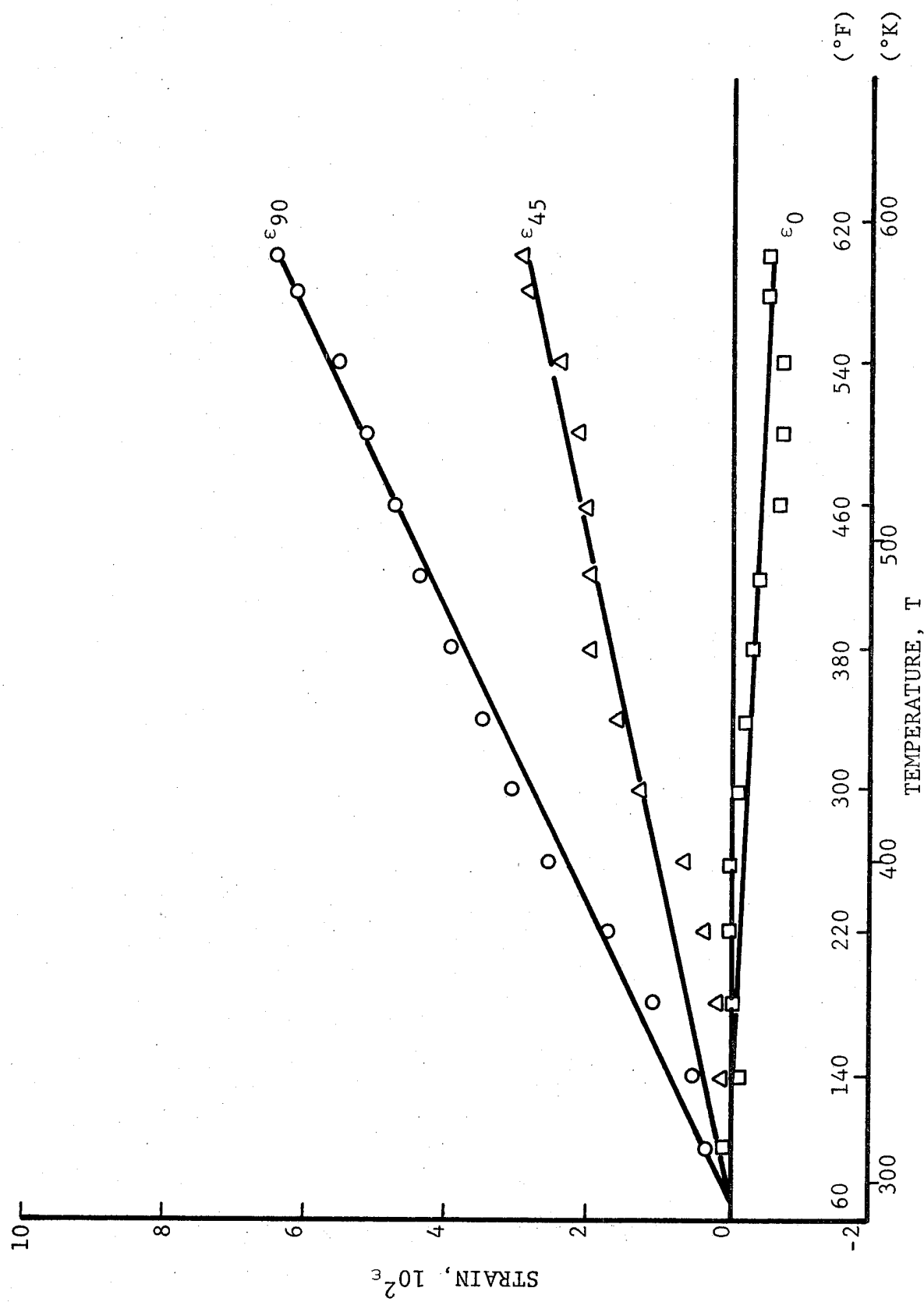
Fig. 6-36 STRAINS IN [0/+45/0/-45]$_s$ GRAPHITE/POLYIMIDE SPECIMEN

6-54
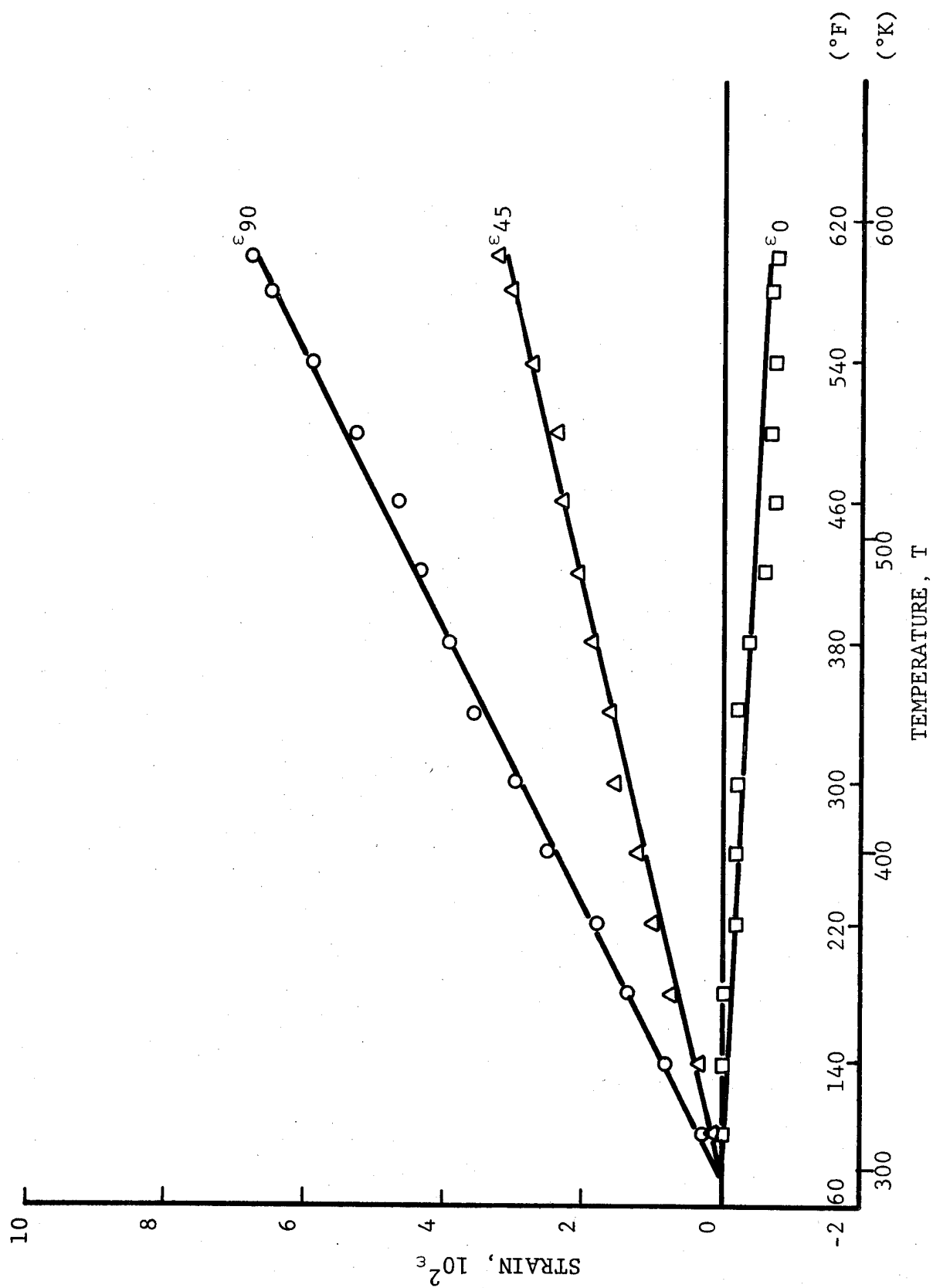
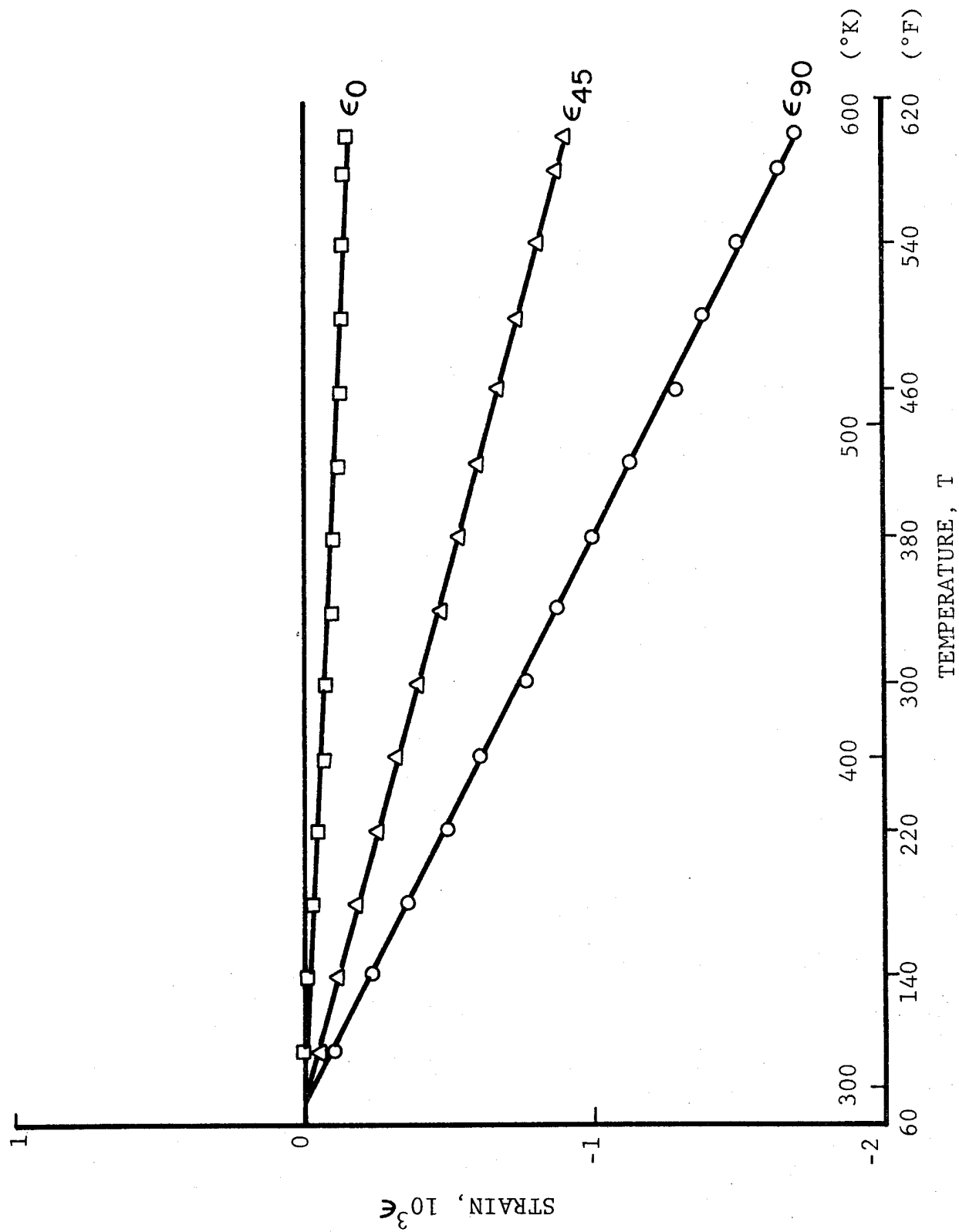Fig. 6-37 STRAINS IN [+45/0₂/-45]ₛ GRAPHITE/POLYIMIDE SPECIMEN
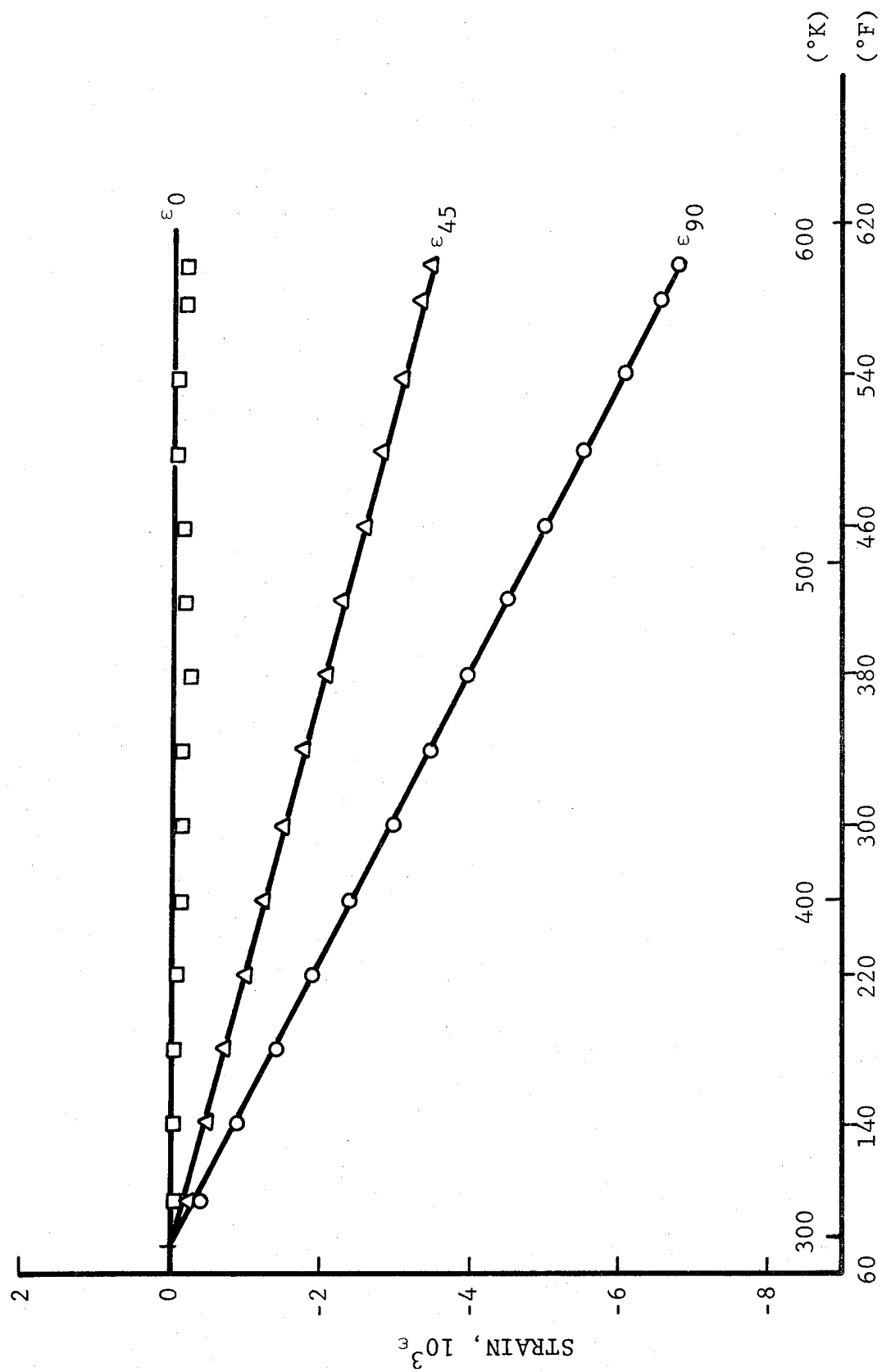
Fig. 6-38 RESTRAINT STRAINS IN 0-DEGREE PLIES OF $[\pm45/0_2]_s$ GRAPHITE/POLYIMIDE SPECIMEN

6-56
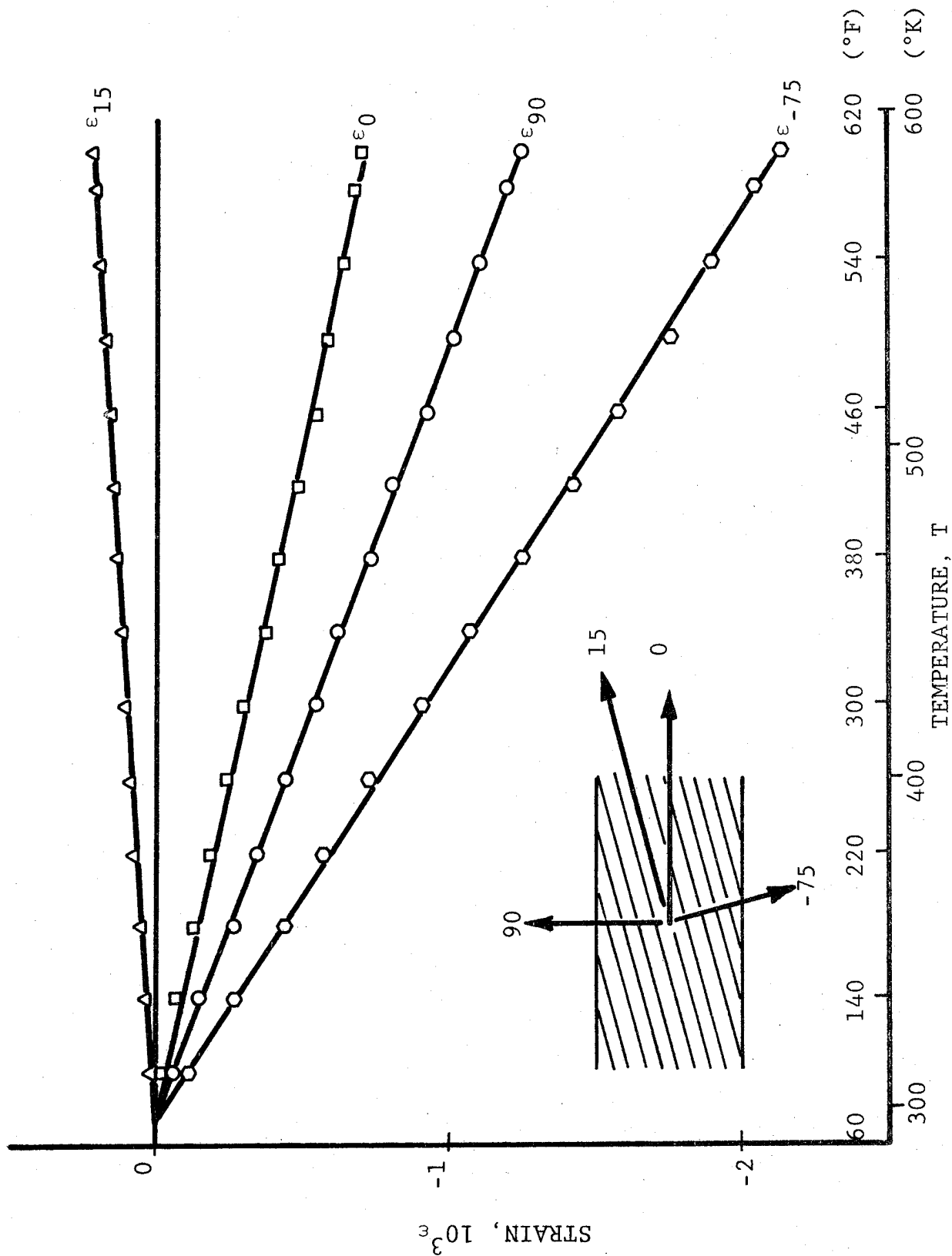
6-9
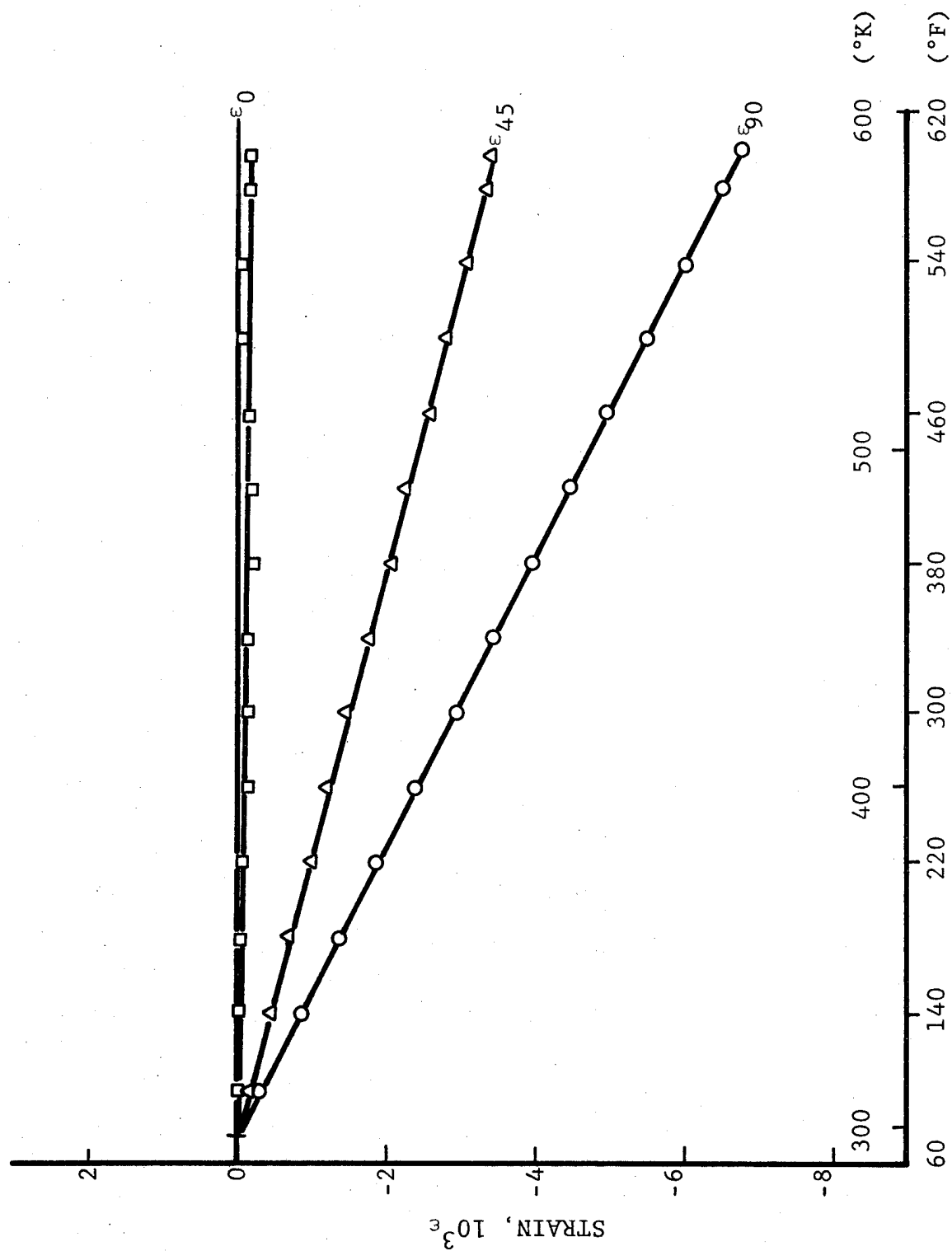
Fig. 6-39 RESTRAINT STRAINS IN 0-DEGREE PLIES OF $[0/+45/0/-45]_s$ GRAPHITE/ POLYIMIDE SPECIMEN
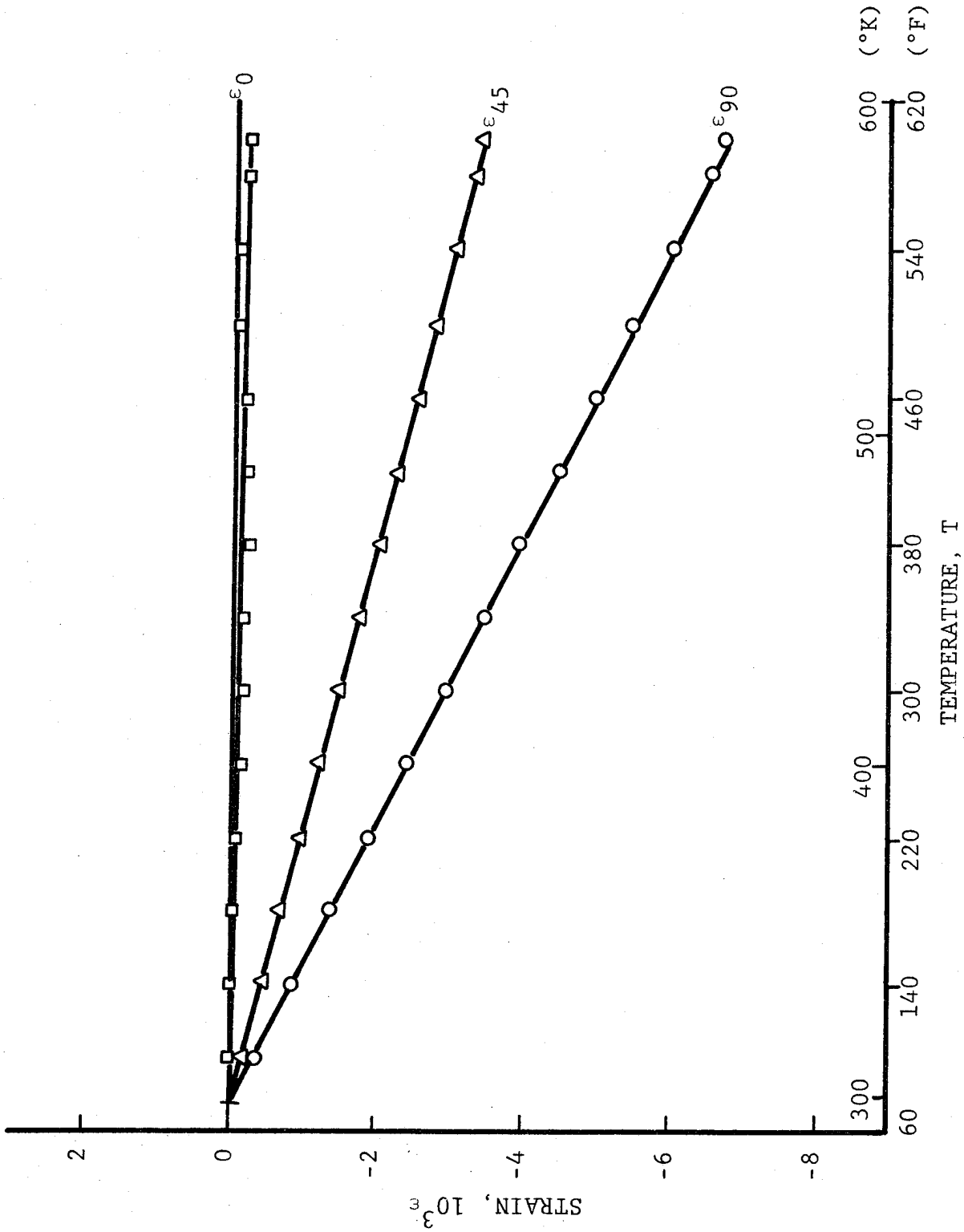
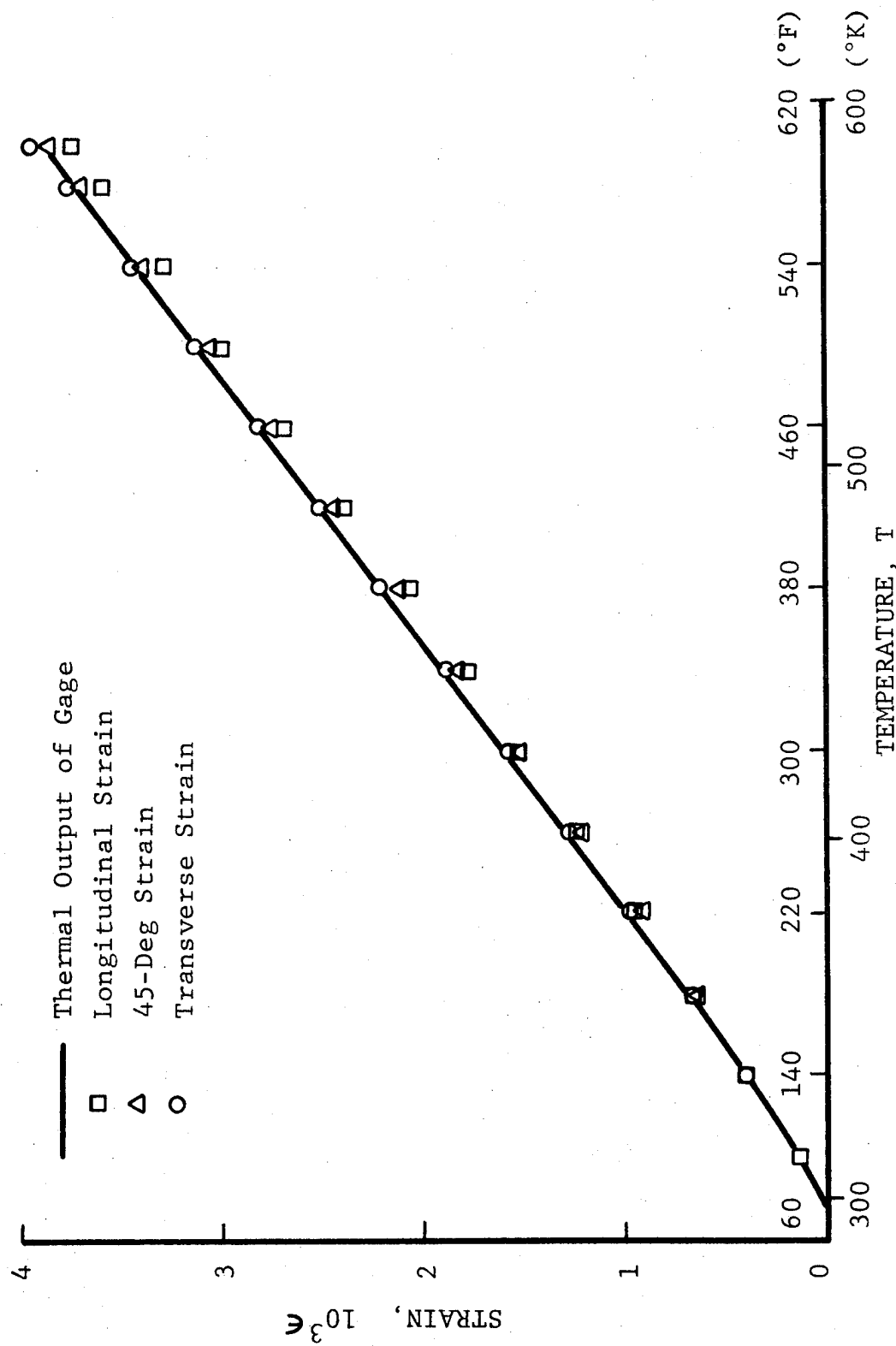Fig. 3-40 RESTRAINT STRAINS IN 0-DEGREE PLIES OF $[+45/0_2/-45]_s$ GRAPHITE/POLYIMIDE SPECIMEN

6-58
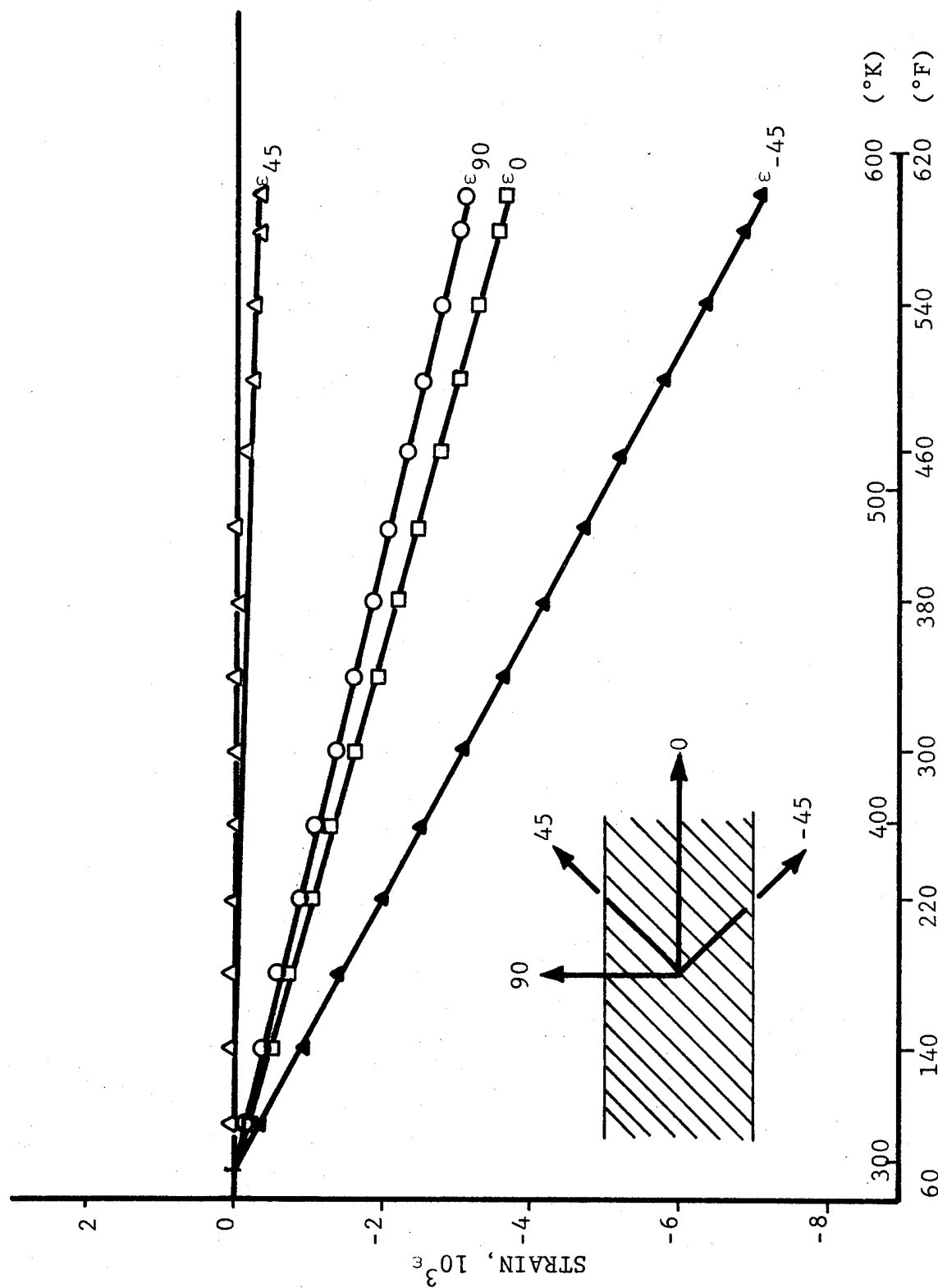
Fig. 6-41 RESTRAINT STRAINS IN 45-DEGREE PLIES OF $[\pm 45/0_2]_s$ GRAPHITE/
POLYIMIDE SPECIMEN
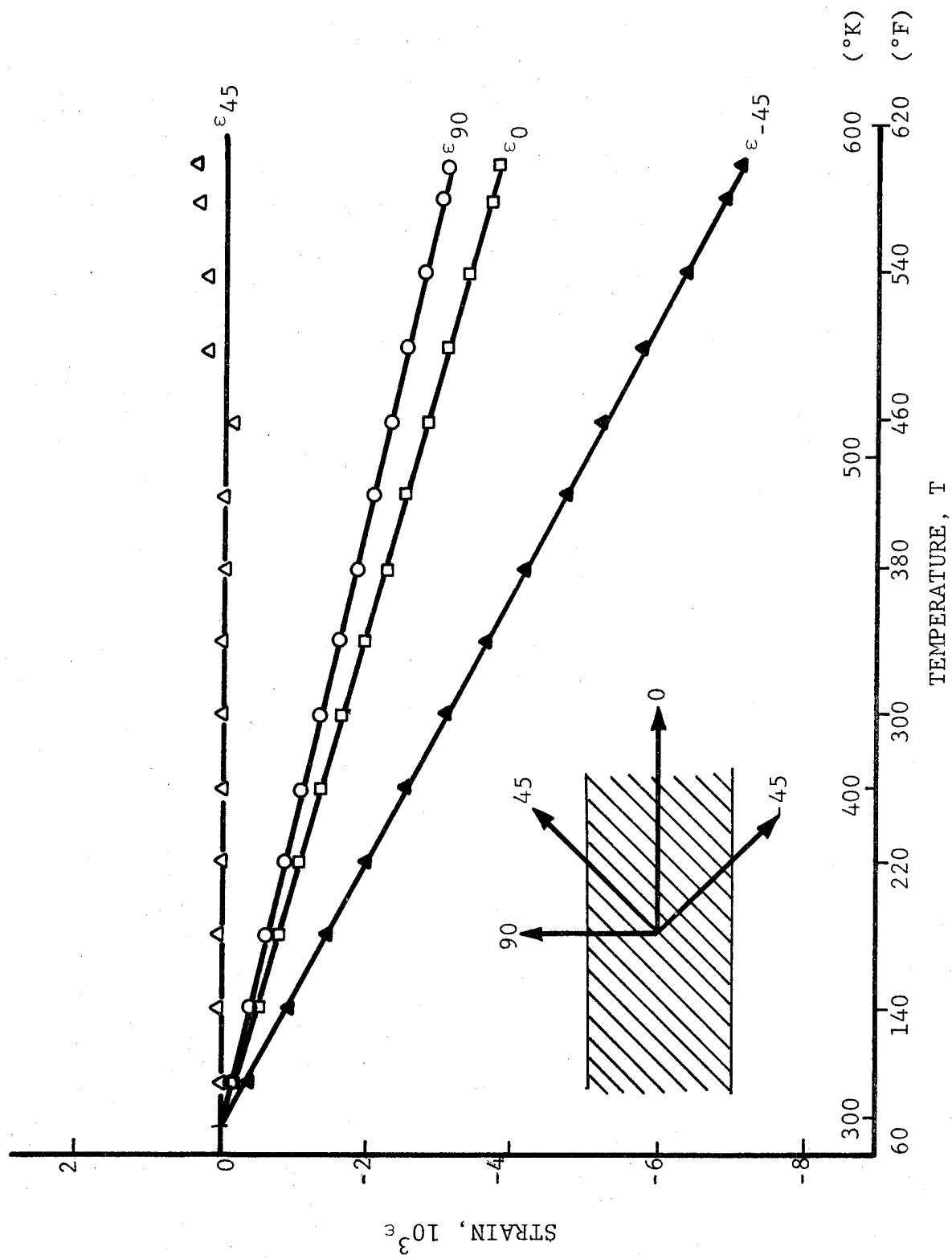
Fig. 6-42 RESTRAINT STRAINS IN 45-DEGREE PLIES OF $[0/+45/0/-45]_s$ GRAPHITE/ POLYIMIDE SPECIMEN

6-60
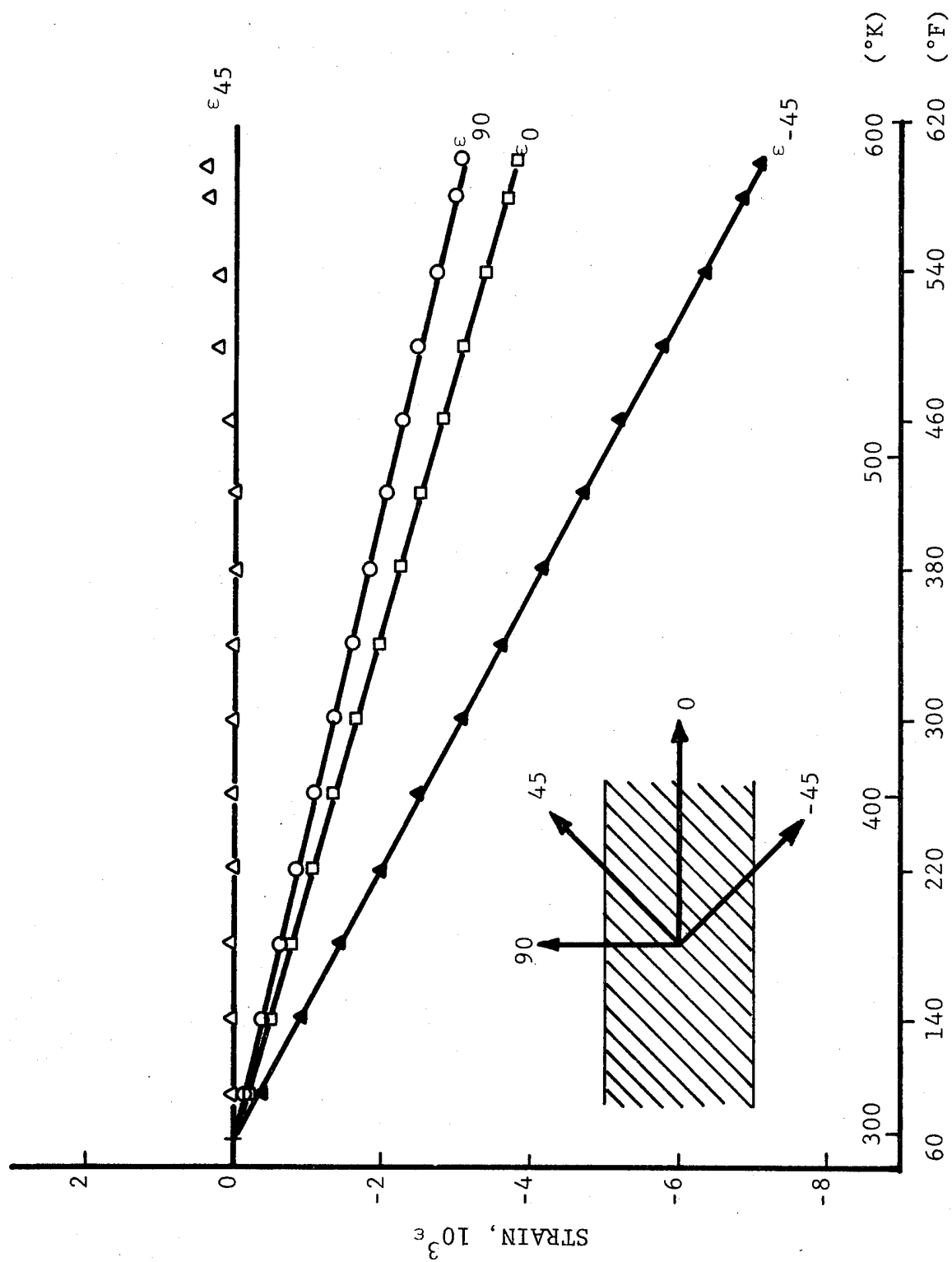
Fig. 6-43 RESTRAINT STRAINS IN 45-DEGREE PLIES OF $[+45/0_2/-45]_s$ GRAPHITE/
POLYIMIDE SPECIMEN
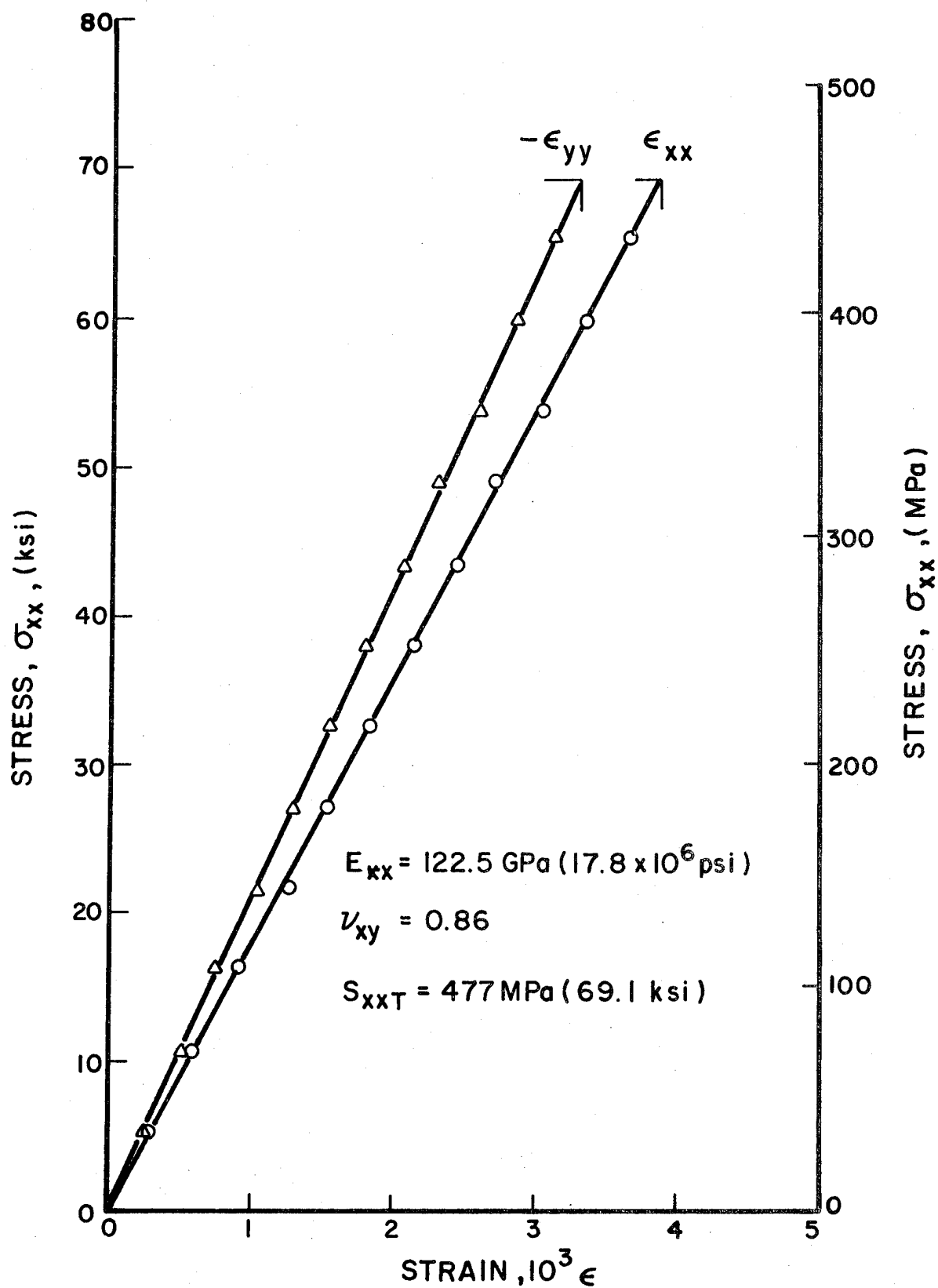
Fig. 6-44 STRAINS IN $[\pm 45/0_2]_s$ GRAPHITE/POLYIMIDE
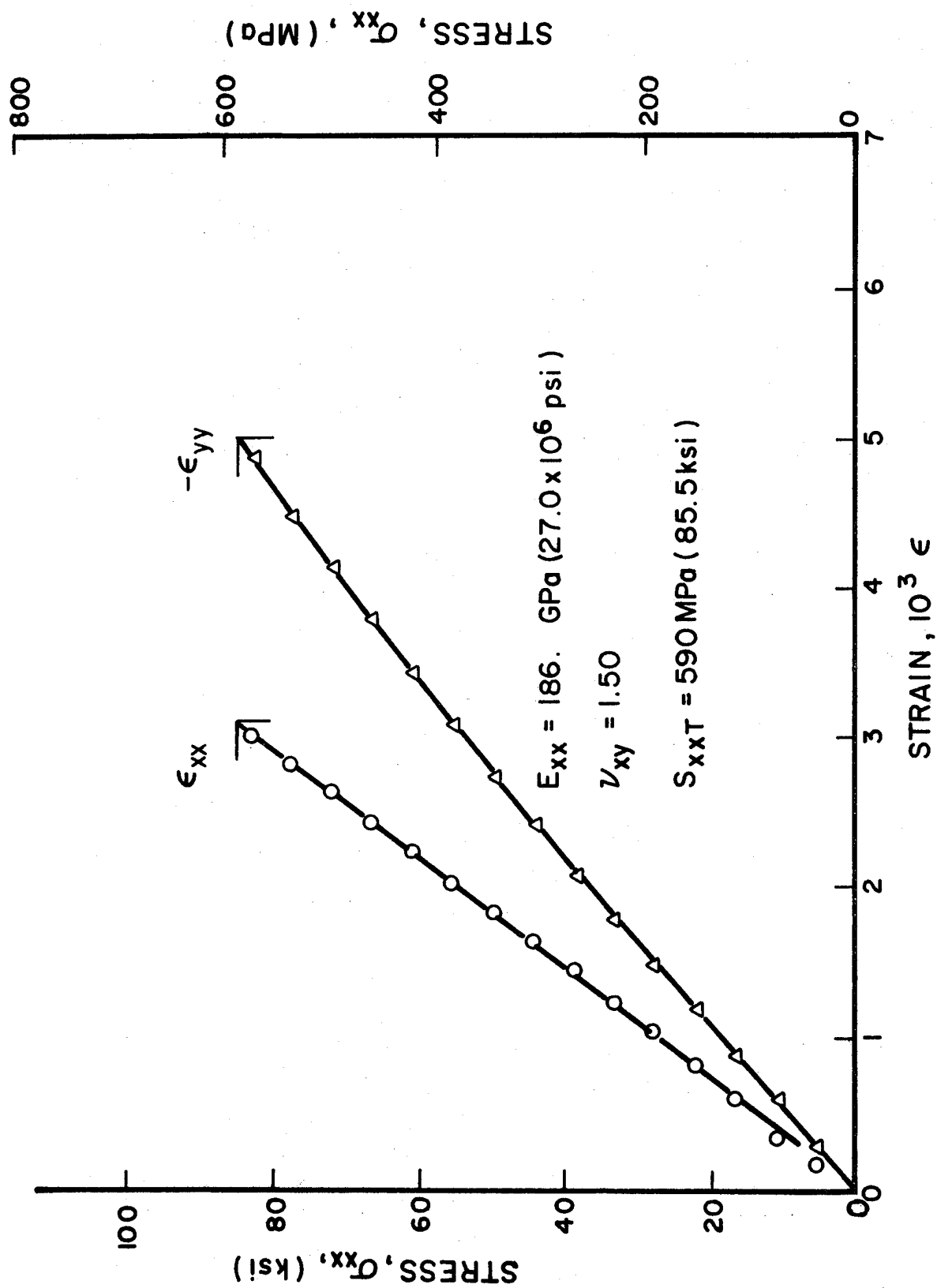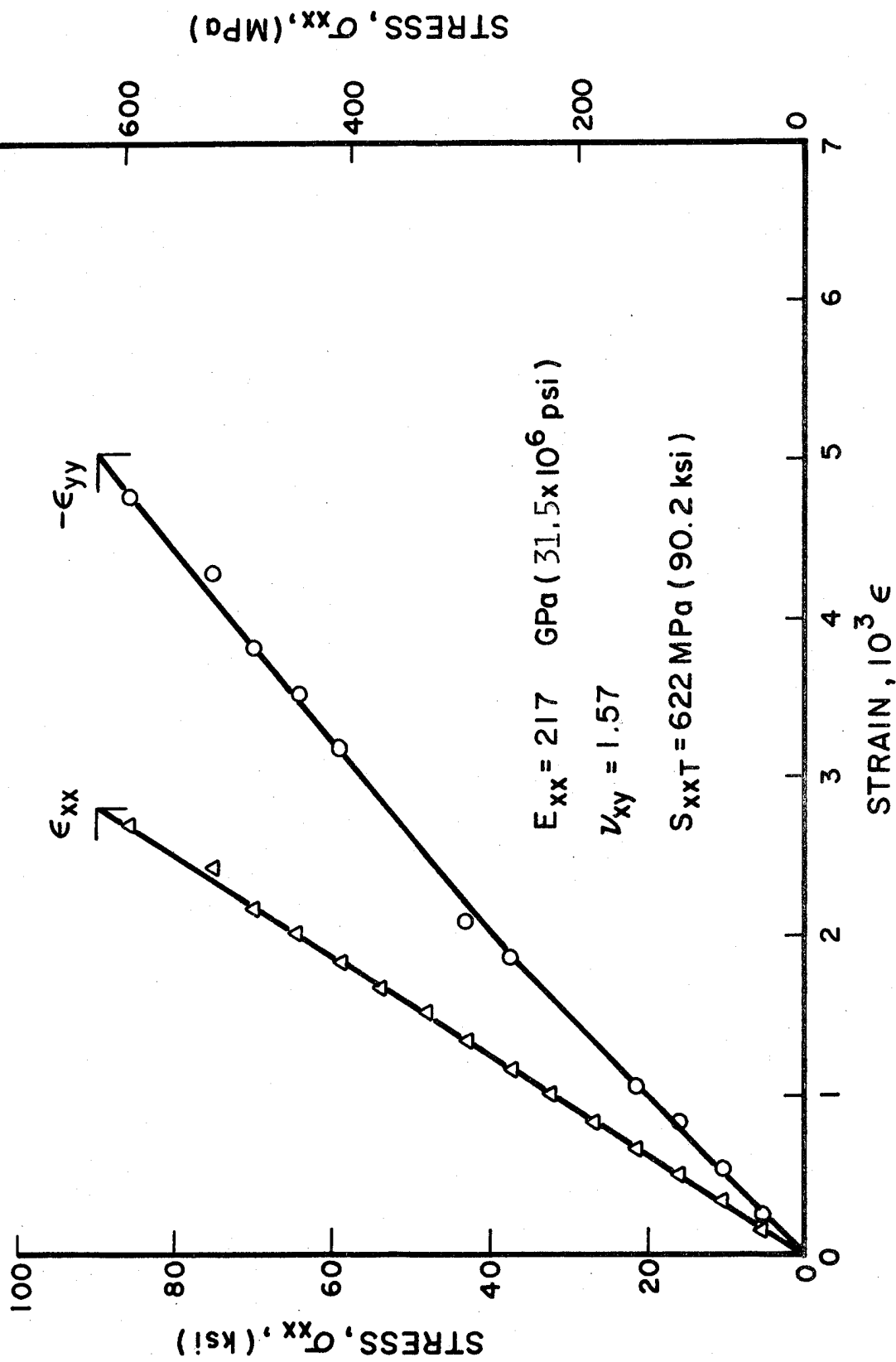SPECIMEN UNDER TENSILE LOADING

6-62
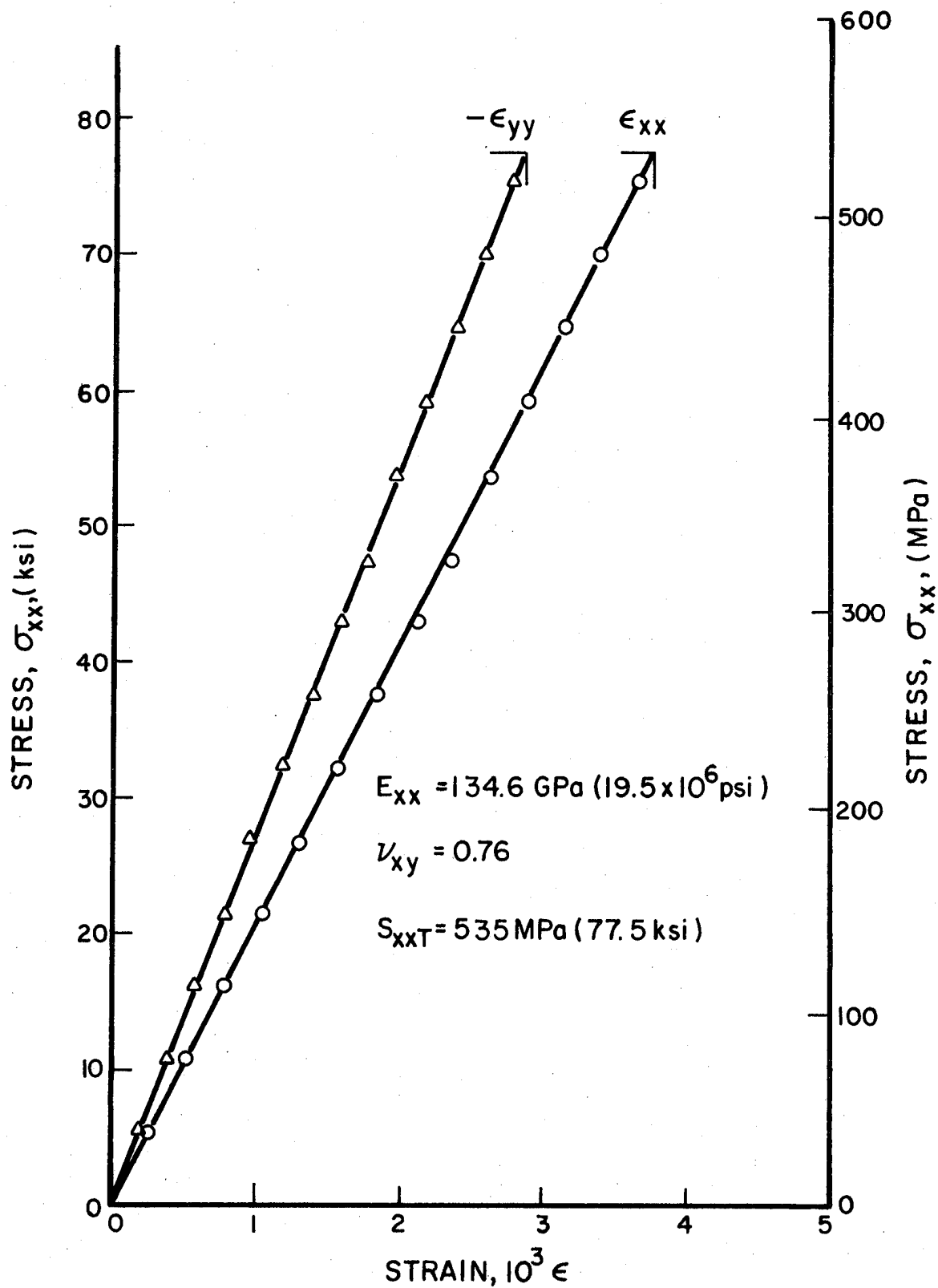
Fig. 6-45 STRAINS IN $[\pm 45/0_2]_s$ GRAPHITE/POLYIMIDE SPECIMEN UNDER TENSILE LOADING
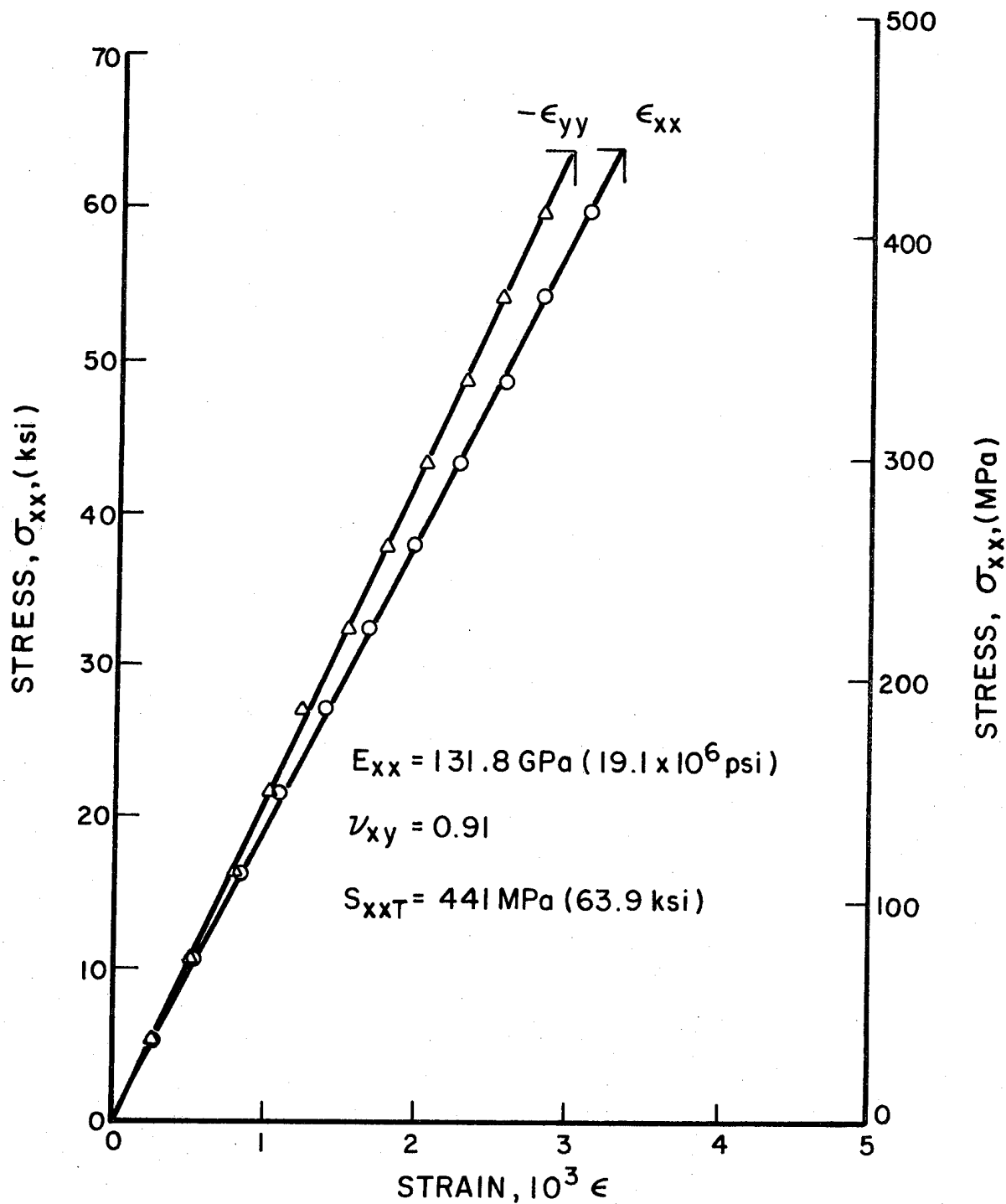
Fig. 6-46   STRAINS IN $[0/+45/0/-45]_s$ GRAPHITE/
POLYIMIDE SPECIMEN UNDER TENSILE LOADING

The figure shows stress vs. strain curves with the following annotations:

$E_{xx} = 131.8 \, GPa \, (19.1 \times 10^6 \, psi)$

$\nu_{xy} = 0.91$

$S_{xxT} = 441 \, MPa \, (63.9 \, ksi)$

Axis labels: STRESS, σ_{xx}, (ksi); STRESS, σ_{xx}, (MPa); STRAIN, $10^3 \epsilon$

Curve labels: $-\epsilon_{yy}$ and ϵ_{xx}
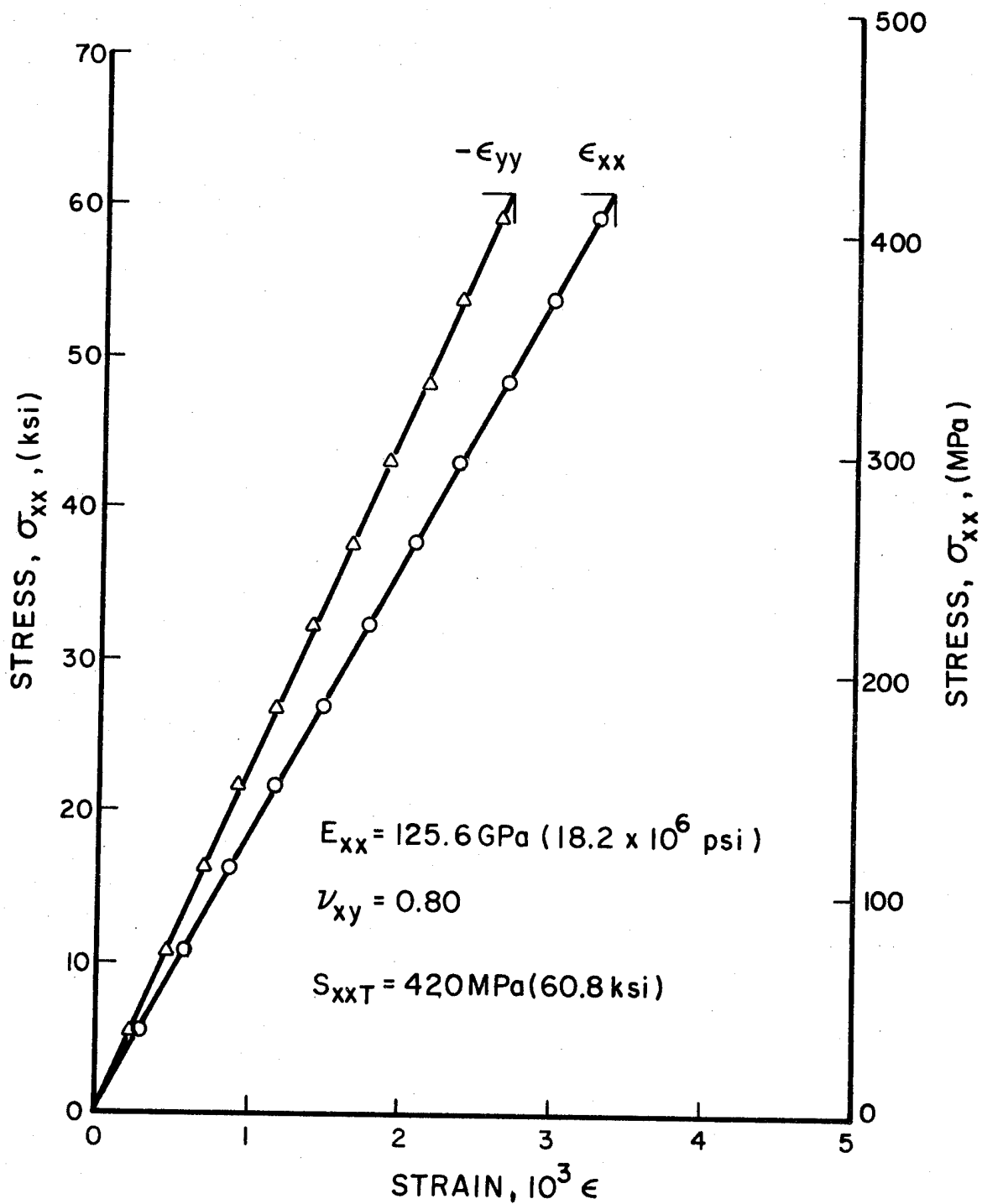
Fig. 6-47   STRAINS IN $[0/+45/0/-45]_s$ GRAPHITE/
POLYIMIDE SPECIMEN UNDER TENSILE LOADING

The figure shows stress-strain curves with:
E_{xx} = 125.6 GPa (18.2 x 10^6 psi)

ν_{xy} = 0.80

S_{xxT} = 420 MPa (60.8 ksi)
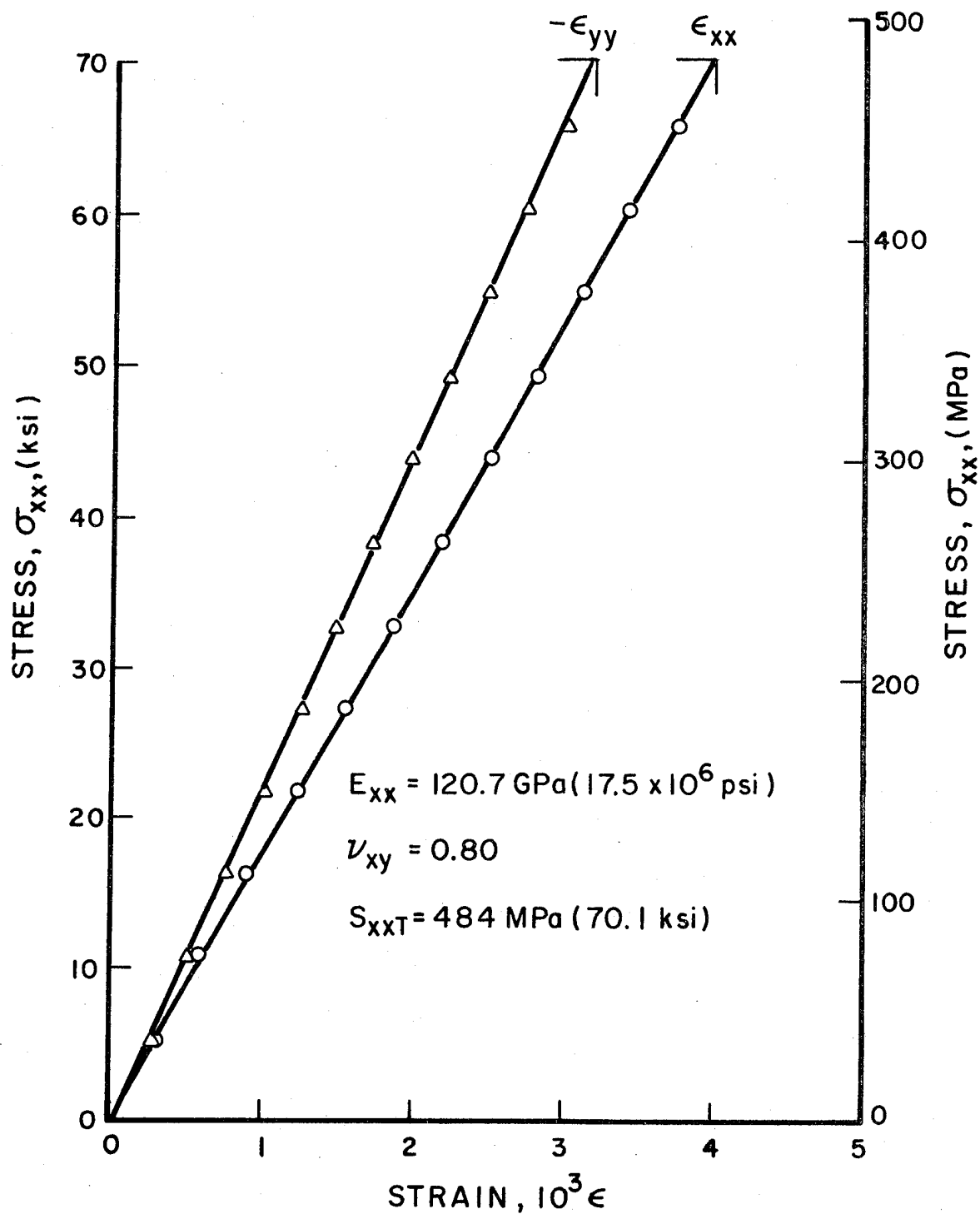
Fig. 6-48 STRAINS IN $[+45/0_2/-45]_s$ GRAPHITE/POLYIMIDE SPECIMEN UNDER TENSILE LOADING

6-66
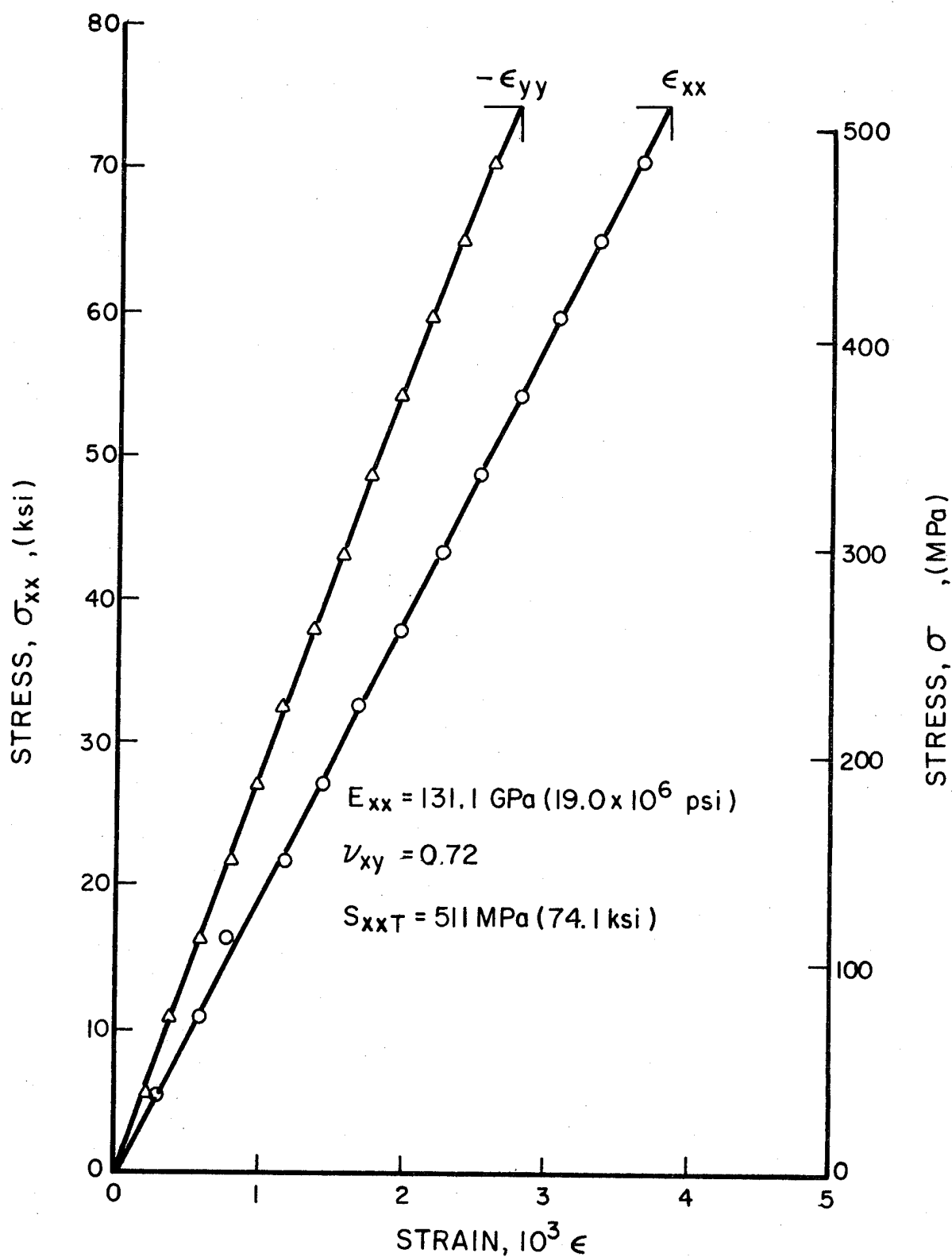
Fig. 6-49 STRAINS IN $[+45/0_2/-45]_s$ GRAPHITE/
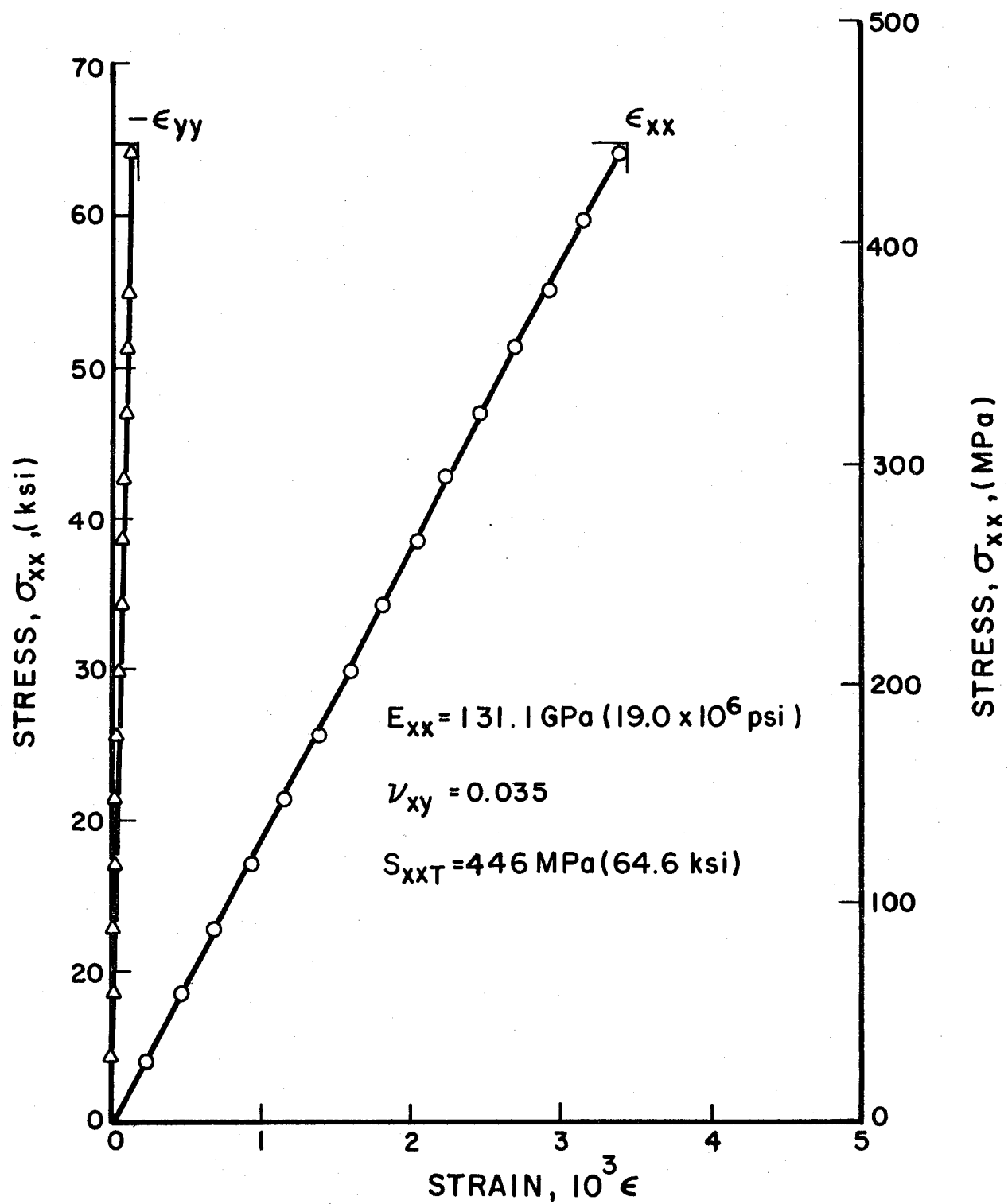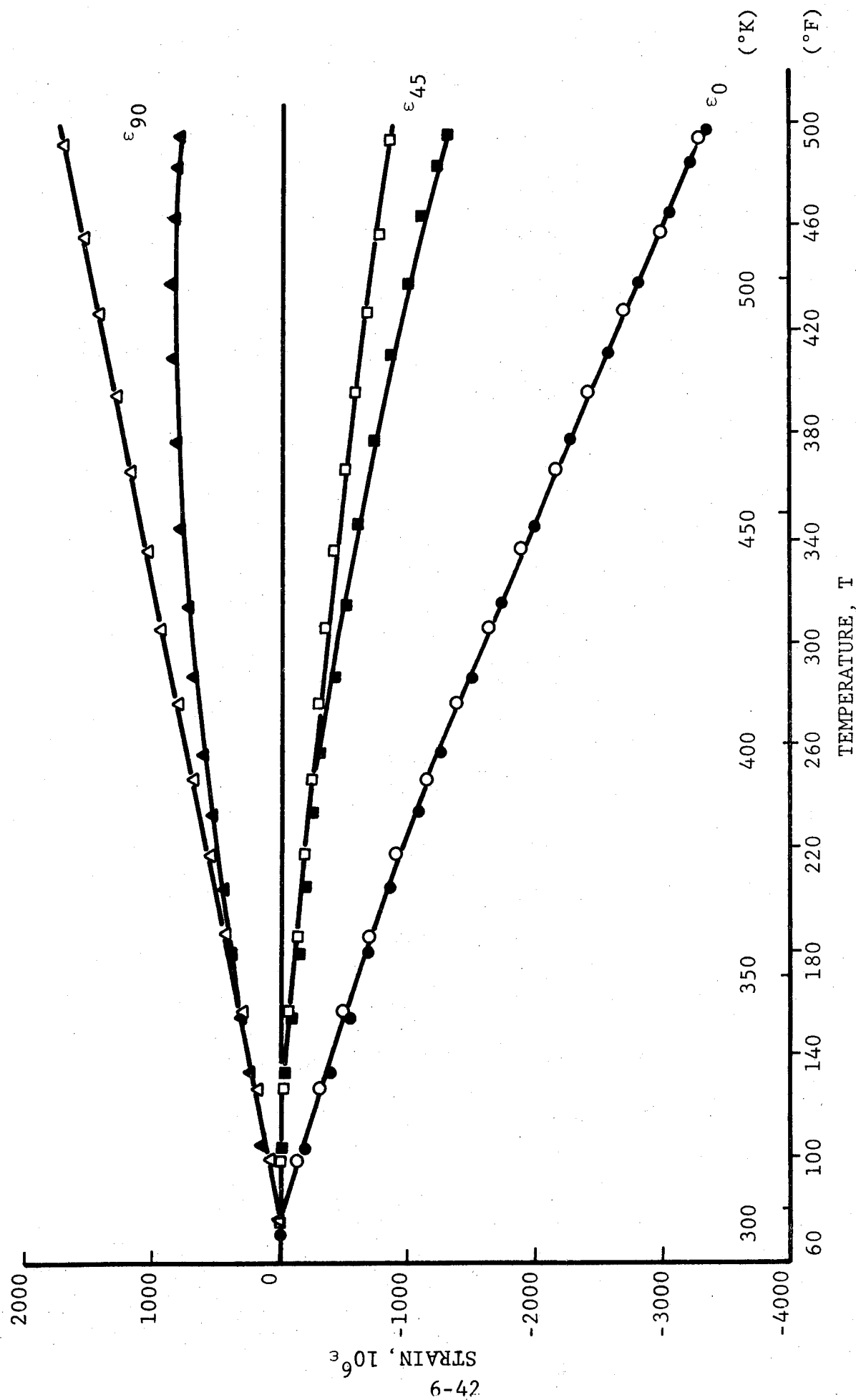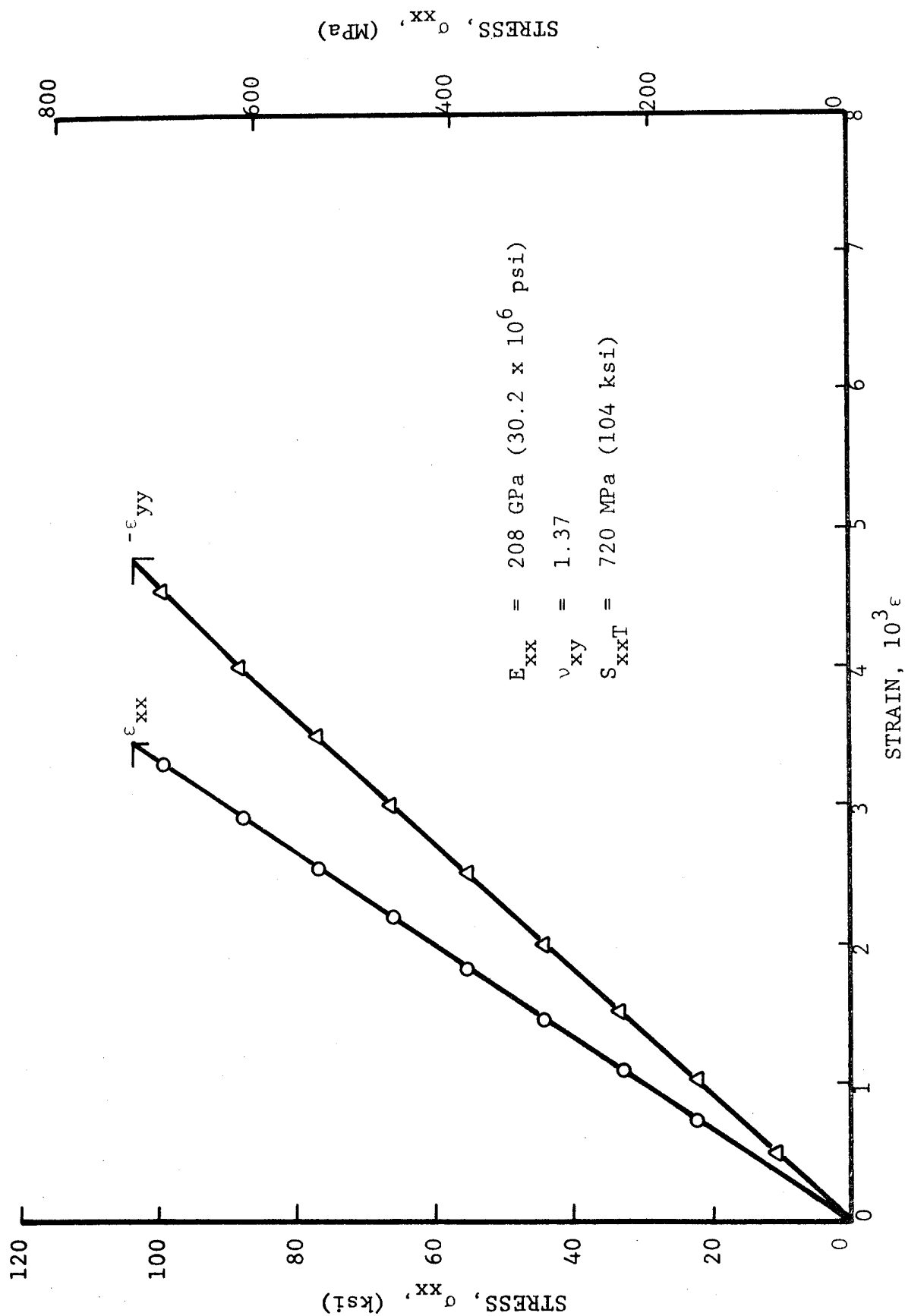POLYIMIDE SPECIMEN UNDER TENSILE LOADING

6-67
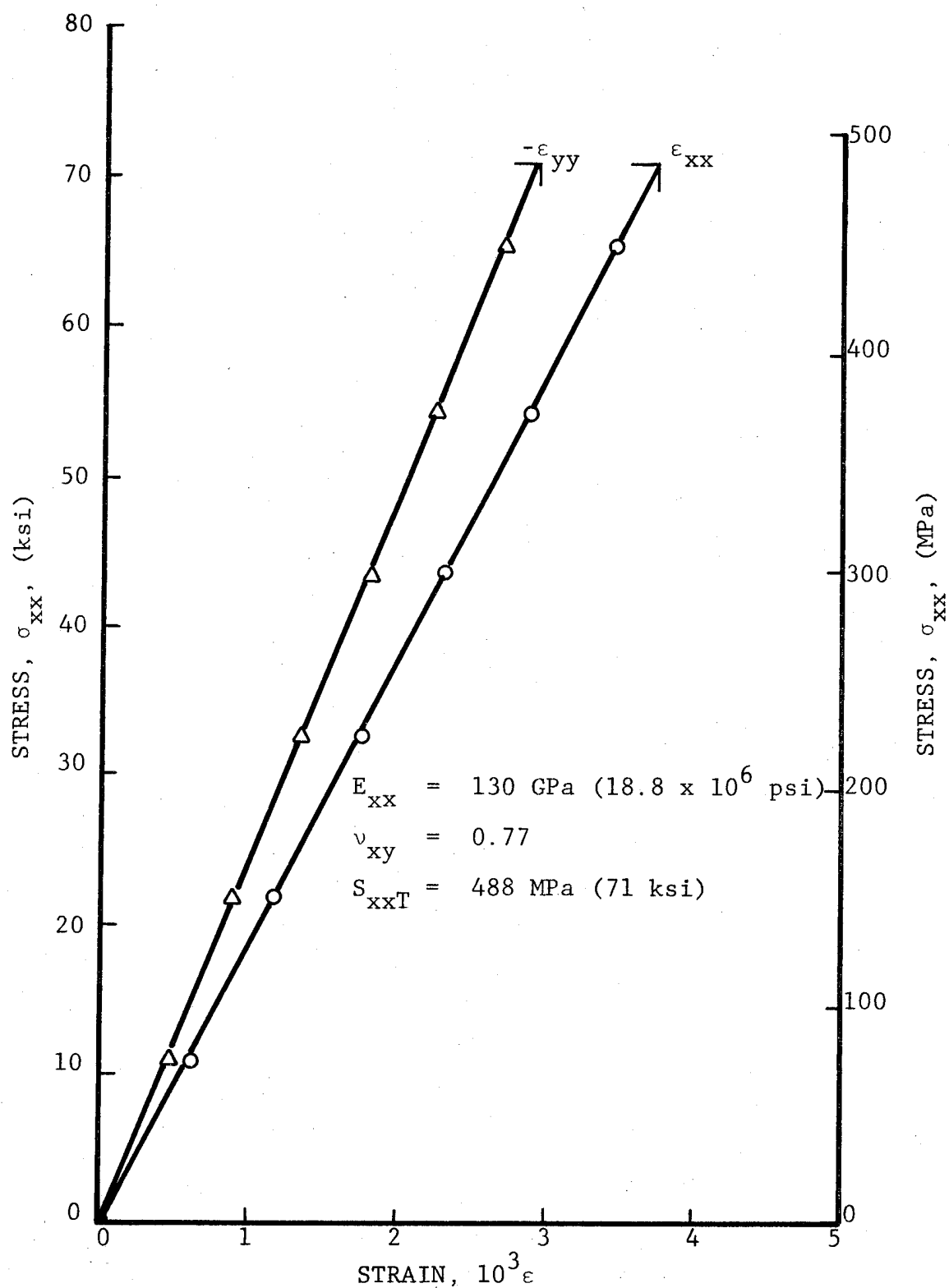
Fig. 6-50   STRAINS IN $[\pm 45/0_2]_s$ GRAPHITE/POLYIMIDE SPECIMEN
UNDER UNIAXIAL TENSILE LOADING AFTER 100 THERMAL
CYCLES BETWEEN ROOM TEMPERATURE AND 533 degK (500°F)
UNDER TENSILE LOADING
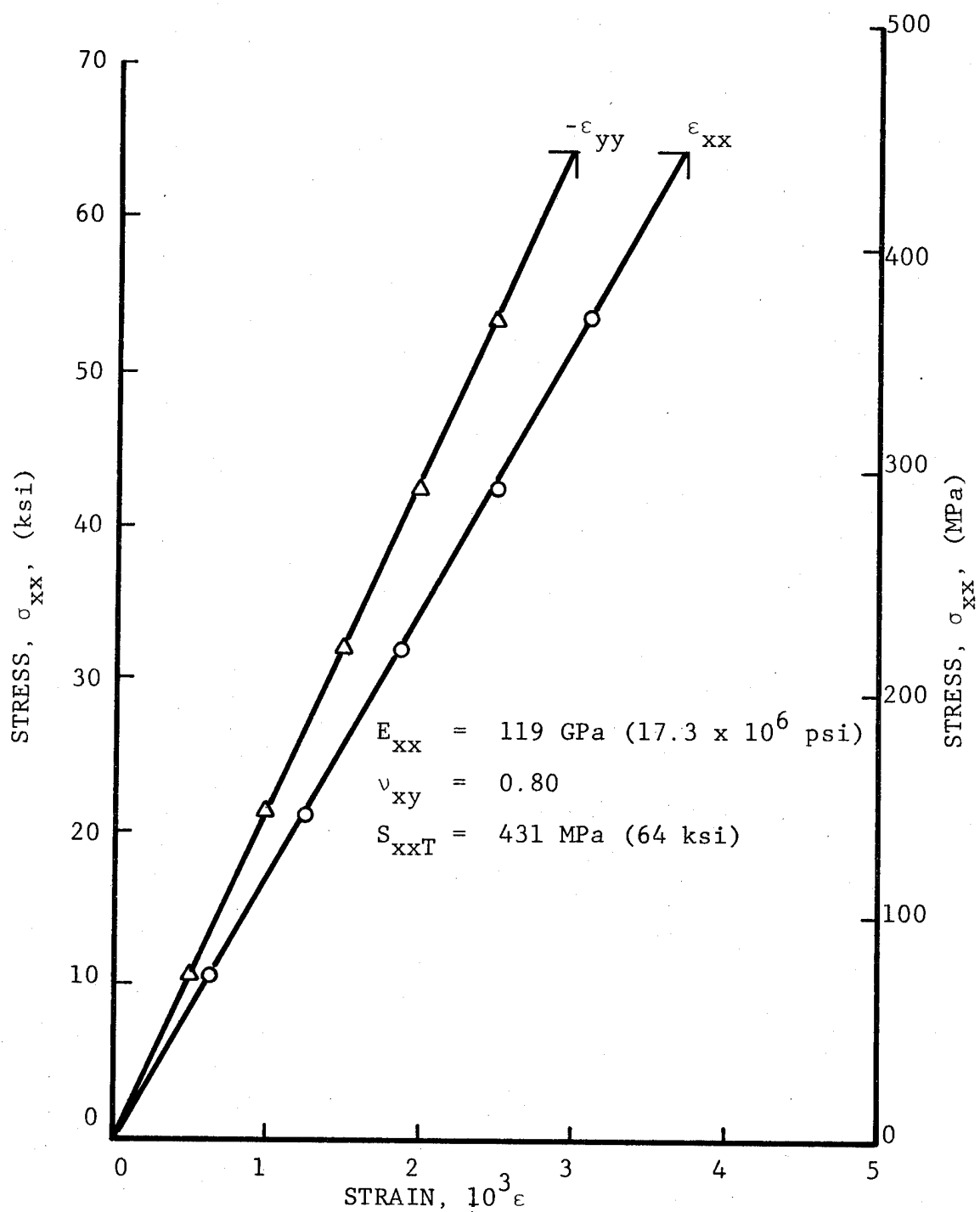
Fig. 6-51 STRAINS IN $[\pm 45/0_2]_s$ GRAPHITE/POLYIMIDE
SPECIMEN UNDER UNIAXIAL TENSILE LOADING
AFTER 100 THERMAL CYCLES BETWEEN ROOM
TEMPERATURE AND 533 degK (500°F) UNDER
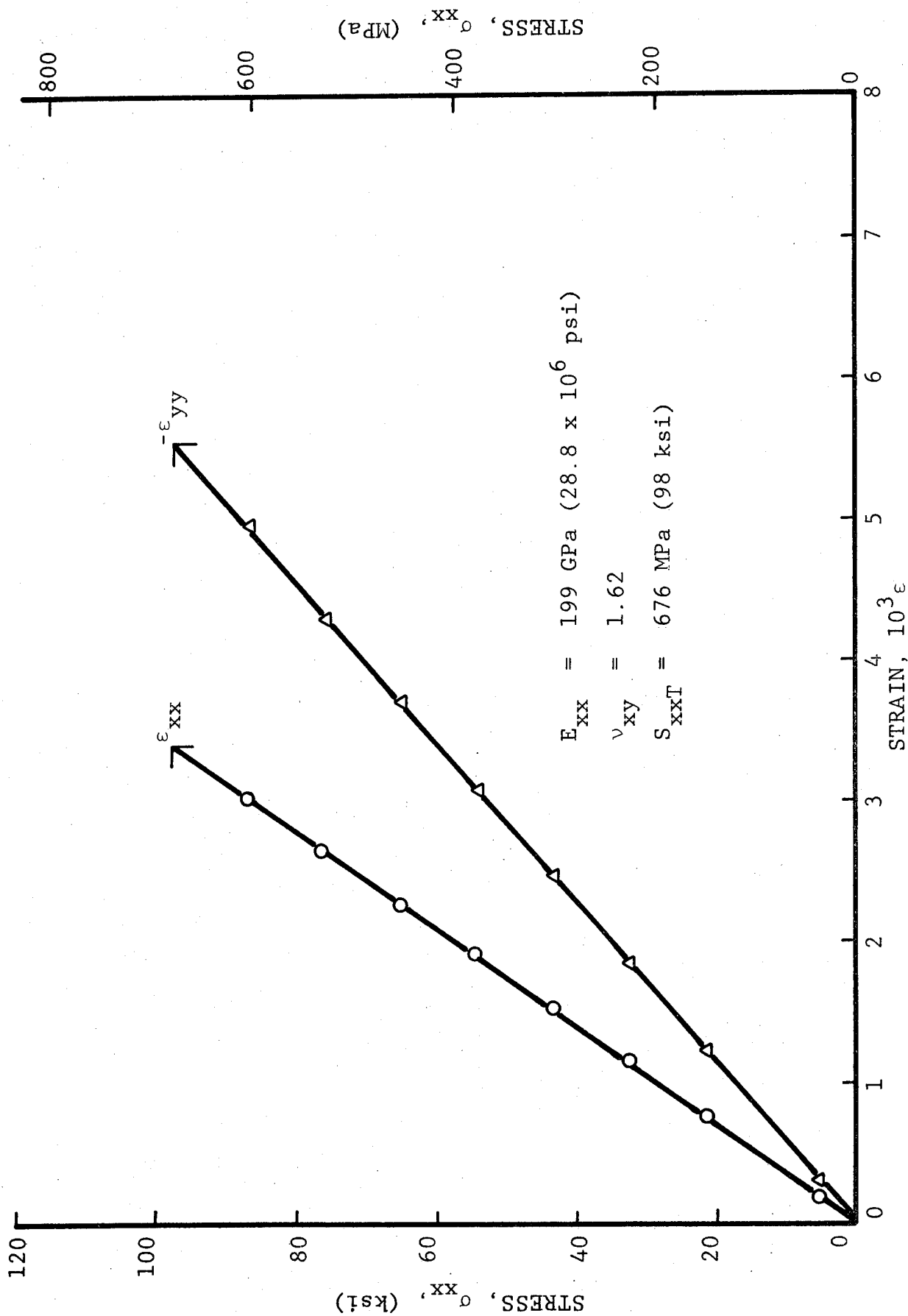TENSILE LOADING

6-69
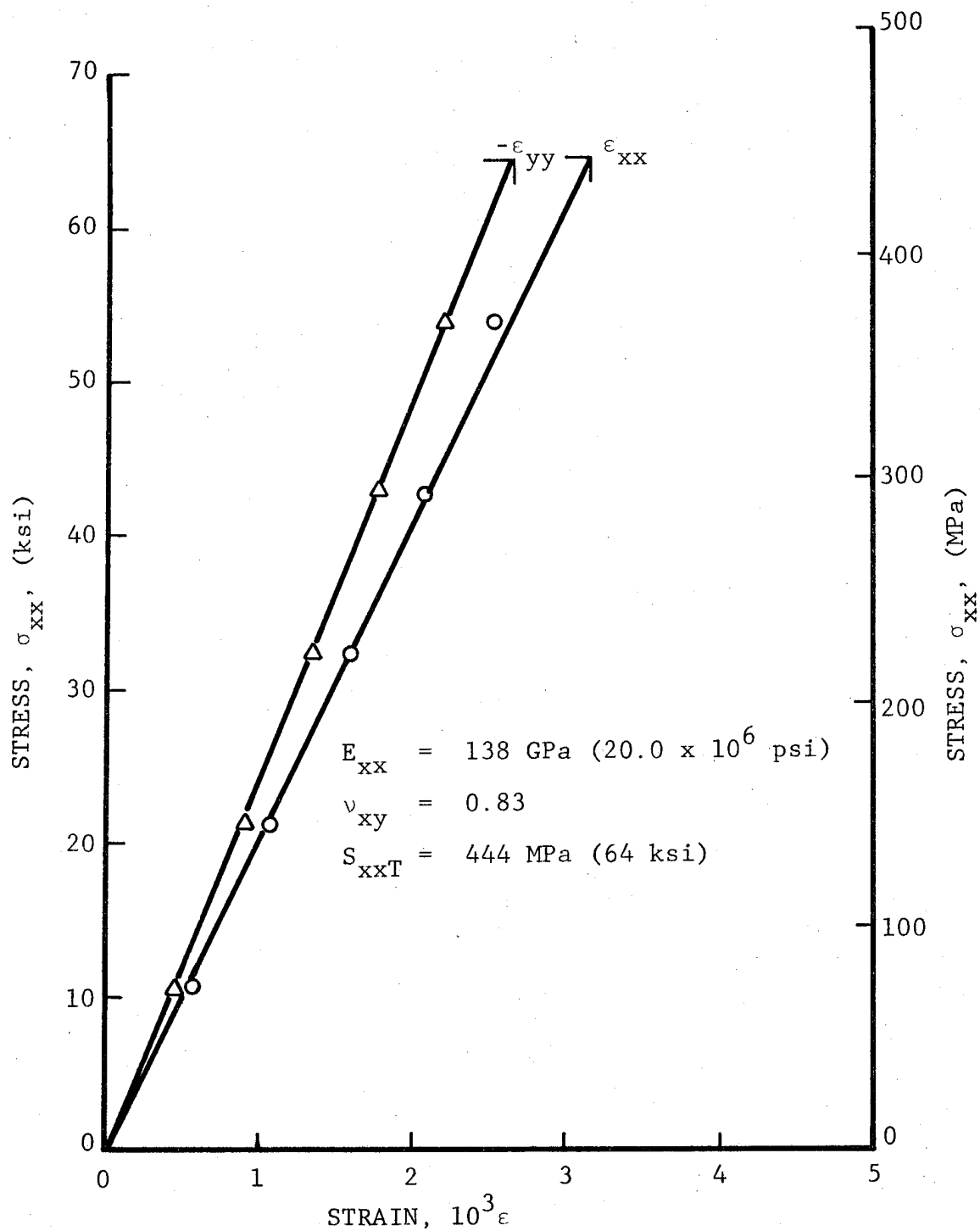
Fig. 6-52   STRAINS IN $[0/+45/0/-45]_s$ GRAPHITE/POLYIMIDE
SPECIMEN UNDER UNIAXIAL TENSILE LOADING AFTER
100 THERMAL CYCLES BETWEEN ROOM TEMPERATURE AND
533 degK (500°F) UNDER TENSILE LOADING
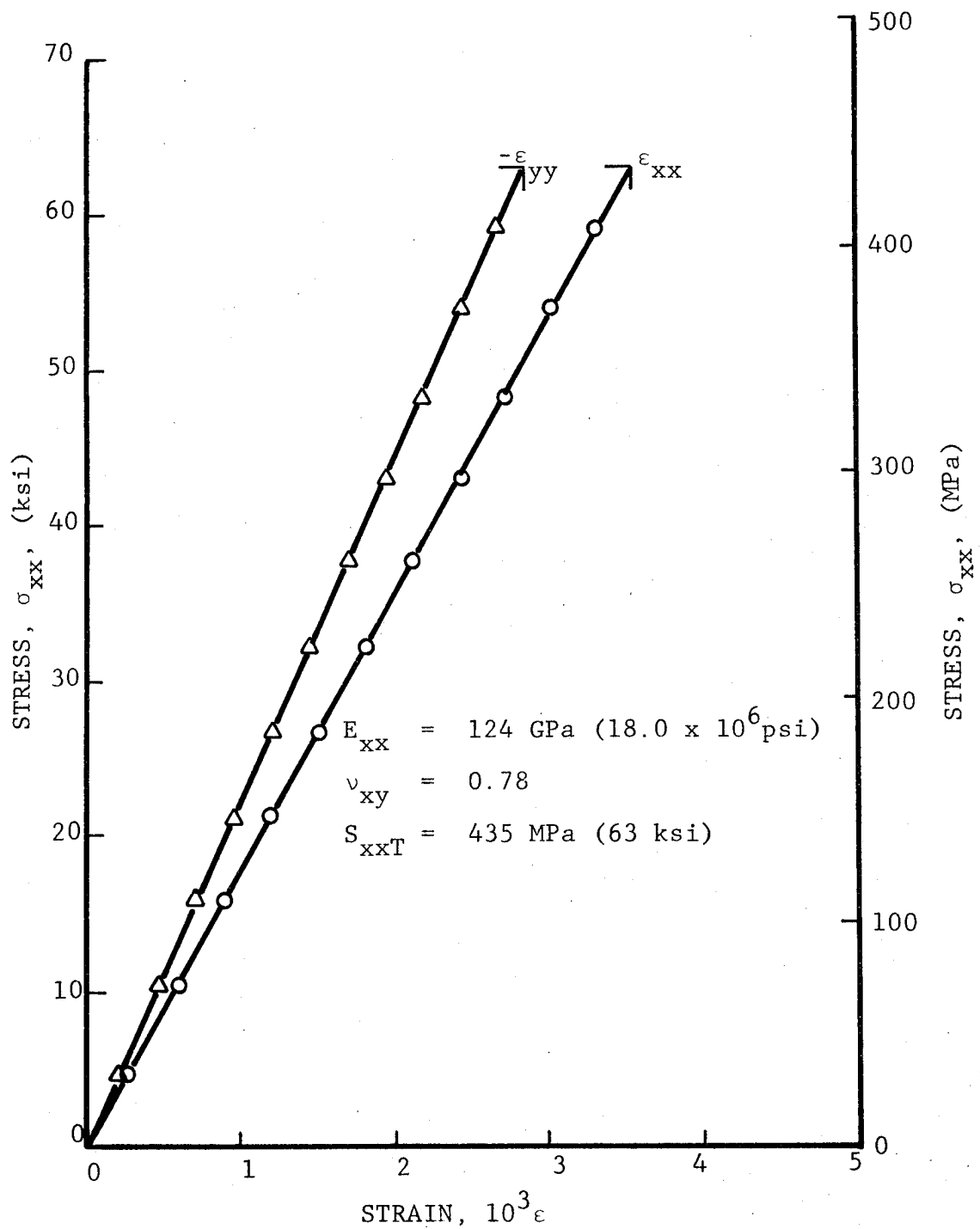
Fig. 6-53 STRAINS IN $[0/+45/0/-45]_s$ GRAPHITE/POLYIMIDE
SPECIMEN UNDER UNIAXIAL TENSILE LOADING AFTER
100 THERMAL CYCLES BETWEEN ROOM TEMPERATURE AND
533 degK (500°F) UNDER TENSILE LOADING
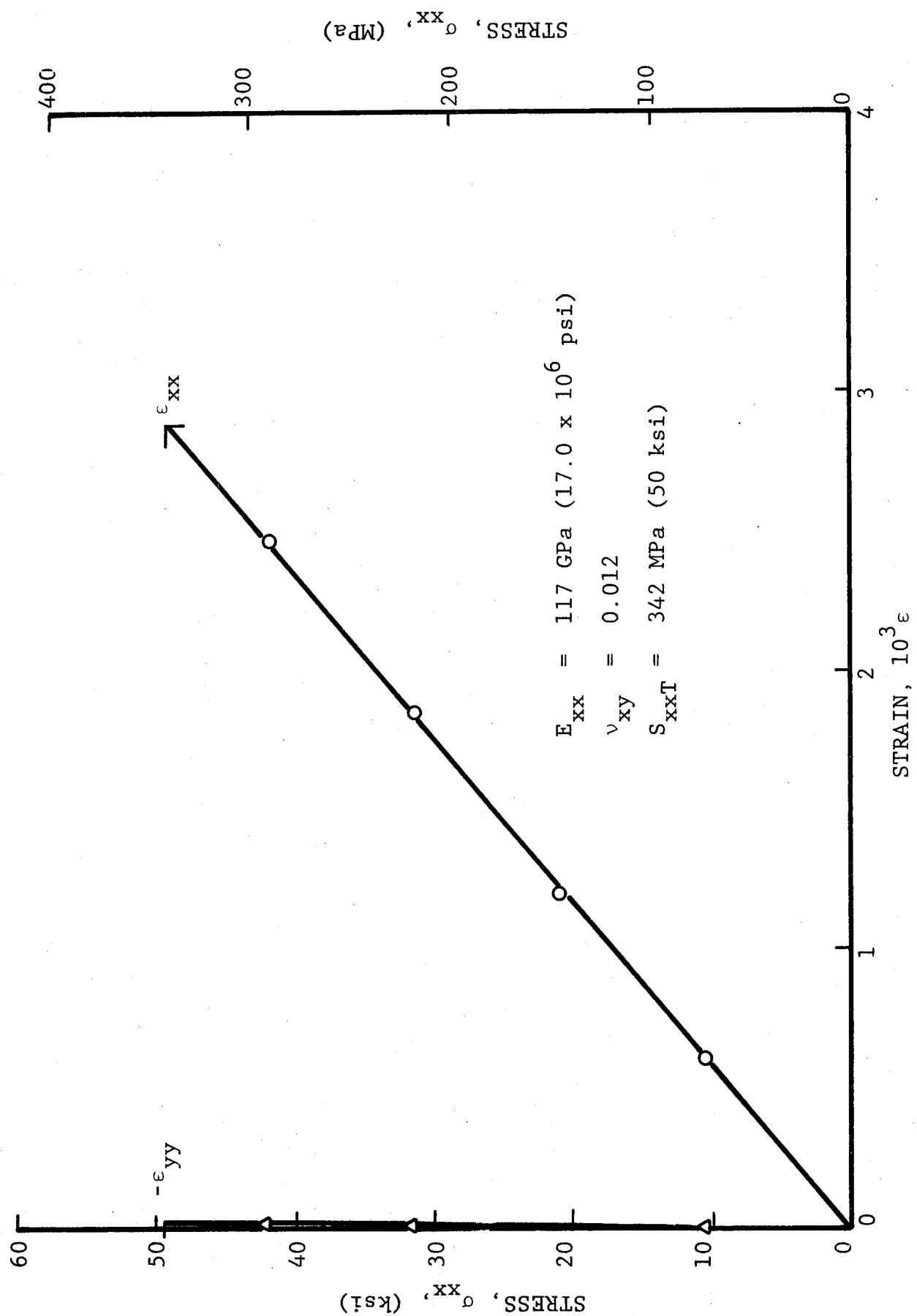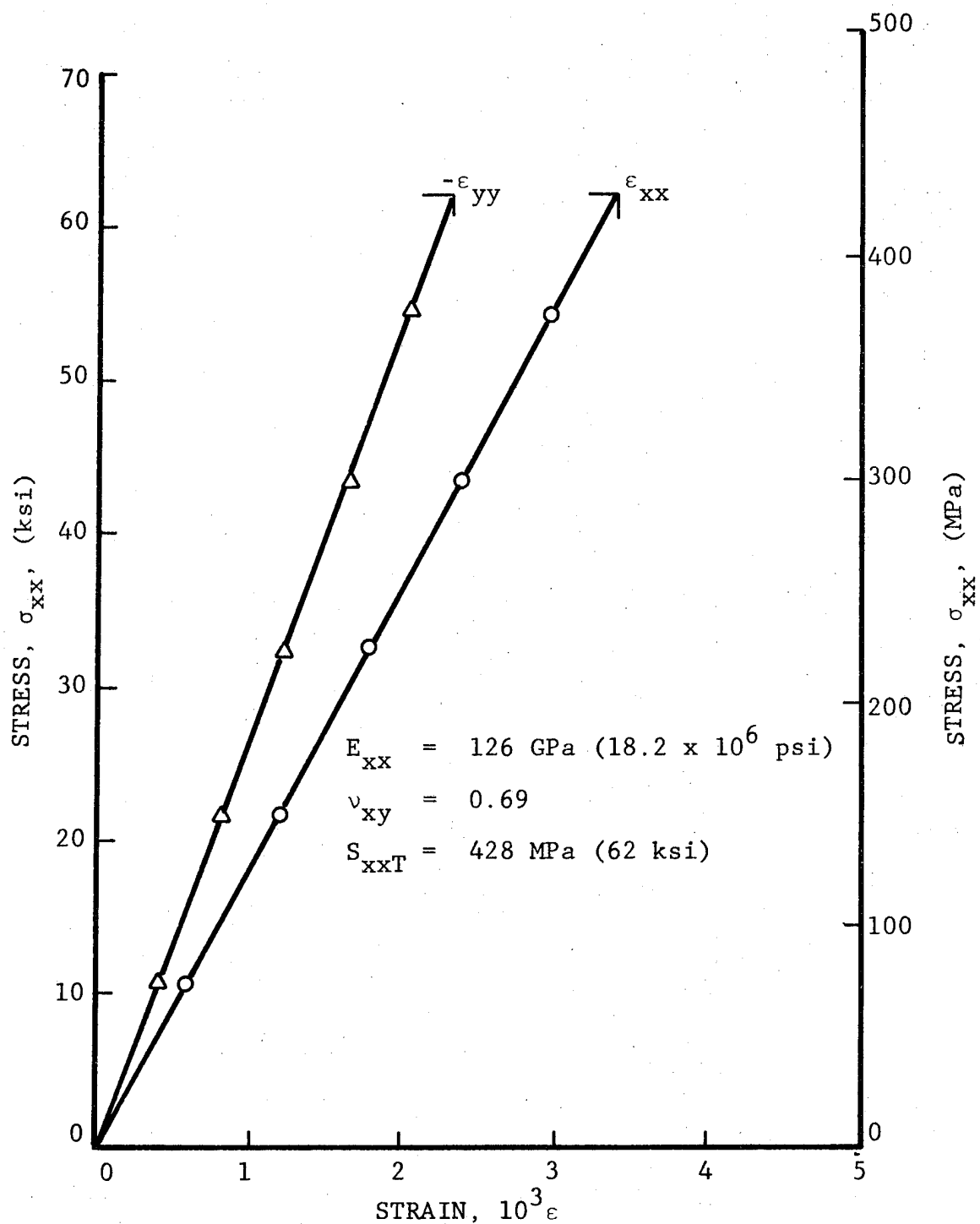
Fig. 6-54   STRAINS IN $[+45/0_2/-45]_s$ GRAPHITE/POLYIMIDE SPECIMEN UNDER UNIAXIAL TENSILE LOADING AFTER 100 THERMAL CYCLES BETWEEN ROOM TEMPERATURE AND 533 degK (500°F) UNDER TENSILE LOADING
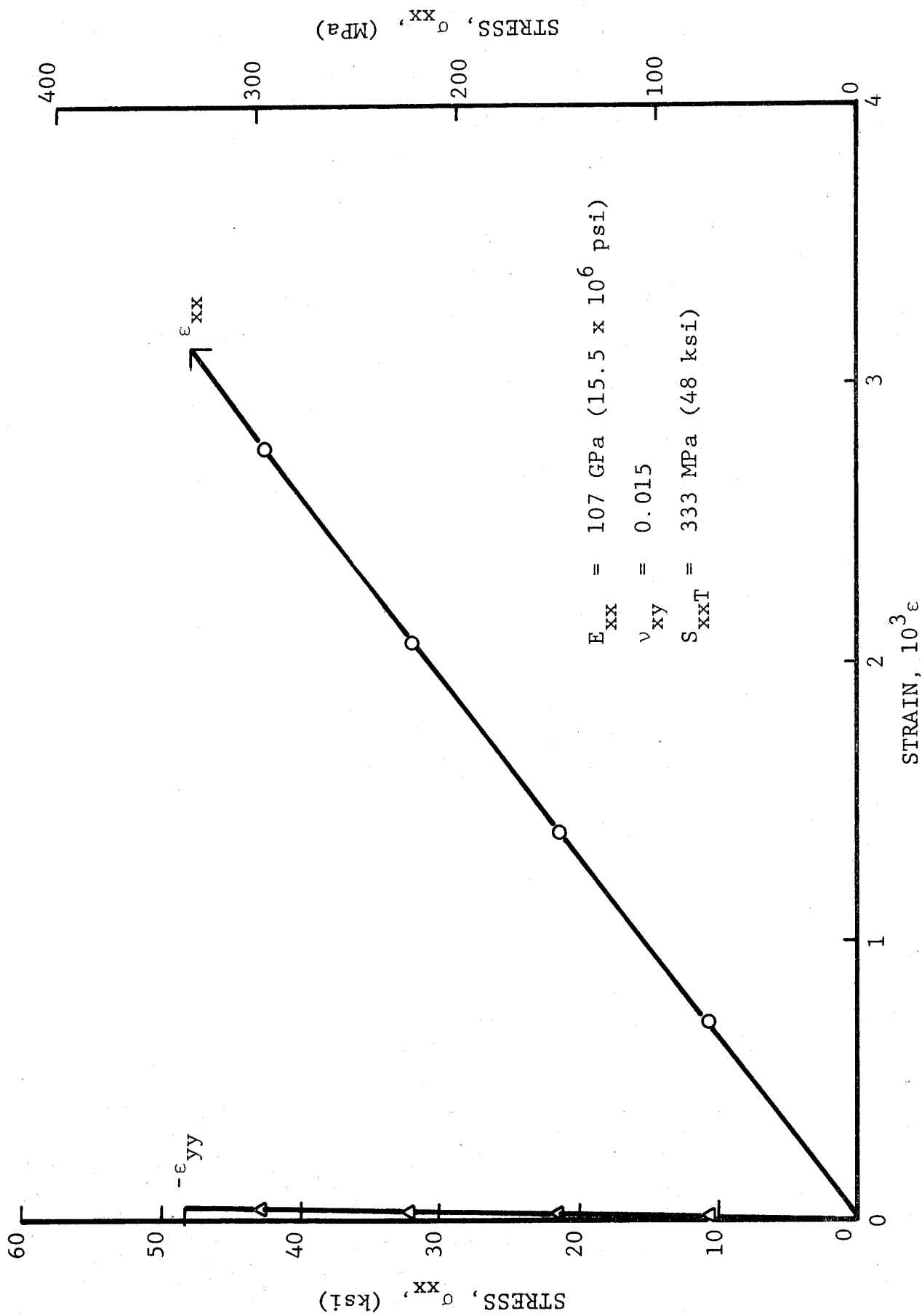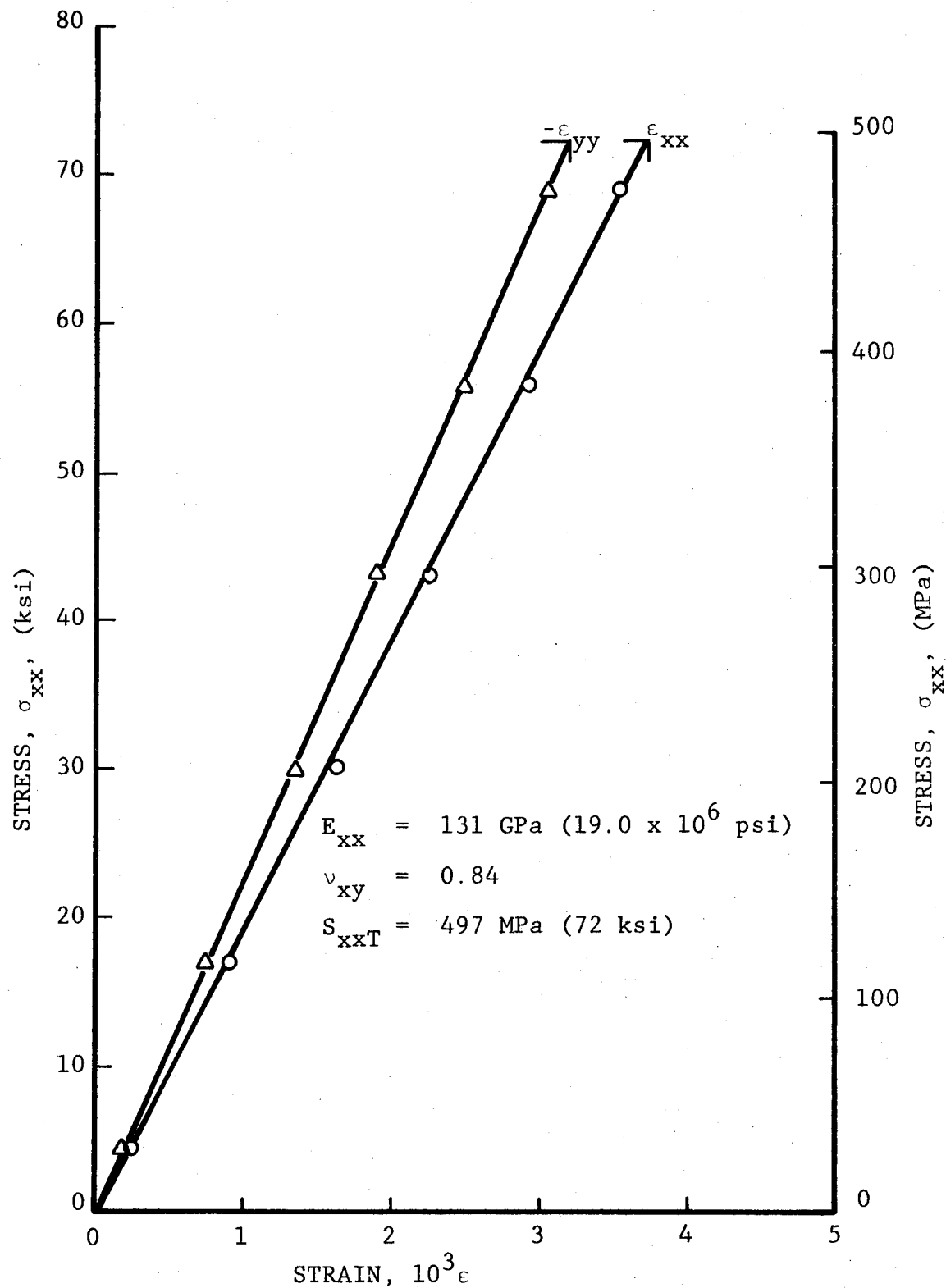
Fig. 6-55 STRAINS IN $[+45/0_2/-45]_s$ GRAPHITE/POLYIMIDE
SPECIMEN UNDER UNIAXIAL TENSILE LOADING AFTER
100 THERMAL CYCLES BETWEEN ROOM TEMPERATURE AND
533 degK (500°F) UNDER TENSILE LOADING
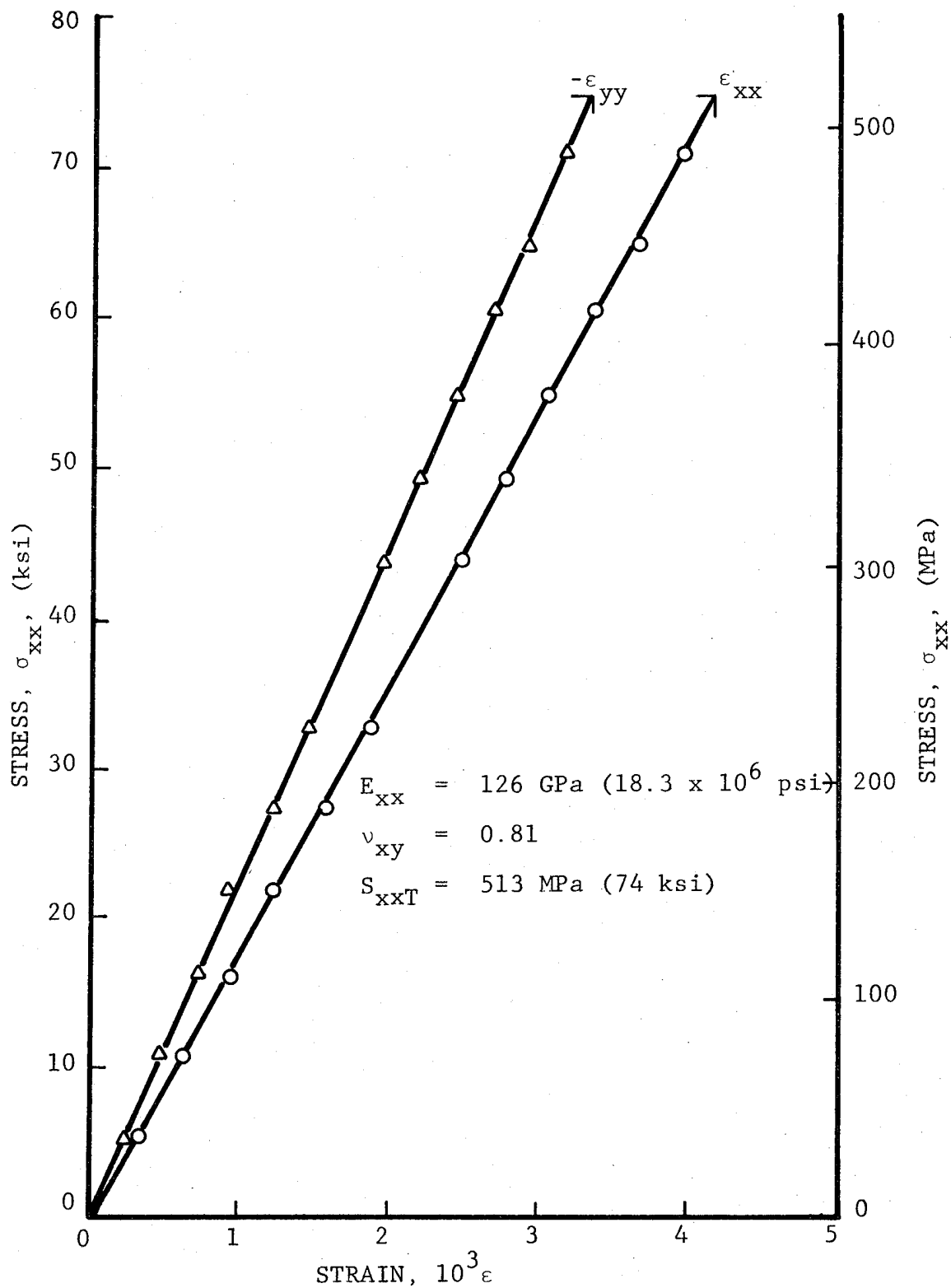
Fig. 6-56 STRAINS IN $[\pm 45/0_2]_s$ GRAPHITE/POLYIMIDE SPECIMEN UNDER UNIAXIAL TENSILE LOADING AFTER 100 THERMAL CYCLES BETWEEN ROOM TEMPERATURE AND 200 degK (-100°F) UNDER TENSILE LOADING
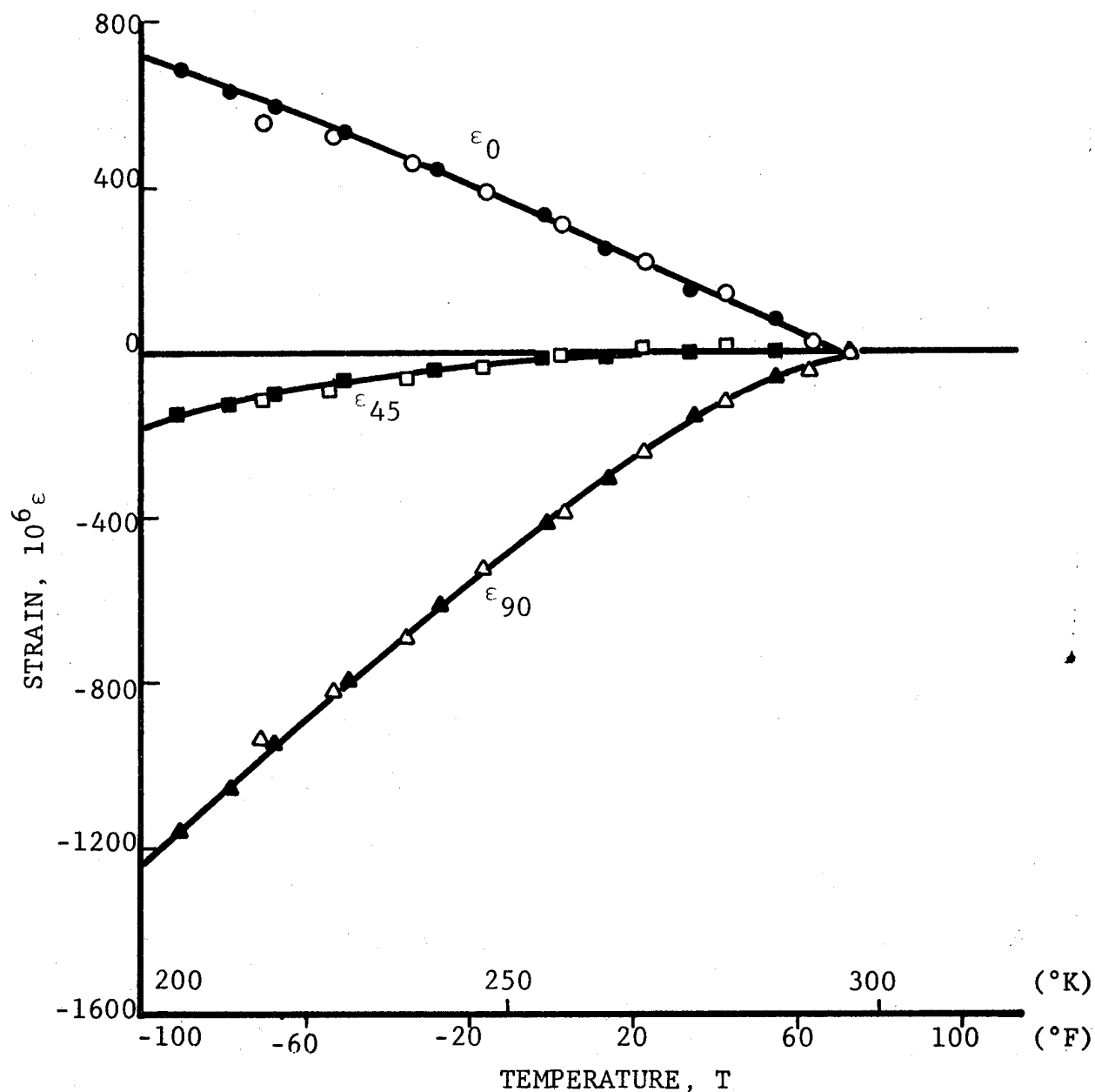
6-74
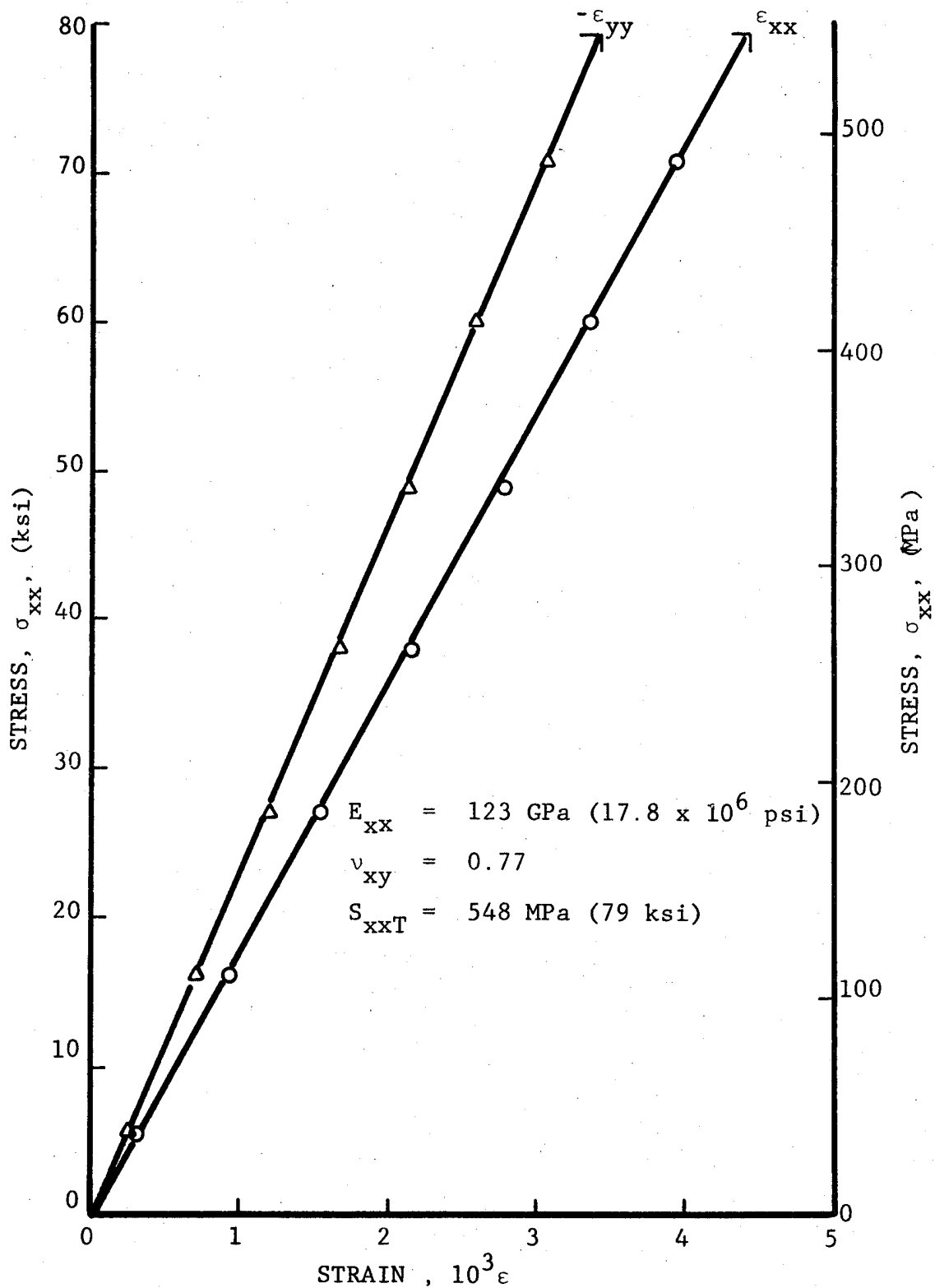
Fig. 6-57 STRAINS IN $[\pm 45/0_2]_s$ GRAPHITE/POLYIMIDE SPECIMEN
UNDER UNIAXIAL TENSILE LOADING AFTER 100 THERMAL
CYCLES BETWEEN ROOM TEMPERATURE AND 200 degK (-100°F)
UNDER TENSILE LOADING

6-75

$$E_{xx} = 128 \text{ GPa } (18.6 \times 10^6 \text{ psi})$$
$$\nu_{xy} = 0.84$$
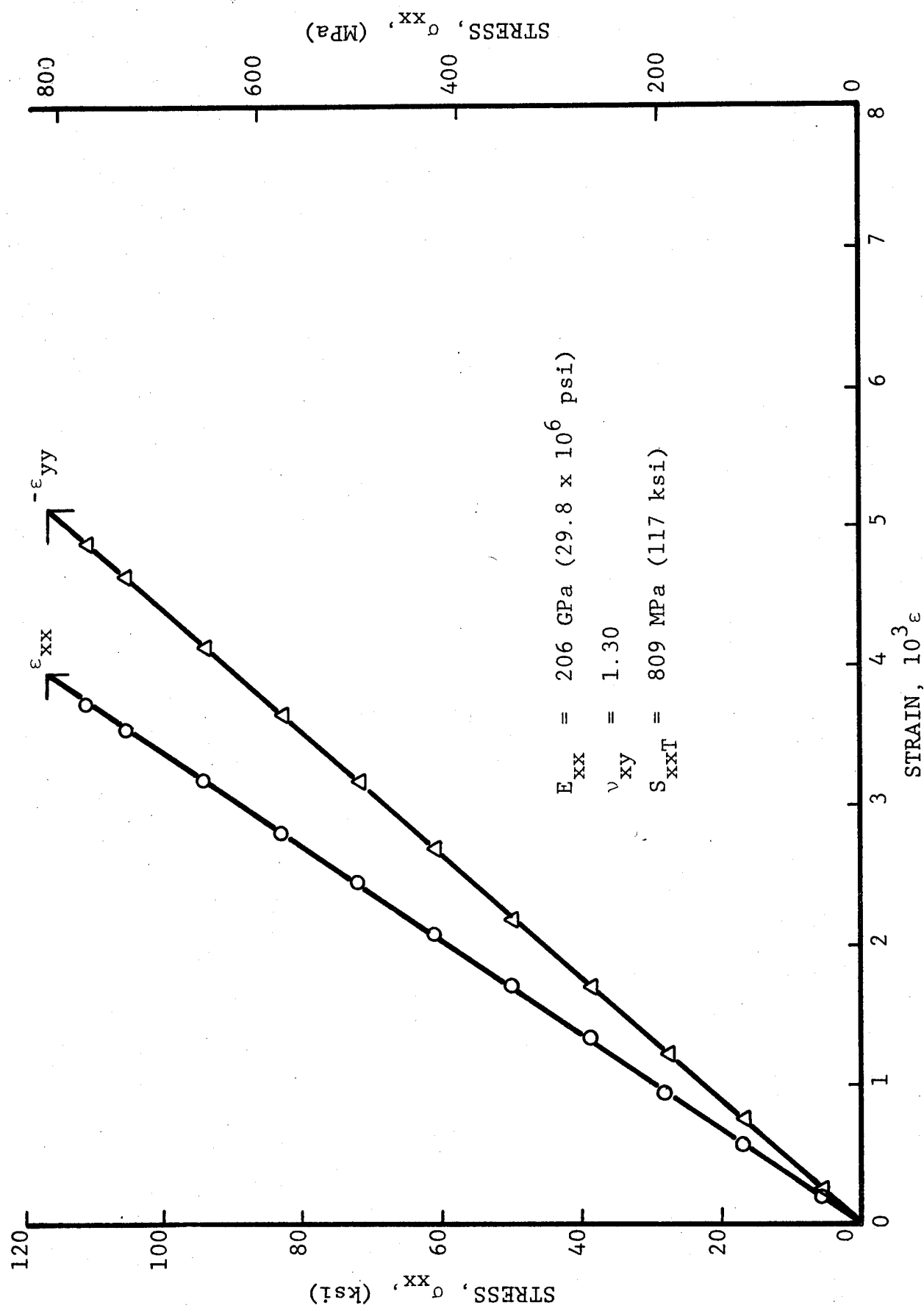$$S_{xxT} = 452 \text{ MPa } (66 \text{ ksi})$$
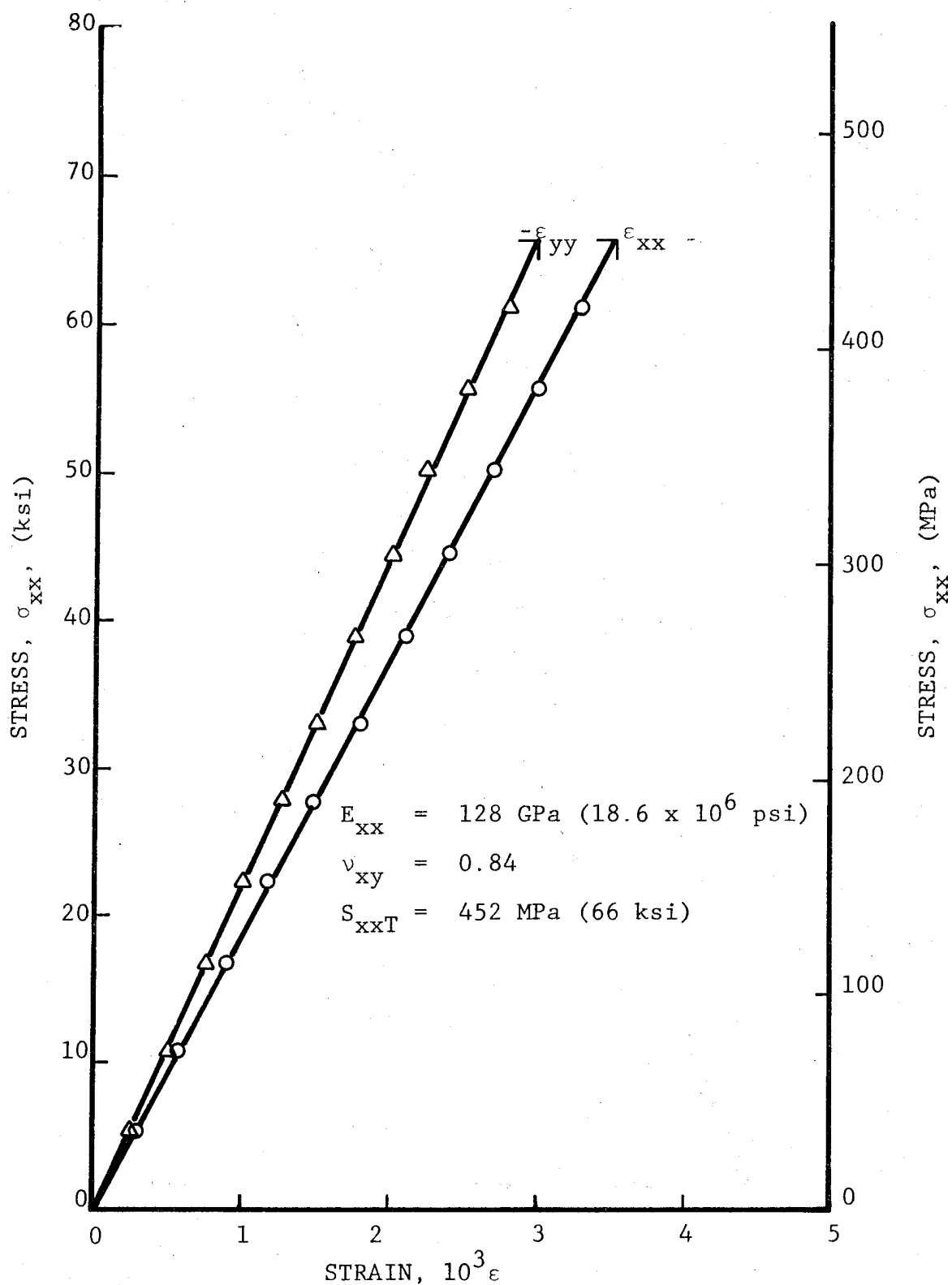
Fig. 6-58   STRAINS IN $[0/+45/0/-45]_s$ GRAPHITE/POLYIMIDE
SPECIMEN UNDER UNIAXIAL TENSILE LOADING AFTER
100 THERMAL CYCLES BETWEEN ROOM TEMPERATURE AND
200 degK (-100°F) UNDER TENSILE LOADING

6-76
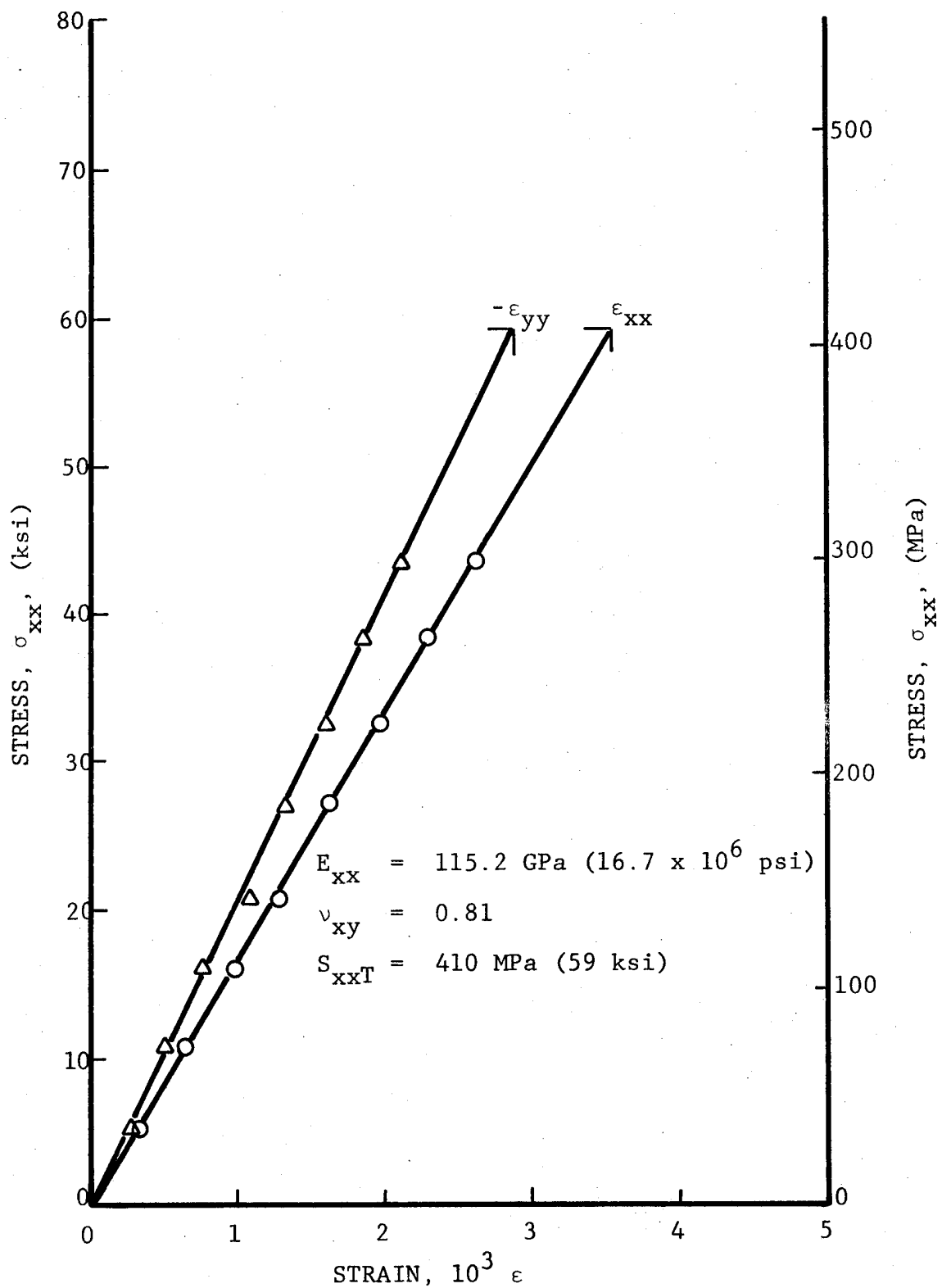
Fig. 6-59 STRAINS IN [0/+45/0/-45]$_s$ GRAPHITE/POLYIMIDE SPECIMEN
UNDER UNIAXIAL TENSILE LOADING AFTER 100 THERMAL CYCLES
BETWEEN ROOM TEMPERATURE AND 200 degK (-100°F) UNDER
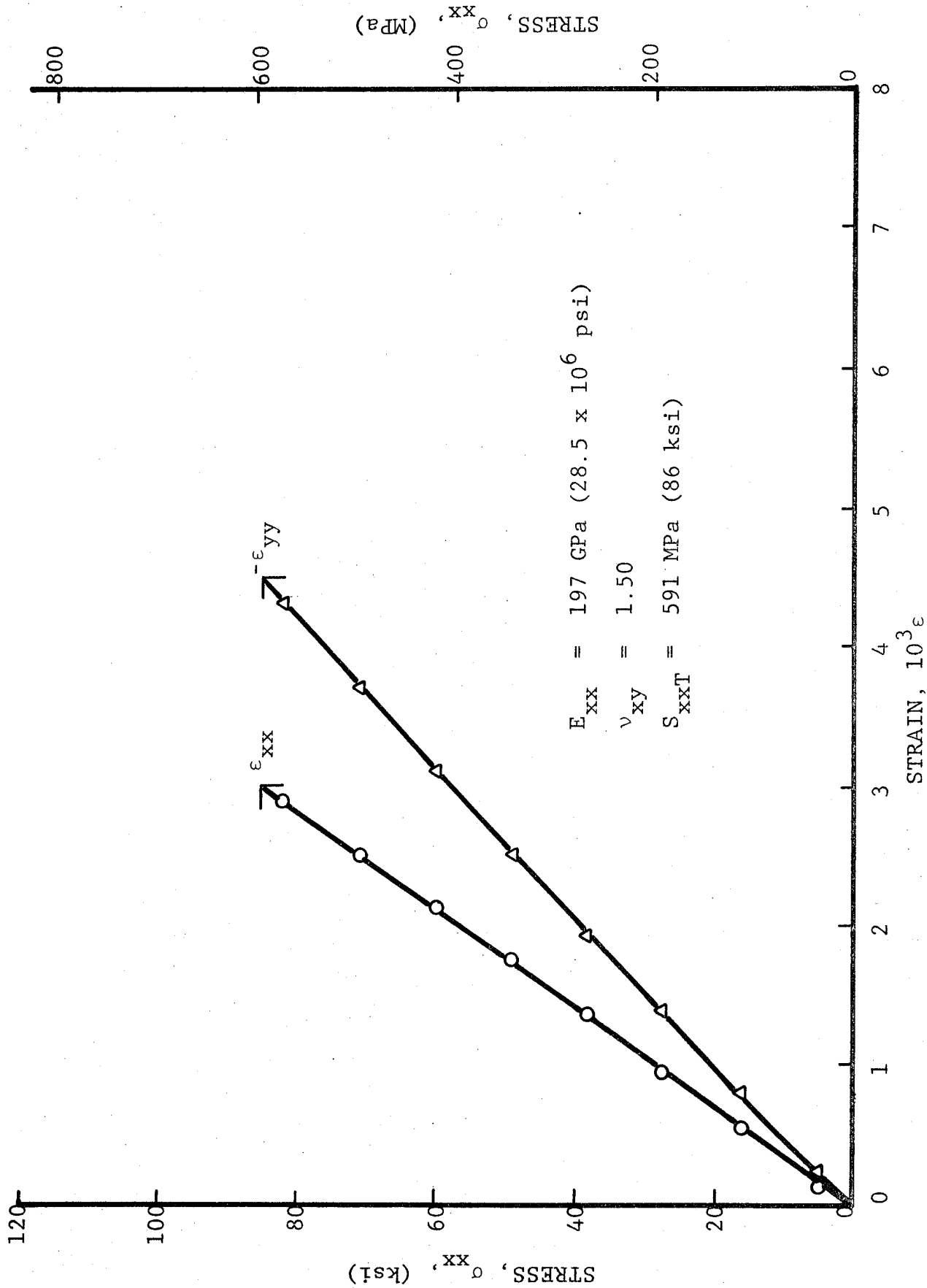TENSILE LOADING
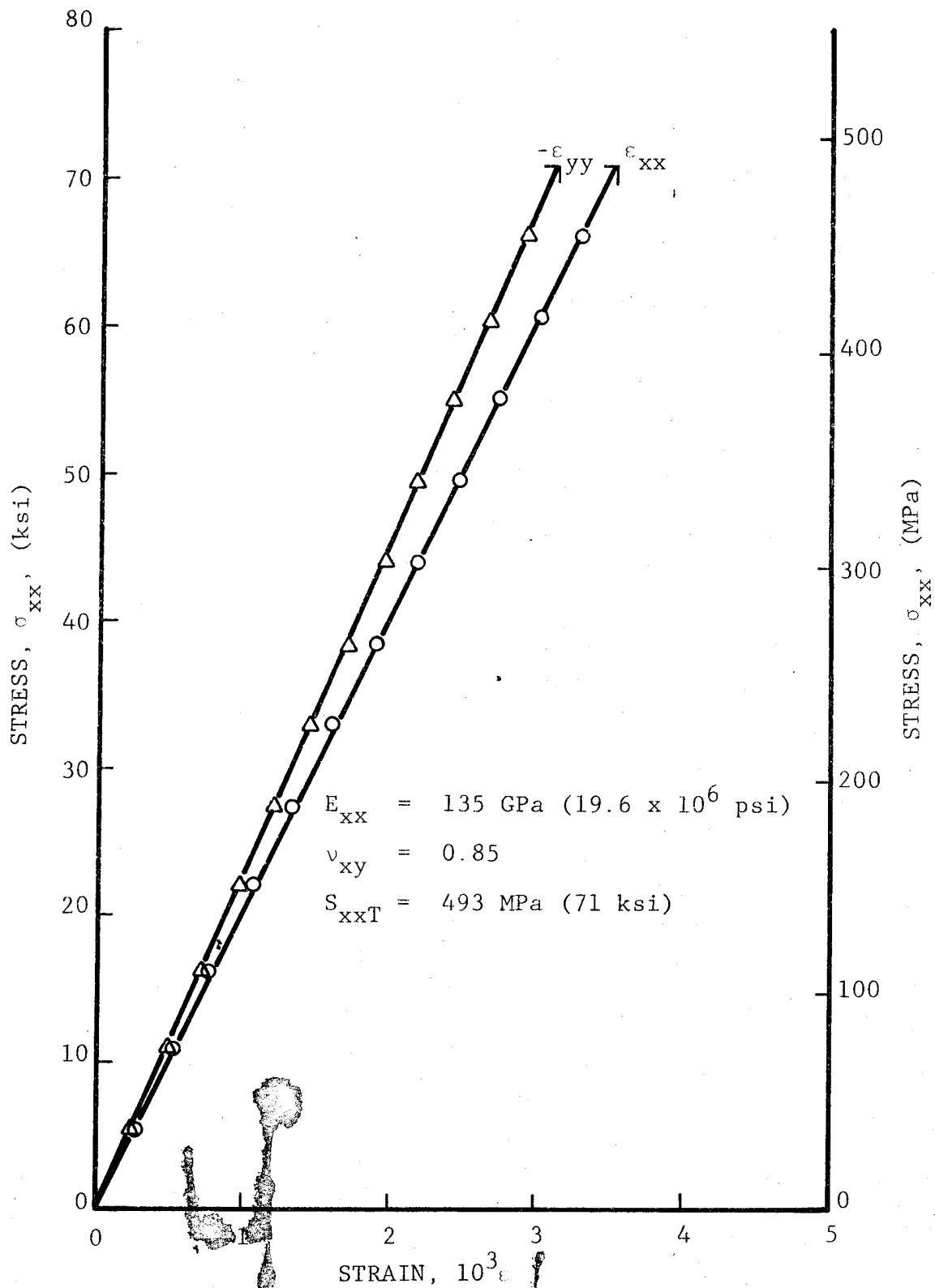
Fig. 6-60 STRAINS IN $[+45/0_2/-45]_s$ GRAPHITE/POLYIMIDE SPECIMEN
UNDER UNIAXIAL TENSILE LOADING AFTER 100 THERMAL CYCLES
BETWEEN ROOM TEMPERATURE AND 200 degK (-100°F) UNDER
TENSILE LOADING
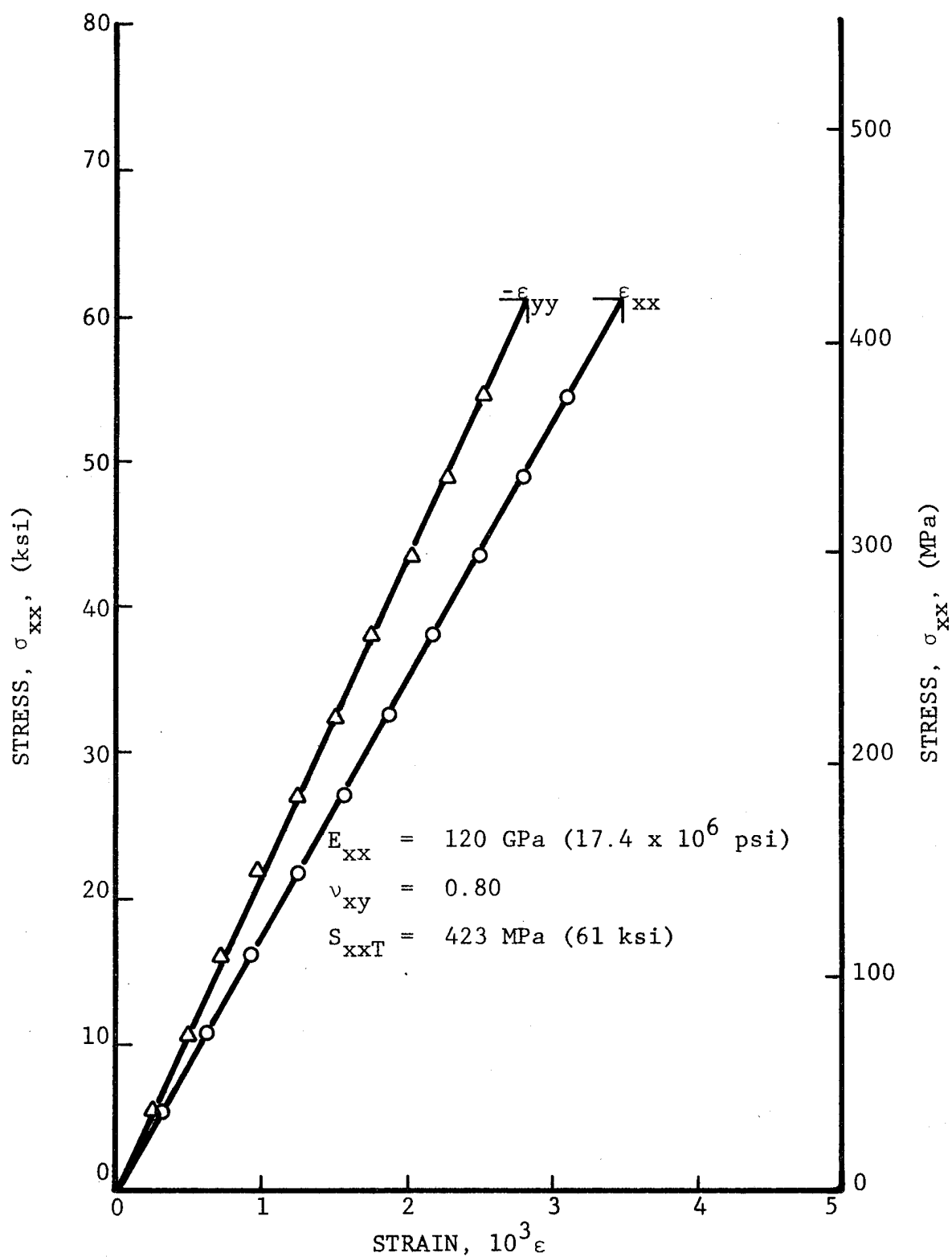
Fig. 6-61 STRAINS IN $[+45/0_2/-45]_s$ GRAPHITE/POLYIMIDE SPECIMEN
UNDER UNIAXIAL TENSILE LOADING AFTER 100 THERMAL
CYCLES BETWEEN ROOM TEMPERATURE AND 200 degK (-100°F)
UNDER TENSILE LOADING

6-79

7.0 SUMMARY, CONCLUSIONS AND RECOMMENDATIONS FOR FUTURE WORK

An experimental investigation was conducted to determine the magnitude of lamination residual stresses in angle-ply composites and to evaluate their effects on composite structural integrity. The investigation consisted of five tasks.

Task I dealt with a selective literature survey to obtain thermal and mechanical properties of unidirectional composites. Six fiber/matrix systems were selected for the experimental investigation: Boron/Epoxy (4 mil Boron/AVCO 5505), Boron/Polyimide (4 mil Boron/ WRD 9371), Graphite/Low Modulus Epoxy (Modmor I/ERLA 4289), Graphite/ High Modulus Epoxy (Modmor I/ERLA 4617), Graphite/Polyimide (Modmor I/ WRD 9371), and S-Glass/Epoxy (Scotchply 1009-26S).

In Task II, the six materials selected were characterized, instrumentation procedures were developed, residual strains were measured during curing, and the static strength measured of $[0_2/\pm45]_s$ angle-ply laminates. Material characterization consisted of determination of longitudinal and transverse tensile and compressive properties, in-plane shear properties, coefficients of thermal expansion, density and fiber volume ratio. Results of this characterization are tabulated in Tables 3-13 through 3-18.

The longitudinal modulus of the polyimide-matrix systems is somewhat higher than that of epoxy-matrix systems with the same fibers. This is not the case for the transverse moduli. The transverse modulus of Boron/Polyimide is appreciably lower than that of Boron/Epoxy and the transverse modulus of Graphite/Polyimide is lower than that of Graphite/High Modulus Epoxy. The S-Glass/Epoxy has the highest transverse modulus as well as the highest ratio of transverse to longitudinal modulus (~ 0.4) and the highest shear modulus. The longitudinal tensile strength of the polyimide matrix systems is noticeably

lower than that of epoxy-matrix systems with the same fibers. Furthermore, the longitudinal tensile strength of the Graphite/ High Modulus Epoxy is significantly lower than that of the Graphite/Low Modulus Epoxy. The transverse tensile strength of the polyimide-matrix systems is appreciably lower than that of the epoxy-matrix systems with the same fibers. The same strength for Graphite/Low Modulus Epoxy is very low (4.15 MPa; 600 psi).

The longitudinal compressive strength for Boron/Epoxy, Boron/Polyimide and Graphite/High Modulus Epoxy is higher, by up to 15 percent, than the tensile strength. This is not the case for the other three systems, but that conclusion is not definite. The measured transverse compressive strength (S_{22C}) is in all cases appreciably higher (2.2 to 5.7 times) than the corresponding tensile strength. As in the case of other strengths, the intralaminar shear strength for the polyimide matrix systems is lower than that of the corresponding epoxy-matrix systems.

Techniques were developed and applied to the measurement of subsurface strains in composite laminates at elevated temperatures. They consist primarily of embedding encapsulated foil strain gages with attached insulated leads between the plies of the composite during lamination, and recording the output during curing and subsequent thermal and mechanical loading. The strain gage output at elevated temperatures was separated into one part due to deformation and another part due to change in resistivity of the gage with temperature (thermal output). The latter part was determined from a reference quartz specimen instrumented with similar strain gages.

Strains during curing and thermal cycling were measured in $[0_2/\pm45]_s$ and $[0_8]$ laminates of the six systems selected. Strains recorded in the first part (heating) of the curing cycle are not significant as they correspond to the fluid state of the matrix.

Strains measured in the second part (cooling) of the curing cycle were in satisfactory agreement with strains measured during subsequent thermal cycling. This indicates that residual stresses are set up during cooldown as a result of differential thermal expansion of the various plies. The strains in most specimens vary linearly with temperature, except for the unidirectional S-Glass/Epoxy and the Graphite/High Modulus Epoxy specimens. Restraint or residual strains were computed for the 0-deg. and 45-deg plies of the $[0_2/\pm45]_s$ laminates by taking the differences of the measured laminate strains and the corresponding unrestrained strains of that ply. These strains vary linearly with temperature for most materials except the Graphite/High Modulus Epoxy and the S-Glass/Epoxy.

Residual stresses as a function of temperature were computed from the residual strains by using the anisotropic constitutive relations and taking into account the temperature dependence of the stiffnesses and strains. In the case of the 0-deg. plies in the Boron/Epoxy laminate a maximum transverse residual stress of 32,400 kPa (4,700 psi) was determined. This means that approximately 50 percent of the transverse strength of these plies has been exhausted in the curing process.

Two $[0_2/\pm45]_s$ specimens of each material, including one with embedded instrumentation were tested statically in tension to failure. Strains and acoustic emission were recorded. The initial Young's modulus, Poisson's ratio and tensile strength are tabulated in Table 3-19. The S-Glass/Epoxy is the strongest but has the lowest modulus. The Boron/Epoxy follows closely in strength and has the second highest modulus. The Boron/Polyimide with the highest modulus has a strength equal to approximately 80 percent of that of Boron/Epoxy. The Graphite/Low Modulus Epoxy seems to be somewhat stronger than the Graphite/High Modulus Epoxy and much stronger than the first batch of Graphite/Polyimide specimens. The average value of Poisson's ratio is 0.72 $\pm$0.02, except for the S-Glass/Epoxy which has a much lower Poisson's ratio (0.52).

The extent of relaxation of lamination residual stresses was investigated in Task III. Three approaches were followed: (1) Direct measurement of strain changes with time, (2) Stress relaxation determination in 90-degree unidirectional specimens, and (3) Elastic and strength properties of laminates as a function of time after curing. The first approach proved to be very insensitive. The measured amount of relaxation in 90-degree specimens after thirty days in most cases ranged between 9.5 and 24.5 percent, except for the Boron/Polyimide where a fracture mechanism was operating. The relaxation measured in the 90-degree specimens is an upper bound to the actual relaxation of residual stresses in an angle-ply laminate. Therefore, it can be concluded that the amount of residual-stress relaxation is small. No significant variations in stiffness or strength were observed in specimens tested over periods from one to twenty-two months after curing.

In Task IV the behavior of angle-ply laminates subjected to thermal cycling, tensile load cycling and thermal cycling with tensile load was investigated. Specimens were subjected to thermal cycling between room temperature and 411 degK (280°F) for the epoxy-matrix composites and between room temperature and -533 degK (500°F) for the polyimide-matrix composites. No visual degradation was evident and no differences were detected in measured strains between the beginning and the end of cycling. Residual moduli were very close to initial values. The residual strengths, with the exception of the Boron/Polyimide, were slightly higher than the initial strengths. Although the differences are too small to be considered significant in view of the small number of specimens tested, they could be attributed to some residual stress relaxation.

Cycling between room temperature and 200 degK (-100°F) did not reveal any apparent degradation or any differences in measured thermal strains between the beginning and the end of cycling. Subsequent static testing showed that the residual moduli and strengths remained

unchanged, except for the Graphite/Low Modulus Epoxy which showed significant reductions in both modulus and strength (approximately 35 percent) due to degradation during cycling.

A group of specimens were subjected to tensile load cycling between 0 and 25 to 90 percent of the static strength. Strains and temperature were monitored during cycling. The Boron/Epoxy and Graphite/ Low Modulus Epoxy survived 10 million cycles to 40 percent of ultimate. The Boron/Polyimide showed runouts at loads of 40 and 70 percent of ultimate. The Graphite/High Modulus Epoxy had runouts at 70 percent of ultimate. The Graphite/Polyimide had the highest endurance with runouts at 70, 80 and, in one case, even 90 percent of ultimate. The S-Glass/Epoxy had the lowest endurance and did not survive 10 million cycles even at 25 percent of ultimate. All surviving specimens were tested statically to failure with no indications of any changes in residual modulus or strength.

A group of specimens were subjected to a static tensile load equal to 70 percent of the ultimate and simultaneously to 100 thermal cycles as the unloaded specimens before. The Graphite/Low Modulus Epoxy and S-Glass/Epoxy did not survive the elevated temperature thermal cycling. The same materials showed visible degradation as a result of the low temperature thermal cycling. The residual modulus and strength remained relatively unchanged, except for significant reductions in strength and modulus in the Graphite/Low Modulus Epoxy and some strength reduction in the S-Glass/Epoxy.

The effects of fiber volume ratio, ply orientation and ply stacking sequence on the magnitudes of residual stress, stiffness and strength of Graphite/Polyimide were investigated in Task V.

Residual strains in the lower fiber volume ratio laminates were approximately the same as those of the standard FVR material. Restraint strains in the 0-degree plies of the $[0_2/\pm15]_s$ are approximately

one-fourth of those in the 0-degree plies of the $[0_2/\pm45]_s$ layup. This is because the ±15-degree plies offer less restraint to transversal contraction of the 0-degree plies than do ±45-degree plies. Restraint strains in the 0-degree plies of the $[0_2/90_2]_s$ laminate are higher than corresponding strains in the $[0_2/\pm45]_s$ laminate by approximately 8 percent. Ply stacking sequence was found to have no measurable effect on the magnitude of residual strains. These strains were almost identical for all four variations of ply stacking sequence: $[0_2/\pm45]_s$, $[\pm45/0_2]_s$, $[0/+45/0/-45]_s$ and $[+45/0_2/-45]_s$.

Results of static tensile tests are tabulated in Table 6-2. The modulus and tensile strength of the low fiber-volume-ratio laminate were lower than corresponding properties of the standard material by approximately the same ratio as the corresponding fiber volume ratios. The ratio of FVR's is 0.45/0.37 = 1.22 and compares closely with the ratio of measured moduli of 18.5/15.6 = 1.19 and the strength ratio of 69/56 = 1.23. This means that the stiffness and strength per ply are not affected by moderate changes in the fiber volume ratio. The modulus of the cross-ply laminate $[0_2/90_2]_s$ is only slightly higher than that of the $[0_2/\pm45]_s$ laminate and its stacking sequence variations, but its strength is lower by approximately 12 percent. The $[0_2/\pm15]_s$ layup showed the most dramatic influences of ply orientation. The modulus of 201 GPa (29.2 x 10^6 psi) approaches that of the unidirectional material and the strength is higher than that of the $[0_2/\pm45]_s$ layups by approximately 28 percent. The most pronounced result is the high value of 1.53 for Poisson's ratio. Stacking sequence variations of the basic $[0_2/\pm45]_s$ had no significant effect on measured modulus and strength, although the $[0/+45/0/-45]_s$ layup displayed consistently lower strength values.

Specimens were subjected to a tensile preload equal to 70 percent of the static strength and to 100 thermal cycles between room temperature and 533 degK (500°F). No changes in measured strains were observed between the beginning and the end of cycling. The low FVR

specimens failed during cycling. Residual properties were measured for the surviving specimens. The $[0_2/\pm 15]_s$ specimens show higher residual strength and unchanged modulus. The $[0_2/90_2]_s$ laminate, having the highest residual stresses, showed a reduction in both strength and stiffness. No significant changes between initial and residual properties were observed in the three stacking sequence variations of the basic $[0_2/\pm 45]_s$ laminate.

Similarly loaded specimens were subjected to 100 cycles between room temperature and 200 degK (-100°F). No strain changes were observed between the beginning and the end of the cycling. The residual strength of the low FVR specimens remained unchanged, but the modulus showed some reduction. The $[0_2/\pm 15]_s$ specimens showed higher residual strength and unchanged modulus. The $[0_2/90_2]_s$ laminate, having the highest residual stresses, showed a reduction in both strength and modulus, as above. The stacking sequence variations of the basic $[0_2/\pm 45]_s$ laminate showed no significant changes between initial and residual properties. Again, as in the case of initial static properties and residual properties after elevated temperature cycling, the $[0/+45/0/-45]_s$ layup showed a somewhat lower strength than the other stacking sequence variations.

One major contribution of this phase of the program is the development and successful application of techniques for measuring residual strains during curing. Residual strains were measured for six composite systems and, in the case of Graphite/Polyimide, for two fiber volume ratios, three layups and four stacking sequence variations of one layup. The same techniques can be readily applied to measurement of residual strains in hybrid angle-ply laminates and evaluate the influence of hybridization on the magnitude of residual stresses and residual strength. Hybridizing Graphite/Epoxy with S-Glass/Epoxy and Kevlar 49/Epoxy should be investigated.

The effect of residual stresses on laminates with defects and damaged areas would be of importance. Specimens with cutouts,

cracks or other defects could be prepared with varying ply configurations resulting in different states of residual stress. Strain concentrations and maximum strain at failure would be determined to evaluate the effect of residual stresses on fracture around defects.

In all the tasks conducted in the present phase of the investigation, the effects of residual stresses are measured in an indirect manner, because there is no comparison with similar residual-stress-free specimens. The independent influence of residual stresses on elastic response and strength can be studied by comparing conventionally fabricated angle-ply laminates with similar stress-free laminates produced by bonding together at room temperature precured plies.

The combination of residual stresses and interlaminar stresses near edges can be beneficial or deleterious. These combined stresses near free edges should be investigated.

Knowledge of the complete relaxation characteristics of unidirectional composites for different fiber orientations and at different temperatures will help in evaluating the exact amount of relaxation of lamination residual stresses. Similar relaxation properties in shear and under states of biaxial stress would help describe the response of individual plies in angle-ply laminates.

The small number of tests described in this report where acoustic emission was used point out the potential of this technique in assessing structural degradation in composites. This technique could be very useful in conjunction with other strain measuring techniques, including embedded strain gages. It could be used effectively in monitoring progressive degradation in thermally or mechanically cycled laminates.

The effects of residual stresses on dynamic response of composite laminates is of great relevance to the foreign-object-damage (FOD) of jet engine turbine blades. Stress wave propagation for a

variety of material and loading parameters, including residual stresses, should be studied. Stress wave studies should include determination of propagation velocities of different types of waves, i.e., dilatational, distortional and flexural waves, and attenuation, reflection and induced fracture types and fracture propagation. Experimental techniques, such as surface and embedded strain gages, photoelastic coatings and moire grids are very suitable.

Impact resistance of composite laminates should be studied as a function of lamination construction, hence residual stresses. The effects of hybridization should also be studied. Ultrasonic techniques are very suitable for damage assessment in such studies.

Proper evaluation of results of dynamic loading of composites requires knowledge of the basic material properties for similar timescales, i.e., at high strain rates. Very little work has been done in the area of dynamic (high strain rate) characterization of composites. Such characterization of unidirectional and angle-ply laminates as a function of strain rate for tensile, compressive and shear loading is greatly needed.

REFERENCES

1. Chamis, C.C., "Lamination Residual Stresses in Cross-Plied Fiber Composites," Proc. of 26th Annual Conference of SPI, Reinforced Plastics/Composites Division, Paper No. 17-D, February 1971.

2. Chamis, C.C., "Design and Analysis of Fiber Composite Structural Components," NASA Report SP227, 1970, pp. 217-228.

3. Ahimaz, F.J., Liber, T. and Daniel, I.M., "Development of Techniques for Determination of Relationship Between Surface and Subsurface Strains in Boron-Epoxy Composites," Tech. Report AFFDL-TR-69-86, August 1970.

4. Grumman Aerospace Corporation, "Advanced Composite Wing Structures - B/E Design Data," Vol. II, Analytical Data, Tech. Report AL-SM-ST-8085, November 1969.

5. "Development of Engineering Data for Advanced Composite Materials," Fourth, Fifth, and Seventh Quarterly Progress Reports for Contract F33615-69-C-1474, General Dynamics/Fort Worth Division, 1969-1970.

6. "Structural Airframe Application of Advanced Composite Materials, Vol. IV - Physical Properties, Environmental," AFML-TR-69-101, General Dynamics/Fort Worth Division, October 1969.

7. Nadler, M.A., Yoshino, S.Y., and Darms, F.J., Jr., "Boron-Epoxy Support Strut for Non-Integral Cryogenic Tankage," Report No. SD68-995-1, North American Rockwell Corp./Space Division, February 1969.

8. "Advanced Composite Wing Structures, Material Qualification Properties," Technical Report AC-ME-ST-8082, Contract F33615-68-C-1301, Grumman Aerospace Corporation, October 1968.

9. Mangiapane, J.A., "Advanced Composite Engine Development Program," AFML TR-70-89, Parts I and II, April 1970.

10. Hercules, Incorporated, Data Sheets Nos. 815, 815-2, 816, 816-1, 823, 824, 828, ACI-3, ACI-4, ACM-5.

11. Narmco Whittaker Data Sheets for Modmor I/WRD 9371 and 4 mil Boron/WRD 9371, Modulite 5206.

12. Monsanto Company Data Sheets for Skybond 700 (5042C), Skybond 703 (T.B. #6236), Skybond 709 (T.B. #6239).

REFERENCES (Cont'd)

13. Ciba-Geigy Data Sheets for P13N Polyimide Laminating Varnish and P105A Polyimide Laminating Varnish.

14. Hertz, J., Christian, J.L., et al., "Advanced Composite Applications for Spacecraft and Missiles," Phase I, Final Report, AFML-TR-71-186, Vol. II, March 1972, pp. 3-122.

15. Cavano, P.J., Jones, R.J., et al., "Resin/Graphite Fiber Composites," NASA-CR-72983, TRWER7396-F, March 1, 1972.

16. Gray, R.M., "Boron and Graphite Reinforced Elevated Temperature Composites," Advanced Comp. Data and Analysis Program, Lockheed Georgia Company Report No. ACDAPRept. 2, July 1971.

17. Browning, C.E., "Mechanical Properties of Epoxy Composites Reinforced with Experimental Graphite Fabrics," AFML TR-69-127, June 1969.

18. Boll, K.G. and Mangiapane, J.A., "Advanced Composite Engine Design Allowables Program," AFML TR-70-320, March 1971.

19. Cole, L.F. and Mulvaney, W.P., "Mechanical Property Correlations Between High Performance Composites and Cast Epoxy Resin Data," SPI 22nd Annual Mtg. Proceedings, Section 4-C.

20. Patterson, C.W., "Epoxy Systems and Applications," for SAMPE, October 15, 1968.

21. Fiberite Co. Data Sheets for hy E1305A, hy E1105 and hy E1305C.

22. Ferro Corporation Data Sheets for Ferro E293, Ferropreg C4010, Ferropreg C5010, Ferropreg C5025.

23. Advanced Composite Technology Fuselage Program, AFML Contract F33615-69-C-1494, General Dynamics/Fort Worth Division, Started April 1969.

24. Flightworthy Graphite Reinforced Aircraft Primary Structural Assemblies, AFML Contract F33615-69-C-1490, Northrop Corp. Aircraft Division, Started April 1969.

25. Varlas, M., "Development of Epoxy-Graphite/Asbestos Laminates," GDC-ERR-1422, Convair Division of General Dynamics, 1969.

26. "Development of Carbon Composite Structural Elements for Missile Interstage Application," AFML Contract F33615-67-C-1641, The Boeing Company.

27. Varlas, M., "Advanced Graphite Reinforced Resin Composites," IRAD 111-7006-111, Convair Division of General Dynamics, 1970.

28. Celanese Corporation, Published Literature, 1970.

29. Private Communication Between Dr. T.P. Airhart, Fort Worth Division of General Dynamics, April 14, 1970 and G.D. Convair (See Ref. 1).

30. Striepens, A.H., "New Data for Production of Graphite/ Polyimide Laminates for Near Zero Thermal Coefficients of Expansion," Contract No. NAS 9-10960, North American Rockwell Corp., Downey, California.

31. "Scotchply" Type 1002-S, Technical Data Sheet No. 4, January 1969, Minnesota Mining and Manufacturing Company.

32. "Scotchply" Type 1009-265, Technical Data Sheet No. 2, October 1963, Minnesota Mining and Manufacturing Company.

33. "Scotchply" Reinforced Plastic XP-251S, Technical Data Sheet No. 5, December 1968, Minnesota Mining and Manufacturing Company.

34. Daniel, I.M., Mullineaux, J.L., Ahimaz, F.J. and Liber, T., "The Embedded Gage Technique for Testing Boron/Epoxy Composites," Composite Materials: Testing and Design (Second Conference), ASTM STP 497, 1972, pp. 257-272.

35. Advanced Composites Design Guide, 3rd edition, Vol. IV, Materials, January 1973 (Prepared by Rockwell International Corporation for the AFML).

36. Kaminski, B.E., Lemon, G.H., and McKague, E.L., "Development of Engineering Data for Advanced Composite Materials - Volume I, Static and Thermophysical Properties," AFML-TR-70-108, Contract F33615-68-C-1474, General Dynamics/Convair Aerospace Division/ Fort Worth, October 1972.

37. "F-15 Composite Wing Flight Test," Second Quarterly Technical Report for Contract F33615-71-C-1536, MDC/MAC Report MDC A1424, McDonnell Douglas/McDonnell Aircraft Company, November 1971.

DISTRIBUTION LIST

Advanced Research Projects Agency
Washington, D.C. 20525
Attn: Library

Advanced Technology Center, Inc.
LTV Aerospace Corporation
P.O. Box 6144
Dallas, Texas 75222
Attn: D.H. Petersen

Air Force Flight Dynamics Laboratory
Wright-Patterson Air Force Base, Ohio 45433
Attn: L.J. Obery (TBP)
       G.P. Sendeckyj (FBC)
       R.S. Sandhu

Air Force Materials Laboratory
Wright-Patterson Air Force Base, Ohio 45433
Attn: J.D. Ray (LTN)
       H.S. Schwartz (LN)
       T.J. Reinhart (MBC)
       G.P. Peterson (LC)
       E.J. Morrisey (LAE)
       A. Hopkins (LLN)
       S.W. Tsai (MBM)
       N.J. Pagano
       J.M. Whitney (MBM)
       J.C. Halpin

Air Force Office of Scientific Research
Washington, D.C. 20333
Attn: J.F. Masi (SREP)

Air Force Office of Scientific Research
1400 Wilson Blvd.
Arlington, VA 22209
Attn: SIGL

Air Force Rocket Propulsion Laboratory
Edwards, CA 93523
Attn: Library

Babcock and Wilcox Co.
Advanced Composites Department
P.O. Box 419
Alliance, Ohio 44601
Attn: K. Lauraitis

Bell Helicopter Co.
P.O. Box 482
Ft. Worth, Texas 76101
Attn: H. Zinberg

The Boeing Company
P.O. Box 3999
Seattle, Washington 98124
Attn: J.T. Hoggatt, MS 88-33

The Boeing Company
Vertol Division
Morton, PA 19070
Attn: W.D. Harris
       R.A. Pinckney

Battelle Memorial Institute
Columbus Laboratories
505 King Avenue
Columbus, Ohio 43201
Attn: E.F. Rybicki
       B. Noton

Brunswick Corporation
Defense Products Division
P.O. Box 4594
43000 Industrial Avenue
Lincoln, Nebraska
Attn: R. Morse

Chemical Propulsion Information Agency
Applied Physics Laboratory
8621 Georgia Avenue
Silver Spring, MD 20910
Attn: Library

Commander
Natick Laboratories
U.S. Army
Natick, MA 01762
Attn: Library

Commander
Naval Air Systems Command
U.S. Navy Department
Washington, D.C. 20360
Attn: M. Stander, AIR-42032D
       C. Bersch

Commander
Naval Ordnance Systems Command
U.S. Navy Department
Washington, D.C. 20360
Attn: B. Drimmer, ORD-033
       M. Kinna, ORD-033A

Cornell University
Dept. Theoretical & Applied Mech.
Thurston Hall
Ithaca, New York 14853
Attn: F.C. Moon

Defense Metals Information Center
Battelle Memorial Institute
Columbus Laboratories
505 King Avenue
Columbus, Ohio 43201

Department of the Army
U.S. Army Material Command
Washington, D.C. 20315
Attn: AMCRD-RC

Department of the Army
U.S. Army Aviation Materials Laboratory
Ft. Eustis, Va. 23604
Attn: I.E. Figge, Sr.
       R. Berrisford

Department of the Army
U.S. Army Aviation Systems Command
P.O. Box 209
St. Louis, Mo. 63166
Attn: R. Vollmer, AMSAV-A-UE

Department of the Army
Plastics Technical Evaluation Center
Picatinny Arsenal
Dover, New Jersey 07801
Attn: H.E. Pebly, Jr.

Department of the Army
Watervliet Arsenal
Watervliet, N.Y. 12189
Attn: F.W. Schmiedershoff

Department of the Army
Watertown Arsenal
Watertown, MA   02172
Attn: A. Thomas

Department of the Army
Redstone Arsenal
Huntsville, AL   35809
Attn: R.J. Thompson, AMSMI-RSS

Department of the Navy
Naval Ordnance Laboratory
White Oak
Silver Spring, MD   20910
Attn: R. Simon

Department of the Navy
U.S. Naval Ship R&D Laboratory
Annapolis, MD   21402
Attn: C. Hersner, Code 2724

Director
Deep Submergence Systems Project
6900 Wisconsin Avenue
Washington, D.C.   20015
Attn: H. Bernstein, DSSP-221

Director
Naval Research Laboratory
Washington, D.C.   20390
Attn: Code 8430
        I. Wolock, Code 8433

E.I. DuPont DeNemours and Co.
DuPont Experimental Station
Wilmington, DE   19898
Attn: C.H. Zweben

Fiber Science, Inc.
245 East 157th Street
Gardena, CA.   90248
Attn: L.J. Ashton

General Dynamics
P.O. Box 748
Ft. Worth, Texas   76100
Attn: J.E. Ashley
        M.E. Waddoups

General Dynamics/Convair
P.O. Box 1128
San Diego, CA   92112
Attn: J.L. Christian

General Electric Co.
Evendale, Ohio   45215
Attn: C. Stotler
        R. Ravenhall
        C.A. Steinhagen

Goldsworthy Engineering Inc.
Lomiter Blvd.
Torrance, CA   90505
Attn: B.H. Jones

General Motors Corp.
Detroit Diesel-Allison Division
Indianapolis, Indiana
Attn: M. Herman

Grumman Aerospace Corporation
Bethpage, Long Island, N.Y.   11714
Attn: S. Dastin
        J.B. Whiteside

Hamilton Standard Division
United Aircraft Corporation
Windsor Locks, CT   06096
Attn: W.A. Percival

Hercules, Inc.
Allegheny Ballistics Laboratory
P.O. Box 210
Cumberland, MD   21052
Attn: A.A. Vicario

Illinois Institute of Technology
10 West 32 Street
Chicago, Illinois 60616
Attn: L.J. Broutman

Jet Propulsion Laboratory
4800 Oak Grove Drive
Pasadena, California 91103
Attn: A.C. Knoell
       W. Jensen

Lawrence Livermore Laboratory
P.O. Box 808, L-421
Livermore, California 94550
Attn: T.T. Chiao

Lockheed-Georgia Co.
Advanced Composites Information Center
Dept. 72-14, Zone 402
Marietta, Georgia 30060

Lockheed Missiles and Space Co.
P.O. Box 504
Sunnyvale, California 94087
Attn: R.W. Fenn

McDonnell Douglas Aircraft Corporation
P.O. Box 516
Lambert Field, MS 63166
Attn: J.C. Watson

McDonnell Douglas Aircraft Corporation
3855 Lakewood Blvd.
Long Beach, California 90810
Attn: L.B. Greszczuk

Massachusetts Institute of Technology
Cambridge, MA 02139
Attn: F.J. McGarry
       J.F. Mandell

Material Sciences Corporation
1777 Walton Road
Blue Bell, PA 19422
Attn: B.W. Rosen

NASA-Ames Research Center
Moffett Field, California 94035
Attn: Library
       D.P. Williams

NASA-Flight Research Center
P.O. Box 273
Edwards, California 93523
Attn: Library

NASA-George C. Marshall Space Flight Center
Huntsville, Alabama 35812
Attn: D.D. Thompson, S&E, ASTN-PPA
       C.E. Cataldo, S&E-ASTN-MX
       Library

NASA-Goddard Space Flight Center
Greenbelt, MD 20771
Attn: Library

NASA-Langley Research Center
Hampton, VA 23365
Attn: E.E. Mathauser, MS 188a
       R.A. Pride, MS 188a
       M.C. Card
       Library

NASA-Lewis Research Center
21000 Brookpark Road
Cleveland, Ohio 44135
Attn: Contracting Officer, MS 500-313
       Tech. Report Control, MS 5-5
       Technical Utilization, MS 3-19
       AFSC Liaison, MS 501-3
       Rel. and Quality Assur., MS 500-211
       R.A. Signorelli, MS 106-1
       M.P. Hanson, MS 501-7
       R.H. Kemp, MS 49-3
       R.F. Lark, MS 49-3
       J.C. Freche, MS 49-1
       R.H. Johns, MS 49-3
       N.T. Saunders, MS 105-1
       C.C. Chamis, MS 49-3 (16 copies)
       T.T. Serafini, MS 49-1
       Library, MS 60-3 (2 copies)
       Director, ASRDI, MS 6-2 (2 copies)

NASA-Lyndon B. Johnson Space Center
Houston, Texas 77001
Attn: R.E. Johnson, SMD-ES5
       S. Glorioso, SMD-ES52
       Library

NASA Headquarters
Washington, D.C. 20546
Attn: G.C. Deutsch

NASA Scientific and Tech. Information Facility
P.O. Box 33
College Park, MD 20740
Attn: Acquisitions Branch (10 copies)

National Aeronautics and Space Administration
Office of Advanced Research and Technology
Washington, D.C. 20546
Attn: L.A. Harris, Code RWS

National Aeronautics and Space Administration
Office of Technology Utilization
Washington, D.C. 20546

National Bureau of Standards
Eng. Mech. Section
Washington, D.C. 20234
Attn: R. Mitchell

National Technology Information Service
Springfield, VA   22151 (6 copies)

National Science Foundation
Engineering Division
1800 G Street, N.W.
Washington, D.C. 20540
Attn: Library

Northrop Space Laboratories
3401 West Broadway
Hawthorne, CA 90250
Attn: D. Stanbarger

Pratt & Whitney Aircraft
East Hartford, CT
Attn: A.J. Dennis

Rockwell International
Los Angeles Division
International Airport
Los Angeles, CA   90009
Attn: L.M. Lackman

Sikorsky Aircraft Division
United Aircraft Corporation
Stratford, CT.   06602
Attn: Library

Southwest Research Institute
8500 Culebra Road
San Antonio, Texas   78284
Attn: G.C. Grimes

Space and Missile Systems Organization
Air Force Unit Post Office
Los Angeles, CA.   90045
Attn: Technical Data Center

Structural Composites Industries, Inc.
6344 N. Irwindale Avenue
Azusa, CA   91702
Attn: E.E. Morris

TRW, Incorporated
23555 Euclid Avenue
Cleveland, Ohio   44117
Attn: W.E. Winters

Union Carbide Corporation
P.O. Box 6116
Cleveland, Ohio   44101
Attn: J.C. Bowman

United Technologies Research Center
East Hartford, CT   06108
Attn: R.C. Novak

University of Dayton Research Institute
Dayton, OH   45409
Attn: W.S. Blain

DISTRIBUTION LIST (Cont'd)

University of Oklahoma
School of Aerospace Mechanical and
  Nuclear Engineering
Norman, OK 73069
Attn: C.W. Bert

U.S. Army Materials and Mechanics
  Research Center
Watertown Arsenal
Watertown, MA   02172
Attn: E.M. Lenoe

V.P.I. and S.U.
Dept. of Eng. Mech.
Blacksburg, VA 24061
Attn: R.H. Heller
       H.F. Brinson

Washington University
Materials Research Laboratory
St. Louis, MO
Attn: E.M. Wu